frontiers | Research Topics

Respiratory microbiome in health and disease

Edited by
Jianmin Chai, Jiangchao Zhao and Tao Ding

Coordinated by
Yimin Zhuang

Published in
Frontiers in Cellular and Infection Microbiology

ISSN 1664-8714
ISBN 978-2-8325-4112-8
DOI 10.3389/978-2-8325-4112-8

About Frontiers

Frontiers is more than just an open access publisher of scholarly articles: it is a pioneering approach to the world of academia, radically improving the way scholarly research is managed. The grand vision of Frontiers is a world where all people have an equal opportunity to seek, share and generate knowledge. Frontiers provides immediate and permanent online open access to all its publications, but this alone is not enough to realize our grand goals.

Frontiers journal series

The Frontiers journal series is a multi-tier and interdisciplinary set of open-access, online journals, promising a paradigm shift from the current review, selection and dissemination processes in academic publishing. All Frontiers journals are driven by researchers for researchers; therefore, they constitute a service to the scholarly community. At the same time, the *Frontiers journal series* operates on a revolutionary invention, the tiered publishing system, initially addressing specific communities of scholars, and gradually climbing up to broader public understanding, thus serving the interests of the lay society, too.

Dedication to quality

Each Frontiers article is a landmark of the highest quality, thanks to genuinely collaborative interactions between authors and review editors, who include some of the world's best academicians. Research must be certified by peers before entering a stream of knowledge that may eventually reach the public - and shape society; therefore, Frontiers only applies the most rigorous and unbiased reviews. Frontiers revolutionizes research publishing by freely delivering the most outstanding research, evaluated with no bias from both the academic and social point of view. By applying the most advanced information technologies, Frontiers is catapulting scholarly publishing into a new generation.

What are Frontiers Research Topics?

Frontiers Research Topics are very popular trademarks of the *Frontiers journals series*: they are collections of at least ten articles, all centered on a particular subject. With their unique mix of varied contributions from Original Research to Review Articles, Frontiers Research Topics unify the most influential researchers, the latest key findings and historical advances in a hot research area.

Find out more on how to host your own Frontiers Research Topic or contribute to one as an author by contacting the Frontiers editorial office: frontiersin.org/about/contact

Respiratory microbiome in health and disease

Topic editors
Jianmin Chai — Foshan University, China
Jiangchao Zhao — University of Arkansas, United States
Tao Ding — Sun Yat-sen University, China

Topic coordinator
Yimin Zhuang — China Agricultural University, China

Citation
Chai, J., Zhao, J., Ding, T., Zhuang, Y., eds. (2023). *Respiratory microbiome in health and disease*. Lausanne: Frontiers Media SA. doi: 10.3389/978-2-8325-4112-8

Table of contents

frontiers | Frontiers in Cellular and Infection Microbiology

TYPE Editorial
PUBLISHED 29 November 2023
DOI 10.3389/fcimb.2023.1335337

OPEN ACCESS

EDITED AND REVIEWED BY
Souhaila Al Khodor,
Sidra Medicine, Qatar

*CORRESPONDENCE
Tao Ding
dingt8@mail.sysu.edu.cn
Jiangchao Zhao
jzhao77@uark.edu
Jianmin Chai
jchai@uark.edu

RECEIVED 08 November 2023
ACCEPTED 21 November 2023
PUBLISHED 29 November 2023

CITATION
Zhuang Y, Ding T, Zhao J and Chai J (2023) Editorial: Respiratory microbiome in health and disease. *Front. Cell. Infect. Microbiol.* 13:1335337. doi: 10.3389/fcimb.2023.1335337

Editorial: Respiratory microbiome in health and disease

Yimin Zhuang[1,2], Tao Ding[3]*, Jiangchao Zhao[4]* and Jianmin Chai[1,4]*

[1]Guangdong Provincial Key Laboratory of Animal Molecular Design and Precise Breeding, College of Life Science and Engineering, Foshan University, Foshan, China, [2]State Key Laboratory of Animal Nutrition, College of Animal Science and Technology, China Agricultural University, Beijing, China, [3]Department of Immunology and Microbiology, Zhongshan School of Medicine, Sun Yat-sen University, Guangzhou, China, [4]Department of Animal Science, Division of Agriculture, University of Arkansas, Fayetteville, AR, United States

KEYWORDS

respiratory microbiome, health, respiratory disease, respiratory tracts, microbe-microbe interaction, microbe-host interaction

Editorial on the Research Topic
Respiratory microbiome in health and disease

Respiratory diseases, such as COVID-19, pneumonia, asthma, chronic obstructive pulmonary disease, and lung cancer, etc., are leading causes of death and disability in the world. With the development of sequencing technology, the critical roles of the respiratory microbiome in health and disease have been understood (Zhao et al., 2012). As we know, a diverse and dynamic community of microbiomes colonizes the inter-surface of the respiratory system. However, compared to the gut ecosystem, fewer studies focus on the respiratory microbiome and its roles in health and disease. Although a changed respiratory microbiome is associated with a specific disease and host inflammation, more studies need to be conducted to broadly investigate the importance of the respiratory microbiome in health and disease.

A total of 15 original studies published in this Research Topic broaden our knowledge of the respiratory microbiome. These studies generally reveal the potential relationship between respiratory microbiome and various diseases, which benefits our understanding of how the airway microbiota maintain respiratory health and resist disease.

In the past years, the coronavirus disease 2019 (COVID-19) epidemic that spread throughout the world has impacted our life and health. Revealing the critical roles of microbiota may contribute to the prevention and treatment the COVID-19. Ferrari et al. found that Shannon's entropy and the nasopharyngeal bacterial microbiota (BMN) Factor1 were positively associated with serum anti-RBD-IgG antibody maintenance, suggesting that BNM composition may influence the immunological memory against SARS-CoV-2 infections. Li et al. examined the changes in stool and oral microbiota from the same individuals during the pre-pandemic (before March 2020) and early pandemic (May–November 2020) phases and found that stool and saliva microbiota from the pre-pandemic to early pandemic periods largely exhibited ecological stability (especially stool microbiota), with most associations in loss of diversity or changes in composition related to more

reported health issues and pandemic-associated worries. Ling et al. assessed longitudinal changes in the upper respiratory microbiome, its association with disease severity, and potential confounders in adult hospitalized patients with COVID-19. Among all covariates, antibiotic treatment had the largest effect on upper airway microbiota. Longitudinal analysis showed that the upper respiratory microbiota alpha and beta diversity was unchanged during hospitalization in the absence of antimicrobial therapy.

Pneumonia, a common lung infection, causes the air sacs, or alveoli, of the lungs to fill up with fluid or pus in one or both lungs. It usually is caused by bacteria, viruses, or fungi. In terms of other diseases, He et al. compared the difference in the lower respiratory tract (LRT) microbiome between patients with hematopoietic stem cell transplantation (HSCT), healthy controls (HC), and patients with community-acquired pneumonia (CAP). The results showed the diversity of the LRT microbiome significantly decreased in patients with post-HSCT pneumonia, and the overall community was different from the CAP and HC groups. At the phylum level, post-HSCT pneumonia samples had a high abundance of Actinobacteria and a relatively low abundance of Bacteroidetes. The same was true for non-survivors compared with survivors in patients with post-HSCT pneumonia. At the genus level, the abundances of *Pseudomonas*, *Acinetobacter*, *Burkholderia*, and *Mycobacterium* were prominent in the pneumonia group after HSCT. On the other hand, gut-associated bacteria, *Enterococcus*, was more abundant in the non-survivors. Some pathways concerning amino acid and lipid metabolism were predicted to be altered in patients with post-HSCT pneumonia. Hu et al. conducted a multi-omics association analysis to detect the interactions between the oropharyngeal microbiome and the metabolome in pediatric patients with influenza A virus pneumonia, and the results indicated that compared to healthy children, children with IAV pneumonia exhibited significant changes in the oropharyngeal macrobiotic structure and significantly lower microbial abundance and diversity. These changes came with significant disturbances in the levels of oropharyngeal metabolites. Intergroup differences were observed in 204 metabolites mapped to 36 metabolic pathways. Significantly higher levels of sphingolipid (sphinganine and phytosphingosine) and propanoate (propionic acid and succinic acid) metabolism were observed in patients with IAV pneumonia than in healthy controls. Using Spearman correlation analysis, correlations between IAV pneumonia-associated discriminatory microbial genera and metabolites were evaluated. The results indicated significant correlations and consistency in variation trends between *Streptococcus* and three sphingolipid metabolites (phytosphingosine, sphinganine, and sphingosine). Besides these three sphingolipid metabolites, the sphinganine-to-sphingosine ratio and the joint analysis of the three metabolites indicated remarkable diagnostic efficacy in children with IAV pneumonia. Xu et al. concluded that metagenomic next-generation sequencing (mNGS) of bronchoalveolar lavage fluid (BALF) improves the sensitivity of pathogen detection and provides guidance in clinical practice for diagnosing lower respiratory tract infections in children. Moreover, the importance of oral microbiota in other respiratory diseases, such as periodontitis, chronic obstructive pulmonary disease (COPD), and comorbid diseases, was classified. Liu et al. found significant differences in the bacterial community and functional characterization of oral microbiota in periodontitis, COPD, and comorbid diseases. Compared to gingival crevicular fluid, subgingival plaque may be more appropriate for reflecting the difference in subgingival microbiota in periodontitis patients with COPD. These results provide a potential path for predicting, screening, and treatment strategies for individuals with periodontitis and COPD.

The respiratory microbiota in animals affected by environmental factors also correlates with respiratory disease (Chai et al., 2022). In addition to human research, publications in this Research Topic also detect the microbial characteristics of bovine respiratory tract. Howe et al., detected the microbial difference between healthy calves and bovine respiratory disease (BRD) calves and found greater variation in microbial diversity in the BRD calves. Consensus approaches-based random forest, DESeq2, and ANCOM-BC2 were successfully applied to identify signature bacteria. Immigration of the microbiota from the upper airways to the lungs has been confirmed in humans (Zhang et al., 2022). In cattle, Zhang et al. found that the microbial connections among the upper and lower airway were observed in beef cattle regardless of geography, although the microbial diversity, structure, and composition in the upper and lower respiratory tract in beef cattle from China, the United States, Canada, and Italy were significantly different. Regarding the spatial dissimilarities among the respiratory niches, the nostril and nasopharynx had a more similar microbiome compared to the lung communities. Additionally, the major bacterial immigration patterns in the bovine respiratory tract were estimated, and some of them were associated with geography.

Except for the associations between the airway microbiota and respiratory disease, gut microbiota interacting with lung disease and health is another hot topic, which might provide a new treatment direction for respiratory disease. Hu et al. found that acute respiratory distress syndrome (ARDS) altered the gut microbiota of the patients. This study confirmed that the *Escherichia–shigella* genus was effective at distinguishing AP-ARDS from AP-nonARDS, which could predict ARDS occurrence in AP patients.

The present Research Topic highlights the tight associations between the respiratory microbiota and disease. It also reveals the microbe–microbe interaction in the respiratory tract, which is influenced by multiple environmental factors. These recent advancements in the field of respiratory microbiome in health and disease of both animals and humans provide insights into how to manipulate respiratory microbiota to improve host health in the future.

Author contributions

YZ: Investigation, Resources, Writing – original draft. TD: Resources, Supervision, Writing – review & editing. JZ: Funding acquisition, Project administration, Visualization, Writing – review & editing. JC: Funding acquisition, Writing – original draft, Writing – review & editing, Project administration.

Funding

The author(s) declare financial support was received for the research, authorship, and/or publication of this article. This project

was supported by Agriculture and Food Research Initiative Competitive Grant No. 20196701629869 from the USDA National Institute of Food and Agriculture, National Natural Science Foundation of China (No. 32170430), Guangdong Provincial Key Laboratory of Animal Molecular Design and Precise Breeding (2019B030301010), and Key Laboratory of Animal Molecular Design and Precise Breeding of Guangdong Higher Education Institutes (2019KSYS011).

Acknowledgments

The editor thanks the Frontiers administration team for their wonderful support with the Research Topic and the numerous peer reviewers.

Conflict of interest

The authors declare that the research was conducted in the absence of any commercial or financial relationships that could be construed as a potential conflict of interest.

Publisher's note

References

Chai, J., Capik, S. F., Kegley, B., Richeson, J. T., Powell, J. G., and Zhao, J. (2022). Bovine respiratory microbiota of feedlot cattle and its association with disease. *Vet. Res.* 53 (1), 4. doi: 10.1186/s13567-021-01020-x

Zhang, J., Wu, Y., Liu, J., Yang, Y., Li, H., Wu, X., et al. (2022). Differential oral microbial input determines two microbiota pneumo-types associated with health status. *Adv. Sci. (Weinh).* 9 (32), e2203115. doi: 10.1002/advs.202203115

Zhao, J., Schloss, P. D., Kalikin, L. M., Carmody, L. A., Foster, B. K., Petrosino, J. F., et al. (2012). Decade-long bacterial community dynamics in cystic fibrosis airways. *Proc. Natl. Acad. Sci. U.S.A.* 109 (15), 5809–5814. doi: 10.1073/pnas.1120577109

frontiers | Frontiers in Cellular and Infection Microbiology

ORIGINAL RESEARCH
published: 06 July 2022
doi: 10.3389/fcimb.2022.882302

Nasopharyngeal Bacterial Microbiota Composition and SARS-CoV-2 IgG Antibody Maintenance in Asymptomatic/ Paucisymptomatic Subjects

Luca Ferrari[1,2], Chiara Favero[1], Giulia Solazzo[1], Jacopo Mariani[1], Anna Luganini[3], Monica Ferraroni[4], Emanuele Montomoli[5], Gregorio Paolo Milani[6,7], Valentina Bollati[1,2] and UNICORN Consortium[1†]*

[1] EPIGET Lab, Department of Clinical Sciences and Community Health, Università degli Studi di Mila-no, Milan, Italy, [2] Department of Preventive Medicine, Fondazione IRCCS Ca' Granda Ospedale Maggiore Policlinico, Milan, Italy, [3] Laboratory of Microbiology and Virology, Department of Life Sciences and Systems Biology, Università degli Studi di Torino, Turin, Italy, [4] Branch of Medical Statistics, Biometry, and Epidemiology "G. A. Maccacaro", Department of Clinical Sciences and Community Health, Università degli Studi di Milano, Milan, Italy, [5] Department of Molecular and Developmental Medicine, Università degli Studi di Siena, Siena, Italy, [6] Department of Clinical Sciences and Community Health, Università degli Studi di Milano, Milan, Italy, [7] Pediatric Unit, Fondazione IRCCS Ca' Granda Ospedale Maggiore Policlinico, Milan, Italy

The severe acute respiratory syndrome coronavirus 2 (SARS-CoV-2) causes the coronavirus disease 2019 (COVID-19), ranging from asymptomatic conditions to severe/fatal lung injury and multi-organ failure. Growing evidence shows that the nasopharyngeal microbiota composition may predict the severity of respiratory infections and may play a role in the protection from viral entry and the regulation of the immune response to the infection. In the present study, we have characterized the nasopharyngeal bacterial microbiota (BNM) composition and have performed factor analysis in a group of 54 asymptomatic/paucisymptomatic subjects who tested positive for nasopharyngeal swab SARS-CoV-2 RNA and/or showed anti-RBD-IgG positive serology at the enrolment. We investigated whether BNM was associated with SARS-CoV-2 RNA positivity and serum anti-RBD-IgG antibody development/maintenance 20–28 weeks after the enrolment. Shannon's entropy α-diversity index [odds ratio (OR) = 5.75, p = 0.0107] and the BNM Factor1 (OR = 2.64, p = 0.0370) were positively associated with serum anti-RBD-IgG antibody maintenance. The present results suggest that BNM composition may influence the immunological memory against SARS-CoV-2 infections. To the best of our knowledge, this is the first study investigating the link between BNM and specific IgG antibody maintenance. Further studies are needed to unveil the mechanisms through which the BNM influences the adaptive immune response against viral infections.

Keywords: UNICORN, SARS-CoV-2, nasopharyngeal bacterial microbiota, immunoglobulins, asymptomatic carriers

OPEN ACCESS

Edited by:
Carlo Contini, University of Ferrara, Italy

Reviewed by:
Sebastien Boutin, Heidelberg University Hospital, Germany
Alba Boix-Amoros, Icahn School of Medicine at Mount Sinai, United States

***Correspondence:**
Valentina Bollati
valentina.bollati@unimi.it

†The full list of UNICORN Consortium members is reported in the ***Supplementary Material***

Specialty section:
This article was submitted to Microbiome in Health and Disease, a section of the journal Frontiers in Cellular and Infection Microbiology

Received: *23 February 2022*
Accepted: *28 April 2022*
Published: *06 July 2022*

Citation:
Ferrari L, Favero C, Solazzo G, Mariani J, Luganini A, Ferraroni M, Montomoli E, Milani GP, Bollati V and UNICORN Consortium (2022) Nasopharyngeal Bacterial Microbiota Composition and SARS-CoV-2 IgG Antibody Maintenance in Asymptomatic/ Paucisymptomatic Subjects. Front. Cell. Infect. Microbiol. 12:882302. doi: 10.3389/fcimb.2022.882302

INTRODUCTION

The severe acute respiratory syndrome coronavirus 2 (SARS-CoV-2) has been infecting millions of people and causing more than five million deaths worldwide since the end of 2019 (Wu and McGoogan, 2020; WHO, 2021). The SARS-CoV-2 virus infection causes the coronavirus disease 2019 (COVID-19), ranging in presentation from asymptomatic to severe lung injury and multi-organ failure, eventually leading to death (Berlin et al., 2020; Gandhi et al., 2020; Vicenzi et al., 2020). The host features influence both the severity and outcomes of SARS-CoV-2 infection (Lauer et al., 2020; Sun et al., 2020), and the local and systemic immune responses play a key role in the reaction to the viral threat especially in the first stage of disease (Tay et al., 2020). Most of the infected individuals experience asymptomatic to mild symptomatic conditions, but only some of them develop antibodies (Milani et al., 2020a; Milani et al., 2020b).

SARS-CoV-2 binds to the host cells through the interaction between the receptor-binding domain (RBD), present in the viral spike (S) glycoprotein, and the angiotensin-converting enzyme 2 (ACE2) on host cells (Hoffmann et al., 2020). Most SARS-CoV-2-infected individuals produce S- and RBD-specific antibodies during the first 2 weeks of the primary response, and RBD-specific antibodies can neutralize the virus *in vitro* and *in vivo* (Rodda et al., 2021).

SARS-CoV-2 virus penetrates the host through the upper airways, and the nasal barrier is the first defensive line to limit infection (Tay et al., 2020). In addition to the epithelial layer and the local immune system, the upper airways harbor a community of microorganisms, the nasopharyngeal microbiota, which is pivotal in maintaining mucosal homeostasis and in the resistance to infections (Man et al., 2017). Growing evidence shows that the nasopharyngeal microbiota composition may help to predict the severity of respiratory infections (de Steenhuijsen Piters et al., 2015; Kumpitsch et al., 2019; Man et al., 2019). However, the role of the upper airway microbiota in COVID-19 is far from being understood and likely goes beyond protection from viral entry to include the regulation of the immune response to the infection (Di Stadio et al., 2020).

The present study was aimed at characterizing the nasopharyngeal bacterial microbiota (BNM) by 16S rRNA gene sequencing in a group of 54 asymptomatic/paucisymptomatic subjects who tested positive for nasopharyngeal swab SARS-CoV-2 RNA and/or showed positive serology for anti-RBD-IgG at the enrolment. We investigated whether the composition of the BNM collected at the enrolment was associated with serum anti-RBD-IgG development and maintenance after 20–28 weeks. This study was part of the UNICORN ("UNIversity against CORoNavirus") project, which was conducted among the personnel of the University of Milan (Milani et al., 2020a; Milani et al., 2020b, Milani et al., 2021).

MATERIALS AND METHODS

The investigated subjects are a subset of the UNICORN study. The enrolment criteria and procedures were previously described (Milani et al., 2021). Briefly, all the participants in the study were volunteers working at the University of Milan. In this specific study, antibiotic consumption up to 1 month before the enrolment was considered an exclusion criterion. Other excluding criteria were fever, any symptoms of flu-like infections or dyspnea at the time of the recruitment or during the preceding 14 days, prolonged and close contact with any subjects positive for SARS-CoV-2, or symptoms suggestive of infection during the previous 14 days. The study was approved by the ethics committee of the University of Milan (approval number 17/20; approval date March 6, 2020; amendment date November 17, 2020) and conducted following the Declaration of Helsinki. All participants signed an informed consent form.

This investigation includes 54 subjects selected among those who tested positive for either SARS-CoV-2 RNA nasopharyngeal swab or serum anti-RBD IgG antibodies in the UNICORN study population. The present study includes the subjects who donated the nasal swab within 3 months from the beginning of the pandemic in Italy (during the first wave of SARS-CoV-2, from March to June 2020) and whose DNA yield and quality were acceptable to perform the 16S sequencing (yield > 100 ng; purity 260/280 ratio > 1.8; 260/230 ratio 1.8–2.1).

Nasopharyngeal Sample Collection and SARS-CoV-2 RNA Detection

Nasopharyngeal swabs were collected from each participant, viral RNA was extracted, and SARS-CoV-2 RNA was detected as previously detailed (Milani et al., 2021). Briefly, RNA was isolated from swabs by using the QIAamp Viral RNA Mini Kit (Qiagen, Hilden, Germany), according to the manufacturer's instructions. SARS-CoV-2 RNA detection was performed by using the multiplex real-time quantitative PCR test TaqPath COVID-19 CE-IVD RT-PCR Kit, Thermo Fisher Scientific (Waltham, MA, USA) following the manufacturer's instructions. In each extracted sample, 10 µl of internal control RNA (i.e., MS2 Phage) and an RNA carrier were added before being stored at −80°C. In the PCR, specific probes were annealed to three specific SARS-CoV-2 sequences: 1) ORF1ab with reporter dye FAM; 2) N protein (nucleocapsid) with reporter dye VIC; and 3) S protein with reporter dye ABY. The MS2 internal control-specific probe (labeled with the JUN dye) was included to verify the efficacy of the sample preparation. After RNA was reverse transcribed into cDNA, samples were amplified using the QuantStudio 12K Flex Real-Time PCR Instruments (Thermo Fisher). The data analysis was performed using the "Design and Analysis Software" (V.2.3.3, Thermo Fisher) setting "Automatic Threshold." The reaction was considered only if the MS2 cycle threshold (Ct) ≤38. If any two of the three SARS-CoV-2 genes were positive (Ct ≤38), the sample was classified as positive; if only one of the assays was positive, the test was repeated. If after repetition the sample tested positive again, the sample was classified as positive for SARS-CoV-2 RNA. If all three of the assays were negative (Ct = undetermined), the subject was classified as negative.

16S rRNA Gene Sequencing

DNA from nasopharyngeal swabs was extracted by using QIAamp® UCP Pathogen Mini (Qiagen, Hilden, Germany) following the manufacturer's guidelines. The extracted DNA

was stored at −20°C and later shipped to the sequencing service facility Personal Genomics Srl (Verona, Italy) for qualitative and quantitative checks, PCR amplification, and second-generation sequencing analysis. Four extraction- and PCR-negative controls were included in the procedure, but library preparation for these control samples failed. Libraries were obtained by following the Illumina 16S Metagenomic Sequencing Library Preparation (Illumina, San Diego, CA, USA). The bacterial microbiome was investigated by amplicon sequencing analysis of the 16S rRNA gene hypervariable regions V3–V4, amplified with the following oligonucleotides: Pro341F (5′-CCTACGGGNBGCASCAG-3′) and Pro805R (5′-GACTACNVGGGTATCTAATCC-3′). Sequencing was performed with the Illumina MiSeq platform (Illumina) by using a paired-end library of 300-bp insert size.

Upstream Analyses and Operational Taxonomic Unit Clustering

Raw read quality and statistics were checked using FastQC v0.11.2 and then imported into QIIME2 v2020.6 (Bolyen et al., 2019) software for the following analysis. Primer sequences were removed from each read with cutadapt plugin using the trim-paired method to improve database read matching. The trimmed files were then joined using Vsearch's merge_pairs function with a minimum overlap length of forward and reverse reads of 80 bp, to cover the 16S V3–V4 region (Rognes et al., 2016). Then, joined reads underwent a quality filtering process to exclude from further analysis those reads with a quality value less than a PHRED score of 20 on a base-slide window of 3 nucleotides. The retained joined reads were then grouped into high-resolution amplicon sequence variants (ASVs) using the Deblur denoiser plugin with an arbitrary minimum length of 400 bp to be retained (Amir et al., 2017). Taxonomic assignment was done through the skylearn-classifier against the SILVA v132_99_16S database, which had been modified to contain only the V3–V4 16S fragments to improve read matching. Mafft-fast-tree method and default setting suggested in the QIIME2 pipeline were applied to align the sequences and to generate rooted and unrooted trees for phylogenetic analysis.

Downstream Analysis

Downstream analyses were carried out using QIIME2 v2020.62 analyzing the above-described ASV or feature table. Taxonomic values within each sample and group were assigned to each ASV from the phylum to the genus level. ASVs that failed genus attribution were tagged as "Unassigned" followed by the specific family label. Before diversity analysis, all samples were rarefied to 10,000 sequences with a seed of 10 in order to avoid the influence of different sequencing depths, as this number of sequences was the minimum identified in the ASVs table. α-Diversity richness, evenness, and genetic distance were calculated using observed ASVs, Shannon, and Faith's phylogenetic diversity (Faith's PD) indices.

Blood Collection and Serum Anti-RBD-IgG Detection

Blood samples were collected in ethylenediamine tetra-acetic acid (EDTA) tubes and processed within 2 h of the phlebotomy. The detection of specific anti-RBD-IgG antibodies was performed by an ELISA approach that was previously described (Mazzini et al., 2021; Milani et al., 2021). Briefly, for the detection of anti-RBD IgG, ELISA plates were coated with purified recombinant spike-RBD HEK-derived protein (Sino Biological, Beijing, China). Serum samples were heat-inactivated at 56°C for 1 h and diluted at 1:100 in Tris-buffered saline (TBS)–0.05% Tween 20 5%. Each serum dilution measuring 100 µl was added to the coated plates with specific antibodies and incubated for 1 h at 37°C. Then, 100 µl/well of Goat anti-Human IgG-Fc horseradish peroxidase (HRP)-conjugated antibody (dilution 1:100,000; Bethyl Laboratories, Montgomery, TX, USA) was added. After incubation at 37°C for 30 min, plates were washed and 100 µl/well of 3,3′,5,5′-tetramethylbenzidine substrate (Bethyl Laboratories) was added in the dark at room temperature for 20 min. After stopping the reaction with 100 µl of ELISA stop solution (Bethyl Laboratories), plates were read at 450 nm, with a cutoff value established as three times the average optical density (OD) values from blank wells (background—no addition of analyte). Borderline samples were defined where one replicate was under the cutoff and the other was above. Sensitivity was reported to be 85.7% and specificity 98.1%.

Statistical Analysis

Descriptive statistics were performed on all variables. Quantitative data were expressed as mean ± SD or as median [first quartile–third quartile] if not normally distributed. Categorical data were presented as frequencies and percentages. Continuous variables were tested for normality and linearity. Factor analysis was applied to reduce a large dimension of microbiome data to a smaller number of latent independent factors to predict microbiome composition at the genus level (**Supplementary Figure S1**). A set of 47 genera, excluding *a priori* two genera (i.e., ":" and "uncultured"), were selected because they did not provide any interpretable results. Next, the correlation matrix of the log-transformed variables was analyzed. Since *Sphingomonas* and *Streptococcus* genera did not correlate (p-value >0.05) with any other genera and correlation coefficients were less than |0.25|, they were not included in the factor analysis. Whether the correlation matrix of the log-transformed relative abundances of 45 genera was factorable was evaluated by visual inspection of the matrix as well as statistical procedures, including Bartlett's test of sphericity, overall [Kaiser–Meyer–Olkin (KMO)], and individual measures of sampling adequacy (**Table 1**). An overall KMO ≤ 0.50 for the factor analysis and genera with a measure of sampling adequacy <0.30 (Rajalahti and Kvalheim, 2011) were considered unacceptable. Thus, 20 genera were excluded, and the method assumption on the correlation matrix was verified again considering the remaining 25 genera. The new correlation matrix was factorable, but six genera (*Staphylococcus*, *Campylobacter*, *Clostridium senso stricto 10*, *Moraxella*, *Escherichia-Shigella*, and *Corynebacterium 1*) were excluded because of their low communality; i.e., they explained less than 15% of variance each. In the last correlation matrix, all the assumptions were satisfied, and factor analysis was applied to obtain the microbiome patterns.

TABLE 1 | Factorability of the correlation matrix of the log-transformed genera: Bartlett's test of sphericity and measures of sampling adequacy.

	from correlation matrix N=45	from correlation matrix N=25	from correlation matrix N=19
Bartlett's test of sphericity:	p-value <0.0001	p-value <0.0001	p-value <0.0001
Kaiser-Meyer-Olkin statistic - Overall measure of sampling adequacy:	0.36	0.69	0.70
Individual measures of sampling adequacy:			
< 0.30	*Paracoccus, Mesorhizobium, Neisseria, Lawsonella, Citrobacter, Ralstonia, Carnobacterium, Dolosigranulum, Micrococcus, Peptoniphilus, Anaerococcus, Acinetobacter, Finegoldia, Geobacillus, Enhydrobacter, Deinococcus, Serratia, Labrys, Gemella, Thermosinus*	–	–
0.30 - 0.40	*Afipia, Staphylococcus, Escherichia Shigella, Caldicellulosiruptor, Vibriomonas, Corynebacterium 1, Sediminbacterium*	*Staphylococcus*	–
0.40 - 0.50	*Thermus, Clostridium senso stricto 10, Cutibacterium, Bacillus, Tepidiphilus, Bradyrhizobium, Moraxella, Campylobacter*	*Afipia, Vibriomonas, Campylobacter*	*Afipia, Vibriomonas*
0.50 - 0.60	*Thermoanaerobacter, Pseudomonas, Aeromonas, Enterococcus*	*Bradyrhizobium, Sediminbacterium, Pseudomonas*	*Bradyrhizobium, Pseudomonas, Sediminbacterium*
0.60 - 0.70	*Gulbenkiania, Thermoanaerobacterium, Tumebacillus, Fervidobacterium, Comamonas*	*Thermus, Thermoanaerobacterium, Caldicellulosiruptor, Clostridium senso stricto 10, Enterococcus*	*Thermus, Thermoanaerobacterium, Caldicellulosiruptor, Enterococcus*
0.70 - 0.80	*Burkholderia Caballeronia Parabulkholderia*	*Cutibacterium, Escherichia Shigella, Tepidiphilus, Moraxella, Thermoanaerobacter, Gulbenkiania, Tumebacillus, Aeromonas, Corynebacterium 1*	*Thermoanaerobacter, Tepidiphilus, Gulbenkiania, Tumebacillus*
0.80 - 0.90	-	*Comamonas, Bacillus, Fervidobacterium, Burkholderia Caballeronia Parabulkholderia*	*Aeromonas, Enterococcus, Bacillus, Thermosinus, Thermoanaerobacter, Comamonas, Gulbenkiania, Burkholderia Caballeronia Parabulkholderia*
≥ 0.90	-	-	-

Overall and individual measures of sampling adequacy range between 0 and 1, with values > 0.50 indicating an acceptable size.

Exploratory principal component factor analysis was performed on the correlation matrix of nineteen selected genera to identify a smaller set of uncorrelated underlying factors. The number of factors to be included in the analysis was chosen considering the following criteria: factor eigenvalues > 1, scree-plot construction, and factor interpretability (Härdle and Simar, 2012). A varimax rotation to the factor-loading matrix was applied to obtain a simpler loadings structure and improve the interpretation. Genera with an absolute rotated factor loading ≥ 0.63 on a given factor were used to name the factor and are indicated as "dominant genera" hereafter (Gudgeon et al., 1994). Factor scores, calculated for each subject and each pattern, indicated how consistent was each participant's microbiome with the identified pattern. To confirm both reproducibility and stability of the identified independent factors, additional exploratory factor analyses were carried out to derive factor scores from all genera (n = 45) and 25 genera with KMO ≥ 0.30. Given the reassuring and consistent results from this check, all the subsequent analyses on the factor scores derived from the subset of 19 genera were carried out. To assess the reliability of microbiome patterns and internal consistency of genera that load more than |0.40| on any factor, Cronbach's coefficient alpha for each factor and coefficient alpha when the item was deleted were calculated. Next, two different outcomes were focused on. First, whether the microbiome

influenced the probability of developing IgG antibodies was verified at both the baseline (i.e., enrolment T1) and the follow-up (T2). Second, whether the microbiome composition modified the probability to maintain anti-RBD IgG antibodies at the T2 (i.e., 20–28 weeks after enrolment) in subjects with IgG+ at the T1 was investigated.

Multiple logistic regression models were applied to estimate the odds ratios (ORs), and their 95% CI for each microbiome pattern was estimated with factor analysis, α-diversity indices, and relative abundance for each taxon at the phylum and genus levels. One model was fitted for each microbiome pattern. All multivariable models were adjusted for age, gender, smoking habit (yes, no, and former), lifestyle (active and sedentary), and the month of enrolment. Due to the high number of comparisons, multiple comparison correction methods based on the Benjamini–Hochberg false discovery rate (FDR) were applied to calculate the FDR p-value. In the second outcome, the models were adjusted also for SARS-CoV-2 RNA detection at the T1 (positive and negative).

To improve the interpretability of microbiome patterns significantly associated with anti-RBD IgG measured at the T2, a score adding the relative abundance of the overall four dominant genera (i.e., *Enterococcus*, *Pseudomonas*, *Bacillus*, and *Burkholderia Caballeronia Paraburkholderia*) was created in the so-called Factor1. A receiver operating characteristic (ROC) curve was generated to evaluate the diagnostic ability of the microbiome score to distinguish between participants maintaining or non-maintaining IgG at T2. The optimum threshold was selected by Youden's index as the one that maximized sensitivity (SE) + specificity (SP) − 1. The area under the ROC curve (AUC) and the corresponding 95% CI, SE, SP, and threshold were reported. Statistical analyses and graphs were performed with SAS software (version 9.4; SAS Institute Inc., Cary, NC, USA) and R software (version 4.1.2; Foundation for Statistical Computing, Vienna, Austria).

RESULTS

Study Population

The study population was composed of 54 asymptomatic/paucisymptomatic subjects who tested positive for nasopharyngeal swab SARS-CoV-2 RNA and/or showed anti-RBD-IgG antibodies for SARS-CoV-2 at the enrolment (defined as T1). At the T1, 19 out of 54 subjects presented positive nasopharyngeal swab for SARS-CoV-2, while 35 tested positive only for serology of anti-RBD-IgG antibodies. Thus, 6 subjects were positive for both the nasopharyngeal swab and serology at the T1 (**Supplementary Table S1**). At the T2, occurring approximately 20–28 weeks after the T1, 32 out of 41 individuals with positive serology at the T1 (i.e., 35 IgG-positive individuals + 6 swab- and IgG-positive individuals) maintained positive serology. All the participants in the study were employed at the University of Milan, Italy, at the time of the enrollment. Subjects who tested positive for SARS-CoV-2 RNA nasopharyngeal swab were completely asymptomatic at enrolment, while subjects who tested positive for serum anti-RBD IgG antibodies reported completely no symptoms (40.7%), or mild-to-moderate symptoms (51.9% at least one episode of upper airway infections; 20.4% with at least one episode of lower airway infections; 44.4% with at least one episode of fever), which occurred from October 2019 to 14 days before the enrolment (none of them with a previous certified COVID-19 diagnosis). The characteristics of the study population are reported in **Table 2**.

Nasopharyngeal Bacterial Microbiota Composition and α-Diversity

Considering the entire study population, the BNM was dominated by Actinobacteria (relative abundance mean 30.6% (SD ± 24.36%), Firmicutes (36.98% ± 17.6%), and Proteobacteria (30.56% ± 21.28%) phyla (**Supplementary Table S2**). Of the 47 genera detected, the most represented in the study population were *Corynebacterium* (21.95% ± 24.4%), *Enterococcus* (9.78% ± 7.51%), *Staphylococcus* (8.15% ± 13.44%), *Dolosigranulum* (8.14% ± 1.65%), *Pseudomonas* (9.23% ± 8.91%), *Cutibacterium* (6% ± 6.52%), *Burkholderia Caballeronia Paraburkholderia* (5.24% ± 4.66%), *Bacillus* (4.19% ± 3.67%), *Moraxella* (3.53% ± 13.94%), and *Gulbenkiania* (3.35% ± 3.07%) (**Figure 1**; **Supplementary Table S3**). BNM compositional diversity (α-diversity) was calculated for each sample in the study. The richness and phylogenetic diversity evaluated in terms of ASVs showed a mean of 36.85 (± 8.15), while the Faith_PD index mean was 3.02 (± 0.58). Shannon index, which combines estimates of richness and evenness within the samples, had a mean of 3.42 (± 0.90). After univariate analysis, among the 47 genera identified, only *Vibrionimonas* median relative abundance was different in the 19 subjects who were positive for SARS-CoV-2 RNA, compared to the 35 who were negative (SARS-CoV-2 RNA positive, 0.44%; SARS-CoV-2 RNA negative, 0.04%, p-value = 0.02), and no differences were observed for α-diversity indices (**Supplementary Table S4**).

In addition, we performed 16S sequencing in a group of 18 healthy negative control subjects who tested negative for both SARS-CoV-2 RNA and anti-RBD SARS-CoV-2 IgG at the T1, were negative for anti-RBD SARS-CoV-2 IgG at T2, and reported no symptoms attributable to SARS-CoV-2 infection. However, as not all asymptomatic subjects with positive SARS-CoV-2 RNA develop IgG (Milani et al., 2020a), we considered that attributing the negative control status (i.e., assuming no contact with the virus) on the basis of the result of the IgG analysis was not adequate. We thus decided to exclude the "negative control group" from the factor analysis. Nonetheless, a descriptive analysis is reported in **Supplementary Figure S2**.

Exploratory Factor Analysis

The correlation matrix of the 19 selected genera (**Figure 2**; **Supplementary Table S5**) was suitable for factor analysis. **Table 1** reports the results of statistical procedures for checking matrix factorability. Bartlett's test of sphericity was significant ($p < 0.001$). The overall measure of sampling adequacy was equal to 0.70, indicating that the sample size was

TABLE 2 | Characteristics of the study participants.

	All subjects N = 54
Age, years mean ± SD	45 ± 12.0
Gender, N (%)	
Male	28 (51.9)
Female	26 (48.1)
BMI, kg/m^2, mean ± SD	23.8 ± 4.1
Smoking, N (%)	
Never	38 (70.3)
Former	9 (16.7)
Current	7 (13.0)
Education, N (%)	
Junior high school	1 (1.9)
High school	10 (18.5)
University	10 (18.5)
Above university	33 (61.1)
Means of transport to and from work, N (%)	
Private means of transport	28 (53.9)
Public means of transport	17 (32.7)
Both	7 (13.4)
Time to and from work, N (%)	
<1 h	43 (82.7)
1–2 h	9 (17.3)
Lifestyle, N (%)	
Sedentary	14 (26.0)
Active	40 (74.0)
Travels (from October 2019), N (%)	
Europe (at least one)	21 (38.9)
America (at least one)	6 (11.5)
Oceania (at least one)	0 (0.0)
Asia (at least one)	3 (5.8)
Africa (at least one)	1 (1.9)
Flu vaccine, N (%)	
Yes	10 (18.5)
From October 2019	
Upper airway infections, N (%)	
Yes	28 (51.9)
Lower airway infections, N (%)	
Yes	11 (20.4)
Fever, N (%)	
Yes	24 (44.4)
At least one of symptoms, N (%)	
Yes	32 (59.3)

Continuous variables are expressed as mean ± SD; discrete variables are expressed as counts (%).
BMI, body mass index.

sufficient, as compared to the number of genera under consideration. In addition, the individual measures of sampling adequacy were satisfactory. **Table 3** shows the factor-loading matrix for the three retained microbiome patterns, the corresponding communality estimates, and the proportion of explained variance. The retained factor explained 72.34% of the total variance in the original dataset. The first factor, named Factor1, had the highest contribution from *Enterococcus*, *Pseudomonas*, *Bacillus*, and *Burkholderia Caballeronia Paraburkholderia*. The second factor, named Factor2, was characterized by the greatest positive loadings on *Comamonas*, *Aeromonas*, *Caldicellulosiruptor*, and *Gulbenkiania* and by the highest negative loadings on *Thermoanaerobacter*, *Thermoanaerobacterium*, and *Tumebacillus*. The third pattern, named Factor3, had the highest factor loadings on *Bradyrhizobium*, *Vibrionimonas*, and *Sediminibacterium*. All the examined genera had at least one-factor loading greater than |0.40|, thus proving an important role of all genera included in this analysis.

Effects of Nasopharyngeal Bacterial Microbiota Composition of Positive Serology Development/Maintenance

We investigated the effects of the bacterial community composition and α-diversity on the probability of developing or maintaining serum anti-RBD-IgG antibodies during the entire period of the study. No associations were observed either between the bacterial community composition or between the α-diversity indices and the probability of developing anti-RBD-IgG antibodies in the 19 participants with a positive nasal swab for SARS-CoV-2 RNA at the T1 (**Table 4** and **Supplementary Table S6**). As a sensitivity analysis, we excluded the three subjects who were negative for anti-RBD SARS-CoV-2 IgG at T1 and missing at T2. Results were comparable to those obtained in the whole group of subjects (**Supplementary Table S7**). The calculated ORs and 95% CIs of the effects of the BNM composition on maintaining a positive serology at T2 in the 41 participants with positive IgG at the T1 and with known serological anti-RBD-IgG status at the T2 are reported in **Table 5**. Shannon's entropy α-diversity showed a positive association with serum anti-RBD-IgG antibody maintenance (OR = 5.75, 95% CI: 1.50–22.01, p = 0.0107). Factor1 pattern was positively associated with the maintenance of anti-RBD-IgG antibodies (OR = 2.64, 95% CI: 1.06–6.56, p = 0.0370). To improve the interpretability of the Factor1 pattern, we created a score by adding the relative abundance of the four Factor1 dominant genera (i.e., *Enterococcus*, *Pseudomonas*, *Bacillus*, and *Burkholderia Caballeronia Paraburkholderia*). This score was associated with a higher probability of maintaining positive IgG at the T2 (OR = 1.09, 95% CI: 1.01–1.17, p = 0.0271). Thus, the probability of maintaining anti-RBD-IgG antibodies increases by 9% for each increment of 1% in the sum of the relative abundances of the four dominant genera. When we considered single genera, only *Enterococcus* showed a positive significant association (OR = 1.21, 95% CI: 1.0–1.42, p = 0.0243) (**Supplementary Table S8**). A ROC curve was fitted to examine the prognostic ability of this score in assessing the probability to maintain anti-RBD-IgG at the T2 (**Figure 3**). The optimal threshold score was 23.3% (p = 0.0084), which yielded maximum discrimination between individuals maintaining or not the positive IgG (sensitivity 0.63, specificity 0.78).

DISCUSSION

Nasal cavities represent the principal entry and infection site of SARS-CoV-2, as most of the inhaled air enters the body through the nose and the nasal epithelium expresses high levels of the ACE2, which act as the coronavirus receptor (Hou et al., 2020). Nasopharyngeal microbiota has a critical role in protecting the host from both viral and pathogenic bacterial infections, thus cooperating with the nasal immune response (Salzano et al.,

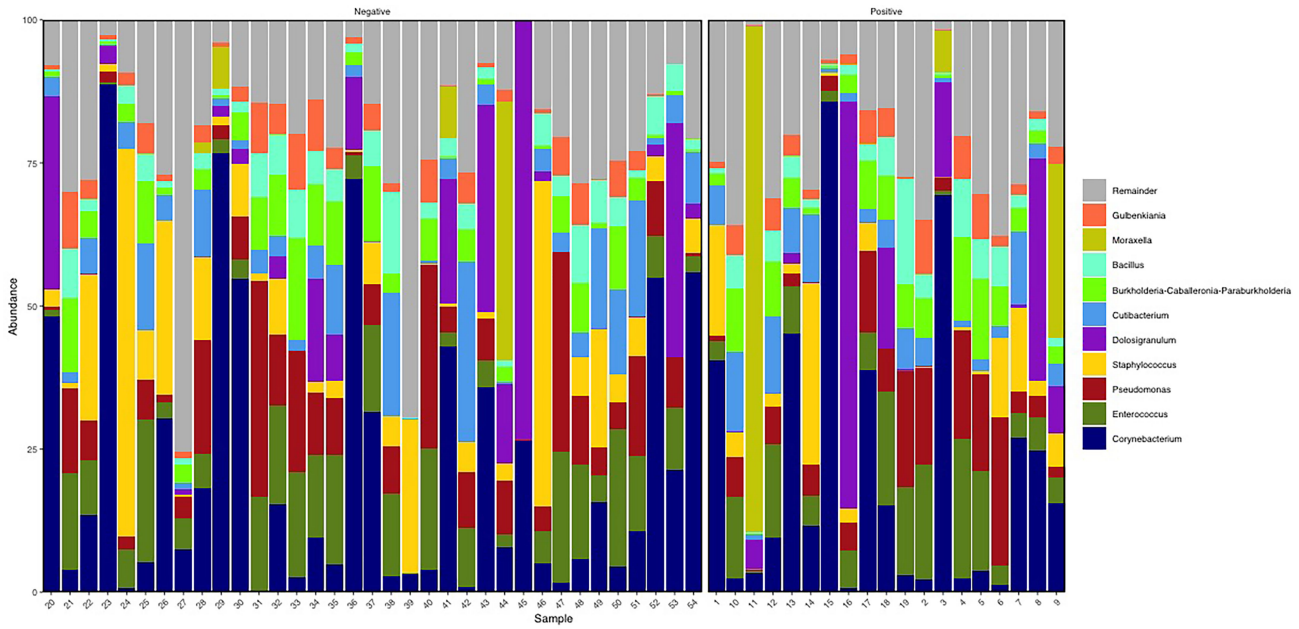

FIGURE 1 | Descriptive nasopharyngeal bacterial microbiota (BNM) genus-profile composition in the two groups SARS-CoV-2 RNA negative (i.e., negative, N = 35) and SARS-CoV-2 RNA positive (i.e., positive, N = 19). Here the top 10 most abundant genera are represented. Figure generated by R software (version 4.1.2 https://www.r-project.org/)

2018). In particular, the nasopharyngeal microbiota influences mucosal homeostasis (Di Stadio et al., 2020) and is involved in the development of the mucosa-associated lymphoid tissue and in the modulation of adaptive responses such as the activation of both cell-mediated and humoral immune responses (Brown et al., 2013; De Rudder et al., 2020; Dimitri-Pinheiro et al., 2020).

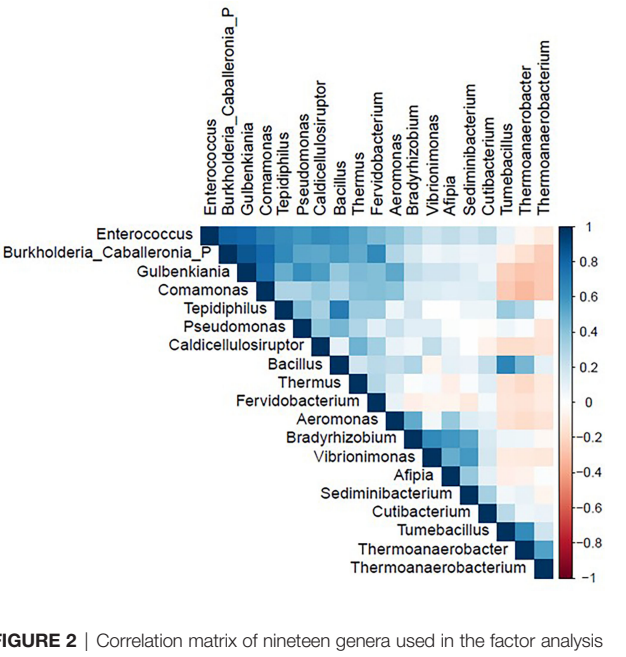

FIGURE 2 | Correlation matrix of nineteen genera used in the factor analysis in the study population (N = 54). Figure generated by R software (version 4.1.2 https://www.r-project.org/).

We characterized the BNM composition in a group of asymptomatic/paucisymptomatic individuals who tested positive for nasopharyngeal swab SARS-CoV-2 RNA and/or serum anti-RBD SARS-CoV-2 IgG at the enrolment. In terms of taxa, the BNM composition was similar to the one reported for healthy (not infected) populations of adult subjects (Man et al., 2017; Bomar et al., 2018; Mariani et al., 2018; Budden et al., 2019). Our results are supported by other previous studies reporting that patients with mild or asymptomatic COVID-19 were characterized by a bNM similar to that of negative healthy controls, suggesting that in asymptomatic/paucisymptomatic subjects who tested positive for SARS-CoV-2 RNA, the BNM composition apparently is not affected by the viral infection (De Maio et al., 2020; Rosas-Salazar et al., 2021; Shilts et al., 2022). The link between BNM composition and SARS-CoV-2 RNA has been investigated by a growing number of case–control studies that specifically focused on SARS-CoV-2-positive patients, either symptomatic or paucisymptomatic, compared to not infected healthy controls. De Maio and colleagues investigated the BNM by 16S rDNA sequencing in a group of 40 patients with mild COVID-19 disease, and no differences were observed in terms of neither the bacterial composition nor α-diversity between those who tested positive compared to those who were tested negative (De Maio et al., 2020). On the contrary, Nardelli et al. reported a significant reduction of Proteobacteria and Fusobacteria relative abundances in symptomatic patients, compared to healthy controls (Nardelli et al., 2021). The study conducted by Rueca and colleagues reported that Shannon's α-diversity index was

TABLE 3 | Factor-loading matrix*, commonalities (COMM), and explained variance for three microbiome patterns identified by factor analysis.

Genera	Factor1	Factor2	Factor3	COMM
Aeromonas	0.39	**0.63**	–	0.55
Afipia	0.16	–	0.42	0.20
Bacillus	**0.96**	–0.11	0.10	0.94
Bradyrhizobium	0.14	–	**0.91**	0.84
Burkholderia Caballeronia Paraburkholderia	**0.83**	0.48	0.10	0.93
Caldicellulosiruptor	0.35	**0.63**	–	0.54
Comamonas	0.34	**0.86**	–	0.85
Cutibacterium	0.53	–	0.22	0.33
Enterococcus	**0.97**	0.17	0.11	0.98
Fervidobacterium	0.52	0.46	–	0.48
Gulbenkiania	0.55	**0.66**	0.17	0.76
Pseudomonas	**0.74**	0.13	–	0.56
Sediminibacterium	–	–	**0.80**	0.66
Tepidiphilus	0.56	–	–	0.32
Thermoanaerobacter	0.22	**–0.86**	–	0.80
Thermoanaerobacterium	–	**–0.66**	–	0.45
Thermus	0.41	0.38	–	0.31
Tumebacillus	0.17	**–0.90**	–	0.84
Vibrionimonas	–	0.13	**0.99**	0.99
Proportion of explained variance (%)	45.23	21.40	17.06	
Cumulative explained variance (%)	45.23	66.63	83.69	

Loadings greater or equal to 0.63 defined dominant genera for each factor and were shown in bold typeface. Loadings smaller than |0.10| were suppressed.
**Estimated from a principal component factor analysis performed on 19 genera. The magnitude of each loading measures the importance of the corresponding genus to the factor.*

reduced only in patients with a severe condition requiring intensive care compared to controls and paucisymptomatic patients, thus partially supporting our results with paucisymptomatic subjects, similar to healthy controls (Rueca et al., 2021). In a recent study conducted on 103 adult subjects, ranging from asymptomatic not infective healthy subjects to very severe SARS-CoV-2-positive patients, BNM composition changes were associated with the severity of the disease, and in particular, *Corynebacterium* consistently decreased as COVID-19 severity increased (Shilts et al., 2022). In a metagenomic analysis conducted on 50 patients under investigation for COVID-19 disease, Mostafa and colleagues did not observe any significant differences at the genus and family levels but identified an α-diversity decrease in COVID-19-confirmed symptomatic patients (Mostafa et al., 2020). The partial inconsistency of these results might be due to different limitations, such as the limited number of studies in the field together with the small samples included in the analyses. Moreover, some confounders might not have been considered, such as the different pharmacological treatments and the possibility that those who were selected as negative healthy controls might have actually encountered the virus before the enrolment.

We also investigated whether BNM composition was associated with the development and/or the maintenance of serum anti-RBD-IgG antibodies. The observed positive association between α-diversity and anti-RBD-IgG antibody maintenance at the T2 suggests that the more diverse the microbiota composition, the more effective the cross-talk with the local immune component, favoring the activation of the systemic adaptive response. Indeed, lower α-diversity and richness were reported in patients with COVID-19 compared to subjects who tested negative for SARS-CoV-2 RNA in the study of Moustafa and colleagues (Mostafa et al., 2020). Since this field of research is still in its infancy, functional studies are needed to clarify the mechanisms underlying our observations.

We further applied factor analysis to group all the microbiome data information into a smaller number of independent factors able to predict the microbiome composition at the genus level by considering the relative

TABLE 4 | Odds ratios for the estimated contribution of each α-diversity index and microbiome pattern to the probability of developing IgG in the entire period of the study.

		OR	95% CI		p-Value	R^2
α-Diversity indices	Faith pd	0.65	0.10	4.03	0.6413	0.26
	Observed features	1.02	0.89	1.16	0.7926	0.26
	Shannon entropy	0.78	0.24	2.54	0.6780	0.26
Microbiome pattern	Factor1	0.69	0.16	2.92	0.6168	0.26
	Factor2	0.05	0.001	9.55	0.2633	0.32
	Factor3	0.85	0.21	3.53	0.8276	0.26

The analysis was performed on 19 participants with positive SARS-CoV-2 RNA at the T1, by a multivariable logistic model adjusted for age, gender, smoking habit, and lifestyle.

TABLE 5 | Odds ratios for the estimated contribution of each α-diversity index and microbiome pattern to the probability of preserving IgG antibodies at follow-up.

		OR	95% CI		p-Value	R^2
α-Diversity indices	Faith pd	2.28	0.46	11.24	0.3113	0.18
	Observed features	1.09	0.97	1.22	0.1565	0.21
	Shannon entropy	5.75	1.50	22.01	0.0107	0.43
Microbiome pattern	Factor1	2.64	1.06	6.56	0.0370	0.33
	Factor2	0.76	0.32	1.83	0.5436	0.15
	Factor3	0.58	0.23	1.43	0.2333	0.19

The analysis was performed on 41 participants with positive IgG at T1, by a multivariable logistic model adjusted for age, gender, smoking habit, lifestyle, microbiome measured in March or May/June, and SARS-CoV-2 RNA.

abundances. The factorial analysis allowed us to identify three different signatures of the BNM. In particular, Factor1 was mainly characterized by *Bacillus*, *Burkholderia*, *Enterococcus*, and *Pseudomonas*, which include several opportunistic strains that may turn pathogenic and cause infections (Kumpitsch et al., 2019). Factor2 was mainly characterized by both opportunistic (such as *Aeromonas*) and environmental microbiota genera (such as *Caldicellulosibacterium* and *Comamonas*). Factor3 included different genera representative of environmental microbiota (Adams et al., 2015; Lai et al., 2017; Duan et al., 2019). In particular, this factor had the highest loading also on *Vibrionimonas*, which was the only genus that was found to be different between SARS-CoV-2 RNA-positive and RNA-negative subjects after univariate analysis. However, Factor3 was not associated either with the development or the maintenance of RBD-IgG antibodies.

Following factor analysis, we observed that the higher relative abundance of the Factor1 dominant genera was positively associated with anti-RBD-IgG maintenance. This evidence suggests that Factor1 components might influence the activation of the immune response, thus promoting the adaptive immunity against new unknown pathogens, such as the SARS-CoV-2 virus. Indeed, several species belonging to the genus *Bacillus*, such as *Bacillus subtilis*, are known stimulators of the immune system, and their colonization promotes the increase of immune cell number in the nasal mucosa, stimulating the activation of the immune response (Yang et al., 2018; Li et al., 2019). According to this hypothesis, the nasal microbiota composition was reported to influence the local host immune response and the severity of symptoms after respiratory syncytial virus bronchiolitis infection (Lynch et al., 2017; Sonawane et al., 2019; Mansbach et al., 2020; Schippa et al., 2020). Indeed, nasopharyngeal-associated lymphoid tissue (NALT), which directly interacts with the nasopharyngeal microbiota community, is constituted by a large variety and number of immune cells, including dendritic cells, macrophages, and lymphocytes (Pabst, 2015). Moreover, the BNM composition was demonstrated to influence the efficacy of a live attenuated influenza vaccine, impacting the host's adaptive immune response and thus modulating the vaccine's therapeutic efficacy (Salk et al., 2016). Thus, occurring shifts in the composition of the nasal microbiota may result in pro- or anti-inflammatory patterns with effects not only on the susceptibility and on the course of infection but also on the modulation of the local and systemic immune response.

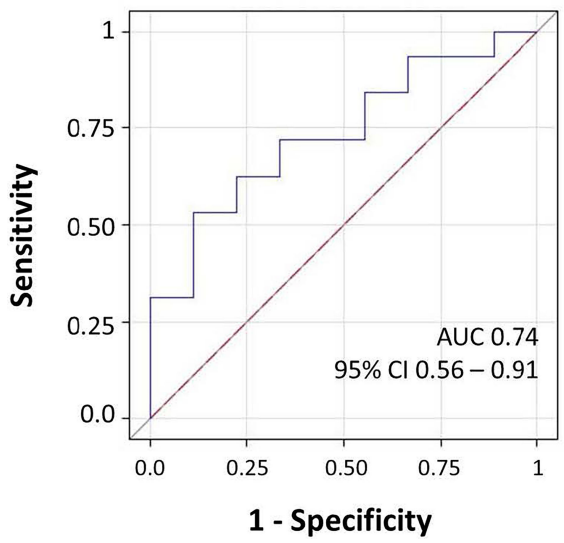

FIGURE 3 | Receiver operating characteristic (ROC) curve for microbiome score for prediction of the presence of IgG at follow-up. The area under the ROC curve (AUC) and 95% CI values were annotated.

We acknowledge some limitations of the present study. First, the small number of samples and the presence of potential confounders that we did not consider may have hindered the identification of distinct signatures between the different subgroups. Second, we did not assess anti-SARS-CoV-2 IgA antibodies, which play an important role in the local mucosal immunity. However, our study aimed to investigate whether the BNM composition might influence long-term immunization, which is related to IgG antibodies. Third, BNM was assessed during or after the infection; thus, we cannot exclude that we are observing the effects of the infection rather than a causal mechanism of antibody maintenance. Moreover, current guidelines are recommending to include in the airway microbiome investigations some negative controls as the gold standard. In particular, the negative sample results meaning negative from the sampling methods, the extraction process, and the PCR step should be included. In the present paper, we included negative controls to exclude any contaminations resulting from the extraction and the PCR amplification. A limitation of the study is that we did not include any sampling control. However, the main results of the paper describe an effect of Factor1, which includes strains that are not usually considered

of environmental origin. Moreover, due to the pandemic context, each sampling was performed in a very controlled environment, to avoid also the SARS-CoV-2 cross-contamination of subjects (e.g., environmental disinfection after each sampling, and FFP3 masks worn by the operator and by the subjects until sampling).

CONCLUSION

In conclusion, BNM is associated with the maintenance of specific anti-RBD IgG antibodies in asymptomatic/paucisymptomatic subjects, suggesting that its composition may be linked to the prompt immune activation, consequently supporting the development of immunological memory against new pathogens. To the best of our knowledge, the present study is the first to investigate the influence of BNM composition on specific IgG antibody maintenance. Further studies are required to confirm the impact of other viral infections and to unveil the mechanisms underlying the cross-talk between the BNM and the adaptive immune response.

DATA AVAILABILITY STATEMENT

The original contributions presented in the study are publicly available. This data can be found here: SRA sequence read archive database, Accession PRJNA839581.

ETHICS STATEMENT

The studies involving human participants were reviewed and approved by the Ethics committee of the University of Milan, Italy (approval number 17/20; approval date March 6, 2020; amendment date November 17, 2020). The patients/participants provided their written informed consent to participate in this study.

AUTHOR CONTRIBUTIONS

LF: study design, literature search, laboratory analysis, data interpretation, and writing. CF: data collection, statistical analysis, and writing. GS: laboratory analysis and microbiome data analysis. JM: DNA extraction and microbiome analysis. AL: microbiome analysis. MF: statistical analysis and supervision. EM: data collection, data analysis, and data interpretation. GM: study design, data collection, and funding. VB: study design, data collection, data analysis, data interpretation, and funding. UNICORN Consortium: subject's enrolment, laboratory analysis, and data interpretation. All authors reviewed the manuscript.

FUNDING

VB and GM received a grant from "Ricerche Emergenza coronavirus", University of Milan, 2020, to support the study (https://lastatalenews.unimi.it/statale-individuati-sette-progetti-ricerca-ad-alta-priorita-contro-covid-19). Funds have been used for purchasing reagents.

ACKNOWLEDGMENTS

We thank all the AVIS-Milano volunteers for their support with blood collection, Patrizia Angi-olillo for electronic questionnaire preparation, Nicla Diomede for informatics security, Elena del Giorgio for support during the subjects' enrolment, and Angelo Casertano and all the University of Milan staff for their precious help. The authors acknowledge the support of the APC central fund of the university of Milan

SUPPLEMENTARY MATERIAL

The Supplementary Material for this article can be found online at: https://www.frontiersin.org/articles/10.3389/fcimb.2022.882302/full#supplementary-material

Supplementary Figure 1 | schematic representation of statistical analysis.

Supplementary Figure 2 | Descriptive analysis of the "negative control group". **(A)** Relative abundance of the most represented genera; **(B)** alpha-diversity scores of the anti-RBD IgG positive group (IgG-pos), healthy control group (negative controls), and SARS-CoV-2 RNA positive (RNA-pos).

Supplementary Table 1 | SARS-CoV-2 RNA positivity and an-ti-RBD-IgG development of the enrolled subjects during the time study title.

Supplementary Table 2 | phyla relative abundance.

Supplementary Table 3 | genera relative abundance.

Supplementary Table 4 | Descriptive statistics of the microbiome in participants.

Supplementary Table 5 | Evaluation of nineteen genera used in the factor analysis in the study population.

Supplementary Table 6 | Odds ratios for the estimated contribution of each taxon at phylum and genus level to the probability of developing IgG in the entire period of the study in the 19 participants with a positive nasal swab for SARS-CoV-2 RNA at the T1.

Supplementary Table 7 | Odds ratios for the estimated contribution of each taxon at phylum and genus level to the probability of developing IgG in the entire period of the study in 16 participants (we excluded the three subjects who were negative for anti-RBD SARS-CoV-2 IgG at T1 and missing at T2).

Supplementary Table 8 | Odds ratios for the estimated contribution of each taxa at phylum and genus level to the probability of preserve IgG antibodies at follow-up. The analysis was performed on 41 participants with positive IgG at baseline, by multivariable logistic model adjusted for age, gender, smoking habit, lifestyle, microbiome measured in March or May/June and SARS-Cov-2 RNA. Estimates were reported for one percent increment in the relative abundance of each taxa.

REFERENCES

Adams, R. I., Bateman, A. C., Bik, H. M., and Meadow, J. F. (2015). Microbiota of the Indoor Environment: A Meta-Analysis. *Microbiome* 3, 49. doi: 10.1186/s40168-015-0108-3

Amir, A., McDonald, D., Navas-Molina, J. A., Kopylova, E., Morton, J. T., Zech Xu, Z., et al. (2017). Deblur Rapidly Resolves Single-Nucleotide Community Sequence Patterns. *mSystems*. 2, 1–7. doi: 10.1128/msystems.00191-16

Berlin, D. A., Gulick, R. M., and Martinez, F. J. (2020). Severe Covid-19. *N. Engl. J. Med.* 383, 2451–2460. doi: 10.1056/nejmcp2009575

Bolyen, E., Rideout, J. R., Dillon, M. R., Bokulich, N. A., Abnet, C. C., Al-Ghalith, G. A., et al. (2019). Reproducible, Interactive, Scalable and Extensible Microbiome Data Science Using QIIME 2. *Nat. Biotechnol.* 37, 852–857. doi: 10.1038/s41587-019-0209-9

Bomar, L., Brugger, S. D., and Lemon, K. P. (2018). Bacterial Microbiota of the Nasal Passages Across the Span of Human Life. *Curr. Opin. Microbiol* 41, 8–14. doi: 10.1016/j.mib.2017.10.023

Brown, A. F., Leech, J. M., Rogers, T. R., and McLoughlin, R. M. (2013). Staphylococcus Aureus Colonization: Modulation of Host Immune Response and Impact on Human Vaccine Design. *Front. Immunol*. 4, 507. doi: 10.3389/fimmu.2013.00507

Budden, K. F., Shukla, S. D., Rehman, S. F., Bowerman, K. L., Keely, S., Hugenholtz, P., et al. (2019). Functional Effects of the Microbiota in Chronic Respiratory Disease. *Lancet Respir. Med*. 7, 907–920. doi: 10.1016/S2213-2600(18)30510-1

De Maio, F., Posteraro, B., Ponziani, F. R., Cattani, P., Gasbarrini, A., and Sanguinetti, M. (2020). Nasopharyngeal Microbiota Profiling of SARS-CoV-2 Infected Patients. *Biol. Proced. Online.* 22, 1–4. doi: 10.1186/s12575-020-00131-7

De Rudder, C., Garcia-Tímermans, C., De Boeck, I., Lebeer, S., Van de Wiele, T., and Calatayud Arroyo, M. (2020). Lacticaseibacillus Casei AMBR2 Modulates the Epithelial Barrier Function and Immune Response in a Donor-Derived Nasal Microbiota Manner. *Sci. Rep*. 10, 1–16. doi: 10.1038/s41598-020-73857-9

de Steenhuijsen Piters, W. A. A., Sanders, E. A. M., and Bogaert, D. (2015). The Role of the Local Microbial Ecosystem in Respiratory Health and Disease. *Philos. Trans. R. Soc B Biol. Sci*. 194, 1104–1115. doi: 10.1098/rstb.2014.0294

Dimitri-Pinheiro, S., Soares, R., and Barata, P. (2020). The Microbiome of the Nose—Friend or Foe? *Allergy Rhinol*. 11, 1–10. doi: 10.1177/2152656720911605

Di Stadio, A., Costantini, C., Renga, G., Pariano, M., Ricci, G., and Romani, L. (2020). The Microbiota/Host Immune System Interaction in the Nose to Protect From COVID-19. *Life* 10, 345. doi: 10.3390/life10120345

Duan, S., Zhou, X., Xiao, H., Miao, J., and Zhao, L. (2019). Characterization of Bacterial Microbiota in Tilapia Fillets Under Different Storage Temperatures. *J. Food Sci.* 84, 1487–1493. doi: 10.1111/1750-3841.14630

Gandhi, R. T., Lynch, J. B., and del Rio, C. (2020). Mild or Moderate Covid-19. *N. Engl. J. Med.* 383, 1757–1766. doi: 10.1056/NEJMcp2009249

Gudgeon, A. C., Comrey, A. L., and Lee, H. B. (1994). A First Course in Factor Analysis. *Stat.* 43, 332. doi: 10.2307/2348352

Härdle, W. K., and Simar, L. (2012). *Applied Multivariate Statistical Analysis* (Berlin, Heidelberg: Springer Berlin Heidelberg). doi: 10.1007/978-3-642-17229-8

Hoffmann, M., Kleine-Weber, H., Schroeder, S., Krüger, N., Herrler, T., Erichsen, S., et al. (2020). SARS-CoV-2 Cell Entry Depends on ACE2 and TMPRSS2 and Is Blocked by a Clinically Proven Protease Inhibitor. *Cell*. 181, 271–280.e8. doi: 10.1016/j.cell.2020.02.052

Hou, Y. J., Okuda, K., Edwards, C. E., Martinez, D. R., Asakura, T., Dinnon, K. H., et al. (2020). SARS-CoV-2 Reverse Genetics Reveals a Variable Infection Gradient in the Respiratory Tract. *Cell*. 182, 429–446.e14. doi: 10.1016/j.cell.2020.05.042

Kumpitsch, C., Koskinen, K., Schöpf, V., and Moissl-Eichinger, C. (2019). The Microbiome of the Upper Respiratory Tract in Health and Disease. *BMC Biol.* 17, 87. doi: 10.1186/s12915-019-0703-z

Lai, P. S., Allen, J. G., Hutchinson, D. S., Ajami, N. J., Petrosino, J. F., Winters, T., et al. (2017). Impact of Environmental Microbiota on Human Microbiota of Workers in Academic Mouse Research Facilities: An Observational Study. *PloS One*. 12, 1–16. doi: 10.1371/journal.pone.0180969

Lauer, S. A., Grantz, K. H., Bi, Q., Jones, F. K., Zheng, Q., Meredith, H. R., et al. (2020). The Incubation Period of Coronavirus Disease 2019 (CoVID-19) From Publicly Reported Confirmed Cases: Estimation and Application. *Ann. Intern. Med*. 172, 577–582. doi: 10.7326/M20-0504

Li, N., Ma, W. T., Pang, M., Fan, Q. L., and Hua, J. L. (2019). The Commensal Microbiota and Viral Infection: A Comprehensive Review. *Front. Immunol*. 10, 1551. doi: 10.3389/fimmu.2019.01551

Lynch, J. P., Sikder, M. A. A., Curren, B. F., Werder, R. B., Simpson, J., Cuív, P.Ó., et al. (2017). The Influence of the Microbiome on Early-Life Severe Viral Lower Respiratory Infections and Asthma—Food for Thought? *Front. Immunol.* 8. doi: 10.3389/fimmu.2017.00156

Man, W. H., de Steenhuijsen Piters, W. A. A., and Bogaert, D. (2017). The Microbiota of the Respiratory Tract: Gatekeeper to Respiratory Health. *Nat. Rev. Microbiol.* 15, 259–270. doi: 10.1038/nrmicro.2017.14

Mansbach, J. M., Luna, P. N., Shaw, C. A., Hasegawa, K., Petrosino, J. F., Piedra, P. A., et al. (2020). Increased Moraxella and Streptococcus Species Abundance After Severe Bronchiolitis is Associated With Recurrent Wheezing. *J. Allergy Clin. Immunol.* 145, 518–527.e8. doi: 10.1016/j.jaci.2019.10.034

Man, W. H., van Houten, M. A., Mérelle, M. E., Vlieger, A. M., Chu, M. L. J. N., Jansen, N. J. G., et al. (2019). Bacterial and Viral Respiratory Tract Microbiota and Host Characteristics in Children With Lower Respiratory Tract Infections: A Matched Case-Control Study. *Lancet Respir. Med*. 7, 417–426. doi: 10.1016/S2213-2600(18)30449-1

Mariani, J., Favero, C., Spinazzè, A., Cavallo, D. M., Carugno, M., Motta, V., et al. (2018). Short-Term Particulate Matter Exposure Influences Nasal Microbiota in a Population of Healthy Subjects. *Environ. Res.* 162, 119–126. doi: 10.1016/j.envres.2017.12.016

Mazzini, L., Martinuzzi, D., Hyseni, I., Benincasa, L., Molesti, E., Casa, E., et al. (2021). Comparative Analyses of SARS-CoV-2 Binding (IgG, IgM, IgA) and Neutralizing Antibodies From Human Serum Samples. *Nat Libr Med*. 489, 112937. doi: 10.1016/j.jim.2020.112937

Milani, G. P., Dioni, L., Favero, C., Cantone, L., Macchi, C., Delbue, S., et al. (2020a). Serological Follow-Up of SARS-CoV-2 Asymptomatic Subjects. *Sci. Rep*. 10, 1–7. doi: 10.1038/s41598-020-77125-8

Milani, G. P., Montomoli, E., Bollati, V., Albetti, B., Bandi, C., Bellini, T., et al. (2020b). SARS-CoV-2 Infection Among Asymptomatic Homebound Subjects in Milan, Italy. *Eur. J. Intern. Med*. 78, 161–163. doi: 10.1016/j.ejim.2020.06.010

Milani, G. P., Rota, F., Favero, C., Dioni, L., Manenti, A., Hoxha, M., et al. (2021). Detection of IgM, IgG and SARS-CoV-2 RNA Among the Personnel of the University of Milan, March Through May 2020: The UNICORN Study. *BMJ Open* 11:1–8. doi: 10.1136/BMJOPEN-2020-046800

Mostafa, H. H., Fissel, J. A., Fanelli, B., Bergman, Y., Gniazdowski, V., Dadlani, M., et al. (2020). Metagenomic Next-Generation Sequencing of Nasopharyngeal Specimens Collected From Confirmed and Suspect Covid-19 Patients. *MBio*. 11, 1–13. doi: 10.1128/mBio.01969-20

Nardelli, C., Gentile, I., Setaro, M., Di Domenico, C., Pinchera, B., Buonomo, A. R., et al. (2021). Nasopharyngeal Microbiome Signature in COVID-19 Positive Patients: Can We Definitively Get a Role to Fusobacterium Periodonticum? *Front. Cell. Infect. Microbiol.* 11. doi: 10.3389/fcimb.2021.625581

Pabst, R. (2015). Mucosal Vaccination by the Intranasal Route. Nose-Associated Lymphoid Tissue (NALT)-Structure, Function and Species Differences. *Vaccine*. 33, 4406–4413. doi: 10.1016/j.vaccine.2015.07.022

Rajalahti, T., and Kvalheim, O. M. (2011). Multivariate Data Analysis in Pharmaceutics: A Tutorial Review. *Int. J. Pharm.* 417, 280–290. doi: 10.1016/j.ijpharm.2011.02.019

Rodda, L. B., Netland, J., Shehata, L., Pruner, K. B., Morawski, P. A., Thouvenel, C. D., et al. (2021). Functional SARS-CoV-2-Specific Immune Memory Persists After Mild COVID-19. *Cell*. 184, 169–183.e17. doi: 10.1016/j.cell.2020.11.029

Rognes, T., Flouri, T., Nichols, B., Quince, C., and Mahé, F. (2016). VSEARCH: A Versatile Open Source Tool for Metagenomics. *PeerJ* 4, e2584. doi: 10.7717/peerj.2584

Rosas-Salazar, C., Kimura, K. S., Shilts, M. H., Strickland, B. A., Freeman, M. H., Wessinger, B. C., et al. (2021). SARS-CoV-2 Infection and Viral Load are Associated With the Upper Respiratory Tract Microbiome. *J. Allergy Clin. Immunol.* 147, 1226–1233.e2. doi: 10.1016/J.JACI.2021.02.001

Rueca, M., Fontana, A., Bartolini, B., Piselli, P., Mazzarelli, A., Copetti, M., et al. (2021). Investigation of Nasal/Oropharyngeal Microbial Community of COVID-19 Patients by 16S rDNA Sequencing. *Int. J. Environ. Res. Public Health* 18, 1–12. doi: 10.3390/IJERPH18042174

Salk, H. M., Simon, W. L., Lambert, N., Kennedy, R. B., Grill, D. E., Kabat, B. F., et al. (2016). Taxa of the Nasal Microbiome are Associated With Influenza-Specificiga Response to Live Attenuated Influenza Vaccine. *PloS One*. 11, 1–13. doi: 10.1371/journal.pone.0162803

Salzano, F. A., Marino, L., Salzano, G., Botta, R. M., Cascone, G., D'Agostino Fiorenza, U., et al. (2018). Microbiota Composition and the Integration of Exogenous and Endogenous Signals in Reactive Nasal Inflammation. *J. Immunol. Res.* 2018, 1–17. doi: 10.1155/2018/2724951

Schippa, S., Frassanito, A., Marazzato, M., Nenna, R., Petrarca, L., Neroni, B., et al. (2020). Nasal Microbiota in RSV Bronchiolitis. *Microorganisms* 8, 731. doi: 10.3390/microorganisms8050731

Shilts, M. H., Rosas-Salazar, C., Strickland, B. A., Kimura, K. S., Asad, M., Sehanobish, E., et al. (2022). Severe COVID-19 Is Associated With an Altered Upper Respiratory Tract Microbiome. *Front. Cell. Infect. Microbiol.* 11. doi: 10.3389/FCIMB.2021.781968

Sonawane, A. R., Tian, L., Chu, C. Y., Qiu, X., Wang, L., Holden-Wiltse, J., et al. (2019). Microbiome-Transcriptome Interactions Related to Severity of Respiratory Syncytial Virus Infection. *Sci. Rep.* 9, 1–14. doi: 10.1038/s41598-019-50217-w

Sun, K., Chen, J., and Viboud, C. (2020). Early Epidemiological Analysis of the Coronavirus Disease 2019 Outbreak Based on Crowdsourced Data: A Population-Level Observational Study. *Lancet Digit. Heal.* 2 e201–e208. doi: 10.1016/S2589-7500(20)30026-1

Tay, M. Z., Poh, C. M., Rénia, L., MacAry, P. A., and Ng, L. F. P. (2020). The Trinity of COVID-19: Immunity, Inflammation and Intervention. *Nat. Rev. Immunol.* 20, 363–374. doi: 10.1038/s41577-020-0311-8

Vicenzi, M., Di Cosola, R., Ruscica, M., Ratti, A., Rota, I., Rota, F., et al. (2020). The Liaison Between Respiratory Failure and High Blood Pressure: Evidence From COVID-19 Patients. *Eur. Respir. J.* 51, 1–4. doi: 10.1183/13993003.01157-2020

WHO (2021). COVID-19 Weekly Epidemiological Update. *World Heal. Organ.*, 1–23. Available at: https://www.who.int/emergencies/diseases/novel-coronavirus-2019/situation-reports

Wu, Z., and McGoogan, J. M. (2020). Characteristics of and Important Lessons From the Coronavirus Disease 2019 (COVID-19) Outbreak in China. *JAMA* 323, 1239. doi: 10.1001/jama.2020.2648

Yang, Y., Jing, Y., Yang, J., and Yang, Q. (2018). Effects of Intranasal Administration With Bacillusï¿½subtilis on Immune Cells in the Nasal Mucosa and Tonsils of Piglets. *Exp. Ther. Med.* 159, 156–166. doi: 10.3892/etm.2018.6093

Conflict of Interest: The authors declare that the research was conducted in the absence of any commercial or financial relationships that could be construed as a potential conflict of interest.

Publisher's Note: All claims expressed in this article are solely those of the authors and do not necessarily represent those of their affiliated organizations, or those of the publisher, the editors and the reviewers. Any product that may be evaluated in this article, or claim that may be made by its manufacturer, is not guaranteed or endorsed by the publisher.

frontiers | Frontiers in Cellular and Infection Microbiology

TYPE Original Research
PUBLISHED 16 August 2022
DOI 10.3389/fcimb.2022.789436

OPEN ACCESS

EDITED BY
Yolanda López-Vidal,
Universidad Nacional Autónoma de México, Mexico

REVIEWED BY
Geraldine Kong,
Peter Doherty Institute for Infection and Immunity, Australia
Selvasankar Murugesan,
Sidra Medicine, Qatar

*CORRESPONDENCE
Susanna Esposito
susannamariaroberta.esposito@unipr.it

SPECIALTY SECTION
This article was submitted to Microbiome in Health and Disease, a section of the journal Frontiers in Cellular and Infection Microbiology

RECEIVED 19 October 2021
ACCEPTED 06 July 2022
PUBLISHED 16 August 2022

CITATION
Esposito S, Ballarini S, Argentiero A, Ruggiero L, Rossi GA and Principi N (2022) Microbiota profiles in pre-school children with respiratory infections: Modifications induced by the oral bacterial lysate OM-85. *Front. Cell. Infect. Microbiol.* 12:789436. doi: 10.3389/fcimb.2022.789436

Microbiota profiles in pre-school children with respiratory infections: Modifications induced by the oral bacterial lysate OM-85

Susanna Esposito[1]*, Stefania Ballarini[2], Alberto Argentiero[1], Luca Ruggiero[3], Giovanni A. Rossi[4] and Nicola Principi[5]

[1]Pediatric Clinic, Department of Medicine and Surgery, University of Parma, Parma, Italy, [2]Medicine and Surgery Department, University of Perugia, Perugia, Italy, [3]Fondazione Istituti di Ricovero e Cura a Carattere Scientifico Cà Granda Ospedale Maggiore Policlinico, Milan, Italy, [4]Department of Pediatrics, Unit of Pediatrics Pulmonology and Respiratory Endoscopy, G. Gaslini University Hospital, Genoa, Italy, [5]Professor Emeritus of Pediatrics, Università degli Studi di Milano, Milan, Italy

To describe microbiota profiles considering potential influencing factors in pre-school children with recurrent respiratory tract infections (rRTIs) and to evaluate microbiota changes associated with oral bacterial lysate OM-85 treatment, we analyzed gut and nasopharynx (NP) microbiota composition in patients included in the OM-85-pediatric rRTIs (OMPeR) clinical trial (https://www.clinicaltrialsregister.eu/ctr-search/trial/2016-002705-19/IT). Relative percentage abundance was used to describe microbiota profiles in all the available biological specimens, grouped by age, atopy, and rRTIs both at inclusion (T0) and at the end of the study, after treatment with OM-85 or placebo (T1). At T0, *Firmicutes* and *Bacteriodetes* were the predominant genera in gut and *Proteobacteria*, *Firmicutes*, and *Actinobacteria* were the predominant genera in NP samples. Gut microbiota relative composition differed with age (<2 vs. ≥2 years) for *Firmicutes, Proteobacteria, Actinobacteria* (phyla) and *Bifidobacterium, Ruminococcus, Lachnospiraceae* (genera) ($p < 0.05$). *Moraxella* was more enriched in the NP of patients with a history of up to three RTIs. Intra-group changes in relative percentage abundance were described only for patients with gut and NP microbiota analysis available at both T0 and T1 for each study arm. In this preliminary analysis, the gut microbiota seemed more stable over the 6-month study in the OM-85 group, whose mean age was lower, as compared to the placebo group ($p = 0.004$). In this latter group, the relative abundance of *Bacteroides* decreased significantly in children ≥2 years. Some longitudinal significant differences in genera relative abundance were also detected in children of ≥2 years for NP *Actinobacteria*, *Haemophilus*, and *Corynebacterium* in the placebo group only. Due to the small number of patients in the different sub-populations, we could not identify significant differences in the clinical outcome and therefore no associations with microbiota changes were searched. The use of bacterial lysates might play a role in microbiota rearrangement, but further data and advanced analysis are needed to prove

this in less heterogeneous populations with higher numbers of samples considering the multiple influencing factors such as delivery method, age, environment, diet, antibiotic use, and type of infections to ultimately show any associations with prevention of rRTIs.

KEYWORDS

children, microbiota, respiratory infection, dysbiosis, bacterial lysates, OM-85

1 Introduction

Respiratory tract infections (RTIs) tend to recur in the pediatric population and, in the first years of life, are associated with increased risk of wheezing illness and asthma (Zomer–Kooijker et al., 2014). The overuse of antibiotics to treat acute RTIs contributes to the increase in the rate of antimicrobial resistance and related lack of efficacy as well as to the disruption of the host microbiota, which is essential for immune homeostasis. Both effects induce a self-perpetuating vicious cycle of infection–inflammation–reinfection that potentially leads to chronic respiratory conditions (Dethlefsen et al., 2008). Because of the above, solutions to address poor respiratory health in young children should be sought around pathogen exposure, commensal colonization, and immune training. Based on the "hygiene hypothesis", the "farm-dust" effect, and the more recent concept of "innate immune training" (Ober et al., 2017; Netea et al., 2020), it has been suggested that the exposure to some microorganisms or microbial-derived components administered orally might influence the development and functions of gut and, secondarily, airway microbiota, mimicking the protective natural exposure that is needed for a healthy respiratory system (Esposito et al., 2018; Rossi et al., 2020). Oral bacterial lysates have been shown to act as immunomodulators able to shape the immune response to protect children from RTIs and associated wheezing (Esposito et al., 2018). An interesting hypothesis is that oral administration of whole bacteria or bacterial component can lead to a change in the gut microbiota composition by colonization and/or outgrowth of "good" strains. This could influence the composition of the airway microbiota either indirectly, by the migration of bacterial components or metabolites to the lungs to favor the outgrowth of "good" bacteria, or directly *via* microaspiration of these from the gastroesophageal tract to the airways. These may lead to the re–establishment of a health–promoting microbiota and have some therapeutic effects (Gollwitzer and Marsland, 2014). As such, an oral respiratory inactivate pathogenic bacterial lysate (manufacturing code name OM–85) could exert its effects by creating the conditions within the mucosal microbiome interface for the growth of beneficial bacteria or for limiting their outgrowth or repletion. This might, in turn, have a positive regulatory effect on airway inflammation such as shown in animal models of viral/bacterial superinfections and asthma (Karimi et al., 2009). The efficacy and safety of OM–85 was investigated in the OM–85–Pediatric rRTIs (OMPeR) study (EudraCT: 2016–002705–19), conducted in pre–school children (n = 288, age 1 to 6 years) with a history of recurrent RTIs (rRTIs) (Esposito et al., 2019). RTIs were significantly lower among patients receiving the standard regimen of OM–85 than among those given placebo (33% vs. 65.1%, $p < 0.0001$). OM–85 is an oral extract of bacterial lysates of 21 strains of eight known respiratory pathogens, *Haemophilus influenzae*, *Streptococcus pneumoniae*, *Klebsiella pneumoniae* subsp. *pneumoniae* and subsp. *ozaena*, *Staphylococcus aureus*, *Streptococcus pyogenes*, *Streptococcus viridans*, and *Moraxella catarrhalis*. The mechanism of action of OM–85 has been deeply reviewed and the main immunological effects have been described, nevertheless, the effect of this lysate on microbiota composition in children with rRTIs remained to be unraveled (Rossi et al., 2019). Therefore, a description of both gut and nasopharynx (NP) microbial composition in this population of children was performed considering common influencing factors reported in the OMPeR study demographics, e.g., age, atopy, and number of RTIs and antibiotics. A particular attention was given to age because children <2 years of age represent a window of opportunity to manipulate the microbiome and, as pointed out by Thomas et al., after 3 years of life, the gut microbiota is relatively more stable (Thomas et al., 2015). Furthermore, an exploratory analysis aimed at identifying any sign of possible microbiota rearrangement associated with the prophylactic use of OM–85 has been conducted. To our knowledge, this is the first study describing microbiota profiles in children with rRTIs receiving an oral bacterial lysate.

2 Materials and methods

2.1 Patient population

Children included in the clinical study OMPeR underwent biological sampling for both the NP and gut microbiome analysis. OMPeR was a phase IV, randomized, double–blind,

placebo–controlled, single–center trial, which enrolled 288 patients and aimed at assessing the efficacy and safety of the oral bacterial lysates OM–85 reducing acute RTIs in pre–school children affected by rRTI defined as at least six acute episodes in the previous year. The active immunotherapy was administered as either 3.5 mg of OM–85 once a day for the first 10 days of the first 3 months of the 6–month study (group A) or once a day for the first 10 days of the 6–month study (group C). Matching placebo was administered to keep the double–blind condition (group B). The randomization 3:3:1 (OM–85, 10 days for 3 months, placebo or OM–85, 10 days for 6 months) was done at the beginning of the infective season (September/October), and the three groups were observed for 6 months. Children with malformations of the cardiovascular system and the respiratory tract, with chronic lung, kidney, or liver diseases, with primary or secondary immunodeficiency, and with cancer, malnutrition, and severe allergic manifestations such as atopic dermatitis and asthma were excluded. In addition, patients who received antibiotics and systemic, inhaled, or oral steroids within 4 weeks before enrollment were not included in the clinical trial and therefore excluded from our microbiome analysis.

2.2 Biological samples collection, processing, and DNA extraction

Both stools and NP swabs were collected at visit 2 (day −1, before the randomization) as baseline, and at V5 (month 6, end of the study) for microbiome essays. Stools were collected by the parents at home, as immediate freezing of fresh sample at -80°C was not possible, the specimens were stored at +4°C in anaerobic atmosphere for a short period (up to 24 h) and then frozen at −80°C in the microbiology laboratory of University of Milan, Pediatrics Clinic. In the same laboratory, NP swabs were obtained. NP samples were collected by trained personnel using sterile dry cotton–headed swabs (MASTASWAB MD 559, MAST Diagnostica GmbH, Reinfeld, Germany) by five circular rubbings about 1 cm from the nares. Secretion and other material were collected from the soft and moving part of the nose. After sampling, the swabs were immediately placed back in the collection tube and stored within 24 h at −80°C. The samples were processed using the kit for DNA isolation MoBio PowerLyzer, PowerSoil DNA isolation kit (Mobio, Loker Ave West, Carlsbad, CA, USA) according to the manufacturer protocol for extraction. A fecal sample of 200 µg was used, suspended in 200 µl of sterile water. The specimen was shaken first using the TISSUE LYZER 30–Hz impulses for 10 s for a total duration of 2 min. The sample was then centrifuged at 13,000*g* for 10 min and the supernatant was discharged. The pellet was transferred into a GLASS BEAD TUBE together with 750 µl of buffer Bead sol. The sample was warmed up first for 10 min at 65°C, then for 10 min more but at a temperature of 95°C. After adding 60 µl of C1 buffer, the sample underwent the proper lytic process by TISSUE LYZER 30–Hz impulses for 5 min + 5 min short bead–beating time, for a total of 10 min. The DNA material extractions were followed by a purification step to avoid that some constituents (e.g., scatols, fecols, and other aromatic acids) might inhibit the sequencing reactions. The commercial sequencing platform kit used for library generation (16S Illumina) included reagents to bind and remove known inhibitory compounds (Terranova et al., 2018). The NP swab samples underwent the processing and extraction process described by the same manufacturer (Mobio, Loker Ave West, Carlsbad, CA, USA). In our lab, the swabs were placed in the extraction tube with 750 µl of Bead sol buffer, and the tube was vortexed for 20 s. The sample could be then temporarily stored at −20°C until further processing (Depner et al., 2017). The sample has been transferred into the GLAS BEAD TUBE with 60 µl of C1 buffer and it underwent the lytic process by TISSUE LYZER 30 Hz impulses for 5 min + 5 min short bead–beating time, for a total of 10 min. Following extraction, DNA was quantified by Qubit® dsDNA HS Assay Kits (Thermo Fisher Scientific Inc., Massachusetts, USA).

2.3 DNA sequencing

In our laboratory, we followed the 16S Illumina MiSeq system protocol (https://support.illumina.com/documents/documentation/chemistry_documentation/16s/16s–metagenomic–library–prep–guide–15044223–b.pdf). Briefly, V3–V4 hypervariable regions of the 16S rRNA gene were amplified with 16S Amplicon PCR Forward Primer = 5' TCGTCGGCAGCGTCAGATGTGTATAAGAGACAGCCTACGGG–NGGCWGCAG and 16S Amplicon PCR Reverse Primer = 5' GTCTCGTGGGCTCGGA–GATGTGTATAAGAGACAGGACTACHVGGGTATCTAATCC. Libraries were generated by dual indexing strategy using the Nextera XT v2 Index Kit (Illumina, California, USA). PCR products were cleaned up using Agencourt AMPure XP beads (Beckman Coulter Genomics, Minnesota, USA) and DNA quantification and quality were assessed by Qubit® dsDNA HS Assay Kits and Bioanalyzer (Agilent Technology, California, USA), respectively. Equimolar DNA amounts from each sample library were pooled together. Finally, the pool was sequenced on the MiSeq sequencing instrument using a 2 × 250 cycle MiSeq Reagent Kit v2 (Illumina, California, USA). Reagent blank samples were subjected to all the steps of library preparation, from DNA extraction to amplification, to avoid contamination bias. Bioanalyzer assay showed no amplification product in the blank samples. During the DNA processing of the raw sequence, data obtained contained sequences corresponding to sequencing adaptors and primers used for amplification, as the first step, these segments were trimmed away. Sequence data with a minimum length of 250 base pairs were processed and analyzed. Quality–control filters were used to identify such poor–quality reads and purge these from the data. Only reads with an average quality score of 30 or above

(which represents an expected error rate of fewer than 1 base for every 1,000 bases) were selected for further analysis. Samples were rarefied to a read depth of 6,700 to ensure that a reasonable number of sequence reads have been obtained for each Operational Taxonomic Units (OTU). We applied the following standards: sequences with >97% of nucleotide identity were assumed to correspond to one or few correlated microorganisms (e.g., species) while a lower level of identity of >95% was used to identify sequence clusters of the same genus. These clusters (OTU) were classified by phylogeny using the classifier from the Greengenes database (https://greengenes.secondgenome.com/).

2.4 Microbiome library

The first step in our microbiome analysis was the elimination of data background noise. We used a 10% cutoff. Bacterial taxa that were present in a few specimens of the same group (<10%) or that were present in very low concentration once the specimens are put all together (i.e., for very few reads, e.g., <0.005% of reads in all) were discharged. The second step was to create the library for each specimen at T0 and T1, to make intra–group comparisons at different time points. For fecal samples, we considered the taxa being represented by at least 2% of all reads per sample. For the NP samples, we kept the taxa being represented by at least 1% of all reads per sample (Sarangi et al., 2019). QIIME Software was used for the initial analysis (Caporaso et al., 2010).

2.5 Data analysis

For this exploratory and descriptive analysis, we chose to present data as the relative abundance of major taxa. Descriptive statistics were reported in terms of means with standard deviations (SD) for quantitative data and in terms of absolute frequencies or percentages for qualitative data. Non–parametric Wilcoxon's signed–rank test for paired quantitative data was used to compare intra–group data, i.e., between two different time points: at visit 2 (day −1, before the randomization) as baseline, and at visit 5 (month 6) at the end of the study. Unpaired Mann–Whitney U test was used to compare quantitative data in two different groups, i.e., age groups. For comparing mean age among the three treatment groups (i.e., OM–85/placebo, OM–85, placebo only), Kruskal–Wallis test followed by Bonferroni *post–hoc* test was used. For comparing qualitative data, Chi–square test or Fisher's exact test in the case of expected frequencies < 5 was used.

3 Results

Out of the 288 children recruited in the OMPeR study, we could only collect and analyze 144 stool and 158 NP swabs samples at baseline (T0), approximately in half of the whole population. At the end of the study (T1), microbiota collection and analysis were performed in stool samples from 98 out of 144 patients and in 137 NP samples out of 158 patients who provided biological specimens at T0. Samples available at both T0 and T1 for each patient were used for longitudinal studies on gut (n = 98) and NP microbiota (n = 137) (Figure 1).

3.1 Age distribution in the study population and in the microbiota study subgroups at T0

Because of the strong influence on the microbiota composition, the age distribution across the studied groups was first verified. As reported in the demographic table of the OMPeR original article (Esposito et al., 2019), the three treatment groups (A, B, and C) were homogeneous for mean age in years ± SD at admission (3.6 ± 1.6, 3.7 ± 1.5, and 3.8 ± 1.7, respectively). In contrast, when looking at the 144 patients with gut microbiota profile available at T0, we found that the mean age of children receiving OM–85 treatment (A and C) was significantly lower compared to the placebo group (B) (p = 0.014) (Table 1). The difference was still significant when the data from active groups (A and C) were combined (p = 0.004) (Table 2), or when data related to infants and pre–school children were analyzed separately (p = 0.041) (Table 3). Similar findings were reported when analyzing the mean age and the distribution by the same age cutoff (infants and pre–schoolers) in the 158 children allocated to OM–85 and placebo groups for which NP microbiota analysis was available at T0 (data not shown).

3.2 Microbiota profiling at T0

3.2.1 Gut microbiota profiling at T0 in the total population and in the different age subgroups

The gut microbiota analysis at T0 was performed in the total population (n = 144), and in the <2 (n = 30) and ≥2 years of age (n = 114) subgroups, regardless of the treatment allocations, as reported in Figures 2 and 3, respectively.

The composition and relative percentage abundance of phyla in the gut were comparable with the one described in the literature for healthy children with *Firmicutes* being predominant followed by *Bacteroidetes* (Figure 2).

In children <2 years of age, *Firmicutes* were less abundant compared to what was observed in older children, while *vice versa*, *Actinobacteria* and *Proteobacteria* were relatively more abundant. Among genera, *Bifidobacterium* and *Lachnospiraceae* were more abundant in children <2 years of age while *Ruminococcus* was less abundant (Figures 3A, B). Other genera

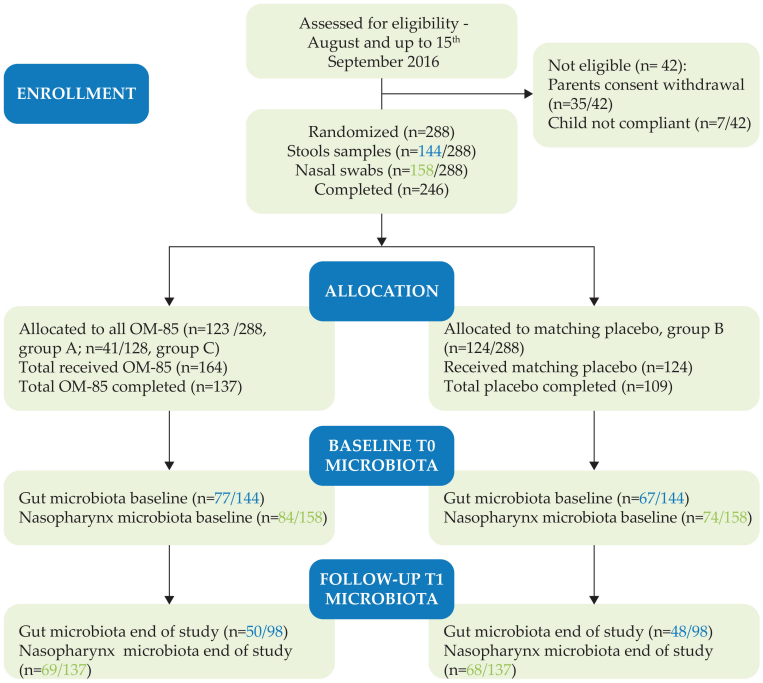

FIGURE 1
CONSORT. Number of gut and nasopharyngeal (NP) samples per treatment allocation (different active treatment groups A and C with OM–85 and group B with placebo) collected and analyzed at T0 and T1.

differed significantly such as *Veillonella* and *Dorea* (data not shown because of their very low relative abundance).

3.2.2 NP microbiota at baseline in the total population and in the different age subgroups

The baseline NP microbial profiles were analyzed first in the total population (n = 158), and phyla and genera are reported in Figure 4.

The relative abundance of phyla was in line with what was described in the literature in children with highest abundance of *Proteobacteria* and *Firmicutes* followed by *Actinobacteria*. The relative abundance of genera was also reported at T0. The profiles in this case were not statistically different in the different age subgroups (data not shown).

3.2.3 Distribution of gut microbiota taxa at T0 by other influencing factors (atopy and prior RTIs)

In the total patient group (n = 144), the baseline gut microbiota profiles were described and evaluated according to the presence or not of atopy and to the number (<3 or ≥3) of RTI episodes over 6 months prior to study entry. The number of atopic children with stool specimen was small (n = 31) compared to the non–atopic ones (n = 113). The mean age in years was higher in atopic children (4.11 ± 1.5) as compared with the non–atopic ones (3.28 ± 1.56, p = 0.006). The numbers of children who experienced <3 or ≥3 RTI episodes were respectively 49 and 95 and their mean ages in years were 3.63 ± 1.73 and 3.37 ± 1.5 (p = 0.43). Because of the very small numbers, we could not show any statistically significant difference in the gut microbial profiles at T0 between these patient subgroups. Furthermore, other influencing factors, such as the type of infections or the use and type of antibiotics prior to the study could not be analyzed because such historical data were not available.

3.2.4 Distribution of NP microbiota taxa at T0 by other influencing factors (atopy and prior RTIs)

The baseline profiles were evaluated also for the NP microbiota in the total patient group (n = 158) and described according to the presence of atopy and to the number of RTI episodes. The mean age

TABLE 1 Mean (SD) age in years at T0 per randomization group (A, OM–85/placebo, B, placebo, C, OM–85) of all patients with available stool specimens and gut microbiota analysis (n = 144).

OM–85/Placebo (A) (n = 62)	Placebo (B) (n = 67)	OM–85 (C) (n = 15)	p–value
3.2 (1.6)	3.9 (1.6)	2.9 (1.4)	0.014

TABLE 2 Mean (SD) age in years at T0 per randomization groups receiving active prophylactic treatment (A, OM−85/placebo and C, OM−85) or placebo (B) of all patients with stool specimens and gut microbiota analysis available (n = 144).

All OM−85 (A + C) (n = 77)	Placebo (B) (n = 67)	p−value
3.1 (1.5)	3.9 (1.6)	0.004

TABLE 3 Number and percentage of patients <2 or ≥2 years of age with stool samples and gut microbiota analysis done at T0 (n = 144).

Age cutoff	All active (A + C) (n = 77)	Placebo (B) (n = 67)	p−value
<2 years [n (%)]	21 (27.3)	9 (13.4)	0.041
≥2 years [n (%)]	56 (72.7)	58 (86.6)	

in years for the atopic (n = 30) and the non−atopic (n = 128) patients was statistically different, being 4.23 ± 1.5 and 3.28 ± 1.56, respectively (p = 0.0023). As described for the gut microbiota relative abundance, we could not observe statistically significant differences in the microbiota relative abundance by atopy.

The number of rRTIs prior to the study was available for 157 out of 158 patients. The mean age was similar in the two groups, i.e., the 53 patients with <3 RTIs and the 104 patients with ≥3 RTIs. Some differences in the relative abundance of each taxon were observed (Figure 5A), but only *Moraxella* was significantly more enriched in the patients that had experienced <3 RTIs in the previous 6 months before the study entry (Figure 5B).

3.3 Gut microbiota profiling changes at T1

3.3.1 Intra−group changes of gut microbiota profiles over the study (T1−T0)

For such longitudinal study, only 98 gut samples were available (n=50 OM-85 and n=48 in placebo groups). Some statistically significant differences in relative abundance of specific taxa were observed, when comparing the two time points (Figure 6A). While the relative abundance of *Bacteroides* genus did not change over time in the OM−85 group, it decreased significantly in the placebo group (p = 0.03). In contrast, while no changes were observed for the *Clostridium XIVa* and *Dorea* in the OM−85 group, the relative abundance was increased with borderline significance for *Clostridium XIVa* and in a statistically significant manner for *Dorea* (p = 0.026) in the placebo group (Figure 6B).

3.3.2 Intra−group changes of gut microbiota profiles over the study (T1−T0) in the different age subgroups

The intra−group comparisons of gut microbiota relative abundance in children <2 and ≥2 years of age were also made. Only 18 children <2 years of age had gut microbiota profiles at T0 and T1, and of these, 13 were in the OM−85 and only 5 were in the placebo subgroup. No statistically significant differences could be seen in this small subgroup of patients (data not shown). Differences were observed instead in the ≥2 years of age subgroup of children (n = 80), of whom 37 were in the OM−85 group and 43 were in the placebo group (Figure 7A). However, statistically significant differences were detected only in the placebo subgroup, with relative abundance reduction of *Bacteroides* and increase in *Streptococcus, Lachnospiraceae_incertae_sedis*, and *Clostridium XIVa* (Figure 7B). The gut microbiota remained more stable in this longitudinal study over the 6 months in the OM−85 subgroup.

3.4 OM−85 and placebo clinical response in the gut microbiota group

In the 98 patients whose stool samples were collected for gut microbiota analysis both at T0 and at T1 (n=50 in OM−85 and n=48 in placebo group), no significant differences were observed in the mean number of RTIs at the end of the study (OM−85 = 1.56 ± 1.66, placebo = 1.19 ± 1.05, p = 0.62), as well as in the mean number of antibiotics (OM−85 = 1.10 ± 1.049, placebo 0.96 ± 0.80, p = 0.62) used during the study. The same analysis conducted using the age cutoff of 2 years showed a statistically significant higher mean number of RTIs and antibiotic use in the <2 years old subgroup at T1, as compared to the ≥ 2 years old subgroup (p = 0.025 and p = 0.013, respectively), but with no significant difference between OM−85 and placebo (Figure 8). No association between gut microbiota profiles and clinical response could be made. It should be noted that the mean number of antibiotics used over the study was very low, as the majority of RTIs were in the upper RT and did not require antibiotic prescription.

3.5 NP microbiota profiling changes at T1

3.5.1 Intra−group changes of NP microbiota profiles over the study (T1−T0)

Analysis of NP microbiota of the 137 patients (n=69 in OM-85 and n=68 in placebo groups) at T1 showed a significant decrease in the placebo group only of *Actinobacteria* phylum, an increase in relative abundance of *Haemophilus* in the OM−85 group, and a near

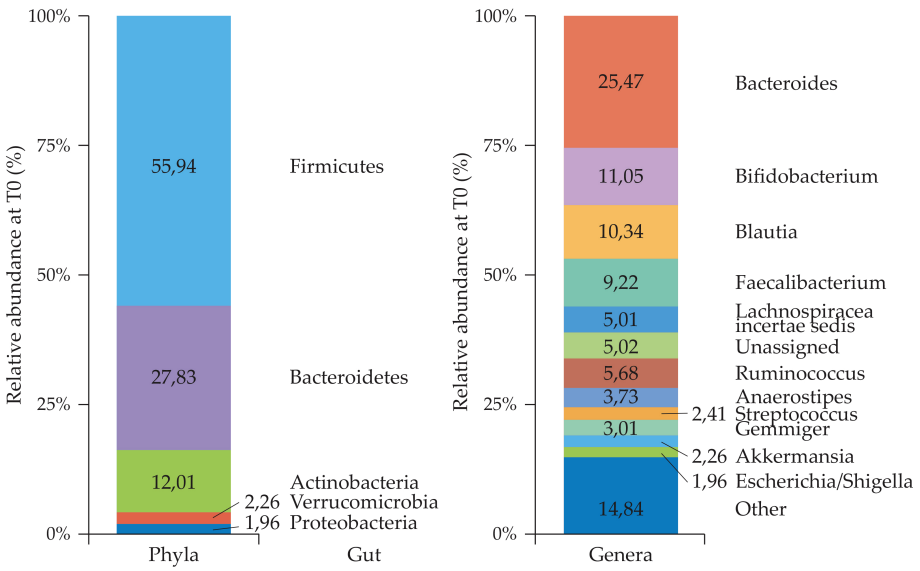

FIGURE 2
Gut microbiota profiles (phyla and genera) in the total population (n = 144) at T0.

to significant decrease of *Corynebacterium* in the placebo group compared to T0. Precisely, the *Actinobacteria* phylum decreased in placebo from 6.60% ± 1.63 to 4.33% ± 1.18 (p = 0.055). In addition, in the OM–85 group, the relative abundance of *Haemophilus* was 11.25% ± 22.47 at T0 and increased to 20.61% ± 22.55 at T1 (p = 0.006). In the placebo group, the relative abundance of *Corynebacterium* was 6.6% ± 13.45 at T0 and decreased to 4.33% ± 9.71 at T1 (p = 0.05) (Figures 9A, B).

3.5.2 Intra–group changes of NP microbiota relative abundance over the study in the different age subgroups

The mean age in years was not homogeneously distributed, with a lower mean age (p = 0.015) as well as a higher number of younger children included in the OM–85 group. We observed some differences in NP microbiota relative abundance at T1 only in children of ≥2 years (n = 111), in OM–85 (n = 52) and placebo groups (n = 59), both at the phylum level and the genus level. The *Actinobacteria* phylum did not change in the OM–85 group, but it decreased in the placebo group (7.36% ± 14.24 to 4.38% ± 10.08, p = 0.0136), and *Haemophilus* increased in the OM–85 group (11.77% ± 22.33 to 22.25% ± 31.08, p = 0.010) while the *Corynebacterium* decreased in the placebo group (7.36% ± 14.24 to 4.38 ± 10.08, p = 0.013), as shown in Figures 10A, B.

3.6 OM–85 and placebo clinical response in the NP microbiota group

No significant difference could be detected between the OM–85 and placebo group in the mean number of RTIs and the number of antibiotics use, during the study in patients with NP swabs both at T0 and at T1 (n = 137). However, when the different age groups were compared, a statistically significant higher mean number and frequency of RTIs and of antibiotic prescriptions were found in the youngest children, both in the OM–85 group and in the placebo group (Table 4). No association between NP microbiota profiles and clinical response could be made.

4 Discussion

RTIs are common in the pediatrics population, especially in young children, because of the relative immaturity of the immune system and the microbiota, as well as the exposure to respiratory pathogens in childcare facilities and schools. Some children are more fragile than others, experiencing higher respiratory morbidity, characterized by RTI recurrence and/or more severe clinical manifestations. It is known that complex inter–talks between environmental and host factors such as immune components and microbiota metabolites move the needle towards a health or disease status in childhood (Man et al., 2017).

It has been hypothesized that reducing the risk for RTIs in infancy could be therapeutically achieved by accelerating early immune maturation/functional competence *via* enhancing the level of appropriate benign microbial–derived signaling to the developing innate immune system. The "immune training" led to a state of broad spectrum enhanced resistance to pathogens (Holt et al., 2019). In addition, a right balance between Th1/Th2

10.3389/fcimb.2022.789436

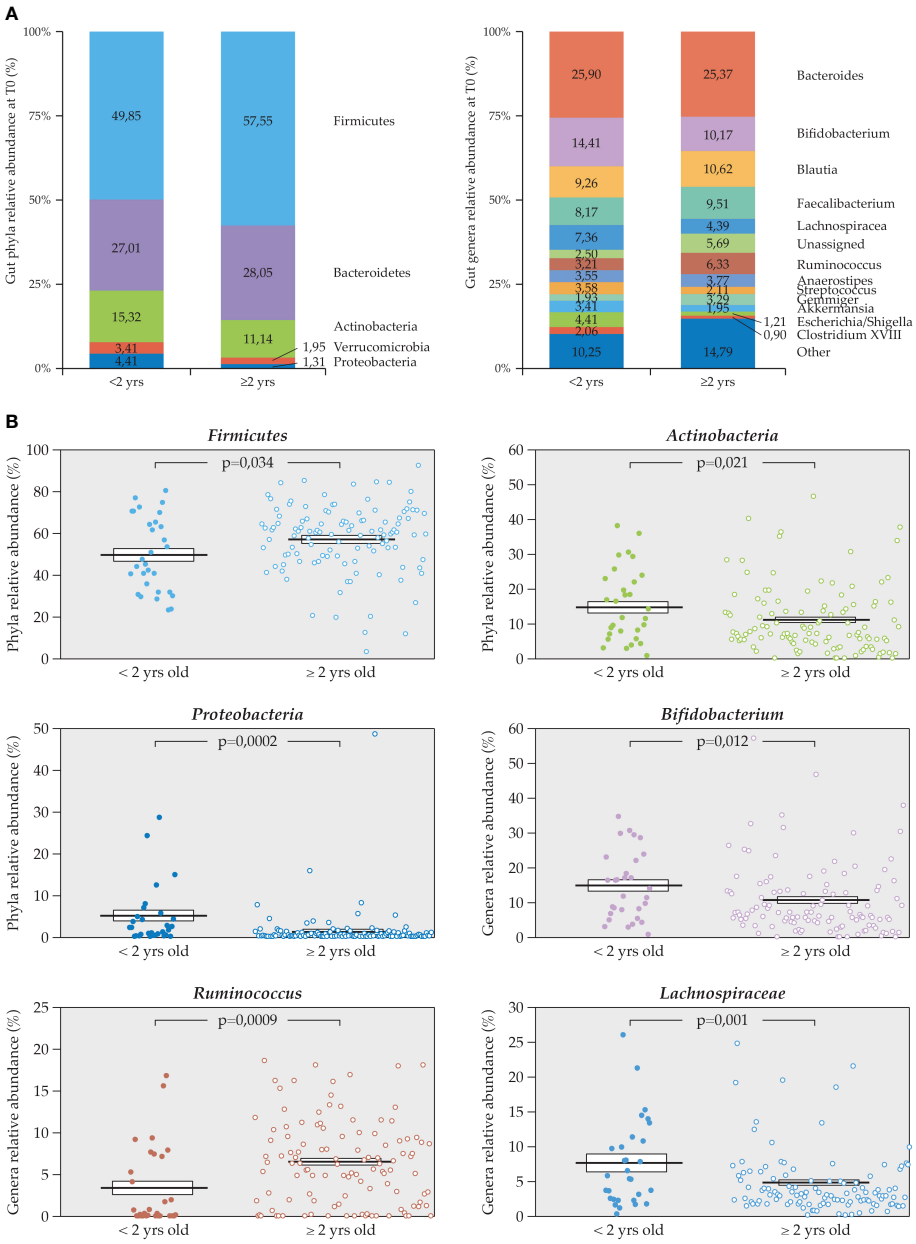

FIGURE 3
Relative percentage abundance of phyla and genera in the gut microbiota at T0. **(A)** Comparison between <2 (*n* = 30) and ≥2 years of age (*n* = 114) subgroups, **(B)** statistically significant differences in relative abundance of specific taxa, *Firmicutes, Proteobacteria*, and *Actinobacteria* (phyla) and *Bifidobacterium, Ruminococcus*, and *Lachnospiraceae* (genera) in the two age subgroups (Mann U Whitney test).

responses is key to avoid more severe LRTIs and sequelae. A few microbial–derived products have been shown to experimentally reproduce immune training effects. The bacterial lysate OM–85 has been extensively investigated, and it has shown to enhance deficient INF responses (Dang et al., 2017) to modulate the interplay between Th1 and Th2 mechanisms (Huber et al., 2005) and to potentially play a role in gut microbiota rearrangement (Rossi et al., 2019).

The aims of our work were to (a) describe microbiota profiles in rRTIs of pre–school children, starting with relative abundance, (b) describe microbiota profile changes associated with common influencing factors such as age, atopy, and number or RTIs, (c) describe any possible sign of effect of the oral bacterial lysate OM–85 when given as prophylaxis on microbiota relative abundance, and (d) make associations, if possible, with its clinical efficacy in prevention of rRTIs.

10.3389/fcimb.2022.789436

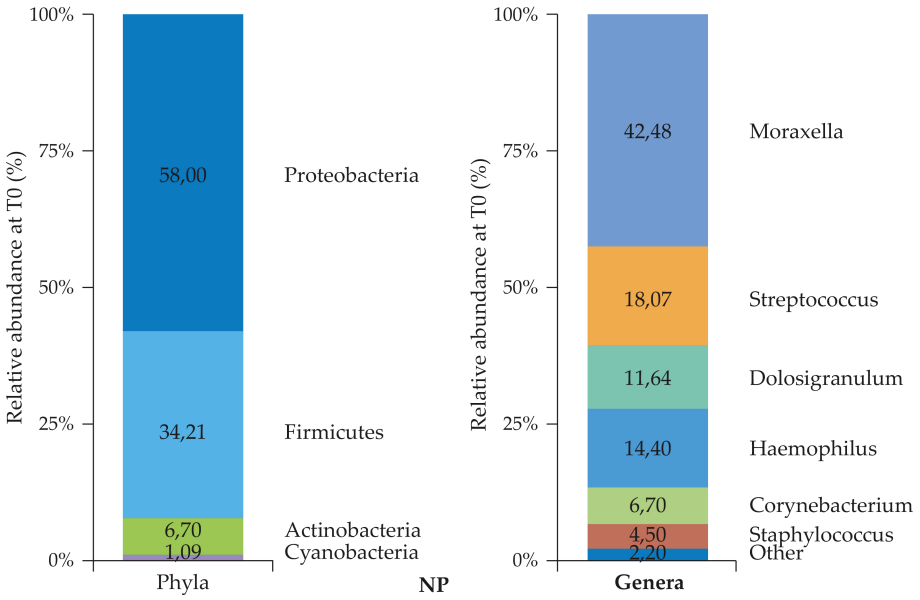

FIGURE 4
NP microbiota profiles (phyla and genera) in the total "NP sample" (n = 158) at T0.

Performing the sub–analysis of the gut and NP microbiota derived from the pre–school children included in the OMPeR clinical study, we realized that the number of stool and NP swabs collected at T0 and analyzed by 16S rRNA sequencing was approximately half of the total enrolled population and that the number of stool samples as well as NP swabs available and analyzed at both T0 and T1 was smaller. This could negatively affect the possibility to reach the statistical significance, when evaluating the results of the study.

Furthermore, in contrast with what was reported in the OMPeR study original population, the demographic characteristics were not homogeneously distributed in the different treatment groups in our studied sub–population. There was a statistically significant difference in the mean age for children included in the "gut" and the "NP" samples groups at T0, with the youngest allocated to the OM–85 treated group, and this could be a bias to keep in mind when evaluating the results of our study. It is well known that the age plays a key role in the microbiota richness in children, indeed, the gut microbiota is relatively less stable (i.e., more influenced by factors such as breast feeding, diet, and past infections antibiotic use) below the 3 years of age (Thomas et al., 2015). Infancy (i.e., <2 years) might represent a better window of opportunity to manipulate the microbiota. Also, when considering the age cutoff of 2 years, a significant higher proportion of younger children was allocated to OM–85 compared to placebo. As expected, more significant differences in the relative abundance of phyla and genera were observed at T0 when comparing microbiota profiles by using the "clinical" age cutoff of 2 years. Therefore, we performed all the microbiota analysis in the total "gut" or "NP" samples, and in the subgroups of children <2 or ≥2 years to minimize the age bias. The sample size in these age subgroups was small, and this was particularly true for the youngest group, which was less represented in the OMPeR study population according to the eligibility criteria (age at enrollment from 1 to 6 years). This negatively affected the analysis especially in group comparisons.

We therefore decided to apply a stepwise approach to our microbiota analysis to minimize the costs. At T0, in the gut microbiota, the phylum *Firmicutes* was predominantly followed by *Bacteroidetes* and *Actinobacteria* phyla, as reported by other authors (Arumugam et al., 2011). In the NP microbiota, *Proteobacteria* and *Firmicutes* were more represented, followed by *Actinobacteria*. Also, these findings were in line with what was reported in the literature for this age group of children (Pichon et al., 2017). Our T0 findings confirmed that the gut microbiota composition is influenced by age, as shown by several statistically significant differences in the microbiota profiles of children <2 years vs. ≥2 years of age.

In NP microbiota analysis, at T0, we could identify only a significant difference in *Moraxella* spp., which was more abundant in children who had <3 RTIs during the study, this was independent of the age, because this was not significantly different in these two subgroups (<2 or ≥2 years). It is important to point out that rRTIs in children are usually defined as at least six to eight over a 12–month period. In the OMPeR study, pediatrics patients were recruited with a history of ≥6 RTIs in the previous year. As not all the episodes over the entire 12–month

10.3389/fcimb.2022.789436

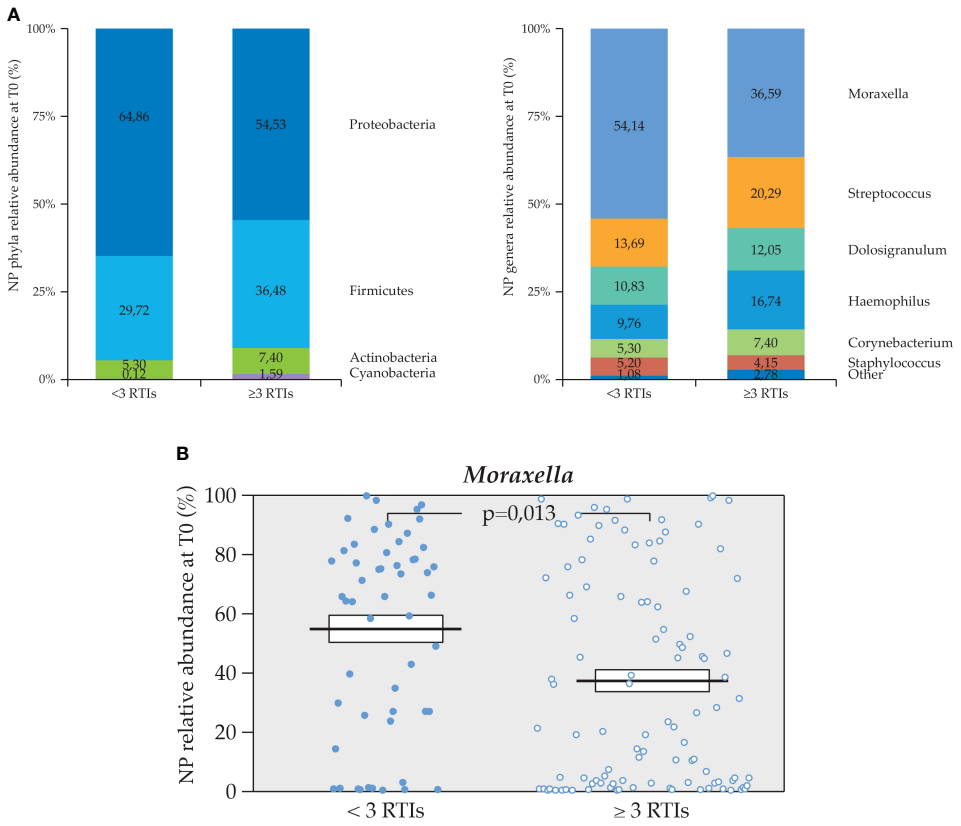

FIGURE 5
Relative percentage abundance of phyla and genera in the NP microbiota at T0. **(A)** Differences of NP microbiota profiles per number of RTIs in the 6 months prior to the study (n=53 <3 and n=104 ≥3 RTIs), **(B)** Statistically significant difference in relative abundance of *Moraxella* spp. between the two subgroups (Mann U Whitney test).

period prior to the study were recorded or dated for all the patients, we defined rRTIs instead by the number of three episodes over 6 months prior to study. We observed that a higher relative abundance of *Moraxella* spp. was associated with less recurrences. Other authors reported that *Moraxella* spp. might be associated with a healthier status in the elderly at risk for RTIs, while in the pediatric populations, the reports on this health–associated taxa (Man et al., 2020) are more conflicting as far as microbiota profile stability and association with RTIs (Bosch and McFall–Ngai, 2011; Biesbroek et al., 2014; Teo et al., 2015; Man et al., 2019). The differences in susceptibility to RTIs likely arise from the complex interplay between mucosa, innate and adaptive immunity, and airway microbiota (van den Munckhof et al., 2020).

Other factors might influence or are being associated with microbiota rearrangements in the pediatric population prone to RTIs, such as atopy and antibiotic use. The number of atopic children was overall smaller compared to the non–atopic ones. The reasons of such imbalance can be found in the exclusion of asthmatics from the study according to OMPeR eligibility criteria. Because of the above, we could not find any association of specific microbiota profiles with atopy. In addition, we could not perform other subgroup analysis by other influencing factors such as the type of infection and of antibiotic use because this kind of anamnestic data was not available.

At T1, the gut microbiota relative abundance showed that *Bacteroides* spp. were significantly decreased while *Dorea* spp. increased compared to T0 in the placebo group only. *Bacteroides* spp. were also statistically decreased in the placebo subgroup of ≥2 years of age, which was the largest age subgroup. Other genera proved to be less stable in the placebo group compared to OM–85 (increased *Streptococcus, Lachnospiraceae_incertae_sedis*, and *Clostridium XIV*). Despite small numbers, the inter–group analysis in this subgroup still showed a statistically significant difference in the change for the *Bacteroides* (borderline significance) and for *Lachnospiraceae_incertae_sedis* spp.

Bacteroides is a Gram–negative, non–spore–forming, obligate anaerobic bacteria normally found in the human intestines, mouth, upper respiratory tract, and genital tract.

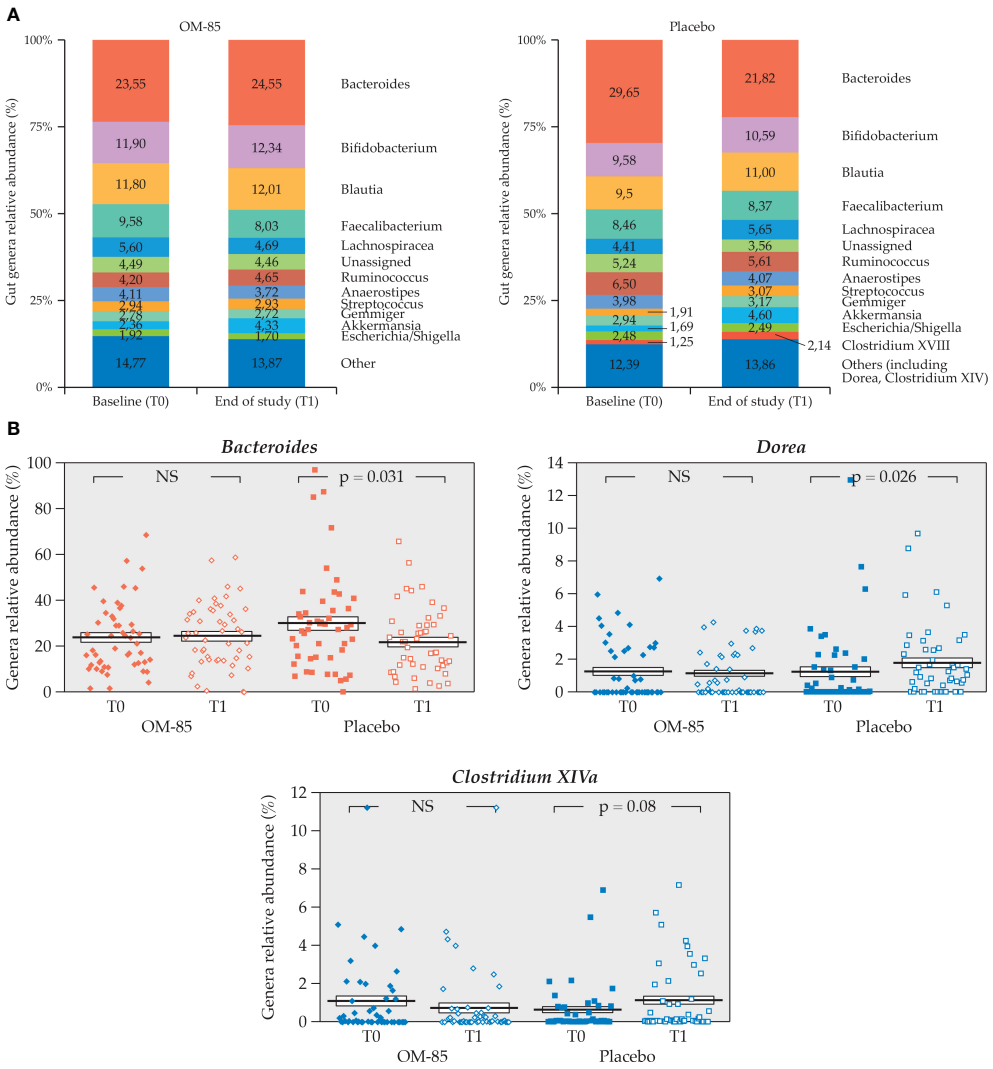

FIGURE 6
Intra–group change of gut microbiota relative abundance in both OM–85 and placebo groups (n=98). **(A)** Gut microbiota profiles at T0 and T1 for both treatment groups (n=50, OM-85 and n=48, placebo). **(B)** Statistically significant intra–group differences for genera *Bacteroides, Dorea*, and *Clostridium XIVa* in placebo (Wilcoxon's signed–rank test). NS: not significant.

Bacteroides expresses polysaccharide A, which can induce regulatory T–cell growth and cytokine expression that are protective against inflammation. A lower level of *Bacteroides* has been associated with some inflammatory diseases such as inflammatory bowel diseases (IBDs) (Zhou and Zhi, 2016). *Bacteroides* has been considered protective by some authors (Lazar et al., 2018), while early colonization of *Bacteroides fragilis* was associated with asthma risk at 3 years of age (Vael et al., 2008). *Bacteroides fragilis* and *Bacteroides uniformis* have been identified to exert anti–inflammatory effects in animal models, and they might be considered as the next generation of probiotics (O'Toole et al., 2017).

Lachnospiraceae belong to the core of gut microbiota, colonizing the intestinal lumen from birth and increasing in terms of species richness and their relative abundances during the host's life. In contrast to *Bacteroides*, *Lachnospiraceae* are in greater abundance in the irritable bowel syndrome (IBS) clone library (Rinninella et al., 2019). *Lachnospiraceae* might influence healthy functions, although different genera and species of this family are increased in diseases. Indeed, some metabolic syndrome, obesity, diabetes, liver diseases, IBD, and chronic kidney disease are all inflammatory conditions involving this family (including *Lachnospiraceae_incertae_sedis* or *Blautia* spp.). In addition, they seemed to play a

10.3389/fcimb.2022.789436

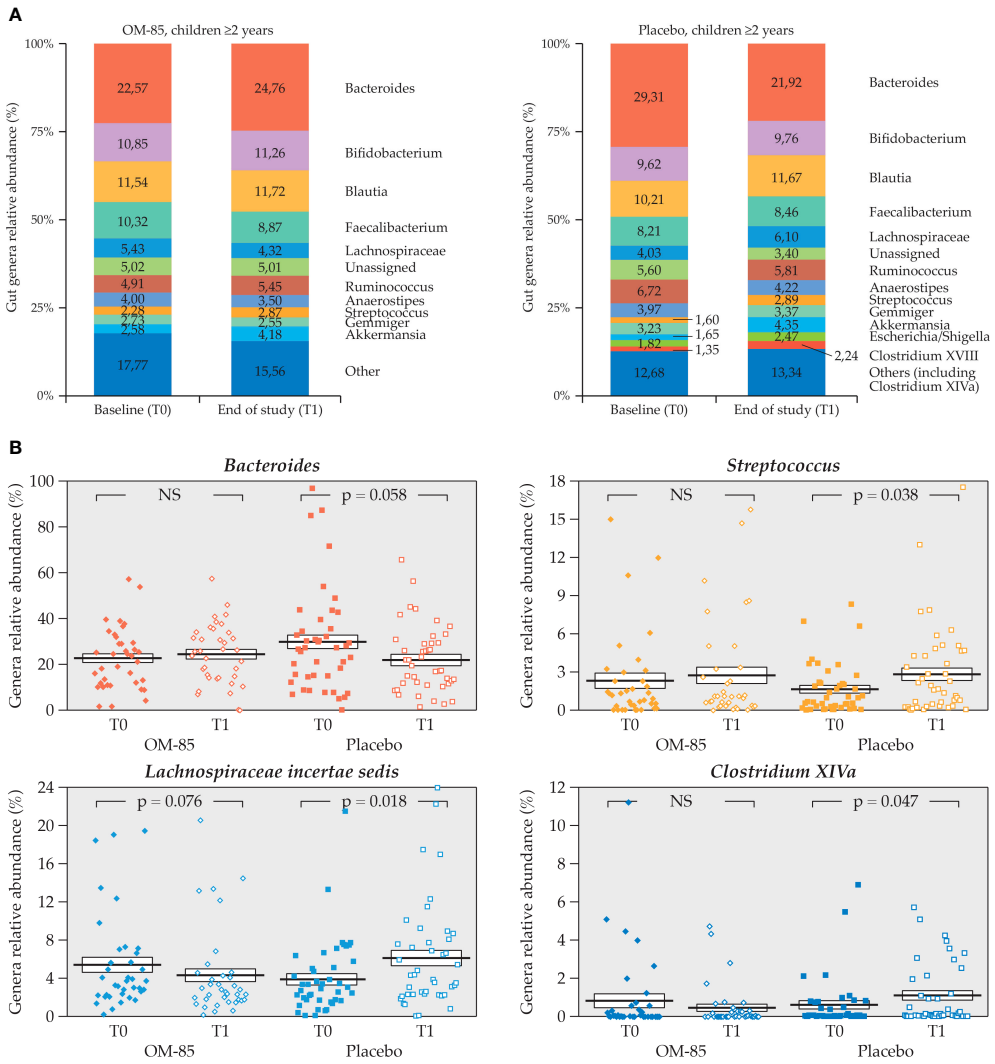

FIGURE 7
Intra–group change of gut microbiota relative abundance in both OM–85 and placebo group in the subgroup of children aged ≥2 years (n=80) **(A)** Gut microbiota profiles at T0 and T1 for both treatment groups (n=37, OM-85 and n=45, placebo). **(B)** Statistically significant intra–group differences in relative abundance of *Bacteroides, Streptococcus, Lachnospiraceae_incertae_sedis*, and *Clostridium XIVa* genera in placebo. (Wilcoxon's signed–rank test). NS: not significant.

role in depressive syndromes and multiple sclerosis syndrome (Vacca et al., 2020).

Diet influences the microbiota in older children, and this factor was not controlled over the study. Furthermore, the role of gut microbiota specific taxa is still controversial in regard to health or disease status, and limited data are available for children with high risk for RTIs.

No direct associations between gut microbiota relative abundance changes at T1 and clinical response (RTIs and antibiotic use during the study) could be detected. This can be explained by a few factors, such as the small samples size for the microbiota OMPeR sub–analysis, the non–homogeneous age distribution in the treatment groups, and the small sample size when analyzing the age subgroups. These limitations can also explain the lack of significant differences for the clinical endpoints (RTIs and antibiotic use) between OM–85 and placebo in the sub–analysis, differences detected in the OMPeR total study population (Esposito et al., 2019). Furthermore, the mean number of RTIs and of antibiotic use was very low probably because the majority of RTIs were in the upper airways and did not require antibiotic prescription.

The NP microbiota relative abundance intra–group analysis at T1 confirmed a more stable microbiota for the OM–85 group compared to placebo. Some statistically significant changes were

10.3389/fcimb.2022.789436

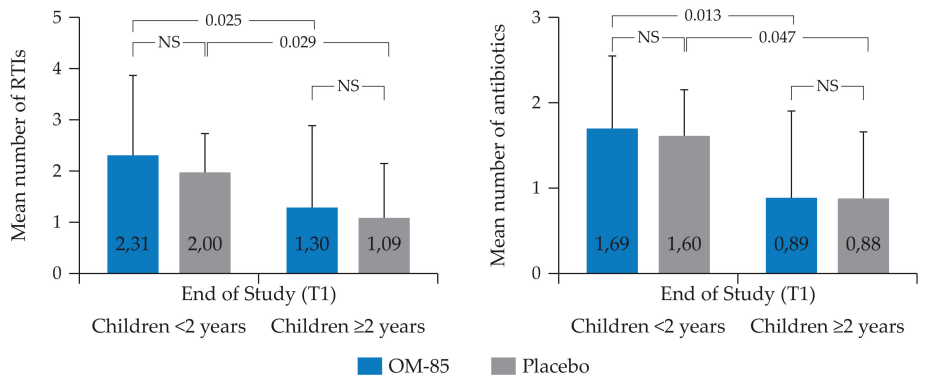

FIGURE 8
Mean number of RTIs and antibiotics used during the study and recorded at T1 in the children (n=98), <2 (n=18) and ≥2 (n=80) years of age (Mann *U* Whitney test). RTIs = LRTIs, URTIs, AOM, and otorrhea. URTIs: upper respiratory tract infections, LRTIs, lower respiratory tract infection; AOM, acute otitis media; NS, not significant.

detected in the placebo group in both the total population and in the larger group of children ≥2 years of age where we observed a decrease for the *Actinobacteria* phylum and *Corynebacterium*. *Haemophilus* increased in the OM–85 group. *Actinobacteria* and *Corynebacterium* seem to be associated with respiratory health, while a relative high colonization of *Haemophilus* is associated with increase of asthma risk (Hufnagl et al., 2020).

As far as the clinical response, when comparing the frequency of RTIs and antibiotic use between OM–85 and placebo during the study, there were less children with RTI and antibiotics in the OM–85 group, but these findings were not statistically significant. Therefore, it was not possible to make associations between NP microbiota profiles and clinical outcomes.

The clinical efficacy of OM–85 treatment shown in the original OMPeR study was lost in our sub–analysis. This was in contrast with the one observed in the OMPeR total study population. Indeed, in OMPeR, there were statistically significant differences in favor of OM–85 for upper RTIs (i.e., common cold/viral pharyngitis) as well as for acute otitis media (AOM). Furthermore, the percentage of patients with recurrent upper RTIs and AOM favored OM–85. Precisely, the number of patients with recurrences was approximately 50% among children given placebo and only 21% among those treated with OM–85. The reduction of the URTIs and ear complications, the most frequent ones in the pre–school pediatric population, was associated with a general lower respiratory disease burden, measured as missed days of schools for children and of work for parents. These parameters were significantly reduced in the OM–85 compared to the placebo group. The reasons for such discrepancy between clinical outcomes in our sub–analysis and the OMPeR total population might be several. Surely, the loss of the effect of the randomization and the reduced sample size can be pointed out.

Our work presents some analysis limitations such as the lack of statistical methods controlling for multiple comparisons and multivariate analysis to assess sources of variation compared to the treatments. We did not apply statistical methods controlling for multiple comparisons because of the relatively small sample size of the subgroups, also considering the population heterogenicity. In addition, important microbiota influencing factors, such as method of delivery, gestational age, food source, and pets, were not assessed and reported in the OMPeR clinical trial, with the microbiota assessment only an ancillary study, and we could have not controlled for them. Furthermore, as far as the clinical endpoint, we could not confirm any significant difference between the subgroups, therefore, no further multivariate analysis to assess sources of variation compared to the treatments was done. The collaboration for metagenomic analysis with another research group on expected additional data will help better define the possible correlation between OM–85–induced changes in microbiome composition and clinical results in children with RTIs.

In conclusion, our study, which is registered in EudraCT: 2016–00705–19, is one of the few clinical trials assessing both gut and NP microbiota in pre–school children at risk for RTIs. In addition, it is, to our knowledge, the first study aimed at describing the microbiota relative abundance in patients treated with the oral bacterial lysate OM–85. Other studies used probiotic and prebiotic, mainly *Lactobacillus*, *Bifidobacterium*, and *Enterococcus*, to modulate gut microbiota, a promising approach against viral RTIs *via* host innate and adaptive immunity regulation (Shi et al., 2021).

Some authors are indeed suggesting that such kind of compounds themselves might mimic and even rearrange the gut and, indirectly, airway microbiota (Ober et al., 2017; Rossi et al., 2019). Others observed that bacterial–derived compounds might play a role in innate training, as it has been published for

10.3389/fcimb.2022.789436

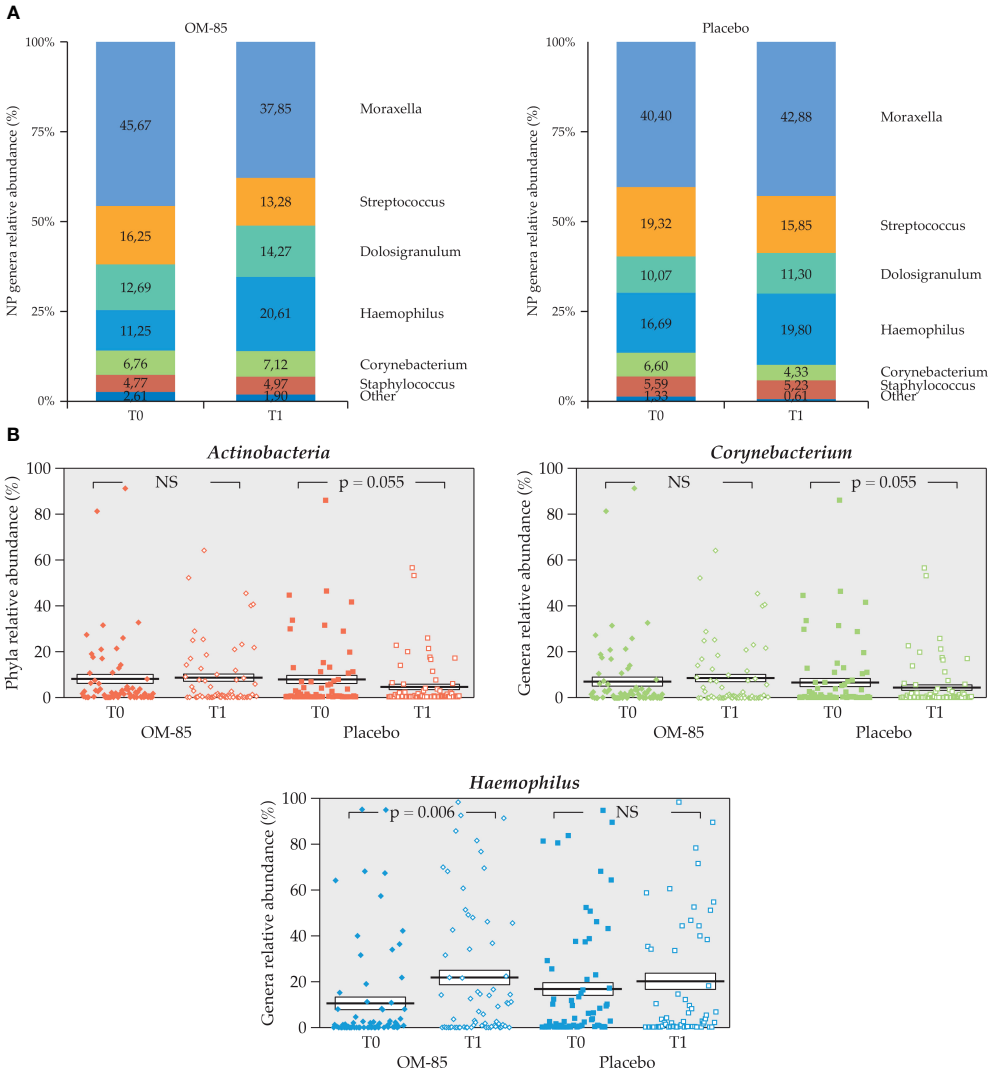

FIGURE 9
Intra–group change of NP microbiota composition in both OM–85 and placebo groups (n=137). **(A)** NP microbiota profiles at T0 and T1 for both treatment groups (n=69, OM-85 and n=68, placebo). **(B)** Statistically significant intra–group difference for *Actinobacteria, Corynebacterium* in placebo, and *Haemophilus* in OM-85 (Wilcoxon's signed–rank test). NS: not significant.

TABLE 4 Mean (SD) number of antibiotic prescriptions and respiratory infections, use of antibiotics (yes, no), and RTI occurrence (yes, no) in subgroups of children <2 years or ≥2 years during the study in the OM–85 and the placebo groups. .

	OM–85 (n = 69)		p–value	Placebo (n = 68)		p–value
	<2 years (n = 17)	≥2 years (n = 52)		<2 years (n = 9)	≥2 years (n = 59)	
Number of antibiotics	1.65 (0.79)	0.92 (0.97)	**0.005**	1.67 (0.71)	0.90 (0.78)	**0.010**
Number of RTIs[1]	2.29 (1.45)	1.29 (1.58)	**0.007**	1.78 (0.97)	1.09 (1.06)	**0.033**
Antibiotics: Yes (%)	16 (94.12%)	30 (57.69%)	**0.007 F**	9 (100%)	39 (66.1%)	**0.0495 F**
No (%)	1 (5.88%)	22 (42.31%)		0	20 (33.9%)	
RTI Yes (%)	16 (94.12%)	29 (55.77%)	**0.003 F**	8 (88.89%)	41 (69.49%)	0.43 F
No (%)	1 (5.88%)	23 (44.23%)		1 (11.11%)	18 (30.51%)	

[1] URTIs, LRTIs, AOM, and otorrhea. URTIs: upper respiratory tract infections, LRTIs, lower respiratory tract infections; AOM, acute otitis media. The bold font means that the value is statistically significant.

10.3389/fcimb.2022.789436

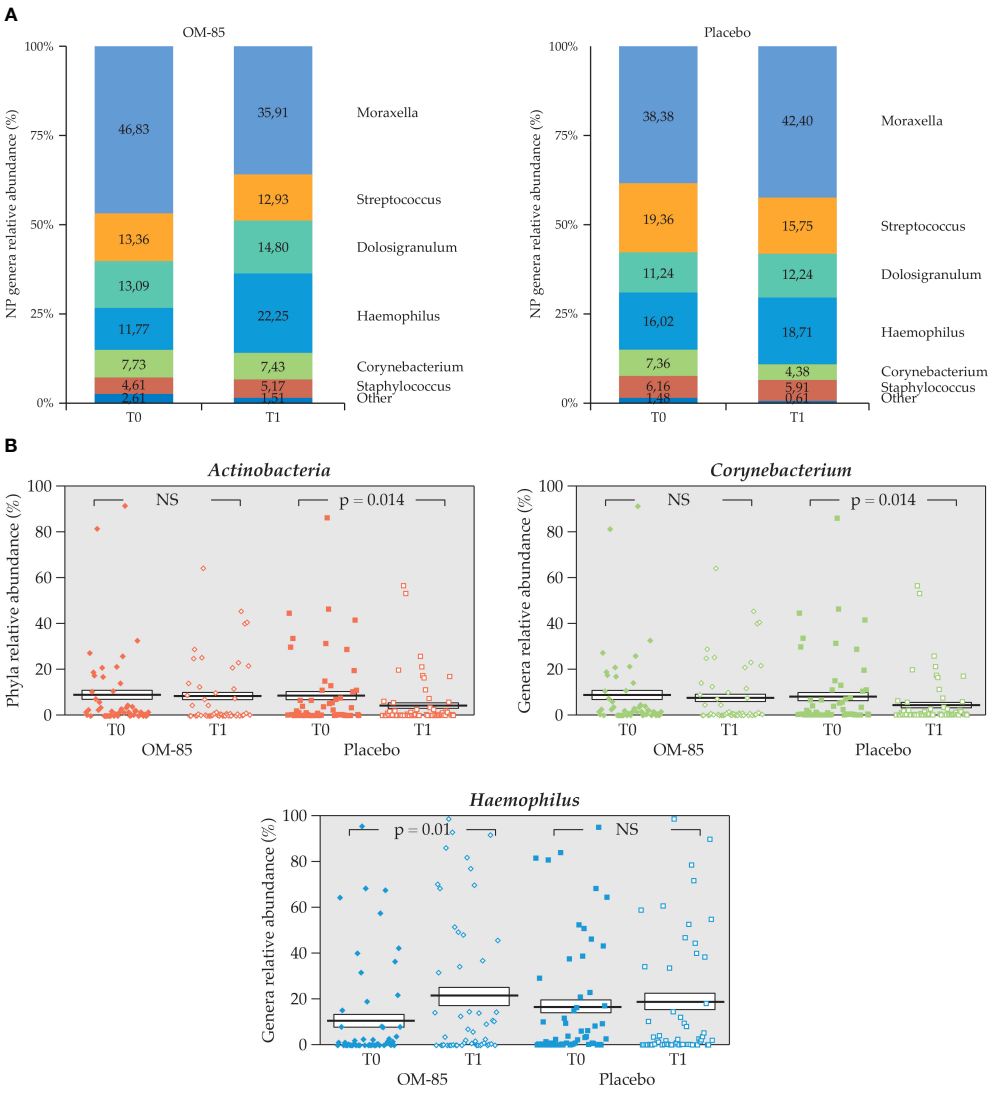

FIGURE 10
Intra–group change of NP microbiota relative abundance in OM–85 and placebo groups in the subgroup of children aged ≥2 years (*n* = 111). **(A)** NP microbiota profiles at T0 and T1 for both treatment groups (n=52, OM-85 and n=59, placebo). **(B)** Statistically significant intra–group difference in relative abundance for *Actinobacteria* phylum, and *Corynebacterium* in placebo and *Haemophilus* genera in OM-85 (Wilcoxon's signed–rank test). NS, not significant.

bacilli Calmette–Guerin (BCG) oral vaccine (Netea et al., 2020). Indeed, Mantovani et al. (Mantovani and Netea, 2020) suggested that the exposure not only to selected vaccines, but also to microbial components, can increase the baseline tone of innate immunity and trigger pathogen–agnostic resistance. Attention has converged on the importance of intervening at early life/stages, with the goal of reducing RTI severity and recurrences as well as preventing the progression to chronicity. To this end, the training of the immune system in early childhood represents an important strategy for preventing RTI–related morbidity and minimizing long–term consequences. Training the immune system with OM–85 might induce long–lasting changes in host microbiota and possibly in innate immunity, resulting in an enhanced response to infection by unrelated pathogens. Further studies are therefore needed in infancy, in a larger patient population, designed for metagenomics analysis and across more viral seasons to clarify its role in microbiota rearrangements.

Data availability statement

The original contributions presented in the study are publicly available. This data can be found here: SRA;

PRJNA488913. In addition, the data presented in the study are deposited in the European Clinical Trial registry (https://www.clinicaltrialsregister.eu/ctr-search/trial/2016-002705-19/IT)", with access number 2016-002705-19.

Ethics statement

The studies involving human participants were reviewed and approved by Fondazione IRCCS Ca' Granda Ospedale Maggiore Policlinico, Milan, Italy. Written informed consent to participate in this study was provided by the participants' legal guardian/next of kind.

Author contributions

Conceptualization: SE and NP. Methodology: SE and NP. Software: SE. Validation: SE and NP. Formal analysis: SE, LR, and AA. Investigation: LR and AA. Resources: SE. Data curation and interpretation: SE, GR, and SB. Writing—original draft preparation: SB. Writing—review and editing: SB, SE, and GR. Visualization: SB. Supervision: SE and NP. Project administration: SE. Funding acquisition: SE. All authors have read and agreed to the published version of the manuscript. SB contributed to microbiota results interpretation and manuscript preparation as an Industrial International PhD student in "System Biology in Immunology and Infectious Pathologies".

Funding

This research was funded by WAidid, Word Association for Infectious Diseases and Immunological Disorders.

Acknowledgments

The investigational medicinal product and placebo were supplied by OMPharma S.A.Meyrin, Switzerland) as an in–kind donation.

Conflict of interest

The authors declare that the research was conducted in the absence of any commercial or financial relationships that could be construed as a potential conflict of interest.

Publisher's note

References

Arumugam, M., Raes, J., Pelletier, E., Le Paslier, D., Yamada, T., Mende Daniel, R., et al. (2011). Enterotypes of the human gut microbiome. *Nature.* 473 (7346), 174–180. doi: 10.1038/nature09944

Biesbroek, G., Tsivtsivadze, E., Sanders, E. A. M., Montijn, R., Veenhoven, R. H., Keijser, B. J. F., et al. (2014). Early respiratory microbiota composition determines bacterial succession patterns and respiratory health in children. *Am. J. Respir. Crit. Care Med.* 190 (11), 1283–1292. doi: 10.1164/rccm.201407-1240OC

Bosch, T. C. G., and McFall–Ngai, M. J. (2011). Metaorganisms as the new frontier. *Zool (Jena)* 114 (4), 185–190. doi: 10.1016/j.zool.2011.04.001

Caporaso, J. G., Kuczynski, J., Stombaugh, J., Bittinger, K., Bushman, F. D., Costello, E. K., et al. (2010). QIIME allows analysis of high–throughput community sequencing data. *Nat. Methods* 7 (5), 335–336. doi: 10.1038/nmeth.f.303

Dang, A. T., Pasquali, C., Ludigs, K., and Guarda, G. (2017). OM–85 is an immunomodulator of interferon–β production and inflammasome activity. *Sci. Rep.* 7:43844. doi: 10.1038/srep43844.

Depner, M., Ege, M. J., Cox, M. J., Dwyer, S., Walker, A. W., Birzele, L. T., et al. (2017). Bacterial microbiota of the upper respiratory tract and childhood asthma. *J. Allergy Clin. Immunol.* 139 (3), 826–834. doi: 10.1016/j.jaci.2016.05.050

Dethlefsen, L., Huse, S., Sogin, M. L., and Relman, D. A. (2008). The pervasive effects of an antibiotic on the human gut microbiota, as revealed by deep 16S rRNA sequencing. *PloS Biol.* 6 (11), E280. doi: 10.1371/journal.pbio.0060280

Esposito, S., Bianchini, S., Bosis, S., Tagliabue, C., Coro, I., Argentiero, A., et al. (2019). A randomized, placebo–controlled, double–blinded, single–centre, phase IV trial to assess the efficacy and safety of OM–85 in children suffering from recurrent respiratory tract infections. *J. Transl. Med.* 17 (1):284. doi: 10.1186/s12967-019-2040-y

Esposito, S., Soto–Martinez, M. E., Feleszko, W., Jones, M. H., Shen, K–L, and Schaad, U. B. (2018). Nonspecific immunomodulators for recurrent respiratory tract infections, wheezing and asthma in children: a systematic review of mechanistic and clinical evidence. *Curr. Opin. Allergy Clin. Immunol.* 18 (3), 198–209. doi: 10.1097/ACI.0000000000000433

Gollwitzer, E. S., and Marsland, B. J. (2014). Microbiota abnormalities in inflammatory airway diseases – potential for therapy. *Pharmacol. Ther.* 141 (1), 32–39. doi: 10.1016/j.pharmthera.2013.08.002

Holt, P. G., Mok, D., Panda, D., Renn, L., Fabozzi, G., deKlerk, N. H., et al. (2019). Developmental regulation of type 1 and type 3 interferon production and risk for infant infections and asthma development. *J. Allergy Clin. Immunol.* 143 (3), 1176–1182. doi: 10.1016/j.jaci.2018.08.035

Huber, M., Mossmann, H., and Bessler, W. G. (2005). Th1–orientated immunological properties of the bacterial extract OM–85–BV. *Eur. J. Med. Res.* 10 (5), 209–217.

Hufnagl, K., Pali–Schöll, I., Roth–Walter, F., and Jensen–Jarolim, E. (2020). Dysbiosis of the gut and lung microbiome has a role in asthma. *Springer Semin. Immunopathol.* 42 (1), 75–93. doi: 10.1007/s00281-019-00775-y

Karimi, K., Inman, M. D., Bienenstock, J., and Forsythe, P. (2009). Lactobacillus reuteri–induced regulatory T cells protect against an allergic airway response in mice. *Am. J. Respir. Crit. Care Med.* 179 (3), 186–193. doi: 10.1164/rccm.200806-951OC

Lazar, V., Ditu, L–M, Pircalabioru, G. G., Gheorghe, I., Curutiu, C., Holban, A. M., et al. (2018). Aspects of gut microbiota and immune system interactions in infectious diseases, immunopathology, and cancer. *Front. Immunol.* 9. doi: 10.3389/fimmu.2018.01830

Man, W. Ho, de Steenhuijsen Piters Wouter, A. A., and Bogaert, D. (2017). The microbiota of the respiratory tract: gatekeeper to respiratory health. *Nat. Rev. Microbiol.* 15 (5), 259–270. doi: 10.1038/nrmicro.2017.14

Man, W. H., Scheltema, N. M., Clerc, M., van Houten, M. A., Nibbelke, E. E., Achten, N. B., et al. (2020). Infant respiratory syncytial virus prophylaxis and nasopharyngeal microbiota until 6 years of life: a subanalysis of the MAKI randomised controlled trial. *Lancet Respir. Med.* 8 (10), 1022–1031. doi: 10.1016/S2213-2600(19)30470-9

Mantovani, A., and Netea, M. G. (2020). Trained innate immunity, epigenetics, and covid–19. *N Engl. J. Med.* 383 (11), 1078–1080. doi: 10.1056/NEJMcibr2011679

Man, W. H., van Houten, M. A., Mérelle, M. E., Vlieger, A. M., Chu, M. L. J. N., Jansen, N. J. G., et al. (2019). Bacterial and viral respiratory tract microbiota and host characteristics in children with lower respiratory tract infections: a matched case–control study. *Lancet Respir. Med.* 7 (5), 417–426. doi: 10.1016/S2213-2600(18)30449-1

Netea, M. G., Domínguez–Andrés, J., Barreiro, L. B., Chavakis, T., Divangahi, M., Fuchs, E., et al. (2020). Defining trained immunity and its role in health and disease. *Nat. Rev. Immunol.* 20 (6), 375–388. doi: 10.1038/s41577-020-0285-6

Ober, C., Sperling, A. I., von Mutius, E., and Vercilli, D. (2017). Immune development and environment: lessons from Amish and Hutterite children. *Curr. Opin. Immunol.* 48, 51–60. doi: 10.1016/j.coi.2017.08.003

O'Toole, P. W., Marchesi, J. R., and Hill, C. (2017). Next–generation probiotics: the spectrum from probiotics to live biotherapeutics. *Nat. Microbiol.* 2, 17057. doi: 10.1038/nmicrobiol.2017.57

Pichon, M., Lina, B., and Josset, L. (2017). Impact of the respiratory microbiome on host responses to respiratory viral infection. *Vaccines (Basel)* 5 (4):40. doi: 10.3390/vaccines5040040

Rinninella, E., Raoul, P., Cintoni, M., Franceschi, F., Miggiano, G., Gasbarrini, A., et al. (2019). What is the healthy gut microbiota composition? a changing ecosystem across age, environment, diet, and diseases. *Microorganisms.* 7 (1), 14. doi: 10.3390/microorganisms7010014

Rossi, G. A., Esposito, S., Feleszko, W., Melioli, G., Olivieri, D., Piacentini, G., et al. (2019). Immunomodulation therapy – clinical relevance of bacterial lysates OM–85. *Eur. Respir. pulmonary dis* 5 (1), 17. doi: 10.17925/ERPD.2019.5.1.17

Rossi, G. A., Pohunek, P., Feleszko, W., Ballarini, S., and Colin, A. A. (2020). Viral infections and wheezing–asthma inception in childhood: is there a role for immunomodulation by oral bacterial lysates? *Clin. Transl. Allergy* 0 (1), 1–11. doi: 10.1186/s13601-020-00322-1

Sarangi, A. N., Goel, A., and Aggarwal, R. (2019). Methods for studying gut microbiota: A primer for physicians. *J. Clin. Exp. Hepatol.* 9 (1), 62–73. doi: 10.1016/j.jceh.2018.04.016

Shi, H. Y., Zhu, X., Li, W. L., Mak, J. W. Y., Wong, S. H., Zhu, S. T., et al. (2021). Modulation of gut microbiota protects against viral respiratory tract infections: a systematic review of animal and clinical studies. *Eur. J. Nutr.*, (8):4151–4174. doi: 10.1007/s00394-021-02519-x

Teo, S. M., Mok, D., Pham, K., Kusel, M., Serralha, M., Troy, N., et al. (2015). The infant nasopharyngeal microbiome impacts severity of lower respiratory infection and risk of asthma development. *Cell Host Microbe* 17 (5), 704–715. doi: 10.1016/j.chom.2015.03.008

Terranova, L., Oriano, M., Teri, A., Ruggiero, L., Tafuro, C., Marchisio, P., et al. (2018). How to process sputum samples and extract bacterial DNA for microbiota analysis. *Int. J. Mol. Sci.* 19 (10), 3256. doi: 10.3390/ijms19103256

Thomas, V., Clark, J., and Dor, J. (2015). L. fecal microbiota analysis: an overview of sample collection methods and sequencing strategies. *Future Microbiol.* 10 (9), 1485–1504. doi: 10.2217/fmb.15.87

Vacca, M., Celano, G., Calabrese, F. M., Portincasa, P., Gobbetti, M., and De Angelis, M. (2020). The controversial role of human gut lachnospiraceae. *Microorganisms.* 8 (4):573. doi: 10.3390/microorganisms8040573

Vael, C., Nelen, V., Verhulst, S. L., Goossens, H., and Desager, K. N. (2008). Early intestinal bacteroides fragilis colonisation and development of asthma. *BMC Pulm Med.*, 8:19. doi: 10.1186/1471-2466-8-19

van den Munckhof, E. H. A., Hafkamp, H. C., de Kluijver, J., Kuijper, E. J., de Koning, M. N. C., Quint, W. G. V., et al. (2020). Nasal microbiota dominated by moraxella spp. is associated with respiratory health in the elderly population: a case control study. *Respir. Res.* 21 (1), 181. doi: 10.1186/s12931-020-01443-8

Zhou, Y., and Zhi, F. (2016). Lower level of bacteroides in the gut microbiota is associated with inflammatory bowel disease: A meta–analysis. *BioMed. Res. Int.*; 2016:5828959. doi: 10.1155/2016/5828959

Zomer–Kooijker, K., van der Ent, C. K., Ermers, M. J. J., Uiterwaal, C. S. P. M., Rovers, M. M., and Bont, L. J. (2014). Increased risk of wheeze and decreased lung function after respiratory syncytial virus infection. *PloS One* 9 (1), E87162. doi: 10.1371/journal.pone.0087162

frontiers | Frontiers in Cellular and Infection Microbiology

TYPE Original Research
PUBLISHED 09 September 2022
DOI 10.3389/fcimb.2022.966361

OPEN ACCESS

EDITED BY
Steven Gill,
University of Rochester, United States

REVIEWED BY
Ruth Serra-Moreno,
University of Rochester Medical Center, United States
Leopoldo Segal,
New York University, United States

*CORRESPONDENCE
Barbara A. Methé
metheba@upmc.edu

†These authors have contributed equally to this work and share first authorship

SPECIALTY SECTION
This article was submitted to Microbiome in Health and Disease, a section of the journal Frontiers in Cellular and Infection Microbiology

RECEIVED 10 June 2022
ACCEPTED 22 August 2022
PUBLISHED 09 September 2022

CITATION
Li K, Methé BA, Fitch A, Gentry H, Kessinger C, Patel A, Petraglia V, Swamy P and Morris A (2022) Gut and oral microbiota associations with viral mitigation behaviors during the COVID-19 pandemic.
Front. Cell. Infect. Microbiol. 12:966361.
doi: 10.3389/fcimb.2022.966361

Gut and oral microbiota associations with viral mitigation behaviors during the COVID-19 pandemic

Kelvin Li[1,2†], Barbara A. Methé[1,2*†], Adam Fitch[1,2], Heather Gentry[1,2], Cathy Kessinger[1,2], Asha Patel[1,2], Vickie Petraglia[1,2], Pruthvi Swamy[1,2] and Alison Morris[1,2]

[1]Center for Medicine and the Microbiome, University of Pittsburgh School of Medicine, Pittsburgh, PA, United States, [2]Division of Pulmonary, Allergy and Critical Care Medicine, Department of Medicine, University of Pittsburgh School of Medicine and University of Pittsburgh Medical Center, Pittsburgh, PA, United States

Imposition of social and health behavior mitigations are important control measures in response to the coronavirus disease 2019 (COVID-19) pandemic caused by the Severe Acute Respiratory Syndrome Coronavirus 2 (SARS-CoV-2). Although postulated that these measures may impact the human microbiota including losses in diversity from heightened hygiene and social distancing measures, this hypothesis remains to be tested. Other impacts on the microbiota and host mental and physical health status associations from these measures are also not well-studied. Here we examine changes in stool and oral microbiota by analyzing 16S rRNA gene sequence taxonomic profiles from the same individuals during pre-pandemic (before March 2020) and early pandemic (May-November 2020) phases. During the early pandemic phase, individuals were also surveyed using questionnaires to report health histories, anxiety, depression, sleep and other lifestyle behaviors in a cohort of predominantly Caucasian adults (mean age = 61.5 years) with the majority reporting at least one underlying co-morbidity. We identified changes in microbiota (stool n = 288; oral n = 89) between pre-pandemic and early pandemic time points from the same subject and associated these differences with questionnaire responses using linear statistical models and hierarchical clustering of microbiota composition coupled to logistic regression. While a trend in loss of diversity was identified between pre-pandemic and early pandemic time points it was not statistically significant. Paired difference analyses between individuals identified fewer significant changes between pre-pandemic and early pandemic microbiota in those who reported fewer comorbidities. Cluster transition analyses of stool and saliva microbiota determined most individuals remained in the same cluster assignments from the pre-pandemic to early pandemic period. Individuals with microbiota that shifted in composition, causing them to depart a pre-pandemic cluster, reported more health issues and pandemic-associated worries. Collectively, our study identified that stool and saliva microbiota from the pre-pandemic to early pandemic periods largely exhibited ecological stability (especially stool

microbiota) with most associations in loss of diversity or changes in composition related to more reported health issues and pandemic-associated worries. Longitudinal observational cohorts are necessary to monitor the microbiome in response to pandemics and changes in public health measures.

KEYWORDS

COVID-19, microbiome, ecological stability, saliva microbiota, gut microbiota, 16S rRNA gene amplicon sequencing

Introduction

The coronavirus disease 2019 (COVID-19) pandemic caused by the Severe Acute Respiratory Syndrome Coronavirus 2 (SARS-CoV-2) is a devastating worldwide event that has precipitated dramatic changes in social and health behaviors in human populations (Atzrodt et al., 2020). Especially in the early pandemic phase in 2020 prior to vaccine and other pharmaceutical prophylaxis interventions, a variety of strategies were implemented to minimize the spread of the virus including social distancing, self-isolation, working from home and increased hygiene measures (Bavel et al., 2020). Substantial efforts have been underway to understand the impacts of these disruptions and COVID-19 related worries on human psychology including stress, and anxiety (Blix et al., 2021), as well as health consequences such as changes in diet, sleep, and exercise (Arora and Grey, 2020). Several, longitudinal studies assessed mental health outcomes within the same individuals before and during the pandemic and determined that general mental distress increased during the pandemic (Daly et al., 2020; Pierce et al., 2020) and effects of COVID-19 on daily life were significant predictors of higher levels of depression, anxiety, and stress during the pandemic (Haliwa et al., 2021). However, the impact of these population-wide viral transmission minimization strategies and other behavioral changes on the human microbiota of individuals non-symptomatic for COVID-19 have not been well-studied despite the substantial and complex interplay between diet, environment factors and the microbiome in human health and disease.

The human microbiota and its collection of genomes (the microbiome) is composed of trillions of cells that interact as microbial communities in multiple ecological niches in and on the human body through mutualistic or symbiotic relationships with the host (Gevers et al., 2012; Sender et al., 2016). More than a decade of research has underscored the multiple, critical roles the microbiome plays in normal development and maintenance of the immune, endocrine, and nervous systems, and healthy metabolism.

As the COVID-19 pandemic has progressed, several groups have speculated on the potential impact of these changes in behavior and lifestyle on the microbiome (Domingues et al., 2020; Burchill et al., 2021; Finlay et al., 2021). In particular, it has been hypothesized that these changes may include the loss of microbial diversity due to increased microbial depletion and reduced transmission resulting from heightened hygiene and social distancing measures, respectively (Domingues et al., 2020; Burchill et al., 2021; Finlay et al., 2021). However, this hypothesis has not been well-studied longitudinally in individuals not infected with COVID-19. Here we used an ongoing large observational cohort (MedBio Cohort) with pre- and early pandemic data and stool and oral specimens from the same individuals to examine associations between human microbiota and changes in social behaviors precipitated during an ongoing pandemic and concomitant changes in public health measures.

Materials and methods

Cohort

Participants were selected without bias from a large ongoing observational cohort (MedBio) consisting of a collection of UPMC patient registries and clinical investigations which facilitates standardized approaches to subject enrollment and specimen processing across multiple studies. These studies span a range of chronic illnesses and disease status. The University of Pittsburgh IRB approved the study, and all participants signed informed consent.

Sample collection

Early pandemic samples were collected from May 2020 through November 2020. Stool specimens were self-collected using the DNA/RNA Shield Fecal Collection tubes (Zymo) for nucleic acid preservation and short-term (two to four weeks) storage at ambient temperature. Oral specimens were self-collected using the OMNIgene·ORAL OM-505 devices. 2 mL of saliva were collected for nucleic acid preservation and short-

term storage at ambient temperature. Specimens were mailed to the University of Pittsburgh. Upon receipt, specimens were sub-aliquoted prior to long-term storage at -80°C.

Early pandemic data collection

During the early pandemic period, subjects participated in an on-phone interview assessing demographics, medical history, smoking history, health status, and COVID-19-related behavior with specimen collection occurring within approximately 10-14 days of the interview. We also administered the General Anxiety Disorder 7 (GAD7) questionnaire (Johnson et al., 2019), Patient Health Questionnaire 9 (PHQ-9) questionnaire (Kroenke et al., 2001), and the Insomnia Severity Index (ISI) (Morin et al., 2011).

The questionnaire consisted of 49 grouped questions: Demographics (Q1-Q6), Past Health History (Q7-Q12, Q12 was an inventory Q12a-Q12q of comorbidities), Smoking History (Q13-Q15), Recent Heath History (Q16-Q19), GAD7 Anxiety (Q20), PHQ-9 Depression (Q21), ISI Sleep Survey (Q22), and Recent Behavior (Q23-Q49). Some questions were excluded from the statistical analyses as they were either regarding the accessibility of UPMC medical resources, or the potential relevance of the question was more directly represented by an alternative question.

Categorical responses were recoded into ordinal responses when necessary, so that 0 (reference) was associated with healthy or no difference. Responses to inventory-style questions were summed up (Q17 General Ailments). (See Supplemental material for a PDF version of the questionnaire.) See Table 1. "Questionnaire Summary Table" for a summary of descriptive statistics for the subset of responses included in the models.

Other subject information

BMI was estimated by linear interpolation using the closest bracketing BMI measurements taken before and after the collection date of the sample. Samples taken before March 15, 2020, were considered pre-pandemic samples, and matching samples from the same subject collected after March 15, 2020, were considered early pandemic samples (when "lockdown" and more intense viral transmission mitigation strategies were in place). Early pandemic samples were collected from May 2020 through November 2020.

DNA extraction

DNA extraction was performed using the Qiagen Powersoil Microbiome Kit EP for automated DNA extraction using an Eppendorf, 5075VTC liquid handling workstation. HEPA filtration was used during sample processing and the workstation was UV sanitized between batches. Specimens were processed per manufacturer's protocol with the following modifications: An approximate aliquot of 300µl of specimen was added to individual bead beating tubes to ensure no carryover between samples during the bead beating process. Aliquots from the individual tubes were then transferred to 96-well blocks for completion of the automated genomic DNA extraction process. Reagent blanks were included as negative controls. Cells and genomic DNA from a microbial community of known composition (ZymoBiomics Microbial Community Standards; Zymo Research, Irvine, CA) served as positives controls. As a component of the QC process, positive controls were evaluated across sample batches to evaluate laboratory and sequencing performance and compared to historical performance of 16S rRNA gene sequencing at the Center for Medicine and the Microbiome (CMM). No significant batch deviation was identified in this project.

Bacterial community sequencing

Extracted genomic DNA (gDNA) was amplified for the V4 region using Q5 HS High-Fidelity polymerase (New England BioLabs, Ipswich, MA) with inline barcode primers design based on the method of Caporaso (2012) (Caporaso et al., 2012). V4 primer sequences were: 515f 5'-GTGCCAGCMGCCGCGGTAA-3' and 806r 5'-GGACTACHVGGGTWTCTAAT-3'. Approximately 5-10 ng of each sample were amplified in 25 µL reactions. Cycle conditions were 98°C for 30 seconds, then 30 cycles of 98°C for 10 seconds, 57°C for 30 seconds, and 72°C for 30 seconds, with a final extension step of 72°C for 2 minutes. Amplicons were purified with AMPure XP beads (Beckman Coulter, Indianapolis, IN) at a 0.8:1 ratio (beads:DNA) to remove primer dimers. Eluted DNA was quantitated on a Qubit fluorimeter (Life Technologies, Grand Island, NY). Sample pooling was performed on ice by combining 40 ng of each purified band. For negative controls and poorly performing samples, 20 µL of each sample was used. The sample pool was purified with the MinElute PCR purification kit (Qiagen, Germantown, MD). The final sample pool underwent 2 more purifications: AMPure XP beads to 0.8:1 to remove primer dimers, and a final cleanup in Purelink PCR Purification Kit (Life Technologies). The purified pool was quantitated in triplicate on the Qubit fluorimeter prior to sequencing.

The sequencing pool was prepared as per Illumina's recommendations (Illumina, Inc., San Diego, CA), with an added incubation at 95°C for 2 minutes immediately following the initial dilution to 20pM. The pool was then diluted to a final concentration of 7pM + 20% PhiX control (Illumina). Sequencing was done on an Illumina MiSeq 500-cycle V2 kit (Illumina).

Bioinformatics

Sequences from the Illumina MiSeq were deconvolved and then processed through the CMM in-house sequence quality control pipeline, which includes dust low complexity filtering, quality value (QV<30) trimming, and trimming of primers used for 16S rRNA gene amplification, and minimum read length filtering. Using the scripts fastq_quality_trimmer and fastq_quality_filter from Hannon's Cold Spring Harbor Laboratory's FASTAX-Toolkit (http://hannonlab.cshl.edu/fastx_toolkit/). Reads were trimmed until the QV was 30 or higher. Trimmed reads shorter than 75bp or those with less than 95% of the bases above a QV of 30 were discarded. Forward and reversed paired reads were merged with a minimum required overlap of 25 bp, proportion overlap mismatch > 0.2, maximum N's allowed = 4, and a read length minimum of 125 bp. Forward and reverse reads were merged into contigs then processed through the CMM's Mothur-based (v1.44.1) (Schloss et al., 2009) 16S rRNA gene sequence clustering and annotation pipeline. Sequence taxonomic classifications were performed with the Ribosomal Database Project's (RDP) naïve Bayesian classifier (Wang et al., 2007) (Quast et al., 2013) with the SILVA 16S rRNA database (v138) (Quast et al., 2013).

Data analysis

Questionnaire Analyses. Selected recoded questionnaire responses (variables), p = 25, were tested with the Shapiro-Wilk test for normality (H_0: values are normally distributed). If the p-value was >0.2, then the original values were utilized. If the p-value <0.2, the values were then logarithm transformed and retested. If the transformation increased the p-value, then the transformation was accepted. Pearson correlations were calculated between responses and a Principal Component Analysis (PCA) was performed. Principal Components (PCs) which represented at least 5% of the total variance were then annotated by identifying the variable with the greatest correlation with the PC. Correlations were reported for those with p-values < 0.001 after a Bonferroni adjustment, assuming the number of tests were m = p(p-1)/2 = 300.

Due to the compositional nature of the taxonomic profiles from 16S rRNA gene sequencing (Gloor et al., 2224), taxonomic abundances were first transformed using the additive log ratio (ALR) transformation (Tarabichi et al., 2015). The top 15 taxa, by average abundance across the experimental samples, were selected to represent the taxa of interest, and the remaining taxa were accumulated into the denominator of the ratio, prior to natural log transformation. Log ratio transformations are crucial when including multiple taxa into linear models to ensure the abundances are normally distributed and independent from each other (Aitchison, 1982).

Analyses involving the calculation of a diversity index utilized the Shannon diversity index and the Tail statistic (Li et al., 2012). The Tail statistic is more sensitive towards the lower abundance taxa than the Shannon diversity index. Analyses requiring the calculation of pair-wise compositional distances between samples used the Manhattan distance, which is also more sensitive towards differences in the lower abundance taxa than the Euclidean distance.

Adjusting for differences in sample collection times

There was a wide range of timespans between the pre- and early pandemic samples. The median and 95% Prediction Intervals (PI) time spans for stool were 526 (164, 1094) days and for saliva, 725 (251, 1046) days. Preliminary analyses to identify a corrective adjustment suggested that over time, paired sample distances approached a limit asymptotically. A non-linear adjustment for each timespan t based on fitting 3 parameters (maximum distance m, rate r, slope s) with the function: adjustment(t) = m*(1-exp(-t*r))+s*t) was calculated, but model comparisons revealed the adjustment was not significantly better than the simpler linear model with an intercept. This is likely due to the lower bound of the timespans being restricted between 5-6 months, so any acute changes to the microbiota composition might have already reached their limits. The correlation between changes in the stool and saliva from the same subject were also examined, but the near 100% correlation of the pre-pandemic to early pandemic timespans between the two sample types confounded the analysis.

Models

Three statistical models were used to associate the microbiota sampling with the questionnaire responses.

The "pre/early pandemic paired" (PEPP) model first identified subjects with both pre-pandemic and early pandemic samples, then used the variables of days pre-pandemic, days early pandemic, pre-BMI, and dBMI (change in BMI) and questionnaire responses to predict the difference between the diversity, abundance or the distance (Stapleton et al., 2021) between pre-pandemic and early pandemic samples with a linear model.

The "pre/early pandemic cluster transition" (PEPCT) model, another type of paired analysis, used a combination of clustering and then logistic regression to associate questionnaire responses to changes in "microbiome type". Pre- and early pandemic samples were first hierarchically clustered together, then clusters were iteratively identified by increasing cuts (k). At each cut k, for each of the resultant clusters identified from 1:k,

the following variables were used to predict the sample's early pandemic cluster: questionnaire responses, pre- and early pandemic days, pre-pandemic BMI and dBMI, and pre-pandemic cluster identifiers. This analysis identified factors that could predispose a subject's sample to change to a specific early pandemic cluster ("arrive"). Similarly, a "departure" analysis was performed for each of the pre-pandemic clusters at each cut *k*. For each pre-pandemic cluster, member subjects were divided into those that remained in the same early pandemic cluster and those that departed. In the departure analysis, dBMI, pre- and early pandemic days, and the questionnaire responses were included in the logistic regression to predict whether a sample stayed in or left the pre-pandemic cluster. To identify which cluster cut *k* to report arrival or departure associations with, the cut *k* with the most significant p-value for each factor was selected. Taxonomic members (cluster unifiers) that differentiate a cluster from other clusters generated at the same cut, were identified with an R^2 ratio analyses (See Supplemental methods). The R^2 ratio analyses estimate the R^2 between two clusters with (full model) and without (reduced model) a taxon of interest, to identify whether the taxon of interest contributed to cluster separation. If the reduced model had a smaller R^2 than the full model, then the taxon left out of the reduced model contributed to cluster separation. Taxa that consistently contributed to a cluster's separation from the other clusters were considered taxa that defined a cluster's microbiota "type".

The "early pandemic cross-sectional" (EPCS) model focused on the early pandemic samples. The questionnaire responses, EP-BMI, and days early pandemic were used to predict the microbiota diversity, inter-sample distancing, or abundance with a linear model.

See Figure 1, "Variables and Models" for a diagram illustrating the relationship between variables and the models that were fit.

Results

Questionnaire

From the 588 questionnaire responders, the mean respondent's age was 61.5 years old, although 95% of the subjects were between 25 and 82 years. 54.5% of respondents were female and 84.5% were Caucasian. The percent of respondents with a smoking history (>100 cigarettes in their lifetime) was 50.2%. The mean and 95% CI of the questionnaire responses can be found in Table 1, "Questionnaire Descriptive Statistics Summary". The breakdown of respondents included in the pre-pandemic to early pandemic time points (PEPP), pre-pandemic to early pandemic cluster transition (PEPCT), and early pandemic cross-sectional (EPCS) models for stool and saliva analyses can be found in Supplemental Table 1, "Sample Exclusions".

Examination of the correlation matrix with Bonferroni adjusted p-values < 0.001 identified several noteworthy correlations. See Supplemental Figure 2, "Questionnaire Response Correlations, Bonferroni Adjusted Significant (p-value < 0.05)" for the heat map and all pairwise correlations. Education level was correlated with health (ρ = 0.23) and exercise (>1x/week, pre-pandemic ρ = 0.29, early pandemic ρ = 0.25). Exercise pre-pandemic was correlated with early pandemic exercise with a coefficient of ρ = 0.6. A clustering of positive correlations was also identified among immune system disease, asthma, (sum of) general ailments, GAD7 anxiety, PHQ9 depression, and ISI sleep. (Sum of) COVID-19 worries was correlated with diet change (ρ = 0.24). The number of cohabitants was correlated with the number of pets (ρ = 0.24). Principal Components Analysis (PCA) revealed that the top 5 PCs each captured greater than 5% of the total variance, but the first 21 (out of 25) PCs would be required to capture 95% of the variance. The top 5 PCs were most closely correlated with: PHQ9 depression (ρ = 0.79), exercise (pre-pandemic) (ρ = 0.58), ethnicity (ρ = 0.67), exercise (early pandemic) (ρ = 0.45), and high blood pressure (ρ = 0.48).

Statistical analyses of microbiota from stool and oral samples

Here results are reported first for the analyses of microbiota from stool then for saliva samples. For each sample type, the paired analysis results for the pre- and early pandemic samples are reported first followed by the cross-sectional results for the early pandemic sample analysis. Both paired and cross-sectional analyses are comprised of a collection of independent sub-analyses that fit statistical models using calculated sample diversity, inter-sample distances, and taxonomic abundances.

Stool specimens for 16S rRNA gene sequencing

The sample size available for stool was 311 samples available for the early pandemic cross-sectional analysis and 288 subjects had both pre- and post-pandemic samples for the paired analyses.

The pre/early pandemic paired analysis of stool sample microbiota

The pre/early pandemic paired (PEPP) analysis of stool sample microbiota was performed on the n = 288 paired pre-pandemic and early pandemic stool samples taken from the

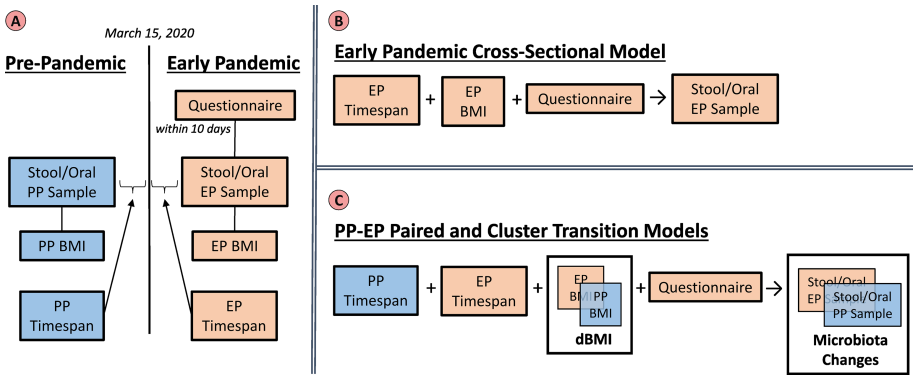

FIGURE 1
Variables and Models. The left panel **(A)** summarizes the groups of variables that were utilized in the analyses. Pre-pandemic (PP) (blue) and Early Pandemic (EP) **(beige)** variables include the taxonomic profiles from sequencing microbiota samples, BMIs interpolated based on the sample collection dates, and timespans relative to March 15, 2020. The questionnaire responses were only collected during the early pandemic. The top right panel **(B)** illustrates the early pandemic cross-sectional model. Here, only the EP variables: timespan, BMI, and questionnaire were utilized to build a model to predict the EP stool or saliva microbiota. The lower right panel **(C)** represents the variables included in the paired and cluster transition models. Both the PP and EP timespans, as well as questionnaire responses were included in the models. The BMI and microbiota profiles were included in the model as their relative changes which could be calculated per subject.

same subject. The median and 95% Prediction Interval (PI) of the pre- and early pandemic days were 342 (25, 912) and 162 (118, 223), respectively. These differences were then associated with the questionnaire responses from these subjects. The number of subjects with both samples available were fewer, so there was less statistical power than the EPCS stool analysis. Overall composition for the pre-pandemic and early pandemic stool samples can be found in Supplemental Figure 1, "Paired Compositional Stacked Bar Plots".

Diversity was stable between time points. When examining stool microbiota, the Shannon diversity index did not identify any significant ($p<0.05$) associations, but the Tail statistic identified a negative association with change in BMI (p–val = 0.0232) and smoking history (p–val = 0.0317). The number of pets was positively associated with an increase in diversity (p–val = 0.0406). The intercept, representing the difference between pre- and early pandemic differences in diversity when controlling for other factors included in the model, was not significantly non-zero for neither the Tail statistic (β_0 = -0.7441, p-val = 0.7341) nor the Shannon diversity index (β_0 = −0.4881, p-val = 0.2297). The increase of BMI of subjects with paired stool samples was not statistically significant in the subjects: median dBMI = 0.0, 95% PI = (-4.326, 3.761).

BMI and health were associated with reduced pre-to-early pandemic inter-sample distances. An analysis of the distance (compositional change) between stool sample pairs found a significant effect of lengthening the distance between pairs (greater change in composition) for pre-pandemic days (p–val = 0.0023) and days into the early pandemic (p–val = 0.0265). See Figure 2, Stool and Saliva Pre- and early pandemic MDS Plots. Pre-pandemic BMI (p–val = 0.0328) and health (p–val = 0.0178) had an effect of shortening the distance between pairs (composition becomes more alike). There was a less significant, but potentially noteworthy, effect of diabetes (p–val = 0.0708) and number of cohabitants (p–val = 0.0907).

Changes in multiple taxonomic abundances were associated with immune system disorders and changes in BMI. The number of days from stool sample collection to the early pandemic period were positively associated with two taxa. The number of pre-pandemic days before sample collection was associated with *Fusicatenibacter* (p–val = 3.33×10^{-4}), and the number of early pandemic days before sample collection was associated with *Lachnoclostridium* (p–val = 5.13×10^{-4}). Immune system disease was associated with the increase of *Alistipes* (p–val = 3.8×10^{-5}), *Lachnospiraceae_uncl* (p–val = 1.02×10^{-3}), *Bacteroides* (p–val = 1.08×10^{-3}), and *Faecalibacterium* (p–val = 5.72×10^{-3}). Asthma was associated with an increase of *Ruminococcus* (p–val = 8.12×10^{-4}). Pre-pandemic BMI was associated with an increase in *Prevotella* (p–val = 3.64×10^{-4}), and changes in BMI between sample collection dates were associated with less *Oscillospiraceae UCG_002* (p–val = 3.84×10^{-4}) and *Subdoligranulum* (p–val = 4.58×10^{-3}), and more *Escherichia_Shigella* (p–val = 4.55×10^{-3}). Diabetes was associated with more *Agathobacter* (p–val = 9.89×10^{-3}) in the early pandemic. In addition, there were associations with depression including a decrease in *Lachnospiraceae_uncl* (p–val = 2.46×10^{-3}) and an increase of *Prevotella* (p–val = 8.78×10^{-3}) with education level in the early pandemic period.

TABLE 1 Questionnaire Descriptive Statistics Summary.

	Variable	Categories	Mean	(95% CI: LB, UB)	[N]	Question ID
1.)	Age		61.505	(60.285, 62.726)	[582]	Q1
2.)	Sex	*Male*	0.455	(0.415, 0.497)	[266]	Q2
		Female	0.545	(0.503, 0.585)	[318]	
3.)	Ethnicity	*Black*	0.068	(0.049, 0.091)	[40]	Q3
		Other	0.087	(0.065, 0.112)	[51]	
4.)	Education Level [1]	*range [0, 5]*	2.642	(2.538, 2.746)	[586]	Q5
5.)	Health [2]	*range [0, 4]*	2.342	(2.265, 2.42)	[587]	Q7
6.)	Fever (past year)	*Yes*	0.128	(0.101, 0.158)	[72]	Q10
7.)	Exercise Pre-Pandemic (>1x/week)	*Yes*	0.642	(0.602, 0.681)	[377]	Q11
8.)	High Blood Pressure	*Yes*	0.453	(0.412, 0.494)	[265]	Q12a
9.)	Diabetes	*Yes*	0.116	(0.091, 0.145)	[68]	Q12b
10.)	Sleep Apnea	*Yes*	0.193	(0.162, 0.228)	[113]	Q12h
11.)	Asthma	*Yes*	0.156	(0.127, 0.188)	[91]	Q12j
12.)	Cancer (active treatment)	*Yes*	0.070	(0.051, 0.094)	[41]	Q12l
13.)	Immune System Disease (excluding HIV)	*Yes*	0.281	(0.245, 0.319)	[164]	Q12n
14.)	Smoking History	*Yes*	0.502	(0.46, 0.543)	[293]	Q13
15.)	Sum of Ailments	*range [0, 10]*	1.053	(0.914, 1.191)	[588]	Q17
16.)	GAD7 Anxiety Score	*range [0, 21]*	2.827	(2.512, 3.141)	[588]	Q20
17.)	PHQ9 Depression Score [3]	*range [0, 24]*	2.621	(2.33, 2.912)	[588]	Q21
18.)	ISI Sleep Survey	*range [0, 28]*	11.316	(10.928, 11.705)	[588]	Q22
19.)	Exercise Early Pandemic (>1x/week)	*Yes*	0.708	(0.668, 0.745)	[402]	Q26
20.)	Sum of COVID-19 Worries	*range [0, 15]*	5.184	(4.958, 5.409)	[588]	Q38, Q39, Q41
21.)	Social Distancing [4]	*Yes*	0.930	(0.907, 0.95)	[547]	Q42
22.)	Change in Diet [5]	*range [0, 4]*	0.683	(0.605, 0.762)	[584]	Q46
23.)	Number Cohabitants [6]	*range [0, 3]*	1.434	(1.338, 1.531)	[587]	Q47
24.)	Number of Pets [6]	*range [0, 3]*	0.920	(0.834, 1.005)	[587]	Q48

[1]Education Level coding: 0 = "did not graduate from high school" to 5 = "doctorate".
[2]Health coding: 0 = "poor" to 4 = "excellent".
[3]Last PHQ9 item (suicide) was omitted from questionnaire.
[4]Either Social Distance or Working From Home.
[5]Coding: 0 = "not at all" to 4 = " a lot".
[6]Coding: 0 = "none" to 3 = "3 or more".
This table contains a summary of the variables included in the analyses that were based on the questionnaire responses. The category or range of values, mean, 95% CI, N, and question identifier have been reported for each variable. Note that the subset of subjects that were used in the stool or saliva analyses depended on matching samples. This table represents the descriptive statistics from all the questionnaire responders, regardless of whether they could be included in the stool or saliva samples analyses.

Pre/early pandemic cluster transition stool analysis identified changes of cluster membership associated with sex, COVID-19 worries, asthma, cancer, and social distancing

A Pre/Early Pandemic Cluster Transition (PEPCT) stool analysis was performed to identify factors that are associated with samples changing their cluster membership between pre- and early pandemic time points. "Departer" samples were defined as those samples that left their starting pre-pandemic cluster for another cluster by their early pandemic time point. "Arriver" samples were defined as those samples that were new additions to a cluster in the early pandemic time point. When the hierarchical clustering was cut to $k = 3$ clusters the departers from the second cluster ($cl = 2$ of $k = 3$) consisted of fewer females (p-val < 0.001). Based on cluster influencer analysis, the distinguishing taxonomic member of this cluster was *Bacteroides*. When the hierarchical clusters were cut to $k = 6$, the departers from the second cluster ($cl = 2$ of $k = 6$) were associated with more COVID-19 worries (p-val = 0.006). The distinguishing members of this cluster were *Akkermansia Oscillospiraceae UCG_002, Bacteroides, Alistipes, Prevotella*, and others. Clusters with arriving samples with significant associations included ($cl = 3$ of $k = 6$) that were associated with fewer COVID-19 worries (p-val < 0.001). This cluster was distinguished by *Bacteroides*, *Faecalibacterium*, and *Agathobacter*. Samples from asthma subjects were associated with arrival in ($cl = 1$ of $k = 2$) (p-val = 0.009). The distinguishing taxa of this cluster were *Prevotella* and *Prevotellaceae*_uncl.

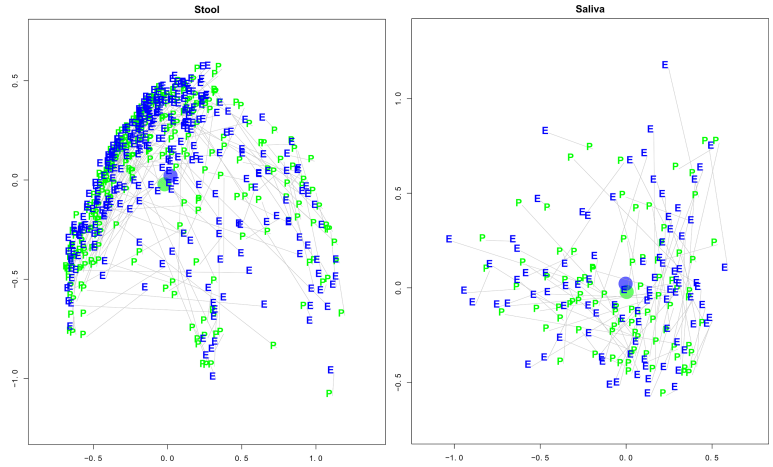

FIGURE 2
Stool and Saliva Pre- and Early Pandemic Paired MDS plots. These multi-dimensional scaling (MDS) plots illustrate each subject's taxonomic compositional similarity between pre- and early pandemic samples in context with the samples of the cohort. The left and right panels represent the intra-cohort separation of stool and saliva samples, respectively. The green "pre" and blue "early" labels indicate the MDS estimated locations of pre- and early pandemic samples, respectively. A grey line connects pre- and early pandemic samples from the same subject. The blue and green circles represent the centroids of the pre- and early pandemic samples. After controlling for questionnaire responses, the bootstrapped regression identified that pre- vs early pandemic samples had a statistically significant separation (coef = 1.1404, p-val < 0.0001), but saliva did not (coef = 0.1421, p-val = 0.8461).

Samples from subjects with cancer, arrived at ($cl = 2$ of $k = 5$) (p-val = 0.005) which was distinguishable by *Akkermansia*, *Oscillospiraceae UCG_002*, *Prevotella*, *Bacteroides*, *Escherichia_Shigella*, and others. Arrivers in cluster ($cl = 1$ of $k = 2$) were positively associated with social distancing (p-val = 0.009). See Supplemental Materials for additional descriptions and figures supporting this analysis. Clusters were considered from $k = 2$ to $k = 6$, after which individual clusters sizes became too small to associate factors with.

Early pandemic cross-sectional analysis for stool

The early pandemic cross-sectional (EPCS) for stool focused on identifying associations between questionnaire responses and changes in the microbiota, while controlling for age, sex, and days into the early pandemic.

Differences in diversity were associated with immune system disease and age. A decrease in diversity was found in association with immune system disease (Tail: p–val = 3.69×10^{-8}; Shannon: p–val = 1.83×10^{-6}). Age was associated with an increase of diversity (Tail: p–val = 0.000263; Shannon: p–val = 0.000301). At less significance, health was associated with increased diversity (Tail: p–val = 0.0246; Shannon: p–val = 0.0282). GAD7 Anxiety was associated with increased Shannon diversity (p–val = 0.0676). Pre-pandemic exercise was associated with increased diversity (Tail: p–val = 0.0886; Shannon: p–val = 0.0689).

Effects on Inter-sample distance were small, but associated with BMI, age, health, sex, and immune system disease. EPCS analysis of stool microbiota using PERMANOVA revealed a number of significant associations, although all the effect sizes were relatively small with the greatest R^2 at 0.0148 for days into the early pandemic (p-val = 3.704×10^{-5}), followed by BMI (p–val = 1.5925×10^{-3}), age (p–val = 3.704×10^{-4}), health (p–val = 5.185×10^{-04}), female (p–val = 3.704×10^{-5}), immune system disease (p–val = 3.704×10^{-5}), social distancing and working from home (p–val = 6.2738×10^{-2}).

Differences in taxonomic abundances were associated with sex, age, immune system disease, and BMI. The EPCS stool microbiota analysis using taxonomic abundance as a response identified many significant associations (p-values < 0.001). These included associations with sex (female): *Prevotellaceae uncl* (negative, p–val = 2.84×10^{-10}), *Prevotella* (negative, p–val = 2.31×10^{-4}), and *Bacteroides* (p–val = 7.91×10^{-4}); an association with Age: *Alistipes* (p–val = 8.09×10^{-6}); immune system disease: *Oscillospiraceae UCG_002* (negative, p–val = 9.17×10^{-6}), *Subdoligranulum* (negative, p–val = 1.57×10^{-5}), *Ruminococcus* (negative, p–val = 1.62×10^{-4}), *Lachnospiraceae_NK4A136_grp* (negative, p–val = 6.28×10^{-4}), and *Fusicatenibacter* (negative, p–val = 8.06×10^{-4}); days into the early pandemic: *Prevotella* (negative, p–val =

1.58×10^{-4}) and *Prevotellaceae_uncl* (negative, p–val = 4.88×10^{-4}) and with BMI: *Bacteroides* (p–val = 6.24×10^{-4}) and *Lachnoclostridium* (p–val = 6.46×10^{-4}).

Saliva specimens for 16S rRNA gene sequencing

The sample size available for saliva was 218 early pandemic cross-sectional subjects and 89 subjects for the pre/early pandemic paired analyses. The decrease of BMI of subjects with paired saliva samples was not statistically significant: median dBMI = 0, 95% PI = (-2.434, 3.002). The median and 95% Prediction Interval (PI) of the pre- and early pandemic days were 520 (55, 907) and 172.5 (117,220), respectively.

The pre/early pandemic paired analysis for saliva

The Pre/Early Pandemic Paired (PEPP) analysis for saliva samples identified fewer significant associations (p-value < 0.1) than the stool samples. Overall composition for the pre-pandemic and early pandemic saliva samples can be found in Supplemental Figure 1, "Paired Compositional Stacked Bar Plots".

Diversity was stable between time points. While multiple associations were identified between saliva microbiota and diversity, only the positive association with immune system disease when measured by the Tail statistic (p–val = 0.0116) was strong. Marginally significant associations (p-value < 0.10) were also found with the Tail statistic that could corroborate significant associations found in other analyses: education level (negative, p–val = 0.06866), depression (p–val = 0.071907), number of cohabitants (negative, p–val = 0.097342), and anxiety (negative, p–val = 0.098607). The intercept was not significantly non-zero for Tail ($\beta_0 = -3.875$, p-val = 0.1759) nor the Shannon diversity index ($\beta_0 = -0.9160$, p-val = 0.147).

Pre-to-early pandemic inter-sample distances were marginally associated with social distancing and COVID-19 worries. The paired distance analysis using saliva samples identified a positive association with social distancing (p-val = 0.0262) and to a lesser extent, a negative association with COVID-19 worries (p-val = 0.0754).

COVID-19 worries associated with Oribacterum and Campylobacter abundances. Increased taxonomic abundances of saliva microbiota were associated between COVID-19 worries and *Oribacterium* (p–val = 0.00299) and *Campylobacter* (p–val = 0.00853).

The cluster transition analysis did not yield any significant associations with p-val < 0.01.

Saliva cross-sectional analyses

Associations with diversity were marginal except for BMI. The EPCS saliva microbiota had marginal associations (p-values < 0.1) with diversity. Early pandemic BMI was associated with increased diversity (Tail: p–val = 0.015042; Shannon: p–val = 0.01897). High blood pressure was associated with decreased diversity (Shannon: p–val = 0.08730). Anxiety was associated with increased diversity (Tail: p-val = 0.02655; Shannon: p-val = 0.05952). Number of pets was associated with less diversity (Shannon: p-val = 0.05164).

Greater inter-sample distances between subjects were associated with health and smoking history. The PLCS saliva microbiota PERMANOVA analysis identified associations with days into early pandemic (p–val = 0.00030), health (p–val = 0.00030), smoking history (p–val = 0.00278), and less significantly with COVID-19 worries (p–val = 0.05685) and the number of pets (p–val = 0.04555).

Differences in taxonomic abundances were associated with health, high blood pressure, diabetes, COVID-19 worries and asthma. The PLCS saliva microbiota analysis using taxonomic abundances identified several associations that could support the underlying differences in diversity and distancing. Days into the early pandemic was found to be negatively associated with *Streptococcus* (p–val < 0.00001), but positively associated with *Bergeyella* (p–val = 0.00063), *Capnocytophaga* (p–val = 0.00165), and *Oribacterium* (p–val = 0.00912). Health was positively associated with *Neisseria* (p–val = 0.00007), *Alloprevotella* (p–val = 0.00613), and *Veillonellaceae_uncl* (p–val = 0.00719). High blood pressure was negatively associated with *Capnocytophaga* (p–val = 0.00039), *Fusobacterium* (p–val = 0.00374) and *Bergeyella* (p–val = 0.00986). Diabetes was associated with increased *Veillonella* (p–val = 0.00294). COVID-19 worries were negatively associated with *Lactobacillus* (p–val = 0.00501). Asthma was positively associated with *Yersinia* (p–val = 0.00557).

Comparison of changes in stool and saliva microbiota profiles between pre-pandemic and early pandemic samples revealed stool microbiota communities were more stable

An analysis of the cluster membership stability was performed separately for stool (n=288) and saliva (n=89) sample types. For each sample type, pre- and early pandemic samples were hierarchically clustered together. The resultant tree was then iteratively cut from $k = 2$ to 7 clusters and resultant memberships were evaluated. When both pre- and early pandemic samples were in the same cluster, for a specific k, then the subjects' early pandemic samples were considered to have "remained" in the same cluster as the pre-pandemic

sample. Figure 3, "Cluster Transition Scatter Plot" illustrates the cluster member relationships between pre- and early pandemic samples. The proportion of samples that remained in the sample cluster is plotted across the cuts (k) in Figure 4, "Samples Remaining in Pre-pandemic Cluster". At k = 2, 93.8% of early pandemic stool samples were clustered with their pre-pandemic sample, while only 74.2% of saliva samples shared their pre-pandemic cluster. At k = 7, 48.6% and 28.1% of stool and saliva samples, respectively, were had their pre-pandemic and early pandemic samples clustered together. Early pandemic stool samples were consistently closer to their pre-pandemic samples than saliva samples.

Please refer to Supplemental Table 2, "Associations with Stool and Saliva Samples" for a complete table of coefficients and p-values for all models reported in this Result section.

Discussion

Although effects of COVID-19 pandemic changes in human social behaviors and hygiene patterns on human microbiota and their potential interactions with the host have been postulated to include loss of diversity, they remain largely understudied. An important outcome of our study design was the ability to examine matched stool and oral sample pairs from the same individual taken from the pre-pandemic to early pandemic time points (PEPP model). Here we examined dynamic changes in alpha (within sample) diversity, and compositional changes using both measures of inter-sample distances (beta diversity) and relative taxonomic abundance. We related these diversity, distance, and abundance measures to participant questionnaire responses to determine associations with the microbiota that may have been potentiated by factors related to pandemic minimization strategies or implicit subject habits. We also examined ecological stability through pre-pandemic to early pandemic cluster transition (PEPCT) analysis. Finally, cross-sectional analyses of early pandemic (EPCS model) microbiota profiles from stool and saliva were examined to elucidate associations with health and lifestyle behavior providing a "snapshot" of these relationships at a time of heightened pandemic awareness and for the identification of study variables that may be proxies of other pre-pandemic behaviors or other lifestyle characteristics not directly measured in this study.

Early during the pandemic (2020), it was quickly established that individuals with certain comorbidities, such as hypertension or diabetes mellitus (Sanyaolu et al., 2020; Zhang et al., 2020), were at a greater risk for COVID-19 complications. As a result, individuals in our cohort (of which over half reported at least one underlying comorbidity) may have followed the recommended precautionary guidelines more strictly. Therefore, effects of the viral transmission strategies may have resulted in more substantial lifestyle changes in these individuals

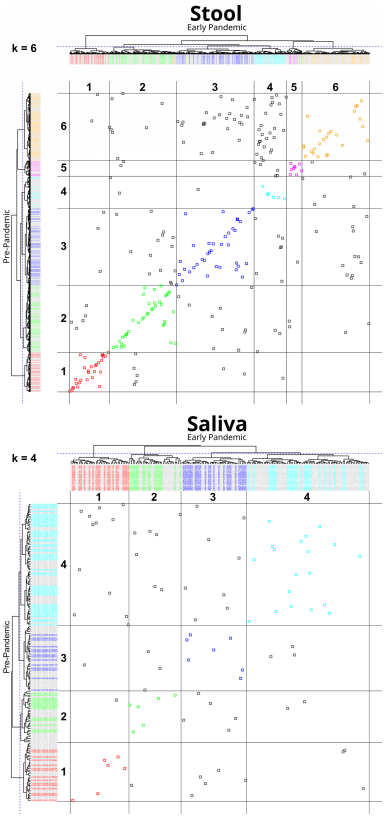

FIGURE 3
Cluster transition plot for Stool at k=6 and Saliva at k=4. Cluster transition plots provide a visualization of the degree to which an early pandemic sample's composition has changed relative to its pre-pandemic composition to warrant a change in its cluster membership. Hierarchical clustering and tree cutting (to form discrete clusters) is inherently an iterative process. In this figure, only one slice at k = 6, for stool, and k = 4, for saliva (labeled on the top left of each plot), were selected for illustrative purposes, although cuts k from 2 to 7 were also calculated. The dendrogram from hierarchically clustering of pre- and early pandemic samples are drawn on the top and left margins. The left margin dendrogram have pre-pandemic samples colored by their cluster identifier, while early pandemic samples are colored grey. Similarly, but complementarily, the top margin dendrogram has early pandemic samples colored by cluster identifier, but pre-pandemic samples are colored grey. In the field of the plot, each point represents the intersection of pre- and early pandemic samples. If both pre- and early pandemic samples are in the same cluster, then they are colored by their cluster identity, otherwise they are colored grey. Gridlines are drawn in the field to help identify cluster boundaries. When pre- to early pandemic samples have changed less in their composition, their points will be colored and lie across a diagonal from bottom-left to top-right. Examples of noteworthy observations from the stool transition plot includes the number of pre-pandemic cluster 6 (*Bacteroides* and *Escherichia Shigella*) members that have moved into cluster 4 (*Bacteroides*, *Faecalibacterium*) early pandemic, or that none of the pre-pandemic members of cluster 1 (*Prevotella*, *Prevotellaceae*, and *Lactobacillus*) have moved into cluster 6. Comparing the stool and saliva cluster transition plots provides a visualization of the stronger coherence of early pandemic samples to their pre-pandemic counterparts in stool.

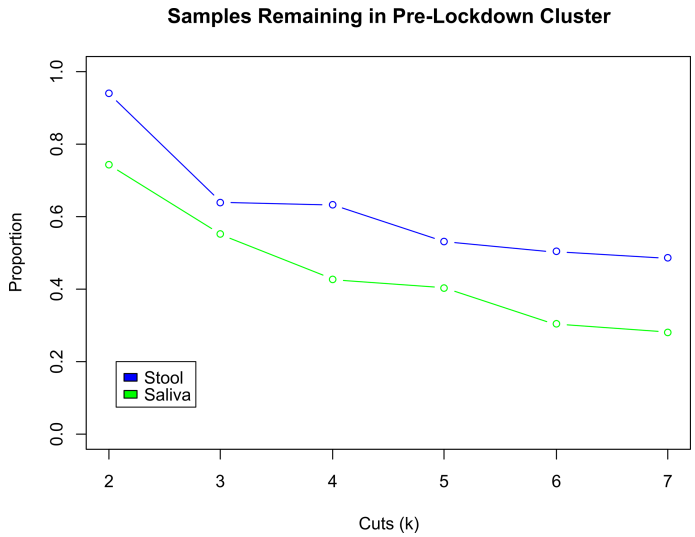

FIGURE 4
Comparison of Proportion of Subjects Changing Clusters between Stool and Saliva. These two curves illustrate the change in the proportion of early pandemic samples that remain in the same cluster as their pre-pandemic sample, for stool (blue) and saliva (green) samples. As the hierarchically clustered samples are cut from k = 2 to 7 clusters, the cluster sizes decrease and become more exclusive. Thus, any two samples that are in the same cluster when k = 7 are more similar to each other, than when k was smaller, e.g., 2. Across all cuts k, the early pandemic stool samples tend to be consistently closer to their pre-pandemic mates, than the saliva samples. At k = 2, the proportion of pre- and early pandemic stool samples that in the same cluster are 93.8%, compared to 74.2% in saliva. At k = 7, 48.6% of stool vs. 28.1% of saliva pre- and early pandemic samples are collocated in the same cluster.

relative to the general population. The analyses of questionnaire responses did not identify a significant correlation between social distancing and work-from-home strategies with COVID-19 worries, as the ability to social distance may have depended more on socio-economic conditions (Garnier et al., 2021) rather than personal choice. From questionnaire responses, social distancing was negatively correlated with age, but positively correlated with asthma and COVID-19 worries.

Although both saliva and stool taxonomic profiles from matched pairs trended towards decreased (alpha) diversity, overall, from the pre-pandemic to early pandemic time points (PEPP) model, the effect was not statistically significant. In part, this finding could be due to the relatively early pandemic sampling dates. Therefore, the associations identified in this study may be limited to those factors with acute effects. In the paired analyses, the median days into the early pandemic were 162 days for stool and 172.5 days for saliva. Nonetheless, this is an interesting finding given that our cohort is older and over half of participants reported at least one comorbidity, as loss of microbiota diversity is often reported to be associated with increasing age and chronic disease (Sun et al., 2021; Ceballos et al., 2021).

Applying the pre-pandemic to early pandemic time points (PEPP) model to stool microbiota, changes in diversity were associated with changes in BMI, smoking history, and pet ownership. From our questionnaire, smoking history was reported, however changes in smoking habits from the pre-pandemic to early pandemic time periods could not be determined. Therefore, it is not clear why smoking history would decrease diversity during the early pandemic unless smoking frequency increased for this group, or if it was a proxy for another behavior. In a separate study, it was reported that during the "lockdown" phase, alcohol consumption increased, but more subjects tried to quit smoking (Jackson et al., 2021). Overall, if we assume that decreased social contact and increased hygiene measures (e.g., hand washing) can decrease diversity, then our study suggests that other factors (e.g., household pets) and those implied but not directly measured (e.g., diet) may offset these potential losses in diversity. It has also been recognized that humans can share microorganisms through social interactions, cohabitation, and exchanges with both the natural and built environments (Tong et al., 2021; Peimbert and Alcaraz, 2022). Previous reports have also identified microbiota associations with pet ownership were also found in conjunction with stool studies (Kates et al., 2020) and our study suggests that pets may be an important reservoir of microbes in humans, a relationship that may be heightened in periods of decreased social contact.

In addition to examining diversity, the pre-pandemic to early pandemic time points (PEPP) model for stool microbiota profiles also examined changes to composition as measured by paired sample distances (beta diversity) or by specific ALR-transformed taxonomic abundances. The analysis of stool microbiota paired distances found associations with pre-pandemic BMI, health, diabetes, immune system pathology, and number of cohabitants.

Multiple changes in specific taxonomic abundances were associated with immune system disease, asthma, pre-pandemic BMI and changes in BMI, diabetes, depression, and education level. These results are consistent with previous findings such as a 2018 study by Rothschild and colleagues (Rothschild et al., 2018) which determined that genetic ancestry or individual polymorphic variants in families were minor contributors to gut microbiome composition (<2%), in contrast to more than 20% of the variance in microbiome diversity attributed to shared environmental, diet and lifestyle factors.

The microorganisms identified by paired sample distances or by specific ALR-transformed taxonomic abundances using the pre-pandemic to early pandemic time points (PEPP) model for stool microbiota profiles were polymicrobial in nature, however the associations almost exclusively consist of genera assigned to the dominant phyla found in the human gut, Bacteroidetes and Firmicutes. This finding suggests that this diverse set of organisms is likely to be involved in multiple human gut metabolic processes. These are likely to include the production of short chain fatty acids (Silva et al., 2020) and secondary bile acids which have been implicated in neuro-immunoendocrine regulation affecting both physical and mental health status (Romaní-Pérez et al., 2021) as well as other metabolic processes that warrant future investigation.

The pre-pandemic to early pandemic time points (PEPP) model used to examine saliva microbiota profiles, identified contrasting associations. Social distancing led to increased changes in composition, while COVID-19 worries were associated with a decrease in compositional distance, between samples from the same individual. The apparent opposition of these associations exemplifies the complexity of these host behaviors in host-microbiota interactions. While many studies have focused on the role of the microbiome in the gut-brain axis, findings in the current study suggest that saliva microbiota may in part be important contributors to, or markers of anxiety, stress, and general mental health. For example, it has been demonstrated that chronic psychological distress can depress diurnal secretion levels of salivary glucocorticoid and catecholamines (Miller et al., 2007) as well as alpha-amylase (Nater et al., 2007). Glucocorticoids, as corticosteroids, are involved in carbohydrate, protein, and fat metabolism and exhibit anti-inflammatory activity. As neurotransmitters, catecholamines, have been shown to moderate gut microorganisms (Huang et al., 2015) and may perform similar roles within the oral cavity.

Overall, paired analyses generally found fewer significant associations with saliva relative to stool microbiota. This result may in part be attributable to the smaller sample size available for the saliva analysis. However, biologically this finding may indicate that the collective effects of the variables measured within the timeframe of this study were less influential or acted more in opposition to one another in saliva microbiota relative to their stool counterparts. In addition, microbiota recovered from saliva represent an amalgam of habitats in the oral cavity, and the oral cavity has direct contact with the external environment, all factors that can result in greater sample variability.

The pre-pandemic to early pandemic cluster transition (PEPCT) analysis identified that overall, from the same subject, the microbiota profiles from both stool and saliva, from an ecological standpoint (Relman, 2012), were largely stable from pre-pandemic to early pandemic time periods with stool more stable relative to saliva. In the stool samples, departers (samples from individuals that left their pre-pandemic cluster assignment) were associated with sex (female) and COVID-19 worries. Most arrivers (samples from individuals that changed to new early pandemic cluster assignments) were associated with asthma and cancer and social distancing. These associations further support the finding that perturbations to the stool microbiota from the pre-pandemic to early pandemic period were associated with individuals reporting more issues with physical health. The association with COVID-19 worries however, may be an indicator of possible changes with mental health status or alternatively, it may be a proxy for other behaviors not measured directly in this study.

Further the pre-pandemic to early pandemic cluster transition (PEPCT) analysis provided an opportunity to identify "local shifts" or changes in microbiota composition from a subset of the cohort in relation to study variables. For instance, increased cancer diagnoses were associated with individuals that departed multiple pre-pandemic clusters but arrived in one early pandemic cluster for which cluster influencing bacteria include *Akkermansia* and *Escherichia-Shigella*. Consistent with these findings, *Escherichia* has been associated with promotion of colorectal and other cancers (Dalmasso et al., 2014), while *Akkermansia* has been linked to the potentiation of anti-CTLA-4 and anti-PD-1 immunotherapy (Miller and Carson, 2020). More recently, both microorganisms (Jayachandran et al., 2020) were found to be increased in abundance in individuals with stable non-small cell lung cancer while undergoing immunotherapy (He et al., 2021).

In a contrasting example, the pre-pandemic to early pandemic cluster transition (PEPCT) analysis was able to provide insights into specific taxa related to changes in COVID-19 worries Here the cluster influencers changed from a diverse pre-pandemic set of bacteria including *Akkermansia*, *Oscillospiraceae UCG_002*, *Bacteroides*, *Alistipes* and *Prevotella*, to a reduced set of cluster influencers consisting of *Bacteroides*, *Faecalibacterium* and *Agathobacter*. *Bacteroides* are well-known for their metabolic complexity and roles in many important metabolic activities in the human colon including a prodigious capacity to catabolize complex host and diet derived carbohydrates, as well as production of propionate, use of proteins and other nitrogenous compounds, and transformation of bile acids and other steroids (Zafar and Saier, 2021). As such, *Bacteroides* often support many interspecies cross-feeding interactions including other short chain fatty acid producers such as *Faecalibacterium* and *Agathobacter* (Rodriguez-Castaño et al., 2019). *Faecalibacterium* (Li et al., 2008) is an important producer of butyrate while *Agathobacter* fermentation

products include butyrate, acetate, hydrogen, and lactate (Rosero et al., 2016). The functional significance of these microbiota compositional patterns in relation to increased COVID-19 related worries cannot ultimately be determined in this study and they could also reflect other behaviors such as pandemic-related dietary changes. However, this shift in microbiota may in part result in changes in the composition and concentration of the gut short chain fatty acid pool and other microbially-mediated metabolites consistent with results from the paired differences analyses (PEPP models). Among other biological functions, short chain fatty acids have been identified as a critical mechanism of gut-brain communication and may be relevant to the increased psychological distress reflected in greater worries about the COVID-19 pandemic (Ortega et al., 2022).

When applying the cross-sectional analyses of early pandemic (EPCS) model to microbiota profiles, contrasting associations were determined both between sample types (stool and oral) and with the previously discussed pre-pandemic to early pandemic time points (PEPP) model from both stool and oral samples. Relationships with stool microbiota largely corroborated previously identified microbiota associations with age (Yatsunenko et al., 2012; de la Cuesta-Zuluaga et al., 2019), anxiety (Foster and McVey Neufeld, 2013), health, exercise (Clauss et al., 2021), and immune system disease in studies undertaken prior to the COVID-19 pandemic. According to inter-sample distance measures, lifestyle changes, as represented by both social distancing and working from home, had a significant effect on the microbiota composition as a whole. Interestingly, these effects were not detected in the paired analyses of pre-pandemic to early pandemic time points. This finding may suggest that these associations instead serve as proxies for other pre-pandemic behavioral or other lifestyle characteristics that could be identified by their subsequent acceptance of advised changes in social distancing or work-from-home patterns during the early pandemic. Regardless of analytical method, changes in stool microbiota diversity and composition from the cross-sectional examinations were consistently related to age and more immune system disturbances. In contrast, cross-sectional analyses of early pandemic microbiota profiles from saliva (EPCS) model, identified fewer significant associations with diversity and a different set of variables related to compositional changes offering novel insights into to the effects of lifestyle and behavioral perturbations on the microbiota with influences from smoking history, COVID-19 related worries and the number of pets per household.

Strengths of our study include the relatively large number of subjects with matching pre- and early pandemic samples for both stool and saliva. The existence of an ongoing microbiome biospecimen collection and surveillance system, allowed us to rapidly integrate a COVID-19 study specific design, both quickly and practically, through sample self-collection and remotely conducted questionnaires. Analogous to long-term ecological monitoring of the environment (Vergin et al., 2013; Karl and Church, 2014), our findings argue for the importance of long-term surveillance of the human microbiome to improve the ability to monitor future potential population-wide perturbations. Further, the collection of subject covariates (e.g., BMI, age, sex, smoking, etc.) that were included into our models and are crucial to control for in microbiome studies, improved the confidence of the associations made with the questionnaire responses. While self-reported responses to questionnaires can have limitations compared to objective biomarkers (Boparai et al., 2018), we confirmed that measures of health status were consistent with clinical records.

We recognize that the study has several limitations. While the use of 16S rRNA gene sequencing, as a means to estimate the taxonomic composition of each sample can be conducted relatively quickly and with use of fewer resources, it does not measure biological function directly and therefore is limited in its ability to identify functional interactions with the host. Additional assays to elucidate potential, latent, and active metabolic process, through additional multi-omics approaches such as metagenomics, metatranscriptomics, metabolomics and personal genomic information, would provide a means to test more narrowly proposed hypotheses governing the underlying the associations determined in this study. In addition, given the rapidly changing nature of the pandemic, there may have been subsequent changes in the microbiome that we did not capture. In future works of this nature, the questionnaire could be refined by including multiple alternatively worded redundant questions that can be later combined for robustness, and by excluding some questions that may have ambiguous or unnecessary distinctions towards hypothetical physiological outcomes. We also lacked data on diet and other factors that might have influenced the microbiome.

In conclusion, our study examined changes in stool and saliva microbiota diversity and composition that may be attributable to social and lifestyle behavior mitigations from pre-COVID-19 to early pandemic time points in individuals who were not infected with SARS-CoV-2. While there was a trend towards a decrease in stool and saliva microbiota diversity, this change was not significant between pre-pandemic and early pandemic periods. Collectively, our analyses support the notion of relative ecological stability in stool and saliva microbiota taxonomic profiles (with higher stability found in stool) from the pre-pandemic to early pandemic periods. Greater changes in microbiota diversity and taxonomic profiles were associated with more questionnaire reported health issues including immune system disturbances, asthma, and cancer, or with greater worries related to the COVID-19 pandemic. Therefore, managing underlying comorbidities and psychological distress such as worries about the pandemic may be important for maintaining beneficial host-microbiome

interactions. Our study highlights the importance of longitudinal sampling of large observational cohorts as a valuable tool to examine the status of the microbiome over time in response to pandemics and changes in public health measures.

Data availability statement

The original contributions presented in the study are publicly available in NCBI using accession number PRJNA847970.

Ethics statement

The studies involving human participants were reviewed and approved by University of Pittsburgh Institutional Review Board under protocol number CR19030104-017. The patients/participants provided their written informed consent to participate in this study.

Author contributions

KL analyzed data and drafted the manuscript. CK and VP completed questionnaires. HG conducted specimen processing. AP and AF performed laboratory processing to generate data. AF and PS conducted data QC and management. AM conceived the study, provided specimen management, clinical review and edited the manuscript. BM generated and analyzed data and drafted and edited the manuscript. All authors contributed to the article and approved the submitted version.

Funding

This work was funded by the UPMC Immune Transplant and Therapy Center (ITTC).

Conflict of interest

The authors declare that the research was conducted in the absence of any commercial or financial relationships that could be construed as a potential conflict of interest.

Publisher's note

All claims expressed in this article are solely those of the authors and do not necessarily represent those of their affiliated organizations, or those of the publisher, the editors and the reviewers. Any product that may be evaluated in this article, or claim that may be made by its manufacturer, is not guaranteed or endorsed by the publisher.

Supplementary material

The Supplementary Material for this article can be found online at: https://www.frontiersin.org/articles/10.3389/fcimb.2022.966361/full#supplementary-material

References

Aitchison, J. (1982). The statistical analysis of compositional data. *J. R. Stat. Society: Ser. B (Methodological)* 44 (2), 139–160. doi: 10.1111/j.2517-6161.1982.tb01195.x

Arora, T., and Grey, I. (2020). Health behaviour changes during COVID-19 and the potential consequences: A mini-review. *J. Health Psychol.* 25 (9), 1155–1163. doi: 10.1177/1359105320937053

Atzrodt, C. L., Maknojia, I., McCarthy, R. D. P., Oldfield, T. M., Po, J., Ta, K. T. L., et al. (2020). A guide to COVID-19: A global pandemic caused by the novel coronavirus SARS-CoV-2. *FEBS J.* 287 (17), 3633–3650. doi: 10.1111/febs.15375

Bavel, J. J. V., Baicker, K., Boggio, P. S., Capraro, V., Cichocka, A., Cikara, M., et al. (2020). Using social and behavioural science to support COVID-19 pandemic response. *Nat. Hum. Behav.* 4 (5), 460–471. doi: 10.1038/s41562-020-0884-z

Blix, I., Birkeland, M. S., and Thoresen, S. (2021). Worry and mental health in the covid-19 pandemic: vulnerability factors in the general Norwegian population. *BMC Public Health* 21 (1), 928. doi: 10.1186/s12889-021-10927-1

Boparai, J. K., Singh, S., and Kathuria, P. (2018). How to design and validate a questionnaire: A guide. *Curr. Clin. Pharmacol.* 13 (4), 210–215. doi: 10.2174/1574884713666180807151328

Burchill, E., Lymberopoulos, E., Menozzi, E., Budhdeo, S., McIlroy, J. R., Macnaughtan, J., et al. (2021). The unique impact of COVID-19 on human gut microbiome research. *Front. Med. (Lausanne)* 8, 652464. doi: 10.3389/fmed.2021.652464

Caporaso, J. G., Lauber, C. L., Walters, W. A., Berg-Lyons, D., Huntley, J., Fierer, N., et al. (2012). Ultra-high-throughput microbial community analysis on the illumina HiSeq and MiSeq platforms. *ISME J.* 6 (8), 1621–1624. doi: 10.1038/ismej.2012.8

Ceballos, D., Hernández-Camba, A., and Ramos, L. (2021). Diet and microbiome in the beginning of the sequence of gut inflammation. *World J. Clin. cases* 9 (36), 11122–11147. doi: 10.12998/wjcc.v9.i36.11122

Clauss, M., Gérard, P., Mosca, A., and Leclerc, M. (2021). Interplay between exercise and gut microbiome in the context of human health and performance. *Front. Nutr.* 8, 637010. doi: 10.3389/fnut.2021.637010

Dalmasso, G., Cougnoux, A., Delmas, J., Darfeuille-Michaud, A., and Bonnet, R. (2014). The bacterial genotoxin colibactin promotes colon tumor growth by modifying the tumor microenvironment. *Gut Microbes* 5 (5), 675–680. doi: 10.4161/19490976.2014.969989

Daly, M., Sutin, A. R., and Robinson, E. (2020). Longitudinal changes in mental health and the COVID-19 pandemic: Evidence from the UK household longitudinal study. *Psychol. Med.* 1–10. doi: 10.1017/S0033291720004432

de la Cuesta-Zuluaga, J., Kelley, S. T., Chen, Y., Escobar, J. S., Mueller, N. T., Ley, R. E., et al. (2019). Age- and sex-dependent patterns of gut microbial diversity in human adults. *mSystems* 4 (4). doi: 10.1128/mSystems.00261-19

Domingues, C. P. F., Rebelo, J. S., Dionisio, F., Botelho, A., and Nogueira, T. (2020). The social distancing imposed to contain COVID-19 can affect our microbiome: a double-edged sword in human health. *mSphere* 5 (5). doi: 10.1128/mSphere.00716-20

Finlay, B. B., Amato, K. R., Azad, M., Blaser, M. J., Bosch, T. C. G., Chu, H., et al. (2021). The hygiene hypothesis, the COVID pandemic, and consequences for the human microbiome. *Proc. Natl. Acad. Sci. U.S.A.* 118 (6). doi: 10.1073/pnas.2010217118

Foster, J. A., and McVey Neufeld, K. A. (2013). Gut-brain axis: How the microbiome influences anxiety and depression. *Trends Neurosci.* 36 (5), 305–312. doi: 10.1016/j.tins.2013.01.005

Garnier, R., Benetka, J. R., Kraemer, J., and Bansal, S. (2021). Socioeconomic disparities in social distancing during the COVID-19 pandemic in the united states: Observational study. *J. Med. Internet Res.* 23 (1), e24591. doi: 10.2196/24591

Gevers, D., Knight, R., Petrosino, J. F., Huang, K., McGuire, A. L., Birren, B. W., et al. (2012). The human microbiome project: A community resource for the healthy human microbiome. *PLoS Biol.* 10 (8), e1001377. doi: 10.1371/journal.pbio.1001377

Gloor, G. B., Macklaim, J. M., Pawlowsky-Glahn, V., and Egozcue, J. J. (2224). Microbiome datasets are compositional: And this is not optional. *Front. Microbiol.* 2017, 8. doi: 10.3389/fmicb.2017.02224

Haliwa, I., Wilson, J., Lee, J., and Shook, N. J. (2021). Predictors of change in mental health during the COVID-19 pandemic. *J. Affect. Disord.* 291, 331–337. doi: 10.1016/j.jad.2021.05.045

He, D., Li, X., An, R., Wang, L., Wang, Y., Zheng, S., et al. (2021). Response to PD-1-Based immunotherapy for non-small cell lung cancer altered by gut microbiota. *Oncol. Ther.* 9 (2), 647–657. doi: 10.1007/s40487-021-00171-3

Huang, E. Y., Inoue, T., Leone, V. A., Dalal, S., Touw, K., Wang, Y., et al. (2015). Using corticosteroids to reshape the gut microbiome: Implications for inflammatory bowel diseases. *Inflammation Bowel Dis.* 21 (5), 963–972. doi: 10.1097/MIB.0000000000000332

Jackson, S. E., Garnett, C., Shahab, L., Oldham, M., and Brown, J. (2021). Association of the COVID-19 lockdown with smoking, drinking and attempts to quit in England: an analysis of 2019-20 data. *Addiction* 116 (5), 1233–1244. doi: 10.1111/add.15295

Jayachandran, M., Chung, S. S. M., and Xu, B. (2020). A critical review of the relationship between dietary components, the gut microbe. *Crit. Rev. Food Sci. Nutr.* 60 (13), 2265–2276. doi: 10.1080/10408398.2019.1632789

Johnson, S. U., Ulvenes, P. G., Øktedalen, T., and Hoffart, A. (2019). Psychometric properties of the general anxiety disorder 7-item (GAD-7) scale in a heterogeneous psychiatric sample. *Front. Psychol.* 10, 1713. doi: 10.3389/fpsyg.2019.01713

Karl, D. M., and Church, M. J. (2014). Microbial oceanography and the Hawaii ocean time-series programme. *Nat. Rev. Microbiol.* 12 (10), 699–713. doi: 10.1038/nrmicro3333

Kates, A. E., Jarrett, O., Skarlupka, J. H., Sethi, A., Duster, M., Watson, L., et al. (2020). Household pet ownership and the microbial diversity of the human gut microbiota. *Front. Cell Infect. Microbiol.* 10, 73. doi: 10.3389/fcimb.2020.00073

Kroenke, K., Spitzer, R. L., and Williams, J. B. (2001). The PHQ-9: validity of a brief depression severity measure. *J. Gen. Intern. Med.* 16 (9), 606–613. doi: 10.1046/j.1525-1497.2001.016009606.x

Li, K., Bihan, M., Yooseph, S., and Methe, B. A. (2012). Analyses of the microbial diversity across the human microbiome. *PLoS One* 7 (6), e32118. doi: 10.1371/journal.pone.0032118

Li, M., Wang, B., Zhang, M., Rantalainen, M., Wang, S., Zhou, H., et al. (2008). Symbiotic gut microbes modulate human metabolic phenotypes. *Proc. Natl. Acad. Sci. U S A.* 105 (6), 2117–2122. doi: 10.1073/pnas.0712038105

Miller, P. L., and Carson, T. L. (2020). Mechanisms and microbial influences on CTLA-4 and PD-1-based immunotherapy in the treatment of cancer: a narrative review. *Gut Pathog.* 12, 43. doi: 10.1186/s13099-020-00381-6

Miller, G. E., Chen, E., and Zhou, E. S. (2007). If it goes up, must it come down? chronic stress and the hypothalamic-pituitary-adrenocortical axis in humans. *Psychol. Bull.* 133 (1), 25–45. doi: 10.1037/0033-2909.133.1.25

Morin, C. M., Belleville, G., Bélanger, L., and Ivers, H. (2011). The insomnia severity index: psychometric indicators to detect insomnia cases and evaluate treatment response. *Sleep* 34 (5), 601–608. doi: 10.1093/sleep/34.5.601

Nater, U. M., Moor, C., Okere, U., Stallkamp, R., Martin, M., Ehlert, U., et al. (2007). Performance on a declarative memory task is better in high than low cortisol responders to psychosocial stress. *Psychoneuroendocrinology* 32 (6), 758–763. doi: 10.1016/j.psyneuen.2007.05.006

Ortega, M. A., Alvarez-Mon, M. A., García-Montero, C., Fraile-Martinez, O., Guijarro, L. G., Lahera, G., et al. (2022). Gut microbiota metabolites in major depressive disorder-deep insights into their pathophysiological role and potential translational applications. *Metabolites* 12 (1). doi: 10.3390/metabo12010050

Peimbert, M., and Alcaraz, L. D. (2022). Where environmental microbiome meets its host: Subway and passenger microbiome relationships. *Mol. Ecol.* doi: 10.1111/mec.16440

Pierce, M., Hope, H., Ford, T., Hatch, S., Hotopf, M., John, A., et al. (2020). Mental health before and during the COVID-19 pandemic: A longitudinal probability sample survey of the UK population. *Lancet Psychiatry* 7 (10), 883–892. doi: 10.1016/S2215-0366(20)30308-4

Quast, C., Pruesse, E., Yilmaz, P., Gerken, J., Schweer, T., Yarza, P., et al. (2013). The SILVA ribosomal RNA gene database project: Improved data processing and web-based tools. *Nucleic Acids Res.* 41, D590–D596. doi: 10.1093/nar/gks1219

Relman, D. A. (2012). The human microbiome: Ecosystem resilience and health. *Nutr. Rev.* 70 Suppl 1, S2–S9. doi: 10.1111/j.1753-4887.2012.00489.x

Rodriguez-Castaño, G. P., Dorris, M. R., Liu, X., Bolling, B. W., Acosta-Gonzalez, A., and Rey, F. E. (2019). Starch utilization promotes quercetin degradation and butyrate production by. *Front. Microbiol.* 10, 1145. doi: 10.3389/fmicb.2019.01145

Romaní-Pérez, M., Bullich-Vilarrubias, C., López-Almela, I., Liébana-García, R., Olivares, M., and Sanz, Y. (2021). The microbiota and the gut-brain axis in controlling food intake and energy homeostasis. *Int. J. Mol. Sci.* 22 (11). doi: 10.3390/ijms22115830

Rosero, J. A., Killer, J., Sechovcova, H., Mrázek, J., Benada, O., Fliegerová, K., et al. (2016). Reclassification of eubacterium rectale (Hauduroy et al. 1937) prévot 1938 in a new genus agathobacter gen. nov. as agathobacter rectalis comb. nov., and description of agathobacter ruminis sp. nov., isolated from the rumen contents of sheep and cows. *Int. J. Systematic Evolutionary Microbiol.* 66 (2), 768–773. doi: 10.1099/ijsem.0.000788

Rothschild, D., Weissbrod, O., Barkan, E., Kurilshikov, A., Korem, T., Zeevi, D., et al. (2018). Environment dominates over host genetics in shaping human gut microbiota. *Nature* 555 (7695), 210–215. doi: 10.1038/nature25973

Sanyaolu, A., Okorie, C., Marinkovic, A., Patidar, R., Younis, K., Desai, P., et al. (2020). Comorbidity and its impact on patients with COVID-19. *SN Compr. Clin. Med.* 2 (8), 1069–1076. doi: 10.1007/s42399-020-00363-4

Schloss, P. D., Westcott, S. L., Ryabin, T., Hall, J. R., Hartmann, M., Hollister, E. B., et al. (2009). Introducing mothur: open-source, platform-independent, community-supported software for describing and comparing microbial communities. *Appl. Environ. Microbiol.* 75 (23), 7537–7541. doi: 10.1128/AEM.01541-09

Sender, R., Fuchs, S., and Milo, R. (2016). Revised estimates for the number of human and bacteria cells in the body. *PLoS Biol.* 14 (8), e1002533. doi: 10.1371/journal.pbio.1002533

Silva, Y. P., Bernardi, A., and Frozza, R. L. (2020). The role of short-chain fatty acids from gut microbiota in gut-brain communication. *Front. Endocrinol. (Lausanne)* 11, 25. doi: 10.3389/fendo.2020.00025

Stapleton, A. L., Shaffer, A. D., Morris, A., Li, K., Fitch, A., and Methé, B. A. (2021). The microbiome of pediatric patients with chronic rhinosinusitis. *Int. Forum Allergy Rhinol.* 11 (1), 31–39. doi: 10.1002/alr.22597

Sun, W., Du, D., Fu, T., Han, Y., Li, P., and Ju, H. (2021). Alterations of the gut microbiota in patients with severe chronic heart failure. *Front. Microbiol.* 12, 813289. doi: 10.3389/fmicb.2021.813289

Tarabichi, Y., Li, K., Hu, S., Nguyen, C., Wang, X., Elashoff, D., et al. (2015). The administration of intranasal live attenuated influenza vaccine induces changes in the nasal microbiota and nasal epithelium gene expression profiles. *Microbiome* 3 (1), 1–16. doi: 10.1186/s40168-015-0133-2

Tong, X., Leung, M. H. Y., Shen, Z., Lee, J. Y. Y., Mason, C. E., and Lee, P. K. H. (2021). Metagenomic insights into the microbial communities of inert and oligotrophic outdoor pier surfaces of a coastal city. *Microbiome* 9 (1), 213. doi: 10.1186/s40168-021-01166-y

Vergin, K. L., Beszteri, B., Monier, A., Thrash, J. C., Temperton, B., Treusch, A. H., et al. (2013). High-resolution SAR11 ecotype dynamics at the Bermuda Atlantic time-series study site by phylogenetic placement of pyrosequences. *ISME J.* 7 (7), 3122–1332. doi: 10.1038/ismej.2013.32

Wang, Q., Garrity, G. M., Tiedje, J. M., and Cole, J. R. (2007). Naive Bayesian classifier for rapid assignment of rRNA sequences into the new bacterial taxonomy. *Appl. Environ. Microbiol.* 73 (16), 5261–5267. doi: 10.1128/AEM.00062-07

Yatsunenko, T., Rey, F. E., Manary, M. J., Trehan, I., Dominguez-Bello, M. G., Contreras, M., et al. (2012). Human gut microbiome viewed across age and geography. *Nature.* 486 (7402), 222–227. doi: 10.1038/nature11053

Zafar, H., and Saier, M. H. (2021). Gut. *Gut Microbes* 13 (1), 1–20. doi: 10.1080/19490976.2020.1848158

Zhang, J., Wang, X., Jia, X., Li, J., Hu, K., Chen, G., et al. (2020). Risk factors for disease severity, unimprovement, and mortality in COVID-19 patients in wuhan, China. *Clin. Microbiol. Infect.* 26 (6), 767–772. doi: 10.1016/j.cmi.2020.04.012

frontiers | Frontiers in Cellular and Infection Microbiology

TYPE Original Research
PUBLISHED 13 September 2022
DOI 10.3389/fcimb.2022.943317

OPEN ACCESS

EDITED BY
Eva Maria Weissinger,
Hannover Medical School, Germany

REVIEWED BY
Philipp Rausch,
University of Kiel, Germany
Kentaro Fukushima,
Osaka University, Japan

*CORRESPONDENCE
Pihua Gong
gardenia1978@163.com
Zhancheng Gao
zcgao@bjmu.edu.cn

SPECIALTY SECTION
This article was submitted to Microbiome in Health and Disease, a section of the journal Frontiers in Cellular and Infection Microbiology

RECEIVED 13 May 2022
ACCEPTED 23 August 2022
PUBLISHED 13 September 2022

CITATION
He Y, Li J, Yu W, Zheng Y, Yang D, Xu Y, Zhao L, Ma X, Gong P and Gao Z (2022) Characteristics of lower respiratory tract microbiota in the patients with post-hematopoietic stem cell transplantation pneumonia. *Front. Cell. Infect. Microbiol.* 12:943317. doi: 10.3389/fcimb.2022.943317

Characteristics of lower respiratory tract microbiota in the patients with post-hematopoietic stem cell transplantation pneumonia

Yukun He[1], Jia Li[1], Wenyi Yu[1], Yali Zheng[1,2], Donghong Yang[1], Yu Xu[1], Lili Zhao[1], Xinqian Ma[1], Pihua Gong[1*] and Zhancheng Gao[1*]

[1]Department of Respiratory and Critical Care Medicine, Peking University People's Hospital, Beijing, China, [2]Department of Respiratory, Critical Care, and Sleep Medicine, Xiang'an Hospital of Xiamen University, School of Medicine, Xiamen University, Xiamen, China

Background: Pneumonia is a leading cause of non-relapse mortality after hematopoietic stem cell transplantation (HSCT), and the lower respiratory tract (LRT) microbiome has been proven to be associated with various respiratory diseases. However, little is known about the characteristics of the LRT microbiome in patients with post-HSCT compared to healthy controls (HC) and community-acquired pneumonia (CAP).

Methods: Bronchoalveolar lavage samples from 55 patients with post-HSCT pneumonia, 44 patients with CAP, and 30 healthy volunteers were used to detect microbiota using 16S rRNA gene sequencing.

Results: The diversity of the LRT microbiome significantly decreased in patients with post-HSCT pneumonia, and the overall community was different from the CAP and HC groups. At the phylum level, post-HSCT pneumonia samples had a high abundance of Actinobacteria and a relatively low abundance of Bacteroidetes. The same is true for non-survivors compared with survivors in patients with post-HSCT pneumonia. At the genus level, the abundances of *Pseudomonas*, *Acinetobacter*, *Burkholderia*, and *Mycobacterium* were prominent in the pneumonia group after HSCT. On the other hand, gut-associated bacteria, *Enterococcus* were more abundant in the non-survivors. Some pathways concerning amino acid and lipid metabolism were predicted to be altered in patients with post-HSCT pneumonia.

Conclusions: Our results reveal that the LRT microbiome in patients with post-HSCT pneumonia differs from CAP patients and healthy controls, which could

be associated with the outcome. The LRT microbiota could be a target for intervention during post-HSCT pneumonia.

KEYWORDS

hematopoietic stem cell transplantation, pneumonia, bronchoalveolar lavage, lower respiratory tract, microbiome

Introduction

Hematopoietic stem cell transplantation (HSCT) is a potentially curative method of treating hematologic and lymphoid malignancies (Harris et al., 2016). Overall survival following HSCT has significantly improved due to advances in transplant management (Gooley et al., 2010). The success of allogeneic HSCT, however, is hindered by certain complications (Bergeron and Cheng, 2017). Of all the organ-specific complications that can occur after HSCT, pneumonia is more complicated and difficult to treat and has been reported in 30-60% of HSCT recipients (Kader et al., 1994; Kotloff et al., 2004; Peters and Afessa, 2005; Lucena et al., 2014). Pneumonia, including community-acquired pneumonia (CAP) and hospital-acquired pneumonia (HAP), can occur early or late after the procedure, including during the pre-engraftment (neutropenic) phase and the early and late post-engraftment phases (Chi et al., 2013; Ahya, 2017; Bondeelle and Bergeron, 2019). Despite advances in posttransplant prevention support care, pneumonia remains a leading cause of non-relapse mortality after HSCT (Nusair et al., 2004; Choi et al., 2014; Harris et al., 2016; Zhou et al., 2019). A growing body of evidence suggests that gut microbiota is associated with pulmonary complications (PCs) after HSCT and transplant-related mortality (Taur et al., 2014; Harris et al., 2016; Golob et al., 2017), yet little is known about how lung microbiota is associated with disease status (Huang et al., 2013).

Advances in molecular methods and the advent of next-generation sequencing technologies have revealed that the lungs harbor complex and diverse bacterial communities (Charlson et al., 2011; Dickson et al., 2017; Huffnagle et al., 2017; Pattaroni et al., 2018). The potential role of the lung microbiome in respiratory pathology is increasingly being recognized (Dickson et al., 2016a; Invernizzi et al., 2020). Several studies have focused on defining lung microbiome composition in both healthy (Dickson et al., 2017) and diseased subsets (Dickson et al., 2014; Jorth et al., 2019; Singanayagam et al., 2019). The composition of the healthy lung microbiome may be depended on the neutral distribution of microbes from the oral cavity. Whereas microbiomes in diseased lungs may be associated strongly with increased selection of specific microbes, potentially reflecting possible microbiome alterations happening in its source environment at the same time (Hubbell, 2010; Venkataraman et al., 2015).

The balance of the lower respiratory tract (LRT) microbiome community in HSCT recipients is affected by multiple factors, including the impairment of host defenses through myeloablative conditioning, derangements in pulmonary immune responses, and multiple treatments, such as corticosteroid usage, and antibiotic usage (Gooley et al., 2010; Harris et al., 2016; Zinter and Hume, 2021), which collectively shape the respiratory microbiome. While the importance of the lung microbiome has already been proposed in the context of HSCT recipients with post-HSCT PCs (O'Dwyer et al., 2018), the characteristics of lung microbiota in HSCT recipients with pneumonia were less reported due to the complex conditions after HSCT. Moreover, the differences in lung microbiota related to the outcomes were undetermined. Therefore, we hypothesize that patients with post-HSCT pneumonia possessed lung microbiota that differs from that of healthy control subjects and CAP patients with normal immune function and lung microbiota could be differed in different clinical outcomes of patients with post-HSCT pneumonia.

To clarify the composition and putative function of the lung microbiota of patients with post-HSCT pneumonia, we applied 16S ribosomal ribonucleic acid (rRNA) gene sequencing to bronchoalveolar lavage fluid (BALF) samples from 55 patients with post-HSCT PCs, 44 patients with CAP, and 30 healthy control subjects (HCs).

Materials and methods

Study population

This study received ethics approval from the Ethical Review Committee of Peking University People's Hospital (No. 2016PHB202-01). The study was performed in accordance with the Declaration of Helsinki. Written informed consent was obtained from all participants prior to clinical data collection and sampling.

A retrospective analysis was conducted for 55 patients with post-HSCT pneumonia (including CAP and HAP). Among

them, patients who died after treatment were defined as non-survivors. Additionally, 30 healthy volunteers from the medical center were enrolled in the HC group voluntarily, and 44 immunocompetent CAP patients were recruited as disease control subjects. All participants were enrolled from Peking University People's Hospital between April 2014 and August 2017. CAP and HAP were defined according to the published standards (Mandell et al., 2007; Kalil et al., 2016; Cao et al., 2018). Subjects with other pulmonary diseases, or tumors were excluded, and healthy volunteers taking antibiotics or hormones for the last three months were excluded (Charlson et al., 2011). General participant demographics, including age, gender, complications, laboratory findings, and clinical treatments, were collected from medical record system using a standard form. BALF was detected for routine microbiological examination, including routine culture, virus quantity polymerase chain reaction (qPCR), GeneXpert, 1,3-β-D glucan test, and galactomannan test. Baseline characteristics and clinical indicators of patients were listed in Table 1 and e-Tables 1-3.

Sample preparation, DNA extraction, and sequencing

For patients diagnosed with pneumonia, bronchoscopy was performed as a part of clinical management within 72 h after hospital admission before the ventilation treatments. Detailed sampling procedures, pretreatment, and storage were performed as described in previous studies (Zheng et al., 2019; He et al., 2022). Sampling controls were collected through simulated bronchoscopy procedures (no patient) using the same instrument and method. BALF was then centrifuged. Total DNA was extracted from the BALF precipitate and 500 μL of the supernatant using the CTAB/SDS method. 16S rRNA genes of the V3-V4 region were amplified with pre-validated primers (Klindworth et al., 2013). Detailed procedure of library construction was provided in the supplementary materials. High-quality libraries were sequenced to 250 bp paired-end raw reads on the HiSeq2500 platform. The V3-V4 regions were not amplified in the sampling control. Besides, contaminants were excluded from this analysis using negative controls containing only sterile ddH_2O and reagents for extraction and PCR amplification. "Decontam" R package was applied to further reduce the potential impact of contamination for low biomass samples using the prevalence method in the "isNotContaminant" function with thresholds at 0.1 (Davis et al., 2018; Karstens et al., 2019) (e-Table 4). While all the steps of sampling, DNA extraction and PCR amplification were controlled with negative reagents, further analysis was performed to ensure that the potential risks of contamination were minimized. The results of this study were compared with the 92 contamination genera detected in the negative sequencing

TABLE 1 Baseline characteristics and clinical indicators of patients with post-HSCT pneumonia, CAP patients, and health control subjects.

	post-HSCT pneumonia (N = 55)	CAP (N = 44)	HC (N = 30)	*P*-value
Age	34 (28-44.5)	53.5 (37-65.5)	60 (47.5-63.5)	<0.001 a,b,
Gender, n, (% male)	40 (72.7)	28 (63.6)	11 (36.7)	<0.001
Smokers, n (%)	4 (7.3)	8 (18.2)	0 (0)	0.009
Comorbidities				
Diabetes Mellitus, n (%)	6 (10.9)	6 (13.6)	3 (10.0)	0.234
Hypertension, n (%)	15 (32.7)	14 (31.8)	11 (36.7)	0.539
Laboratory Findings				
Peripheral blood				
WBC (× 10^9/L)	4.31 (2.80-7.00)	6.40 (5.13-9.73)	6.87 (5.68-8.31)	<0.001 a,b
Neutrophils (%)	73.40 (59.80-86.30)	71.87 (63.02-83.02)	61.60 (53.72-64.77)	<0.001 a,c
Lymphocytes (%)	16.50 (7.70-27.1)	15.96 (8.92-27.19)	29.98 (24.93-36.83)	<0.001 a,c
BAL related				
PMN percentages (%)	14.00 (2.00-28.50)	18.00 (1.75-65.50)	1.00 (0.50-2.00)	<0.001 a,c
Lymphocyte percentages (%)	33.00 (17.00-53.50)	21.00 (11.00-43.50)	12.00 (8.00-30.75)	<0.001 a,
Eosinophil percentages (%)	0.00 (0.00-1.00)	0.00 (0.00-1.00)	0.00 (0.00-1.00)	0.042
Macrophages percentages (%)	42.00 (21.00-67.00)	37.00 (13.50-60.00)	86.50 (64.50-91.00)	<0.001 a,c
Inflammatory markers				
PCT (μg/L)	0.20 (0.11-0.50)	0.16 (0.05-1.02)	0.05 (0.05-0.09)	<0.001 a,c
CRP (mg/L)	30.09 (6.64-76.63)	40.75 (12.12-132.75)	1.37 (0.78-2.81)	<0.001 a,c
ESR (mm)	57.00 (27.75-89.00)	39.00 (19.00-61.00)	8.50 (6.00-13.50)	<0.001 a,c
PSI	74 (65-88)	72 (51-104)	–	0.235

a, HSCTvs.HC; b, HSCTvs.CAP; c, CAPvs.HC; HSCT hematopoietic stem cell transplantation; CAP community-acquired pneumonia; CRP, C-reactive protein; ESR, erythrocyte sedimentation rate; PCT procalcitonin; PSI, pneumonia severity index; PMN, polymorphonuclear leukocyte; WBC, white blood cell.

blank controls in previous study (Salter et al., 2014). We failed to detect 61 out of the contaminant genera in our result (e-Table 5). Among the remaining 31 genera found in our data, 6 genera were not reported in samples from the respiratory tract but none had an average relative abundance greater than 0.0002.

Bioinformatics analysis

The high-quality sequencing data was generated by removing low-quality reads (the quality control rate is less than 1%), primers, barcodes, and dereplication using VSEARCH (Rognes et al., 2016). After removing the chimeric sequences with the UCHIME algorithm (Edgar et al., 2011), effective reads were obtained and denoised to generate amplicon sequence variants (ASVs) using unoise3 (Edgar, 2016). Taxonomy assignment was performed on ASVs based on the RDP database (v 11.5) (Cole et al., 2014) and the GreenGene database (DeSantis et al., 2006).The microbiome phenotypes were predicted by BugBase based on GreenGene annotation (Ward et al., 2017). PICRUSt2 was used to identify the predicted associated pathways from the inferred metagenomes of taxa with the 'stratified' mode (Douglas et al., 2020).

Statistical analysis

The abundance-based coverage estimator (ACE) index and Shannon index were calculated to evaluate alpha diversity using rarefied data using vegan R package (Jari Oksanen et al., 2020). The nearest taxon index (NTI) and net-relatedness index (NRI) were applied to estimate phylogenetic structure of the community using picante R package (Kembel et al., 2010). The algorithm was run using 999 randomizations of the community within the mega-phylogeny applying the "taxa.labels". Beta diversity was assessed by permutational multivariate analysis of variance (PERMANOVA) test, and visualized using principal coordinate analysis (PCoA). Adonis test was conducted based on Bray-Curtis distances and Jaccard distances. ASV abundances were centered with log-ratio transformation prior to analysis. Differential bacterial taxa among groups were assessed using the edgeR R package based on centered log-ratio-transformed genome relative abundance (Robinson et al., 2010). A multifactorial design within the edgeR R package was used to adjust confounding factors, such as age, gender, and smoking. Statistically significant genera differences (LDA > 2, P < 0.05) associated with different groups were explored using linear discriminant analysis (LDA) effect size (LEfSe) (Segata et al., 2011). Spearman's rho was calculated using the 'corr.test' function within the R package. Network analysis was performed based on read count data at the genus level using SpeciEasi (Kurtz et al., 2015). The density of the networks was calculated by the "graph.density" function in the igraph R package.

For clinical indicators, all categorical variables are presented as numbers (percentages), parametric continuous variables are presented as the mean ± SD, and nonparametric continuous variables are presented as median and interquartile ranges (25th and 75th percentiles). Student's t-test or analysis of variance (ANOVA) with *post hoc* Tukey HSD test were used to analyze continuous parametric data. Continuous nonparametric data were analyzed using Mann–Whitney U or a Kruskal–Wallis test. All categorical data were analyzed using a chi-square or Fisher's exact test. All tests were two-sided, p-values were corrected using Benjamin-Hochberg false discovery rate (FDR), and $p < 0.05$ was considered statistically significant. Statistical analyses were performed using SPSS version 23 software.

Results

Clinical characteristics of the study population

To explore the clinical characteristics of post-HSCT pneumonia, we summarized clinical information from 55 subjects. For HSCT patients with pneumonia, the median age was 34 years old, and 72.7% of them were male. A total of 47.3% of patients underwent transplantation for acute myelocytic leukemia (AML). e-Table 1 showed that 18 (32.7%) patients died. Pneumonia occurred at late post-engraftment phases in 35 (63.6%) patients, and occurred at pre-engraftment (neutropenic) phase in 4 (7.3%) patients (e-Table 1). The median time from transplant to the onset of pneumonia was 165 days. The PMN percentages in the BALF and PCT were significantly elevated in non-survivors (e-Table 2), suggesting that exacerbated inflammation may result in poor outcomes in patients with post-HSCT pneumonia.

Demographic information on the three groups is displayed in Table 1, along with comorbidities, blood cell counts, BALF cell counts, inflammatory markers, and the pneumonia severity index (PSI). Neutrophil percentage, C-reactive protein (CRP), procalcitonin (PCT) and erythrocyte sedimentation rate (ESR) levels, and the percentage of polymorphonuclear leukocytes (PMNs) in the BALF were higher in patients with pneumonia than in the HC group. In contrast, the lymphocyte percentage in the peripheral blood and the macrophage percentage in the BALF were significantly lower. Pathogens were detected in 47.3% of BALF samples with conventional hospital-based microbiology tests in patients with post-HSCT pneumonia and 65.9% in patients with CAP (e-Table 3). 89.1%, 81.8%, and 54.5% patients with post-HSCT pneumonia received the antibiotics, antifungals, and *Pneumocystis carinii* prophylaxis,

respectively (e-Table 3). Moreover, there was no difference in the proportion of patients taking antibiotics in the last three months between the two diseased groups (e-Table 3). and the mortality is higher in the post-HSCT pneumonia group.

Disturbance of the LRT microbiome

Species accumulation curves and the read counts of samples revealed that the sequencing was sufficient to describe associated microbial community (e-Figure 1; e-Table 6). After filtering for sequence variants in at least two samples with a minimum relative abundance of 0.05% (Bowerman et al., 2020), 2396 sequence variants were retained for community analysis. In terms of alpha diversity, no significant differences were observed in the ACE index, whereas the Shannon index showed significant decreases in diversity in patients with post-HSCT pneumonia compared to the HC and CAP groups (Figures 1A, B). The mean values of NTI and NRI in all groups was greater than 0, indicating the samples clustering in each group (Figures 1C, D). The NTI values in samples with post-HSCT pneumonia were less positive compared to the CAP and HC samples, which indicated that phylogenetic clustering was weakest in the post-HSCT pneumonia samples. The PERMANOVA test demonstrated that the bacterial community of the post-HSCT pneumonia group significantly differs from that of the CAP or HC group (Figure 1E). The Adonis tests based on Bray-Curtis distances and Jaccard distances revealed that significant differences existed in both composition and abundance of tax among groups (Figures 1F, G). Besides, we found no significant difference in the microbiota composition in terms of smoking status ($p = 0.297$) in all subjects and in the HC group, there is no difference in sex ($p = 0.19$), age ($p = 0.052$) or comorbidity groups. Similarly, antibiotic usage ($p = 0.278$) or corticosteroid usage ($p = 0.552$) had no effect in the microbiota composition of patients (e-Figures 2A–G). These results indicate that patients with post-HSCT pneumonia had decreased diversity and have a different LRT microbiome composition compared with the HC or CAP group.

To determine specific bacterial taxa correlated with patients with post-HSCT pneumonia, we compared the relative

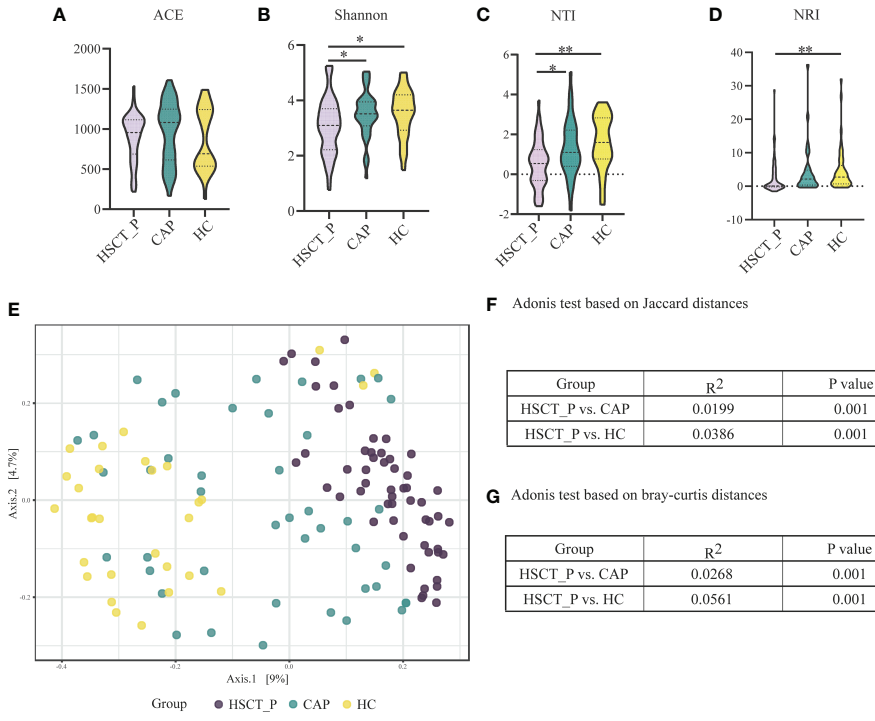

F Adonis test based on Jaccard distances

Group	R^2	P value
HSCT_P vs. CAP	0.0199	0.001
HSCT_P vs. HC	0.0386	0.001

G Adonis test based on bray-curtis distances

Group	R^2	P value
HSCT_P vs. CAP	0.0268	0.001
HSCT_P vs. HC	0.0561	0.001

FIGURE 1
Alpha and Beta diversity of the lower respiratory tract microbiome in the post-HSCT pneumonia (HSCT_P), community-acquired pneumonia (CAP), and healthy controls (HC) groups. **(A)** Comparison of abundance-based coverage estimator (ACE) index in different groups for assessment of microbiome richness of three groups. **(B)** Comparison of Shannon index in different groups for assessment of microbiome diversity of three groups. * represents $p < 0.05$ based on Kruskal–Wallis test. **(C)** Comparison of the mean nearest taxon distance (MNTD) index in different groups for assessment of phylogenetic diversity of three groups. ** represents $p < 0.01$ based on Kruskal–Wallis test. **(D)** Comparison of the nearest taxon index (NTI) in different groups for assessment of microbiome diversity of three groups. * represents $p < 0.05$, and ** represents $p < 0.0$ based on Kruskal–Wallis test. **(E)** Beta diversity was assessed by PERMANOVA test based on Jaccard distances using principal coordinate analysis (PCoA). *P* value of post-HSCT pneumonia vs. CAP and post-HSCT pneumonia vs. HC were both 0.001. **(F)** Adonis test based on Jaccard distances. **(G)** Adonis test based on bray-curtis distances.

abundances (RA) of microbiota among groups. As shown in Figure 2A, the five most abundant phyla included Proteobacteria, Firmicutes, Bacteroidetes, Fusobacteria, and Actinobacteria. Specifically, post-HSCT pneumonia samples had a higher RA of Actinobacteria and a relatively low RA of Fusobacteria and Bacteroidetes. The top 30 genera in RA were shown in Figure 2B. Obviously, the RA of *Sphingomonas*, and *prevotella* decreased in the post-HSCT pneumonia group (Figure 2B; e-Tables 7, 8), whereas the RA of *Bacillus*, *Bifidobacterium*, and *Enterococcus* were significantly increased. According to the Lefse analysis, the RA of *Pseudomonas*, *Acinetobacter*, *Burkholderia*, and *Mycobacterium* were prominent in the pneumonia group after HSCT (Figure 2C).

Potential function of the LRT microbiome

Predicted phenotypes based on taxonomic classification were analyzed with BugBase, which indicated that aerobic bacteria were more abundant in patients with post-HSCT pneumonia than in the CAP and HC groups, while the abundance of anaerobic bacteria was the opposite (e-Figures 3A, B, $p < 0.05$). Additionally, the results suggested that Gram-positive bacteria were more abundant in both post-HSCT pneumonia and CAP groups than in the HC group, while the abundance of Gram-negative bacteria was lower (e-Figures 3C, D, $p < 0.05$).

To explore differences in potential function, we annotated the 16S reads using PICRUSt2 based on the Kyoto Encyclopedia of Genes and Genomes (KEGG) (Kanehisa et al., 2021), and obtained 193 KEGG pathways. Through a Wilcoxon Rank Sum Test, we found that 99 and 107 pathways may be differentially expressed in the post-HSCT pneumonia group compared with CAP and HC groups, respectively (e-Tables 9, 10). The expression of multiple pathways concerning amino acid metabolism, such as arginine, histidine, and tyrosine, was elevated in patients with post-HSCT pneumonia compared to the two control groups (Figure 3A). The pathways "biosynthesis of unsaturated fatty acids" and "pyruvate metabolism" were predicted to be more enriched in patients with post-HSCT pneumonia (Figure 3B). Compared with the HC group, pathways associated with "cytokine-cytokine receptor interaction" were more abundant in patients with post-HSCT pneumonia, but the predicted "NOD-like receptor signaling" pathway decreased (Figure 3B). These results suggest that the

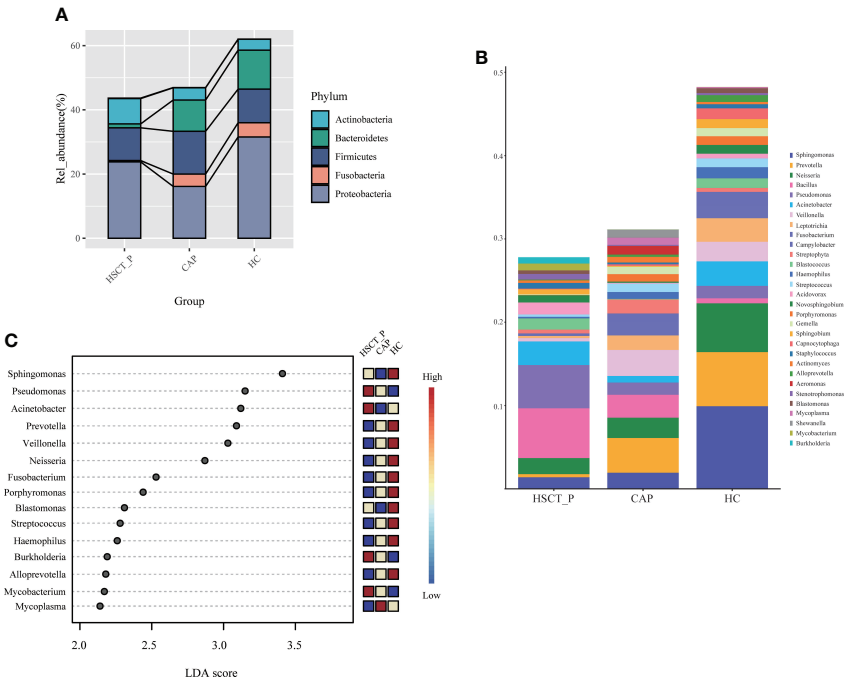

FIGURE 2
Taxonomic analysis of lower respiratory tract microbiome in the post-HSCT pneumonia (HSCT_P), community-acquired pneumonia (CAP), and healthy controls (HC) groups. **(A)** The relative abundance of microbial communities at the level of phylum among groups. **(B)** The top 30 genera in three groups. **(C)** LDA shows distinct lung microbiome composition associated with HSCT_P, CAP, and HC group. LDA scores as calculated by LEfSe of taxa differentially abundant in different group.

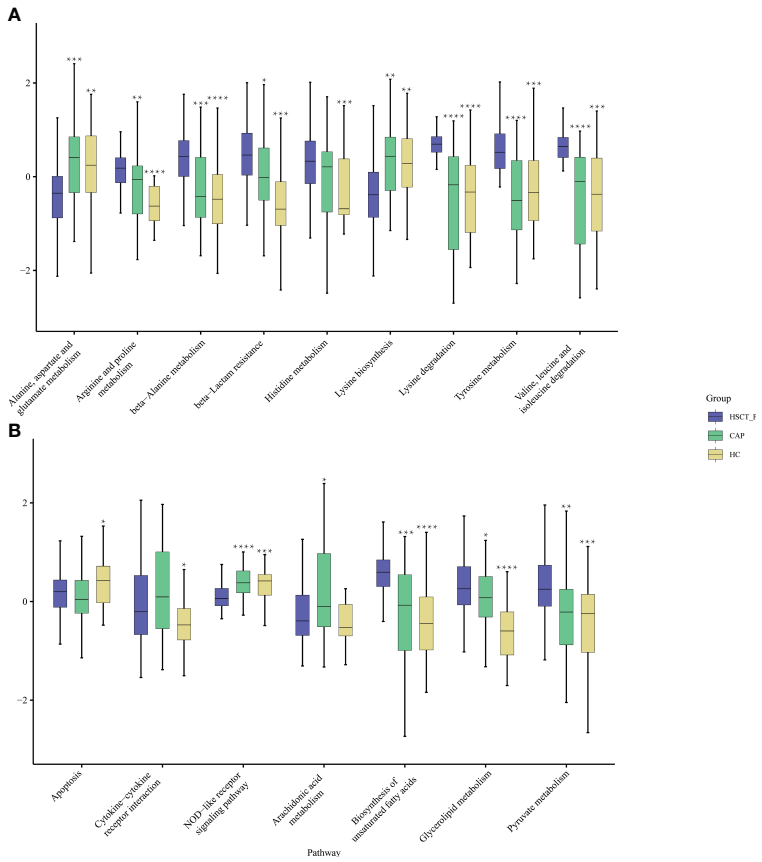

FIGURE 3
Functional characterization of different groups based on PICRUSt analysis. The abundance of pathways concerning amino acid metabolism among three groups **(A)** and the abundance of pathways concerning lipid metabolism and immune reaction among three groups **(B)**. Black stars upon the boxes indicate significant results for CAP or group compared with post-HSCT pneumonia patients. (* P < 0.05, ** P < 0.01, *** P<0.001, ****P < 0.0001).

predicted microbial functions of amino acids, lipid metabolism, and inflammatory reactions may change in the patients with post-HSCT pneumonia.

The LRT microbiome in non-survivors

To explore the structure of the flora in patients with post-HSCT pneumonia, we compared subgroups within the 55 samples. No significant difference was observed in microbiota composition or diversity in terms of pathogen detection (e-Figure 4) or post-HSCT period (neutropenic phase, early and late post-engraftment phase, e-Figure 5) or outcome (survivors vs. non-survivors) (Figures 4A, B). However, a higher RA of Actinobacteria and a lower RA of Bacteroidetes were found in non-survivors (e-Figure 6), and 45 genera were identified as differential taxa between survivors and non-survivors (e-Table 11). The RAs of the genera *Enterococcus*, *Acinetobacter*, *Burkholderia*, *Mycobacterium*, and *Escherichia* all significantly increased in non-survivors, while the RAs of the genera *Neisseria*, *Bacillus*, and *Veillonella* decreased in non-survivors (Figure 4C). Among them, the RA of *Enterococcus* was positively correlated with PCT levels, and *Mycobacterium* was positively correlated with PMN percentage in the BALF numerically (Figure 4D; e-Table 12). The RA of *Veillonella* was negatively correlated with the neutrophil percentage. Through phenotype prediction, potentially pathogenic and aerobic bacteria were enriched in non-survivors (e-Figure 7, all $p < 0.05$).

Discussion

The LRT microbiota is crucial for the host immune system, and the imbalance between microbial migration and removal is correlated with alveolar and systematic inflammation (O'Dwyer et al., 2016). Understanding the composition of the LRT microbiota under different diseases is essential for identifying potential mechanisms underlying the pathogenesis of post-

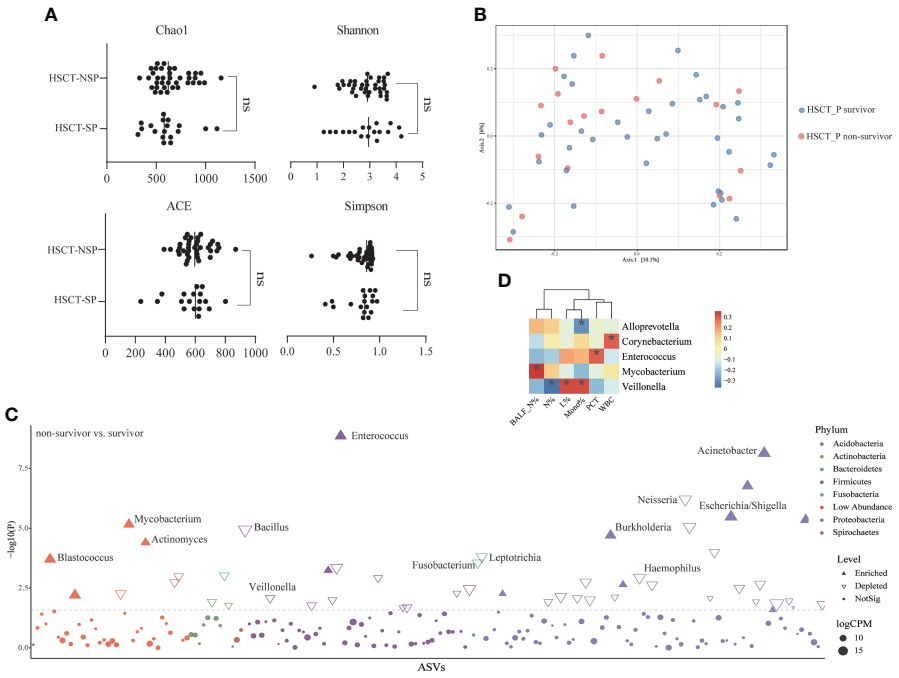

FIGURE 4
Differences in lung microbial composition between survivors and non-survivors of post HSCT pneumonia patients **(A)** Comparison of Chao1, ACE, Shannon and Simpson diversity index in different groups for assessment of microbiome alpha diversity of survivors and non-survivors. ns, no significant differences were observed between the groups. **(B)** Beta diversity was assessed by PERMANOVA test based on Jaccard distances using principal coordinate analysis (PCoA) (p = 0.361). **(C)** Differential genera between survivors and non-survivors using edgeR package. CPM, counts per million. **(D)** Spearman's rho calculated between ASVs and clinical indicators. Black stars within heatmap boxes indicate significant results (*$p < 0.05$), Benjamini–Hochberg adjustment for multiple comparisons. ASV abundances were centered with log-ratio transformation prior to analysis.

HSCT pneumonia and could offer crucial insights into therapeutic targets. Although sputum sample is noninvasive and was used to explore the microbiome in diverse pulmonary diseases, it is difficult to collect for some patients and all healthy controls. Besides, the location of the respiratory tract represented by the sputum sample cannot be determined and sputum sample is highly likely to be contaminated by the oral microbiota. On the contrary, BALF has been believed to be a viable option for the lung microbiome (Cheng et al., 2020). Thus, in this study, we characterized the LRT microbiome of 55 patients with post-HSCT pneumonia and provided evidence for significant alterations in the bacterial community, utilizing the remaining BALF samples from clinical testing.

Previous studies have found that intestinal microbiota and dental biofilm microbiota dysbiosis occurred during HSCT, marked by a gradual loss of bacterial diversity (Heidrich et al., 2021). Our results also showed a significantly decreased alpha diversity in patients with post-HSCT pneumonia compared to the CAP and HC groups. The composition of the LRT microbiome in post-HSCT pneumonia patients was characterized by a decreased abundance of commensal genera and an overgrowth of opportunistic pathogens, such as *Acinetobacter* (Du et al., 2021) and *Mycobacterium* (Meehan et al., 2021). Thus, under the state of immune defects and chronic inflammation, the bacterial community was likely to be seriously altered in patients after HSCT, which elicited epithelial and luminal inflammation, which may further alter the conditions in the lung microenvironment, perpetuating dysbiosis and increasing the susceptibility to infection. However, although Nearing et al. reported that edgeR and LEfSe often identified the most significant differential ASVs than any other tools, they have relatively high false discovery rate (Nearing et al., 2022).

According to the predicted phenotypes, the abundance of anaerobic bacteria decreased in patients with post-HSCT pneumonia, and at the phylum level, a relatively low abundance of Bacteroidetes was observed compared with the HC group. The same results were also observed in non-survivors of the post-HSCT pneumonia group compared to the survivors. Marsland et al. reported that Bacteroidetes are strictly anaerobic and that most Bacteroidetes are sensitive to low pH (Marsland and Gollwitzer, 2014). Robustly disturbed and reduced anaerobic bacteria could be caused by chemotherapy, antibiotics, mechanical ventilation, or HSCT itself, and inflammatory response could lower the local PH in

the LRT. Antibiotics targeting anaerobic pathogens have been revealed to increase GVHD-related mortality in humans (Shono et al., 2016). Therefore, dysbiosis and the decrease of anaerobic bacteria in the LRT could be the cause of post-HSCT pneumonia and poor prognosis. However, the exact mechanisms must be further studied.

The predicted functions of the LRT microbiome were significantly different among groups. The relative abundances of microbiome genes associated with histidine metabolism were increased in patients with post-HSCT pneumonia, and the bioavailable histidine in the lung could promote *Acinetobacter* pathogenesis and serve as a crucial nitrogen source during infection (Lonergan et al., 2020). The "cytokine-cytokine receptor interaction" function was predicted to be more evident in patients with post-HSCT pneumonia, but the abundance of genes related to "NOD-like receptor signaling" decreased. This may indicate a stronger inflammatory response and impaired innate immune responses in the LRT of patients with post-HSCT pneumonia. However, the predictive ability of PICRUSt2 is limited and the actual functions can substantially differ. Meanwhile, inaccuracies in pathway annotation or assignments of gene function may be present. Thus, further experiments are required to verify changes in these functions.

Our data further demonstrated that some genera were correlated with the prognosis of patients with post-HSCT pneumonia. The RA of *Enterococcus* was more abundant in non-survivors, which agrees with recent studies reporting that the enrichment of gut-associated bacteria in the lung suggested poor outcomes for critical patients (Dickson et al., 2016b; Dickson et al., 2020; Martin-Loeches et al., 2020). This suggests that increased intestinal permeability is involved in the gut-lung translocation of bacteria and inflammatory products to distant organs in non-survivors, which should be investigated further using paired gut and lung specimens.

There are some limitations to our study. First, clinical heterogeneity is a major concern in patients with post-HSCT pneumonia (including the primary disease, pretreatment methods, and transplant types). Meanwhile, nearly all HSCT recipients were received therapy such as antibiotics, corticosteroids and cytotoxic drugs inevitably, so the lung microbiome in the post-HSCT pneumonia group was shaped by a variety of factors. Thus, the direct cause of the differences in the lung microbiome between the post-HSCT pneumonia group and HC group is unclear. Therefore, further experiment is needed to explore lung microbiome characteristics in this population and the effects of each variability. Second, the causal relationship between the observed alterations in the LRT microbiome and the development of post-HSCT pneumonia is uncertain, which should be further explored using animal models. Third, the 16s resolution is lower, and only relative abundances of specific bacteria were described, meaning that further research to detection of absolute abundances of microorganisms are needed. Lastly, despite the efforts made in contamination control, the potential sources of oral or environmental pollution may be not completely excluded.

Despite these limitations, our study explored the LRT microbiome in patients with post-HSCT pneumonia and raises some interesting questions worthy of further investigation. Our results support the findings of larger cohorts evaluating the value of the airway microbiome and its immune interactions and propose potential targets for preventing and treating pneumonia in post-HSCT patients.

Conclusions

Our results demonstrate that the LRT microbiome in post-HSCT pneumonia, which is characterized by decreases in species diversity, the enrichment of pathogens, and reduced biotic interactions, differs from CAP patients and healthy controls. The composition of the LRT microbiome is different with outcomes in patients with post-HSCT pneumonia.

Data availability statement

The names of the repository/repositories and accession number(s) can be found below: https://www.ncbi.nlm.nih.gov/, PRJNA791752 and PRJNA751994.

Ethics statement

The studies involving human participants were reviewed and approved by the Ethical Review Committee of Peking University People's Hospital. The patients/participants provided their written informed consent to participate in this study.

Author contributions

YH was responsible for investigation, methodology, analyzation, and writing-original draft. JL was responsible for investigation, methodology, analyzation. WY, YZ, DY, YX, LZ, and XM were responsible data collection, experiment and analyzation. PG and ZG were responsible for investigation, methodology, provision of in-house control data, project administration, resources, supervision, funding acquisition, writing-review and editing. All authors read and approved the final manuscript.

Funding

This work was supported by the National Natural Science Foundation of China (No. 82000019, No. 81870010), and the

National and Provincial Key Clinical Specialty Capacity Building Project 2020 (Department of the Respiratory Medicine).

Acknowledgments

The authors wish to thank staff members of the hospital for assistance with samples and clinical data collection.

Conflict of interest

The authors declare that the research was conducted in the absence of any commercial or financial relationships that could be construed as a potential conflict of interest.

Publisher's note

Supplementary material

The Supplementary Material for this article can be found online at: https://www.frontiersin.org/articles/10.3389/fcimb.2022.943317/full#supplementary-material

References

Ahya, V. N. (2017). Noninfectious acute lung injury syndromes early after hematopoietic stem cell transplantation. *Clin. Chest Med.* 38 (4), 595–606. doi: 10.1016/j.ccm.2017.07.002

Bergeron, A., and Cheng, G. S. (2017). Bronchiolitis obliterans syndrome and other late pulmonary complications after allogeneic hematopoietic stem cell transplantation. *Clin. Chest Med.* 38 (4), 607–621. doi: 10.1016/j.ccm.2017.07.003

Bondeelle, L., and Bergeron, A. (2019). Managing pulmonary complications in allogeneic hematopoietic stem cell transplantation. *Expert Rev. Respir. Med.* 13 (1), 105–119. doi: 10.1080/17476348.2019.1557049

Bowerman, K. L., Rehman, S. F., Vaughan, A., Lachner, N., Budden, K. F., Kim, R. Y., et al. (2020). Disease-associated gut microbiome and metabolome changes in patients with chronic obstructive pulmonary disease. *Nat. Commun.* 11 (1), 5886. doi: 10.1038/s41467-020-19701-0

Cao, B., Huang, Y., She, D. Y., Cheng, Q. J., Fan, H., Tian, X. L., et al. (2018). Diagnosis and treatment of community-acquired pneumonia in adults: 2016 clinical practice guidelines by the Chinese thoracic society, Chinese medical association. *Clin. Respir. J.* 12 (4), 1320–1360. doi: 10.1111/crj.12674

Charlson, E. S., Bittinger, K., Haas, A. R., Fitzgerald, A. S., Frank, I., Yadav, A., et al. (2011). Topographical continuity of bacterial populations in the healthy human respiratory tract. *Am. J. Respir. Crit. Care Med.* 184 (8), 957–963. doi: 10.1164/rccm.201104-0655OC

Cheng, C., Wang, Z., Wang, J., Ding, C., Sun, C., Liu, P., et al. (2020). Characterization of the lung microbiome and exploration of potential bacterial biomarkers for lung cancer. *Transl. Lung Cancer Res.* 9 (3), 693–704. doi: 10.21037/tlcr-19-590

Chi, A. K., Soubani, A. O., White, A. C., and Miller, K. B. (2013). An update on pulmonary complications of hematopoietic stem cell transplantation. *Chest* 144 (6), 1913–1922. doi: 10.1378/chest.12-1708

Choi, M. H., Jung, J. I., Chung, W. D., Kim, Y. J., Lee, S. E., Han, D. H., et al. (2014). Acute pulmonary complications in patients with hematologic malignancies. *Radiographics* 34 (6), 1755–1768. doi: 10.1148/rg.346130107

Cole, J. R., Wang, Q., Fish, J. A., Chai, B., McGarrell, D. M., Sun, Y., et al. (2014). Ribosomal database project: data and tools for high throughput rRNA analysis. *Nucleic Acids Res.* 42 (Database issue), D633–D642. doi: 10.1093/nar/gkt1244

Davis, N. M., Proctor, D. M., Holmes, S. P., Relman, D. A., and Callahan, B. J. (2018). Simple statistical identification and removal of contaminant sequences in marker-gene and metagenomics data. *Microbiome* 6 (1), 226. doi: 10.1186/s40168-018-0605-2

DeSantis, T. Z., Hugenholtz, P., Larsen, N., Rojas, M., Brodie, E. L., Keller, K., et al. (2006). Greengenes, a chimera-checked 16S rRNA gene database and workbench compatible with ARB. *Appl. Environ. Microbiol.* 72 (7), 5069–5072. doi: 10.1128/AEM.03006-05

Dickson, R. P., Erb-Downward, J. R., Freeman, C. M., McCloskey, L., Falkowski, N. R., Huffnagle, G. B., et al. (2017). Bacterial topography of the healthy human lower respiratory tract. *mBio* 8 (1), e02287–16. doi: 10.1128/mBio.02287-16

Dickson, R. P., Erb-Downward, J. R., Martinez, F. J., and Huffnagle, G. B. (2016a). The microbiome and the respiratory tract. *Annu. Rev. Physiol.* 78, 481–504. doi: 10.1146/annurev-physiol-021115-105238

Dickson, R. P., Martinez, F. J., and Huffnagle, G. B. (2014). The role of the microbiome in exacerbations of chronic lung diseases. *Lancet* 384 (9944), 691–702. doi: 10.1016/S0140-6736(14)61136-3

Dickson, R. P., Schultz, M. J., van der Poll, T., Schouten, L. R., Falkowski, N. R., Luth, J. E., et al. (2020). Lung microbiota predict clinical outcomes in critically ill patients. *Am. J. Respir. Crit. Care Med.* 201 (5), 555–563. doi: 10.1164/rccm.201907-1487OC

Dickson, R. P., Singer, B. H., Newstead, M. W., Falkowski, N. R., Erb-Downward, J. R., Standiford, T. J., et al. (2016b). Enrichment of the lung microbiome with gut bacteria in sepsis and the acute respiratory distress syndrome. *Nat. Microbiol.* 1 (10), 16113. doi: 10.1038/nmicrobiol.2016.113

Douglas, G. M., Maffei, V. J., Zaneveld, J. R., Yurgel, S. N., Brown, J. R., Taylor, C. M., et al. (2020). PICRUSt2 for prediction of metagenome functions. *Nat. Biotechnol.* 38 (6), 685–688. doi: 10.1038/s41587-020-0548-6

Du, B., Shen, N., Tao, Y., Sun, S., Zhang, F., Ren, H., et al. (2021). Analysis of gut microbiota alteration and application as an auxiliary prognostic marker for sepsis in children: a pilot study. *Transl. Pediatr.* 10 (6), 1647–1657. doi: 10.21037/tp-21-51

Edgar, R. C. (2016). UNOISE2: Improved error-correction for illumina 16S and ITS amplicon sequencing. *BioRxiv*. Available at: https://www.biorxiv.org/content/10.1101/081257v1

Edgar, R. C., Haas, B. J., Clemente, J. C., Quince, C., and Knight, R. (2011). UCHIME improves sensitivity and speed of chimera detection. *Bioinformatics* 27 (16), 2194–2200. doi: 10.1093/bioinformatics/btr381

Golob, J. L., Pergam, S. A., Srinivasan, S., Fiedler, T. L., Liu, C., Garcia, K., et al. (2017). Stool microbiota at neutrophil recovery is predictive for severe acute graft vs host disease after hematopoietic cell transplantation. *Clin. Infect. Dis.* 65 (12), 1984–1991. doi: 10.1093/cid/cix699

Gooley, T. A., Chien, J. W., Pergam, S. A., Hingorani, S., Sorror, M. L., Boeckh, M., et al. (2010). Reduced mortality after allogeneic hematopoietic-cell transplantation. *N Engl. J. Med.* 363 (22), 2091–2101. doi: 10.1056/NEJMoa1004383

Harris, B., Morjaria, S. M., Littmann, E. R., Geyer, A. I., Stover, D. E., Barker, J. N., et al. (2016). Gut microbiota predict pulmonary infiltrates after allogeneic hematopoietic cell transplantation. *Am. J. Respir. Crit. Care Med.* 194 (4), 450–463. doi: 10.1164/rccm.201507-1491OC

Heidrich, V., Bruno, J. S., Knebel, F. H., de Molla, V. C., Miranda-Silva, W., Asprino, P. F., et al. (2021). Dental biofilm microbiota dysbiosis is associated with the risk of acute graft-Versus-Host disease after allogeneic hematopoietic stem cell transplantation. *Front. Immunol.* 12. doi: 10.3389/fimmu.2021.692225

He, Y., Yu, W., Ning, P., Luo, Q., Zhao, L., Xie, Y., et al. (2022). Shared and specific lung microbiota with metabolic profiles in bronchoalveolar lavage fluid between infectious and inflammatory respiratory diseases. *J. Inflammation Res.* 15, 187–198. doi: 10.2147/JIR.S342462

Huang, Y. J., Charlson, E. S., Collman, R. G., Colombini-Hatch, S., Martinez, F. D., and Senior, R. M. (2013). The role of the lung microbiome in health and disease. a national heart, lung, and blood institute workshop report. *Am. J. Respir. Crit. Care Med.* 187 (12), 1382–1387. doi: 10.1164/rccm.201303-0488WS

Hubbell, S. P. (2010). Neutral Theory and the Theory of Island Biogeography. Princeton: Princeton University Press.

Huffnagle, G. B., Dickson, R. P., and Lukacs, N. W. (2017). The respiratory tract microbiome and lung inflammation: A two-way street. *Mucosal Immunol.* 10 (2), 299–306. doi: 10.1038/mi.2016.108

Invernizzi, R., Lloyd, C. M., and Molyneaux, P. L. (2020). Respiratory microbiome and epithelial interactions shape immunity in the lungs. *Immunology* 160 (2), 171–182. doi: 10.1111/imm.13195

Jari Oksanen, F. G. B., Frienly, M., Kindt, R., Legendre, P., McGlinn, D., R.Minchin, P., et al. (2020) *Vegan: Community ecology package*. Available at: https://github.com/vegandevs/vegan.

Jorth, P., Ehsan, Z., Rezayat, A., Caldwell, E., Pope, C., Brewington, J. J., et al. (2019). Direct lung sampling indicates that established pathogens dominate early infections in children with cystic fibrosis. *Cell Rep.* 27 (4), 1190–1204.e1193. doi: 10.1016/j.celrep.2019.03.086

Kader, H. A., Khanna, S., Hutchinson, R. M., Aukett, R. J., and Archer, J. (1994). Pulmonary complications of bone marrow transplantation: the impact of variations in total body irradiation parameters. *Clin. Oncol. (R Coll. Radiol)* 6 (2), 96–101. doi: 10.1016/s0936-6555(05)80111-6

Kalil, A. C., Metersky, M. L., Klompas, M., Muscedere, J., Sweeney, D. A., Palmer, L. B., et al. (2016). Management of adults with hospital-acquired and ventilator-associated pneumonia: 2016 clinical practice guidelines by the infectious diseases society of America and the American thoracic society. *Clin. Infect. Dis.* 63 (5), e61–e111. doi: 10.1093/cid/ciw353

Kanehisa, M., Furumichi, M., Sato, Y., Ishiguro-Watanabe, M., and Tanabe, M. (2021). KEGG: integrating viruses and cellular organisms. *Nucleic Acids Res.* 49 (D1), D545–D551. doi: 10.1093/nar/gkaa970

Karstens, L., Asquith, M., Davin, S., Fair, D., Gregory, W. T., Wolfe, A. J., et al. (2019). Controlling for contaminants in low-biomass 16S rRNA gene sequencing experiments. *mSystems* 4 (4), e00290-19. doi: 10.1128/mSystems.00290-19

Kembel, S. W., Cowan, P. D., Helmus, M. R., Cornwell, W. K., Morlon, H., Ackerly, D. D., et al. (2010). Picante: R tools for integrating phylogenies and ecology. *Bioinformatics* 26 (11), 1463–1464. doi: 10.1093/bioinformatics/btq166

Klindworth, A., Pruesse, E., Schweer, T., Peplies, J., Quast, C., Horn, M., et al. (2013). Evaluation of general 16S ribosomal RNA gene PCR primers for classical and next-generation sequencing-based diversity studies. *Nucleic Acids Res.* 41 (1), e1. doi: 10.1093/nar/gks808

Kotloff, R. M., Ahya, V. N., and Crawford, S. W. (2004). Pulmonary complications of solid organ and hematopoietic stem cell transplantation. *Am. J. Respir. Crit. Care Med.* 170 (1), 22–48. doi: 10.1164/rccm.200309-1322SO

Kurtz, Z. D., Muller, C. L., Miraldi, E. R., Littman, D. R., Blaser, M. J., and Bonneau, R. A. (2015). Sparse and compositionally robust inference of microbial ecological networks. *PloS Comput. Biol.* 11 (5), e1004226. doi: 10.1371/journal.pcbi.1004226

Lonergan, Z. R., Palmer, L. D., and Skaar, E. P. (2020). Histidine utilization is a critical determinant of acinetobacter pathogenesis. *Infect. Immun.* 88 (7), e00118–20. doi: 10.1128/IAI.00118-20

Lucena, C. M., Torres, A., Rovira, M., Marcos, M. A., de la Bellacasa, J. P., Sanchez, M., et al. (2014). Pulmonary complications in hematopoietic SCT: A prospective study. *Bone Marrow Transplant.* 49 (10), 1293–1299. doi: 10.1038/bmt.2014.151

Mandell, L. A., Wunderink, R. G., Anzueto, A., Bartlett, J. G., Campbell, G. D., Dean, N. C., et al. (2007). Infectious diseases society of America/American thoracic society consensus guidelines on the management of community-acquired pneumonia in adults. *Clin. Infect. Dis.* 44 Suppl 2, S27–S72. doi: 10.1086/511159

Marsland, B. J., and Gollwitzer, E. S. (2014). Host-microorganism interactions in lung diseases. *Nat. Rev. Immunol.* 14 (12), 827–835. doi: 10.1038/nri3769

Martin-Loeches, I., Dickson, R., Torres, A., Hanberger, H., Lipman, J., Antonelli, M., et al. (2020). The importance of airway and lung microbiome in the critically ill. *Crit. Care* 24 (1), 537. doi: 10.1186/s13054-020-03219-4

Meehan, C. J., Barco, R. A., Loh, Y. E., Cogneau, S., and Rigouts, L. (2021). Reconstituting the genus mycobacterium. *Int. J. Syst. Evol. Microbiol.* 71 (9), 004922. doi: 10.1099/ijsem.0.004922

Nearing, J. T., Douglas, G. M., Hayes, M. G., MacDonald, J., Desai, D. K., Allward, N., et al. (2022). Microbiome differential abundance methods produce different results across 38 datasets. *Nat. Commun.* 13 (1), 342. doi: 10.1038/s41467-022-28034-z

Nusair, S., Breuer, R., Shapira, M. Y., Berkman, N., and Or, R. (2004). Low incidence of pulmonary complications following nonmyeloablative stem cell transplantation. *Eur. Respir. J.* 23 (3), 440–445. doi: 10.1183/09031936.04.00053004

O'Dwyer, D. N., Dickson, R. P., and Moore, B. B. (2016). The lung microbiome, immunity, and the pathogenesis of chronic lung disease. *J. Immunol.* 196 (12), 4839–4847. doi: 10.4049/jimmunol.1600279

O'Dwyer, D. N., Zhou, X., Wilke, C. A., Xia, M., Falkowski, N. R., Norman, K. C., et al. (2018). Lung dysbiosis, inflammation, and injury in hematopoietic cell transplantation. *Am. J. Respir. Crit. Care Med.* 198 (10), 1312–1321. doi: 10.1164/rccm.201712-2456OC

Pattaroni, C., Watzenboeck, M. L., Schneidegger, S., Kieser, S., Wong, N. C., Bernasconi, E., et al. (2018). Early-life formation of the microbial and immunological environment of the human airways. *Cell Host Microbe* 24 (6), 857–865.e854. doi: 10.1016/j.chom.2018.10.019

Peters, S. G., and Afessa, B. (2005). Acute lung injury after hematopoietic stem cell transplantation. *Clin. Chest Med.* 26 (4), 561–569, vi. doi: 10.1016/j.ccm.2005.06.009

Robinson, M. D., McCarthy, D. J., and Smyth, G. K. (2010). edgeR: a bioconductor package for differential expression analysis of digital gene expression data. *Bioinformatics* 26 (1), 139–140. doi: 10.1093/bioinformatics/btp616

Rognes, T., Flouri, T., Nichols, B., Quince, C., and Mahe, F. (2016). VSEARCH: a versatile open source tool for metagenomics. *PeerJ* 4, e2584. doi: 10.7717/peerj.2584

Salter, S. J., Cox, M. J., Turek, E. M., Calus, S. T., Cookson, W. O., Moffatt, M. F., et al. (2014). Reagent and laboratory contamination can critically impact sequence-based microbiome analyses. *BMC Biol.* 12, 87. doi: 10.1186/s12915-014-0087-z

Segata, N., Izard, J., Waldron, L., Gevers, D., Miropolsky, L., Garrett, W. S., et al. (2011). Metagenomic biomarker discovery and explanation. *Genome Biol.* 12 (6), R60. doi: 10.1186/gb-2011-12-6-r60

Shono, Y., Docampo, M. D., Peled, J. U., Perobelli, S. M., Velardi, E., Tsai, J. J., et al. (2016). Increased GVHD-related mortality with broad-spectrum antibiotic use after allogeneic hematopoietic stem cell transplantation in human patients and mice. *Sci. Transl. Med.* 8 (339), 339ra371. doi: 10.1126/scitranslmed.aaf2311

Singanayagam, A., Glanville, N., Cuthbertson, L., Bartlett, N. W., Finney, L. J., Turek, E., et al. (2019). Inhaled corticosteroid suppression of cathelicidin drives dysbiosis and bacterial infection in chronic obstructive pulmonary disease. *Sci. Transl. Med.* 11 (507), eaav3879. doi: 10.1126/scitranslmed.aav3879

Taur, Y., Jenq, R. R., Perales, M. A., Littmann, E. R., Morjaria, S., Ling, L., et al. (2014). The effects of intestinal tract bacterial diversity on mortality following allogeneic hematopoietic stem cell transplantation. *Blood* 124 (7), 1174–1182. doi: 10.1182/blood-2014-02-554725

Venkataraman, A., Bassis, C. M., Beck, J. M., Young, V. B., Curtis, J. L., Huffnagle, G. B., et al. (2015). Application of a neutral community model to assess structuring of the human lung microbiome. *mBio* 6 (1), e02284–14. doi: 10.1128/mBio.02284-14

Ward, T., Larson, J., Meulemans, J., Hillmann, B., Lynch, J., Sidiropoulus, D, et al. (2017). BugBase predicts organism-level microbiome phenotypes. *BioRxiv*. Available at: https://www.biorxiv.org/content/10.1101/133462v1.

Zheng, Y., Ning, P., Luo, Q., He, Y., Yu, X., Liu, X., et al. (2019). Inflammatory responses relate to distinct bronchoalveolar lavage lipidome in community-acquired pneumonia patients: A pilot study. *Respir. Res.* 20 (1), 82. doi: 10.1186/s12931-019-1028-8

Zhou, X., O'Dwyer, D. N., Xia, M., Miller, H. K., Chan, P. R., Trulik, K., et al. (2019). First-onset herpesviral infection and lung injury in allogeneic hematopoietic cell transplantation. *Am. J. Respir. Crit. Care Med.* 200 (1), 63–74. doi: 10.1164/rccm.201809-1635OC

Zinter, M. S., and Hume, J. R. (2021). Effects of hematopoietic cell transplantation on the pulmonary immune response to infection. *Front. Pediatr.* 9. doi: 10.3389/fped.2021.634566

frontiers | Frontiers in Cellular and Infection Microbiology

TYPE Original Research
PUBLISHED 28 October 2022
DOI 10.3389/fcimb.2022.1011254

OPEN ACCESS

EDITED BY
Yolanda López-Vidal,
Universidad Nacional Autónoma de México, Mexico

REVIEWED BY
Xiang Wang,
Nanjing University, China
Shigefumi Okamoto,
Kanazawa University, Japan

*CORRESPONDENCE
Wenjian Wang
wwjxx@126.com
Uet Yu
cloveringo69@hotmail.com

SPECIALTY SECTION
This article was submitted to Extra-intestinal Microbiome, a section of the journal Frontiers in Cellular and Infection Microbiology

RECEIVED 04 August 2022
ACCEPTED 03 October 2022
PUBLISHED 28 October 2022

CITATION
Hu Q, Liu B, Fan Y, Zheng Y, Wen F, Yu U and Wang W (2022) Multi-omics association analysis reveals interactions between the oropharyngeal microbiome and the metabolome in pediatric patients with influenza A virus pneumonia. *Front. Cell. Infect. Microbiol.* 12:1011254.
doi: 10.3389/fcimb.2022.1011254

Multi-omics association analysis reveals interactions between the oropharyngeal microbiome and the metabolome in pediatric patients with influenza A virus pneumonia

Qian Hu[1], Baiming Liu[1], Yanqun Fan[2], Yuejie Zheng[1], Feiqiu Wen[3], Uet Yu[3]* and Wenjian Wang[1]*

[1]Department of Respiratory Diseases, Shenzhen Children's Hospital, Shenzhen, China, [2]Department of Trans-omics Research, Biotree Metabolomics Technology Research Center, Shanghai, China, [3]Department of Hematology and Oncology, Shenzhen Children's Hospital, Shenzhen, China

Children are at high risk for influenza A virus (IAV) infections, which can develop into severe illnesses. However, little is known about interactions between the microbiome and respiratory tract metabolites and their impact on the development of IAV pneumonia in children. Using a combination of liquid chromatography tandem mass spectrometry (LC-MS/MS) and 16S rRNA gene sequencing, we analyzed the composition and metabolic profile of the oropharyngeal microbiota in 49 pediatric patients with IAV pneumonia and 42 age-matched healthy children. The results indicate that compared to healthy children, children with IAV pneumonia exhibited significant changes in the oropharyngeal macrobiotic structure ($p = 0.001$), and significantly lower microbial abundance and diversity ($p < 0.05$). These changes came with significant disturbances in the levels of oropharyngeal metabolites. Intergroup differences were observed in 204 metabolites mapped to 36 metabolic pathways. Significantly higher levels of sphingolipid (sphinganine and phytosphingosine) and propanoate (propionic acid and succinic acid) metabolism were observed in patients with IAV pneumonia than in healthy controls. Using Spearman's rank-correlation analysis, correlations between IAV pneumonia-associated discriminatory microbial genera and metabolites were evaluated. The results indicate significant correlations and consistency in variation trends between *Streptococcus* and three sphingolipid metabolites (phytosphingosine, sphinganine, and sphingosine). Besides these three sphingolipid metabolites, the sphinganine-to-sphingosine ratio and the joint analysis of the three metabolites indicated remarkable diagnostic efficacy in children with IAV pneumonia. This study confirmed significant changes in the characteristics and metabolic profile of the oropharyngeal microbiome in pediatric patients with IAV pneumonia, with high synergy between the two factors. Oropharyngeal sphingolipid metabolites may serve as potential diagnostic biomarkers of IAV pneumonia in children.

KEYWORDS
influenza A viruses, pneumonia, pediatric, oropharyngeal, microbiota, metabolites

Introduction

Influenza A virus (IAV) is a common pathogen causing respiratory tract infections in children. Seasonal influenza epidemics are caused by the H1N1 and H3N2 IAV subtypes (Fouchier et al., 2005). Most infected children show mild symptoms, but this infection can lead to severe and life-threatening lung disease (Iuliano et al., 2018; Ratre et al., 2020). In children with IAV infection, secondary bacterial infections can lead to more severe diseases, such as pneumonia, pulmonary edema, and lung abscess, and morbidity and mortality are also significantly higher in children with combined *Streptococcus* pneumoniae infections compared to influenza alone (Dawood et al., 2014; Hsing et al., 2022). The potential mechanisms underlying IAV infection have not been fully explored. Early detection can considerably improve disease management and overall survival of children. New evidence suggests that the pathogenesis of IAV infection involves complicated interactions among viral invasion processes, the respiratory tract microbiome, and host mucosal immune responses (Lim et al., 2016; Gounder and Boon, 2019). During IAV infection, microbiota colonizing different ecological niches are closely associated with disease severity, duration, and prognosis (Söderholm et al., 2016). The oropharyngeal mucosa is colonized by various microorganisms, such as *Streptococcus* spp., *Neisseria* spp., and *Rothschild* spp., which maintain a dynamic balance with the lower respiratory tract to ensure the physical health of the host. The oropharyngeal mucosa is an integral part of the mucosal epithelial barrier, which isolates numerous bacteria, but is a notable site of virus entrance into the body, proliferation, and transmission (Man et al., 2017; Shannon et al., 2021).

To date, little is known about the mechanisms underlying the impact of the microbiota and its metabolites on inflammatory responses and mucosal immune function in pediatric patients. A metabolite is an intermediate or final product of a cellular regulatory process. Therefore, the level of a macrobiotic metabolite can reflect the cellular biochemical activities associated with infections (Jaurila et al., 2020). Direct metabolite testing has become a valuable method for identifying biomarkers of various diseases and exploring potential pathogeneses. Metabolite analyses can distinguish active infections from latent ones, thus addressing the shortcomings of available diagnostic tests, such as polymerase chain reaction (PCR), in disease diagnosis and treatment (Bowler et al., 2017; Zurfluh et al., 2018). Previous studies have reported that infections can induce changes in *in vivo* metabolites and affect the microbiotic structure, exacerbating respiratory diseases (Gu et al., 2019; Mendez et al., 2019). The microbiota can participate in host physiological and pathological processes by converting nutrients provided by the host into metabolites (Anand et al., 2016). Through the direct or indirect stimulation of the host immune system, IAV can disrupt cellular metabolic pathways by obtaining the components necessary for its self-replication from host cells (Smallwood et al., 2017).

However, most studies focus on mono-omics, cell culture, or animal models (Wen et al., 2018; Gierse et al., 2021). Therefore, the interactions between the microbiome and the respiratory tract and their correlations with susceptibility to IAV infection and disease severity in children remain unclear. Therefore, our objective was to identify changes in the oropharyngeal microbiome and metabolite profile of pediatric patients and to analyze the association between the two omics. Our findings may elucidate the etiology of IAV-related pneumonia in children and provide more accessible and valuable information for early risk prediction.

Materials and methods

Study participants and sample collection

Study participants comprised 49 children with IAV pneumonia hospitalized at Shenzhen Children's Hospital (Shenzhen, China) and 42 age- and sex-matched healthy controls (<16 years of age) who underwent a health examination from January 2018 to January 2020. The age difference between the two groups was maintained at <6 months to reduce potential confounding differences in the metabolome and microbiome between different age groups. Participants in both study groups were Han Chinese, with similar dietary habits and geographical proximity (Shenzhen, China). Participants in the IAV pneumonia group met the following criteria: 1) epidemiological history, clinical symptoms, and radiological signs of acute IAV pneumonia were present; 2) IAV positive status was confirmed using multiplex kits for the detection of 13 respiratory pathogens

(PCR capillary electrophoresis fragment analysis; Haiers Gene Technology Co., Ltd., Ningbo, China); and 3) the pediatric patient joined the clinical pathway for pneumonia immediately after hospital admission and received unified and standardized treatment. Furthermore, pediatric patients were included in the severe pneumonia group based on their clinical symptoms and whether they were admitted to the Pediatric Intensive Care Unit (PICU). Exclusion criteria included: 1) The presence of any medical conditions including acute upper and lower respiratory tract infections (rhinitis, tonsillitis, bronchitis, and pneumonia, as well as severe odontogenic, oral, and maxillofacial infections), within one month before enrollment, may affect the oropharyngeal microbiota and metabolome. Chronic diseases include asthma and cystic fibrosis. 2) Nutritional status was judged by experienced pediatricians according to 2006 child growth standard (WHO and Multicentre Growth Reference Study Group, 2006), using weight-for-age growth curves directly for children under five years and body mass index (BMI) for children over five years (de Onis et al., 2007). BMI (kg/m^2) = $weight/height^2$. The 5th percentile ≤ BMI < 85th percentile is defined as normal weight. Malnutrition and obesity were excluded.3)Use of drugs that affect the microbiome and metabolome, such as immunosuppressants, probiotics, traditional Chinese medicine, and glucocorticoids, within 1 month before enrollment. 4) Essential data were missing because of refusal of laboratory tests after admission. 5) Patients with delayed consent for enrollment (>24 hours after hospitalization) (Stewart et al., 2017). The study flowchart, from enrollment to analysis, is shown in Supplementary Figure 1. The Medical Ethics Committee of Shenzhen Children's Hospital of China Medical University approved this study (registration number: 202009202). All parents of children who took part in the study provided us with their written, informed consent.

On the day of the health examination, oropharyngeal specimens were collected from healthy controls and patients with IAV pneumonia sterile swabs (155C, COPAN, Murrieta, CA, USA) within 24 h after hospital admission (Hogan et al., 2021; Ma et al., 2021). We collected samples in the morning, and participants refrained from brushing their teeth 12 hours before sampling, rinsed or drank water two hours before sampling to remove oral debris, followed by a two-hour fast to reduce the impact on the oropharyngeal microbiota and metabolome. A sterile tongue depressor was inserted to fully expose the deep pharynx. Then the swab was inserted into the pharynx and rotated twice against the posterior pharyngeal wall or the pharyngeal-palatal arch, avoiding contact with other areas such as the tongue, uvula, and gingiva. An experienced pediatrician or nurse performed all procedures. The oropharyngeal swab samples were immediately put on ice and sent to a biological specimen bank, where they were stored at -80°C until further analysis. Unused swabs were used as blank controls to assess contamination during the experiment.

Oropharyngeal DNA extraction for microbiome analysis

Using the power soil DNA isolation kit (Mo Bio Laboratories, Carlsbad, CA, USA) and following the manufacturer's instructions, total genomic DNA was isolated from oropharyngeal swab samples (Wen et al., 2018). A Thermo NanoDrop 2000 spectrophotometer (Thermo Fisher Scientific, New York, NY, USA) was used to measure the DNA concentration. 2% agarose gel electrophoresis was used to confirm the DNA's integrity and fragment size. Total DNA was stored in an elution buffer at -80°C until PCR sequencing was performed.

16S ribosomal RNA gene sequencing with high throughput

The V3-V4 region of the 16S ribosomal RNA (rRNA) gene was amplified using the PCR primers (341F: 5′-CCTACGGGNGGCWGCAG-3′ and 805R: 5′-GACTACHVGGGTATCTAATCC-3′). The PCR products were measured using Qubit (Invitrogen Ltd., Carlsbad, CA, USA) after being purified with AMPure XT beads (Beckman Coulter Genomics, Danvers, MA, USA). The Illumina sequencing Library Quantification Kit (Kapa Biosciences, Woburn, MA, USA) and an Agilent 2100 Bioanalyzer (Agilent Technologies, Inc., Santa Clara, CA, USA) were used to confirm the amplicon library before up-sequencing the qualifying libraries. We performed 2 × 250 bp double-end sequencing on the NovaSeq 6000 platform (Illumina, San Diego, CA, USA), using the NovaSeq 6000 SP Reagent Kit (500 cycles); all was done following the manufacturer's instructions. The assembled miseq sequence was submitted to NCBI's open-access sequence to read the archive.

Sequencing data analysis

Pair-end reads obtained after sequencing were divided into samples for data separation based on their unique barcode information. In addition, the primer sequence and barcode were removed. The raw reads were quality filtered according to fqtrim (v0.94) (Magoč and Salzberg, 2011), and the double-ended sequences that passed the primary quality screening were pairwise linked based on overlapping bases using FLASH (v1.2.8). The Vsearch software (v2.3.4) was used to identify and reject chimeric sequences. The feature abundance table and the feature sequence of the amplicon sequence variants (ASVs) were obtained using a divisive amplicon denoising algorithm 2 (DADA2). Bioinformatic analysis of the oropharyngeal microbiome was performed using QIIME 2 software. The annotation was performed using the SILVA database (Release 138) and the NT-16S database based on the ASV feature sequence (Quast et al., 2013). The abundance of each species was determined according to the ASV abundance table. The confidence threshold for the annotation was >0.7.

Preparation of oropharyngeal samples for metabolomics analysis

Ultra-high performance liquid chromatography mass spectrometry (UHPLC-MS/MS) was used to determine the metabolite composition of oropharyngeal swab samples. Oropharyngeal swabs were transferred to Eppendorf (EP) tubes; 1000 ml of the extraction solution was added to the EP tube in an acetonitrile: methanol: water ratio of 2:2:1 (V:V:V). The tubes were then vortexed for 30 s and placed in an ice-water bath for 30 min of sonication. After removing the swabs, the supernatant was stored at -40°C for 1 h. The samples were then centrifuged at 4°C and 13,800 ×*g* for 15 min, and the supernatant obtained was transferred to a new injection vial for onboard detection.

Liquid chromatography mass spectrometry/mass spectrometry analysis

In both positive and negative-ion modes, all oropharyngeal samples were subjected to metabolite separation using a UHPLC system (Vanquish, Thermo Fisher Scientific). The target compounds were separated using a Waters ACQUITY UPLC BEH Amide (2.1 mm × 100 mm, 1.7 μm) liquid chromatography column. Mobile phase A was an aqueous phase with a pH of 9.75. It contained 25 mmol/L of ammonium acetate and 25 mmol/L of ammonia hydroxide, whereas mobile phase B comprised acetonitrile. The temperature of the sample tray was 4°C, and the injection volume was 2μL.

The organic phase was injected into the column at 30°C. The elution gradients were set to 95% B, 0–0.5 min; 95–65% B, 0.5–7.0 min; 65–40% B, 7.0–8.0 min; 40% B, 8.0–9.0 min; 40–95% B, 9.0–9.1 min; and 95% B, 9.1–12.0 min. The data was gathered using Xcalibur (Thermo Fisher Scientific) on the Orbitrap Exploris 120 mass spectrometer, which can collect primary and secondary mass spectrometry data in the information-dependent acquisition mode. Other conditions for the electrospray ionization source were established as follows: capillary temperature, 320°C; collision energy, 10/30/60 in NCE mode; MS/MS resolution, 15,000; full MS resolution, 60,000; auxiliary gas flow rate, 15 Arb; and sheath gas flow rate, 50 Arb. The spray voltage was set to 3.8 and -3.4 kV for the positive-ion and negative-ion modes, respectively.

Data analysis

The raw data were transformed into the mzXML format using the ProteoWizard software. The R package, XCMS (v3.8.2), was used to perform peak identification, peak alignment, peak extraction, and integration. The algorithm scoring cutoff value was set to 0.3. The online Human Metabolome Database and Kyoto Encyclopedia of Genes and Genomes (KEGG) database were used to compare molecular weight data (m/z) for the identification of metabolites. The deviation values were filtered according to the coefficient of variation, the missing values in the data were filled by one-half of the minimum value, the individual peaks were filtered, and the peak area of the internal standard in each sample was normalized. In over 50% of the samples, missing ions were considered low-mass ions and were removed. Finally, 9820 peaks were retained; the raw data were uploaded to the MetaboLights website.

Statistical analyses

Data were statistically analyzed using R (v3.6.3, R Foundation for Statistical Computing, Vienna, Austria) and SPSS (v22.0, Statistical Product and Service Solutions, IBM, Chicago, IL, USA). Data are presented as mean ± standard deviation, and the Mann-Whitney U test was performed to compare two independent samples having a non-normal distribution. The count data are expressed as the number of cases or percentages (%), and the Chi-square test was used to compare groups. The R vegan package was used to perform the permutational multivariate analysis of variance (PERMANOVA), and 1,000 permutations were used to calculate the adonis p-value (Zhou et al., 2020; Frau et al., 2021). Spearman rank-correlation analysis was used to determine the associations between the microbiome and metabolites. The final data set from the LC-MS/MS analysis was imported into the SIMCA 16.0.2 software package (Sartorius Stedim Data Analytics AB, Umea, Sweden). The importance of the variable in the projection (VIP) of the first principal component of each metabolite was calculated by building an orthogonal partial least squares discriminant analysis model (OPLS-DA). Seven-fold cross-validation was used to obtain R^2 and Q^2 to assess model validity. The Mann-Whitney U test was used to determine differences between the two groups; differences defined as $p < 0.05$ and VIP > 1 were considered significant. The Benjamini-Hochberg correction method was used to adjust the P values.

Results

Clinical characteristics

Children <6 years accounted for 89.8% (44/49 cases) of the patients in the IAV pneumonia group, with children aged 3–6 years accounting for most cases (53.1%, 26/49 cases). No significant differences were observed between the age, gender, exposure to cigarettes at home, antibiotics use before sampling,

and child delivery method of the two groups ($p > 0.05$) (Supplementary Table 1). Furthermore, PERMANOVA was performed to adjust for these and found that IAV pneumonia was the main factor contributing to the difference in microbiota and metabolome between the two groups (permutated $p = 0.001$). Moreover, there was no statistically significant difference between antibiotics on microbiota or metabolome (permutated $p = 0.774$ and $p = 0.352$, respectively). The average time from the onset of influenza symptoms to hospital admission was 7.08 ± 3.13 days (Supplementary Table 1). Seventeen pediatric patients were admitted to the PICU for further treatment, as required for their disease conditions, and classified as patients with severe pneumonia.

Oropharyngeal microbiota profile

Oropharyngeal swab samples collected from the 49 pediatric patients with IAV pneumonia and 42 healthy individuals were subjected to 16S rRNA sequencing. Two samples (FG20 and HG20) were removed due to a failure to detect the microbiota, leaving 89 samples for the final analysis. A total of 5,049,593 high-quality sequences were obtained (average: 58,385 sequences per sample; range: 49,637.50–64,538.50). After species annotation was performed, 4,133 usable ASVs were obtained (Supplementary Table 2; average, 176 ASVs per sample; range: 103.5–225.0), and the data of these ASVs were subjected to a structural analysis of the oropharyngeal microbiome. The rarefaction curves for the two groups of samples leveled or plateaued, indicating that the sequencing depth was adequate for identifying the features of most bacteria in the samples and the subsequent structural analysis (Supplementary Figure 2A–E). The rank abundance distribution curves suggested that the IAV pneumonia group had a significant decrease in abundance and microbiota imbalance compared to the healthy group (Supplementary Figure 2F).

The sequences were analyzed to estimate the alpha and beta diversity and measure variations in microbial diversity between the two groups. Alpha diversity analysis indicated significant intergroup differences in the Shannon index (3.92 ± 1.45 versus 5.39 ± 0.56, $p < 0.001$), observed species (147.75 ± 72.55 versus 196.53 ± 63.37, $p < 0.001$), chao1 (150.77 ± 73.40 versus 199.99 ± 65.85, $p < 0.001$), and Simpson index (0.79 ± 0.22 versus 0.94 ± 0.05, $p < 0.001$), suggesting significantly lower abundance and diversity of the oropharyngeal microbiota in the IAV pneumonia group than in the healthy volunteer group (Figure 1A). Beta diversity describes the intergroup differences in species. The beta diversity analysis indicated substantial changes in the composition and richness of the oropharyngeal microbial community between the two groups (Bray–Curtis $p = 0.001$; Figure 1B). Based on an analysis of similarity, we found that the differences between groups were significantly greater than those within groups. We observed a higher beta diversity in the oropharyngeal microbiota of children with IAV pneumonia, indicating that the microbiota structure of the IAV pneumonia group was more heterogeneous than that of the control group Figure 1C).

Influenza A pneumonia-associated changes in the oropharyngeal microbiota

The species abundance table for each taxonomic level was obtained based on the ASV annotations and abundance tables for the analysis and comparison of the species composition of the two groups. The IAV pneumonia group exhibited significantly differential abundances of 12 bacterial phylum, 12 classes, 33 orders, 46 families, 63 genera, 63 species, and 838 individual ASVs (Supplementary Table 3). At the phylum level, bacteria belonging to 11 phyla were identified in the healthy volunteer group, whereas 14 phyla were identified in the IAV pneumonia group. Firmicutes, Bacteroidota, Proteobacteria, Fusobacteriota, and Actinobacteria were the dominant bacterial phyla in both groups (Figure 1D). However, intergroup differences were observed in the proportions of the oropharyngeal microbiota represented by these predominant phyla. The differences in the proportion of Firmicutes were the most notable (Figure 1E). In the IAV pneumonia group, Firmicutes represented 53.04% of bacteria, whereas in the healthy volunteer group, Firmicutes accounted for 21.18%. In contrast, Bacteroidota and Proteobacteria represented higher proportions in the healthy volunteer group (28.85% vs. 19.57% and 31.77% vs. 15.22%, respectively).

Further evaluation of differences between the microbiota at different taxonomic levels revealed that Firmicutes ($p < 0.001$) and Actinobacteriota ($p < 0.001$) were more abundant in the IAV pneumonia group than in the healthy volunteer group at the phylum level. However, the abundance of Proteobacteria ($p < 0.001$), Fusobacteriota ($p < 0.001$), and Bacteroidota ($p < 0.001$) was significantly higher in the healthy volunteer group (Supplementary Figure 3A). At the genus level, there were significant intergroup differences for 63 genera (FDR $p < 0.05$); the abundance levels of *Streptococcus* ($p < 0.001$) and *Actinomyces* ($p < 0.001$) were significantly higher in the IAV pneumonia group, whereas the abundance levels of *Haemophilus* ($p < 0.001$), *Neisseria* ($p < 0.001$), *Alloprevotella* ($p < 0.001$), and *Leptotrichia* ($p < 0.001$) were significantly higher in the healthy volunteer group (Supplementary Figure 3B). The heatmap of the relative abundance of the 63 genera, listed in Supplementary Table 4, is shown in Figure 2. We also analyzed PICU admission; however, intergroup differences were not observed at any taxonomic level (all FDR > 0.05).

We generated a cladogram using linear discriminant analysis (LDA) effect size analysis to identify the oropharynx-specific microbiota associated with pediatric IAV pneumonia by visually presenting all strata of differential species in the two groups

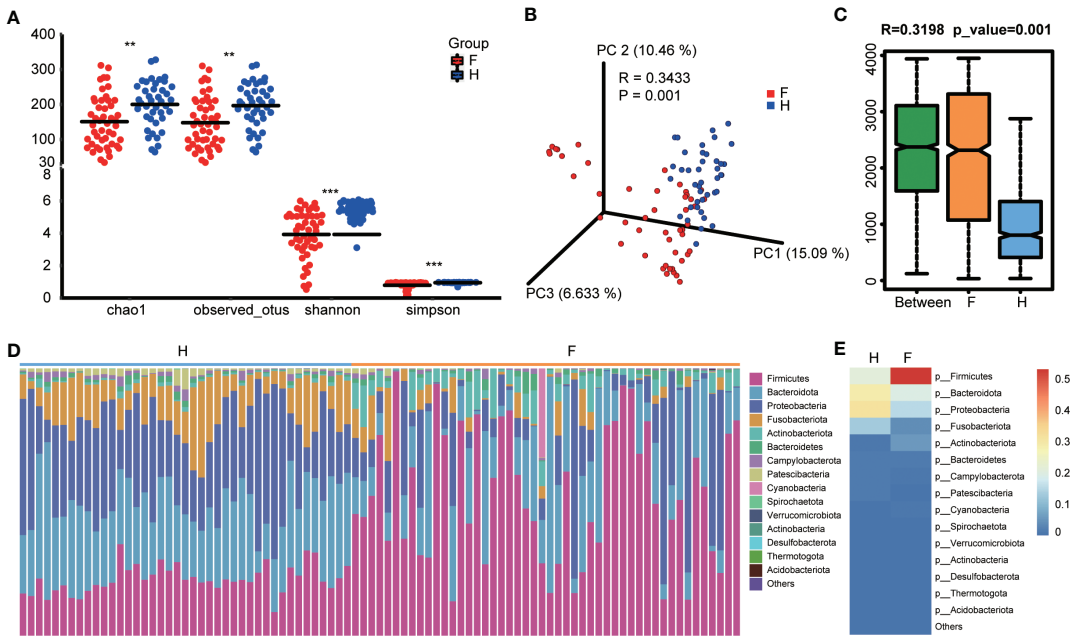

FIGURE 1
Diversity and structural analysis of the oropharyngeal microbiota. **(A)** Alpha diversity differences between the two groups were observed using the Simpson index, Shannon index, observed species, and chao1. $^{**}p < 0.05$; $^{***}p < 0.001$; F, IAV pneumonia group (red); H, healthy group (blue). **(B)** PCoA plot based on the Bray–Curtis distance matrix reflects the difference in bacterial structure between the two groups. F, IAV pneumonia group (red); H, healthy group (blue). **(C)** Through unweighted unifrac analysis of similarity, we discovered that the difference between groups was significantly greater than within groups. F, IAV pneumonia group (yellow); H, healthy group (blue). **(D)** Relative abundances of the top 15 phyla in each group. F, IAV pneumonia group (yellow); H, healthy group (blue). **(E)** The heatmap reflects the similarities and differences in phylum composition between the two groups in terms of color gradients. IAV, influenza A virus.

(Figure 3A). Significant differences were observed between the oropharyngeal microbiota of the two groups in 48 ASVs (LDA > 4), with relatively high abundances of *Actinomyces*, *Streptococcus*, *Lactobacillales*, and *Veillonellaceae* (all LDA scores $\log_{10} > 4$) in the IAV pneumonia group. In contrast, the abundances of *Bacteroidales*, *Porphyromonas*, *Haemophilus*, *Neisseria*, *Streptobacillus*, and *Prevotella* were significantly higher in the healthy volunteer group (all LDA scores $\log_{10} > 4$) than in the IAV pneumonia group. Thirty-two ASVs were enriched in the healthy volunteer group and sixteen ASVs in the IAV pneumonia group, suggesting higher abundances in the healthy volunteer group. These results indicate a lower abundance of microbiota in the IAV pneumonia group. Hence, there was a difference in the abundance of the oropharyngeal microbiota between the two groups (Figure 3B).

General characteristics of the oropharyngeal metabolome in each group

We expected that the oropharyngeal microbiota in children with IAV pneumonia would partially influence oropharyngeal metabolic pathways, based on previous mono-omics studies that demonstrated a high correlation between IAV infection and the microbiome and metabolome (Ohno et al., 2020; Gierse et al., 2021). Therefore, LC-MS/MS-based untargeted metabolomics were used to identify and quantify 591 metabolites from 91 oropharyngeal samples from the two groups (Supplementary Table 5).

Discriminatory oropharyngeal metabolites

Significant variations in metabolic phenotypes were detected between the two groups in the OPLS-DA model, implying that patients with IAV pneumonia had a distinct metabolic profile (R^2X (cum) = 0.357, R^2Y (cum) = 0.985, Q^2 (cum) = 0.974, $p < 0.001$) (Figure 4A). The permutation test revealed no overfitting and that the OPLS-DA model was remarkably robust(n = 200; Figure 4B). In order to see the general distribution, we displayed the results of the differential metabolite screening as volcano plots. The IAV pneumonia group had relatively high abundances of 86 metabolites and relatively low abundances of 118 metabolites ($p < 0.05$; VIP > 1; Supplementary Table 6, Figure 4C). Sphingosine, L-valine, 3,4-dimethylbenzoic acid, and N-acetyl-L-tyrosine were

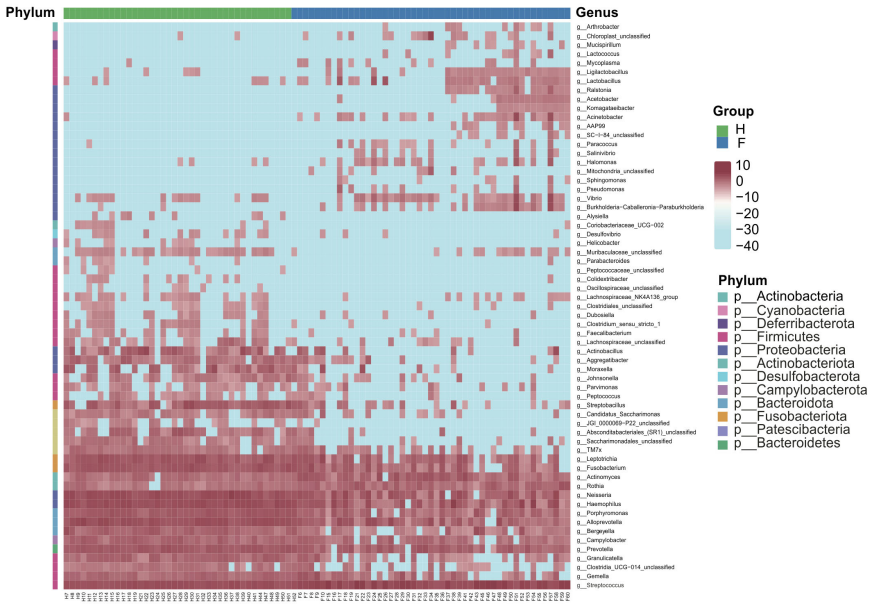

FIGURE 2
The two groups have similarities and differences in composition at the phyla and genera levels. The data after Z-transformation showed the abundance of genera, which was lower in the blue section and higher in the red section. F, IAV pneumonia group (blue); H, healthy group (green). IAV, influenza A virus.

significantly reduced in the IAV pneumonia group, according to a matchstick graph of differential metabolites. In contrast, phytosphingosine, sphinganine, succinic acid, pyruvic acid, propionic acid, and hydroxypropionic acid increased significantly in the IAV pneumonia group (Figure 4D).

Revealing discriminatory metabolites by different analytical methods

The identified discriminatory metabolites were usually functionally similar and biologically complementary to each other. Hierarchical cluster analysis (HCA) revealed that in the healthy volunteer group, abundant metabolites were glycerophosphocholine {PC[16:1(9Z)/20:1(11Z)]}, amino acid metabolites (beta-tyrosine, L-valine, and N-acetyl-L-tyrosine), and lipids and lipid-like molecules (bauerenyl acetate, isohyodeoxycholic acid, lithocholic acid, and alpha-tocopherol acetate). In contrast, the IAV pneumonia group displayed relatively high levels of amino acid metabolites (L-arginine, leucyl-isoleucine, and N-ethylglycine), sphingolipid metabolites (sphinganine and phytosphingosine), propanoate metabolites (propionic acid, succinic acid, and hydroxypropionic acid), and alpha hydroxy acids and derivatives (D-lactic acid). Significant changes in the oropharyngeal metabolome occurred in the disease group, with lipid metabolism being the most pronounced. Lipid metabolites represented 31.4% of the 204 discriminatory metabolites (64/204; Figure 5). Total oropharyngeal metabolites were mapped to 47 KEGG metabolic pathways *via* KEGG annotation and classification of metabolites. The enriched metabolites were associated with propanoate metabolism (4 metabolites), sphingolipid metabolism (5 metabolites), ABC transporters (23 metabolites), tyrosine metabolism (10 metabolites), and nicotinate and nicotinamide metabolism (9 metabolites). We identified the differential metabolic pathways involved in IAV pneumonia by KEGG annotation. Compared to healthy controls, metabolic pathway analysis of patients with IAV pneumonia revealed 36 pathways with differently abundant metabolites (Figure 6A). The results of the metabolic pathway analysis are shown in the bubble plots in Figure 6B, where the differences in propanoate and sphingolipid metabolism are significant ($p < 0.05$; Supplementary Tables 7, 8).

Based on previous results and the known importance of the role of sphingolipid metabolites in viral infectious diseases, we defined discriminatory metabolites in the sphingolipid metabolic pathway as potential biomarkers for IAV pneumonia (Avota et al., 2021). Sphinganine (area under curve [AUC], 0.857; $p < 0.001$), phytosphingosine (AUC, 0.810; $p < 0.001$), and sphingosine (AUC, 0.798; $p < 0.001$) were significantly related to IAV pneumonia. A previous study revealed that an elevated sphinganine-to-sphingosine (S_a/S_o) ratio indicated a disturbance

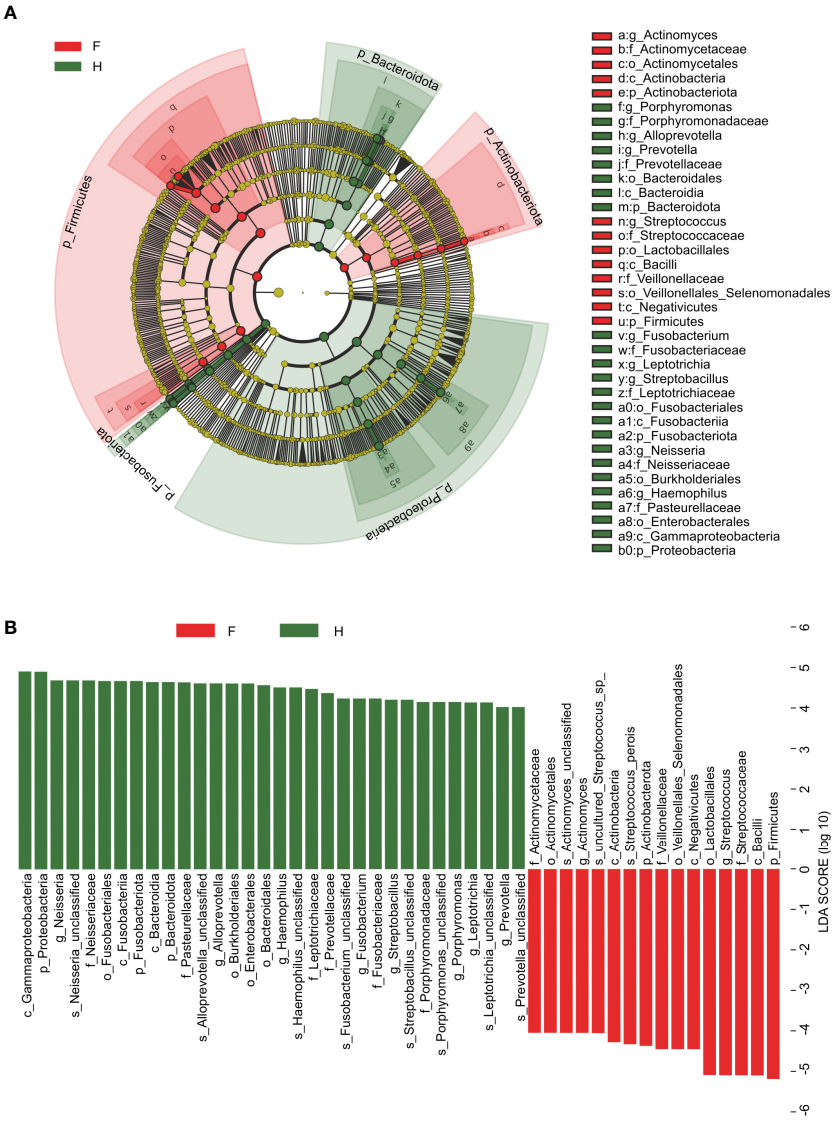

FIGURE 3
Linear discriminant analysis (LDA) and LDA effect size. **(A)** The cladogram visually indicates the differential species in each level in each group. F, IAV for abstract pneumonia group (red); H, healthy group (green). **(B)** Histogram of LDA scores for different abundant genera between groups H and (F) Red, enriched in the F group; Green, enriched in the H group. F, IAV pneumonia group; H, healthy group; IAV, influenza A virus.

in sphingolipid biosynthesis, which was correlated with the host's inflammatory response (Antonissen et al., 2015). Our investigation indicated that the S_a/S_o ratio (AUC, 0.916; $p < 0.001$) was also associated substantially with IAV pneumonia. Furthermore, analysis of the combined diagnosis using sphingosine, phytosphingosine, and sphinganine yielded an AUC of 0.939 ($p < 0.001$), indicating a close correlation between the three metabolites and IAV pneumonia in children. Therefore, oropharyngeal sphingolipid metabolites could serve as another powerful diagnostic tool and biomarkers for IAV pneumonia in children (Figure 7).

Multi-omics analysis method reveals the association between the oropharyngeal microbiome and metabolites for the two groups

Based on the results of our study, 10 genera (LEfSe LDA > 4and p <0.05) and 26 metabolites differentially expressed (VIP >1 and p <0.05) were used to verify the changes in the correlation between genera and metabolites in the oropharynx of children with IAV pneumonia. Most discriminatory oropharyngeal metabolites were significantly correlated with differential

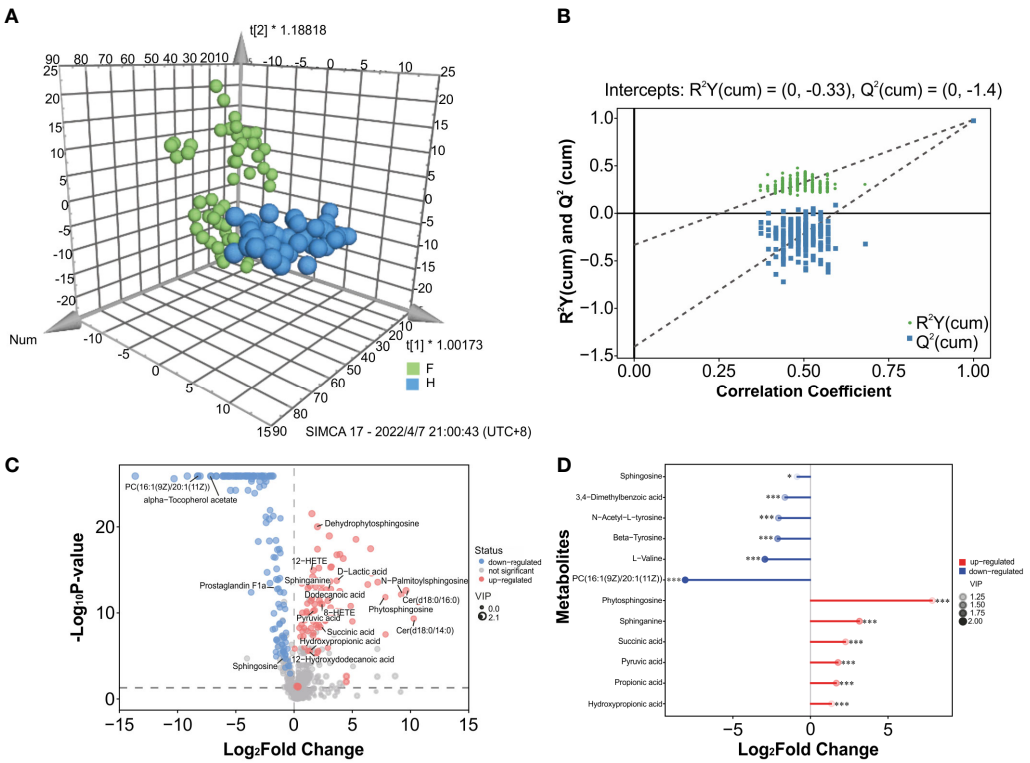

FIGURE 4
Metabolite differences between the IAV pneumonia group F and the healthy group H. **(A)** The OPLS-DA 3D plot of the oropharyngeal samples from both groups ($p < 0.001$) are shown. F, IAV pneumonia group (green circle); H, healthy group (blue circle). **(B)** The OPLS-DA permutation test indicates good model robustness, with no overfitting (n = 200). **(C)** Volcano plots showing differences in oropharyngeal metabolites between children with IAV pneumonia and healthy controls: upregulated metabolites (red circles), downregulated metabolites (blue circles). **(D)** Important discriminatory metabolites are displayed on the matchstick diagram. *p < 0.05; ***p < 0.001. The abscissa shows the log-transformed change multiple, and the dot color depth represents the VIP value size. IAV, influenza A virus.

microbiomes and the trends in their variations were consistent (|r| >0.3 and p <0.05). The significantly increased abundance of the genus, *Streptococcus*, was positively correlated with the significantly increased metabolites in the IAV pneumonia group, including sphinganine (r = 0.3255, p = 0.0019), phytosphingosine (r = 0.3560, p = 0.0007), N-palmitoylsphingosine (r = 0.3476, p = 0.0009), and L-arginine (r = 0.5021, p < 0.001), and negatively correlated with the significantly less abundant metabolites in the IAV pneumonia group, including β–tyrosine (r = -0.4305, p < 0.001) and PC (16:1 (9Z)/20:1(11Z)) (r = -0.3867, p = 0.0002). Furthermore, the higher abundance of the genus, *Actinomyces*, in the IAV pneumonia group was positively correlated with significantly more abundant metabolites in this group, including succinic acid (r = 0.3232, p = 0.0020) and propionic acid (r = 0.3416, p = 0.0011). However, there were no significant correlations between *Actinomyces* and phytosphingosine, and between sphinganine and N-palmitoylsphingosine. Moreover, the genera enriched in the healthy volunteer group, such as *Haemophilus*, were positively correlated with the most abundant metabolites from this group, including β-tyrosine (r = 0.5890, p < 0.001), L-valine (r = 0.5274, p < 0.001), and prostaglandin F1a (r = 0.4594, p < 0.001), and negatively correlated with the least abundant metabolites in this group, including sphinganine (r = -0.4163, p < 0.001) and phytosphingosine (r = -0.4082, p < 0.001; Figure 8, Supplementary Table 9).

Discussion

This study confirmed that IAV pneumonia in pediatric patients is associated with changes in the structure of the oropharyngeal microbiota and its metabolites and that these two factors are significantly correlated and consistent in terms of variation trends. Therefore, we combined two omics to identify potential biomarkers associated with IAV pneumonia in children. There are four types of influenza viruses, among which IAV infection (especially H1N1) causes more severe

FIGURE 5
Hierarchical cluster analysis (HCA) was performed using quantitative values of differential metabolites in two groups. The horizontal coordinates represent the grouping, and the vertical coordinates represent the differential metabolites in the group. Red indicates high expression, whereas blue indicates low expression. F, IAV pneumonia group (blue); H, healthy group (green). IAV, influenza A virus.

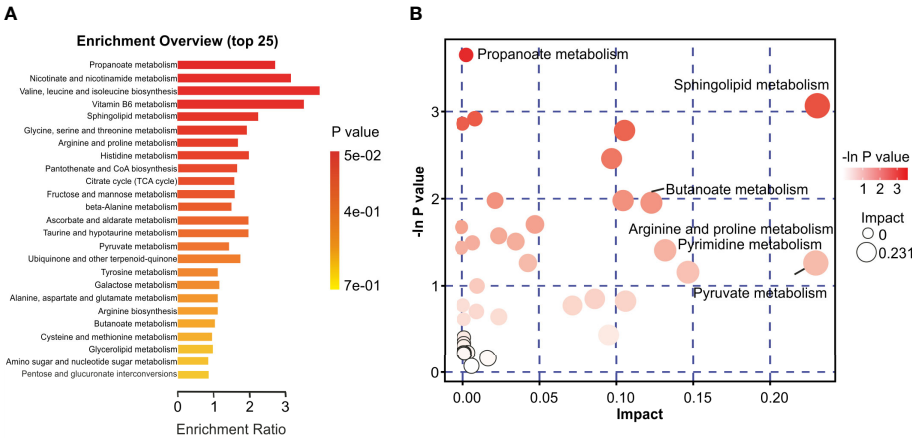

FIGURE 6
Characteristics of the oropharyngeal metabolome in IAV pneumonia and healthy volunteer groups. **(A)** Differential Pathway enrichment analysis based on differential metabolites between the two groups. **(B)** The crucial pathway with the highest correlation with metabolite differences between groups F and H was identified following metabolic pathway analysis of differential metabolites. In the bubble chart, each bubble represents a metabolic pathway. The X-axis and bubble size indicate the size of the impact value of the pathway; the Y-axis and bubble color indicate the p-value ($-\ln_p$) of the enrichment analysis. F, IAV pneumonia group; H, healthy group; IAV, influenza A virus.

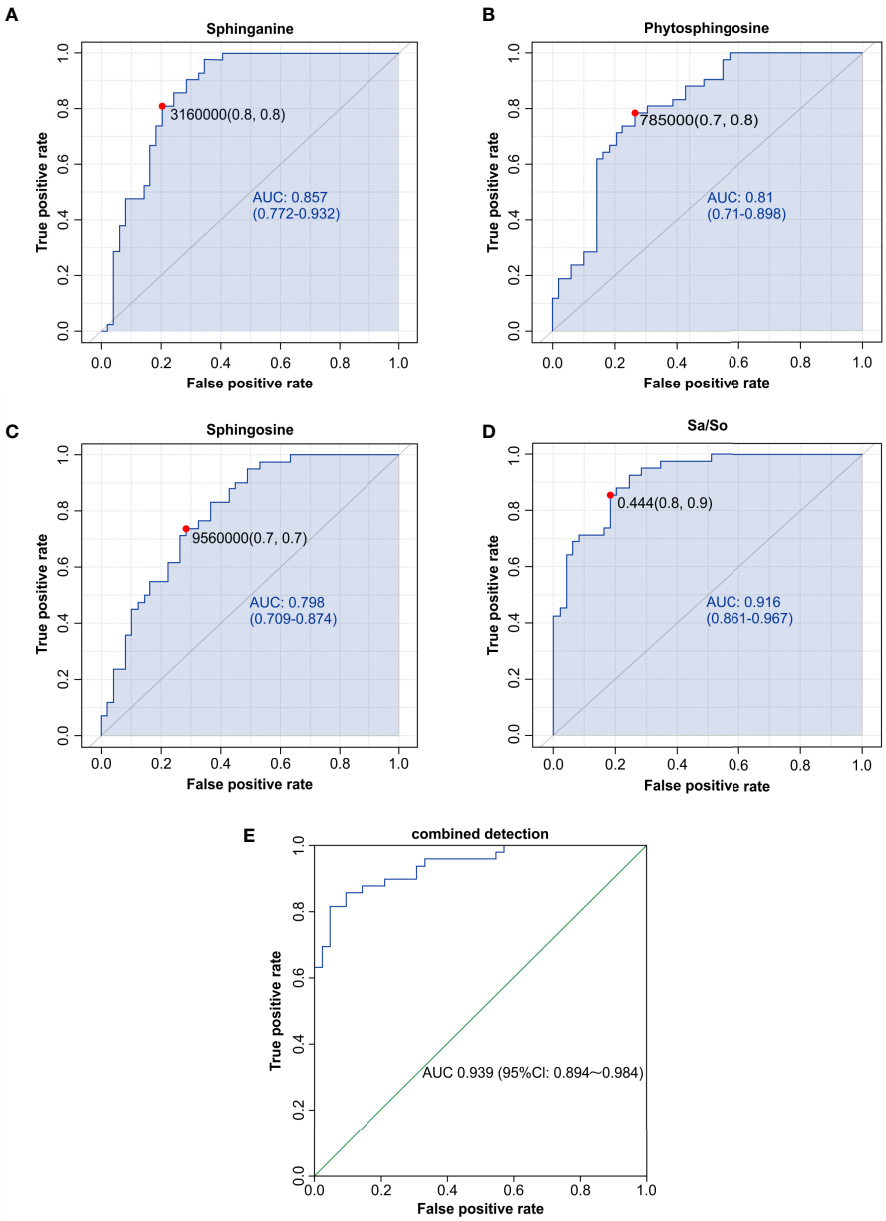

FIGURE 7
Sphingolipid metabolites, such as sphinganine **(A)**, phytosphingosine **(B)**, sphingosine **(C)**, the Sa/So ratio **(D)**, and the combination of multiple indicators **(E)**, were discovered to have high AUCs by ROC analysis and could be used as biomarkers for influenza-induced pneumonia in children. AUC, area under the curve; ROC, receiver operating characteristic.

illness in patients (Drews et al., 2019; Gaitonde et al., 2019). Viruses have applied multiple strategies to evade the host's immune response, including an antigenic shift to evade vaccine protection. Furthermore, first line anti-influenza drugs are limited in terms of time of administration and drug resistance; this requires the development of drugs that target the metabolic mechanisms (Hurt, 2014; Zumla et al., 2016). The oropharynx is a space shared by the external environment, the respiratory system, and the digestive system, and serves as a major source of the microbiome in the lower respiratory tract, explains the striking similarity between the composition of the microbiota in the oropharynx and that in the lower respiratory tract (Sahin-Yilmaz and Naclerio, 2011; Bassis et al., 2015). The oropharyngeal mucosal epithelium is a vital defense barrier of the human body that can protect directly or indirectly against invading pathogens. With technological advancements, studies of oropharyngeal and nasopharyngeal microbiomes and metabolomes have become feasible (Marangoni et al., 2020;

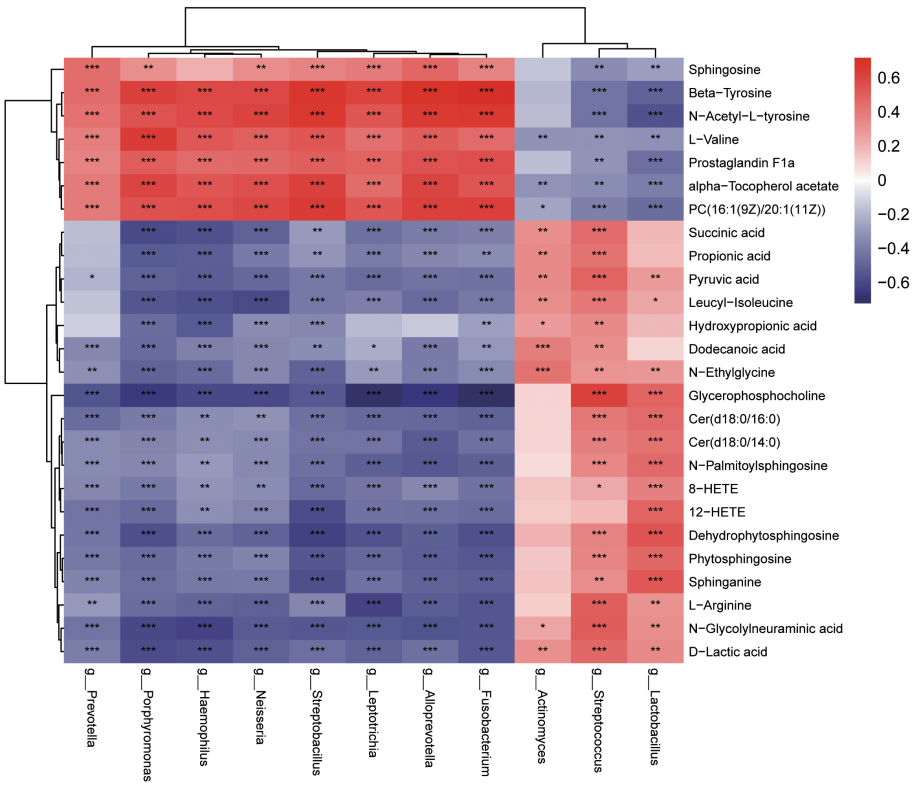

FIGURE 8
Heatmaps indicate the Spearman rank-correlation coefficients for the relative abundance of differential oropharyngeal microbiota at the genus level and differential metabolites in children with IAV pneumonia and healthy controls. Positive correlation is depicted using red, whereas negative correlation is depicted using blue. *$p < 0.05$; **$p < 0.01$; ***$p < 0.001$; IAV, influenza A virus.

Ma et al., 2021). Pediatric patients and their family members relatively comply with oropharyngeal swab sampling due to its non-invasive nature (Huang et al., 2020).

Our study showed significant changes in the composition of the oropharyngeal microbiota of pediatric patients with IAV pneumonia, such as a significant decrease in the abundance and diversity of the microbiota and an increase in the heterogeneity of the bacterial community structure, which is consistent with previous findings. (Hanada et al., 2018). The disease group showed higher Firmicutes at the phylum level, while the healthy group showed higher Bacteroidota and Proteobacteria. Studies on the oropharyngeal microbiota in adult patients with IAV pneumonia have also revealed significantly higher abundances of Firmicutes and Proteobacteria, consistent with this study (Leung et al., 2013). At the genus level, the abundances of *Streptococcus* and *Actinomyces* were significantly higher in the IAV pneumonia group. Previous studies suggest that specific microbial communities in the respiratory mucosa directly or indirectly influence the host's defense against viral infections. The microbiota can influence viral infections through various mechanisms, including the promotion of viral replication, such as stabilization of viral particles, modulation of the host immune response to viral infections, and the promotion of adenovirus reactivation by metabolites of bacterial short-chain fatty acids (SCFAs), which cause recurrent respiratory infections in children (Wang et al., 2021; Wirusanti et al., 2022).In childhood, IAV infections that are more dependent on innate immune responses, the immune system preferentially uses T helper 2 cell (Th-2) responses associated with γ δ T cells, which may be less favorable than the Th-1 antiviral immune response in adults; also, this is influenced to some extent by the gut microbiome (Sakleshpur and Steed, 2022). Furthermore, viral infection-induced host antiviral immune responses can disrupt the microbiota structure and function (Hanada et al., 2018). Viral infections usually increase glucose uptake and fermentation processes, thus altering the composition of the microbiota and clinical symptoms (Shibata et al., 2020). Studies have shown that IAV inhibits bacterial-induced interleukin-1β (IL-1β) production and impairs host defense against bacterial infection. IL-10 production by regulatory T (T Reg) cells has the potential to induce susceptibility to secondary bacterial infections, and serum levels of IL-1β and IL-10 are elevated in children secondary to Streptococcus pyogenes infection one week after IAV infection, while decreasing with symptom

improvement, which seems to indicate that IAV infection and secondary Streptococcus infection also enhance pulmonary toxicity in children, but this needs to be confirmed by further studies (Bedoya et al., 2013; Ochi et al., 2018). According to these investigations, bacterial-viral interactions play an important role in disease development (Bai et al., 2022; Mirzaei et al., 2022).

Interestingly, the study discovered that the IAV pneumonia group had much greater levels of *Streptococcus* and *Actinomycetes* at the genus level. However, in previous studies, children infected with IAV show a higher abundance of *Streptococcus* in the nasopharynx and lower abundances of *Streptococcus* and *Neisseria* in the oropharynx during the early phase of infection (Wen et al., 2018). Using a decision tree evaluation by random forest analysis, Zhou et al. (2020) demonstrated that elevated Ralstonia and Acidobacteria in oropharyngeal samples could better distinguish between healthy groups and respiratory infections groups such as IAV and Mycoplasma pneumoniae infections, consistent with our study. Existing studies suggested that nasopharyngeal secretions can drip down the posterior part of the nasal cavity into the oropharynx or lungs, resulting in migration of nasal microbes into the lungs. The immune barrier and the indigenous microbiota in the respiratory tract gradually eliminate nasal microbes to restore homeostasis (Gu et al., 2019). Entering virus particles can bind to the respiratory colonization microbiota and stimulate local microbiota reproduction and diffusion to the upper and lower respiratory tracts when infected with IAV; however, this follows viral infection by a few days and correlates with lower respiratory macrophage loss (Mina et al., 2015). Dynamic changes in the structure of the gut microbiota over time and an increase in the abundance of several bacterial genera, including *Acinetobacter* and *Streptococcus*, were observed on day 7 after infection in mouse models infected with influenza A (Gu et al., 2019). In children, the vulnerability to secondary bacterial superinfection often manifests one week after influenza infection, and much research has sought to understand the immunological mechanism of IAV exacerbated by bacterial superinfection (Ochi et al., 2018). In our study, the mean time to the onset of influenza symptoms was seven days at the time of admission of children with IAV pneumonia, and the patients had a significant increase in oropharyngeal *Streptococcus*. These studies suggest that the abundance of oropharyngeal *Streptococcus* in children is altered following IAV infection, which may exacerbate lung injury and the disease. However, more studies are needed to understand how changes in the microbiota in children affect different responses of the immune system to IAV infection and the mechanisms by which lung injury occurs. There is the potential to confer beneficial immunomodulatory effects through microbiological interventions and to assist in targeted clinical treatment.

Significant changes in the oropharyngeal metabolome of study participants with IAV pneumonia were observed, the most significant changes in lipid metabolism. Pathway enrichment analyses revealed significant changes in propanoate and sphingolipid metabolism. Previous studies in human lung epithelial cells and animal models revealed alterations in lipids, carbohydrates, and related molecules, nucleosides, and other metabolites following influenza virus infection, which follows the present findings (Cui et al., 2016; Tisoncik-Go et al., 2016; Tian et al., 2019). Sphingolipid metabolites are essential components of the lipid bilayer and the extracellular fluid. They serve as signaling molecules in normal cellular physiological processes and pathological inflammatory conditions (Avota et al., 2021). sphingosine, sphinganine, and phytosphingosine are categorized as long-chain sphingolipid bases and are essential in cellular apoptosis as sphingolipid structural analogs (Nagahara et al., 2005). Therefore, sphingosine, phytosphingosine, sphinganine, the S_a/S_o ratio, and the combination of the three metabolites showed good diagnostic value in children with IAV pneumonia.

IAV primarily targets mucosal epithelial cells in the respiratory tract (Lee et al., 2018). Viruses must interact with cell membranes to attach and infiltrate cells as specialized intracellular pathogens. Sphingolipid metabolites perform various functions in virus-host interactions, including the promotion of virus binding and the entrance, reproduction, and release of new particles (Konan and Sanchez-Felipe, 2014; Drake et al., 2017). This study revealed a significantly lower abundance of sphingosine and significantly higher abundances of sphinganine and phytosphingosine in the IAV pneumonia group than in the healthy volunteer group. A previous study showed that phytosphingosine and sphingosine exert different levels of antimicrobial activity against several species of bacteria (Fischer et al., 2012). Adult patients with severe IAV infections also exhibit changes in the sphingolipid metabolites in their blood plasma, which is closely associated with respiratory failure and death. The bronchial mucosal epithelium acts as the host's first line of defense against respiratory infections, and sphingosine is a component of this epithelium. Sphingosine can inhabit various bacterial species *in vivo* and *in vitro*, serving as a natural antiseptic agent in the airways (Wendt et al., 2021). Sphingosine expression levels are significantly reduced in patients with cystic fibrosis and mouse models, resulting in an increased incidence of pulmonary infections, which are ameliorated by the sphingosine pathway or by inhalation of exogenous sphingosine (Grassmé et al., 2017). In addition, sphinganine protects lung tissue from invading pathogens, and significantly elevated serum levels of sphinganine in mouse models infected with SARS-CoV-2 are correlated with disease severity (Vitner et al., 2022). As a result, oropharyngeal sphingolipid metabolites may be useful as both diagnostic and therapeutic targets for childhood IAV pneumonia. Furthermore, pediatric patients with IAV had significantly elevated levels of propionic acid and succinic acid, resulting from propanoate metabolism and lower levels of L-valine. Propionic acid induces insulin resistance and hyperinsulinemia by

activating the sympathetic nervous system in mice (Tirosh et al., 2019). In addition, significantly higher serum levels of propionic acid were observed in patients with SARS-CoV-2 pneumonia, which could act as a potential biomarker of metabolic disorders related to COVID-19 (He et al., 2021). Elevated levels of succinic acid indicate an increased turn of the TCA cycle, whereas increased TCA turn rates and mitochondrial dysfunction can lead to oxidative stress in patients (Bolukbas et al., 2005; Li et al., 2015).

We also performed a multi-omics association analysis and discovered that discriminatory oropharyngeal microbiota was closely associated with discriminatory metabolites. For example, *Streptococcus* was positively correlated with sphinganine, phytosphingosine, and N-palmitoylsphingosine, suggesting that oropharyngeal microbiota and metabolites had consistent variation trends. Some investigations have discovered a strong correlation between elevated *Streptococcus* levels and the change in sphingolipid metabolites. Previous investigations on nasopharyngeal samples from infants with severe bronchiolitis found that the sphingolipid pathway is the most enriched sub-pathway positively correlated with abundance of Streptococcus (Stewart et al., 2017). In adult patients with community-acquired pneumonia, changes in *Streptococcus* in the respiratory tract were significantly correlated with pneumonia severity and were associated with changes in serum metabolites, including sphingolipid, pyruvate, and inositol phosphate (To et al., 2016). Studies indicate that the abundance of many species of *Streptococcus* has significantly increased in patients with chronic obstructive pulmonary disease (COPD). The increased abundance of the glucosyltransferase and LP_XTG-anchored adhesion domain in *streptococcus* enrichment suggests that the ability to the stick to surfaces was essential for increased abundance (Bowerman et al., 2020). Furthermore, bioactive sphingolipids are becoming evident in the regulation of cell adhesion, migration, and invasion, with sphinganine, phytosphingosine and sphingosine modulating bacterial adhesion, which may be a key point of interaction between Streptococcus and sphingolipid metabolites (Hannun and Obeid, 2018; Cukkemane et al., 2015). Metagenomic data analysis confirmed that *Streptococcus* produces serine, the substrate for sphinganine and the fundamental building block of all sphingolipids; therefore, exogenous serine produced by *Streptococcus* can contribute to a significant increase in airway metabolism (Stewart et al., 2017).However, the mechanisms involved need to be further explored. Furthermore, in this study, Lactobacillus and D-lactate in the oropharynx of children with IAV pneumonia were significantly elevated and positively correlated. Lactobacillus-produced D-lactic acid in the oropharynx may play a vital role in inhibiting *Streptococcus* colonization and proliferation (Yildiz et al., 2020). These results demonstrate that pediatric patients with IAV pneumonia show changes in the oropharyngeal microbiota and its metabolites during acute infections and that significant correlations between the oropharyngeal microbiota and oropharyngeal metabolites can be identified. Combining these findings, we found that IAV pneumonia leads to an altered abundance of specific microbiota in the airways and alters host cell metabolism. On the one hand, the oropharyngeal microbiota can contribute to the altered severity of IAV pneumonia by modulating host cell function and metabolism (e.g., sphingolipid metabolism). However, the abundance of specific microbiota (e.g., *Streptococcus*) is altered following changes in host metabolism. Our findings should support future research into the potential processes relating these changes in the microbiota, host immune system, and airway metabolism to IAV development. These findings are highly significant for early disease prediction, evaluation, and intervention.

We adopted a multi-omics analytical approach and revealed significant changes in the oropharyngeal microbiota and metabolites, as well as significant correlations between the two factors in pediatric patients with IAV pneumonia. Oropharyngeal swabbing serves as a convenient, effective, and non-invasive sampling method that facilitates scientific evaluation. However, this study has several limitations. Because our findings are based on data collected from a single center with a relatively small sample size, more multicenter studies that use larger datasets are needed to validate our metagenomic and metabolomic findings. Furthermore, we performed comparative analyzes between pediatric patients with IAV infection only and healthy children; therefore, the generalizability of the findings of our study to pediatric patients with mixed infections is unclear. In subsequent studies, other important respiratory viruses should be included in comparative analyzes to optimize the evaluation of the available molecular diagnostic approaches. Finally, although the selection of subjects included in this study was rigorous, ethically,children with pneumonia are required to receive medication as soon as possible.There may still be various potential factors affecting the microbiome and metabolome. In a subsequent investigation, we will set up a more thorough longitudinal study to reduce confounders and dynamically track changes in the respiratory microbiome and metabolome of IAV-infected children. However, the results of this preliminary study provide important clues for understanding the respiratory microbiome and metabolome associations in children with IAV pneumonia and to explore potential predictors and more effective treatment options.

Conclusions

This study comprehensively analyzes the mechanism of the oropharyngeal microbiota and its metabolites compared to previous mono-omics studies of IAV pneumonia among pediatric patients. Oropharyngeal samples from pediatric patients with IAV pneumonia can be successfully differentiated from those of healthy children using LC-MS/MS-based untargeted metabolomics and high throughput 16S rRNA gene

sequencing-based microbiome analysis. Pediatric patients with IAV pneumonia had significantly lower abundance and diversity of the oropharyngeal microbiota than healthy children, with significant changes in the abundance of bacterial species such as *Streptococcus*, *Rothia*, and *Haemophilus*. Furthermore, significant intergroup differences in oropharyngeal metabolites were observed. Among them, the sphingolipid metabolites, sphingosine, sphinganine, and phytosphingosine were identified as important discriminatory oropharyngeal metabolites. These three metabolites, the S_a/S_o ratio, and the combination of these three metabolites showed high diagnostic efficacy in pediatric patients with IAV pneumonia. The characteristic changes in the oropharyngeal microbiota and metabolites indicate they can serve as efficient and non-invasive diagnostic biomarkers, and even therapeutic targets for pediatric patients with IAV pneumonia. More long-term confirmatory studies are required in a larger patient population across different geographic regions and ethnic groups to validate these hypotheses.

Data availability statement

The datasets presented in this study can be found in online repositories. The names of the repository/repositories and accession number(s) can be found in the article/Supplementary Material.

Ethics statement

The studies involving human participants were reviewed and approved by The Medical Ethics Committee of Shenzhen Children's Hospital, China Medical University (registration number: 202009202). Written informed consent to participate in this study was provided by the participants' legal guardian/next of kin.

Author contributions

Conceptualization: QH, FW, and WW. Methodology: QH and UY. Formal analysis: QH and YF. Data curation: BL and QH. Software: YF. Writing-original draft preparation: QH and YF. Writing-review and editing: YZ, UY, and WW. All authors contributed to the article and approved the submitted version.

Funding

This study was supported by the Shenzhen Fundamental Research Program (JCYJ20190809170007587), Shenzhen Fund for Guangdong Provincial High-level Clinical Key Specialties (SZGSP012), Shenzhen Key Medical Discipline Construction Fund (SZXK032) and the Shenzhen Science and Technology Innovation Commission (RCBS20200714114858018).

Acknowledgments

We thank the recruited children and their parents who participated in the research. We thank Editage (www.editage.cn) for English language editing.

Conflict of interest

The authors declare that the research was conducted in the absence of any commercial or financial relationships that could be construed as a potential conflict of interest.

Publisher's note

Supplementary material

The Supplementary Material for this article can be found online at: https://www.frontiersin.org/articles/10.3389/fcimb.2022.1011254/full#supplementary-material

References

Anand, S., Kaur, H., and Mande, S. S. (2016). Comparative in silico analysis of butyrate production pathways in gut commensals and pathogens. *Front. Microbiol.* 7. doi: 10.3389/fmicb.2016.01945

Antonissen, G., Croubels, S., Pasmans, F., Ducatelle, R., Eeckhaut, V., Devreese, M., et al. (2015). Fumonisins affect the intestinal microbial homeostasis in broiler chickens, predisposing to necrotic enteritis. *Vet. Res.* 46 (1), 98. doi: 10.1186/s13567-015-0234-8

Avota, E., Bodem, J., Chithelen, J., Mandasari, P., Beyersdorf, N., and Schneider-Schaulies, J. (2021). The manifold roles of sphingolipids in viral infections. *Front. Physiol.* 12. doi: 10.3389/fphys.2021.715527

Bai, G. H., Lin, S. C., Hsu, Y. H., and Chen, S. Y. (2022). The human virome: Viral metagenomics, relations with human diseases, and therapeutic applications. *Viruses* 14 (2), 278. doi: 10.3390/v14020278

Bassis, C. M., Erb-Downward, J. R., Dickson, R. P., Freeman, C. M., Schmidt, T. M., Young, V. B., et al. (2015). Analysis of the upper respiratory tract microbiotas as the source of the lung and gastric microbiotas in healthy individuals. *mBio* 6 (2), e00037. doi: 10.1128/mBio.00037-15

Bedoya, F., Cheng, G. S., Leibow, A., Zakhary, N., Weissler, K., Garcia, V., et al. (2013). Viral antigen induces differentiation of Foxp3+ natural regulatory T cells in influenza virus-infected mice. *J. Immunol.* 190 (12), 6115–6125. doi: 10.4049/jimmunol.1203302

Bolukbas, C., Bolukbas, F. F., Horoz, M., Aslan, M., Celik, H., and Erel, O. (2005). Increased oxidative stress associated with the severity of the liver disease in various forms of hepatitis b virus infection. *BMC Infect. Dis.* 5, 95. doi: 10.1186/1471-2334-5-95

Bowerman, K. L., Rehman, S. F., Vaughan, A., Lachner, N., Budden, K. F., Kim, R. Y., et al. (2020). Disease-associated gut microbiome and metabolome changes in patients with chronic obstructive pulmonary disease. *Nat. Commun.* 11 (1), 5886. doi: 10.1038/s41467-020-19701-0

Bowler, R. P., Wendt, C. H., Fessler, M. B., Foster, M. W., Kelly, R. S., Lasky-Su, J., et al. (2017). New strategies and challenges in lung proteomics and metabolomics. an official American thoracic society workshop report. *Ann. Am. Thorac. Soc* 14 (12), 1721–1743. doi: 10.1513/AnnalsATS.201710-770WS

Cui, L., Zheng, D., Lee, Y. H., Chan, T. K., Kumar, Y., Ho, W. E., et al. (2016). Metabolomics investigation reveals metabolite mediators associated with acute lung injury and repair in a murine model of influenza pneumonia. *Sci. Rep.* 6, 26076. doi: 10.1038/srep26076

Cukkemane, N., Bikker, F. J., Nazmi, K., Brand, H. S., Sotres, J., Lindh, L., et al. (2015). Anti-adherence and bactericidal activity of sphingolipids against streptococcus mutans. *Eur. J. Oral. Sci.* 123 (4), 221–227. doi: 10.1111/eos.12200

Dawood, F. S., Chaves, S. S., Pérez, A., Reingold, A., Meek, J. , Farley, M. M., et al. (2014). Emerging infections program network. complications and associated bacterial coinfections among children hospitalized with seasonal or pandemic influenza, united states 2003-2010. *J. Infect. Dis.* 209 (5), 686–694. doi: 10.1093/infdis/jit473

de Onis, M., Onyango, A. W., Borghi, E., Siyam, A., Nishida, C., and Siekmann, J. (2007). Development of a WHO growth reference for school-aged children and adolescents. *Bull. World Health Organ* 85 (9), 660–667. doi: 10.2471/blt.07.043497

Drake, M. J., Brennan, B., Briley, K. J., Bart, S. M., Sherman, E., Szemiel, A. M., et al. (2017). A role for glycolipid biosynthesis in severe fever with thrombocytopenia syndrome virus entry. *PloS Pathog.* 13 (4), e1006316. doi: 10.1371/journal.ppat.1006316

Drews, K., Calgi, M. P., Harrison, W. C., Drews, C. M., Costa-Pinheiro, P., Shaw, J. J. P., et al. (2019). Glucosylceramidase maintains influenza virus infection by regulating endocytosis. *J. Virol.* 93 (12), e00017–e00019. doi: 10.1128/jvi.00017-19

Fischer, C. L., Drake, D. R., Dawson, D. V., Blanchette, D. R., Brogden, K. A., and Wertz, P. W. (2012). Antibacterial activity of sphingoid bases and fatty acids against gram-positive and gram-negative bacteria. *Antimicrob. Agents. Chemother.* 56 (3), 1157–1161. doi: 10.1128/aac.05151-11

Fouchier, R. A., Munster, V., Wallensten, A., Bestebroer, T. M., Herfst, S., Smith, D., et al. (2005). Characterization of a novel influenza a virus hemagglutinin subtype (H16) obtained from black-headed gulls. *J. Virol.* 79 (5), 2814–2822. doi: 10.1128/jvi.79.5.2814-2822.2005

Frau, A., Ijaz, U. Z., Slater, R., Jonkers, D., Penders, J., Campbell, B. J., et al. (2021). Inter-kingdom relationships in crohn's disease explored using a multi-omics approach. *Gut Microbes* 13 (1), 1930871. doi: 10.1080/19490976.2021.1930871

Gaitonde, D. Y., Moore, F. C., and Morgan, M. K. (2019). Influenza: Diagnosis and treatment. *Am. Fam. Phys.* 100 (12), 751–758.

Gierse, L. C., Meene, A., Schultz, D., Schwaiger, T., Schröder, C., Mücke, P., et al. (2021). Influenza a H1N1 induced disturbance of the respiratory and fecal microbiome of German landrace pigs - a multi-omics characterization. *Microbiol. Spectr.* 9 (2), e0018221. doi: 10.1128/Spectrum.00182-21

Gounder, A. P., and Boon, A. C. M. (2019). Influenza pathogenesis: The effect of host factors on severity of disease. *J. Immunol.* 202 (2), 341–350. doi: 10.4049/jimmunol.1801010

Grassmé, H., Henry, B., Ziobro, R., Becker, K. A., Riethmüller, J., Gardner, A., et al. (2017). β1-integrin accumulates in cystic fibrosis luminal airway epithelial membranes and decreases sphingosine, promoting bacterial infections. *Cell Host Microbe* 21 (6), 707–718.e8. doi: 10.1016/j.chom.2017.05.001

Gu, L., Deng, H., Ren, Z., Zhao, Y., Yu, S., Guo, Y., et al. (2019). Dynamic changes in the microbiome and mucosal immune microenvironment of the lower respiratory tract by influenza virus infection. *Front. Microbiol.* 10. doi: 10.3389/fmicb.2019.02491

Hanada, S., Pirzadeh, M., Carver, K. Y., and Deng, J. C. (2018). Respiratory viral infection-induced microbiome alterations and secondary bacterial pneumonia. *Front. Immunol.* 9. doi: 10.3389/fimmu.2018.02640

Hannun, Y. A., and Obeid, L. M. (2018). Sphingolipids and their metabolism in physiology and disease. *Nat. Rev. Mol. Cell Biol.* 19 (3), 175–191. doi: 10.1038/nrm.2017.107

He, X., Liu, C., Peng, J., Li, Z., Li, F., Wang, J., et al. (2021). COVID-19 induces new-onset insulin resistance and lipid metabolic dysregulation *via* regulation of secreted metabolic factors. *Signal Transduction Targeting Ther.* 6 (1), 427. doi: 10.1038/s41392-021-00822-x

Hogan, C. A., Rajpurkar, P., Sowrirajan, H., Phillips, N. A., Le, A. T., Wu, M., et al. (2021). Nasopharyngeal metabolomics and machine learning approach for the diagnosis of influenza. *EBio Med.* 71, 103546. doi: 10.1016/j.ebiom.2021.103546

Hsing, T. Y., Lu, C. Y., Chang, L. Y., Liu, Y. C., Lin, H. C., Chen, L. L., et al. (2022). Clinical characteristics of influenza with or without streptococcus pneumoniae co-infection in children. *J. Formos Med. Assoc.* 121 (5), 950–957. doi: 10.1016/j.jfma.2021.07.012

Huang, N., Perez, P., Kato, T., Mikami, Y., Okuda, K., Gilmore, R. C., et al. (2020)Integrated single-cell atlases reveal an oral SARS-CoV-2 infection and transmission axis (Accessed July 11, 2022).

Hurt, A. C. (2014). The epidemiology and spread of drug resistant human influenza viruses. *Curr. Opin. Virol.* 8, 22–29. doi: 10.1016/j.coviro.2014.04.009

Iuliano, A. D., Roguski, K. M., Chang, H. H., Muscatello, D. J., Palekar, R., Tempia, S., et al. (2018). Estimates of global seasonal influenza-associated respiratory mortality: a modelling study. *Lancet* 391 (10127), 1285–1300. doi: 10.1016/s0140-6736(17)33293-2

Jaurila, H., Koivukangas, V., Koskela, M., Gäddnäs, F., Myllymaa, S., Kullaa, A., et al. (2020). ^{1}H NMR based metabolomics in human sepsis and healthy serum. *Metabolites* 10 (2), 70. doi: 10.3390/metabo10020070

Konan, K. V., and Sanchez-Felipe, L. (2014). Lipids and RNA virus replication. *Curr. Opin. Virol.* 9, 45–52. doi: 10.1016/j.coviro.2014.09.005

Lee, S., Hirohama, M., Noguchi, M., Nagata, K., and Kawaguchi, A. (2018). Influenza a virus infection triggers pyroptosis and apoptosis of respiratory epithelial cells through the type I interferon signaling pathway in a mutually exclusive manner. *J. Virol.* 92 (14), e00396–e00418. doi: 10.1128/jvi.00396-18

Leung, R. K., Zhou, J. W., Guan, W., Li, S. K., Yang, Z. F., and Tsui, S. K. (2013). Modulation of potential respiratory pathogens by pH1N1 viral infection. *Clin. Microbiol. Infect.* 19 (10), 930–935. doi: 10.1111/1469-0691.12054

Lim, M. Y., Yoon, H. S., Rho, M., Sung, J., Song, Y. M., Lee, K., et al. (2016). Analysis of the association between host genetics, smoking, and sputum microbiota in healthy humans. *Sci. Rep.* 6, 23745. doi: 10.1038/srep23745

Li, H., Zhu, W., Zhang, L., Lei, H., Wu, X., Guo, L., et al. (2015). The metabolic responses to hepatitis b virus infection shed new light on pathogenesis and targets for treatment. *Sci. Rep.* 5, 8421. doi: 10.1038/srep08421

Magoč, T., and Salzberg, S. L. (2011). FLASH: fast length adjustment of short reads to improve genome assemblies. *Bioinformatics* 27 (21), 2957–2963. doi: 10.1093/bioinformatics/btr507

Man, W. H., de Steenhuijsen, P. W. A., and Bogaert, D. (2017). The microbiota of the respiratory tract: gatekeeper to respiratory health. *Nat. Rev. Microbiol.* 15 (5), 259–270. doi: 10.1038/nrmicro.2017.14

Marangoni, A., Ceccarani, C., Camboni, T., Consolandi, C., Foschi, C., Salvo, M., et al. (2020). Pharyngeal microbiome alterations during neisseria gonorrhoeae infection. *PloS One* 15 (1), e0227985. doi: 10.1371/journal.pone.0227985

Ma, S., Zhang, F., Zhou, F., Li, H., Ge, W., Gan, R., et al. (2021). Metagenomic analysis reveals oropharyngeal microbiota alterations in patients with COVID-19. *Signal Transduction Targeting Ther.* 6 (1), 191. doi: 10.1038/s41392-021-00614-3

Mendez, R., Banerjee, S., Bhattacharya, S. K., and Banerjee, S. (2019). Lung inflammation and disease: A perspective on microbial homeostasis and metabolism. *IUBMB Life* 71 (2), 152–165. doi: 10.1002/iub.1969

Mina, M. J., Klugman, K. P., Rosch, J. W., and McCullers, J. A. (2015). Live attenuated influenza virus increases pneumococcal translocation and persistence within the middle ear. *J. Infect. Dis.* 212 (2), 195–201. doi: 10.1093/infdis/jiu804

Mirzaei, R., Dehkhodaie, E., Bouzari, B., Rahimi, M., Gholestani, A., Hosseini-Fard, S. R., et al. (2022). Dual role of microbiota-derived short-chain fatty acids on host and pathogen. *BioMed. Pharmacother.* 145, 112352. doi: 10.1016/j.biopha.2021.112352

Nagahara, Y., Shinomiya, T., Kuroda, S., Kaneko, N., Nishio, R., and Ikekita, M. (2005). Phytosphingosine induced mitochondria-involved apoptosis. *Cancer Sci.* 96 (2), 83–92. doi: 10.1111/j.1349-7006.2005.00012.x

Ochi, F., Tauchi, H., Jogamoto, T., Miura, H., Moritani, T., Nagai, K., et al. (2018). Sepsis and pleural empyema caused by streptococcus pyogenes after influenza a virus infection. *Case Rep. Pediatr.* 2018, 4509847. doi: 10.1155/2018/4509847

Ohno, M., Sekiya, T., Nomura, N., Daito, T. J., Shingai, M., and Kida, H. (2020). Influenza virus infection affects insulin signaling, fatty acid-metabolizing enzyme expressions, and the tricarboxylic acid cycle in mice. *Sci. Rep.* 10 (1), 10879. doi: 10.1038/s41598-020-67879-6

Quast, C., Pruesse, E., Yilmaz, P., Gerken, J., Schweer, T., Yarza, P., et al. (2013). The SILVA ribosomal RNA gene database project: improved data processing and

web-based tools. *Nucleic Acids Res.* 41 (Database issue), D590–D596. doi: 10.1093/nar/gks1219

Ratre, Y. K., Vishvakarma, N. K., Bhaskar, L. , and Verma, H. K. (2020). Dynamic propagation and impact of pandemic influenza A, (2009 H1N1) in children: A detailed review. *Curr. Microbiol.* 77 (12), 3809–3820. doi: 10.1007/s00284-020-02213-x

Sahin-Yilmaz, A., and Naclerio, R. M. (2011). Anatomy and physiology of the upper airway. *Proc. Am. Thorac. Soc* 8 (1), 31–39. doi: 10.1513/pats.201007-050RN

Sakleshpur, S., and Steed., A. L. (2022). Influenza: Toward understanding the immune response in the young. *Front. Pediatr.* 10. doi: 10.3389/fped.2022.953150

Shannon, J. P., Vrba, S. M., Reynoso, G. V., Wynne-Jones, E., Kamenyeva, O., Malo, C. S., et al. (2021). Group 1 innate lymphoid-cell-derived interferon-γ maintains anti-viral vigilance in the mucosal epithelium. *Immunity* 54 (2), 276–290.e5. doi: 10.1016/j.immuni.2020.12.004

Shibata, T., Makino, A., Ogata, R., Nakamura, S., Ito, T., Nagata, K., et al. (2020). Respiratory syncytial virus infection exacerbates pneumococcal pneumonia *via* Gas6/Axl-mediated macrophage polarization. *J. Clin. Invest.* 130 (6), 3021–3037. doi: 10.1172/JCI125505

Smallwood, H. S., Duan, S., Morfouace, M., Rezinciuc, S., Shulkin, B. L., Shelat, A., et al. (2017). Targeting metabolic reprogramming by influenza infection for therapeutic intervention. *Cell Rep.* 19 (8), 1640–1653. doi: 10.1016/j.celrep.2017.04.039

Söderholm, S., Fu, Y., Gaelings, L., Belanov, S., Yetukuri, L., Berlinkov, M., et al. (2016). Multi-omics studies towards novel modulators of influenza a virus-host interaction. *Viruses* 8 (10), 269. doi: 10.3390/v8100269

Stewart, C. J., Mansbach, J. M., Wong, M. C., Ajami, N. J., Petrosino, J. F., Camargo, C. A.Jr., et al. (2017). Associations of nasopharyngeal metabolome and microbiome with severity among infants with bronchiolitis. a multiomic analysis. *Am. J. Respir. Crit. Care Med.* 196 (7), 882–891. doi: 10.1164/rccm.201701-0071OC

Tian, X., Zhang, K., Min, J., Chen, C., Cao, Y., Ding, C., et al. (2019). Metabolomic analysis of influenza a virus A/WSN/1933 (H1N1) infected A549 cells during first cycle of viral replication. *Viruses* 11 (11), 1007. doi: 10.3390/v11111007

Tirosh, A., Calay, E. S., Tuncman, G., Claiborn, K. C., Inouye, K. E., Eguchi, K., et al. (2019). The short-chain fatty acid propionate increases glucagon and FABP4 production, impairing insulin action in mice and humans. *Sci. Transl. Med.* 11 (489), eaav0120. doi: 10.1126/scitranslmed.aav0120

Tisoncik-Go, J., Gasper, D. J., Kyle, J. E., Eisfeld, A. J., Selinger, C., Hatta, M., et al. (2016). Integrated omics analysis of pathogenic host responses during pandemic H1N1 influenza virus infection: The crucial role of lipid metabolism. *Cell Host Microbe* 19 (2), 254–266. doi: 10.1016/j.chom.2016.01.002

To, K. K., Lee, K. C., Wong, S. S., Sze, ,. K. H., Ke, Y. H., Lui, Y. M., et al. (2016). Lipid metabolites as potential diagnostic and prognostic biomarkers for acute community acquired pneumonia. *Diagn. Microbiol. Infect. Dis.* 85 (2), 249–254. doi: 10.1016/j.diagmicrobio.2016.03.012

Vitner, E. B., Avraham, R., Politi, B., Melamed, S., and Israely, T. (2022). Elevation in sphingolipid upon SARS-CoV-2 infection: possible implications for COVID-19 pathology. *Life Sci. Alliance.* 5 (1), e202101168. doi: 10.26508/lsa.202101168

Wang, L., Xu, D., Huang, Q., Yang, G., Zhang, M., Bi, J., et al. (2021). Characterization of tonsil microbiota and their effect on adenovirus reactivation in tonsillectomy samples. *Microbiol. Spectr.* 9 (2), e0124621. doi: 10.1128/Spectrum.01246-21

Wendt, C. H., Castro-Pearson, S., Proper, J., Pett, S., Griffin, T. J., Kan, V., et al. (2021). Metabolite profiles associated with disease progression in influenza infection. *PloS One* 16 (4), e0247493. doi: 10.1371/journal.pone.0247493

Wen, Z., Xie, G., Zhou, Q., Qiu, C., Li, J., Hu, Q., et al. (2018). Distinct nasopharyngeal and oropharyngeal microbiota of children with influenza a virus compared with healthy children. *BioMed. Res. Int.* 2018, 6362716. doi: 10.1155/2018/6362716

WHO and Multicentre Growth Reference Study Group (2006). *WHO child growth standards: length/height-for-age, weight-for-age, weight-for-length, weight-for-height and body mass index-for-age: methods and development* (Geneva: World Health Organization).

Wirusanti, N. I., Baldridge, M. T., and Harris, V. C. (2022). Microbiota regulation of viral infections through interferon signaling. *Trends Microbiol.* 30 (8), 778–792. doi: 10.1016/j.tim.2022.01.007

Yildiz, S., Pereira, B. L. J. P., Bergé, M., González-Ruiz, V., Baud, D., Kloehn, J., et al. (2020). Respiratory tissue-associated commensal bacteria offer therapeutic potential against pneumococcal colonization. *Elife* 9, e53581. doi: 10.7554/eLife.53581

Zhou, Q., Xie, G., Liu, Y., Wang, H., Yang, Y., Shen., K., et al. (2020). Different nasopharynx and oropharynx microbiota imbalance in children with mycoplasma pneumoniae or influenza virus infection. *Microb. Pathog.* 144, 104189. doi: 10.1016/j.micpath.2020.104189

Zumla, A., Rao, M., Wallis, R. S., Kaufmann, S. H., Rustomjee, R., Mwaba, P., et al. (2016). Host-directed therapies for infectious diseases: current status, recent progress, and future prospects. *Lancet Infect. Dis.* 16 (4), e47–e63. doi: 10.1016/s1473-3099(16)00078-5

Zurfluh, S., Baumgartner, T., Meier, M. A., Ottiger, M., Voegeli, A., Bernasconi, L., et al. (2018). The role of metabolomic markers for patients with infectious diseases: implications for risk stratification and therapeutic modulation. *Expert Rev. Anti Infect. Ther.* 16 (2), 133–142. doi: 10.1080/14787210.2018.1426460

frontiers | Frontiers in Cellular and Infection Microbiology

TYPE Original Research
PUBLISHED 09 February 2023
DOI 10.3389/fcimb.2023.1121399

OPEN ACCESS

EDITED BY
Eva Maria Weissinger,
Hannover Medical School, Germany

REVIEWED BY
Eija Könönen,
University of Turku, Finland
Mustafa Yilmaz,
Biruni University, Türkiye

*CORRESPONDENCE
Shuming Guo
kyzx@linfench.com
Yudong Hou
bycgk@126.com
Zhancheng Gao
zcgao@bjmu.edu.cn

†These authors share first authorship

‡These authors have contributed equally to this work

SPECIALTY SECTION
This article was submitted to Microbiome in Health and Disease, a section of the journal Frontiers in Cellular and Infection Microbiology

RECEIVED 11 December 2022
ACCEPTED 30 January 2023
PUBLISHED 09 February 2023

CITATION
Liu S, Xie G, Chen M, He Y, Yu W, Chen X, Mao W, Liu N, Zhang Y, Chang Q, Qiao Y, Ma X, Xue J, Jin M, Guo S, Hou Y and Gao Z (2023) Oral microbial dysbiosis in patients with periodontitis and chronic obstructive pulmonary disease. *Front. Cell. Infect. Microbiol.* 13:1121399. doi: 10.3389/fcimb.2023.1121399

Oral microbial dysbiosis in patients with periodontitis and chronic obstructive pulmonary disease

Siqin Liu[1†], Guofang Xie[2†], Meifeng Chen[3†], Yukun He[4], Wenyi Yu[4], Xiaobo Chen[2], Weigang Mao[2], Nanxia Liu[2], Yuanjie Zhang[2], Qin Chang[3], Yingying Qiao[3], Xinqian Ma[4], Jianbo Xue[4], Mengtong Jin[5], Shuming Guo[6*‡], Yudong Hou[1*‡] and Zhancheng Gao[4*‡]

[1]School of Stomatology, Binzhou Medical University, Yantai, China, [2]Department of Stomatology, Linfen Central Hospital, Linfen, China, [3]Department of Respiratory and Critical Care Medicine, Linfen Central Hospital, Linfen, China, [4]Department of Respiratory and Critical Care Medicine, Peking University People's hospital, Beijing, China, [5]Department of Science and Education, Linfen Central Hospital, Linfen, China, [6]Nursing department, Linfen Central Hospital, Linfen, China

Background: Oral microbiota is closely related to the homeostasis of the oral cavity and lungs. To provide potential information for the prediction, screening, and treatment strategies of individuals, this study compared and investigated the bacterial signatures in periodontitis and chronic obstructive pulmonary disease (COPD).

Materials and methods: We collected subgingival plaque and gingival crevicular fluid samples from 112 individuals (31 healthy controls, 24 patients with periodontitis, 28 patients with COPD, and 29 patients with both periodontitis and COPD). The oral microbiota was analyzed using 16S rRNA gene sequencing and diversity and functional prediction analysis were performed.

Results: We observed higher bacterial richness in individuals with periodontitis in both types of oral samples. Using LEfSe and DESeq2 analyses, we found differentially abundant genera that may be potential biomarkers for each group. *Mogibacterium* is the predominant genus in COPD. Ten genera, including *Desulfovibrio*, *Filifactor*, *Fretibacterium*, *Moraxella*, *Odoribacter*, *Pseudoramibacter Pyramidobacter*, *Scardovia*, *Shuttleworthia* and *Treponema* were predominant in periodontitis. *Bergeyella*, *Lautropia*, *Rothia*, *Propionibacterium* and *Cardiobacterium* were the signature of the healthy controls. The significantly different pathways in the Kyoto Encyclopedia of Genes and Genomes (KEGG) between healthy controls and other groups were concentrated in genetic information processing, translation, replication and repair, and metabolism of cofactors and vitamins.

Conclusions: We found the significant differences in the bacterial community and functional characterization of oral microbiota in periodontitis, COPD and comorbid diseases. Compared to gingival crevicular fluid, subgingival plaque

may be more appropriate for reflecting the difference of subgingival microbiota in periodontitis patients with COPD. These results may provide potentials for predicting, screening, and treatment strategies for individuals with periodontitis and COPD.

KEYWORDS

periodontal disease, COPD, oral microbiome, 16S rRNA, subgingival plaque, gingival crevicular fluid, inflammation, chronic obstructive pulmonary disease

1 Introduction

The oral microenvironment is complicated and comprises more than 700 bacterial species (Dewhirst et al., 2010). Among them, 400 species have been identified in periodontal pockets. Oral microbial dysbiosis is known to impact chronic inflammatory diseases (Thomas et al., 2021). Microbial migration from the oral cavity appears to be a significant source of the lung microbiome through microaspiration and inhalation (Bassis et al., 2015). Thus, the oral microbiota is closely related to the homeostasis of the oral cavity and lungs.

Periodontitis , a chronic infectious disease caused by periodontal pathogens, is characterized by the loss of gingiva, bone, and ligament and deep periodontal pockets between the tooth and gingiva (Kinane et al., 2017). Periodontitis is a highly prevalent oral disease in China, with a prevalence of up to 52.8% (Jiao et al., 2021). Emerging evidence has revealed that periodontitis is closely related to the oral microbiota, which can increase the risk of the development of chronic inflammatory conditions, thereby leading to coronary artery disease, systemic lupus erythematosus, and respiratory disease (Gomes-Filho et al., 2010; Preshaw et al., 2012; Slocum et al., 2016; Li et al., 2020). Chronic obstructive pulmonary disease (COPD) is one of the most common respiratory diseases characterized by progressive and non-reversible airflow limitation (Barnes et al., 2015a). Recurrent episodes of exacerbations in COPD lead to significant mortality worldwide (Barnes et al., 2015b; Caramori et al., 2016; Rabe and Watz, 2017). Disturbed lung microbiome and abnormal inflammatory reactions are the two main causes of acute exacerbation of COPD (Mammen and Sethi, 2016).

Gram-negative bacteria, such as *Porphyromonas gingivalis*, *Treponema denticola*, and species are believed to be the main oral microbiome in the periodontal inflammatory response (Gaeckle et al., 2020). Compared with the control group, the abundance of *P.gingivalis*, *Klebsiella pneumoniae*, *Pseudomonas aeruginosa* and *Streptococcus pneumoniae* increased in participants with COPD (Tan et al., 2019). Moreover, *Veillonella*, *Rothia*, and *Actinomyces* were more enriched in patients with COPD and periodontitis than in HCs(Lin et al., 2020). Treating periodontitis significantly reduced exacerbation frequency in patients with COPD (Kucukcoskun et al., 2013). Although most recent studies have explored the relationship and influence mechanism of periodontitis or COPD, research on the alteration of the oral microbiome in patients with periodontitis, COPD or both, remains insufficient. Moreover, previous studies have mainly focused on saliva samples; however, the bacterial composition differs between saliva and subgingival pockets (Jakubovics and Kolenbrander, 2010; Jia et al., 2018). As the main accumulation site of periodontal pathogens, subgingival plaque more directly reflects the status of the subgingivalmicrobiome.

In this study, we investigated the shared and specific alterations in the oral microbiomes of participants with periodontitis, COPD, or both, through 16S rRNA gene sequencing.

2 Material and methods

2.1 Study participants

The present study was approved by the ethics committee of Linfen Central Hospital (Ethics Approval No. 2021-42-1) and was performed in accordance with the Declaration of Helsinki. Written informed consent was obtained from all participants prior to clinical data collection and sampling.

A total of 112 participants were recruited at Linfen Central Hospital, including 31 healthy controls (HC group), 24 periodontitis patients without COPD (P group), 28 COPD patients without periodontitis (COPD group), and 29 patients with both periodontitis and COPD (P_COPD group). The diagnosis and assessment of the severity of COPD were made according to the recommendations of the Global Initiative for Chronic Obstructive Lung Disease (GOLD) committee (Vogelmeier et al., 2017). The diagnosis and assessment of the periodontitis were based on the new classification, Classification of Periodontal and Peri-implant Diseases and Conditions (Tonetti et al., 2018). Other inclusion criteria included: (1) aged ≥18 years; and (2) Periodontitis from stage II to IV, grade B. The exclusion criteria were antibiotic using before during the last three months, other systemic diseases, administration of periodontal therapy during the last three months (Cai et al., 2021). General participant demographics, including age, gender, blood routine records, pulmonary function test results and clinical treatments were collected from medical record system using a standard form.

2.2 Sample collection

Before sample collection, the participants were asked to rinse their mouth for removing the food residues and debris. We obtained oral samples from four first incisor teeth and four first molar teethof each participant. The first molars and incisors are the main sites of periodontal lesions, and we selected 11, 21, 31, 41, 16, 26, 36, 46 as the main sampling sites based on previous periodontal microbiology studies (Zhou et al., 2020). Clinical examination was performed before sampling to ensure that the sampling site clinical attachment loss (CAL) ≥ 3mm, probing

depth (PD) ≥ 4mm and bleeding on probing. If one of these teeth was missing, the adjacent tooth was collected. After drying the target sites, gingival crevicular fluid (GCF) samples were collected with sterile absorbent paper points from gingival sulcus of each tooth. After removal of supragingival plaque, subgingival plaque (SP) samples were collected with sterile Gracey curettes from the buccal and lingual sides of each tooth. The sample of each participant was collected in the eppendorf tube. All oral specimens (subgingival plaque and gingival crevicular fluid) were stored in -80°C until DNA extraction.

2.3 DNA extraction, 16S rRNA gene amplification, and sequencing

Total bacterial DNA was extracted from oral samples using SteadyPure Bacterial Genomic DNA Extraction Kit(Accurate Biotechnology(Hunan)Co,Ltd,China) following the manufacturer's instructions. Hypervariable regions (V2, V3, V4, V6-7, V8 and V9) of the 16S rRNA were amplified using two primer sets in the Ion 16STM Metagenomics Kit (ThermoFisher Scientific, UK). XP beads were used to purify the amplification products and quantified by Qubit4 (ThermoFisher Scientific, USA). Purified amplicons were ligated with barcodes and then generated for the libraries. Then the libraries were pooled in equimolar amounts on chip 530 and sequenced to single-end, 250-base-pair reads on an Ion GeneStudio S5 System (ThermoFisher Scientific, USA) based on Ion Reporter metagenomics workflow (Ion 16S mNGS). Quality filtering, trimming and dereplication of raw sequencing reads were conducted automatically on Ion Reporter metagenomics workflow, relying on default parameters. Unaligned binary data files (Binary Alignment Map, BAM) generated by the Ion Torrent PGM were uploaded to Ion Reporter and analyzed using default settings (Malczynski et al., 2021).

2.4 Statistical analysis

Quantitative variables conforming to normal distribution were presented as the mean ± SD analyzed by Student's t test and analysis of variance (ANOVA), while Quantitative variables of non-normal distribution were presented as median and interquartile ranges (25th and 75th percentiles) and analyzed by Mann-Whitney U or Kruskal-Wallis test. Categorical variables were presented as rate or percentage, and chi-square test or Fisher test were used to analysis. The alpha diversity was evaluated using the Chao-1, Shannon, abundance-based coverage estimator (ACE) and Simpson indices, respectively. The beta diversity has been evaluated through principal coordinates analysis (PCoA) ordination of variance and compared using Bray-Curtis dissimilarity. Differential species among groups was explored with the linear discriminant analysis (LDA) effect size (LEfSe) method (Shi et al., 2021) and DESeq2 analysis (Lu et al., 2022). The microbiome phenotypes were predicted by BugBase (Ward et al., 2017). The BugBase phenotype predictions were implemented using the online web page https://bugbase.cs.umn.edu/index.html. Prediction of the abundances of functional categories was conducted using PICRUSt2 (Douglas et al., 2020). Statistics and visualization of functional data were depicted using STAMP (Chowdhry et al., 2018). $P<0.05$ was considered as statistically significant.

3 Results

3.1 Clinical characteristics of the study population

A total of 112 participants were enrolled in our study, and the basic characteristics of each group are listed in Table 1. There were no differences among the groups except for gender, age and smoking. The healthy control (HC) group's median age was significantly younger than the diseased groups. The median age of the comorbid (P_COPD) group was highest. Moreover, the healthy group had a higher proportion of female participants. Significant difference of smoking was only existed between healthy control group and periodontitis group. Gender, age and smoking status were treated as confounding factors which were corrected in the difference analysis

TABLE 1 Demographical and Clinical Features of Included Subjects.

	HC(n=31)	P(n=24)	COPD(n=28)	P_COPD(n=29)	*p*-value
Age	25(23-38)	53.5(47.25-61.25)	61(51.75-67.75)	66(60.5-72.5)	<0.005[a]
Gender,n (%)					<0.001[b]
female	19(61.3%)	9(37.5%)	5(17.9%)	4(13.8%)	
male	12(38.7%)	15(62.5%)	23(82.1%)	25(86.2%)	
Somkers,n (%)					
Current smoker	3(9.7%)	12(50%)	7(25%)	7(24.1%)	<0.001[c]
Former smoker	0	0	7(25%)	15(51.7%)	>0.05
Nonsmoker	28(90.3%)	12(50%)	14(50%)	7(24.1%)	<0.001[d]
PD(mm)	2(1-2)	6.33(4.33-6.92)	2(1.25-2)	6.33(5-6.67)	<0.001[e]
BOP%	2.08(2.08-4.17)	78.13(71.35-83.33)	2.08(2.08-4.17)	81.25(68.75-87.5)	<0.001[f]
Stage(%)					0.612

(Continued)

TABLE 1 Continued

	HC(n=31)	P(n=24)	COPD(n=28)	P_COPD(n=29)	*p*-value
II	—	9(37.5%)	—	8(27.6%)	
III	—	10(41.7%)	—	16(55.2%)	
IV	—	5(20.8%)	—	5(17.2%)	
GOLD(%)					0.712
I	—	—	3(10.7%)	6(20.7%)	
II	—	—	11(39.3%)	10(34.5%)	
III	—	—	9(32.1%)	7(24.1%)	
IV	—	—	5(17.9%)	6(20.7%)	
BMI(kg/m^2)	—	—	27.35(23.43-29.3)	23.5(22.1-25.75)	0.007
FVC(L)	—	—	2.88(2.51-3.56)	2.82(2.34-3.67)	0.943
FEV1(L)	—	—	1.43(0.99-2.18)	1.34(0.92-2.12)	0.472
FEV1%	—	—	58.31(35.71-73.54)	53.08(33.56-75.52)	0.576
Peripheral blood					
WBC(x10^9/L)	—	—	6.3 ± 2.1	6.5 ± 1.7	0.675
RBC(x10^{12}/L)	—	—	4.7 ± 0.4	4.7 ± 0.4	0.797
HGB(g/L)	—	—	143.4 ± 11.2	142.8 ± 12.1	0.848
Neutrophil percentages(%)	—	—	57.2 ± 8.1	58.6 ± 10.4	0.578
Lymphocyte percentages(%)	—	—	31.1 ± 6.7	30.5 ± 9.9	0.799
Monocytes percentages(%)	—	—	7.5(6.45-10)	7.7(6.65-9)	0.958
Eosinophil percentages(%)	—	—	2.3(1.45-3.85)	2.3(1.25-2.85)	0.409
Basophil percentages(%)	—	—	0.5 ± 0.3	0.5 ± 0.2	0.706
Neutrophil(x10^9/L)	—	—	2.99(2.62-5.125)	3.8(2.675-4.67)	0.482
Lymphocyte(x10^9/L)	—	—	1.9 ± 0.5	2.0 ± 0.7	0.719
Monocytes(x10^9/L)	—	—	0.43(0.375-0.565)	0.54(0.48-0.615)	0.147
Eosinophil(x10^9/L)	—	—	0.15(0.08-0.22)	0.12(0.08-0.205)	0.567
Basophil (x10^9/L)	—	—	0.03(0.02-0.04)	0.03(0.02-0.05)	0.333

[a]Significant difference exists among healthy control group and other groups, significant difference exists between periodontitis group and COPD with periodontitis group.
[b]Significant differences exists among healthy control group and other three groups.
[c,d]Significant difference exists between healthy control group and periodontitis group.
[e,f]Significant difference exists between healthy control group and periodontitis group, significant difference exists between COPD group and periodontitis group, significant difference exists between COPD group and COPD with periodontitis group.
BMI, body mass index; GOLD, grading of pulmonary function; WBC, white blood cell; RBC, red blood cell; PD, probing depth; BOP, bleeding on probing.
HC, health controls; P, patients with periodontitis; COPD, patients with chronic obstructive pulmonary disease; P_COPD, patients with comorbid diseases.

(Figure S4A). There were no significant differences in the GOLD grade and clinical indicators between the COPD and P_COPD groups.

3.2 The oral microbial community in the periodontal pocket and crevice

All sequencing data for the four groups reached saturation at approximately 50,000 reads (Figure S1). For alpha diversity, the Chao1 index in the subgingival plaque (SP) samples from the periodontitis group was significantly higher than that in the HC group (Figure 1A, $P = 0.0245$). In the gingival crevicular fluid (GCF) samples, the Chao1 index of periodontitis group was significantly higher than that of the COPD group (Figure 1C, $P = 0.0068$) and P_COPD group (Figure 1C, $P = 0.0063$). However, no significant difference was found in the Shannon, Simpson and ACE indices among the four groups in the different sample types (Figures 1A, C, $P > 0.05$). To evaluate similarities among the four groups, PCoA was based on unweighted UniFrac distances. Regardless of the SP or GCF samples, beta diversity was different in the HC and diseased groups (Figures 1B, D). However, in the SP samples, the bacterial compositions in the periodontitis, COPD, and P_COPD groups were indistinguishable (Figure 1B, $P>0.05$). For the GCF samples, beta diversity was different between theperiodontitis and P_COPD groups (Figure 1D).

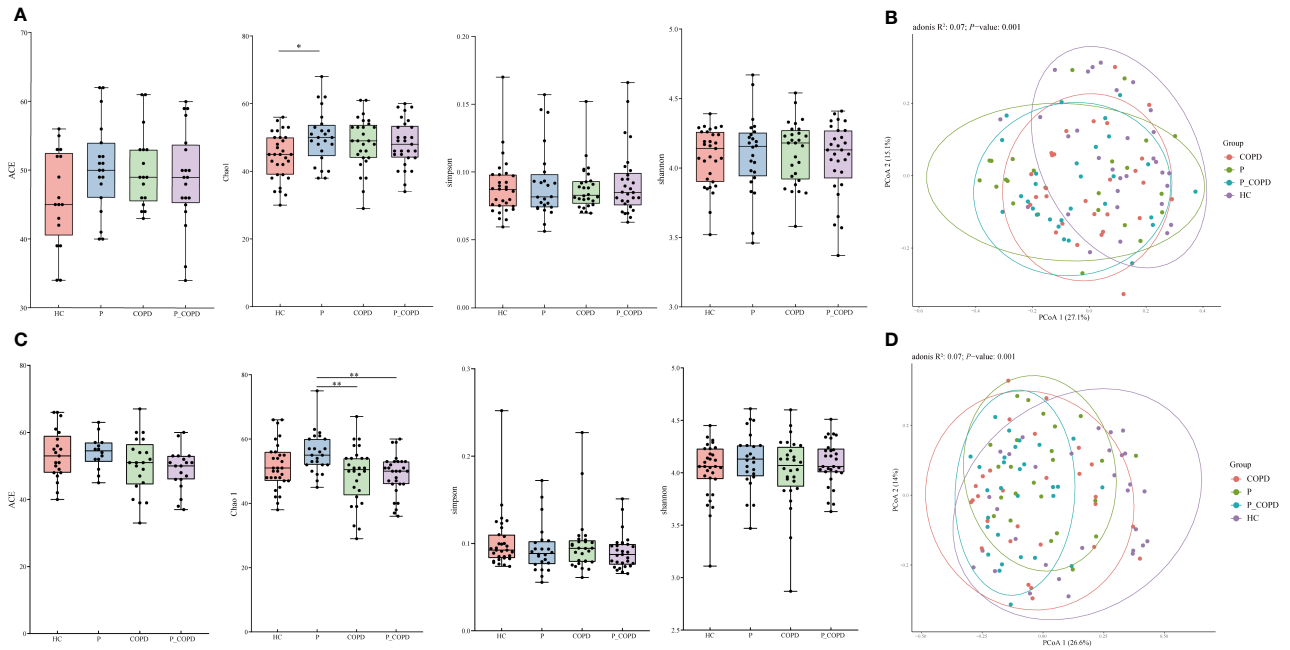

FIGURE 1
Alpha diversity analysis of healthy controls (HC), periodontitis (P) group, chronic obstructive pulmonary disease (COPD) group and comorbid diseases (P_COPD) group. Chao1, Shannon, abundance-based coverage estimator (ACE) and Simpson indices of each group, **(A)** in subgingival plaque samples and **(C)** in gingival crevicular fluid samples. Under Chao1 index, significant difference between HC and P was observed in subgingival plaque samples, significant differences between P and COPD, P and P_COPD were observed in gingival crevicular fluid samples. Principal coordinate analysis (PCoA) among healthy controls (HC), periodontitis (P) group, chronic obstructive pulmonary disease (COPD) group and comorbid diseases (P_COPD) group. **(B)** The PCoA plot showed a separation of samples from HC and other diseased groups in subgingival plaque samples. **(D)** The PCoA plot showed a separation of samples from HC and other diseased groups in gingival crevicular fluid samples. The samples of P_COPD were separated from P group.*: $p < 0.05$ **: $p < 0.01$.

Eight phyla, 50 families, 98 genera were detected in the SP samples. The most abundant genera were *Prevotella*, *Corynebacterium*, *Capnocytophaga*, *Fusobacterium*, *Streptococcus and Porphyromonas* (Figure 2A). *Actinomyces*, *Campylobacter*, *Capnocytophaga*, *Neisseria*, *Prevotella* and *Streptococcus* were present in all SP samples (Figure 2B). Nine phyla, 57 families and 118 genera were identified in the GCF samples. The most abundant genera were *Streptococcus*, *Prevotella*, *Fusobacterium*, *Porphyromonas*, *Neisseria* and *Capnocytophaga* (Figure 2C). The core microbiota of the GCF samples were *Actinomyces*, *Campylobacter*, *Fusobacterium*, *Leptotrichia*, *Porphyromonas*, *Prevotella*, *Streptococcus* and *Tannerella* (Figure 2D).

In periodontitis group, we explored the differential taxa among stages of periodontitis. In both types of oral samples, no significant difference was found in the alpha diversity analysis and beta diversity analysis among the different stages of periodontitis. There were no difference in the taxa among stages of periodontitis (Figure S4B, S4C, $P > 0.05$).

3.3 Microbial alterations in different diseases

To further identify the differential taxa among these groups, LEfSe and DESeq2 analyses were conducted. According to the LEfSe analysis, in the SP samples, eight genera were predominant in the HC group, including *Actinomyces*, *Bergeyella*, *Brachymonas*, *Cardiobacterium*, *Lautropia*, *Mannheimia*, *Propionibacterium* and *Rothia*. In contrast, the abundance of *Haemophilus*, *Filifactor*, and *Moraxella* increased in the periodontitis group. The abundance of *Atopobium* and *Lachnoanaerobaculum* were higher in the COPD group and the abundance of *Stomatobaculum*, *Anaeroglobus*, *Bifidobacterium*, and *Clostridium* were higher in the P_COPD group. (Figure 3A, LDA score (log10) >2, $P < 0.05$). According to DESeq2 analysis (Table S1), there were significant differences in the oral microbiota of the three diseased groups in the SP samples but no common change among these groups. Twenty-nine genera were predominant in the periodontitis group, including *Filifactor*, *Mogibacterium*, *Scardovia*, *Murdochiella* and *Odoribacter*. *Abiotrophia* and *Gemella* were more abundant in the COPD group and the abundance of *Cardiobacterium* was higher in the P_COPD group. The abundance of *Bergeyella* decreased in the periodontitis and COPD groups. The abundance of *Pasteurella* and *Propionicicella* decreased in the periodontitis group. The abundance of *Desulfobulbus*, *Soonwooa* and *Johnsonella* decreased in the COPD group (Figure 3C).

According to LEfSe analysis, in the GCF samples, the abundance of eight genera: *Bergeyella*, *Cardiobacterium*, *Kingella*, *Lautropia*. *Propionibacterium*, *Rothia*, *Serratia* and *Staphylococcus* were more abundant in the HC group. *Desulfovibrio*, *Dorea*, *Filifactor*, *Fretibacterium*, *Moraxella*, *Pseudoramibacter* and *Treponema* were more abundant in the P group, while the abundance of *Mogibacterium* increased in the COPD group. The abundance of *Phocaeicola* and *Schwartzia* was higher in the P_COPD group. (Figure 3B, LDA score (log10) >2, $P < 0.05$). According to DESeq2

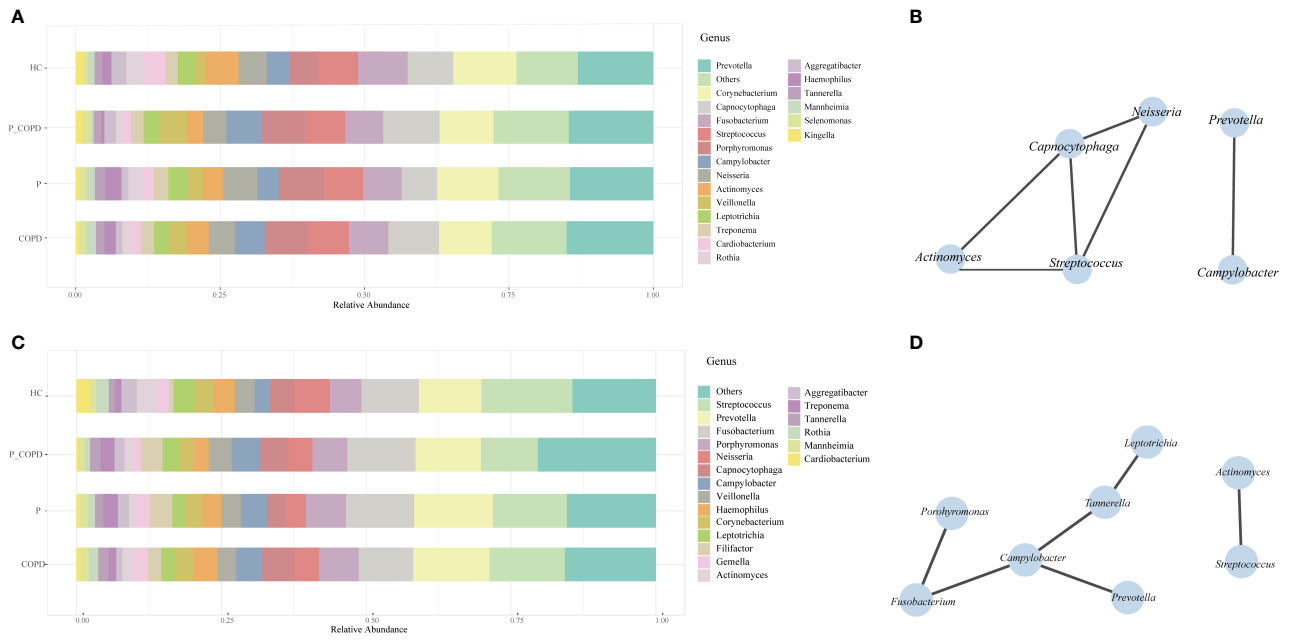

FIGURE 2
Relative abundances of the oral microbiota in healthy controls (HC), periodontitis (P) group, chronic obstructive pulmonary disease (COPD) group and comorbid diseases (P_COPD) group. Stacked bar plots showing relative abundances of the oral microbiota at the genus level **(A)** in subgingival plaque samples, **(C)** in gingival crevicular fluid samples. The correlation network analysis of the core microbiota based on SparCC. The core microbiota was defined as which covering 100% of all samples. **(B)** In subgingival plaque samples. **(D)** In gingival crevicular fluid samples.

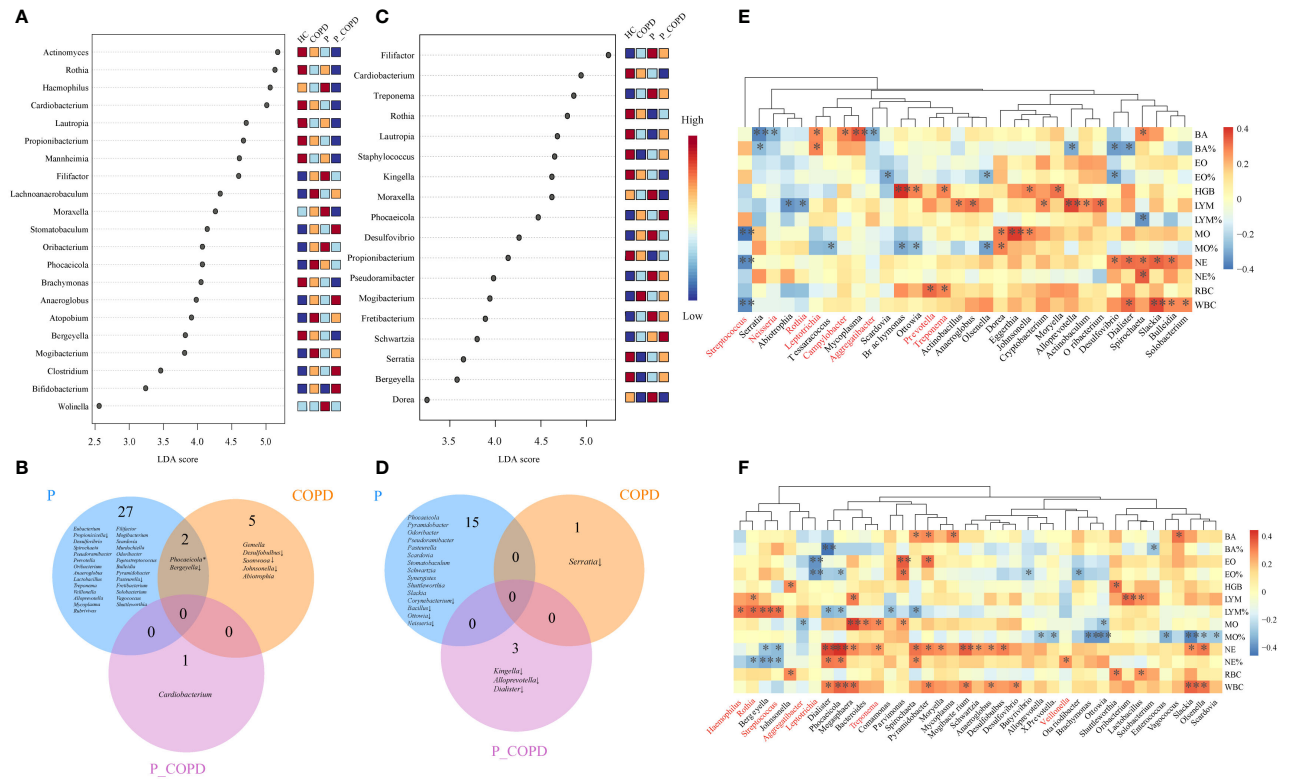

FIGURE 3
Linear discriminant analysis of effect size (LEfSe) of oral microbiota at the genus level enriched in healthy controls (HC), periodontitis (P) group, chronic obstructive pulmonary disease (COPD) group and comorbid diseases (P_COPD) group. LDA score (log10) <2, $P < 0.05$) **(A)** In subgingival plaque samples. **(C)** In gingival crevicular fluid samples. DESeq2 analysis of oral microbiota. Oral microbiota with significantly difference from the diseased groups compared with healthy controls **(B)** in subgingival plaque samples, **(D)** in gingival crevicular fluid samples. * The relative abundances of *Phocaeicola* was more abundant in CP group, while the relative abundance of *Phocaeicola* in COPD group was lower than HC groups. ↓, decreased. Spearman's coefficient calculated between oral microbiota and clinical indicators. The taxa analyzed were the top 20 genera in terms of abundance **(E)** in subgingival plaque samples, **(F)** in gingival crevicular fluid samples. Black stars within heatmap boxes indicate significant results (*: $P \leq 0.05$, **: $P \leq 0.01$), Benjamini–Hochberg adjustment for multiple comparisons.

analysis (Table S2), there were significant differences in the oral microbiota of the three diseased groups, but no common changes were observed among these groups. Fifteen genera were predominant in the periodontitis group: *Pasteurella*, *Phocaeicola*, *Pseudoramibacter*, *Pseudoramibacter*, *Pyramidobacter*, *Scardovia*, *Schwartzia*, *Shuttleworthia*, *Slackia*, *Stomatobaculum* and *Synergistes*. The abundance of *Corynebacterium*, *Bacillus*, *Ottowia* and *Neisseria* decreased in the periodontitis group. The abundance of *Serratia* decreased in the COPD group. The abundance of *Kingella*, *Alloprevotella* and *Dialister* decreased in the P_COPD group (Figure 3D).

3.4 Association between genera and blood routine indicators

The observed links between the respiratory microbial community and disease prompted us to examine the interactions between the taxa and their clinical features. The taxa analyzed were the top 20 genera regarding abundance. For SP samples, the relative abundance of *Streptococcus* was negatively correlated with neutrophil, white blood cell and monocyte counts. The relative abundance of *Rothia* was negatively correlated with lymphocyte counts. The relative abundance of *Leptotrichia* and *Campylobacter* were positively correlated with the basophil counts, and the relative abundance of *Aggregatibacter* and *Neisseria* were negatively correlated with the basophil counts (Figure 3E). In the GCF samples, the relative abundance of *Rothia*, *Streptococcus*, and *Haemophilus* was positively correlated with the lymphocyte percentages. The relative abundance of *Streptococcus* and *Rothia* was negatively correlated with the neutrophil percentages, and the relative abundance of *Veillonella* was positively correlated with neutrophil percentages. The relative abundance of *Treponema* was positively correlated with neutrophil counts. In addition, the relative abundance of *Leptotrichia* was negatively correlated with the eosinophil percentages (Figure 3F).

3.5 Potential function of oral microbiome

We analyzed the predicted phenotypes based on taxonomic classification using BugBase. In different sample types, the relative abundance of aerobic bacteria in the HC group was higher than that in the diseased groups (Figure S2A, S2F). In comparison, the relative abundance of anaerobic bacteria was lower in the HC group than that in the diseased groups (Figure S2B, S2G). The ability to form biofilms in the HC group was greater than that in the diseased groups (Figure S2C, S2H). The potential pathogenicity in the HC group was lower than that in the diseased groups in the SP samples (Figure S2D). In the GCF samples, the potential pathogenicity in the P group was lower than that in the other groups (Figure S2I). In addition, in the SP samples, the relative abundance of gram-positive bacteria in the HC group was higher than that in the other diseased groups, whereas gram-negative bacteria showed the opposite trend (Figures S2E, S2J).

Through PICRUSt2, putative biological functions of the microbiota of the four groups were illustrated. No significant differences were observed between the GCF samples. As shown in Figure 4A, the periodontitis group exhibited significantly enriched metabolism of cofactors and vitamins (thiamine metabolism, nicotinate and nicotinamide metabolism), translation, protein families: genetic information processing (translation factors), amino acid related enzymes, and carbon fixation in photosynthetic organisms. The COPD group showed significantly enriched protein families: genetic information processing (transfer RNA biogenesis, ribosome, mitochondrial biogenesis, DNA replication proteins, translation factors), translation (ribosome, aminoacyl-tRNA biosynthesis, RNA transport), replication and repair (homologous recombination, mismatch repair, DNA replication), protein families: metabolism (peptidases and inhibitors, amino acid related enzymes, peptidoglycan biosynthesis and degradation proteins), glycan biosynthesis and metabolism(peptidoglycan biosynthesis, other glycan degradation, other types of O-glycan biosynthesis and mannose type O-glycan biosynthesis) (Figure 4B). The P_COPD group showed significantly enriched protein families: genetic information processing (DNA repair and recombination proteins, transfer RNA biogenesis, ribosome, chromosome and associated proteins), protein families: metabolism (amino acid related enzymes, peptidases and inhibitors, peptidoglycan biosynthesis and degradation proteins), translation (ribosome, aminoacyl-tRNA biosynthesis, RNA transport), glycan biosynthesis and metabolism (peptidoglycan biosynthesis, other glycan degradation, lipopolysaccharide biosynthesis), metabolism of cofactors and vitamins(lipoic acid metabolism, porphyrin and chlorophyll metabolism, riboflavin metabolism, thiamine metabolism) and other functions (Figure 4C).

The HC group showed significantly enriched signal transduction (two-component system), lipid metabolism (biosynthesis of unsaturated fatty acids), and metabolism of other amino acids (glutathione metabolism, phosphonate and phosphinate metabolism), compared to the other three groups (Figure S3).

4 Discussion

The alteration of oral microecosystem in patients with systemic diseases has been the subject of intense research for several years (Thomas et al., 2021). An increasing amount of evidence from microbiological studies indicates a significant ecological connection between oral microecosystems, periodontitis and COPD (Wu et al., 2022). Here we explored the oral microbiota of SP and GCF in periodontitis, COPD, comorbid patients, and healthy controls. In this study, we collected oral microbial samples of two types. Compared with the GCF, differences in the microbial community compositions of SP more clearly expressed the varieties of oral microecology in periodontitis and COPD, indicating that it may be more appropriate for reflecting the difference of subgingival microbiota between periodontitis and COPD.

This study observed higher bacterial richness in individuals suffering from periodontitis in the two types of oral samples, suggesting that microbial dysbiosis were existed in the process of periodontitis (Lin et al., 2020).

Using LEfSe analysis, we identified differentially abundant genera associated with different diseases. In the present study,periodontitis group had a higher abundance of *Desulfovibrio*, *Filifactor*, *Fretibacterium*, *Moraxella*, *Odoribacter*, *Pseudoramibacter*,

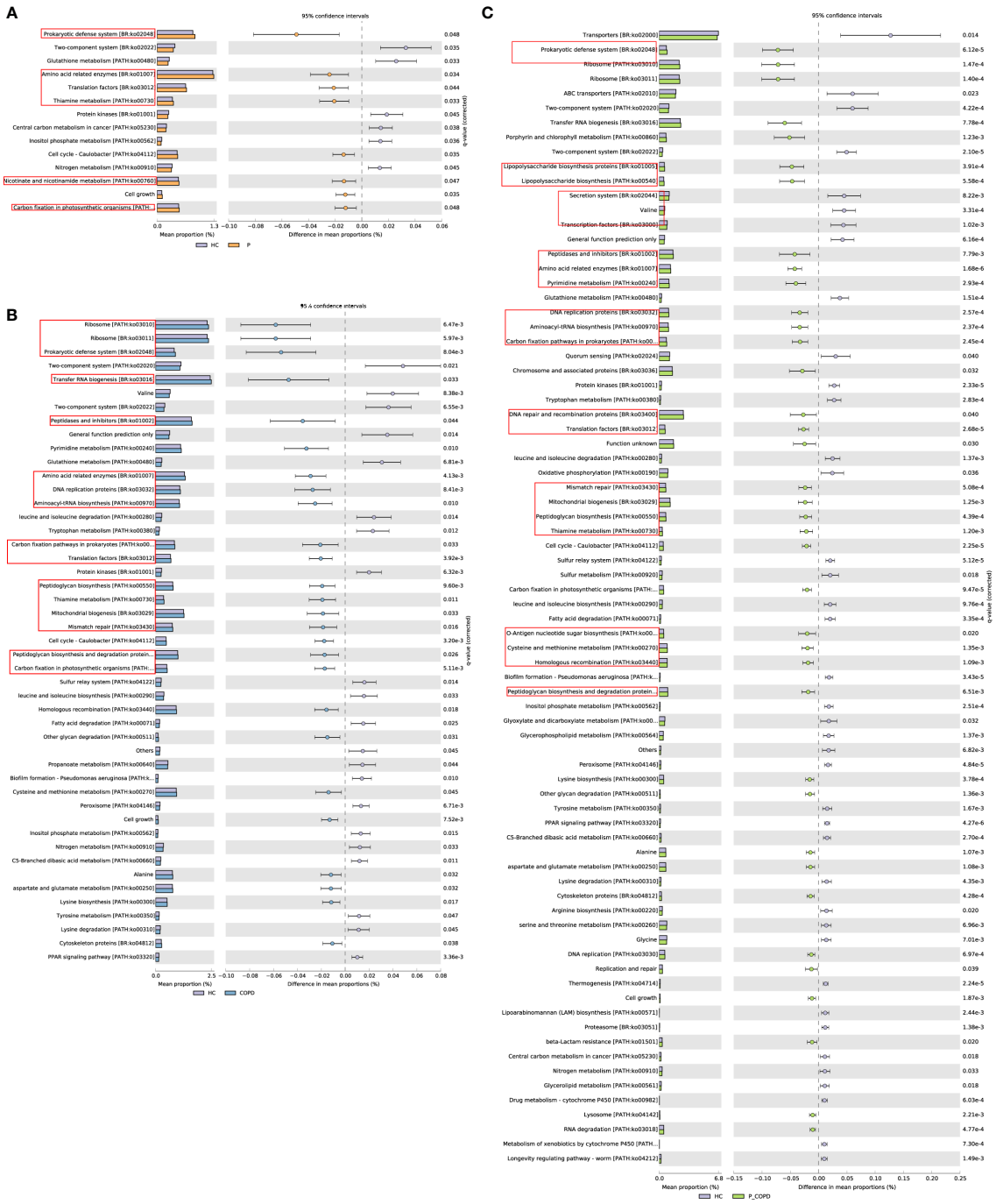

FIGURE 4
PICRUSt analysis in the KEGG pathways. Functional predictions for the oral microbiome of the diseased groups and healthy control group. Significant KEGG pathways at level 3 for the oral microbiome of the diseased groups and healthy control group in subgingival plaque samples were identified by STAMP software. Bar chart showing the functional difference (corrected *p*-value < 0.05) between periodontitis **(A)**, chronic obstructive pulmonary disease **(B)** and comorbid diseases **(C)** versus healthy controls. PICRUSt, Phylogenetic Investigation of Communities by Reconstruction of Unobserved States; KEGG, Kyoto Encyclopedia of Genes and Genomes.

Pyramidobacter, *Scardovia*, *Shuttleworthia* and *Treponema* in the two types of samples. *Pseudoramibacter, Pyramidobacter, Scardovia, Shuttleworthia* and *Desulfovibrio* have been recognized as periodontitis-associated genera (Colombo et al., 2009; Huynh et al., 2017; Shi et al., 2018). *Treponema denticola*, *Porphyromonas gingivalis*, and *Tannerella forsythia* have been designated as 'red-complex' periopathogens and have shown a strong association with periodontitis (Darveau, 2010). . It has been reported that patients with COPD tend to have relatively higher ranked means of *Treponema denticola* than healthy participants (Zhou et al., 2020). The COPD group had a higher abundance of *Mogibacterium* in both sample types. The abundance of *Abiotrophia, Atopobium, Gemella* and *Phocaeicola* also increased in SP samples. In the previous studies, *Abiotrophia*, *Atopobium*, *Mogibacterium* and *Phocaeicola* were common periodontitis-associated genera (Mikkelsen et al., 2000; Camelo-Castillo et al., 2015; Zhang et al., 2015; Coretti et al., 2017).

Besides, we found that no study has adequately described the connection and characteristics of these genera in patients with COPD; *Mogibacterium* is associated with persistent generalized disease (Nibali et al., 2020). . Patients in the P_COPD group had high proportions of the genera *Anaeroglobus, Bifidobacterium* and *Clostridium* in SP samples and *Phocaeicola* and *Schwartzia* in the GCF samples. *Phocaeicola* and *Schwartzia* have been previously identified in periodontitis (Camelo-Castillo et al., 2015). *Bergeyella*, *Lautropia*, *Rothia*, *Propionibacterium* and *Cardiobacterium* were more abundant in the healthy participants. *Bergeyella* was considered as putative periodontal protectors in periodontal swabs from the participants (Zorina et al., 2014). *Lautropia mirabilis*, *Propionibacterium propionicum*, *Rothia dentocariosa/mucilagenosa* and *Cardiobacterium hominis* were significantly more prevalent in the healthy group than in the periodontitis patients (Colombo et al., 2009; Ikeda et al., 2020).

This study and observed the association between genera and blood routine indicators. The inflammatory mediators produced by pathogenic microorganisms promote the development of periodontal inflammation and enter the systemic blood circulation, which affects the inflammatory development of systemic diseases (Kumar, 2017). Here we explored the association between genera and blood routine indicators. *Anaeroglobus geminatus* is positively correlated with different lipid mediators which are related to the inflammatory process of periodontitis (Lee et al., 2021). We also observed that the relative abundance of *Anaeroglobus* was positively correlated with lymphocyte counts, indicating that dysbiosis of periodontal-associated microorganisms may accelerate the process of inflammatory between periodontitis and COPD. In our study, the relative abundance of *Treponema* and *Filifactor* were significantly increased in periodontitis group. The relative abundance of *Treponema* was positively correlated with neutrophil counts in GCF samples. In the previous study, *Filifactor, Treponema, and Fretibacterium*, which were more abundant in patients with periodontitis, were proved connected with inflammatory mediators (Lundmark et al., 2019). *Treponema* sp. and cytokines chitinase 3-like 1, sIL-6Rα, sTNF-R1, and gp130/sIL-6Rβ were positively correlated, a negative correlation was identified between IL-10 and *Filifactor alocis*. We discovered that the relative abundance of *Streptococcus* and *Rothia* was negatively correlated with the neutrophil percentages in the GCF samples. In previous study, as a common microorganism of the oral cavity, the presence of *Rothia mucilaginosa* in the lower airways potentially mitigates inflammation (Rigauts et al., 2022). The levels of *Rothia* and *Streptococcus* were significantly lower in oropharyngeal microbiota composition, in both the COVID-19 and flu patients than in the healthy control group, which indicated oropharyngeal microbiota composition may influence the severity of the disease and the progression of inflammation (Ma et al., 2021).The results of our study were similar to previous studies, which partly proved that alterations of periodontal-associated microorganisms may impact the progression of inflammation in respiratory disorders, and indicated that the specific high-abundance bacteria in the four groups may have vital clinical significance for the early diagnosis and treatment of periodontitis and COPD.

The differences in metabolic pathways and functions caused by alteration of microbiota were evident in the SP samples. We performed functional predictions based on the KEGG database. Genetic information processing and translation were significantly different between the periodontitis, COPD, and P_COPD groups. It is worth noting that the functions related to bacteria proliferation were higher in these groups. This may partly explain the higher diversity and density of patients with periodontitis and COPD (Shi et al., 2021). The metabolism of cofactors and vitamins was significantly enriched in the periodontitis and P_COPD groups. Nicotinate and nicotinamide metabolism is associated with the important metabolic pathways in the keystone periodontal pathogen, *Porphyromonas gingivalis* (Hutcherson et al., 2016). Thiamine is essential for several important enzymes involved in carbohydrate metabolism and associated with the key nutrient for *Treponema denticola* survival (Bian et al., 2015). The metabolism of glutathione, phosphonate and phosphinate was significantly decreased in the periodontitis, COPD, and P_COPD groups similar to observations from previous studies. Glutathione is an antioxidant that can moderate host cell damage and reduce inflammatory response (Ghezzi, 2011). *Treponema denticola* is connected to the catabolism of glutathione to H2S (Chu et al., 2020) and the diseased periodontal pockets of periodontitis patients have lower glutathione levels than healthy sites. Glutathione metabolism may be a key pathway for inflammatory damage in COPD.

This study had several limitations. First, compared to the healthy and periodontitis groups, fewer female individuals were recruited for the COPD, and P_COPD groups because of the difficulty in recruiting older female individuals with COPD. Second, this study was not a longitudinal study which limited the exploration of variations in the oral microbiota during disease progression. Then, the detectable microbial diversity is limited in our sample types, we used 16S rRNA gene amplification which limited our ability to identify specific bacteria at the species level. We will refine this in subsequent studies. Finally, the lower airway microbiota samples were not collected in this study. Studies on association between periodontal bacteria and bacteria in the lower airway are insufficient.

5 Conclusion

The present study discovered that the presence of periodontitis and COPD altered the compositions and functional characterization of oral microbiomes. These diversities in microecology were correlated with the pathological change in diseases. These results may have vital clinical significance in the screening and treatment of individuals with periodontitis and COPD.

Data availability statement

The datasets presented in this study can be found in online repositories. The names of the repository/repositories and accession number(s) can be found below: NCBI, BioProject ID: PRJNA910319.

Ethics statement

The present study was approved by the ethics committee of Linfen Central Hospital (Ethics Approval No. 2021-42-1) and was performed in accordance with the Declaration of Helsinki. Written informed consent was obtained from all participants prior to clinical data collection and sampling.

Author contributions

SL, YHo and ZG designed the research project. GX, MC, YZ, QC and YQ practiced sample collection. SL, XM, JX and MJ performed DNA extraction and sequencing data analysis. SG, YHo and ZG conducted experiments and contributed significantly to analysis and manuscript preparation. SL, YHe and WY performed the data analyses and wrote the manuscript. XC, WM and NL helped perform the analysis with constructive discussions. All authors contributed to manuscript revision, read, and approved the submitted version.

Funding

This study was partially supported by Clinical and molecular mechanisms of the dynamic evolution of chronic obstructive pulmonary disease and asthma (No. 2021157), Clinical Medical Research Center of Linfen Central Hospital, Key Medical Research Project of Shanxi Province (No. 2021XM19), and Key Research and Development Plan of Linfen Science and technology (No. 2111).

Acknowledgments

We thank the Linfen Central Hospital for assistance with samples and data collection.

Conflict of interest

The authors declare that the research was conducted in the absence of any commercial or financial relationships that could be construed as a potential conflict of interest.

Publisher's note

Supplementary material

The Supplementary Material for this article can be found online at: https://www.frontiersin.org/articles/10.3389/fcimb.2023.1121399/full#supplementary-material

References

Barnes, P. J., Burney, P. G., Silverman, E. K., Celli, B. R., Vestbo, J., Wedzicha, J. A., et al. (2015a). Chronic obstructive pulmonary disease. *Nat. Rev. Dis. Primers* 1, 15076. doi: 10.1038/nrdp.2015.76

Barnes, P. J., Burney, P. G., Silverman, E. K., Celli, B. R., Vestbo, J., Wedzicha, J. A., et al. (2015b). Chronic obstructive pulmonary disease. *Nat. Rev. Dis. Primers* 1, 1–21. doi: 10.1038/nrdp.2015.76

Bassis, C. M., Erb-Downward, J. R., Dickson, R. P., Freeman, C. M., Schmidt, T. M., Young, V. B., et al. (2015). Analysis of the upper respiratory tract microbiotas as the source of the lung and gastric microbiotas in healthy individuals. *Mbio* 6 (2), 10. doi: 10.1128/mBio.00037-15

Bian, J., Tu, Y., Wang, S. M., Wang, X. Y., and Li, C. (2015). Evidence that TP_0144 of treponema pallidum is a thiamine-binding protein. *J. Bacteriol.* 197 (7), 1164–1172. doi: 10.1128/jb.02472-14

Cai, Z., Lin, S., Hu, S., and Zhao, L. (2021). Structure and function of oral microbial community in periodontitis based on integrated data. *Front. Cell Infect. Microbiol.* 11. doi: 10.3389/fcimb.2021.663756

Camelo-Castillo, A. J., Mira, A., Pico, A., Nibali, L., Henderson, B., Donos, N., et al. (2015). Subgingival microbiota in health compared to periodontitis and the influence of smoking. *Front. Microbiol.* 6. doi: 10.3389/fmicb.2015.00119

Caramori, G., Casolari, P., Barczyk, A., Durham, A. L., Di Stefano, A., and Adcock, I. (2016). COPD immunopathology. *Semin. Immunopathol.* 38 (4), 497–515. doi: 10.1007/s00281-016-0561-5

Chowdhry, R., Singh, N., Sahu, D. K., Tripathi, R. K., Mishra, A., Singh, A., et al. (2018). 16S rRNA long-read sequencing of the granulation tissue from nonsmokers and smokers-severe chronic periodontitis patients. *BioMed. Res. Int.* 2018, 4832912. doi: 10.1155/2018/4832912

Chu, L., Wu, Y., Xu, X., Phillips, L., and Kolodrubetz, D. (2020). Glutathione catabolism by treponema denticola impacts its pathogenic potential. *Anaerobe* 62, 102170. doi: 10.1016/j.anaerobe.2020.102170

Colombo, A. P., Boches, S. K., Cotton, S. L., Goodson, J. M., Kent, R., Haffajee, A. D., et al. (2009). Comparisons of subgingival microbial profiles of refractory periodontitis, severe periodontitis, and periodontal health using the human oral microbe identification microarray. *J. Periodontol.* 80 (9), 1421–1432. doi: 10.1902/jop.2009.090185

Coretti, L., Cuomo, M., Florio, E., Palumbo, D., Keller, S., Pero, R., et al. (2017). Subgingival dysbiosis in smoker and non–smoker patients with chronic periodontitis. *Mol. Med. Rep.* 15 (4), 2007–2014. doi: 10.3892/mmr.2017.6269

Darveau, R. P. (2010). Periodontitis: A polymicrobial disruption of host homeostasis. *Nat. Rev. Microbiol.* 8 (7), 481–490. doi: 10.1038/nrmicro2337

Dewhirst, F. E., Chen, T., Izard, J., Paster, B. J., Tanner, A. C. R., Yu, W. H., et al. (2010). The human oral microbiome. *J. Bacteriol.* 192 (19), 5002–5017. doi: 10.1128/jb.00542-10

Douglas, G. M., Maffei, V. J., Zaneveld, J. R., Yurgel, S. N., Brown, J. R., Taylor, C. M., et al. (2020). PICRUSt2 for prediction of metagenome functions. *Nat. Biotechnol.* 38 (6), 685–688. doi: 10.1038/s41587-020-0548-6

Gaeckle, N. T., Pragman, A. A., Pendleton, K. M., Baldomero, A. K., and Criner, G. J. (2020). The oral-lung axis: The impact of oral health on lung health. *Respir. Care* 65 (8), 1211–1220. doi: 10.4187/respcare.07332

Ghezzi, P. (2011). Role of glutathione in immunity and inflammation in the lung. *Int. J. Gen. Med.* 4, 105–113. doi: 10.2147/ijgm.S15618

Gomes-Filho, I. S., Passos, J. S., and Seixas da Cruz, S. (2010). Respiratory disease and the role of oral bacteria. *J. Oral. Microbiol.* 2. doi: 10.3402/jom.v2i0.5811

Hutcherson, J. A., Gogeneni, H., Yoder-Himes, D., Hendrickson, E. L., Hackett, M., Whiteley, M., et al. (2016). Comparison of inherently essential genes of porphyromonas gingivalis identified in two transposon-sequencing libraries. *Mol. Oral. Microbiol.* 31 (4), 354–364. doi: 10.1111/omi.12135

Huynh, H. T. T., Pignoly, M., Drancourt, M., and Aboudharam, G. (2017). A new methanogen "Methanobrevibacter massiliense" isolated in a case of severe periodontitis. *BMC Res. Notes* 10 (1), 657. doi: 10.1186/s13104-017-2980-3

Ikeda, E., Shiba, T., Ikeda, Y., Suda, W., Nakasato, A., Takeuchi, Y., et al. (2020). Japanese Subgingival microbiota in health vs disease and their roles in predicted functions associated with periodontitis. *Odontology* 108 (2), 280–291. doi: 10.1007/s10266-019-00452-4

Jakubovics, N. S., and Kolenbrander, P. E. (2010). The road to ruin: the formation of disease-associated oral biofilms. *Oral. Dis.* 16 (8), 729–739. doi: 10.1111/j.1601-0825.2010.01701.x

Jia, G., Zhi, A., Lai, P. F. H., Wang, G., Xia, Y., Xiong, Z., et al. (2018). The oral microbiota - a mechanistic role for systemic diseases. *Br. Dent. J.* 224 (6), 447–455. doi: 10.1038/sj.bdj.2018.217

Jiao, J., Jing, W., Si, Y., Feng, X., Tai, B., Hu, D., et al. (2021). The prevalence and severity of periodontal disease in mainland China: Data from the fourth national oral health survey, (2015-2016). *J. Clin. Periodontol.* 48 (2), 168–179. doi: 10.1111/jcpe.13396

Kinane, D. F., Stathopoulou, P. G., and Papapanou, P. N. (2017). Periodontal diseases. *Nat. Rev. Dis. Primers* 3, 17038. doi: 10.1038/nrdp.2017.38

Kucukcoskun, M., Baser, U., Oztekin, G., Kiyan, E., and Yalcin, F. (2013). Initial periodontal treatment for prevention of chronic obstructive pulmonary disease exacerbations. *J. Periodontol.* 84 (7), 863–870. doi: 10.1902/jop.2012.120399

Kumar, P. S. (2017). From focal sepsis to periodontal medicine: a century of exploring the role of the oral microbiome in systemic disease. *J. Physiol.* 595 (2), 465–476. doi: 10.1113/jp272427

Lee, C. T., Li, R., Zhu, L., Tribble, G. D., Zheng, W. J., Ferguson, B., et al. (2021). Subgingival microbiome and specialized pro-resolving lipid mediator pathway profiles are correlated in periodontal inflammation. *Front. Immunol.* 12. doi: 10.3389/fimmu.2021.691216

Li, B. Z., Zhou, H. Y., Guo, B., Chen, W. J., Tao, J. H., Cao, N. W., et al. (2020). Dysbiosis of oral microbiota is associated with systemic lupus erythematosus. *Arch. Oral. Biol.* 113, 10. doi: 10.1016/j.archoralbio.2020.104708

Lin, M., Li, X., Wang, J., Cheng, C., Zhang, T., Han, X., et al. (2020). Saliva microbiome changes in patients with periodontitis with and without chronic obstructive pulmonary disease. *Front. Cell Infect. Microbiol.* 10. doi: 10.3389/fcimb.2020.00124

Lu, C., Zhao, Q., Deng, J., Chen, K., Jiang, X., Ma, F., et al. (2022). Salivary microbiome profile of diabetes and periodontitis in a Chinese population. *Front. Cell Infect. Microbiol.* 12. doi: 10.3389/fcimb.2022.933833

Lundmark, A., Hu, Y. O. O., Huss, M., Johannsen, G., Andersson, A. F., and Yucel-Lindberg, T. (2019). Identification of salivary microbiota and its association with host inflammatory mediators in periodontitis. *Front. Cell Infect. Microbiol.* 9. doi: 10.3389/fcimb.2019.00216

Ma, S., Zhang, F., Zhou, F., Li, H., Ge, W., Gan, R., et al. (2021). Metagenomic analysis reveals oropharyngeal microbiota alterations in patients with COVID-19. *Signal Transduct Target Ther.* 6 (1), 191. doi: 10.1038/s41392-021-00614-3

Malczynski, M., Zhu, A., Zembower, T., and Qi, C. (2021). Diagnostic performance of ion 16S metagenomics kit and ion reporter metagenomics workflow for bacterial pathogen detection in culture-negative clinical specimens from sterile sources. *Diagn. Microbiol. Infect. Dis.* 101 (2), 115451. doi: 10.1016/j.diagmicrobio.2021.115451

Mammen, M. J., and Sethi, S. (2016). COPD and the microbiome. *Respirology* 21 (4), 590–599. doi: 10.1111/resp.12732

Mikkelsen, L., Theilade, E., and Poulsen, K. (2000). Abiotrophia species in early dental plaque. *Oral. Microbiol. Immunol.* 15 (4), 263–268. doi: 10.1034/j.1399-302x.2000.150409.x

Nibali, L., Sousa, V., Davrandi, M., Spratt, D., Alyahya, Q., Dopico, J., et al. (2020). Differences in the periodontal microbiome of successfully treated and persistent aggressive periodontitis. *J. Clin. Periodontol.* 47 (8), 980–990. doi: 10.1111/jcpe.13330

Preshaw, P. M., Alba, A. L., Herrera, D., Jepsen, S., Konstantinidis, A., Makrilakis, K., et al. (2012). Periodontitis and diabetes: a two-way relationship. *Diabetologia* 55 (1), 21–31. doi: 10.1007/s00125-011-2342-y

Rabe, K. F., and Watz, H. (2017). Chronic obstructive pulmonary disease. *Lancet* 389 (10082), 1931–1940. doi: 10.1016/S0140-6736(17)31222-9

Rigauts, C., Aizawa, J., Taylor, S. L., Rogers, G. B., Govaerts, M., Cos, P., et al. (2022). R othia mucilaginosa is an anti-inflammatory bacterium in the respiratory tract of patients with chronic lung disease. *Eur. Respir. J.* 59 (5). doi: 10.1183/13993003.01293-2021

Shi, C., Cai, L., Xun, Z., Zheng, S., Shao, F., Wang, B., et al. (2021). Metagenomic analysis of the salivary microbiota in patients with caries, periodontitis and comorbid diseases. *J. Dent. Sci.* 16 (4), 1264–1273. doi: 10.1016/j.jds.2020.12.002

Shi, M., Wei, Y., Hu, W., Nie, Y., Wu, X., and Lu, R. (2018). The subgingival microbiome of periodontal pockets with different probing depths in chronic and aggressive periodontitis: A pilot study. *Front. Cell Infect. Microbiol.* 8. doi: 10.3389/fcimb.2018.00124

Slocum, C., Kramer, C., and Genco, C. A. (2016). Immune dysregulation mediated by the oral microbiome: potential link to chronic inflammation and atherosclerosis. *J. Intern. Med.* 280 (1), 114–128. doi: 10.1111/joim.12476

Tan, L., Tang, X., Pan, C., Wang, H., and Pan, Y. (2019). Relationship among clinical periodontal, microbiologic parameters and lung function in participants with chronic obstructive pulmonary disease. *J. Periodontol.* 90 (2), 134–140. doi: 10.1002/jper.17-0705

Thomas, C., Minty, M., Vinel, A., Canceill, T., Loubieres, P., Burcelin, R., et al. (2021). Oral microbiota: A major player in the diagnosis of systemic diseases. *Diagnostics* 11 (8), 29. doi: 10.3390/diagnostics11081376

Tonetti, M. S., Greenwell, H., and Kornman, K. S. (2018). Staging and grading of periodontitis: Framework and proposal of a new classification and case definition. *J. Periodontol.* 89, S159–S172. doi: 10.1002/jper.18-0006

Vogelmeier, C. F., Criner, G. J., Martinez, F. J., Anzueto, A., Barnes, P. J., Bourbeau, J., et al. (2017). Global strategy for the diagnosis, management, and prevention of chronic obstructive lung disease 2017 report. GOLD executive summary. *Am. J. Respir. Crit. Care Med.* 195 (5), 557–582. doi: 10.1164/rccm.201701-0218PP

Ward, T., Larson, J., Meulemans, J., Hillmann, B., Lynch, J., Sidiropoulos, D., et al. (2017). BugBase predicts organism-level microbiome phenotypes. *bioRxiv* 5. doi: 10.1101/133462

Wu, Z. S., Xiao, C., Chen, F. H., Wang, Y., and Guo, Z. D. (2022). Pulmonary disease and periodontal health: a meta-analysis. *Sleep Breathing* 12. doi: 10.1007/s11325-022-02577-3

Zhang, Q., Qin, X. Y., Jiang, W. P., Zheng, H., Xu, X. L., and Chen, F. (2015). Comparison of subgingival and peri-implant microbiome in chronic periodontitis. *Chin. J. Dent. Res.* 18 (3), 155–162.

Zhou, X., Wang, J., Liu, W., Huang, X., Song, Y., Wang, Z., et al. (2020). Periodontal status and microbiologic pathogens in patients with chronic obstructive pulmonary disease and periodontitis: A case-control study. *Int. J. Chron Obstruct Pulmon Dis.* 15, 2071–2079. doi: 10.2147/copd.S266612

Zorina, O. A., Petrukhina, N. B., Basova, A. A., Shibaeva, A. V., Trubnikova, E. V., and Shevelev, A. B. (2014). Identification of key markers of normal and pathogenic microbiota determining health of periodontium by NGS-sequencing 16S-rDNA libraries of periodontal swabs. *Stomatologiia (Mosk)* 93 (6), 25–31. doi: 10.17116/stomat201493625-31

frontiers | Frontiers in Cellular and Infection Microbiology

TYPE Original Research
PUBLISHED 06 March 2023
DOI 10.3389/fcimb.2023.1127369

OPEN ACCESS

EDITED BY
Leticia Reyes,
University of Wisconsin-Madison,
United States

REVIEWED BY
Fons Van Den Berg,
Amsterdam University Medical Center,
Netherlands
Peng Ge,
Dalian Medical University, China

*CORRESPONDENCE
Huijun Shu
shjpumch2002@aliyun.com
Dong Wu
wudong@pumch.cn

†These authors have contributed equally to this work and share first authorship

SPECIALTY SECTION
This article was submitted to Microbiome in Health and Disease, a section of the journal Frontiers in Cellular and Infection Microbiology

RECEIVED 19 December 2022
ACCEPTED 20 February 2023
PUBLISHED 06 March 2023

CITATION
Hu X, Han Z, Zhou R, Su W, Gong L, Yang Z, Song X, Zhang S, Shu H and Wu D (2023) Altered gut microbiota in the early stage of acute pancreatitis were related to the occurrence of acute respiratory distress syndrome.
Front. Cell. Infect. Microbiol. 13:1127369.
doi: 10.3389/fcimb.2023.1127369

Altered gut microbiota in the early stage of acute pancreatitis were related to the occurrence of acute respiratory distress syndrome

Xiaomin Hu[1,2†], Ziying Han[2†], Ruilin Zhou[3†], Wan Su[4†], Liang Gong[2], Zihan Yang[2], Xiao Song[5], Shuyang Zhang[3], Huijun Shu[2*] and Dong Wu[2*]

[1]Department of Medical Research Center, State Key Laboratory of Complex Severe and Rare Diseases, Peking Union Medical College Hospital, Chinese Academy of Medical Sciences and Peking Union Medical College, Beijing, China, [2]Department of Gastroenterology, State Key Laboratory of Complex Severe and Rare Diseases, Peking Union Medical College Hospital, Chinese Academy of Medical Sciences and Peking Union Medical College, Beijing, China, [3]Department of Cardiology, Peking Union Medical College Hospital, Chinese Academy of Medical Science and Peking Union Medical College, Beijing, China, [4]Department of Endocrinology, Peking Union Medical College Hospital, Peking Union Medical College, Chinese Academy of Medical Sciences, Beijing, China, [5]Department of Emergency Medicine, Peking Union Medical College Hospital, Peking Union Medical College, Chinese Academy of Medical Sciences, Beijing, China

Background: Acute respiratory distress syndrome (ARDS) is the most common cause of organ failure in acute pancreatitis (AP) patients, which associated with high mortality. Specific changes in the gut microbiota have been shown to influence progression of acute pancreatitis. We aimed to determine whether early alterations in the gut microbiota is related to and could predict ARDS occurrence in AP patients.

Methods: In this study, we performed 16S rRNA sequencing analysis in 65 AP patients and 20 healthy volunteers. The AP patients were further divided into two groups: 26 AP-ARDS patients and 39 AP-nonARDS patients based on ARDS occurrence during hospitalization.

Results: Our results showed that the AP-ARDS patients exhibited specific changes in gut microbiota composition and function as compared to subjects of AP-nonARDS group. Higher abundances of Proteobacteria phylum, *Enterobacteriaceae* family, *Escherichia-Shigella* genus, and *Klebsiella pneumoniae*, but lower abundances of *Bifidobacterium* genus were found in AP-ARDS group compared with AP-nonARDS groups. Random forest modelling analysis revealed that the *Escherichia-shigella* genus was effective to distinguish AP-ARDS from AP-nonARDS, which could predict ARDS occurrence in AP patients.

Conclusions: Our study revealed that alterations of gut microbiota in AP patients on admission were associated with ARDS occurrence after hospitalization, indicating a potential predictive and pathogenic role of gut microbiota in the development of ARDS in AP patients.

KEYWORDS

acute pancreatitis, acute respiratory distress syndrome, gut microbiota, disease prediction, biomarker

Introduction

Acute pancreatitis (AP), one of the most common gastrointestinal diseases, is an acute inflammatory disease with an increasing incidence worldwide (Tenner et al., 2013; Greenberg et al., 2016). In patients with AP, persistent organ failure (OF) can reach 35% and is a key determinant of mortality (Johnson and Abu-Hilal, 2004; Shah and Rana, 2020). The most common cause of OF in AP is acute respiratory distress syndrome (ARDS) (Garg et al., 2005). ARDS is a type of acute, diffuse inflammatory lung injury that can lead to a high mortality rate of up to 48% (Schmandt et al., 2021). Even after five years of rehabilitation, surviving ARDS patients still suffer from poor long-term quality of life; including exercise limitation, difficulty in returning to work, and high medical costs (Herridge et al., 2011). However, missed or delayed diagnosis of ARDS remains a common and challenging problem worldwide. Nearly two-thirds of patients had a delayed or missed diagnosis of ARDS. The miss rate was approximately 40%, and the diagnosis of half of mild ARDS patients was delayed (Bellani et al., 2020). Early recognition of ARDS ensures that patients receive appropriate treatment which relieves lung injury and improves prognosis, therefore, effective prediction methods for ARDS are urgently required (Fan et al., 2018; Pan et al., 2018; Bellani et al., 2020).

AP is strongly associated with gut microbiota imbalance and an impaired epithelial barrier (Besselink et al., 2009). Compared with the healthy group, the diversity of the gut microbiota decreased; with a greater abundance of pathogenic bacteria in AP patients and lower numbers of commensal beneficial genera (Zhang et al., 2018; Zhu et al., 2019). According to the revised Atlanta classification 2012, AP can be divided into three grades: mild AP (MAP), moderately severe AP (MSAP) with transient OF, and severe AP (SAP) with persistent OF (Banks et al., 2013). In AP patients with different degrees of severity, the dominant gut microbiota also varied; with *Bacteroides* in MAP, *Escherichia-Shigella* in MSAP, and Enterococcus in SAP (Yu et al., 2020). Similar results have been reported in animal models; gut microbiota-depleted AP rats were found to have lower levels of inflammatory factors (Zheng et al., 2019; Li et al., 2020). The degree of gut barrier injury and bacterial translocation are important prognostic factors for AP (Besselink et al., 2009).

Disorganized microbiota and damaged intestinal epithelium in AP patients make it easier for the endotoxin diffusion, immune cell migration, and bacteria translocation. The lung environment may be more susceptible to the gut microbiota in patients with AP. Owing to the increased gut permeability, inflammatory factors and activated trypsin could function as the gut-lung axis, thus triggering and promoting lung disease in patients with AP (Shah and Rana, 2020). In addition, gram-negative infections promote release of endotoxins and these can translocate through high-permeability gut mucosa and contribute to the development of ARDS in AP patients (AP-ARDS; "ARDS" mean for ARDS in general, "AP-ARDS" mean for ARDS in acute pancreatitis.) (Gray et al., 2003). Bacteria can also translocate from the gut to the lung (Mukherjee and Hanidziar, 2018). Previous studies also found evidence of bacteria translocation in ARDS patients (Dickson et al., 2016; Dickson et al., 2020). The composition of gut-associated bacteria, especially *Bacteroidetes* and *Enterobacteriaceae*, increased in the lower respiratory tract of ARDS patients (Dickson et al., 2016; Siwicka-Gieroba and Czarko-Wicha, 2020). Further study found that the increase of Escherichia coli in lung was related to higher mortality of ARDS patients (Zhang et al., 2021). Studies have confirmed that the lung microbiota is associated with alveolar inflammation in ARDS (Dickson et al., 2016). Michihito et al. revealed that alterations in lung microbiota are correlated with serum IL-6 levels and hospital mortality in patients with ARDS (Kyo et al., 2019). Therefore, the gut microbiota may be involved in the pathogenesis of AP-ARDS, however, the relationship between the gut microbiota and AP-ARDS remains unknown. If early changes in gut microbiota in AP-ARDS patients can be found, they may help in the early recognition of AP-ARDS, promote early intervention, and even improve patient outcomes.

Therefore, we wanted to investigate the relationship between gut microbiota and AP-ARDS by comparing the microbiota among three groups: healthy controls, AP patients without ARDS (AP-nonARDS), and AP-ARDS patients. By collecting the gut microbiota at the early stage of AP, we investigated whether gut

Abbreviations: AP, acute pancreatitis; AP-ARDS, acute pancreatitis with acute respiratory distress syndrome; AP-nonARDS, acute pancreatitis without acute respiratory distress syndrome; ARDS, acute respiratory distress syndrome; ASV, amplicon sequence variant; BAL, bronchoalveolar lavage fluid; BMI, body mass index; ICU, intensive care unit; IQR, interquartile range; LDA, linear discriminant analysis; MAP, mild acute pancreatitis; MARDS, mild acute respiratory distress syndrome; MSAP, moderate severe pancreatitis; OF, organ failure; PCoA, principal coordinate analysis; SAP, severe acute pancreatitis; SCFAs, short-chain fatty acids; SD, standard deviation.

microbiota was related to and could help predict and recognize AP-ARDS. Our study explored the potential effect of the gut-lung axis in AP-ARDS and provide identify biomarkers for prediction and early recognition of AP-ARDS.

Methods

Study population

This prospective and observational cohort study was conducted at Peking Union Medical College Hospital, Beijing, China. Twenty healthy volunteers and 75 patients were enrolled between June 2018 and July 2021. Ten AP patients were excluded due to history of comorbidities and medicine intake. All patients fulfilled the AP diagnostic criteria according to the 2012 revised Atlanta criteria and were admitted within 24 h of onset (Banks et al., 2013).

The exclusion criteria were as follows: patients with chronic pancreatitis, immunosuppressive disease, inflammatory bowel disease, cancer, irritable bowel syndrome, gastroenteritis, or necrotizing enterocolitis; and use of antibiotics, probiotics, laxatives, or Chinese herbs within two months before symptom onset. Informed consent was obtained from all participants. This study was approved by the Ethics Committee of PUMCH (Identifier: JS1826; date of approval:20th February 2018. Period of validity: February 2018 to August 2020)

For all patients, no ARDS was diagnosed during the first fecal sampling; however, some patients developed ARDS during hospitalization. Patients were diagnosed with ARDS according to the Berlin definition (Ranieri et al., 2012). According to PaO2/FiO2 levels, patients with ARDS were divided into three groups: mild ARDS (MARDS), moderate ARDS, and severe ARDS (Ranieri et al., 2012). Considering the higher rate of mechanical ventilation in moderate ARDS and severe ARDS patients (Fan et al., 2018) as well as the small sample size of severe ARDS group (n=5), we combined moderate ARDS and severe ARDS as non-MARDS group for subgroup analysis.

Collection and analysis of clinical characteristics

Demographic and clinical data were collected from medical record libraries, including age, sex, body mass index (BMI), smoking history, drinking history, combined diseases, disease severity-related scores, local complications, systematic complications, and clinical outcomes. Definitions of local and systematic complications can be found in previous studies (Yu et al., 2020; Hu et al., 2021b; Yu et al., 2021).

Statistical analysis of clinical characteristics was performed using SPSS Statistics 26.0 (IBM Corp., Armonk, NY, USA). The mean ± standard deviation (SD) was used to represent the data distribution. However, when the data did not fit a normal distribution, the median (interquartile range [IQR]) was used. For categorical variables, we performed the $\chi 2$ test or Fisher's exact test; while for continuous variables, we performed the nonparametric Mann-Whitney test. A difference was considered significant when the two-sided p value was less than 0.05.

Sample collection, DNA extraction, and 16S rRNA gene sequencing

Patients with AP have difficulty defecating owing to fasting and water deprivation. Therefore, we used rectal swabs for fecal sampling, as previous studies have described (Yu et al., 2020; Yu et al., 2021). The fecal samples were immediately collected after admission, and all samples were collected within 24 h of AP onset. Then, these samples were stored at − 80°C, and microbial DNA was extracted as soon as possible. We then performed PCR amplification, library construction, Illumina (San Diego, CA, USA) MiSeq sequencing, and sequence quality control, using previously reported methods (Yu et al., 2020; Yu et al., 2021).

Bioinformatics analysis

Amplicon sequence variant (ASV) analysis was performed using EasyAmplicon (Version 1.10). We use the -derep_fullength command in VSEARCH (version 2.15) to create dereplication, denoised these unique sequences into ASVs by the -unoise3 algorithm in USEARCH (Version 10.0), created an ASVs table using the -usearch_global command, and then completed the ASVs classification using the Sintax algorithm command.

Microbiota composition

Alpha diversity analysis, including the Chao and Simpson indices, was performed using Mothur software (1.30.2). The dilution curve was plotted using R software to calculate the microbial diversity at different numbers of sequences. In the beta diversity analysis, principal coordinate analysis (PCoA) was performed using the R package vegan (v2.5-6).

Based on taxonomic information, community structure analysis can be performed at various taxonomic levels. The composition of microbiota at the phylum, family, genus, and species levels was determined using the stat package in R software. Relevant analytical methods were used to detect variation in microbes between the different groups and pairwise comparisons were calculated using the Wilcoxon rank-sum test.

Functional annotation

Linear discriminant analysis (LDA) effect size (LefSe; http://huttenhower.sph.harvard.edu/galaxy) was performed to identify potential biomarkers in the different groups (LDA score>2, p<0.05). Microbiota phenotypes were predicted using BugBase, based on normalized ASVs. The significance of the functional difference was evaluated using the Wilcoxon rank-sum test in the BugBase prediction analysis. The Random Forest R package was

used to build a random forest regression model. We randomly divided the 65 samples into training sets (70%) and testing sets (30%) according to the 16S amplicon sequence and clinical characteristics. Bioinformatics analysis and visualization were performed using the R software. Detailed analysis methods can be found in our previous studies (Hu et al., 2021a; Hu et al., 2021b).

Results

Clinical characteristics of AP-ARDS patients

Sixty-five AP patients and 20 healthy individuals were included in the study. Rectal swabs were collected before the occurrence of ARDS. Twenty-six patients with AP developed ARDS (AP-ARDS; mild ARDS: n=12; moderate ARDS: n=9; severe ARDS: n=5) and 39 patients did not (AP-nonARDS). The average diagnosis time of ARDS was 3.46 ± 1.92 d after AP onset. Table 1 shows the demographic and clinical characteristics of the two groups. Demographic characteristics were generally balanced, however, patients with ARDS had more severe symptoms than those without ARDS (Table 1). The AP-ARDS group had a higher proportion of SAP (2.56% vs. 73.08%; $p<0.001$) and higher disease severity-related scores compared to the AP-nonARDS group. The occurrence of acute peripancreatic fluid collection (35.90% vs. 92.31%; $p<0.001$), systematic complications, organ failure (10.26% vs. 100.00%; $p<0.001$), and ICU admission (0.00% vs. 73.08%; $p<0.001$) was also significantly increased in the AP-ARDS group, except for bowel obstruction and mental status. Furthermore, the total duration of organ failure (median 0.00, IQR 0.00–0.00; vs median 85.00, IQR 41.50–276.00; $p<0.001$); ICU stay (0.00 ± 0.00 vs. 7.15 ± 6.59; $p<0.001$) and hospital stay (8.26 ± 6.65 vs. 23.04 ± 11.52; $p<0.001$) were both longer in AP-ARDS group.

Taxonomic features of gut microbiota in AP-ARDS patients

We analyzed 745,895 reads that were clustered into 1910 ASVs. No statistically significant differences in the richness and diversity of the gut microbiota were noted between the AP-nonARDS and AP-ARDS groups. In the alpha diversity analysis, there were no significant differences in the Chao index ($p>0.05$ between any two groups; Figure 1A). Compared with healthy controls, the Simpson index decreased in both the AP-nonARDS and AP-ARDS groups, but no differences were found between the AP-nonARDS and AP-ARDS groups (Figure 1B). In the rarefaction curve analysis, the curve tended to plateau as the number of reads increased, demonstrating that microbiota in the healthy control, AP-nonARDS, and AP-ARDS groups were abundant

TABLE 1 Demographic and clinical characteristics of health control, AP-nonARDS, and AP-ARDS group.

	CONTROL (n=20)	AP-nonARDS (n=39)	AP-ARDS (n=26)	P value (AP-nonARDS vs AP-ARDS)
Age (years), mean ± SD	37.20 ± 12.00	44.15 ± 15.02	48.69 ± 13.99	0.135
Male, n (%)	11(55.00)	17(43.59)	17(65.38)	0.085
BMI (kg/m2), mean ± SD	22.80 ± 2.89	26.19 ± 3.63	26.48 ± 3.88	0.794
Smoking, n (%)		9(23.07)	9(34.62)	0.308
Drinking, n (%)		9(23.07)	7(26.92)	0.724
Comorbid abnormalities, n (%)				
Hypertension		10(25.64)	13(50.00)	0.044
Diabetes		9 (23.07)	8(30.77)	0.489
Fatty liver		27(69.23)	16(61.54)	0.521
Etiology, n (%)				0.538
Biliary		18(46.15)	9(34.62)	
Hypertriglyceridemia		17(43.59)	15(57.69)	
Alcohol consumption		4(10.26)	2(7.69)	
Disease severity, n (%)				<0.001
MAP		21(53.85)	0(0.00)	
MSAP		17(43.59)	7(26.92)	
SAP		1(2.56)	19(73.08)	
APACHE II, mean ± SD		3.13 ± 2.25	9.96 ± 4.17	<0.001

(Continued)

10.3389/fcimb.2023.1127369

TABLE 1 Continued

	CONTROL (n=20)	AP-nonARDS (n=39)	AP-ARDS (n=26)	P value (AP-nonARDS vs AP-ARDS)
SOFA score, mean ± SD; median (IQR)		0.54 ± 0.64; 0.00 (0.00,1.00)	6.12 ± 4.09; 4.00(3.00, 7.25)	<0.001
Balthazar score E, mean ± SD		2.90 ± 1.02	4.04 ± 0.72	<0.001
Local complications, n (%)				
Acute peripancreatic fluid collection (APFC)		14(35.90)	24(92.31)	<0.001
Pancreatic pseudocyst (PP)		3(7.69)	2(7.69)	>0.999
Acute necrotic collection (ANC)		2(5.13)	12(46.15)	<0.001
Walled off necrosis (WON)		0(0.00)	2(7.69)	0.079
Infected necrosis		0(0.00)	8(30.77)	0.001
Systematic complication, n (%)				
Systemic inflammatory response syndrome (SIRS)		13(33.33)	22(84.62)	<0.001
Acute kidney injury		1(2.56)	12(46.15)	<0.001
Shock		0(0.00)	10(38.46)	<0.001
Liver damage		1(2.56)	11(42.31)	<0.001
Myocardial injury		1(2.56)	6(23.08)	0.009
Sepsis		1(2.56)	14(53.85)	<0.001
Abdominal compartment syndrome (ACS)		1(2.56)	7(26.92)	0.003
Bowel obstruction		3(7.69)	7(26.92)	0.035
Outcome				
Organ failure, n (%)		4(10.26)	26 (100.0)	<0.001
Organ failure duration (h), mean ± SD; median (IQR)		2.59 ± 8.30; 0.00(0.00,0.00)	164.65 ± 159.85; 85.00(41.50,276.00)	<0.001
ICU, n (%)		0(0.00)	19(73.08)	<0.001
ICU stay (days), mean ± SD;		0.00 ± 0.00	7.15 ± 6.59	<0.001
Hospital stay (days), mean ± SD		8.26 ± 6.65	23.04 ± 11.52	<0.001
Death, n (%)		0(0.00)	1(3.85)	0.217

and evenly distributed (Figure 1C). PCoA for the beta diversity results clearly distinguished the three groups, but overlap did occur between the AP-nonARDS group and AP-ARDS group. This indicated a significant difference in the microbiota structure between healthy controls and patients with AP, possible similarities between the AP-nonARDS group and AP-ARDS group (Figure 1D).

The composition of the gut microbiota was significantly different among the three groups. At the phylum level, *Proteobacteria* and *Bacteroidetes* were both increased in patients with AP compared to healthy controls. *Proteobacteria* showed a gradually increase with disease progression (Figure 2A). At the family level, *Enterobacteriaceae*, *Enterococcaceae*, *Bacteroidaceae*, *Clostridiales Incertae Sedis XI*, and *Prevotellaceae* increased, while *Ruminococcaceae* decreased in patients with AP compared to healthy controls. In particular, the abundance of *Enterobacteriaceae* and *Enterococcaceae* increased with disease progression (Figure 2B). At the genus level, *Escherichia-Shigella*, *Bacteroides*, and *Enterococcus* were more abundant in patients with AP, while *Bifidobacterium* and *Blautia* were more abundant in healthy controls. *Escherichia-Shigella* and *Enterococcus* gradually increased while *Bifidobacterium* decreased with disease progression (Figure 2C). Compared to the AP-nonARDS group, 25 ASVs were enriched and 22 ASVs were depleted in the AP-ARDS group (Figure 2D). Figure 2E shows the top 11 different bacteria between the AP-ARDS and AP-nonARDS groups at the species level. *Klebsiella pneumoniae* (ASV_101, p<0.001; ASV_71, p<0.001), *Prevotella copri* (ASV_30, p<0.001; ASV_111, p=0.002), and *Clostridium ramosum* (ASV_150, p=0.002) showed a significant increase; and *Bifidobacterium longum* (ASV_14, p=0.003) decreased in the AP-ARDS group compared to the AP-nonARDS group. Among these microbiota, *Clostridium ramosum* (ASV_150) showed a gradual increase in the healthy to AP-nonARDS to AP-ARDS groups, whereas *Bifidobacterium longum* (ASV_40) showed a gradual decrease (Figure 2E).

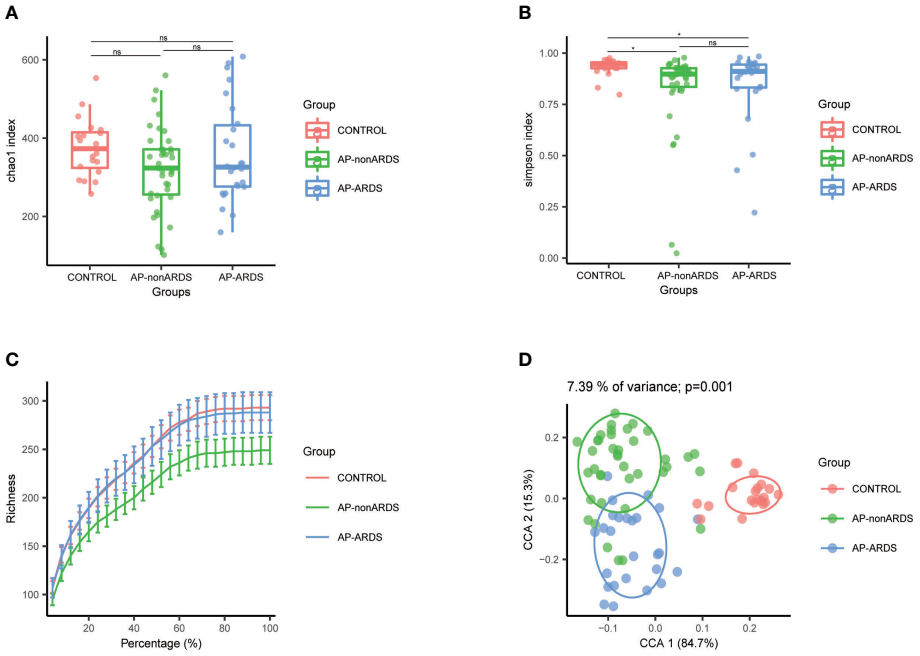

FIGURE 1
Diversity analysis of Control, AP-nonARDS and AP-ARDS group. **(A)** Chao index of α analysis; **(B)** Simpson index of α analysis. There are significant differences between the Control group and AP patients, but no significant difference between AP-nonARDS and AP-ARDS group. **(C)** Rarefaction curves analysis. **(D)**. Principal coordinate analysis (PCoA). CONTROL, healthy population; AP-nonARDS, AP patients without ARDS; AP-ARDS, AP patients with ARDS. * P < 0.05; ns: not significant.

We performed a subgroup analysis according to ARDS severity, and identified some microbiota showing similar trends. At the phylum level, *Proteobacteria* increased in the non-MARDS group compared to that in the MARDS group (Figure 3A). At the family level, *Enterobacteriaceae* increased in the non-MARDS group (Figure 3B). At the genus level, *Escherichia-Shigella* was more abundant in the non-MARDS group (Figure 3C).

Alterations of gut microbiota in AP-ARDS patients are associated with more severe manifestations

LEFSe analysis also revealed that *Enterobacteriaceae* and *Escherichia-Shigella* were dominant in AP-ARDS group while *Enterococcaceae* and *Enterococcus* were dominant in AP-nonARDS group (Figure 4A).

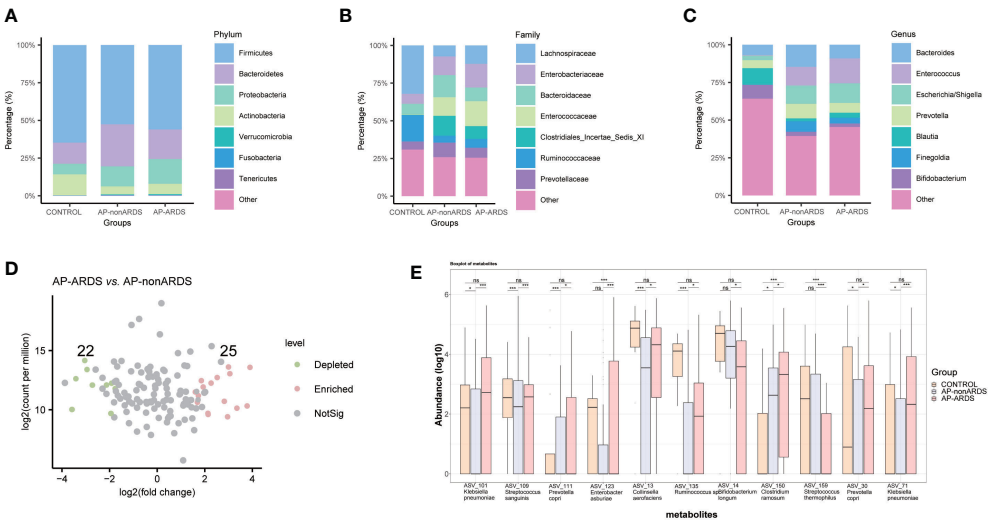

FIGURE 2
Gut microbiota composition at **(A)** phylum, **(B)** family, **(C)** genus levels. **(D)** Different amplicon sequence variants (ASVs) between AP-ARDS and AP-nonARDS group. (green= depleted in AP-ARDS group; red = enriched in AP-ARDS group; gray = no significantly difference). **(E)** Relative abundances of different species between AP-nonARDS and AP-ARDS groups. * P < 0.05; *** P < 0.001; ns: not significant.

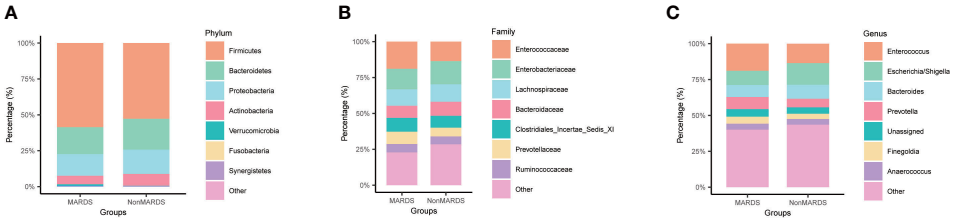

FIGURE 3
Subgroup analysis of gut microbiota composition at phylum **(A)**, family **(B)**, and genus **(C)** levels. MARDS, mild ARDS; NonMARDS, moderate ARDS and severe ARDS.

BugBase functional analysis predicted oxygen utilizing, gram staining, oxidative stress tolerance, biofilm forming, pathogenic potential, mobile element containing, and oxygen tolerance. Compared with healthy controls, anaerobic bacteria decreased in the AP-nonARDS and AP-ARDS groups (CONTROL vs. AP-nonARDS, CONTROL vs. AP-ARDS, both $p<0.001$). Although there was no significant difference, anaerobic bacteria showed a decreasing trend in AP-ARDS compared with AP-nonARDS (Figure 4B). In contrast, aerobic bacteria increased in the AP-nonARDS and AP-ARDS groups (Figure 4C).

Spearman correlation analysis was performed to investigate the relationship between microbiota and clinical outcomes. Two subspecies of *Klebsiella pneumoniae*, ASV_101 and ASV_71, were positively correlated with multiple clinical characteristics, including organ failure, bowel obstruction, sepsis, infection, and acute peripancreatic fluid collection. *Prevotella copri* (ASV_30) was positively correlated with the occurrence and duration of organ failure. Clostridium ramosum (ASV_150) was associated with ICU admission and length of hospital stay. As a probiotic, *Bifidobacterium longum* (ASV_14) negatively correlated with organ failure, Sequential Organ Failure Assessment score (SOFA score), and Acute Physiology And Chronic Health II score (APACHII score) (Figure 4D).

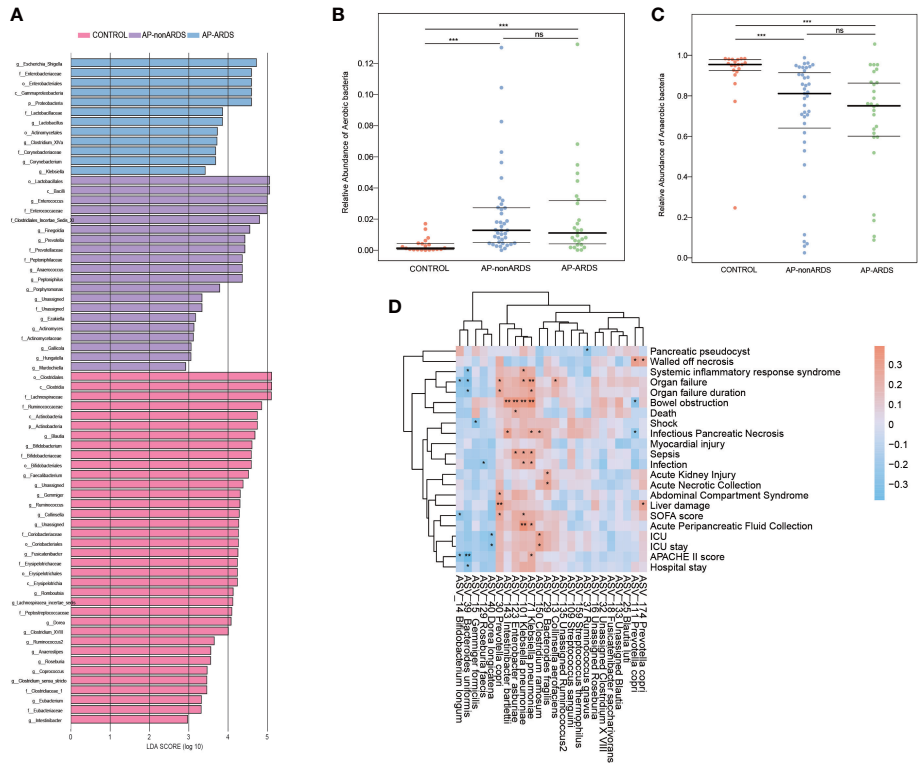

FIGURE 4
Microbial Function Analysis and Clinical Correlation Analysis. **(A)**. Linear discriminant analysis (LDA) Effect Size (LEfSe) analysis. **(B)**. Relative abundance of aerobic bacteria in BugBase analysis. **(C)**. Relative abundance of anaerobic bacteria in BugBase analysis. **(D)**. Spearman correlation of clinical characteristics and different species between AP-ARDS and AP-nonARDS group. * P < 0.05; *** P < 0.001, ns: not significant.

The progression of AP-ARDS is closely associated with Enterobacteriaceae

Considering the significant increase in *Enterobacteriaceae* and its potential pathogenicity, we performed further analyses of *Enterobacteriaceae*. Figure 5A shows the relative abundance of *Enterobacteriaceae* increased with disease progression. Further analysis revealed that almost all genera of the *Enterobacteriaceae* family were increased in the AP-ARDS group (Figure 5B). Random forest identified *Escherichia-shigella* as the most significant feature for distinguishing AP-ARDS from AP-nonARDS (Figure 5C).

Discussion

To our knowledge, this is the first study to explore the relationship between gut microbiota and AP-ARDS and reveals gut microbiota as a predictive biomarker for ARDS. The 16S rRNA sequencing analysis revealed differences of microbiota composition and function between the AP-ARDS and AP-nonARDS groups. Subgroup analysis suggested that gut microbiota composition was also related to the severity of ARDS. Before patients were diagnosed with AP-ARDS, the gut microbiota already had the characteristics of ARDS in AP patients. This indicates that the gut microbiota can be a potential biomarker for prediction and early recognition of AP-ARDS, thereby improving AP-ARDS diagnosis and treatment.

In our characteristics analysis, AP patients with ARDS were more serious than that in the non-ARDS group. AP-severity-associated changes in the gut microbiota were also observed in the AP-ARDS group compared with the AP-nonARDS group. However, we also observed some microbiota changes that might be related to the occurrence and development of AP-ARDS. The enrichment of *Enterobacteriaceae* and *Escherichia-Shigella*, and the reduction of *Bifidobacterium* were associated with AP-ARDS. Previous studies have focused on the lung microbiota of ARDS patients and found that the composition was affected by the gut microbiota (Dickson et al., 2016; Dickson, 2018; Dickson et al., 2020). In our study, similar changes in composition were also observed in the lung microbiota.

In the normal population, the most dominant phylum in the gut microbiota is *Firmicutes*, followed by *Bacteroidetes*, *Actinobacteria*, and *Proteobacteria* (Bozzi Cionci et al., 2018). In our study, the composition of healthy controls was consistent with the normal population; but in AP patients, *Proteobacteria* significantly increased with disease severity. Previous studies have found *Proteobacteria* overgrowth in patients with AP, particularly SAP (Zhu et al., 2019; Yu et al., 2020; Zhu et al., 2021). In addition, *Proteobacteria* in the lung microbiota are closely associated with inflammatory lung disease and positively related to alveolar TNF-α (Dickson et al., 2016). A higher abundance of *Proteobacteria* was a distinguishing feature of ventilator-associated pneumonia (Fromentin et al., 2021). The enrichment of *Proteobacteria* might be a biomarker of inflammatory status in patients.

In our study, *Enterobacteriaceae* and *Escherichia-Shigella* were dominant in AP-ARDS patients. The overall levels of *Enterobacteriaceae*, and the individual *Enterobacteriaceae* genera, increased significantly in patients with ARDS. *Escherichia-Shigella*, a genus of *Enterobacteriaceae* family, is an opportunistic pathogen and more abundant in the sicker group. Random forest analysis identified *Escherichia-Shigella* as the most significant feature for distinguishing ARDS from non-ARDS. Multiple studies have shown that gut-associated bacteria in the lung microbiota, especially *Enterobacteriaceae*, are more abundant in ARDS patients. The abundance of *Enterobacteriaceae* in the lung microbiota was strongly associated with serum IL-6 level and the development of ARDS (Dickson et al., 2016; Dickson, 2018; Mukherjee and Hanidziar, 2018; Kyo et al., 2019). The composition of *Enterobacteriaceae* in the lung can help to identify ARDS patients

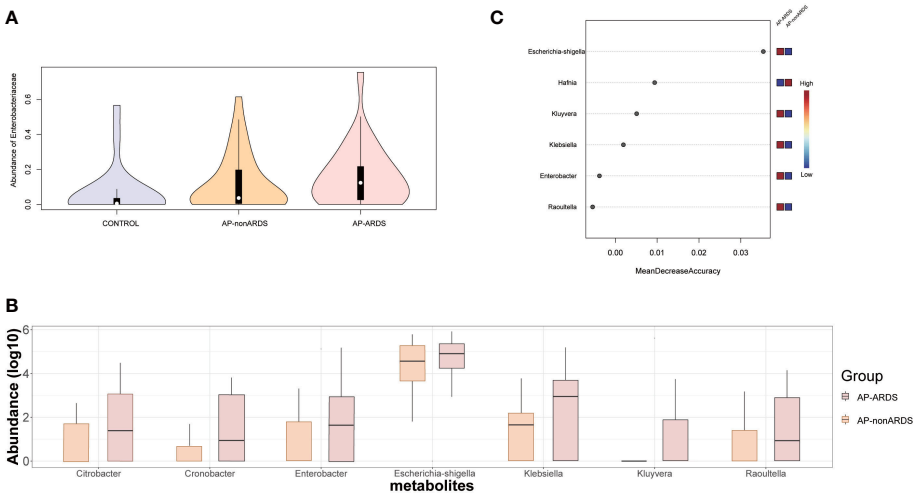

FIGURE 5
Enterobacteriaceae Analysis and Model Predicting. **(A)** The relative abundance of *Enterobacteriaceae* in Control, AP-nonARDS, and AP-ARDS group. **(B)** Major genus in *Enterobacteriaceae* family between AP-nonARDS, and AP-ARDS group. **(C)** Random forest model predicting. It screened out the *Escherichia-shigella* genus as the most significant feature for predicting ARDS.

(Dickson et al., 2020). The enrichment of gut-associated bacteria could also be a biomarker for ARDS patients (Fromentin et al., 2021). Suppression of the gut microbiota could improve the prognosis of critically ill patients (Silvestri et al., 2012).

At the species level, potentially pathogenic bacteria, including *Klebsiella pneumoniae*, *Prevotella copri*, and *Clostridium ramosum*, increased significantly in AP-ARDS patients. *Klebsiella pneumoniae*, a common pathogen of the *Enterobacteriaceae* family, normally colonizes respiratory tract and gut (Chen et al., 2021; Wolff et al., 2021). Dickson et al. revealed that *Klebsiella pneumoniae* overgrowth in the lung was strongly associated with ARDS (Dickson et al., 2020). In addition, *Klebsiella pneumoniae* infection can influence both the gut microbiome and lung metabolome (Wu et al., 2020; Jiang et al., 2022). After inoculation of mice with *Klebsiella pneumoniae*, the diversity and composition of the gut microbiota changed and contributed to lung microbiota dysbiosis within several hours (Jiang et al., 2022). Therefore, *Klebsiella pneumoniae* in the gut may influence lung inflammation through bacterial translocation. *Prevotella* could increase the host sensitivity to intestinal inflammation (Iljazovic et al., 2021). *Prevotella copri* is the most well-known of the Prevotella genus and is positively correlated with many inflammatory diseases, such as rheumatoid arthritis and ankylosing spondylitis (Tett et al., 2021). Transplantation of *Prevotella copri* induces dysbiosis of inflammatory and immune functions and can induce arthritis in mice (Maeda et al., 2016; Qian et al., 2022). Although less well studied, *Clostridium ramosum* has been proven to be positively correlated with Covid-19 disease severity, as well as infection and bacteremia (Zuo et al., 2020).

In our study, the levels of probiotics, such as *Bifidobacterium* and *Bifidobacterium longum*, decreased in patients with ARDS. *Bifidobacterium longum* was negatively correlated with organ failure and disease severity scores. As a beneficial bacterium, *Bifidobacterium* can help maintain gut barrier function, inhibit bacterial translocation, reduce lung inflammation, and therefore improve prognosis (Akshintala et al., 2019; Zhu et al., 2019; Zhu et al., 2021). In the current study, *Bifidobacterium* decreased in both AP patients and mice (Chen et al., 2017; Huang et al., 2017; Zhu et al., 2019; Li et al., 2020). *Bifidobacterium longum* can inhibit viral-induced lung inflammation and injury in mice (Groeger et al., 2020). Supplementation with *Bifidobacterium longum* has shown promising benefits for many diseases, such as irritable bowel syndrome, atopic dermatitis, and obesity (Schellekens et al., 2021; Fang et al., 2022; Sabaté and Iglicki, 2022). Therefore, probiotics have been used in the treatment of AP despite controversy.

Previous studies found the enrichment of gut-associated bacteria in the lung is closely associated with ARDS. However, whether the changes in the gut and lung microbiota are consistent has never been studied. In our study, the variation in gut microbiota in ARDS patients is similar to those seen in lung microbiota in previous studies, which suggests that changes in the lung microbiota might be due to the translocation of the gut microbiota in ARDS patients.

The gut-lung axis is a potential mechanism by which the gut microbiota influences lung inflammation. Gut microbiota can influence local immunity, systemic inflammation, and host immune suppression (Budden et al., 2017; Mukherjee and Hanidziar, 2018; Siwicka-Gieroba and Czarko-Wicha, 2020). Gut microbiota activate immune cells, which can migrate from the gut to the lung and assist in resisting systemic inflammatory disease (He et al., 2017; Mjösberg and Rao, 2018), and release metabolites and endotoxins to influence host immune response (Segain et al., 2000; Artis, 2008; Lin and Zhang, 2017). Additionally, gut microbiota dysbiosis damages the integrity of the intestinal barrier and enables bacterial translocation (Wang et al., 2022). Bacteria in the gut can translocate to the lung through the lymphatic or blood circulation systems and thus mediate lung inflammation (Mukherjee and Hanidziar, 2018). *Enterobacteriaceae*, *Escherichia-Shigella*, and several gut-associated bacteria have been detected in pancreatic fluid which suggested bacteria translocation could occur in AP patients and lead to infected pancreatic necrosis (Li et al., 2013; Hanna et al., 2014; Schmidt et al., 2014). Further studies have revealed that the composition of the lung microbiota can be easily changed, even if the immigration of gut-associated bacteria is transient (Dickson et al., 2016).

Gut microbiota could be transferred to the lung by several possible mechanisms. First, intestinal mucosal permeability may be impaired owing to dysbiosis of the microbiota. In our functional analysis, there was a difference in anaerobic bacterial composition between the AP-ARDS and AP-nonARDS groups. Dysbiosis of anaerobic bacteria is correlated with intestinal epithelial integrity and promotes overgrowth of pathogenic bacteria (Hong et al., 2018; Zhou and Liao, 2021). The proliferation of pathogenic bacteria can consume fatty acids, change intestinal pH, inhibit the growth of probiotics, and damage the gut chemical barrier (Wang et al., 2022). In addition, the overgrowth of pathogens restricts the function of immune cells, such as Tregs, Th2, and B cells; promotes the production of inflammatory factors, such as IL-1β, IL-6, and TNF-α; and thus damages the gut immune barrier (Zhou and Liao, 2021; Wang et al., 2022). As a normal pathogen, *Escherichis-Shigella* is associated with epithelial cell injury and is strongly correlated with AP and ARDS severity (Zhu et al., 2019; Pan et al., 2021). Through reduced butyrate production and increased oxidative stress, *Escherichis-Shigella* could penetrate the intestinal barrier, reach the basolateral layer, and spread rapidly to adjacent cells (Fokam Tagne et al., 2018; Dong et al., 2020). A second possible mechanism may involve the lung microenvironment which is important for bacterial colonization; normally, the alveolar ecosystem is not appropriate for bacterial reproduction (Dickson et al., 2017), however, the lung barrier could be damaged in AP patients. Previous studies have shown that inflammatory factors can migrate from the gut to the lung, recruit neutrophils in the blood, and cause lung inflammation (Mjösberg and Rao, 2018; Zhou and Liao, 2021). The inflammatory cascade amplified the inflammatory response and provided a more favorable inflammatory lung microenvironment for bacterial colonization. In ARDS patients, the influx of nutrient-rich edema and establishment of stark oxygen gradients will damage the local host defenses of the lung and make it easier for bacteria to translocate from the gut to the lung (Dickson, 2018). Therefore, patients may be more sensitive to disruption of the gut microbiota. However, these hypotheses have not been fully confirmed.

The translocation of bacteria from the gut to the lung has important clinical implications. Previous studies have proposed that the lung microbiota from *bronchoalveolar lavage fluid* (*BAL*) could help distinguish ARDS. However, rectal swabs are simpler to collect than BAL, therefore, gut microbiota data are easier to acquire than the lung; making gut microbiota a better prospect. In addition, our study found that the gut microbiota changed before the ARDS diagnosis. Prior to the occurrence of AP-ARDS, the gut microbiota already had characteristics relating to ARDS. Therefore, gut microbiota can be an important predictor of ARDS. Among them, *Proteobacteria*, *Enterobacteriaceae*, and *Escherichia-Shigella* were also found increased in lung microbiota in previous studies. These bacteria may help build prediction models for AP-ARDS that could assist clinicians in decision-making and prevent the occurrence and development of AP-ARDS.

Considering the potential function of microbiota dysbiosis, restoring immune competence and disturbing microbiota is a promising therapy for AP-ARDS (Mukherjee and Hanidziar, 2018). However, the effects of probiotics on patients with AP remain controversial. Some trials have revealed that probiotic supplements may have no benefit in the clinical outcomes of AP patients (Isenmann et al., 2004; Mazaki et al., 2006; Dellinger et al., 2007; de Vries et al., 2007) and probiotic treatment may even worsen the prognosis of patients with AP. Probiotics could cause bacteremia despite the rarity and transfer of antibiotic resistance from probiotics to pathogenic bacteria may worsen infection (Salminen et al., 2002; Cannon et al., 2005; Connolly et al., 2005; Feld et al., 2008). Besselink et al. illustrated that probiotic supplementation increases the occurrence of organ failure and mortality in patients with SAP (Besselink et al., 2008).

According to our study results, this poor response might be related to the overgrowth of pathogens and a disrupted intestinal mucosal barrier. For example, *Klebsiella pneumoniae* infection can inhibit *Bifidobacterium* production (Jiang et al., 2022) and the abundance of *Prevotella* is negatively associated with *Bacteroides* (Tett et al., 2021). Therefore, reducing pathogenic bacteria may promote the growth of probiotics, reduce barrier damage, and thus improve the efficacy of probiotic supplements. Targeted antibiotics are an effective strategy. Germ-free or antibiotic-treated animals are consistently protected from ARDS, and prophylactic administration of antibiotics decreases both mortality and multiple organ dysfunction syndromes, including ARDS (Dickson, 2016; Dickson, 2018). Supplementation with short-chain fatty acids (SCFAs) is another effective treatment option. Studies have found that oral supplementation with SCFAs could decrease susceptibility to bacterial infection, indicating that adjusting the gut microbiota could prevent bacterial pneumonia (Seki et al., 2021). These treatment concepts can be applied for AP patients to prevent ARDS (Siwicka-Gieroba and Czarko-Wicha, 2020). However, considering the potential harm caused by probiotics and antibiotics, targeted therapy should be provided to high-risk ARDS patients. Therefore, the prediction or early recognition of ARDS is essential. Collecting gut microbiota in the early stages of AP could help recognize and diagnose ARDS, and thus guide clinical management.

Gut microbiota could help identify high risk population for developing ARDS. Early identification gives time for appropriate intervention which could help improve prognosis. However, our study has some limitations. First, the specific role of microbiota changes in the disease is unclear. Our study can only provide correlations and suggest that the microbiota might help predict ARDS. However, the mechanism by which microbiota causes pathological conditions remains unknown. Zhang et al. found that different initial sites of infection could influence lung microbiota in patients with septic ARDS. ARDS patients with initial intrapulmonary infection tend to have higher abundance of gut-associated in lung (Zhang et al., 2022). To determine the specific role of gut-lung axis, it is better to make a more nuanced classification in the future. Second, the 16S rRNA sequence analysis could not predict the real composition and function of the microbiota community because it is based on the 16S rRNA sequence library. 16S rRNA analysis cannot completely replace metagenomic analysis but can help guide further studies. Third, the detection time 16S rRNA is long now. For clinical application, quick PCR kit target to specific bacteria is still needed.

In conclusion, this is the first study to report the relationship between gut microbiota and AP-ARDS. Gut microbiota showed a potential predicting ability for AP-ARDS. Dysbiosis of gut microbiota is strongly correlated with AP-ARDS. *Enterobacteriaceae* and *Escherichia-Shigella* are important prediction biomarkers for AP-ARDS. In the future, gut microbiota in early stage of patients with AP may help predict and allow early recognition of AP-ARDS, aid therapy planning, and thus improve patients' quality of life and reduce morbidity of ARDS in AP patients. Further studies will improve our understanding of the role of microbiota in ARDS.

Data availability statement

The datasets presented in this study can be found in online repositories. The names of the repository/repositories and accession number(s) can be found below: https://www.ncbi.nlm.nih.gov/, PRJNA893348.

Ethics statement

The studies involving human participants were reviewed and approved by Ethics Committee of PUMCH (JS1826). The patients/participants provided their written informed consent to participate in this study.

Author contributions

XH and ZH conceived this study and drafted the manuscript. RZ and WS performed data analysis and reviewed the manuscript. ZH, RZ, WS, LG, ZY, and XS collected rectal swabs and clinical data. SZ revised the manuscript. HS and DW contributed to the study design, managed this study and revised the manuscript. All authors contributed to the article and approved the submitted version.

Funding

This study was supported by grants from Chinese Natural Science Foundation, grant number 82270405 and 32170788, National Key Clinical Specialty Construction Project, grant number ZK108000, National High Level Hospital Clinical Research Funding, grant number 2022-PUMCH-A-026, 2022-PUMCH-B-016, 2022-PUMCH-B-023, and Beijing Nova Program.

Acknowledgments

This work was supported by Public Laboratory Platform, National Science and Technology Key Infrastructure on Translational Medicine in Peking Union Medical College Hospital.

Conflict of interest

The authors declare that the research was conducted in the absence of any commercial or financial relationships that could be construed as a potential conflict of interest.

Publisher's note

References

Akshintala, V. S., Talukdar, R., Singh, V. K., and Goggins, M. (2019). The gut microbiome in pancreatic disease. *Clin. Gastroenterol. Hepatol.* 17 (2), 290–295. doi: 10.1016/j.cgh.2018.08.045

Artis, D. (2008). Epithelial-cell recognition of commensal bacteria and maintenance of immune homeostasis in the gut. *Nat. Rev. Immunol.* 8 (6), 411–420. doi: 10.1038/nri2316

Banks, P. A., Bollen, T. L., Dervenis, C., Gooszen, H. G., Johnson, C. D., Sarr, M. G., et al. (2013). Classification of acute pancreatitis–2012: revision of the Atlanta classification and definitions by international consensus. *Gut* 62 (1), 102–111. doi: 10.1136/gutjnl-2012-302779

Bellani, G., Pham, T., and Laffey, J. G. (2020). Missed or delayed diagnosis of ARDS: a common and serious problem. *Intensive Care Med.* 46 (6), 1180–1183. doi: 10.1007/s00134-020-06035-0

Besselink, M. G., van Santvoort, H. C., Boermeester, M. A., Nieuwenhuijs, V. B., van Goor, H., Dejong, C. H., et al. (2009). Timing and impact of infections in acute pancreatitis. *Br. J. Surg.* 96 (3), 267–273. doi: 10.1002/bjs.6447

Besselink, M. G., van Santvoort, H. C., Buskens, E., Boermeester, M. A., van Goor, H., Timmerman, H. M., et al. (2008). Probiotic prophylaxis in predicted severe acute pancreatitis: A randomised, double-blind, placebo-controlled trial. *Lancet* 371 (9613), 651–659. doi: 10.1016/s0140-6736(08)60207-x

Bozzi Cionci, N., Baffoni, L., Gaggìa, F., and Di Gioia, D. (2018). Therapeutic microbiology: The role of bifidobacterium breve as food supplement for the Prevention/Treatment of paediatric diseases. *Nutrients* 10 (11), 1–27. doi: 10.3390/nu10111723

Budden, K. F., Gellatly, S. L., Wood, D. L., Cooper, M. A., Morrison, M., Hugenholtz, P., et al. (2017). Emerging pathogenic links between microbiota and the gut-lung axis. *Nat. Rev. Microbiol.* 15 (1), 55–63. doi: 10.1038/nrmicro.2016.142

Cannon, J. P., Lee, T. A., Bolanos, J. T., and Danziger, L. H. (2005). Pathogenic relevance of lactobacillus: A retrospective review of over 200 cases. *Eur. J. Clin. Microbiol. Infect. Dis.* 24 (1), 31–40. doi: 10.1007/s10096-004-1253-y

Chen, J., Huang, C., Wang, J., Zhou, H., Lu, Y., Lou, L., et al. (2017). Dysbiosis of intestinal microbiota and decrease in paneth cell antimicrobial peptide level during acute necrotizing pancreatitis in rats. *PloS One* 12 (4), e0176583. doi: 10.1371/journal.pone.0176583

Chen, C. M., Wang, M., Li, X. P., Li, P. L., Tian, J. J., Zhang, K., et al. (2021). Homology analysis between clinically isolated extraintestinal and enteral klebsiella pneumoniae among neonates. *BMC Microbiol.* 21 (1), 25. doi: 10.1186/s12866-020-02073-2

Connolly, E., Abrahamsson, T., and Björkstén, B. (2005). Safety of d(-)-lactic acid producing bacteria in the human infant. *J. Pediatr. Gastroenterol. Nutr.* 41 (4), 489–492. doi: 10.1097/01.mpg.0000176179.81638.45

Dellinger, E. P., Tellado, J. M., Soto, N. E., Ashley, S. W., Barie, P. S., Dugernier, T., et al. (2007). Early antibiotic treatment for severe acute necrotizing pancreatitis: a randomized, double-blind, placebo-controlled study. *Ann. Surg.* 245 (5), 674–683. doi: 10.1097/01.sla.0000250414.09255.84

de Vries, A. C., Besselink, M. G., Buskens, E., Ridwan, B. U., Schipper, M., van Erpecum, K. J., et al. (2007). Randomized controlled trials of antibiotic prophylaxis in severe acute pancreatitis: relationship between methodological quality and outcome. *Pancreatology* 7 (5-6), 531–538. doi: 10.1159/000108971

Dickson, R. P. (2016). The microbiome and critical illness. *Lancet Respir. Med.* 4 (1), 59–72. doi: 10.1016/s2213-2600(15)00427-0

Dickson, R. P. (2018). The lung microbiome and ARDS. it is time to broaden the model. *Am. J. Respir. Crit. Care Med.* 197 (5), 549–551. doi: 10.1164/rccm.201710-2096ED

Dickson, R. P., Erb-Downward, J. R., Freeman, C. M., McCloskey, L., Falkowski, N. R., Huffnagle, G. B., et al. (2017). Bacterial topography of the healthy human lower respiratory tract. *mBio* 8 (1), 1–12. doi: 10.1128/mBio.02287-16

Dickson, R. P., Schultz, M. J., van der Poll, T., Schouten, L. R., Falkowski, N. R., Luth, J. E., et al. (2020). Lung microbiota predict clinical outcomes in critically ill patients. *Am. J. Respir. Crit. Care Med.* 201 (5), 555–563. doi: 10.1164/rccm.201907-1487OC

Dickson, R. P., Singer, B. H., Newstead, M. W., Falkowski, N. R., Erb-Downward, J. R., Standiford, T. J., et al. (2016). Enrichment of the lung microbiome with gut bacteria in sepsis and the acute respiratory distress syndrome. *Nat. Microbiol.* 1 (10), 16113. doi: 10.1038/nmicrobiol.2016.113

Dong, R., Bai, M., Zhao, J., Wang, D., Ning, X., and Sun, S. (2020). A comparative study of the gut microbiota associated with immunoglobulin a nephropathy and membranous nephropathy. *Front. Cell Infect. Microbiol.* 10. doi: 10.3389/fcimb.2020.557368

Fan, E., Brodie, D., and Slutsky, A. S. (2018). Acute respiratory distress syndrome: Advances in diagnosis and treatment. *Jama* 319 (7), 698–710. doi: 10.1001/jama.2017.21907

Fang, Z., Pan, T., Li, L., Wang, H., Zhu, J., Zhang, H., et al. (2022). Bifidobacterium longum mediated tryptophan metabolism to improve atopic dermatitis *via* the gut-skin axis. *Gut Microbes* 14 (1), 2044723. doi: 10.1080/19490976.2022.2044723

Feld, L., Schjørring, S., Hammer, K., Licht, T. R., Danielsen, M., Krogfelt, K., et al. (2008). Selective pressure affects transfer and establishment of a lactobacillus plantarum resistance plasmid in the gastrointestinal environment. *J. Antimicrob. Chemother.* 61 (4), 845–852. doi: 10.1093/jac/dkn033

Fokam Tagne, M. A., Noubissi, P. A., Fankem, G. O., and Kamgang, R. (2018). Effects of oxalis barrelieri l. (Oxalidaceae) aqueous extract on diarrhea induced by shigella dysenteriae type 1 in rats. *Health Sci. Rep.* 1 (2), e20. doi: 10.1002/hsr2.20

Fromentin, M., Ricard, J. D., and Roux, D. (2021). Respiratory microbiome in mechanically ventilated patients: A narrative review. *Intensive Care Med.* 47 (3), 292–306. doi: 10.1007/s00134-020-06338-2

Garg, P. K., Madan, K., Pande, G. K., Khanna, S., Sathyanarayan, G., Bohidar, N. P., et al. (2005). Association of extent and infection of pancreatic necrosis with organ failure and death in acute necrotizing pancreatitis. *Clin. Gastroenterol. Hepatol.* 3 (2), 159–166. doi: 10.1016/s1542-3565(04)00665-2

Gray, K. D., Simovic, M. O., Chapman, W. C., Blackwell, T. S., Christman, J. W., May, A. K., et al. (2003). Endotoxin potentiates lung injury in cerulein-induced pancreatitis. *Am. J. Surg.* 186 (5), 526–530. doi: 10.1016/j.amjsurg.2003.07.010

Greenberg, J. A., Hsu, J., Bawazeer, M., Marshall, J., Friedrich, J. O., Nathens, A., et al. (2016). Clinical practice guideline: Management of acute pancreatitis. *Can. J. Surg.* 59 (2), 128–140. doi: 10.1503/cjs.015015

Groeger, D., Schiavi, E., Grant, R., Kurnik-Łucka, M., Michalovich, D., Williamson, R., et al. (2020). Intranasal bifidobacterium longum protects against viral-induced lung inflammation and injury in a murine model of lethal influenza infection. *EBioMedicine* 60, 102981. doi: 10.1016/j.ebiom.2020.102981

Hanna, E. M., Hamp, T. J., McKillop, I. H., Bahrani-Mougeot, F., Martinie, J. B., Horton, J. M., et al. (2014). Comparison of culture and molecular techniques for microbial community characterization in infected necrotizing pancreatitis. *J. Surg. Res.* 191 (2), 362–369. doi: 10.1016/j.jss.2014.05.003

He, Y., Wen, Q., Yao, F., Xu, D., Huang, Y., and Wang, J. (2017). Gut-lung axis: The microbial contributions and clinical implications. *Crit. Rev. Microbiol.* 43 (1), 81–95. doi: 10.1080/1040841x.2016.1176988

Herridge, M. S., Tansey, C. M., Matté, A., Tomlinson, G., Diaz-Granados, N., Cooper, A., et al. (2011). Functional disability 5 years after acute respiratory distress syndrome. *N Engl. J. Med.* 364 (14), 1293–1304. doi: 10.1056/NEJMoa1011802

Hong, G., Zheng, D., Zhang, L., Ni, R., Wang, G., Fan, G. C., et al. (2018). Administration of nicotinamide riboside prevents oxidative stress and organ injury in sepsis. *Free Radic. Biol. Med.* 123, 125–137. doi: 10.1016/j.freeradbiomed.2018.05.073

Hu, X., Fan, Y., Li, H., Zhou, R., Zhao, X., Sun, Y., et al. (2021a). Impacts of cigarette smoking status on metabolomic and gut microbiota profile in Male patients with coronary artery disease: A multi-omics study. *Front. Cardiovasc. Med.* 8. doi: 10.3389/fcvm.2021.766739

Hu, X., Gong, L., Zhou, R., Han, Z., Ji, L., Zhang, Y., et al. (2021b). Variations in gut microbiome are associated with prognosis of hypertriglyceridemia-associated acute pancreatitis. *Biomolecules* 11 (5), 1–16. doi: 10.3390/biom11050695

Huang, C., Chen, J., Wang, J., Zhou, H., Lu, Y., Lou, L., et al. (2017). Dysbiosis of intestinal microbiota and decreased antimicrobial peptide level in paneth cells during hypertriglyceridemia-related acute necrotizing pancreatitis in rats. *Front. Microbiol.* 8. doi: 10.3389/fmicb.2017.00776

Iljazovic, A., Roy, U., Gálvez, E. J. C., Lesker, T. R., Zhao, B., Gronow, A., et al. (2021). Perturbation of the gut microbiome by prevotella spp. enhances host susceptibility to mucosal inflammation. *Mucosal Immunol.* 14 (1), 113–124. doi: 10.1038/s41385-020-0296-4

Isenmann, R., Rünzi, M., Kron, M., Kahl, S., Kraus, D., Jung, N., et al. (2004). Prophylactic antibiotic treatment in patients with predicted severe acute pancreatitis: a placebo-controlled, double-blind trial. *Gastroenterology* 126 (4), 997–1004. doi: 10.1053/j.gastro.2003.12.050

Jiang, Q., Xu, Q., Kenéz, Á., Chen, S., and Yang, G. (2022). Klebsiella pneumoniae infection is associated with alterations in the gut microbiome and lung metabolome. *Microbiol. Res.* 263, 127139. doi: 10.1016/j.micres.2022.127139

Johnson, C. D., and Abu-Hilal, M. (2004). Persistent organ failure during the first week as a marker of fatal outcome in acute pancreatitis. *Gut* 53 (9), 1340–1344. doi: 10.1136/gut.2004.039883

Kyo, M., Nishioka, K., Nakaya, T., Kida, Y., Tanabe, Y., Ohshimo, S., et al. (2019). Unique patterns of lower respiratory tract microbiota are associated with inflammation and hospital mortality in acute respiratory distress syndrome. *Respir. Res.* 20 (1), 246. doi: 10.1186/s12931-019-1203-y

Li, X. Y., He, C., Zhu, Y., and Lu, N. H. (2020). Role of gut microbiota on intestinal barrier function in acute pancreatitis. *World J. Gastroenterol.* 26 (18), 2187–2193. doi: 10.3748/wjg.v26.i18.2187

Li, Q., Wang, C., Tang, C., He, Q., Li, N., and Li, J. (2013). Bacteremia in patients with acute pancreatitis as revealed by 16S ribosomal RNA gene-based techniques*. *Crit. Care Med.* 41 (8), 1938–1950. doi: 10.1097/CCM.0b013e31828a3dba

Lin, L., and Zhang, J. (2017). Role of intestinal microbiota and metabolites on gut homeostasis and human diseases. *BMC Immunol.* 18 (1), 2. doi: 10.1186/s12865-016-0187-3

Maeda, Y., Kurakawa, T., Umemoto, E., Motooka, D., Ito, Y., Gotoh, K., et al. (2016). Dysbiosis contributes to arthritis development *via* activation of autoreactive T cells in the intestine. *Arthritis Rheumatol* 68 (11), 2646–2661. doi: 10.1002/art.39783

Mazaki, T., Ishii, Y., and Takayama, T. (2006). Meta-analysis of prophylactic antibiotic use in acute necrotizing pancreatitis. *Br. J. Surg.* 93 (6), 674–684. doi: 10.1002/bjs.5389

Mjösberg, J., and Rao, A. (2018). Lung inflammation originating in the gut. *Science* 359 (6371), 36–37. doi: 10.1126/science.aar4301

Mukherjee, S., and Hanidziar, D. (2018). More of the gut in the lung: How two microbiomes meet in ARDS. *Yale J. Biol. Med.* 91 (2), 143–149.

Pan, L. L., Li, B. B., Pan, X. H., and Sun, J. (2021). Gut microbiota in pancreatic diseases: possible new therapeutic strategies. *Acta Pharmacol. Sin.* 42 (7), 1027–1039. doi: 10.1038/s41401-020-00532-0

Pan, C., Liu, L., Xie, J. F., and Qiu, H. B. (2018). Acute respiratory distress syndrome: Challenge for diagnosis and therapy. *Chin. Med. J. (Engl)* 131 (10), 1220–1224. doi: 10.4103/0366-6999.228765

Qian, X., Zhang, H. Y., Li, Q. L., Ma, G. J., Chen, Z., Ji, X. M., et al. (2022). Integrated microbiome, metabolome, and proteome analysis identifies a novel interplay among commensal bacteria, metabolites and candidate targets in non-small cell lung cancer. *Clin. Transl. Med.* 12 (6), e947. doi: 10.1002/ctm2.947

Ranieri, V. M., Rubenfeld, G. D., Thompson, B. T., Ferguson, N. D., Caldwell, E., Fan, E., et al. (2012). Acute respiratory distress syndrome: The Berlin definition. *Jama* 307 (23), 2526–2533. doi: 10.1001/jama.2012.5669

Sabaté, J. M., and Iglicki, F. (2022). Effect of bifidobacterium longum 35624 on disease severity and quality of life in patients with irritable bowel syndrome. *World J. Gastroenterol.* 28 (7), 732–744. doi: 10.3748/wjg.v28.i7.732

Salminen, M. K., Tynkkynen, S., Rautelin, H., Saxelin, M., Vaara, M., Ruutu, P., et al. (2002). Lactobacillus bacteremia during a rapid increase in probiotic use of lactobacillus rhamnosus GG in Finland. *Clin. Infect. Dis.* 35 (10), 1155–1160. doi: 10.1086/342912

Schellekens, H., Torres-Fuentes, C., van de Wouw, M., Long-Smith, C. M., Mitchell, A., Strain, C., et al. (2021). Bifidobacterium longum counters the effects of obesity: Partial successful translation from rodent to human. *EBioMedicine* 63, 103176. doi: 10.1016/j.ebiom.2020.103176

Schmandt, M., Glowka, T. R., Kreyer, S., Muders, T., Muenster, S., Theuerkauf, N. U., et al. (2021). Secondary ARDS following acute pancreatitis: Is extracorporeal membrane oxygenation feasible or futile? *J. Clin. Med.* 10 (5), 1–11. doi: 10.3390/jcm10051000

Schmidt, P. N., Roug, S., Hansen, E. F., Knudsen, J. D., and Novovic, S. (2014). Spectrum of microorganisms in infected walled-off pancreatic necrosis - impact on organ failure and mortality. *Pancreatology* 14 (6), 444–449. doi: 10.1016/j.pan.2014.09.001

Segain, J. P., Raingeard de la Blétière, D., Bourreille, A., Leray, V., Gervois, N., Rosales, C., et al. (2000). Butyrate inhibits inflammatory responses through NFkappaB inhibition: implications for crohn's disease. *Gut* 47 (3), 397–403. doi: 10.1136/gut.47.3.397

Seki, D., Mayer, M., Hausmann, B., Pjevac, P., Giordano, V., Goeral, K., et al. (2021). Aberrant gut-microbiota-immune-brain axis development in premature neonates with brain damage. *Cell Host Microbe* 29 (10), 1558–1572.e1556. doi: 10.1016/j.chom.2021.08.004

Shah, J., and Rana, S. S. (2020). Acute respiratory distress syndrome in acute pancreatitis. *Indian J. Gastroenterol.* 39 (2), 123–132. doi: 10.1007/s12664-020-01016-z

Silvestri, L., de la Cal, M. A., and van Saene, H. K. (2012). Selective decontamination of the digestive tract: the mechanism of action is control of gut overgrowth. *Intensive Care Med.* 38 (11), 1738–1750. doi: 10.1007/s00134-012-2690-1

Siwicka-Gieroba, D., and Czarko-Wicha, K. (2020). Lung microbiome - a modern knowledge. *Cent Eur. J. Immunol.* 45 (3), 342–345. doi: 10.5114/ceji.2020.101266

Tenner, S., Baillie, J., DeWitt, J., and Vege, S. S. (2013). American College of gastroenterology guideline: management of acute pancreatitis. *Am. J. Gastroenterol.* 108 (9), 1400–1415; 1416. doi: 10.1038/ajg.2013.218

Tett, A., Pasolli, E., Masetti, G., Ercolini, D., and Segata, N. (2021). Prevotella diversity, niches and interactions with the human host. *Nat. Rev. Microbiol.* 19 (9), 585–599. doi: 10.1038/s41579-021-00559-y

Wang, Z., Li, F., Liu, J., Luo, Y., Guo, H., Yang, Q., et al. (2022). Intestinal microbiota - an unmissable bridge to severe acute pancreatitis-associated acute lung injury. *Front. Immunol.* 13. doi: 10.3389/fimmu.2022.913178

Wolff, N. S., Jacobs, M. C., Wiersinga, W. J., and Hugenholtz, F. (2021). Pulmonary and intestinal microbiota dynamics during gram-negative pneumonia-derived sepsis. *Intensive Care Med. Exp.* 9 (1), 35. doi: 10.1186/s40635-021-00398-4

Wu, T., Xu, F., Su, C., Li, H., Lv, N., Liu, Y., et al. (2020). Alterations in the gut microbiome and cecal metabolome during klebsiella pneumoniae-induced pneumosepsis. *Front. Immunol.* 11. doi: 10.3389/fimmu.2020.01331

Yu, S., Xiong, Y., Fu, Y., Chen, G., Zhu, H., Mo, X., et al. (2021). Shotgun metagenomics reveals significant gut microbiome features in different grades of acute pancreatitis. *Microb. Pathog.* 154, 104849. doi: 10.1016/j.micpath.2021.104849

Yu, S., Xiong, Y., Xu, J., Liang, X., Fu, Y., Liu, D., et al. (2020). Identification of dysfunctional gut microbiota through rectal swab in patients with different severity of acute pancreatitis. *Dig Dis. Sci.* 65 (11), 3223–3237. doi: 10.1007/s10620-020-06061-4

Zhang, P., Chen, Y., Zheng, W., Wu, M., Wu, Z., Lu, Y., et al. (2021). Changes of lung microbiome of acute respiratory distress syndrome before and after treatment under open airway. *Zhonghua Wei Zhong Bing Ji Jiu Yi Xue* 33 (9), 1063–1068. doi: 10.3760/cma.j.cn121430-20210414-00558

Zhang, P., Liu, B., Zheng, W., Chen, Y., Wu, Z., Lu, Y., et al. (2022). Pulmonary microbial composition in sepsis-induced acute respiratory distress syndrome. *Front. Mol. Biosci.* 9. doi: 10.3389/fmolb.2022.862570

Zhang, X. M., Zhang, Z. Y., Zhang, C. H., Wu, J., Wang, Y. X., and Zhang, G. X. (2018). Intestinal microbial community differs between acute pancreatitis patients and healthy volunteers. *BioMed. Environ. Sci.* 31 (1), 81–86. doi: 10.3967/bes2018.010

Zheng, J., Lou, L., Fan, J., Huang, C., Mei, Q., Wu, J., et al. (2019). Commensal escherichia coli aggravates acute necrotizing pancreatitis through targeting of intestinal epithelial cells. *Appl. Environ. Microbiol.* 85 (12), 1–15. doi: 10.1128/aem.00059-19

Zhou, X., and Liao, Y. (2021). Gut-lung crosstalk in sepsis-induced acute lung injury. *Front. Microbiol.* 12. doi: 10.3389/fmicb.2021.779620

Zhu, Y., He, C., Li, X., Cai, Y., Hu, J., Liao, Y., et al. (2019). Gut microbiota dysbiosis worsens the severity of acute pancreatitis in patients and mice. *J. Gastroenterol.* 54 (4), 347–358. doi: 10.1007/s00535-018-1529-0

Zhu, Y., Mei, Q., Fu, Y., and Zeng, Y. (2021). Alteration of gut microbiota in acute pancreatitis and associated therapeutic strategies. *BioMed. Pharmacother.* 141, 111850. doi: 10.1016/j.biopha.2021.111850

Zuo, T., Zhang, F., Lui, G. C. Y., Yeoh, Y. K., Li, A. Y. L., Zhan, H., et al. (2020). Alterations in gut microbiota of patients with COVID-19 during time of hospitalization. *Gastroenterology* 159 (3), 944–955.e948. doi: 10.1053/j.gastro.2020.05.048

frontiers | Frontiers in Cellular and Infection Microbiology

TYPE Original Research
PUBLISHED 25 April 2023
DOI 10.3389/fcimb.2023.1166389

OPEN ACCESS

EDITED BY
Jianmin Chai,
Foshan University, China

REVIEWED BY
Meng Zhou,
Wenzhou Medical University, China
Wenbin Lei,
The First Affiliated Hospital of Sun Yat-sen University, China

*CORRESPONDENCE
Jingting Wang
5433@hrbmu.edu.cn
Yanan Sun
76202920@qq.com

†These authors have contributed equally to this work

SPECIALTY SECTION
This article was submitted to Microbiome in Health and Disease, a section of the journal Frontiers in Cellular and Infection Microbiology

RECEIVED 15 February 2023
ACCEPTED 03 April 2023
PUBLISHED 25 April 2023

CITATION
Che Y, Wang N, Ma Q, Liu J, Xu Z, Li Q, Wang J and Sun Y (2023) Microbial characterization of the nasal cavity in patients with allergic rhinitis and non-allergic rhinitis.
Front. Cell. Infect. Microbiol. 13:1166389.
doi: 10.3389/fcimb.2023.1166389

Microbial characterization of the nasal cavity in patients with allergic rhinitis and non-allergic rhinitis

Yanlu Che, Nan Wang, Qianzi Ma, Junjie Liu, Zhaonan Xu, Qiuying Li, Jingting Wang*† and Yanan Sun*†

Department of Otorhinolaryngology, Head and Neck Surgery, The Second Affiliated Hospital of Harbin Medical University, Harbin, China

Introduction: Although recent studies have shown that the human microbiome is involved in the pathogenesis of allergic diseases, the impact of microbiota on allergic rhinitis (AR) and non-allergic rhinitis (nAR) has not been elucidated. The aim of this study was to investigate the differences in the composition of the nasal flora in patients with AR and nAR and their role in the pathogenesis.

Method: From February to September 2022, 35 AR patients and 35 nAR patients admitted to Harbin Medical University's Second Affiliated Hospital, as well as 20 healthy subjects who underwent physical examination during the same period, were subjected to 16SrDNA and metagenomic sequencing of nasal flora.

Results: The microbiota composition of the three groups of study subjects differs significantly. The relative abundance of Vibrio vulnificus and Acinetobacter baumanni in the nasal cavity of AR patients was significantly higher when compared to nAR patients, while the relative abundance of Lactobacillus murinus, Lactobacillus iners, Proteobacteria, Pseudomonadales, and Escherichia coli was lower. In addition, Lactobacillus murinus and Lacttobacillus kunkeei were also negatively correlated with IgE, while Lacttobacillus kunkeei was positively correlated with age. The relative distribution of Faecalibacterium was higher in moderate than in severe AR patients. According to KEGG functional enrichment annotation, ICMT(protein-S-isoprenylcysteine O-methyltransferase,ICMT) is an AR microbiota-specific enzyme that plays a role, while glycan biosynthesis and metabolism are more active in AR microbiota. For AR, the model containing Parabacteroides goldstemii, Sutterella-SP-6FBBBBH3, Pseudoalteromonas luteoviolacea, Lachnospiraceae bacterium-615, and Bacteroides coprocola had the highest the area under the curve (AUC), which was 0.9733(95%CI:0.926-1.000) in the constructed random forest prediction model. The largest AUC for nAR is 0.984 (95%CI:0.949–1.000) for the model containing Pseudomonas-SP-LTJR-52, Lachnospiraceae bacterium-615, Prevotella corporis, Anaerococcus vaginalis, and Roseburia inulinivorans.

Conclusion: In conclusion, patients with AR and nAR had significantly different microbiota profiles compared to healthy controls. The results suggest that the nasal microbiota may play a key role in the pathogenesis and symptoms of AR and nAR, providing us with new ideas for the treatment of AR and nAR.

KEYWORDS

allergic rhinitis, non-allergic rhinitis, microecology, 16SrDNA, macrogenome

1 Introduction

The prevalence of Chronic rhinitis (CR) is increasing, and it is reported that more than 500 million people worldwide suffer from the disease (Agnihotri and McGrath, 2019). There are two types of CR: allergic rhinitis (AR) and non-allergic rhinitis (nAR). AR is a Th2 immune response disease caused by IgE-mediated inhalation of allergens, with symptoms such as nasal itching, sneezing, runny nose, and nasal congestion (Sahoyama et al., 2022), which relies on positive skin prick test (SPT) or specific immunoglobulin E (sIgE) teats for diagnosis (Roberts et al., 2016). NAR is a heterogeneous nasal disease with symptoms of nasal itching, sneezing, rhinorrhea, and nasal congestion, but no systemic allergic symptoms, negative sIgE and/or SPT, affecting over 200 million people worldwide (Hellings et al., 2017). At present, the etiologies of AR and NAR are still being further explored (Bousquet et al., 2008).

The study of microbiomes has revealed the importance of microbiota in maintaining human health over the last few decades (Ver Heul et al., 2019). The term "microbiota" refers to all microorganisms that live in the body, including bacteria, fungi, viruses, protozoa, and archaea, among others, and are found in large numbers and varying proportions (Koidl and Untersmayr, 2021). This ratio is dynamic during the first two years of life, after which it tends to balance, and early colonization of this "balanced" and "healthy" microbiota lays the groundwork for lifelong health (Grier et al., 2018). Although most current research has focused on the gut microbiota, the role of microbiota elsewhere in the body in human disease is becoming more recognized (Ver Heul et al., 2019). According to research, microbial diversity can play a positive or negative role in allergic diseases. Staphylococcus nasal colonization was found to be significantly higher in asthmatic patients' respiratory extracts than in healthy controls, which induced human nasal epithelial cells to release inflammatory factors and aggravated Th2 cell-mediated inflammatory response (Durack et al., 2018). According to research, the abundance of Faecalibacterium in the intestines of asthmatic children is significantly reduced, and the short-chain fatty acids it produces inhibit the accumulation of peripheral Treg cells *via* HDAC, thereby reducing allergic airway diseases (Koidl and Untersmayr, 2021). However, no studies have been conducted to determine whether there are differences in nasal microbiota between nAR and AR patients. As a result, we used high throughput 16S rDNA and metagenomic sequencing to compare the nasal microbiota characteristics of AR, nAR, and healthy controls. The purpose of this study is to determine nasal microbiota distribution differences, specific nasal microbiota and functions related to AR and nAR environmental factors, and functional analysis of key gene pathways and enzymes.

2 Material and methods

2.1 Research objects and experimental design

From February 2022 to September 2022, patients were consulted in the nasal outpatient department of the Second Affiliated Hospital of Harbin Medical University. 35 cases in the AR group, 35 in the nAR group, and 20 in the healthy control group were selected. A total of 95 subjects were sequenced and analyzed for 16SrDNA of nasal secretions, and 3 were selected in each group. Macro genome sequencing analysis was carried out. This trial was approved by the Ethics Review Committee of the Second Affiliated Hospital of Harbin Medical University (license number: KY2021-360) and registered with the China Clinical Trial Registration Center (registration number ChiCTR2200057919). All subjects and control groups have informed consent, and the case conforms to the ethical norms of the Helsinki Declaration (World MA, 2013).

2.1.1 Incorporate the criteria

The control group: (1) healthy people selected for the physical examination of the Second Affiliated Hospital of Harbin Medical University and the examination results are normal; (2) there is no history of allergies or family allergies; (3) There are no allergy-related symptoms; (4) After a comprehensive physical examination such as allergen testing, no factors that may cause deviation from the results of this test have been found; (5) Voluntary participation in this study.

AR group: (1) Comply with the diagnostic criteria of AR in the Guidelines for the Diagnosis and Treatment of Allergic Rhinitis (2022, Revised Edition) (Subspecialty Group of Rhinology et al., 2022), paroxysmal sneezing, clear water-like runny nose, itch, sneezing, and other symptoms appear 2 or more, and the daily symptoms persist or accumulate more than 1 hour; (2) At least one of the 19 SIgE test result is positive (>=0.35kU/L, household dust mite, house dust, mulberry tree, cat dandruff, dog dandruff,

cockroach, amaranth, egg white, milk, shrimp, beef, shellfish, crab, mango, cashew nuts, pineapple, mixed mold, mixed grass, tree pollen); (3) 10 allergens to One less SPT result was positive (house dust mite, dust mite, cockroach, dendritic spores, artemisia annua, birch, cloves, cat hair, dog hair); (4) Total serum IgE positive (>100IU/mL); (5) Voluntary participation in this study.

nAR group: (1) Have different degrees of clinical symptoms such as nasal congestion, runny nose, nasal itching, sneezing, etc.; (2) All SIgE test results are negative (<35kU/L); (3) All SPT test results are negative; (4) Total serum IgE negative (<100IU/mL); (5) Negative for nasal allergen provocation test (NAPT);(6) Participate in this study voluntarily.

2.1.2 Exclusion criteria

The above subjects met the following exclusion criteria: (1) Patients on systemic or topical antibiotics, immune agents, glucocorticoids, and antihistamines within 3 months.; (2) Other related diseases in the nasal cavity: sinusitis, nasal polyps, benign and malignant tumors, nasal boils, carbuncles, intranasal infections, Nose bleeding within 1 month; (3) Other respiratory diseases: chronic obstructive pulmonary disease, asthma, bronchiectasis, tuberculosis, pneumonia, pulmonary heart disease, pulmonary malignant tumors; (4) Hypertension, coronary heart disease, hyperthyroidism, hypothyroidism, liver and kidney dysfunction, blood system diseases, etc.; 5) The patient has a history of mental and neurological diseases; (6) The abnormal examination results of clinical signs before the trial may deviate the results of this trial according to the judgment of the researchers; (7) Patients with nasal irrigation within 2 weeks.

2.2 Nasal symptom score table (TNSS) and quality of life questionnaire for nasal conjunctivitis (RQLQ)

Use the total score of nasal symptoms (TNSS) to evaluate the severity of the symptoms. TNSS score: 0 to 3 (0 = asymptomatic; 1 = mild; 2 = moderate; 3 = severe). Mild: no symptoms that cause obvious discomfort; Moderate: Symptoms cause discomfort but do not affect daily life or interfere with sleep; Severe: Symptoms interfere with daily activities and sleep status. Add the points of each symptom, and get a total score is TNSS (Kang et al., 2017). RQLQ is limited by activity restrictions, sleep disorders, non- Eye/nasal symptoms, practical problems, nasal symptoms, eye symptoms, and emotional composition includes a total of 28 items, each dimension is scored separately, and the cumulative total score is the total score of RQLQ (Juniper et al., 1996; Blaiss et al., 2022).

2.3 Sample collection

Guide the swab to the lower turbinate area under the nasal endoscope, rotate at least six times until the swab is saturated, remove it, put it in a liquid nitrogen bottle, and refrigerate at -80°C for 15 minutes until DNA is extracted.

2.4 16SrDNA and macrogenome sequencing analysis

2.4.1 16SrDNA sequencing analysis

The genomic DNA of the sample is extracted by CTAB or SDS method, then use agarose gel electrophoresis to detect the purity and concentration of DNA, and use sterile water to dilute an appropriate amount of sample to 1ng/μL. Using diluted genomic DNA as a template, select the V3-V4 area and use specific primers with Barcode and high-efficiency high-fidelity enzymes for PCR. The PCR products that passed the test were purified by magnetic beads, quantified by enzyme labeling, and mixed with the same amount of samples according to the concentration of PCR products. After full mixing, use 2% agarose gel electrophoresis to detect the PCR products and construct the library. The constructed library was checked with Qubit and Q-PCR for quantification, and the qualified library will be sequenced.

2.4.2 Macrogenome sequencing analysis

Use 1% agarose gel electrophoresis (AGE) to analyze the purity and integrity of DNA, and use Qubit® dsDNA Assay Kit in Qubit® 2.0 Fluorometer (Life Technologies, CA, USA) to check DNA for quantification. Take an appropriate amount of sample into a centrifuge tube, and dilute the sample with sterile water until the OD value is between 1.8-2.0. Take 1μg genome DNA of the sample and use NEBNext® Ultra, DNA Library Prep Kit for Illumina (NEB, USA) to construct the library. The genomic DNA was randomly sheared into fragments with a length of about 350 bp using Covaris ultrasonic crusher. The obtained fragments were end-repaired, A-tailed, and further ligated with a sequence adapter. The fragments with adapters were PCR amplified, size selected, and purified to construct the library. The constructed library was checked with Qubit2.0 for quantification, diluted to 2ng/ul, and then the insert size of the library was detected with Agilent 2100. After the insert size meets the expectation, the Q-PCR method is used to accurately quantify effective library concentration (effective library concentration is>3nM) to ensure the quality of the library. Quantified libraries will be pooled and sequenced on Illumina PE150 platforms, according to effective library concentration and data amount required.

2.5 Statistical analysis

2.5.1 16 SrDNA sequencing statistical analysis

Use the Uparse algorithm to cluster sequences into OTUs and annotate species, use Qiime software to calculate Chao1, Shannon, Simpson and ace indexes, draw diluted curves and species accumulation curves, and analyze differences between Alpha diversity index groups. R software is used to analyze the

differences between Beta diversity index groups, including LEfSe analysis, MetaStat analysis, and t.test_bar_plot analysis to compare the differences between groups, calculate the Spearman correlation coefficient values of species and environmental factors and test their significance. Based on species abundance, the correlation coefficient value between each genus is calculated using graphviz-2.38.0 to draw a network diagram, and MeanDecreeAccuracy chose a meaningful genus to build a random forest model.

2.5.2 Statistical analysis of macrogenome sequencing

Use MetaGeneMark for ORF prediction, and use Bowtie2 (Bowtie2.2.4) to compare the Clean Data of each sample to the initial gene catalog for basic information statistics, core-pan gene Analysis, correlation analysis between samples, and gene number Wayne diagram analysis. The sequence extracted from the NR database of NCBI is compared with Unigenes, the LCA algorithm is used to determine the species annotation information, Krona analysis is carried out, and then Metastats and LEfSe analysis are used to find different species between groups. Unigenes were compared with the KEGG database using DIAMOND software for annotated gene number statistics, relative abundance profile display, abundance clustering heat map display, comparative metabolic pathway analysis, and Metastat and LEfSe analysis of functional differences between groups based on abundance at each taxonomic level.

3 Results

3.1 clinical characteristics of the subjects

The mean age of the AR group was 21.03 ± 9.94, the TNSS score was 10.03 ± 3.67, the RQLQ score was 102.8 ± 29.64; the mean age of the nAR group was 33.73 ± 10.73, the TNSS score 8.77 ± 2.24, RQLQ score 89.67 ± 26.43, mean age of control group: 29.7 ± 12.25, AR group was significantly younger than the nAR group ($p<0.001$), and TNSS score and RQLQ score did not differ between the two groups ($p>0.05$) (Table 1).

TABLE 1 Clinical characteristics of AR and non-AR subjects.

Group	AR	nAR	B
Subjects (n)	30	30	20
Gender			
Male	14	13	8
Female	16	17	12
Age	21.03 ± 9.94	33.73 ± 10.73	29.7 ± 12.25
SPT (%)	100	0	0
TNSS	10.03 ± 3.67	8.77 ± 2.24	0
Nasal obstruction	3.13 ± 1.07	2.37 ± 1.89	0
Rhinorrhea	2.5 ± 0.97	2.4 ± 1.07	0
Nasal itching	1.87 ± 1.14	1.53 ± 0.9	0
Sneezing	2.53 ± 1.14	2.47 ± 1.07	0
RQLQ	102.8 ± 29.64	89.67 ± 26.43	NA

SPT, skin prick test, TNSS, Total Nasal Symptom Score; RQLQ, Rhinoconjunctivitis Quality of Life Questionnaire, NA: Not available.

3.2 16SrDNA sequencing analysis

3.2.1 Comparison of microbial diversity among patients with AR and nAR

A total of 18,364 OTUs were obtained from the three groups by 16SrDNA assay, with 2515 OTUs specific to the AR group and 3512 OTUs specific to the nAR group, and a total of 8476 OTUs in the two groups. There were fewer specific OTU in the AR group than in the nAR group (Figure 1A). A total of 98 bacteria phyla and 1476 genera were detected in the three groups. The common dominant groups were Firmicutes, Actinobacteria, Proteobacteria, Bacteroidota, and cyanobacteria. In AR and nAR groups, the average relative abundance of Actinobacteria was lower than that of the control group (Figure 1B), and the average relative abundance of Proteobacteria was higher than that of the control group. Staphylococcus, Corynebacterium, Doloigranulum, Cutibacterium, Moraxella, Lawsonella, Prevotella, Lacticaseibacillus, Pseudomonas, and an unidentified_Chloroplsat were the top 10 genera with the highest relative abundance (Figure 1C). There were significant differences in α-diversity Shannon index and Simpson index between AR group and nAR group. The results showed that the microbial diversity of the two groups was significantly different. There was a significant difference in the Chao1 index and ACE index between the nAR group and control group, but there was no significant difference between the AR group and nAR group. The results showed that there were significant differences in microbial abundance between the two groups (Figure 1D).

3.2.2 Analysis of microbial β diversity in AR and nAR groups

The results of LEfSe analysis in β-diversity showed that the relative abundance of Vibrio, Moraxellaceae, and Corynebacterium_propinquum was higher within the AR group, while the relative abundance of Proteobacteria, Gammaproteobacteria, Clostridia, and Pseudomonadales was higher within the nAR group (Figure 2A). In the t-test test, the relative abundance of S. aureus was higher within the AR group, and the relative abundance of Lactobacillus murinus, Turicibacter sp H121, Lactobacillus reutrei, Lactobacillus kunkeei, Romboutsia ilealis, Enterococcus faecium, and Lactobacillus iners was higher within the nAR group (Figure 2B).

3.2.3 AR group and nAR group have similar network complex patterns

The modularity, clustering coefficient, and average degree of the AR group were 0.0956, 0.7359, and 185.54, while in the nAR group, they were 0.319, 0.622, and 155.43. The two groups had similar network complexity patterns, but the main focusing nodes of the two groups were completely different. The focusing nodes of the AR

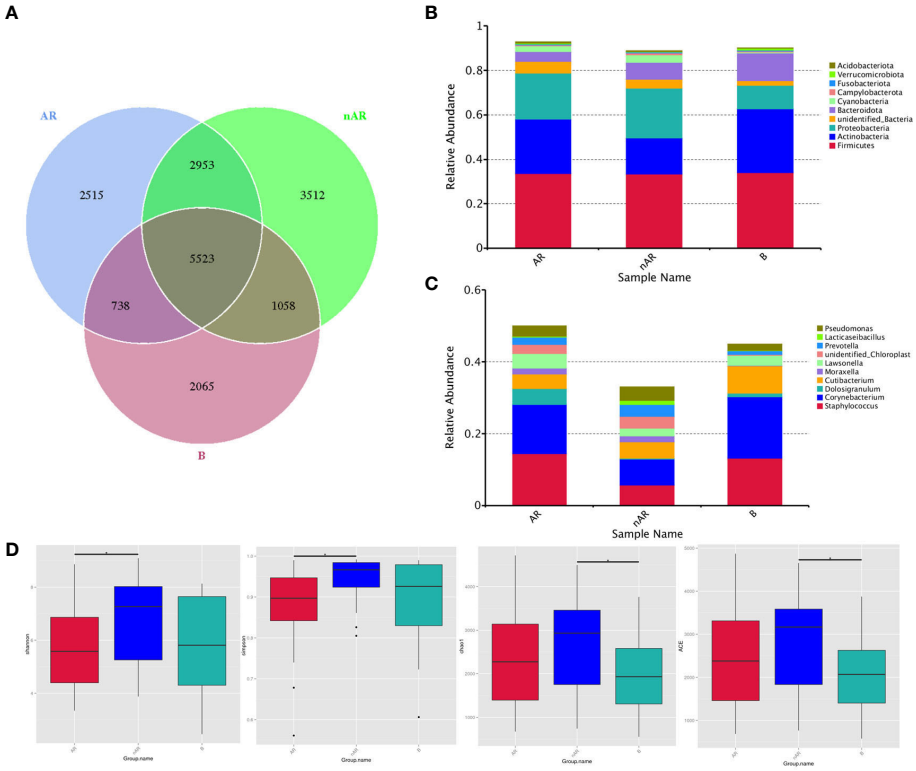

FIGURE 1
Wayne diagrams were made according to OTU **(A)**. bacterial structure comparisons between AR and non-AR at the phylum **(B)** and genus **(C)** levels, including the top ten genera. bacterial diversity comparisons between AR and non-AR patients. Comparison of bacterial alpha diversity indices, including Shannon, Simpson, Chao1, and ACE **(D)**.

group mainly included Firmicutes, Gemmatimonadetes, Planctomycetes, and Nitrospirota (Figure 3A), while the focused nodes in the nAR group were Proteobacteria, Deferribacteres, Verrucomicrobiota (Figure 3B).

3.2.4 Environmental factor correlation analysis

The TNSS score was calculated based on the sum of nasal congestion, nasal leakage, nasal itching, and sneezing and represents the severity of AR and nAR symptoms, a higher score means more severe symptoms. the RQLQ score reflects the disease-related quality of life status, therefore, we used spearman rank correlation analysis to correlate age, sex, TNSS and RQLQ scores, EOS, IgE, and bacterial genus correlations were analyzed.

The results showed that Lactobacillus kunkeei, Corynebacterium accolens, Lactobacillus murinus, and Romboutsia ilealis were positively correlated with age; Prevotella bivia and Aerococcus urinaeequi were negatively correlated with eosinophil (EOS); Corynebacterium propinquum and Prevotella buccalis were positively correlated with IgE, and Lactobacillus murinus and Lactobacillus kunkeei were negatively correlated with IgE

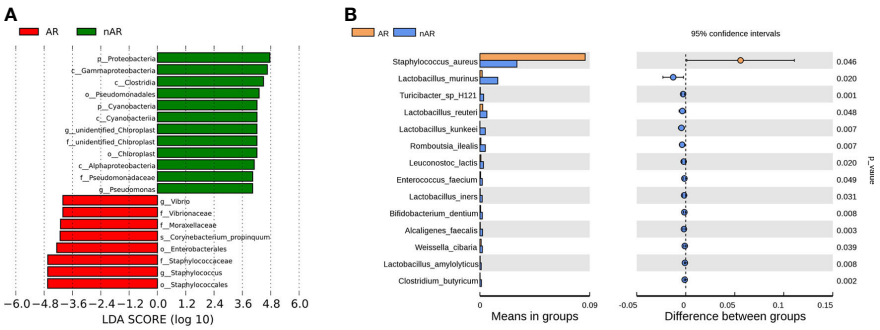

FIGURE 2
Species difference analysis was performed on the nasal flora of patients with allergic rhinitis and non-allergic rhinitis. lefSe analysis screened for different species with LDA>4 **(A)**, and t.test analysis screened for different species with p<0.05 **(B)**.

(Figure 4A), and gender, TNSS, and RQLQ scores were not significantly correlated with There was no significant correlation between gender, TNSS and RQLQ scores and flora. When performing spearman analysis of nasal congestion, nasal leakage, nasal itching, and sneezing in TNSS with flora, we found that Corynebacterium accolens was positively correlated with sneezing (Figure 4B).

3.2.5 Comparison of microbial communities in patients with moderate and severe symptoms

Based on the TNSS score, we divided 60 AR and nAR patients into moderate (score 0-7) and severe (8-16) groups and compared bacterial diversity and community differences to explore the role of bacterial community structure in the progression of AR. Results show that diversity was not significantly different, and LEfSe analysis showed that the mean relative abundance of Faecalibacterium was higher in the moderate group than in the severe group, and the mean relative abundance of Ralstonia pickettii and Cupriavidus was lower than in the severe group, suggesting a role for specific flora in the progression of the disease (Figure 5).

3.2.6 A predictive model of nasal microbial distribution for AR and nAR

This is a classical machine learning model based on a classification tree algorithm that provides further support for differentiating AR groups, nAR groups, and control groups. Based on the analysis of OTU features, a random forest prediction model with 5 genera was constructed. Mean Decree Accuracy selected meaningful genera, performed 10-fold cross-validation of the model, plotted working characteristic (ROC) curves, and calculated the area under the curve (AUC) to score the predictive power.

The results showed that mainly Parabacteroides goldstemii, Lachnospiraceae bacterium 615, Sutterella-SP-6FBBBH3, Pseudoalteromonas luteoviolacea, and Bacteroides coprocola were observed in the models of AR and healthy controls (see Figure 6A) with an AUC of 0.9733 (95% CI: 0.926-1.000) (Figure 6B); nAR and healthy controls model was observed mainly for Pseudomonas sp-LTJR-52, Lachnospiraceae bacterium-615, Prevotella corporis, Anaeroicoccus vaginalis, and Roseburia inulinivorans (Figure 6C) with an AUC of 0.984 (95% CI: 0.949-1.000) (Figure 6D), suggesting that the combined nasal biota has the potential to diagnose AR and nAR and could potentially be used as a diagnostic biomarker one, but the random forest model is only a prediction and further trials are needed to validate it.

3.3 Metagenomic sequencing analysis

3.3.1 Species composition and variability analysis of AR and nAR groups

By macrogenomics analysis, we obtained a total of 57,140.83 raw data and 56,962.55 post-cleaning data, including 19,771.66 for

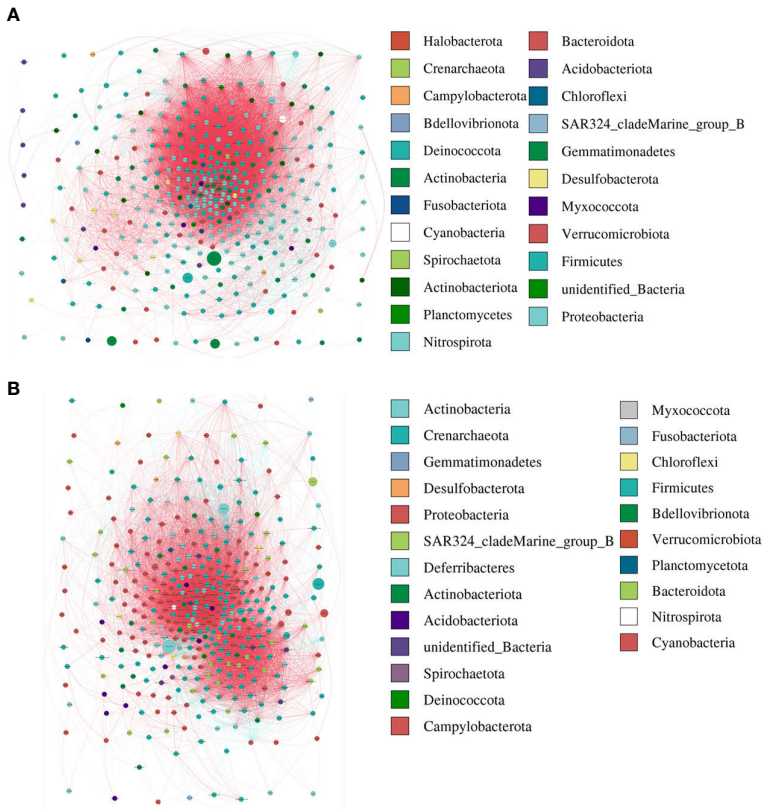

FIGURE 3
The network analysis between bacterial taxa for AR **(A)** and nAR **(B)** group. Different node color denotes varied phyla taxa and the weighted node size was based on the relative abundance. The weighted edges indicate the correlation coefficient.

10.3389/fcimb.2023.1166389

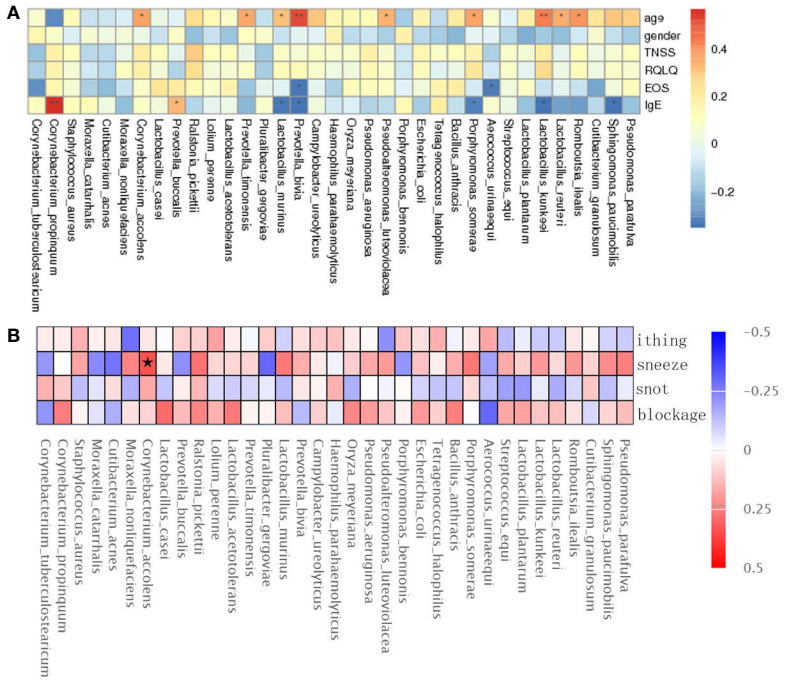

FIGURE 4
Spearman rank correlation analysis was used to correlate age, sex, TNSS, RQLQ scores, EOS, IgE **(A)**, and TNSS score details **(B)** with bacterial species. Correlation significance,* denotes $p < 0.05$ and **$p < 0.01$.

the AR group and 18,313.67 for the nAR group. the α-diversity analysis did not show positive results, which may be related to the selection of samples. In the species distribution heatmap, we found that the mean relative abundance of Pseudoalteromonas luteoviolacea, E.coli and Dolosigranulum was higher in the nAR group, and the mean relative abundance of Vibrio vulnificus and Streptococcus pneumoniae was higher within the AR group (Figure 7A); in the species annotation of the LEfSe analysis, the mean abundance of Neisseria polysaccharea, Mycobacterium szulgai and Thioflexothrix within the nAR group was higher than in the AR group, and Streptococcus sp GMD6S and Acinetobacter baumannii were lower than AR ($p < 0.05$) (Figure 7B).

3.3.2 Differential analysis of specific microbial functions in AR and nAR groups

To characterize the different functions of the nasal microbiota, we annotated the KEGG database for macrogenomic functions. Microbial genes for processing of environmental information, metabolism of nucleotides, metabolism of amino acids, metabolic cofactors, and vitamins, metabolism of carbohydrates, metabolism of lipids, biosynthesis, and metabolism of glycans were found to be increased within the AR group; in the nAR group, microbial genes for cell growth and death, processing of environmental information including signal transduction and interaction of signaling molecules, transport, and catabolism, processing of genetic

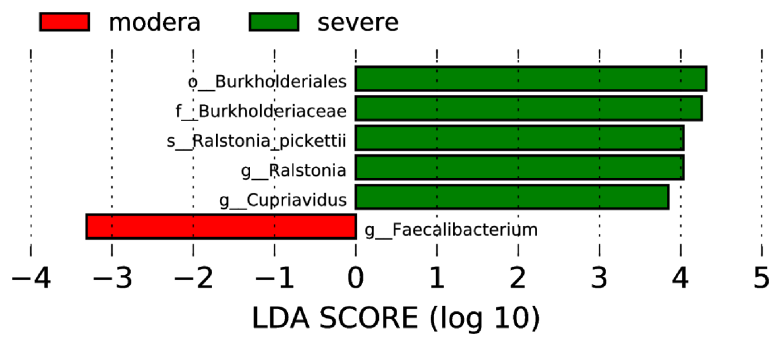

FIGURE 5
Nasal microbiological differences between moderate and severe patients.

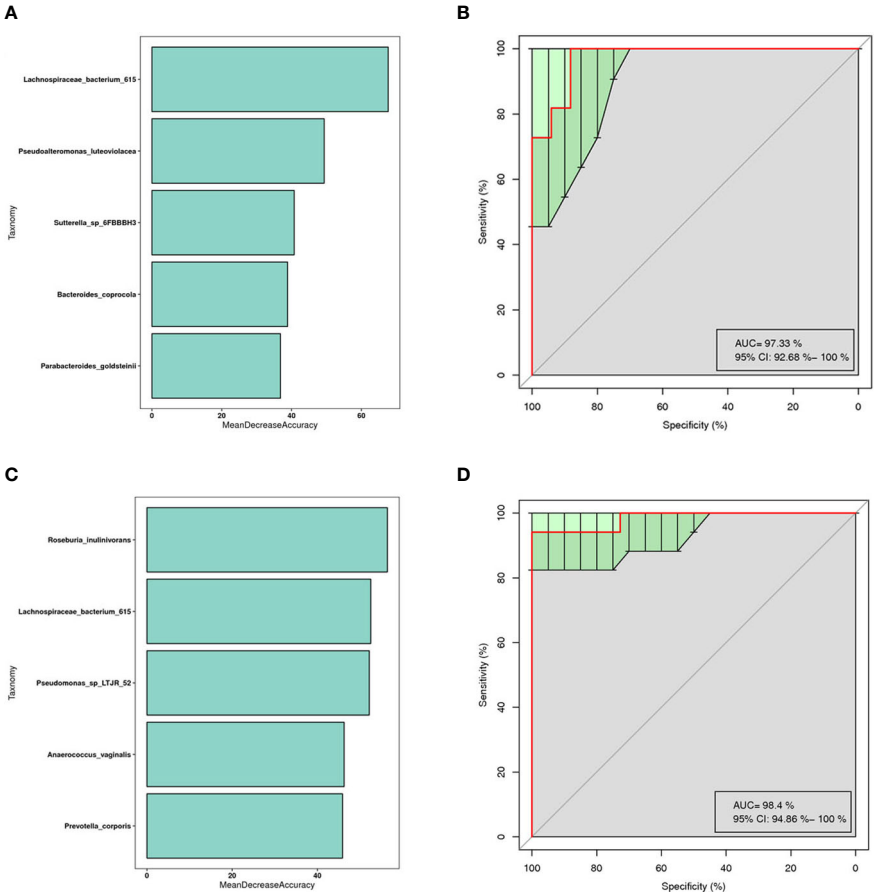

FIGURE 6
Prediction model of the airway microbiota for AR status based on the species-level relative abundances using random forests.AR **(A)** and nAR **(C)** group of variable importance ranking plots, MeanDecreeAccuracy measures the degree to which the predictive accuracy of the random forest is reduced by changing the values of the variables to random numbers. Higher values indicate more important variables. ROC curves of the AR **(B)** and nAR **(D)** model using 5 discriminatory species.

information: folding, sorting and metabolism, microbial genes for biosynthesis and metabolism of glycans were decreased (Figure 8).

3.3.3 Pathway detection of microorganisms in AR and nAR groups

By performing pathway assays on the AR and nAR groups, we found that 6-phospho-3-hexuloisomerase, cystathionine beta-synthase, aspartate–ammonia ligase, farnesyl-diphosphate farnesyltransferase, and protein-S-isoprenylcysteine O-methyltransferase were key enzymes specific to the AR group, whereas threonine aldolase, O-ureido-L-serine synthase, tryptophan-7-halogenase, and penicillin acylase were key enzymes specific to the nAR group (Additional file).

3.3.4 Differential analysis of carbohydrase in AR and nAR groups

Using macrogene annotation from the CAZY database, we found that the number of genes for the glycosyltransferase system, carbohydrate esterase system, and glycoside hydrolase system was significantly increased within the AR group and decreased within the nAR group compared with healthy controls (Figure 9A), and LefSe analysis showed that within the AR group N-acetylglucosaminyltransferase I, dolichyl-phosphate-mannose—protein, mannosyltransferase, N-acetylglucosaminyl-proteoglycan 4-beta-glucuronosyl transferase significantly increased within the AR group and amylo-alpha-1,6-glucosidase, ceramide glucosyltransferase significantly increased within the nAR group (Figure 9B).

4 Discussion

The human microbiota is important for the host immune response, metabolism, and disease progression (Blaser et al., 2013). In the present study, we discovered that the nasal microbiota of AR, nAR, and control patients differed significantly in composition and function at multiple microbial levels.

The average relative abundance of vibrio vulnificus and Acinetobacter baumanni increased significantly in the AR group. Vibrio vulnificus is a Gram-negative, halophilic marine bacterium (Blake et al., 1979). It can activate mTOR by recruiting and activating neutrophils, monocytes, and macrophages (Weichhart

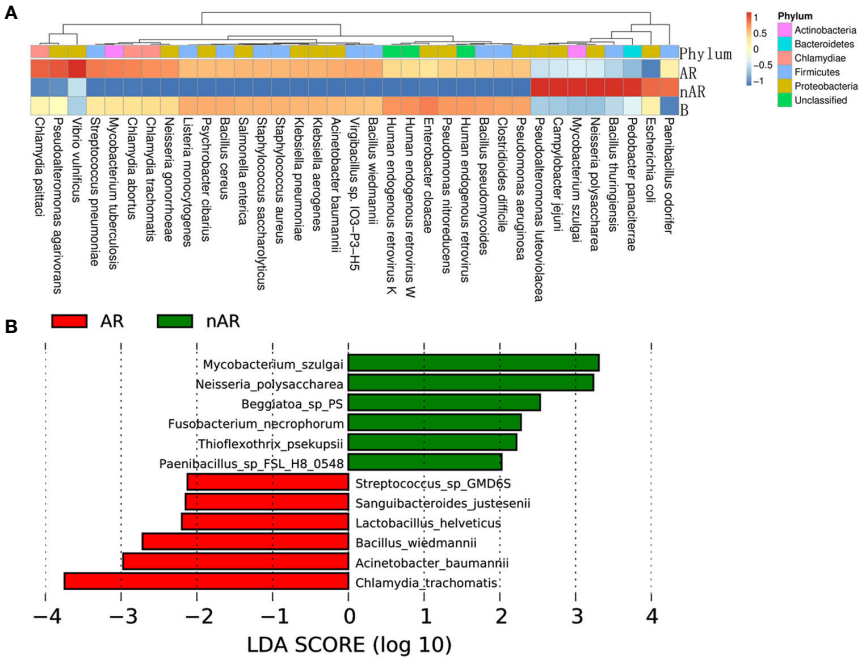

FIGURE 7
Differences in bacterial composition between AR and nAR in the heat map **(A)** and LEfSe analysis **(B)** by macrogenome sequencing.

et al., 2008), activate the NF-kβ signaling pathway *via* TLRs or NLRs, and induce allergic reactions *via* GM-CSF, IFNβ, IL-27, and IL-1β production (Xie et al., 2017). Simultaneously, vibrio vulnificus has an anti-inflammatory effect by inhibiting Kupffer cell proliferation (Blériot et al., 2015), which is consistent with the pathogenesis of AR. According to research, Acinetobacter baumanni activates the Nod-like receptor NLRP3 *via* caspase-1 to promote the release of IL-1β and TNFα from macrophages, thereby inducing asthma (Chai et al., 2022). Simultaneously, Acinetobacter has several virulence factors, including toxins that form pores, and its outer membrane protein A induces dendritic cells to produce ROS, which can activate NLRP3 and promote immune responses such as asthma and allergic rhinitis (Kang et al., 2017).

We observed that Lactobacillus murinus, Lactobacillus iners, and Escherichia coli increased significantly in the nAR patients. Lactobacillus murinus regulates T lymphocyte activity, which helps to maintain intestinal immune homeostasis in a mouse model of colitis (Tang et al., 2015). Lactobacillus murinus and Lactobacillus iners can stimulate macrophage IL-10 release *via* TLR2 signaling, thereby controlling inflammation and preventing immune

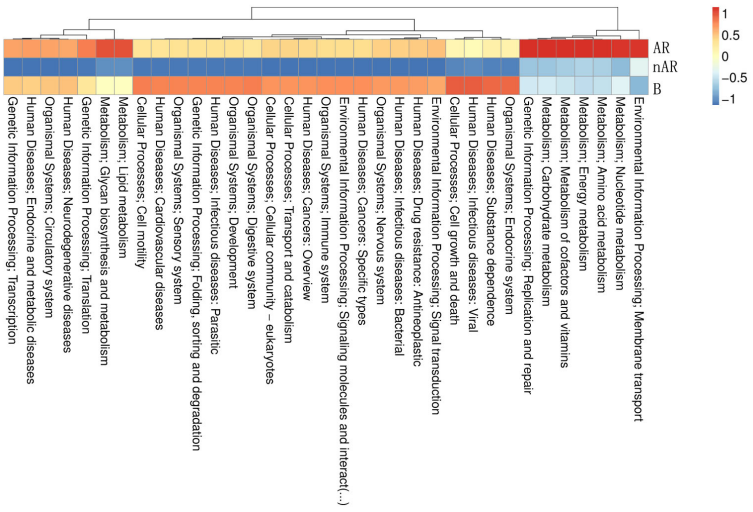

FIGURE 8
Differential analysis of specific microbial functions in AR and nAR groups compared by KEGG database.

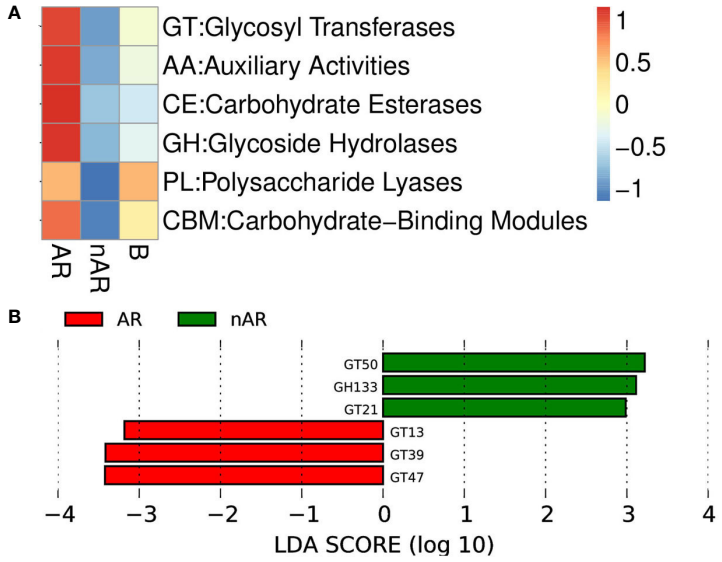

FIGURE 9
Differences between enzymes within the AR and nAR groups in the heat map **(A)** and LEfSe analysis **(B)** compared by CAZY database.

responses (Hu et al., 2022). Through the inhibition of CD23, Escherichia coli has been shown to promote the transformation of T and B cell subsets to Th1 cells and reduce IgE-mediated allergen presentation (Weise et al., 2011). Previous research found increased numbers of FoxP3+ cells as well as increased production of anti-inflammatory factors TGF-β and IL-10 in the skin of Escherichia coli-treated mice (Cukrowska et al., 2002). Simultaneously, Escherichia coli can increase IgA secretion and inhibit mast cell degranulation to suppress the immune response (Dölle et al., 2014). As a result, we believe that vibrio vulnificus and Acinetobacter baumanni have pathogenic effects in the AR group, whereas in the nAR group, patients did not show Th2-mediated allergic reactions due to the anti-inflammatory effects of Lactobacillus murinus, Lactobacillus iners, and Escherichia coli. Spearman analysis confirmed that IgE was negatively correlated with Lactobacillus murinus and Lacttobacillus kunkeei.

Furthermore, studies have revealed that allergy-induced inflammatory responses occur not only in the IgE/mast cell/basophil axis, but also in macrophages, neutrophils, platelets, endothelial cells, complement initiation, neuropeptide release, and can result in anaphylaxis-like reactions (Cianferoni, 2021). In our study, we discovered that the relative abundance of Proteobacteria and Pseudomonadales increased significantly in the nAR group. Proteobacteria and Pseudomonadales were also found to be significantly enriched in intestinal CD14+CD11c+ macrophage samples from Crohn's disease patients. Its LPS binds to CD14 and TLR4 to activate the TIRAP-MyD88 pathway, resulting in the release of inflammatory cytokines, and activation of the TLR4 receptor on the endosomal membrane can also produce type 1 interferon *via* the TRAM-TRIF pathway, inducing even more inflammation (Sekido et al., 2020). Human microbiota species are largely similar, but their relative abundance ratio varies with habit anatomic locations and can influence and interact with one another. According to Jakubczyk D et al., intestinal flora imbalance affects the relative abundance of respiratory tract flora (Jakubczyk and Górska, 2021). In our experiments, we obtained similar results. The majority of the bacteria with significant differences in nasal secretions of nAR patients were intestinal resident bacteria, indicating that nasal and intestinal microbes communicate. As a result, we believe that the rise in Proteobacteria and Pseudomonadales is one of the primary causes of nAR.

According to the KEGG database, ICMT is a unique enzyme in the microbiota of AR patients. The TLR-mediated inflammatory response is regulated by ICMT and its substrate Ras protein. Through the MAPK pathway, methylated Ras protein promotes the production of pro-inflammatory factors IL-1β, IL-1α, IL-5, IL-9, IL-17, and TGF-β, which are also common inflammatory factors in AR (Yang et al., 2020). This suggests that we could use ICMT inhibitors to block Ras methylation and thus prevent the occurrence of AR, which will be the goal of our next investigation. Through KEGG functional annotation, we also found that the glycan biosynthesis and metabolism of microbiota increased in AR patients but decreased in nAR patients. Glycans on the cell surface control and participate in cellular interactions and recognition between functional molecules and cells *via* carbohydrate-binding protein (CBP) (Schnaar, 2015). Galectin is the most common CBP, and it promotes immune cell maturation, survival, and activation by binding to target glycans on surface glycoproteins such as TCR, CD45, and CD43 (Rabinovich and Toscano, 2009). GBP can also inhibit T cell activation and promote Th1-to-Th2 transition by inhibiting IFNγ expression and promoting the production of cytokines such as IL-4, IL-5, IL-9, IL-10, and IL-13 (Sanjurjo et al., 2022). Therefore, we believe that glycan biosynthesis and metabolism play a role in the pathogenesis of AR.

We discovered that Lacttobacillus kunkeei was positively correlated with age using correlation analysis. In this study, the average age of onset in the AR group was 21.03 ± 9.94 years, while it was 33.73 ± 10.73 years in the nAR group. The relative abundance of Lacttobacillus kunkeei increased in the nAR group, implying that increased pathogenicity manifested by microbiota changes may be age-related. Previous studies have shown an association between Lactobacillus and age, with increased abundance with age (Sanjurjo et al., 2022) and that Lactobacillus increases levels of the anti-inflammatory cytokine IL-10 and decreases levels of the pro-inflammatory cytokines TNF-α and ROS (Hu et al., 2022). Therefore, we suggest that the gradual increase of Lactobacillus kunckii with age limits the occurrence of allergic reactions. Using the TNSS score, we discovered a significant difference in the composition of the microbiota between the moderate and severe disease groups. The moderate group had a higher average relative abundance of Faecalibacterium, which could be related to its anti-inflammatory effect (Martín et al., 2017). Faecalibacterium can secrete MAM, which interacts with the ZO-1 protein to maintain the integrity of the tight junction complex by connecting cohesin, occludin, and cytoskeleton protein, thereby preventing systemic complications caused by pathogens and bacterial toxins entering the blood (Xu et al., 2020). As a result, Faecalibacterium may be beneficial in the process of CR disease.

Previous research has shown that random forest analysis can predict the occurrence of AR (Yuan et al., 2022). Our findings suggest that combining the detection of Parabacteroides goldstemii, Sutterella-SP-6FBBBBH3, Pseudoalteromonas luteoviolacea, Lachnospiraceae bacterium-615, and Bacteroides coprocola can be used as a diagnostic biomarker for AR, whereas Pseudomonas-SP-LTJR-52, Prevotella corporis, Anaerococcus vaginalis, Lachnospiraceae bacterium-615, and Roseburia inulinivorans can be used for nAR.

Currently, there is growing interest in the application of probiotics to modulate microecological balance in the treatment of AR, defined by the World Health Organization as living microorganisms that, when administered in adequate amounts, provide health benefits to the host. This beneficial effect was initially thought to stem from improved gut microbial balance, but there is now substantial evidence that probiotics can also provide benefits by modulating immune function (Cortes-Perez et al., 2021). In animal models, probiotic supplementation can protect the organism from spontaneous and chemically induced colitis by downregulating inflammatory cytokines or inducing regulatory mechanisms in a strain-specific manner; in animal models of allergen sensitization and murine models of asthma and allergic rhinitis, oral probiotics can reduce allergen-specific IgE production in an allergen-dependent manner by modulating systemic cytokine production (Ballan et al., 2020), Ahmed et al. demonstrated the same effect of cetirizine and Lactobacillus casei in children under 5 years of age with perennial AR. Children given daily intake of Lactobacillus casei (2×10^9 CFU) or cetirizine (2.5-5 mg) showed significant improvement in baseline AR symptoms in more than 95% of participants after 6 weeks of intervention (Ahmed et al., 2019). This validates our results that microbial homeostasis imbalance plays a key role in the development of disease, that regulating microbial diversity will improve the symptoms of AR, and that the prospect of probiotic applications needs to be explored in more depth, which provides a direction for our future research.

5 Conclusion

In conclusion, this study establishes nasal microecological regulation as a potential therapeutic target for AR and nAR. We discovered that AR patients differed significantly from nAR patients and healthy controls in terms of nasal bacterial α and β diversity. AR is closely associated with an increase in the relative abundance of vibrio vulnificus and Acinetobacter baumanni, and an increase in the relative abundance of Lactobacillus iners, Lactobacillus murinus, and Escherichia coli may also be a key factor in the occurrence of nAR. The anti-inflammatory effect of probiotics such as Lacttobacillus kunkeei and Escherichia iners and the antagonism of ICMT could be a future treatment strategy for AR. Glycan biosynthesis and metabolism may play a role in the pathogenesis of AR, which will be investigated further in the following step. The joint detection of microbiota based on random forest results may also provide us with new ideas for future AR and nAR diagnosis.

Data availability statement

The data presented in the study are deposited in the NCBI repository, accession number PRJNA936719.

Ethics statement

The studies involving human participants were reviewed and approved by China Clinical Trial Registration Center, CHINA. The patients/participants provided their written informed consent to participate in this study.

Author contributions

JW and YS conceived and designed the research. YC, NW, and QM conducted the experiments. JL and ZX analyzed the data. YC and QL wrote and edited the manuscript. All authors contributed to the article and approved the submitted version.

Funding

This work was supported by the Young and Innovative Science Research Foundation of the Second Affiliated Hospital of Harbin Medical University (KYCX2019-04), the Fundamental Research Found for the Provincial Universities (2017LCZX58), the Heilongjiang Postdoctoral Foundation (LBH-Z16247), the Natural

Science Foundation of Heilongjiang Province of China (H2017018), the Heilongjiang Postdoctoral Startup Found (LBH-Q21028).

Acknowledgments

We thank our coworkers for their assistance and all the study participants for their support and active cooperation.

Conflict of interest

The authors declare that the research was conducted in the absence of any commercial or financial relationships that could be construed as a potential conflict of interest.

Publisher's note

Supplementary material

The Supplementary Material for this article can be found online at: https://www.frontiersin.org/articles/10.3389/fcimb.2023.1166389/full#supplementary-material

References

Agnihotri, N. T., and McGrath, K. G. (2019). Allergic and nonallergic rhinitis. *Allergy Asthma Proc.* 40 (6), 376–379. doi: 10.2500/aap.2019.40.4251

Ahmed, M., Billoo, A. G., and Iqbal, K. (2019). Efficacy of probiotic in perennial allergic rhinitis under five year children: a randomized controlled trial. *Pak J. Med. Sci.* 35 (6), 1538–1543. doi: 10.12669/pjms.35.6.744

Ballan, R., Battistini, C., Xavier-Santos, D., and Saad, S. M. I. (2020). Interactions of probiotics and prebiotics with the gut microbiota. *Prog. Mol. Biol. Transl. Sci.* 171, 265–300. doi: 10.1016/bs.pmbts.2020.03.008

Blaiss, M. S., Gronskyte Juhl, R., Siew, L. Q. C., Hammerby, E., and Devillier, P. (2022). Determining the minimal important differences in the RQLQ score with grass and tree allergy immunotherapy versus placebo in adults with moderate-to-severe allergy. *Allergy* 77 (6), 1843–1851. doi: 10.1111/all.15207

Blake, P. A., Merson, M. H., Weaver, R. E., Hollis, D. G., and Heublein, P. C. (1979). Disease caused by a marine vibrio. clinical characteristics and epidemiology. *N Engl. J. Med.* 300 (1), 1–5. doi: 10.1056/NEJM197901043000101

Blaser, M., Bork, P., Fraser, C., Knight, R., and Wang, J. (2013). The microbiome explored: recent insights and future challenges. *Nat. Rev. Microbiol.* 11 (3), 213–217. doi: 10.1038/nrmicro2973

Blériot, C., Dupuis, T., Jouvion, G., Eberl, G., Disson, O., and Lecuit, M. (2015). Liver-resident macrophage necroptosis orchestrates type 1 microbicidal inflammation and type-2-mediated tissue repair during bacterial infection. *Immunity* 42 (1), 145–158. doi: 10.1016/j.immuni.2014.12.020

Bousquet, J., Fokkens, W., Burney, P., Durham, S. R., Bachert, C., Akdis, C. A., et al. (2008). Important research questions in allergy and related diseases: nonallergic rhinitis: a GA2LEN paper. *Allergy* 63 (7), 842–853. doi: 10.1111/j.1398-9995.2008.01715.x

Chai, L., Wang, Q., Si, C., Gao, W., and Zhang, L. (2022). Potential association between changes in microbiota level and lung diseases: a meta-analysis. *Front. Med. (Lausanne)* 8. doi: 10.3389/fmed.2021.723635

Cianferoni, A. (2021). Non-IgE-mediated anaphylaxis. *J. Allergy Clin. Immunol.* 147 (4), 1123–1131. doi: 10.1016/j.jaci.2021.02.012

Cortes-Perez, N. G., de Moreno de LeBlanc, A., Gomez-Gutierrez, J. G., LeBlanc, J. G., and Bermúdez-Humarán, L. G. (2021). Probiotics and trained immunity. *Biomolecules.* 11 (10), 1402. doi: 10.3390/biom11101402

Cukrowska, B., LodInová-ZádnIková, R., Enders, C., Sonnenborn, U., Schulze, J., and Tlaskalová-Hogenová, H. (2002). Specific proliferative and antibody responses of premature infants to intestinal colonization with nonpathogenic probiotic e. coli strain nissle 1917. *Scand. J. Immunol.* 55 (2), 204–209. doi: 10.1046/j.1365-3083.2002.01005.x

Dölle, S., Berg, J., Rasche, C., and Worm, M. (2014). Tolerability and clinical outcome of coseasonal treatment with escherichia coli strain nissle 1917 in grass pollen-allergic subjects. *Int. Arch. Allergy Immunol.* 163 (1), 29–35. doi: 10.1159/000356328

Durack, J., Huang, Y. J., Nariya, S., Christian, L. S., Ansel, K. M., Beigelman, A., et al. (2018). Bacterial biogeography of adult airways in atopic asthma. *Microbiome* 6 (1), 104. doi: 10.1186/s40168-018-0487-3

Grier, A., McDavid, A., Wang, B., Qiu, X., Java, J., Bandyopadhyay, S., et al. (2018). Neonatal gut and respiratory microbiota: coordinated development through time and space. *Microbiome* 6 (1), 193. doi: 10.1186/s40168-018-0566-5

Hellings, P. W., Klimek, L., Cingi, C., Agache, I., Akdis, C., Bachert, C., et al. (2017). Non-allergic rhinitis: position paper of the European academy of allergy and clinical immunology. *Allergy* 72 (11), 1657–1665. doi: 10.1111/all.13200

Hu, J., Deng, F., Zhao, B., Lin, Z., Sun, Q., Yang, X., et al. (2022). Lactobacillus murinus alleviate intestinal ischemia/reperfusion injury through promoting the release of interleukin-10 from M2 macrophages *via* toll-like receptor 2 signaling. *Microbiome* 10 (1), 38. doi: 10.1186/s40168-022-01227-w

Jakubczyk, D., and Górska, S. (2021). Impact of probiotic bacteria on respiratory allergy disorders. *Front. Microbiol.* 12. doi: 10.3389/fmicb.2021.688137

Juniper, E. F., Guyatt, G. H., and Griffith, L. E. (1996). Interpretation of rhinoconjunctivitis quality of life questionnaire data. *J. Allergy Clin. Immunol.* 98 (4), 843–845. doi: 10.1016/S0091-6749(96)70135-5

Kang, M. J., Jo, S. G., Kim, D. J., and Park, J. H. (2017). NLRP3 inflammasome mediates interleukin-1β production in immune cells in response to acinetobacter baumannii and contributes to pulmonary inflammation in mice. *Immunology.* 150 (4), 495–505. doi: 10.1111/imm.12704

Koidl, L., and Untersmayr, E. (2021). The clinical implications of the microbiome in the development of allergy diseases. *Expert Rev. Clin. Immunol.* 17 (2), 115–126. doi: 10.1080/1744666X.2021.1874353

Martín, R., Miquel, S., Benevides, L., Bridonneau, C., Robert, V., Hudault, S., et al. (2017). Functional characterization of novel faecalibacterium prausnitzii strains isolated from healthy volunteers: a step forward in the use of f. prausnitzii as a next-generation probiotic. *Front. Microbiol.* 8, 1226. doi: 10.3389/fmicb.2017.01226

Rabinovich, G. A., and Toscano, M. A. (2009). Turning 'sweet' on immunity: galectin-glycan interactions in immune tolerance and inflammation. *Nat. Rev. Immunol.* 9, 338–352. doi: 10.1038/nri2536

Roberts, G., Ollert, M., Aalberse, R., Austin, M., Custovic, A., DunnGalvin, A., et al. (2016). A new framework for the interpretation of IgE sensitization tests. *Allergy* 71 (11), 1540–1551. doi: 10.1111/all.12939

Sahoyama, Y., Hamazato, F., Shiozawa, M., Nakagawa, T., Suda, W., Ogata, Y., et al. (2022). Multiple nutritional and gut microbial factors associated with allergic rhinitis: the Hitachi health study. *Sci. Rep.* 12 (1), 3359. doi: 10.1038/s41598-022-07398-8

Sanjurjo, L., Broekhuizen, E. C., Koenen, R. R., and Thijssen, V. L. J. L. (2022). Galectokines: the promiscuous relationship between galectins and cytokines. *Biomolecules.* 12 (9), 1286. doi: 10.3390/biom12091286

Schnaar, R. L. (2015). Glycans and glycan-binding proteins in immune regulation: a concise introduction to glycobiology for the allergist. *J. Allergy Clin. Immunol.* 135 (3), 609–615. doi: 10.1016/j.jaci.2014.10.057

Sekido, Y., Nishimura, J., Nakano, K., Osu, T., Chow, C. T., Matsuno, H., et al. (2020). Some gammaproteobacteria are enriched within CD14+ macrophages from intestinal lamina propria of crohn's disease patients versus mucus. *Sci. Rep.* 10 (1), 2988. doi: 10.1038/s41598-020-59937-w

Subspecialty Group of Rhinology, Editorial Board of Chinese Journal of Otorhinolaryngology-Head and Neck Surgery; Subspecialty Group of Rhinology, Society of Otorhinolaryngology Head and Neck Surgery and Chinese Medical Association. (2022). Chinese Guideline for diagnosis and treatment of allergic

rhinitis (2022, revision). *Zhonghua Er Bi Yan Hou Tou Jing Wai Ke Za Zhi* 57 (2), 106–129. doi: 10.3760/cma.j.cn115330-20211228-00828

Tang, C., Kamiya, T., Liu, Y., Kadoki, M., Kakuta, S., Oshima, K., et al. (2015). Inhibition of dectin-1 signaling ameliorates colitis by inducing lactobacillus-mediated regulatory T cell expansion in the intestine. *Cell Host Microbe* 18 (2), 183–197. doi: 10.1016/j.chom.2015.07.003

Ver Heul, A., Planer, J., and Kau, A. L. (2019). The human microbiota and asthma. *Clin. Rev. Allergy Immunol.* 57 (3), 350–363. doi: 10.1007/s12016-018-8719-7

Weichhart, T., Costantino, G., Poglitsch, M., Rosner, M., Zeyda, M., Stuhlmeier, KM., et al. (2008). The TSC-mTOR signaling pathway regulates the innate inflammatory response. *Immunity* 29 (4), 565–577. doi: 10.1016/j.immuni.2008.08.012

Weise, C., Zhu, Y., Ernst, D., Kühl, A. A., and Worm, M. (2011). Oral administration of escherichia coli nissle 1917 prevents allergen-induced dermatitis in mice. *Exp. Dermatol.* 20 (10), 805–809. doi: 10.1111/j.1600-0625.2011.01326.x

World MA. (2013). World medical association declaration of Helsinki: ethical principles for medical research involving human subjects. *JAMA* 310 (20), 2191–2194.

Xie, D. L., Zheng, M. M., Zheng, Y., Gao, H., Zhang, J., Zhang, T., et al. (2017). Vibrio vulnificus induces mTOR activation and inflammatory responses in macrophages. *PloS One* 12 (7), e0181454. doi: 10.1371/journal.pone.0181454

Xu, J., Liang, R., Zhang, W., Tian, K., Li, J., Chen, X., et al. (2020). Faecalibacterium prausnitzii-derived microbial anti-inflammatory molecule regulates intestinal integrity in diabetes mellitus mice *via* modulating tight junction protein expression. *J. Diabetes* 12 (3), 224–236. doi: 10.1111/1753-0407.12986

Yang, W. S., Kim, H. G., Kim, E., Han, S.Y., Aziz, N., Yi, Y. S., et al. (2020). Isoprenylcysteine carboxyl methyltransferase and its substrate ras are critical players regulating TLR-mediated inflammatory responses. *Cells.* 9 (5), 1216. doi: 10.3390/cells9051216

Yuan, Y., Wang, C., Wang, G., Guo, X., Jiang, S., Zuo, X., et al. (2022). Airway microbiome and serum metabolomics analysis identify differential candidate biomarkers in allergic rhinitis. *Front. Immunol.* 12. doi: 10.3389/fimmu.2021.771136

frontiers | Frontiers in Cellular and Infection Microbiology

TYPE Original Research
PUBLISHED 03 July 2023
DOI 10.3389/fcimb.2023.1175747

OPEN ACCESS

EDITED BY
Jianmin Chai,
Foshan University, China

REVIEWED BY
Karthik Subramanian,
Rajiv Gandhi Centre for Biotechnology, India
Rachele Invernizzi,
Broad Institute, United States

*CORRESPONDENCE
Hongling Hou
hlhou@yzu.edu.cn
Qing Shan
qingshan@yzu.edu.cn

RECEIVED 28 February 2023
ACCEPTED 12 June 2023
PUBLISHED 03 July 2023

CITATION
Sun G, Liu W, Zheng Q, Shan Q and Hou H (2023) Ratio of procalcitonin/Simpson's dominance index predicted the short-term prognosis of patients with severe bacterial pneumonia.
Front. Cell. Infect. Microbiol. 13:1175747.
doi: 10.3389/fcimb.2023.1175747

Ratio of procalcitonin/Simpson's dominance index predicted the short-term prognosis of patients with severe bacterial pneumonia

Guoxian Sun[1], Weili Liu[2], Qingbin Zheng[2], Qing Shan[1]* and Hongling Hou[3]*

[1]Department of Infection Control, Affiliated Hospital of Yangzhou University, Yangzhou, China, [2]Department of Critical Care Unit, Affiliated Hospital of Yangzhou University, Yangzhou, China, [3]Department of Neurology, Affiliated Hospital of Yangzhou University, Yangzhou, China

Objective: The aim of this study was to explore the predictive value of the ratio of procalcitonin (PCT) in serum to Simpson's dominance index (SDI) in bronchoalveolar lavage fluid (BALF), in short-term prognosis of patients with severe bacterial pneumonia (SBP).

Methods: This is a retrospective review of case materials of 110 patients with SBP who selected BALF metagenomic next-generation sequencing technique in the intensive care unit (ICU) of the Affiliated Hospital of Yangzhou University from January 2019 and July 2022. Based on the acute physiology and chronic health status score II, within 24 h after admission to the ICU, patients were divided into a non-critical group (n = 40) and a critical group (n = 70). Taking death caused by bacterial pneumonia as the endpoint event, the 28-day prognosis was recorded, and the patients were divided into a survival group (n = 76) and a death group (n = 34). The SDI, PCT, C-reactive protein (CRP), PCT/SDI, and CRP/SDI were compared and analyzed.

Results: Compared with the non-critical group, the critical group had a higher PCT level, a greater PCT/SDI ratio, a longer ventilator-assisted ventilation time (VAVT), and more deaths in 28 days. Compared with the survivors, the death group had a higher PCT level, a lower SDI level, and a greater PCT/SDI ratio. The SDI level was significantly negatively correlated with the VAVT (r = –0.675, p < 0.05), while the PCT level, ratio of PCT/SDI, and ratio of CRP/SDI were remarkably positively correlated with VAVT (r = 0.669, 0.749, and 0.718, respectively, p < 0.05). The receiver operating characteristic (ROC) curves analysis showed that the area under ROC curves of PCT/SDI predicting patient death within 28 days was 0.851, followed by PCT + SDI, PCT, SDI, and CRP/SDI (0.845, 0.811, 0.778, and 0.720, respectively). The sensitivity and specificity of

PCT/SDI for predicting death were 94.1% and 65.8%, respectively, at the optimal value (11.56). Cox regression analysis displayed that PCT/SDI (HR = 1.562; 95% CI: 1.271 to 1.920; p = 0.039) and PCT (HR = 1.148; 95% CI: 1.105 to 1.314; p = 0.015) were independent predictors of death in patients.

Conclusion: The ratio of PCT/SDI was a more valuable marker in predicting the 28-day prognosis in patients with SBP.

KEYWORDS

bacterial pneumonia, bronchoalveolar lavage fluid, procalcitonin, Simpson's dominance index, predictive

Introduction

Severe bacterial pneumonia (SBP) is one of the main causes of death in intensive care unit (ICU) patients, with a mortality rate of 15.5%–38.2% (Shi et al., 2019). Corresponding treatment guidelines recommend that early identification of the causative agent and treatment is an effective way to improve the patient's prognosis (Kalil et al., 2016; Metlay et al., 2019). Patients with SBP have a severe inflammatory response in the lungs, with a massive release of inflammatory cytokines and a disruption of the original immune system balance, which leads to changes in the respiratory flora. Alterations in the respiratory flora, in turn, further promote disease progression and poor prognosis (Panzer et al., 2018). Thus, altered respiratory flora secondary to SBP may increase the risk of death in patients with pulmonary infections(Guo et al., 2021).

Understanding the composition of the respiratory flora is necessary to inform clinical decisions. Previous studies (Dima et al., 2019) have shown that respiratory flora is associated with the development and progression of several diseases, such as chronic obstructive pulmonary disease and acute respiratory distress syndrome. Simpson's dominance index (SDI) is currently a sensitive indicator for studying differences in animal, plant, and soil flora, and has been shown to be a natural marker for bacterial infections in studies involving human respiratory flora (Langelier et al., 2018). It has been shown (Langelier et al., 2018) that SDI values are lower in patients with pulmonary infections compared to uninfected individuals. The more severe the patient's lung bacterial infection, the lower the SDI value, as shown by the trend of SDI. The SDI decreases and PCT increases in SBP, and the ratio of the two indices (SDI/PCT) theoretically better reflects the predictive ability of the disease. Therefore, we proposed a method combining SDI and PCT for the first time exploratively.

The aim of the study was to analyze the ratio of serum PCT in ICU patients with bacterial pneumonia to SDI values obtained by the metagenomic next-generation sequencing technique (mNGS), and then compared with SDI, PCT, C-reactive protein (CRP), and CRP/SDI to evaluate the value of PCT/SDI in the short-term prognosis of ICU patients with SBP.

Materials and methods

Patients and study design

Adult patients (aged ≥ 18 years) with bacterial pneumonia selected for diagnosis with the aid of the bronchoalveolar lavage fluid (BALF) mNGS technique from the Affiliated Hospital of Yangzhou University between January 2019 and July 2022 were retrospectively reviewed. Age, gender, PCT, CRP, mNGS, patient outcomes and acute physiology, and chronic health evaluation (APACHE-II) within 24 h of admission were recorded. Diagnostic criteria for bacterial pneumonia refer to the guidelines for the diagnosis and treatment of hospital-acquired pneumonia and ventilator-associated pneumonia in adults in China (2018). Patients who met criterion 4 or any two or more of the first three criteria were included, as described below: (1) Newly developed cough, sputum, or aggravation of existing respiratory symptoms with purulent airway secretions, with or without chest pain; (2) body temperature >38°C; (3) peripheral blood leukocyte count (WBC) $>10\times10^9$/L or $<4\times10^9$/L, with or without left shift of nuclei; (4) lung imaging showing a new or progressive patchy infiltrative shadow, consolidation, or with or without pleural effusion. A total of 110 patients were enrolled in the study and bronchoscopy was performed to obtain BALF samples. The mNGS of BALF was used to detect bacteria. All patients were treated with appropriate antibiotics and steroid users were excluded. Based on APACHE-II within 24 h of admission to the ICU, all patients were divided into two groups: a non-critical group (APACHE-II <20, n = 40) and a critical group (APACHE-II ≥20, n = 70). The endpoints were bacterial pneumonia causing death of the patients, and 28-day prognosis was recorded. According to the endpoint outcomes, the patients were divided into two groups: a survival group (n = 76) and a death group (n = 34). This study was approved by the Ethics Committee of the Affiliated Hospital of Yangzhou University. Owing to a retrospective study, the ethics committee approved the waiver of informed consent. All research materials were conducted anonymously.

Case definition and positive mNGS result criteria

Two independent physicians reviewed the anonymized data material for all patients. The likelihood of the infection source as suggested by clinical symptoms was determined. The bacteria that may have caused the infection were then identified based on the mNGS results. For rare reported bacteria, unless mNGS results were consistent with the clinical characteristics of the patient, the detected reads were classified as non-pathogenic bacteria sequences. This study excluded the case of viral, fungal, and atypical pathogenic bacteria infections. Finally, an infectious diagnosis was established.

Owing to the lack of interpretation criteria for mNGS, the following criteria were used to define positive bacterial results: (1) Pathogenic bacteria reported in the literature; (2) ≥3 reads of highly pathogenic bacteria at the species level; (3) >30% relative abundance at the genus level for opportunistic bacteria; and (4) ≥1 read for *Mycobacterium tuberculosis* and non-tuberculous mycobacteria.

Sample processing

BALF was collected in accordance with standard operating procedures. The Vision Medicals' Patho-NET technology was used to remove host gDNA. Then, we obtained up to 600-ml samples. DNA was extracted using a Pathogen DNA Kit (Tiangen Biotech, Beijing, China) following the manufacturer's instructions, and DNA libraries were constructed by transposase-mediated ways (Vision Medicals, China). Prior to sequencing, the quality of the libraries was evaluated using the Qsep1 Biofragment Analyzer (BiOptic. Co., La Canada Flintridge, CA) to measure adapter and fragment size. The size of final library was 300 to 500 bp and the library concentration was greater than 0.5 ng/μl. Finally, the Nextseq 550 Dx sequencing platform (Illumina, San Diego, CA) was used for sequencing. High-quality data were obtained by removing short (less than 40 bp) reads. Human sequence was removed by mapping to human reference genome (hg38 and YH sequences) using Burrows–Wheeler Alignment. The remaining microbial sequence was classified by aligning to Microbial Genome Databases, which were downloaded from the NCBI Nucleotide and Genome databases. Finally, multiple parameters of bacteria, such as relative abundance, were exported, and the results were interpreted by microbiologists and clinicians.

SDI calculation

The SDI was calculated using the number of bacterial nucleic acid sequences detected by mNGS with the following formula (Hunter, 1988):

$$\mathrm{SDI} = 1 - \frac{\sum n(n-1)}{N(N-1)}$$

where n is the number of nucleic acid sequences detected for a strain and N is the total number of nucleic acid sequences detected for all strains.

Statistical analysis

Mann–Whitney U test (non-normally distributed variables) and independent-samples t-tests (normally distributed variables) were utilized to compare the quantitative data between the groups. Chi-square tests were used to compare categorical variables. The Spearman method was utilized for correlation analysis. Binary logistic regression analysis was applied to identify independent risk factors associated with patient death in 28 days. Receiver operating curves (ROCs) were used to obtain cutoff values for the best sensitivity and specificity of factors for patient death in 28 days. Multivariate Cox regression analysis was carried out to explore whether the variables can effectively predict the short-term prognosis of patients. All analyses were performed using SPSS 17.0 (SPSS Inc., Chicago, IL, USA), and figures were constructed using MedCalc version 20 software (MedCalc Software Ltd., Ostend, Belgium). $p< 0.05$ was considered significant.

Results

Patient characteristics

A total of 110 patients with SBP (70 male and 40 female patients) with a median age of 65 (62, 71) years were enrolled in this study. The median SDI, PCT, and CRP for all patients were 0.460 (0.350, 0.588), 5.050 (3.845, 7.813) ng/ml, and 21.320 (16.863, 27.533) mg/L, respectively, and the median duration of ventilator-assisted ventilation time (VAVT) was 9.0 (7.0, 14.0) days. All patients were followed up with a 28-day prognosis and 34 patients eventually died. The bacterial test results and clinical characteristics of patients are shown in Table 1.

Comparison of the indicators between the critical group and the non-critical group

The critical patients had significantly lower SDI levels; higher PCT/SDI, PCT, and CRP/SDI values; longer VAVT; and more deaths compared with the non-survival group ($p < 0.01$), while the age, gender, and CRP were not statistically significant ($p > 0.05$) (Table 2).

Comparison of the indicators between the death group and the survival group

Patients with death had higher PCT/SDI, PCT, and CRP/SDI values, and lower SDI values compared with the survival group (all $p < 0.05$), while the age, gender, and CRP were not statistically significant ($p > 0.05$) (Table 3).

TABLE 1 Clinical characteristics and laboratory and bacterial results of patients.

Characteristics	Overall (n = 110)
Gender (male/female)	70/40
Age, years	65.0 (62.0, 71.0)
VAVT, days	9.0 (7.0, 14.0)
Laboratory examination	
SDI	0.460 (0.350, 0.588)
PCT, ng/ml	5.050 (3.845, 7.813)
CRP, mg/L	21.320 (16.863, 27.533)
Bacteria	
Acinetobacter baumannii	20
Klebsiella pneumoniae	16
Pseudomonas aeruginosa	14
Streptococcus pneumoniae	13
Escherichia coli	11
Burkholderia cepacia	9
Stenotrophomonas maltophilia	7
Aspergillus	5
Staphylococcus aureus	5
Listeria	5
Haemophilus influenzae	4
Mycoplasma	4
Pneumocystis carinii	3
Aerobacter cloacae	1
Mycobacterium tuberculosis	1
Legionella pneumophila	1

Continuous variables are presented as median and interquartile range; binary variables are presented as number and percentage. VAVT, ventilator-assisted ventilation time; SDI, Simpson's dominance index; PCT, procalcitonin; CRP, C-reactive protein.

Correlation of indicators with the VAVT

SDI was negatively correlated with VAVT (Spearman's correlation coefficient; $r = -0.675$, $p < 0.001$), and PCT, PCT/SDI, and CRP/SDI were positively correlated with VAVT (Spearman's correlation coefficient; $r = 0.669$, 0.749, and 0.718, respectively, $p < 0.001$). Gender, age, and CRP were not correlated with VAVT (Spearman's correlation coefficient; $r = 0.031$, −0.020, and 0.080, respectively, $p > 0.05$) (Figure 1).

ROC curve analysis for indicators

We included statistically significant PCT, SDI, PCT/SDI, PCT +SDI, and CRP/SDI in the survival group compared with the death group in the ROC curve analysis. The results showed that the area under the ROC curves for PCT/SDI predicting patient death in 28 days was 0.851, followed by PCT+SDI (0.845), PCT (0.811), SDI (0.778), and CRP/SDI (0.720). Pairwise comparisons of the area under the ROC curve for each variables showed that SDI ~ PCT/SDI, $Z = 1.191$, $p = 0.234$; SDI ~ PCT, $Z = 0.810$, $p = 0.418$; SDI ~ CRP/SDI, $Z = 1.910$, $p = 0.056$; SDI ~ PCT+SDI, $Z = 1.908$, $p = 0.056$; PCT/SDI ~ PCT, $Z = 2.081$, $p = 0.038$; PCT/SDI ~ CRP/SDI, $Z = 0.603$, $p = 0.547$; PCT ~ CRP/SDI, $Z = 2.058$, $p = 0.040$; PCT ~ PCT+SDI, $Z = 0.974$, $p = 0.330$; CRP/SDI ~ PCT/SDI, $Z = 3.531$, $p < 0.001$. When the cutoff value of PCT/SDI was 11.56, the best sensitivity for predicting patient death in 28 days was 94.1% and the specificity was 65.8% (Figure 2).

Multivariate Cox regression analysis for 28-day survival in patients with SBP

The survival time is defined as the time from the patient's admission to the ICU to death or the end of follow-up. After removing irrelevant features, age, sex, SDI, PCT/SDI, PCT, CRP/SDI, and PCT+SDI were taken as independent variables, and multivariate Cox regression analysis was performed. The

TABLE 2 Various indicators of the critical group and non-critical group.

Indicators	Non-critical group (n = 40)	Critical group (n = 70)	p-value
Gender (male/female)	28/12	42/28	0.294
Age, years	67.5 (62.0, 72.0)	64.0 (62.0, 70.0)	0.076
SDI	0.625 (0.553, 0.663)	0.410 (0.270, 0.460)	<0.001*
PCT/SDI	6.090 (5.113, 8.283)	17.010 (11.640, 24.690)	<0.001*
PCT, ng/ml	3.775 (3.388, 4.690)	7.120 (4.925, 8.240)	<0.001*
CRP/SDI	33.360 (28.900, 42.520)	65.810 (45.753, 97.958)	<0.001*
CRP, mg/L	24.165 (22.245, 26.725)	24.170 (21.433, 30.563)(20.125,28.220)	0.177
VAVT, days	7.0 (4.8, 8.3)	11.0 (8.0, 16.8)	<0.001*
28-day prognosis(die/survival)	6/34	28/42	0.006*

Continuous variables are presented as median and interquartile range; binary variables are presented as number and percentage. VAVT, ventilator-assisted ventilation time; SDI, Simpson's dominance index; PCT, procalcitonin; CRP, C-reactive protein.

TABLE 3 Various indicators of the survivor group and death group.

Indicators	Survivor group (n = 76)	Death group (n = 34)	p-value
Gender (male/female)	52/24	18/16	0.119
Age, years	65.5 (61.0, 71.0)	64.5 (63.0, 69.3)	0.314
SDI	0.485 (0.430, 0.630)	0.320 (0.270, 0.460)	<0.001*
PCT/SDI	9.250 (5.800, 16.500)	21.420 (13.798, 33.900)	<0.001*
PCT, ng/ml	4.700 (3.640, 5.970)	7.900 (5.403, 9.970)	<0.001*
CRP/SDI	44.140 (23.860, 63.070)	76.440 (42.560, 118.008)	0.004*
CRP, mg/L	21.165 (15.030, 27.120)	22.020 (20.120, 29.230)	0.064

Continuous variables are presented as median and interquartile range; binary variables are presented as number and percentage. SDI, Simpson's dominance index; PCT, procalcitonin; CRP, C-reactive protein.

multivariate Cox regression analysis showed PCT/SDI and PCT as continuous variables and were independent risk factors for 28-day death in patients with SBP (Figures 3A, B).

Discussion

It is now generally accepted that the human body has a complex micro-ecosystem in all the cavities that are connected to the outside world. The imbalance of the microecosystem in the luminal tract and the inflammatory state due to bacterial infection are the main factors for the poor prognosis of patients with severe infections. Multiple studies on the relationship between intestinal flora and disease have shown that the incidence of acute respiratory distress syndrome and ventilator-associated pneumonia is significantly higher once intestinal flora is imbalanced (Dickson et al., 2020; Zanza et al., 2022). In many cases, the pathological changes of the lung, such as parenchymal fibrosis, is considered to be associated

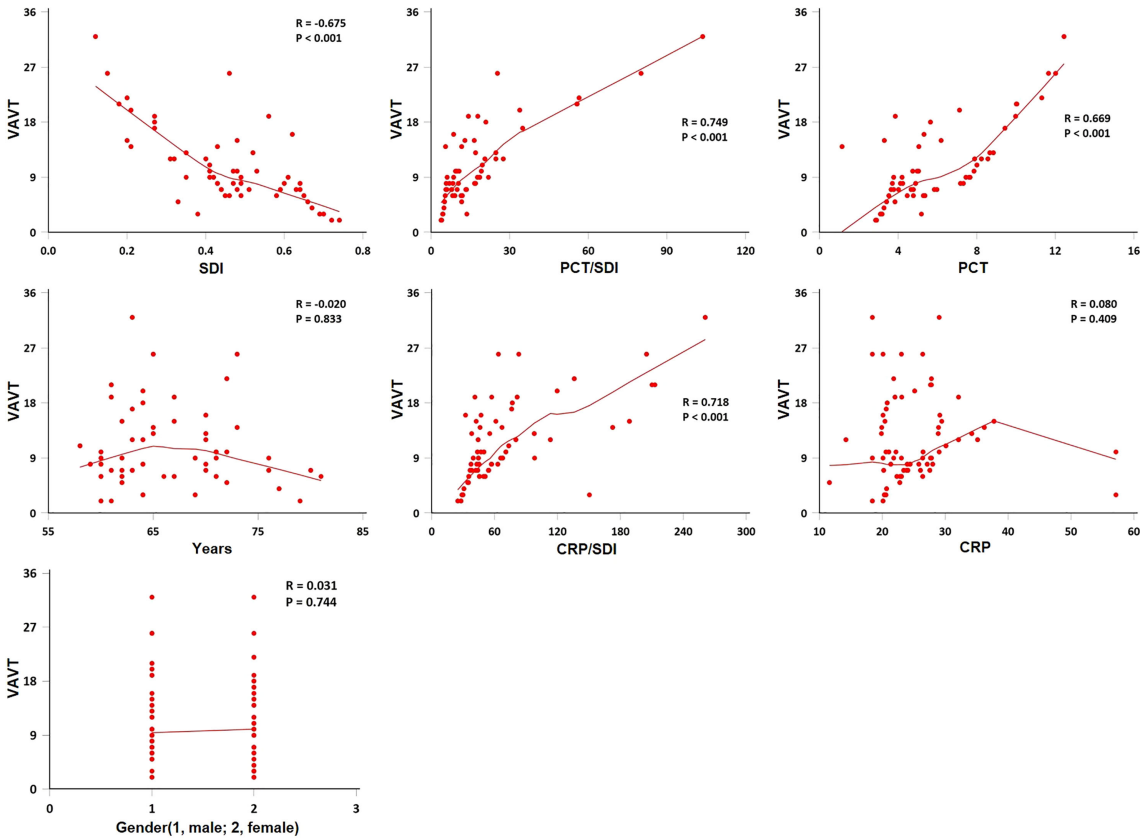

FIGURE 1
Spearman method for correlation of ventilator-assisted ventilation time (VAVT) with indexes. The VAVT by age, gender, Simpson's diversity index (SDI), procalcitonin (PCT), C-reactive protein (CRP), PCT/SDI, and CRP/SDI (n = 110). SDI was negatively correlated with VAVT (p < 0.001), and PCT, PCT/SDI, and CRP/SDI were positively correlated with VAVT (p < 0.001). Gender, age and CRP were not correlated with VAVT (p > 0.05).

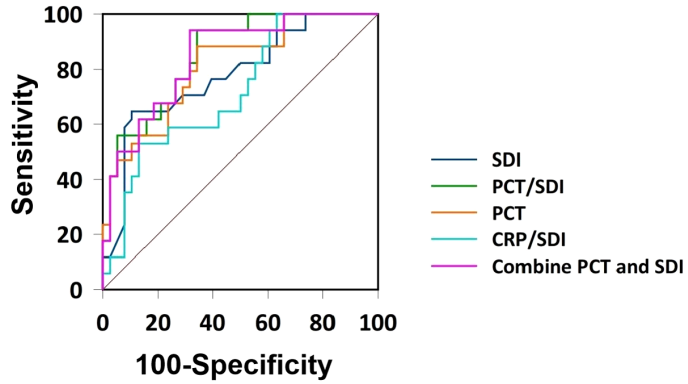

Variables	AUC	95% CI	*P*-value	Sensitivity (%)	Specificity (%)	cutoff	Yoden index
SDI	0.778	0.683-0.874	0.001*	0.647	0.895	0.390	0.542
PCT/SDI	0.851	0.780-0.922	0.001*	0.941	0.658	11.560	0.559
PCT	0.811	0.726-0.896	0.001*	0.882	0.658	5.040	0.540
CRP/SDI	0.720	0.620-0.819	0.001*	0.529	0.868	74.915	0.397
PCT+SDI	0.845	0.770-0.920	0.001*	0.941	0.684	0.215	0.625

FIGURE 2
Receiver operating characteristic curves. SDI, Simpson's dominance index; PCT, procalcitonin; CRP, C-reactive protein; AUC, area under the ROC curves.

with altered microbial communities in the patient's lungs (Dickson and Huffnagle, 2015; Woo et al., 2020). The composition of the intrapulmonary microbial community varies significantly with the progression of the disease. ICU patients with SBP often have advanced age, underlying diseases, and immune deficiencies that can lead to physiological dysfunction and disruption of the body's microecological balance. Previous studies have shown that alterations in microbial communities increase the incidence of infectious diseases through their metabolite-mediated immune regulation (Segal et al., 2017). Further studies suggest that an imbalanced microbial community increases immune-related metabolite production pathways, such as the pentose phosphate pathway and the glycolytic pathway (Hong et al., 2021). As can be expected, alterations in the intrapulmonary microbial community play a special role in the recognition and treatment of infectious diseases. Therefore, simultaneous monitoring of intrapulmonary microbial communities and inflammatory indicators in patients with SBP may be of more clinical value.

SDI was proposed by the British scholar Simpson in 1949 as a measure of the number of biological species within a species community and the relative abundance among species, the principle of which can be derived from probability theory (Simpson, 1949). SDI can reflect the status and role of dominant species in the community, and the larger its value, the higher the ecological dominance. According to previous research (Yang et al., 2018; Pimple, 2020), SDI can elucidate differences in species (flora) such as animals and plants within a given region; however, most recent studies have dealt with human respiratory and intestinal flora (Langelier et al., 2018). Clinical studies have shown (Pimple, 2020) that a subgroup comparison of 22 adult hospitalized patients after hematopoietic stem cell transplantation had significantly lower SDI values in the infected group relative to the uninfected group (p = 0.017). This is similar to the results of our previous unpublished study with a small sample. PCT and CRP are commonly used biomarkers that have the potential to differentiate infectious and non-infectious inflammatory conditions. For the severity and prognosis of bacterial pneumonia, in conjunction with other clinical examination, PCT levels have been shown to be more advantages than CRP (Covington et al., 2018). The results of this study showed that the PCT values of patients in the survival and non-critical groups were significantly lower than those in the death and critical groups (p< 0.001), while CRP was not significantly different in any of the groups (p > 0.05). The PCT levels of patients with bacterial pneumonia were positively correlated with the VAVT. The greater the PCT value, the more severe the disease and the higher the risk of death.

Previous research have shown that the ratio of PCT and CRP to indicators such as serum prealbumin or erythrocyte sedimentation rate (ESR) has clinical significance in the diagnosis, management, and prognosis, such as the study by Christopher et al. (2021), which showed that ESR/CRP helps to determine the duration of periprosthetic joint infection and informs the physician's treatment choice. Another study showed that serum prealbumin/PCT was negatively associated with time in intensive care and death, and could be used as an indicator of patient severity and short-term prognosis (Wang et al., 2022). Given the high and low variability of PCT, CRP, and SDI in the context of bacterial infection in patients, the ratio of inflammatory indexes to SDI was used exploratively in this study. In contrast to PCT for short-term prognosis of patients with bacterial pneumonia, SDI values were taken independent of a variety of clinical factors such as renal insufficiency, autoimmune disease, and neutropenia (Covington et al., 2018). In addition, early

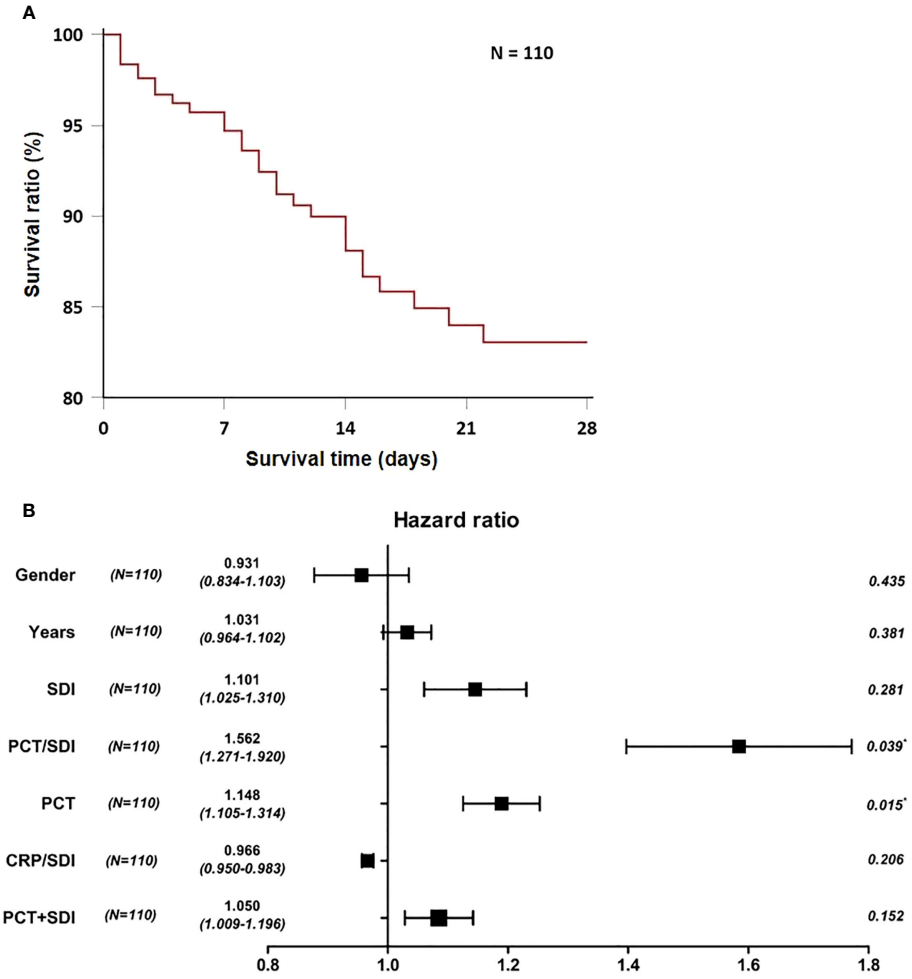

FIGURE 3
Construction of short-term prognostic features of patients with bacterial pneumonia. **(A)** Twenty-eight-day survival curve for patients with SBP. **(B)** Forest plots of multivariate Cox regression analysis for 28-day mortality in patients with SBP. SDI, Simpson's dominance index; PCT, procalcitonin; CRP, C-reactive protein.

and effective antimicrobial therapy in patients can lead to a decrease in the accuracy of PCT as an indicator of prognosis. Therefore, PCT/SDI can be more sensitive to the trend of ratio results. According to our study data, PCT/SDI and CRP/SDI were higher in the critical group than in the non-critical group, and the former group had longer VAVT and more cases of death within 28 days. The SDI values of patients in the death group were lower than those in the survival group, while PCT/SDI and CRP/SDI were higher than those in the survival group, and PCT/SDI was positively correlated with the VAVT. SDI was negatively correlated with the VAVT; SDI was negatively correlated with the VAVT, while age, sex, and CRP were not statistically significant when compared between groups, suggesting that PCT/SDI and CRP/SDI were correlated with the severity of disease in patients with SBP in the ICU.

The ROC curve showed that the area under the curve of PCT/SDI for predicting 28-day death in patients with SBP was 0.851, which was better than PCT (0.811), SDI (0.778), CRP/SDI (0.720), and PCT +SDI (0.845), indicating that the highest accuracy in determining the 28-day prognosis of patients with SBP was observed with a PCT/SDI ratio of 11.56, with a sensitivity and specificity of 94.1% and 65.8%, respectively. The multivariate Cox regression analysis demonstrated that PCT/SDI (HR = 1.562; 95% CI: 1.271 to 1.920; p = 0.039) and PCT (HR = 1.148; 95% CI: 1.105 to 1.134; p = 0.015) were independent risk factors for the 28-day death of patients with bacterial pneumonia in the ICU. Given the impact of multiple diseases on PCT values, such as renal insufficiency, organ transplantation, and autoimmune diseases, it is reasonable to confirm that PCT/SDI can be a more sensitive indicator of a patient's short-term prognosis (Covington et al., 2018).

Some limitations of the study should be considered. First, given its retrospective nature, only 110 patients was included. Second, patients were not divided into subgroups according to their ventilation mode, such as invasive ventilation and noninvasive ventilation. These factors may affect the validity of the PCT/SDI ratio in determining the prognosis of patients with SBP. Third, considering the study methodology and the cost of SDI, this study did not perform dynamic monitoring and evaluation of PCT/SDI to further explore the dynamic change pattern of the index. We expect the cost of SDI to decrease, so that the sample size can be expanded to further evaluate PCT/SDI.

Conclusions

In conclusion, although the PCT/SDI ratio is a tool to predict the 28-day prognosis of patients with SBP and may help to reduce the impact of various diseases on the monitoring results, the ratio is not a perfect method to replace PCT for clinical use. However, as a monitoring method with a sensitivity close to 90%, this method will still help clinicians to assess the short-term prognosis of patients with SBP. Given that the accuracy of PCT and CRP are affected by several factors, the use of antimicrobial drugs can also lead to a decrease in the accuracy of PCT and CRP results. This study indicates the high potential value of PCT/SDI ratio as a method to assess the short-term prognosis of these patients.

Data availability statement

The datasets presented in this study can be found in online repositories. The names of the repository/repositories and accession number(s) can be found below CNSA, CNP0003255.

Ethics statement

The studies involving human participants were reviewed and approved by Ethics Committee of Affiliated Hospital of Yangzhou University. Written informed consent for participation was not required for this study in accordance with the national legislation and the institutional requirements.

Author contributions

HH and QS conceived and designed this study. WL, QZ, and GS collected the data. GS drafted and critically revised the manuscript. All authors have read and approved the final manuscript. All authors contributed to the article and approved the submitted version.

Funding

This work was supported by grants from the Hengrui Pharmacy Service Special Research Grant Project of Jiangsu Province Pharmaceutical Association, China (H202129) and the Pharmaceutical Research Project Sponsored by Tianqing Hospital of Jiangsu Province Pharmaceutical Association, China (Q202050).

Conflict of interest

The authors declare that the research was conducted in the absence of any commercial or financial relationships that could be construed as a potential conflict of interest.

Publisher's note

Supplementary material

The Supplementary Material for this article can be found online at: https://www.frontiersin.org/articles/10.3389/fcimb.2023.1175747/full#supplementary-material

References

Christopher, Z. K., McQuivey, K. S., Deckey, D. G., Haglin, J., Spangehl, M. J., and Bingham, J. S. (2021). Acute or chronic periprosthetic joint infection? using the ESR / CRP ratio to aid in determining the acuity of periprosthetic joint infections. *J. Bone Jt Infect.* 6 (6), 229–234. doi: 10.5194/jbji-6-229-2021

Covington, E. W., Roberts, M. Z., and Dong, J. (2018). Procalcitonin monitoring as a guide for antimicrobial therapy: a review of current literature. *Pharmacotherapy* 38 (5), 569–581. doi: 10.1002/phar.2112

Dickson, R. P., and Huffnagle, G. B. (2015). The lung microbiome: new principles for respiratory bacteriology in health and disease. *PloS Pathog.* 11 (7), e1004923. doi: 10.1371/journal.ppat.1004923

Dickson, R. P., Schultz, M. J., van der Poll, T., Schouten, L. R., Falkowski, N. R., Luth, J. E., et al. (2020). Lung microbiota predict clinical outcomes in critically ill patients. *Am. J. Respir. Crit. Care Med.* 201 (5), 555–563. doi: 10.1164/rccm.201907-1487OC

Dima, E., Kyriakoudi, A., Kaponi, M., Vasileiadis, I., Stamou, P., Koutsoukou, A., et al. (2019). The lung microbiome dynamics between stability and exacerbation in chronic obstructive pulmonary disease (COPD): current perspectives. *Respir. Med.* 157, 1–6. doi: 10.1016/j.rmed.2019.08.012

Guo, M. Y., Chen, H. K., Ying, H. Z., Qiu, F. S., and Wu, J. Q. (2021). The role of respiratory flora in the pathogenesis of chronic respiratory diseases. *BioMed. Res. Int.* 2021. doi: 10.1155/2021/6431862

Hong, L. L., Chen, Y. Q., and Ye, L. (2021). Characteristics of the lung microbiota in lower respiratory tract infections with and without history of pneumonia. *Bioengineered* 12 (2), 10480–10490. doi: 10.1080/21655979.2021.1997563

Hunter, P. (1988). Numerical index of the discriminatory ability of typing systems: an application of simpson's index of diversity. *J. Clin. Microbiol.* 26.

Kalil, A. C., Metersky, M. L., Klompas, M., Muscedere, J., Sweeney, D. A., Palmer, L. B., et al. (2016). Management of adults with hospital-acquired and ventilator-associated pneumonia: 2016 clinical practice guidelines by the infectious diseases society of America and the American thoracic society. *Clin. Infect. Dis.* 63 (5), e61–e111. doi: 10.1093/cid/ciw353

Langelier, C., Zinter, M. S., Kalantar, K., Yanik, G. A., Christenson, S., O'Donovan, B., et al. (2018). Metagenomic sequencing detects respiratory pathogens in hematopoietic cellular transplant patients. *Am. J. Respir. Crit. Care Med.* 197 (4), 524–528. doi: 10.1164/rccm.201706-1097LE

Metlay, J. P., Waterer, G. W., Long, A. C., Anzueto, A., Brozek, J., Crothers, K., et al. (2019). Diagnosis and treatment of adults with community-acquired pneumonia. an official clinical practice guideline of the American thoracic society and infectious diseases society of America. *Am. J. Respir. Crit. Care Med.* 200 (7), e45–e67. doi: 10.1164/rccm.201908-1581ST

Panzer, A. R., Lynch, S. V., Langelier, C., Christie, J. D., McCauley, K., Nelson, M., et al. (2018). Lung microbiota is related to smoking status and to development of acute

respiratory distress syndrome in critically ill trauma patients. *Am. J. Respir. Crit. Care Med.* 197 (5), 621–631. doi: 10.1164/rccm.201702-0441OC

Pimple, U. (2020). Dataset on plot inventories of species diversity and structural parameters of natural and rehabilitated mangrove forest in the trat province of Thailand. *Data Brief* 30, 105500. doi: 10.1016/j.dib.2020.105500

Segal, L. N., Clemente, J. C., Li, Y., Ruan, C., Cao, J., Danckers, M., et al. (2017). Anaerobic bacterial fermentation products increase tuberculosis risk in antiretroviral-Drug-Treated HIV patients. *Cell Host Microbe* 21 (4), 530–537.e534. doi: 10.1016/j.chom.2017.03.003

Shi, Y., Huang, Y., Zhang, T. T., Cao, B., Wang, H., Zhuo, C., et al. (2019). Chinese Guidelines for the diagnosis and treatment of hospital-acquired pneumonia and ventilator-associated pneumonia in adults, (2018 edition). *J. Thorac. Dis.* 11 (6), 2581–2616. doi: 10.21037/jtd.2019.06.09

Simpson, E. H. (1949). Measurement of diversity nature 163. *ghgt.*

Wang, J., Zheng, N., Chang, X., Qian, H., and Han, Y. (2022). Nutritional risk factors for all-cause mortality of critically ill patients: a retrospective cohort study. *BMJ Open* 12 (11), e066015. doi: 10.1136/bmjopen-2022-066015

Woo, S., Park, S. Y., Kim, Y., Jeon, J. P., Lee, J. J., and Hong, J. Y. (2020). The dynamics of respiratory microbiota during mechanical ventilation in patients with pneumonia. *J. Clin. Med.* 9 (3). doi: 10.3390/jcm9030638

Yang, B., Pang, X., Bao, W., and Zhou, K. (2018). Thinning-induced canopy opening exerted a specific effect on soil nematode community. *Ecol. Evol.* 8 (8), 3851–3861. doi: 10.1002/ece3.3901

Zanza, C., Romenskaya, T., Thangathurai, D., Ojetti, V., Saviano, A., Abenavoli, L., et al. (2022). Microbiome in critical care: an unconventional and unknown ally. *Curr. Med. Chem.* 29 (18), 3179–3188. doi: 10.2174/0929867328666210915115056

frontiers | Frontiers in Cellular and Infection Microbiology

TYPE Original Research
PUBLISHED 04 July 2023
DOI 10.3389/fcimb.2023.1205401

OPEN ACCESS

EDITED BY
Jianmin Chai,
Foshan University, China

REVIEWED BY
Kelvin Li,
University of Pittsburgh, United States
Wong Kon Ken,
National University of Malaysia, Malaysia
Benjamin G. Wu,
New York University, United States

*CORRESPONDENCE
Lowell Ling
lowell.ling@cuhk.edu.hk
Zigui Chen
zigui.chen@cuhk.edu.hk

†These authors have contributed equally to this work

RECEIVED 13 April 2023
ACCEPTED 13 June 2023
PUBLISHED 04 July 2023

CITATION
Ling L, Lai CKC, Lui G, Yeung ACM, Chan HC, Cheuk CHS, Cheung AN, Chang LC, Chiu LCS, Zhang JZ, Wong W-T, Hui DSC, Wong CK, Chan PKS and Chen Z (2023) Characterization of upper airway microbiome across severity of COVID-19 during hospitalization and treatment. *Front. Cell. Infect. Microbiol.* 13:1205401. doi: 10.3389/fcimb.2023.1205401

Characterization of upper airway microbiome across severity of COVID-19 during hospitalization and treatment

Lowell Ling[1*†], Christopher K.C. Lai[2], Grace Lui[3], Apple Chung Man Yeung[2], Hiu Ching Chan[2], Chung Hon Shawn Cheuk[4], Adonia Nicole Cheung[4], Lok Ching Chang[1], Lok Ching Sandra Chiu[1], Jack Zhenhe Zhang[1], Wai-Tat Wong[1], David S. C. Hui[3,5], Chun Kwok Wong[6], Paul K. S. Chan[2,5] and Zigui Chen[2*†]

[1]Department of Anaesthesia and Intensive Care, Faculty of Medicine, The Chinese University of Hong Kong, Hong Kong, Hong Kong SAR, China, [2]Department of Microbiology, Faculty of Medicine, The Chinese University of Hong Kong, Hong Kong, Hong Kong SAR, China, [3]Department of Medicine and Therapeutics, Faculty of Medicine, The Chinese University of Hong Kong, Hong Kong, Hong Kong SAR, China, [4]Faculty of Medicine, The Chinese University of Hong Kong, Hong Kong, Hong Kong SAR, China, [5]Stanley Ho Centre for Emerging Infectious Diseases, Faculty of Medicine, The Chinese University of Hong Kong, Hong Kong, Hong Kong SAR, China, [6]Department of Chemical Pathology, Faculty of Medicine, The Chinese University of Hong Kong, Hong Kong, Hong Kong SAR, China

Longitudinal studies on upper respiratory tract microbiome in coronavirus disease 2019 (COVID-19) without potential confounders such as antimicrobial therapy are limited. The objective of this study is to assess for longitudinal changes in the upper respiratory microbiome, its association with disease severity, and potential confounders in adult hospitalized patients with COVID-19. Serial nasopharyngeal and throat swabs (NPSTSs) were taken for 16S rRNA gene amplicon sequencing from adults hospitalized for COVID-19. Alpha and beta diversity was assessed between different groups. Principal coordinate analysis was used to assess beta diversity between groups. Linear discriminant analysis was used to identify discriminative bacterial taxa in NPSTS taken early during hospitalization on need for intensive care unit (ICU) admission. A total of 314 NPSTS samples from 197 subjects (asymptomatic = 14, mild/moderate = 106, and severe/critical = 51 patients with COVID-19; non–COVID-19 mechanically ventilated ICU patients = 11; and healthy volunteers = 15) were sequenced. Among all covariates, antibiotic treatment had the largest effect on upper airway microbiota. When samples taken after antibiotics were excluded, alpha diversity (Shannon, Simpson, richness, and evenness) was similar across severity of COVID-19, whereas beta diversity (weighted GUniFrac and Bray–Curtis distance) remained different. Thirteen bacterial genera from NPSTS taken within the first week of hospitalization were associated with a need for ICU admission (area under the receiver operating characteristic curve, 0.96; 95% CI, 0.91–0.99). Longitudinal analysis showed that the upper respiratory microbiota alpha and beta diversity was unchanged during hospitalization in the absence of antimicrobial therapy.

KEYWORDS

COVID-19, SARS-CoV-2, 16S rRNA, upper airway microbiome, intensive care unit

1 Introduction

Coronavirus disease 2019 (COVID-19) is a respiratory illness caused by a novel coronavirus (SARS-CoV-2) (Huang et al., 2020). The clinical presentation of patients with COVID-19 varies from asymptomatic to critical, which can result in severe pneumonia, acute respiratory distress syndrome, multi-organ failure, and death (Lui et al., 2020). Age and baseline comorbidities such as renal failure, cardiovascular disease, and obesity have been established as the major risk factors of severe COVID-19 infection (Dessie and Zewotir, 2021). Host genetic variants are also associated with COVID-19 mortality (Pairo-Castineira et al., 2021). Although the current omicron variant is much weaker than the original variants of SARS-CoV-2, understanding of host–virus interaction remains incomplete (Esper et al., 2022).

Recent insight into the role of microbiome in human disease has opened up potential new therapeutic avenues (Sorbara and Pamer, 2022). Once thought to be sterile, the dynamic microbiome in the lung has only been recently recognized (Hilty et al., 2010). Furthermore, asthma, cystic fibrosis, and pneumonia are associated with changes in lung microbiome different to that of healthy lungs (Dickson et al., 2016a; Goldman et al., 2018). It remains controversial whether altered microbiome is the result of lung disease, contributes to the disease process itself, or both (Dickson et al., 2014). Nevertheless, modifying the lung microbiota with probiotics has already shown promise in reducing exacerbations in cystic fibrosis (Weiss et al., 2010).

Because SARS-CoV-2 is primarily a respiratory infection, upper airway respiratory dysbiosis-inflammation may play a role in determining severity of COVID-19. Indeed, it has been shown that the respiratory tract microbiome is different in patients with COVID-19 compared with healthy ones (Mostafa et al., 2020; Xu et al., 2020; Rhoades et al., 2021). Furthermore, some studies have shown that COVID-19 severity is associated with progressive changes in upper airway respiratory microbiota (Merenstein et al., 2021; Shilts et al., 2021; Ventero et al., 2021). However, current evidence is often conflicting, likely due to small sample sizes and differences in cohort selection, sampling time points, and site of sampling (Mostafa et al., 2020; Braun et al., 2021; Llorens-Rico et al., 2021; Shilts et al., 2021; Wu et al., 2021; Merenstein et al., 2022). In addition, many studies did not report or account for antimicrobial use in patients hospitalized for COVID-19 (Ma et al., 2021; Merenstein et al., 2021; Rueca et al., 2021; Ventero et al., 2021; Chen et al., 2022). As up to 75% of patients with COVID-19 were given antimicrobial therapy early on during the pandemic, this may have affected the respiratory microbiome independent of SARS-CoV-2 infection (Langford et al., 2021). Last, longitudinal studies of dynamic changes in COVID-19 respiratory microbiome are scarce (Llorens-Rico et al., 2021; Merenstein et al., 2021; Ren et al., 2021; Xu et al., 2021; Candel et al., 2023). We hypothesized that changes in upper respiratory microbiota in hospitalized patients with COVID-19 over the course of hospitalization are greatly affected by treatments such as antimicrobial therapy. Nevertheless, as COVID-19 is associated with respiratory inflammation, we postulate that upper respiratory microbiota may be related to COVID-19 severity, viral load, and plasma cytokines. The primary objective of this prospective observational study on adult patients hospitalized for COVID-19 is to assess for longitudinal changes in the upper respiratory microbiome during hospitalization and COVID-19 treatment. The secondary objectives of the study are to determine association between upper respiratory tract microbiome and severity of COVID-19 as well as its potential confounders and to compare SARS-CoV-2 viral load and plasma cytokine with upper respiratory tract microbiota in COVID-19.

2 Methods

2.1 Study design and subject recruitment

This was a prospective observational study on adult (age ≥ 18 years old) hospitalized patients who tested positive for SARS-CoV-2 on reverse transcription polymerase chain reaction (RT-PCR). Patients were included if they had at least one nasopharyngeal swab and throat swab (NPSTS) sample taken during hospitalization within 3 weeks of hospital admission after informed consent. Patients who were previously vaccinated against SARS-CoV-2, received antibiotics 3 months prior to hospitalization, or had missing data on clinical severity or antimicrobial therapy were excluded. Samples that were inadequate for DNA extraction and 16S rRNA gene amplicon sequencing for microbiota profiling were also excluded. Blood samples for cytokine profiling were taken as early as possible after hospital admission. Mechanically ventilated intensive care unit (ICU) patients without COVID-19 and healthy volunteers working in the same hospital environment were recruited for controls. This study was approved by The Joint Chinese University of Hong Kong – New Territories East Cluster Clinical Research Ethics Committee (2020.076).

2.2 Severity of COVID-19

COVID-19 severity was classified as asymptomatic, mild/moderate, or severe/critical based on the highest severity level at hospital discharge as previously described (28). Medical records including clinical notes, imaging, laboratory results, and observation charts were manually reviewed to determine the severity of COVID-19 according to the following criteria: Asymptomatic patients had no symptoms despite SARS-CoV-2 infection. Mild/moderate group included patients who had symptoms of fever, cough, myalgia, sore throat, and rigors related to SARS-CoV-2 infection but did not require oxygen therapy. Severe/critically ill patients with COVID-19 included those who had dyspnea, respiratory rate ≥ 30, or required oxygen therapy or mechanical ventilation for SARS-CoV-2 infection due to respiratory failure.

2.3 Respiratory sampling

Serial NPSTSs were collected for SARS-CoV-2 viral load quantification and 16S rRNA sequencing analysis. During the early COVID-19 pandemic, all patients with confirmed COVID-19 were hospitalized as part of the Hong Kong public health strategy. Patients were only discharged after testing negative for SARS-CoV-2 on RT-PCR. Patients who were asymptomatic or had mild disease were, sometimes, hospitalized for longer than 2 weeks despite clinical recovery. Therefore, serial NPSTS samples could be collected from all severity groups during hospitalization. The time points used in this study were the first sample within the first week of hospitalization and the second sample between the second and third weeks of hospitalization. Samples were stored in −80°C for 0.1–2.5 years until completion of recruitment for further analysis.

2.4 SARS-CoV-2 viral load quantification

Total RNA was extracted from mixed NPSTSs using the QIAamp Viral RNA Mini Kit (QIAGEN, Hilden, Germany). Primer–probe set targeting the N gene (2019-nCoV_N1-F: 5′-GAC CCC AAA ATC AGC GAA AT-3′; 2019-nCoV_N1-R: 5′-TCT GGT TAC TGC CAG TTG AAT CTG-3′; and 2019-nCoV_N1-P: 5′-FAM-ACC CCG CAT TAC GTT TGG TGG ACC-BHQ1-3′) was used to detect SARS-CoV-2 RNA by real-time RT-PCR as previously described (Lui et al., 2020). The detection limit of real-time RT-PCR was 694 copies/ml, and samples were considered negative if Ct values exceeded 39.9 cycles.

2.5 16S rRNA sequencing

Total DNA was extracted from mixed NPSTS using the QIAamp DNA Mini Kit (QIAGEN, Hilden, Germany) to characterize respiratory microbiota using 16S rRNA gene amplicon sequencing. The molecular process, including the DNA extraction, 16S PCR amplification, and library preparation, were performed at separate locations to avoid contamination. For quality control, negative controls (blank DNA extraction and PCR controls), positive controls (ZymoBIOMICS Microbial Community DNA Standard, catalog no. D6305), and technical replicates (randomly selected DNA samples) were also included. In brief, the 16S rRNA gene hypervariable V3-V4 region (~450 bp) was targeted (341F: 5′-CCT ACG GGN GGC WGC AG-3′; 806R: 5′-GGA CTA CNV GGG TWT CTA AT-3′), with barcodes indexed to each amplicon set for multiplexing sequencing on an Illumina MiSeq for PE300 reads (Chen et al., 2019). QIIME2 (v2022.2) with the latest SILVA ribosomal RNA database (v138 SSU Ref NR 99 dataset) was used to classify amplicon sequence variants (ASVs), with operational taxonomic table showing the proportion of bacterial reads per sample at different taxonomic levels after removing reads assigned to archaea, mitochondria, or chloroplasts.

2.6 Microbiota data analysis

Data distribution was assessed using Shapiro–Wilk test, and descriptive statistics such as mean and standard error as well as median and interquartile range (IQR) were used to summarize data. A phylogenetic tree was generated by inserting the representative reads into the SILVA 128 reference tree using the SATe-enabled phylogenetic placement method. Alpha diversity was assessed using Shannon, Simpson, richness, and evenness, and Wilcoxon rank sum test was used for assessing the pairwise difference between the defined groups. Beta diversity was assessed using unweighted and weighted GuniFrac and Bray–Curtis distance. Principal coordinate analysis was used to assess beta diversity between different groups using permutational multivariate analysis of variance (PERMANOVA) with 9,999 permutations using the *adonis2* in the Vegan R package (v2.6-4). In the effect size analysis using a single multivariable model, antibiotic-controlled association between metadata variables, including intubation, ICU, severity, peak CRP, hospitalized time, antivirus, peak viral load, Charlson comorbidity index, age, and gender, was tested by adding antibiotics into the model formula. An exploratory analysis on discriminative bacterial taxa between patients who required ICU admission and those that did not was estimated using linear discriminant analysis (LDA) effect size (LEfSe) with the default setting, with further comparisons of the relative abundances using nonparametric Mann–Whitney–Wilcoxon rank sum test and Tukey's honest significant difference *post-hoc* test (Segata et al., 2011). Logistic regression and receiver operating characteristic (ROC) curve with the calculation of area under the ROC curve (AUC) were used to evaluate the potential markers identified for prediction of need for ICU admission. Delong's test was used to assess the differences in AUCs. All other data visualization was performed using the ggplot package in R. A two-sided p-value < 0.05 or a false discovery rate–adjusted p-value (p_{adj} or q) < 0.1 was used as the threshold for statistical significance.

2.7 Cytokine profile

A 3 ml of EDTA blood sample was taken from recruited patients with COVID-19 and immediately cooled and transported to the laboratory for processing. Plasma was separated by centrifugation (2,000g for 10 min) at 4°C and stored in 300 µl of aliquots at −70°C until analysis. Milliplex human cytokine multiplex assay using the Bio-plex 200 System (Bio-Rad Laboratories, Inc. CA, USA) was used to determine levels of 32 cytokines including sCD40L, EGF, Eotaxin, FGF-2, Flt-3L, Fractalkine, GRO-α, IFN-α2, IFN-γ, IL-1β, IL-1RA, IL-3, IL-5, IL-6, IL-7, IL-8, IL-10, IL-12 p40, IL-12 p70, IL-13, IL-15, IL-18, IP-10, MCP-1, MCP-3, MDC, MIG, MIP-1β, TGF-α, TNF-α, TNF-β, and VEGF (Ling et al., 2021). Associations of cytokine factors with clinical variants and bacterial genera were analyzed by Fit a Negative Binomial Generalized Linear Model using the glm.nb in the MASS R package and a Spearman's rank-order correlation test using the cor.test in the Stats R package, respectively.

10.3389/fcimb.2023.1205401

3 Results

3.1 Cohort characteristics

A total of 314 NPSTS samples from 197 subjects that generated high-quality 16S sequence reads were analyzed (Figure S1). COVID-19 group consisted of 171 adult hospitalized patients (asymptomatic = 14, mild/moderate = 106, and severe/critical = 51) (Table 1). Meanwhile, 11 mechanically ventilated ICU adult hospitalized patients without COVID-19 and 15 adult healthy volunteers who worked in the same hospital as healthcare workers or departmental staff were included as controls. The baseline characteristics of the recruited subjects are shown in Table 1 and Table S1. Overall, patients with severe/critical COVID-19 were older and were more likely to have comorbidities. Peak median viral load was similar across different COVID-19 severity (Table 1, $p = 0.086$). Antibiotic use was highest in patients with severe/

TABLE 1 Cohort characteristics.

	Asymptomatic (N = 14)	Mild/Moderate (N = 106)	Severe/Critical (N = 51)	Non–COVID-19 ICU (N = 11)	Healthy Controls (N = 15)	p
Median Age, years	32 (25–40)	49.0 (33–61)	66 (57–73)	62 (49–69)	42 (35–48)	<0.001
Female Gender (%)	6 (42.9)	60 (56.6)	16 (31.4)	3 (27.3)	10 (66.7)	0.012
Charlson Comorbidity Index						
None	11 (78.6)	49 (46.2)	3 (5.9)	2 (18.2)	12 (80.0)	<0.001
Mild (1–2)	3 (21.4)	42 (39.6)	20 (39.2)	5 (45.5)	3 (20.0)	0.397
Moderate (3–4)	0 (0)	10 (9.4)	21 (39.2)	4 (36.4)	0 (0.0)	<0.001
Severe (≥5)	0 (0)	5 (4.7)	8 (15.7)	0 (0.0)	0 (0.0)	0.036
Comorbidity (%)						
Good past health	11 (78.6)	65 (61.3)	14 (27.5)	4 (36.4)	14 (93.3)	<0.001
Cardiovascular diseases	2 (14.3)	31 (29.2)	32 (62.8)	6 (54.5)	0 (0)	<0.001
Chronic kidney diseases	0 (0)	3 (2.8)	3 (5.9)	0 (0)	0 (0)	0. 616
Chronic lung diseases	1 (7.1)	3 (2.8)	2 (3.9)	0 (0)	0 (0)	0.779
Diabetes mellitus	0 (0)	15 (14.2)	20 (39.2)	3 (27.3)	1 (6.7)	<0.001
Immunodeficiency	0 (0)	1 (0.9)	0 (0)	0 (0)	0 (0)	0.93
Liver diseases	1 (7.1)	6 (5.7)	5 (9.8)	1 (9.1)	0 (0)	0.703
Malignancy	0 (0)	2 (1.9)	4 (7.8)	0 (0)	0 (0)	0.222
Bacterial Coinfection (%)	0 (0)	1 (0.9)	9 (17.6)	1 (9.1)	–	0.0149
Median Peak Viral Load (Ct)	27.3 (20.3–29.6)	21.5 (17.1–27.6)	20.2 (18.2–25.5)	–	–	0.086
Treatment (%) [b]						
Antibiotics	1 (7.1)	17 (16.0)	38 (74.5)	10 (90.9)	0 (0)	<0.001
Dexamethasone	0 (0.0)	7 (6.6)	47 (92.2)	0 (0)	0 (0)	<0.001
Remdesivir	0 (0.0)	9 (8.5)	38 (74.5)	0 (0)	0 (0)	<0.001
Lopinavir/ritonavir	0 (0.0)	28 (26.4)	14 (27.5)	0 (0)	0 (0)	0.009
Tocilizumab	0 (0.0)	2 (1.9)	2 (3.9)	0 (0)	0 (0)	0.78
Interferon beta-1b	0 (0.0)	39 (36.8)	23 (45.1)	0 (0)	0 (0)	<0.001
Outcomes (%)						
ICU admission	0 (0.0)	0 (0.0)	32 (62.7)	11 (100)	–	<0.001
Vasopressors	0 (0.0)	0 (0.0)	20 (39.2)	4 (36.4)	0 (0)	<0.001
Mechanical ventilation	0 (0.0)	0 (0.0)	20 (39.2)	11 (100)	0 (0)	<0.001
Hospital mortality	0 (0.0)	0 (0.0)	6 (11.8)	1 (9.1)	0 (0)	0.001

Bacterial coinfection was defined as positive growth of a bacterial pathogen in respiratory tract or blood culture samples within 48 hours of hospitalization. Values are expressed as median and (interquartile range) unless otherwise specified.

critical COVID-19 and non–COVID-19 ICU patients. Use of specific COVID-19 treatments varied across the spectrum of COVID-19 severity.

3.2 Upper airway microbiota in earliest samples of all subjects

We selected the earliest collected NPSTS samples from each subject (hospitalized COVID-19 = 171, non–COVID-19 ICU = 11, and healthy = 15) to profile the upper airway microbial communities. The median time interval between time of hospitalization and sampling time of first sample was 3 days. A total of 2,649,726 high-quality 16S rRNA V3-V4 reads were generated, ranging between 1,026 and 118,093 reads per sample (13,450 ± 11,799). As shown in Figure 1 and Figure S2, *Firmicutes* was the most abundant microbial phyla in the surveyed samples (mean relative abundance ± SD of 34.70 ± 1.20%), followed by *Bacteroidota* (30.06 ± 1.30%), *Proteobacteria* (17.86 ± 1.32%), and 11 other phyla. *Proteobacteria* were lower in both hospitalized COVID-19 (17.70 ± 1.44%, Mann–Whitney U-test, $p < 0.01$) and non–COVID-19 ICU (6.52 ± 2.10%, $p < 0.001$) patients compared with healthy volunteers (27.95 ± 3.62%). In contrast, *Bacteroidetes* was higher in both in both hospitalized COVID-19 (30.47 ± 1.30%, $p < 0.001$) and non–COVID-19 ICU (44.09 ± 8.78%, $p < 0.01$) patients compared with healthy volunteers (30.06 ± 1.30%).

Alpha diversity at the ASV level as measured by Shannon, Simpson, and evenness was progressively reduced as severity of COVID-19 increased (Figure 2A, Figure S3A). Similarly, distinct clustering of the microbial communities from patients with COVID-19, particularly those with severe/critical severity, from healthy controls was observed in weighted GUniFrac, unweighted GUniFrac, and Bray–Curtis distance at the ASV level ($p < 0.001$). Antibiotic treatment (yes vs. no) was consistently the most significant covariate that had the largest effect on the overall structure of the upper airway microbiota in all beta diversity metrics (unweighted GUniFrac: $R^2 = 0.0442$, $p < 0.001$; weighted GUniFrac: $R^2 = 0.0307$, $p < 0.001$; and Bray–Curtis: $R^2 = 0.0216$, $p < 0.001$) (Figure 2A, Figure S3B, Table S2). Similarly, the microbial community was also significantly affected by intubation (yes vs. no) and ICU admission (yes vs. no). The effect of severity (severe/critical vs. non-severe/critical), peak CRP (≤ 7 vs. > 7), hospitalized time (≤ 1 vs. ≥ 2 weeks), and antivirus treatment (yes vs. no) on structure of microbial community was not detected in all measures of beta diversity (Figure 2A, Figure S3C). Notably, 86.7% (OR = 40.3; 95% CI, 8.3–392.5; $p < 0.001$) and 62.5% (OR = 14.5; 95% CI, 5.5–40.6; $p < 0.001$) of hospitalized patients with COVID-19 who were intubated and admitted to the ICU, respectively, were treated with antibiotics prior to NPSTS sample collection in this study.

3.3 Upper airway microbiota in samples without antimicrobial use

Because antimicrobial use was the most significant factor that affected upper airway microbiota dysbiosis, we further assessed the difference in microbiota without the effect of antimicrobials. Removal of NPSTS samples taken after antimicrobial use resulted in 157 samples from 137 antibiotic-naïve hospitalized patients with COVID-19 (14 asymptomatic, 98 mild/moderate, and 25 severe/critical cases), five non–COVID-19 ICU patients, and 15 healthy volunteers. The median time interval between time of hospitalization and sampling time of first sample was 3 days. All measures of alpha diversity were no longer significantly different across COVID-19 severity groups when confounding by antimicrobial was removed (Figure 2B, Figure S4A). After exclusion of the samples taken after antimicrobials, microbiota from patients with severe/critical COVID-19 still showed dispersive distribution by beta diversity analysis when compared with other groups, but the differences were reduced (Figure 2B, Figure S4B). After removal of the samples taken after antimicrobial use, the confounding effect of intubation and ICU admission on upper respiratory microbiota in COVID-19 was no longer consistently found (Figure S4C).

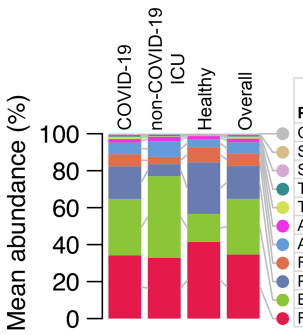

Phylum	COVID-19	P	non-COVID-19 ICU	P	Healthy	Overall
Others	0.01±0.00		0.00±0.00		0.00±0.00	0.00±0.00
Synergistetes	0.09±0.03		0.10±0.05		0.09±0.05	0.09±0.02
Spirochaetes	0.62±0.08		0.45±0.13		0.65±0.18	0.61±0.08
Tenericutes	0.90±0.39		0.76±0.20	*	0.19±0.09	0.84±0.34
Thermotogae	1.25±0.15	*	0.30±0.16		0.29±0.10	1.13±0.13
Armatimonadetes	1.94±0.36		2.44±1.86		1.77±0.67	1.95±0.34
Actinobacteria	6.32±0.74		8.47±4.79		4.26±0.81	6.29±0.69
Fusobacteria	6.50±0.48		3.94±1.24		8.21±2.30	6.48±0.46
Proteobacteria	17.70±1.44	**	6.52±2.10	***	27.95±3.62	17.86±1.32
Bacteroidetes	30.47±1.30	***	44.09±8.78	**	15.10±3.27	30.06±1.30
Firmicutes	34.21±1.24		32.93±7.52		41.47±4.60	34.69±1.20

FIGURE 1
Comparison of the upper airway microbiota summarized at the phylum level from COVID-19 (n = 171), non–COVID-19 ICU patients (n = 11), and healthy controls (n = 15). Values in the table are mean abundance ± standard error of the mean. Phyla with a mean total relative abundance < 0.1% are grouped as others (Deinococcus_Thermus, Chlamydiae, Planctomycetes, and Chloroflexi). Wilcoxon rank sum (MWU) tests for the difference in relative abundance between hospitalized patients with COVID and healthy controls, and between non–COVID-19 ICU patients and healthy controls were performed. *$p < 0.05$, **$p < 0.01$, and ***$p < 0.001$.

FIGURE 2
Alpha (Shannon) and beta (weighted GUniFrac) diversity of upper airway microbiota across cohort groups from all samples **(A)** and inclusion of only samples taken prior to antimicrobial therapy **(B)**. Panel **(A)** included samples from hospitalized patients with COVID-19 (n = 171, including 14 asymptomatic, 106 mild/moderate, and 51 severe/critical), non–COVID-19 patients (n = 11), and healthy controls (n = 15). Panel **(B)** shows difference in alpha and beta diversity when samples taken after antimicrobial therapy were excluded, which consisted of hospitalized COVID patients (n = 137, including 14 asymptomatic, 98 mild/moderate, and 25 severe/critical patients), non–COVID-19 ICU patients (n = 5), and healthy controls (n = 15). Difference in Shannon index was assessed by pairwise differences between groups using Wilcoxon rank sum test. Principal coordinate analysis was based on weighted GUniFrac inferred from amplicon sequence variants. Difference in weighted GUniFrac among groups was evaluated using permutational multivariate analysis of variance (PERMANOVA) with 9,999 permutations. Effect size (R^2 value) of covariates on upper airway microbiota structure in patients with COVID-19 in the multivariable model. Antibiotic-controlled association between metadata variables (intubation, ICU, severity, peak CRP, hospitalized time, antivirus, peak viral load, Charlson comorbidity index, age, and gender) was tested by adding antibiotics into the multivariable model formula. *p < 0.05, **p < 0.01, ***p < 0.001, and ****p < 0.0001.

3.4 Longitudinal changes in microbiota during hospitalization

Because upper airway microbiota is significantly confounded by use of antimicrobial use, longitudinal change in microbiota during hospitalization was assessed after exclusion of samples taken after antimicrobial therapy (102 samples). Assessment of these samples showed that upper airway microbiota alpha and beta diversity did not change overtime during 2 weeks of hospitalization in antibiotic-naïve hospitalized patients with COVID-19 and healthy individuals (Figure 3, Figure S5).

3.5 Association of upper airway microbiota dysbiosis with clinical features and ICU admission of patients with COVID-19

Differentially abundant bacterial genera associated with demographic and clinical variants were characterized using LDA by LEfSe in the surveyed NPSTS samples from patients with COVID-19 in an exploratory analysis (n = 171) (LDA score > 2, p < 0.05) (Figure 4, Table S3). Interestingly, 15 and 10 bacterial genera showed consistent increase or decrease in the relative abundance in patients with antimicrobial use, intubation, and/or ICU admission. Among these, the enrichment of four bacterial genera (*Enterococcus*, *Limosilactobacillus*, *Sneathia*, and *Pseudomonas*) and the depression of eight bacterial genera (*Alloprevotella*, *Prevotella*, *Butyrivibrio*, *Hespellia*, *Lachnoanaerobaculum*, *Oribacterium*, *Solobacterium*, and *Centipeda*) were also significantly associated with the severity of patients with COVID-19. Because 63% (32 of 51) of patients with severe/critical COVID-19 in this study were admitted to the ICU, we further selected early NPSTS samples prior to antimicrobial use within the first week of hospitalization (n = 116) to identify bacterial markers that may be used to predict need for ICU admission (Figure 5). A total 13 discriminative bacterial genera were observed using LDA, with *Enterobacter*, *Mageeibacillus*, *Fannyhessea*, *Scardovia*, *Howardella*, and *Bulleidia* being higher but with *Alloprevotella*, *Campylobacter*, *Leptotrichia*, *Centipeda*, *Hespellia*, *Catonella*, and *Acinetobacter* being lower in patients who required ICU admission. The differential abundances of these 13 bacterial genera in the upper airway tract within the first week of hospitalization predicted the need for ICU admission with a combined AUC of 0.95 (95% CI of 0.91–0.99). Comparatively, prediction based on clinical demographics and comorbidity (age, gender, and Charlson comorbidity index) only achieved a combined

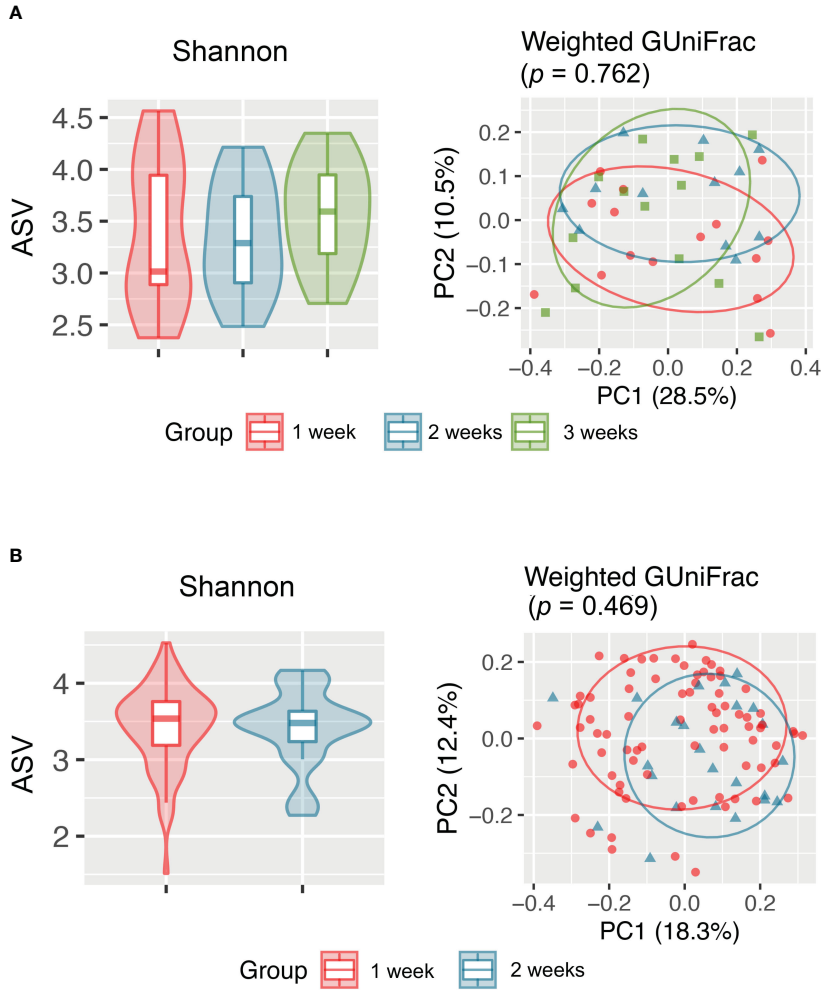

FIGURE 3
Alpha (Shannon index) and beta (weighted GUniFrac) diversity analyses revealed no significant difference in the upper respiratory tract microbiota between samples collected at different time points from **(A)** healthy individuals and **(B)** antibiotic-naïve patients with COVID-19.

AUC of 0.71 (95% CI of 0.57–0.85). Combination of clinical and microbiota (AUC of 0.96 (95% CI 0.93–1.00) did not improve on the predictive performance compared with the use of microbiota alone (Figure S6, $p = 0.486$).

3.6 Upper airway microbiota and plasma cytokine

Plasma was collected from 90 patients with COVID-19 to measure the levels of 32 cytokines. Median (IQR) time to cytokine profiling was 4 (2–8) days after hospital admission. Using the Negative Binomial Generalized Linear Model, changes in numerous cytokine factors were significantly associated with clinical factors (Figure 6). For example, increased IL-5, IL-6, IL-10, and MIG but deceased MIP-1β were observed in patients with severe/critical COVID-19 or those admitted to ICU, with satisfactory AUCs for predictive performance (Table S4). Those patients with higher IL-6 also had a higher chance of intubation and antibiotics and/or antivirus use. Older patients or those with higher Charlson comorbidity had higher levels of IL-6, IL-10, IP-10, MCP-1, and MIG, but lower levels of Fractalkine, IFN-χ, IL-12 p70, IL-13, and TGF-α. To understand the potential of upper airway microbiota dysbiosis on plasma cytokine levels, Spearman correlations between bacterial genera and cytokines were explored (Figure S7, Table S5). Next, we focused on the 13 bacterial genera that were associated with a need for ICU admission and found that only *Acinetobacter*, *Hespellia*, and *Campylobacter* were associated with MIG, IL-18, Fractalkine, and IL-1β after removal of samples taken after antimicrobial therapy (Figure 7).

4 Discussion

In this prospective, longitudinal observational study on upper airway microbiota in adult hospitalized patients with COVID-19, antimicrobial use accounted for most of the observed differences in microbiota during hospitalization and across severity groups. Alpha diversity in the upper airway was similar across severity of COVID-19 in the absence of antimicrobial use. In contrast, beta diversity

10.3389/fcimb.2023.1205401

FIGURE 4
Linear discriminant analysis (LDA) effect size (LEfSe) identified discriminative bacterial genera associated with clinical variants in hospitalized patients with COVID-19 (n = 171). Names in red and green indicate bacterial genera with increased and decreased abundance, respectively, that were commonly associated with antibiotics, intubation, and ICU admission. Differences in the relative abundances of two representative bacterial genera (*Prevotella* and *Pseudomonas*) associated with antibiotics, intubation, ICU admission, and severe/critical COVID-19 are shown in the right panel of the figure. *$p < 0.05$, **$p < 0.01$,and ***$p < 0.001$.

was different between asymptomatic and severe/critical COVID-19 even in the absence of antimicrobial use. Upper airway microbiota in patients with COVID-19 remained unchanged during 2 weeks of hospitalization if antimicrobials were not used. Peak viral load was not associated with upper airway microbiota in COVID-19. Early hospitalization upper airway microbiota may be associated with severity of COVID-19.

Many studies have implicated that reduced alpha diversity in upper respiratory microbiome is a hallmark of higher severity of COVID-19 (Hernandez-Teran et al., 2021; Ma et al., 2021; Merenstein et al., 2021; Ren et al., 2021; Shilts et al., 2021; Ventero et al., 2021; Bradley et al., 2022; Chen et al., 2022; de Castilhos et al., 2022; Hurst et al., 2022; Merenstein et al., 2022). However, mechanical ventilation, duration of ICU admission, and antimicrobial use account for a substantial portion of the variations seen in upper respiratory tract microbiome in COVID-19 (Llorens-Rico et al., 2021; Ren et al., 2021; de Castilhos et al., 2022). Our study corroborates with these findings, as there was no difference alpha diversity between severe/critical and asymptomatic COVID-19 when confounding by use of antimicrobial was removed. These results are consistent with animal and human non–COVID-19 studies that generally demonstrated that antimicrobial use reduces

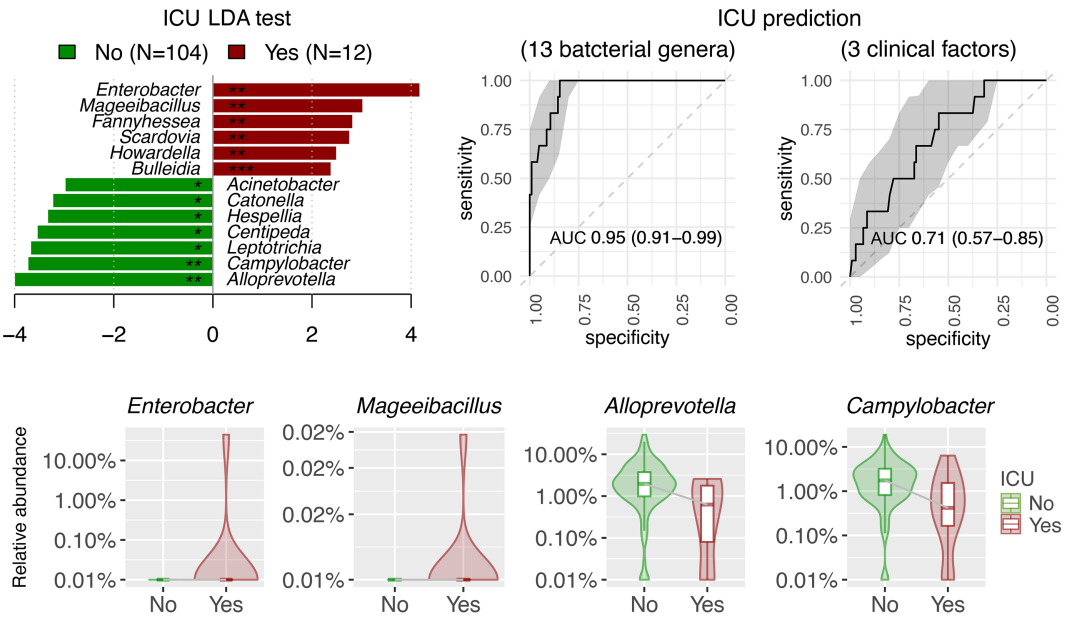

FIGURE 5
Linear discriminant analysis (LDA) effect size (LEfSe) showed the potential of 13 discriminative bacterial genera taken within the first week of hospitalization as predictor for ICU admission in antibiotic-naïve patients with COVID-19 (n = 116). Three clinical factors for ICU prediction included Charlson comorbidity index, age, and gender. AUC were expressed as AUC (95%CI).

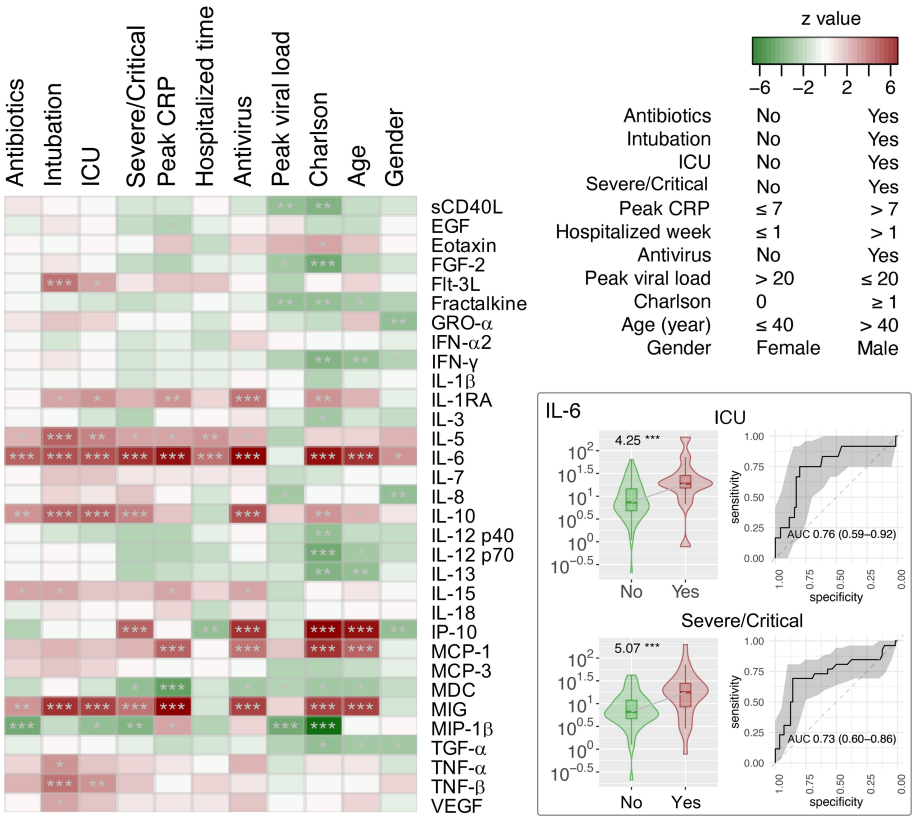

FIGURE 6
Association of cytokine factors with clinical variants in hospitalized patients with COVID-19 (n = 90). The z scores by the Fit a Negative Binomial Generalized Linear Model analysis using the glm.nb in the MASS R package were shown in the heat map. Relative abundance and receiver operating characteristic (ROC) analysis and area under the ROC curve (AUC) of IL-6 cytokine associated with ICU admission and severe/critical COVID-19 are shown in the right panel of the figure. *$p < 0.05$, **$p < 0.01$, and ***$p < 0.001$. AUC were expressed as AUC (95%CI).

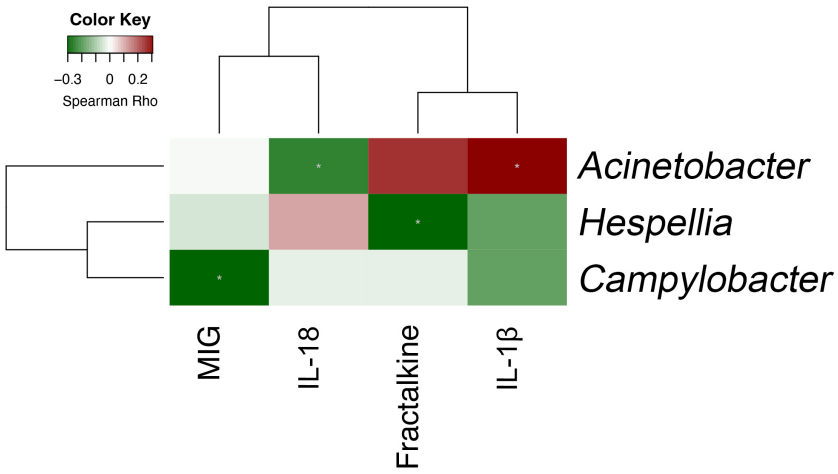

FIGURE 7
Spearman correlation between bacterial genera and plasma cytokines that are both individually associated with critical COVID-19 (n = 90).

bacterial alpha diversity (Huang et al., 2022; Kwon et al., 2022; Lekang et al., 2022). However, exclusion or statistical adjustment of samples for antimicrobial use was often not done or reported in COVID-19–related microbiome studies (Ma et al., 2021; Merenstein et al., 2021; Rueca et al., 2021; Ventero et al., 2021; Chen et al., 2022; Gauthier et al., 2022). As antimicrobial use is more common as COVID-19 severity increases, this may explain why many studies reported reduced alpha diversity as COVID-19 severity increased (Langford et al., 2021). Together, careful considerations on study design and data interpretation are required when assessing the validity of COVID-19–related microbiota study results.

Unlike alpha diversity that was mostly related to use of antimicrobials, we found that beta diversity was different across severity of COVID-19 even after removal of samples taken after antimicrobials. Overall, beta diversity of asymptomatic COVID-19 and severe/critical COVID-19 were closet and furthest from that of healthy individuals, respectively. In this study, *Enterococcus* in the upper airway was associated with COVID-19 severity and mechanical ventilation. Interestingly, this parallels the finding of increased relative abundance of *Enterococcus* in lungs of murine sepsis (Dickson et al., 2016b).

Nevertheless, association between specific bacterial genera and severity of COVID-19 has been inconsistently reported across different cohort studies (Merenstein et al., 2022; Candel et al., 2023). In our exploratory analysis, 13 bacterial genera from the upper airway microbiota were associated with a need for ICU admission. Although we were unable to perform internal validation, the lower abundance of upper airway *Alloprevotella* and *Campylobacter* in patients with COVID-19 requiring ICU admission found in this study was consistent other reports (Shilts et al., 2021; Smith et al., 2021; Chen et al., 2022; Hurst et al., 2022). Along the same lines, we found a lower abundance of *Acinetobacter* when COVID-19 severity was higher (Feehan et al., 2021; Smith et al., 2021). However, this has been inconsistently reported as some have found a higher abundance of *Acinetobacter* in upper airway microbiota in severe COVID-19 (Ma et al., 2021; Ren et al., 2021; Chen et al., 2022). Last, we showed that *Enterobacter* abundance was relatively higher in patients with COVID-19 admitted to ICU. Although this was also reported by Chen et al., not all studies supported the positive correlation between *Enterobacter* abundance and COVID-19 severity (Feehan et al., 2021; Chen et al., 2022; Gauthier et al., 2022). The reasons for these disparities are manifold. First, most of these studies did not exclude samples that were taken after antimicrobial therapy that may have confounded their findings. Second, tracheal intubation itself is associated with changes in upper and lower respiratory microbial diversity and may introduce bias in data interpretation (Kelly et al., 2016; Alagna et al., 2023). Third, there are baseline variations in microbiome composition and diversity among different ethnicity and geographic locations (Gupta et al., 2017).

Although some longitudinal studies reported changes in upper airway microbiota over time, many were confounded by medical interventions such as antimicrobial use and tracheal intubation (Llorens-Rico et al., 2021; Merenstein et al., 2021; Ren et al., 2021; Xu et al., 2021). In contrast, we showed that, in the absence of antimicrobial use, upper airway respiratory microbiome remained stable over 2 weeks of hospitalization in COVID-19 and healthy volunteers. Similarly, although some studies suggest viral load is associated with respiratory microbiome, we found that upper airway microbiota was unrelated to peak viral load. This maybe because we used serial samples to define peak viral load, whereas viral loads in other studies were determined by a single time point (Miller et al., 2021). It should be noted that severity of COVID-19 is more related to duration of viral shedding than peak viral load (Lui et al., 2020; Zheng et al., 2020).

The positive association between plasma cytokines such as IL-6, IL-10, IP-10, and MIG with COVD-19 severity is consistent with previous studies (Chi et al., 2020; Hadjadj et al., 2020; Zhao et al., 2020; Ling et al., 2021; Ochoa-Ramirez et al., 2022). In addition, specific correlations between upper respiratory tract microbiota and plasma cytokine levels were identified. Similar to previous reports,

most of the pairwise associations were not directly between microbiota and cytokines that were individually associated with COVID-19 severity (Ren et al., 2021). This may have been due to confounding by antimicrobial therapy. Indeed, when effect of antimicrobial therapy was removed, the correlations were different between upper respiratory tract microbiota and plasma cytokine. Nevertheless, we found that only three of the 13 bacterial genera that may predict ICU admission were associated with plasma cytokines that were themselves associated with critical COVID-19. Furthermore, neither were the associations particularly strong. For example, we found that *Campylobacter* in the upper respiratory tract was inversely related to MIG and COVID-19 severity, but the relationship was relatively weak. Overall, the likely explanation is that plasma cytokine levels may not directly reflect the local inflammation profile in upper respiratory tract dysbiosis in COVID-19.

The main strength of this study is the comprehensive matching between all COVID-19 severity phenotypes, timing and type of medical intervention, and serial microbiota sampling. This enabled a robust analysis on relationship between microbiota and COVID-19 severity after exclusion of samples that may be affected by medical interventions. However, our study has several limitations. First, this was a single-center study on patients of Southeast Asian descent, which may limit the generalizability of our results. Second, we did not analyze viral or fungal microbiota. Third, we did not analyze lower respiratory tract samples that may be more closely related to severity of COVID-19. Fourth, like many COVID-19 microbiome studies, viral culture medium was used during sample collection rather than fresh sampling, which may have affected the results (Merenstein et al., 2022). Fifth, we did not analyze microbiota according to SARS-CoV-2 strain as variant typing was not performed for all cases. However, the omicron variant first circulated in Hong Kong only during first half-year of 2022. If variant type was defined by study recruitment date, then patients with omicron would represent less than 6% of the study cohort. Although the omicron variant is associated with less severe phenotype, our results are unlikely to be significantly confounded as most of the COVID-19 cases were of alpha and delta variants (Esper et al., 2022). Furthermore, all included cases were unvaccinated against SARS-CoV-2. Sixth, although this resulted in one of the largest studies on respiratory microbiota in COVID-19, the sample size was still relatively modest and may have limited the power to detect subtle differences in microbiota. Moreover, the exploratory findings on association between upper respiratory bacterial genera and severity of COVID-19 require future validation. Last, an absolute abundance was not assessed, and a subsequent compositional approach to assess respiratory microbiota in COVID-19 may be helpful (Gloor et al., 2017).

5 Conclusion

Upper respiratory microbiota in adult patients hospitalized for COVID-19 remains stable during the first two weeks of hospitalization in the absence of antimicrobial use. Beta diversity is different across spectrum of COVID-19 severity, whereas alpha diversity is similar. Early hospitalization upper airway microbiota may be associated with severity of COVID-19. Peak viral load was not associated with upper airway microbiota in COVID-19.

Data availability statement

All sequence reads generated in this study have been deposited to the NCBI Sequence Read Archive (SRA) under Bioproject accession PRJNA934153.

Ethics statement

The studies involving human participants were reviewed and approved by The Joint Chinese University of Hong Kong – New Territories East Cluster Clinical Research Ethics Committee. The patients/participants provided their written informed consent to participate in this study.

Author contributions

LL, PC, CW, and ZC conceived and supervised the study. LL, W-TW, CL, and GL recruited study participants. SC, AC, LCC, LCSC, and JZ collected clinical information. AY and HC performed laboratory investigations. LL, PC, and ZC analyzed data and visualized results. LL and ZC wrote original draft. DH, CW, and PC reviewed and edited manuscript. All authors contributed to the article and approved the submitted version.

Funding

The study was supported, in part, by the Research Grants Council of Hong Kong SAR, China (project no. CUHK 24105721 to LL), and the Food and Health Bureau, Hong Kong SAR, China (reference no. COVID19F06 to PC). ZC thanks the support by the Project Impact Enhancement Fund (Project number PIEF/Ph2/COVID/11) from Faculty of Medicine, The Chinese University of Hong Kong, Hong Kong SAR, China. The funders had no role in study design, data collection and analysis, decision to publish, or preparation of the manuscript.

Acknowledgments

The authors would like to thank the participants who provided samples for this study. We also thank the Core Utilities of Cancer Genomics and Pathobiology (CUCGP) at the Department of Anatomical and Cellular Pathology of the Chinese University of Hong Kong for the service of 16S rRNA gene next-generation sequencing.

Conflict of interest

The authors declare that the research was conducted in the absence of any commercial or financial relationships that could be construed as a potential conflict of interest.

Publisher's note

Supplementary material

The Supplementary Material for this article can be found online at: https://www.frontiersin.org/articles/10.3389/fcimb.2023.1205401/full#supplementary-material

SUPPLEMENTARY FIGURE 1
Study recruitment flow chart showing inclusion and exclusion of study participants.

SUPPLEMENTARY FIGURE 2
Phylum abundance per subjective (n = 171) including hospitalized COVID-19 patients (14 asymptomatic, 106 mild/moderate, 51 severe/critical), 11 mechanically ventilated adult ICU patients without COVID-19 (non-COVID-19 ICU), and 15 adult healthy volunteers (Healthy).

SUPPLEMENTARY FIGURE 3
Upper airway microbiota dysbiosis associated with hospitalized COVID-19 patients (n = 171, including 14 asymptomatic, 106 mild/moderate and 51 severe/critical), non-COVID-19 patients (n = 11) and healthy controls (n = 15). **(A)** Comparison of the upper airway microbiota alpha diversity summarized at the amplicon sequence variant (ASV) level. Pairwise differences between groups were performed using Wilcoxon rank-sum test. **(B)** Principal coordinate analysis based on unweighted and weighted GUniFrac and Bray-Curtis distance metrics inferred from ASVs. Beta diversity among groups was evaluated using permutational multivariate analysis of variance (PERMANOVA) with 9,999 permutations. **(C)** Effect size (R^2 value) of variables on the upper airway microbiota in the hospitalized COVID-19 patients. Antibiotic-controlled association between metadata variables (intubation, ICU, severity, peak CRP, hospitalized time, antivirus, peak viral load, Charlson's comorbidity index, age and gender) were tested by adding antibiotics into the model formula. *$p < 0.05$, **$p < 0.01$, ***$p < 0.001$ and ****$p < 0.0001$.

SUPPLEMENTARY FIGURE 4
Upper airway microbiota dysbiosis associated with antibiotic-naïve hospitalized COVID-19 patients (n = 137, including 14 asymptomatic, 98 mild/moderate, and 25 severe/critical patients), non-COVID-19 ICU patients (n = 5) and healthy controls (n = 15) at the time when samples were collected. **(A)** Comparison of the upper airway microbiota alpha diversity summarized at the amplicon sequence variant (ASV) level. Pairwise differences between groups were performed using Wilcoxon rank-sum test. **(B)** Principal coordinate analysis based on unweighted and weighted GUniFrac and Bray-Curtis distance metrics inferred from ASVs. Beta diversity among groups was evaluated using permutational multivariate analysis of variance (PERMANOVA) with 9,999 permutations. **(C)** Effect size (R^2 value) of variables on the upper airway microbiota in the antibiotic-naïve hospitalized COVID-19 patients. *, $p < 0.05$; **, $p < 0.01$; ***, $p < 0.001$.

SUPPLEMENTARY FIGURE 5
Alpha and beta diversity analyses revealed no significant difference in the upper respiratory tract microbiota between samples collected at different time points from **(A)** healthy individuals and **(B)** antibiotic-naïve hospitalized COVID-19 patients.

SUPPLEMENTARY FIGURE 6
Predictive performance of 13 discriminative bacterial genera in upper respiratory tract microbiota and clinical factors (age, gender, Charlson's comorbidity index) on need for ICU admission in hospitalized patients with COVID-19. Samples taken after antimicrobial therapy were excluded in this analysis. AUC were expressed as AUC (95%CI).

SUPPLEMENTARY FIGURE 7
Spearman correlation between bacterial genera and plasma cytokine in adult hospitalized COVID-19 patients (n = 90).

References

Alagna, L., et al. (2023). Changes in upper airways microbiota in ventilator-associated pneumonia. *Intensive Care Med. Exp.* 11 (1), 17. doi: 10.1186/s40635-023-00496-5

Bradley, E. S., Zeamer, A. L., Bucci, V., Cincotta, L., Salive, M. C., Dutta, P., et al. (2022). Oropharyngeal microbiome profiled at admission is predictive of the need for respiratory support among COVID-19 patients. *Front. Microbiol.* 13, 1009440. doi: 10.3389/fmicb.2022.1009440

Braun, T., Halevi, S., Hadar, R., Efroni, G., Saar Glick, E., Keller, N., et al. (2021). SARS-CoV-2 does not have a strong effect on the nasopharyngeal microbial composition. *Sci. Rep.* 11 (1), 8922. doi: 10.1038/s41598-021-88536-6

Candel, S., Tyrkalska, S. D., Alvarez-Santacruz, C., and Mulero, V.. (2023). The nasopharyngeal microbiome in COVID-19. *Emerg. Microbes Infect.* 12 (1), e2165970. doi: 10.1080/22221751.2023.2165970

Chen, Z., Hui, P. C., Hui, M., Yeoh, Y. K., Wong, P. Y., Chan, M. C. W., et al. (2019). Impact of preservation method and 16S rRNA hypervariable region on gut microbiota profiling. *mSystems* 4 (1), e00271–18. doi: 10.1128/mSystems.00271-18

Chen, J., Liu, X., Liu, W., Yang, C., Jia, R., Ke, Y., et al. (2022). Comparison of the respiratory tract microbiome in hospitalized COVID-19 patients with different disease severity. *J. Med. Virol.* 94 (11), 5284–5293. doi: 10.1002/jmv.28002

Chi, Y., Ge, Y., Wu, B., Zhang, W., Wu, T., Wen, T., et al. (2020). Serum cytokine and chemokine profile in relation to the severity of coronavirus disease 2019 in China. *J. Infect. Dis.* 222 (5), 746–754. doi: 10.1093/infdis/jiaa363

de Castilhos, J., Zamir, E., Hippchen, T., Rohrbach, R., Schmidt, S., Hengler, S., et al. (2022). Severe dysbiosis and specific haemophilus and neisseria signatures as hallmarks of the oropharyngeal microbiome in critically ill coronavirus disease 2019 (COVID-19) patients. *Clin. Infect. Dis.* 75 (1), e1063–e1071. doi: 10.1093/cid/ciab902

Dessie, Z. G., and Zewotir, T. (2021). Mortality-related risk factors of COVID-19: a systematic review and meta-analysis of 42 studies and 423,117 patients. *BMC Infect. Dis.* 21 (1), 855. doi: 10.1186/s12879-021-06536-3

Dickson, R. P., Erb-Downward, J. R., , F. J., and Huffnagle Martinez, G. B.. (2016a). The microbiome and the respiratory tract. *Annu. Rev. Physiol.* 78, 481–504. doi: 10.1146/annurev-physiol-021115-105238

Dickson, R. P., Singer, B. H., Newstead, M. W., Falkowski, N. R., Erb-Downward, J. R., Standiford, T. J., et al. (2016b). Enrichment of the lung microbiome with gut bacteria in sepsis and the acute respiratory distress syndrome. *Nat. Microbiol.* 1 (10), 16113. doi: 10.1038/nmicrobiol.2016.113

Dickson, R. P., Martinez, F. J., and Huffnagle, G. B. (2014). The role of the microbiome in exacerbations of chronic lung diseases. *Lancet* 384 (9944), 691–702. doi: 10.1146/annurev-physiol-021115-105238

Esper, F. P., Adhikari, T. M., Tu, Z. J., Cheng, Y. W., El-Haddad, K., Farkas, D. H., et al. (2022). Alpha to omicron: disease severity and clinical outcomes of major SARS-CoV-2 variants. *J. Infect. Dis.* 227 (3), 344–352. doi: 10.1093/infdis/jiac411

Feehan, A. K., Rose, R., Nolan, D. J., Spitz, A. M., Graubics, K., Colwell, R. R., et al. (2021). Nasopharyngeal microbiome community composition and structure is associated with severity of COVID-19 disease and breathing treatment. *Appl. Microbiol.* 1 (2), 177–188. doi: 10.3390/applmicrobiol1020014

Gauthier, N. P. G., Locher, K., MacDonald, C., Chorlton, S. D., Charles, M., Manges, A. R., et al. (2022). Alterations in the nasopharyngeal microbiome associated with SARS-CoV-2 infection status and disease severity. *PloS One* 17 (10), e0275815. doi: 10.1371/journal.pone.0275815

Gloor, G. B., Macklaim, J. M., Pawlowsky-Glahn, V., and Egozcue, J. J.. (2017). Microbiome datasets are compositional: and this is not optional. *Front. Microbiol.* 8, 2224. doi: 10.3389/fmicb.2017.02224

Goldman, D. L., Chen, Z., Shankar, V., Tyberg, M., Vicencio, A., Burk, R., et al. (2018). Lower airway microbiota and mycobiota in children with severe asthma. *J. Allergy Clin. Immunol.* 141 (2), 808–811.e7. doi: 10.1016/j.jaci.2017.09.018

Gupta, V. K., Paul, S., and Dutta, C. (2017). Geography, ethnicity or subsistence-specific variations in human microbiome composition and diversity. *Front. Microbiol.* 8, 1162. doi: 10.3389/fmicb.2017.01162

Hadjadj, J., Yatim, N., Barnabei, L., Corneau, A., Boussier, J., Smith, N., et al. (2020). Impaired type I interferon activity and inflammatory responses in severe COVID-19 patients. *Science* 369 (6504), 718–724. doi: 10.1126/science.abc6027

Hernandez-Teran, A., Mejia-Nepomuceno, F., Herrera, M. T., Barreto, O., Garcia, E., Castillejos, M., et al. (2021). Dysbiosis and structural disruption of the respiratory microbiota in COVID-19 patients with severe and fatal outcomes. *Sci. Rep.* 11 (1), 21297. doi: 10.1038/s41598-021-00851-0

Hilty, M., Burke, C., Pedro, H., Cardenas, P., Bush, A., Bossley, C., et al. (2010). Disordered microbial communities in asthmatic airways. *PLoS One* 5 (1), e8578. doi: 10.1371/journal.pone.0008578

Huang, C., Wang, Y., Li, X., Ren, L., Zhao, J., Hu, Y., et al. (2020). Clinical features of patients infected with 2019 novel coronavirus in wuhan, China. *Lancet* 395 (10223), 497–506. doi: 10.1016/S0140-6736(20)30183-5

Huang, C., Feng, S., Huo, F., and Liu, H.. (2022). Effects of four antibiotics on the diversity of the intestinal microbiota. *Microbiol. Spectr.* 10 (2), e0190421. doi: 10.1128/spectrum.01904-21

Hurst, J. H., McCumber, A. W., Aquino, J. N., Rodriguez, J., Heston, S. M., Lugo, D.J., et al. (2022). Age-related changes in the nasopharyngeal microbiome are associated with severe acute respiratory syndrome coronavirus 2 (SARS-CoV-2) infection and symptoms among children, adolescents, and young adults. *Clin. Infect. Dis.* 75 (1), e928–e937. doi: 10.1093/cid/ciac184

Kelly, B. J., Imai, I., Bittinger, K., Laughlin, A., Fuchs, B. D., Bushman, F.D., et al. (2016). Composition and dynamics of the respiratory tract microbiome in intubated patients. *Microbiome* 4, 7. doi: 10.1186/s40168-016-0151-8

Kwon, Y., Cho, Y. S., Lee, Y. M., Kim, S. J., Bae, J., and Jeong, S. J.. (2022). Changes to gut microbiota following systemic antibiotic administration in infants. *Antibiotics (Basel)* 11 (4), 470. doi: 10.3390/antibiotics11040470

Langford, B. J., So, M., Raybardhan, S., Leung, V., Soucy, J. R., Westwood, D., et al. (2021). Antibiotic prescribing in patients with COVID-19: rapid review and meta-analysis. *Clin. Microbiol. Infect.* 27 (4), 520–531. doi: 10.1016/j.cmi.2020.12.018

Lekang, K., Shekhar, S., Berild, D., Petersen, F. C., and Winther-Larsen, H. C.. (2022). Effects of different amoxicillin treatment durations on microbiome diversity and composition in the gut. *PLoS One* 17 (10), e0275737. doi: 10.1371/journal.pone.0275737

Ling, L., Chen, Z., Lui, G., Wong, C. K., Wong, W. T., Ng, R. W. Y., et al. (2021). Longitudinal cytokine profile in patients with mild to critical COVID-19. *Front. Immunol.* 12, 763292. doi: 10.3389/fimmu.2021.763292

Llorens-Rico, V., Gregory, A. C., Weyenbergh Van, J., Jansen, S., Buyten Van, T., Qian, J., et al. (2021). Clinical practices underlie COVID-19 patient respiratory microbiome composition and its interactions with the host. *Nat. Commun.* 12 (1), 6243. doi: 10.1038/s41467-021-26500-8

Lui, G., Ling, L., Lai, C.K., Tso, E.Y., Fung, K.S., Chan, V., et al. (2020). Viral dynamics of SARS-CoV-2 across a spectrum of disease severity in COVID-19. *J. Infect.* 81 (2), 318–356. doi: 10.1016/j.jinf.2020.04.014

Ma, S., Zhang, F., Zhou, F., Li, H., Ge, W., Gan, R., et al. (2021). Metagenomic analysis reveals oropharyngeal microbiota alterations in patients with COVID-19. *Signal Transduct Target Ther.* 6 (1), 191. doi: 10.1038/s41392-021-00614-3

Merenstein, C., Bushman, F. D., and Collman, R. G. (2022). Alterations in the respiratory tract microbiome in COVID-19: current observations and potential significance. *Microbiome* 10 (1), 165. doi: 10.1186/s40168-022-01342-8

Merenstein, C., Liang, G., Whiteside, S. A., Cobián-Güemes, A. G., Merlino, M. S., Taylor, L. J., et al. (2021). Signatures of COVID-19 severity and immune response in the respiratory tract microbiome. *medRxiv*. 12 (4), e0177721 doi: 10.1128/mBio.01777-21

Miller, E. H., Annavajhala, M. K., Chong, A. M., Park, H., Nobel, Y. R., Soroush, A., et al. (2021). Oral microbiome alterations and SARS-CoV-2 saliva viral load in patients with COVID-19. *Microbiol. Spectr.* 9 (2), e0005521. doi: 10.1128/Spectrum.00055-21

Mostafa, H. H., Fissel, J. A., Fanelli, B., Bergman, Y., Gniazdowski, V., Dadlani, M., et al. (2020). Metagenomic next-generation sequencing of nasopharyngeal specimens collected from confirmed and suspect COVID-19 patients. *mBio* 11 (6), e01969–20. doi: 10.1128/mBio.01969-20

Ochoa-Ramirez, L. A., Ramos-Payan, R., Jimenez-Gastelum, G. R., Rodriguez-Millan, J., Aguilar-Medina, M., Rios-Tostado, J.J., et al. (2022). The chemokine MIG is associated with an increased risk of COVID-19 mortality in Mexican patients. *Iran J. Immunol.* 19 (3), 311–320. doi: 10.22034/iji.2022.92641.2162

Pairo-Castineira, E., Clohisey, S., Klaric, L., Bretherick, A. D., Rawlik, K., Pasko, D., et al. (2021). Genetic mechanisms of critical illness in COVID-19. *Nature* 591 (7848), 92–98. doi: 10.1038/s41586-020-03065-y

Ren, L., Wang, Y., Zhong, J., Li, X., Xiao, Y., Li, J., et al. (2021). Dynamics of the upper respiratory tract microbiota and its association with mortality in COVID-19. *Am. J. Respir. Crit. Care Med.* 204 (12), 1379–1390. doi: 10.1164/rccm.202103-0814OC

Rhoades, N. S., Pinski, A. N., Monsibais, A. N., Jankeel, A., Doratt, B. M., Cinco, I.R., et al. (2021). Acute SARS-CoV-2 infection is associated with an increased abundance of bacterial pathogens, including pseudomonas aeruginosa in the nose. *Cell Rep.* 36 (9), 109637. doi: 10.1016/j.celrep.2021.109637

Rueca, M., Fontana, A., Bartolini, B., Piselli, P., Mazzarelli, A., Copetti, M., et al. (2021). Investigation of Nasal/Oropharyngeal microbial community of COVID-19 patients by 16S rDNA sequencing. *Int. J. Environ. Res. Public Health* 18 (4), 2174. doi: 10.3390/ijerph18042174

Segata, N., Izard, J., Waldron, L., Gevers, D., Miropolsky, L., Garrett, W. S., et al. (2011). Metagenomic biomarker discovery and explanation. *Genome Biol.* 12 (6), R60. doi: 10.1186/gb-2011-12-6-r60

Shilts, M. H., Rosas-Salazar, C., Strickland, B. A., Kimura, K. S., Asad, M., Sehanobish, E., et al. (2021). Severe COVID-19 is associated with an altered upper respiratory tract microbiome. *Front. Cell Infect. Microbiol.* 11, 781968. doi: 10.3389/fcimb.2021.781968

Smith, N., Goncalves, P., Charbit, B., Grzelak, L., Beretta, M., Planchais, C., et al. (2021). Distinct systemic and mucosal immune responses during acute SARS-CoV-2 infection. *Nat. Immunol.* 22 (11), 1428–1439. doi: 10.1038/s41590-021-01028-7

Sorbara, M. T., and Pamer, E. G. (2022). Microbiome-based therapeutics. *Nat. Rev. Microbiol.* 20 (6), 365–380. doi: 10.1038/s41579-021-00667-9

Ventero, M. P., Cuadrat, R. R. C., Vidal, I., Andrade, B. G. N., Molina-Pardines, C., Haro-Moreno, J. M., et al. (2021). Nasopharyngeal microbial communities of patients infected with SARS-CoV-2 that developed COVID-19. *Front. Microbiol.* 12, 637430. doi: 10.3389/fmicb.2021.637430

Weiss, B., Bujanover, Y., Yahav, Y., Vilozni, D., Fireman, E., and Efrati, O.. (2010). Probiotic supplementation affects pulmonary exacerbations in patients with cystic fibrosis: a pilot study. *Pediatr. Pulmonol* 45 (6), 536–540. doi: 10.1002/ppul.21138

Wu, Y., Cheng, X., Jiang, G., Tang, H., Ming, S., Tang, L., et al. (2021). Altered oral and gut microbiota and its association with SARS-CoV-2 viral load in COVID-19 patients during hospitalization. *NPJ Biofilms Microbiomes* 7 (1), 61. doi: 10.1038/s41522-021-00232-5

Xu, Z. S., Shu, T., Kang, L., Wu, D., Zhou, X., Liao, B.W., et al. (2020). Temporal profiling of plasma cytokines, chemokines and growth factors from mild, severe and fatal COVID-19 patients. *Signal Transduct Target Ther.* 5 (1), 100. doi: 10.1038/s41392-020-0211-1

Xu, R., Lu, R., Zhang, T., Wu, Q., Cai, W., Han, X., et al. (2021). Temporal association between human upper respiratory and gut bacterial microbiomes during the course of COVID-19 in adults. *Commun. Biol.* 4 (1), 240. doi: 10.1038/s42003-021-01796-w

Zhao, Y., Qin, L., Zhang, P., Li, K., Liang, L., , J, et al. (2020). Longitudinal COVID-19 profiling associates IL-1RA and IL-10 with disease severity and RANTES with mild disease. *JCI Insight* 5 (13), e139834. doi: 10.1172/jci.insight.139834

Zheng, S., Fan, J., Yu, F., Feng, B., Lou, B., Zou, Q., et al. (2020). Viral load dynamics and disease severity in patients infected with SARS-CoV-2 in zhejiang province, China, January-march 2020: retrospective cohort study. *BMJ* 369, m1443. doi: 10.1136/bmj.m1443

frontiers | Frontiers in Cellular and Infection Microbiology

TYPE Original Research
PUBLISHED 21 July 2023
DOI 10.3389/fcimb.2023.1200157

OPEN ACCESS

EDITED BY
Jianmin Chai,
Foshan University, China

REVIEWED BY
Yafeng Qiu,
Chinese Academy of Agricultural Sciences, China
Wang Ke,
Guangxi Medical University, China

*CORRESPONDENCE
Min Zhou
2326150072@qq.com

RECEIVED 04 April 2023
ACCEPTED 26 June 2023
PUBLISHED 21 July 2023

CITATION
Yuan X, Xie L, Shi Z and Zhou M (2023) Application of mNGS in the study of pulmonary microbiome in pneumoconiosis complicated with pulmonary infection patients and exploration of potential biomarkers.
Front. Cell. Infect. Microbiol. 13:1200157.
doi: 10.3389/fcimb.2023.1200157

Application of mNGS in the study of pulmonary microbiome in pneumoconiosis complicated with pulmonary infection patients and exploration of potential biomarkers

Xingya Yuan[1], Linshen Xie[1], Zhenzhen Shi[2] and Min Zhou[1]*

[1]Department of Respiratory Medicine, West China Fourth Hospital, Sichuan University, Chengdu, Sichuan, China, [2]Dinfectome Inc., Nanjing, Jiangsu, China

Background: Pneumoconiosis patients have a high prevalence of pulmonary infections, which can complicate diagnosis and treatment. And there is no comprehensive study of the microbiome of patients with pneumoconiosis. The application of metagenomic next-generation sequencing (mNGS) fills the gap to some extent by analyzing the lung microbiota of pneumoconiosis population while achieving accurate diagnosis.

Methods: We retrospectively analyzed 44 patients with suspected pneumoconiosis complicated with pulmonary infection between Jan 2020 and Nov 2022. Bronchoalveolar lavage fluid (BALF) specimens from 44 patients were collected and tested using the mNGS technology.

Results: Among the lung microbiome of pneumoconiosis patients with complicated pulmonary infection (P group), the most frequently detected bacteria and fungi at the genus level were *Streptococcus* and *Aspergillus*, at the species level were *Streptococcus pneumoniae* and *Aspergillus flavus*, respectively, and the most frequently detected DNA virus was *Human gammaherpesvirus 4*. There was no significant difference in α diversity between the P group and the non-pneumoconiosis patients complicated with pulmonary infection group (Non-P group) in pulmonary flora, while $P< 0.01$ for β diversity analysis, and the differential species between the two groups were *Mycobacterium colombiense* and *Fusobacterium nucleatum*. In addition, we monitored a high distribution of *Malassezia* and *Pneumocystis* in the P group, while herpes virus was detected in the majority of samples.

Conclusions: Overall, we not only revealed a comprehensive lung microbiome profile of pneumoconiosis patients, but also compared the differences between their microbiome and that of non-pneumoconiosis complicated with pulmonary infection patients. This provides a good basis for a better understanding of the

relationship between pneumoconiosis and microorganisms, and for the search of potential biomarkers.

KEYWORDS

pneumoconiosis, microbiome, metagenomic next-generation sequencing, pulmonary infection, biomarker

1 Introduction

Pneumoconiosis is a group of lung diseases caused by the inhalation of inorganic mineral particles, usually because of certain occupations. Its main pathological features include chronic lung inflammation and progressive pulmonary fibrosis (Perret et al., 2017), which can lead to respiratory and/or cardiac failure and eventually death. Pneumoconiosis is prevalent worldwide, with more than 60,000 new cases reported worldwide in 2017 (Shi et al., 2020). With the development and optimization of the industry in recent years, the pneumoconiosis population has decreased from 23.33% before 1970 to 2.29% in 2020 (Liu et al., 2022). However, the mortality rate of pneumoconiosis is relatively high (GBD 2017 Disease and Injury Incidence and Prevalence Collaborators, 2018; GBD 2013 Mortality and Causes of Death Collaborators, 2015), which is a serious threat to global public health.

Patients with pneumoconiosis are susceptible to microbial invasion such as *Mycobacterium tuberculosis* (Jun et al., 2013), *nontuberculous mycobacteria* (*NTM*) (McGrath and Bardsley, 2009) and *Aspergillus*(Vangara et al., 2022), leading to pulmonary infection. And many patients with advanced pneumoconiosis die of respiratory failure due to pulmonary infections (Barnes et al., 2019; Qi et al., 2021). Traditional etiologic methods such as microscopy, smear, and culture have low sensitivity, subjectivity, and contamination, which can lead to missed or false detection and affect patient outcomes (Dahyot et al., 2017). It is very important for patients with pulmonary infections to identify the etiology and use accurate drugs, especially for patients with lung damage such as pneumoconiosis. Many studies have revealed that the abundance and composition of microbial communities vary in different body habitats, with strong links to health status and human disease (Dickson et al., 2020; Wu et al., 2020). However, current analysis of bacterial community diversity in pneumoconiosis mostly uses sputum culture and 16S rRNA, which are not sufficient for microbiome analysis, and in most cases, microorganisms cannot be identified to species level (Mingjing Chen et al., 2017; Zhimin Ma, 2020; Druzhinin et al., 2022).

Metagenomic next-generation sequencing (mNGS) has the advantages of broad coverage, unbiased and unpredictable, and can simultaneously identify bacteria, fungi and viruses in a single sample (Chiu and Miller, 2019; Chen et al., 2021; D'Humières et al., 2021). It has been widely used in clinical practice in recent years, playing an important role in assisting clinical diagnosis, guiding rational drug use, reducing patient burden, and improving patient clinical outcome (Qian et al., 2020). In addition, mNGS does not require culture and pathogen detection results are typically available within 24-48 hours and are less susceptible to antibiotics than culture (Miao et al., 2018). Early diagnosis of pneumoconiosis complicated with pulmonary infection patients is very important due to the poor prognosis (Barnes et al., 2019; Qi et al., 2021), while the use of mNGS technique has not been reported for these patients. This study retrospectively examines pulmonary microbiome (bacterial, fungal, viral) characteristics in pneumoconiosis patients with pulmonary infection (P group), compares the pulmonary microbiome to non-pneumoconiosis patients with pulmonary infection (Non-P group), analyzes differential microbiome, and explores potential diagnostic biomarkers of pneumoconiosis.

2 Methods

2.1 Study population

Patients with suspected pneumoconiosis complicated with pulmonary infection were recruited, the diagnostic criteria for pulmonary infection was shown in Figure 1 (Cao et al., 2018; Shi et al., 2019), and pneumoconiosis was diagnosed with pneumoconiosis by the Chinese diagnostic standard GBZ 70-2015 and the International Labor Organization's classification standard for pneumoconiosis (Honma et al., 2004), Recruitment was carried out at a single site in West China Fourth Hospital Sichuan University, Chengdu between Jan 2020-Nov 2022, Patients who were under 18 years of age, unable to obtain bronchoalveolar lavage fluid (BALF), and had incomplete information were excluded from our study. Besides, some of the collected samples have been tested by G test, GM test or culture before mNGS. Data were collected on the demographics, underlying diseases and clinical features of the patients enrolled and were listed in Table 1.

2.2 Specimen collection

BALF was obtained from 44 participants. The purpose of collecting BALF is to make an etiologic diagnosis of the patient's infection. Samples were collected from patients according to standard procedures (Levy et al., 2018). After local anesthesia of the patient's throat, the fiberoptic bronchoscope was introduced. The lung was lavaged with room temperature sterile saline several times through the fiberoptic bronchoscope, 20-60 mL each time. 10 mL of the sample was removed from the recovered solution, place 2

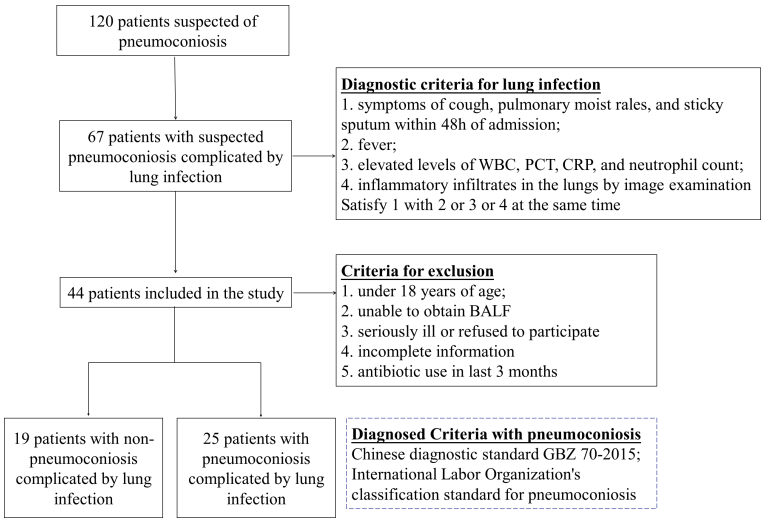

FIGURE 1
Inclusion and exclusion flowchart of study.

mL of it into a sampling tube with RNA protection solution (Sigma-Aldrich) and the rest into a sterile nucleic acid-free DNA sampling tube and store immediately at -80°C.

2.3 Sample DNA and RNA extraction

BALF DNA was extracted using methods previously described (Mac Aogáin et al., 2021; Ju et al., 2022), take 50 µL of proteinase k and 1 mL of BALF sample, digest at 60°C for 20 min, and then leave at 4°C for 5 min to lower the reaction temperature. Transfer the sample to a sterile test tube and centrifuge briefly followed by DNA extraction using the TIANamp Magnetic DNA Kit (DP710-t2, Tiangen, China) according to the manufacturer's protocol. Sputum was liquefied by 0.1% DTT (dithiothreitol) for 20 min at 56°C before extraction. The QIAamp Viral RNA Mini Kit (Qiagen) was used to extract RNA from the BALF (Langelier et al., 2018).

DNA libraries were prepared using the KAPA Hyper Prep Kit (KAPA Biosystems) according to the manufacturer's protocol. Libraries were constructed after Qubit quantification. For RNA extraction samples, rRNA was removed from total RNA and libraries were constructed after purification as described for DNA library construction. Agilent 2100 was used for quality control and then DNA libraries were sequenced on the Dif seq platform for 50 bp paired end sequencing (Dinfectome Medical Technology Inc, Nanjing, China).

2.4 Bioinformatics analysis

For pathogen identification, we used an in-house developed bioinformatics pipeline (Zeng et al., 2022). Briefly, low quality reads, adapter contamination, duplicated and shot (length <36 bp) reads were removed to generate high quality sequencing data. Sequences from the human host were identified by mapping to the human reference genome (hs37d5) using the bowtie2 software (Langmead and Salzberg, 2012). Reads that could not be mapped to the human genome were retained. They were aligned to the microorganism genome database for pathogen identification. Our microorganism genome database contained the genome sequences of bacteria, fungi, viruses, and parasites (can be downloaded from https://www.ncbi.nlm.nih.gov/) (Wood et al., 2019).

2.5 Interpretation and reporting

The mNGS pathogen detection pipeline was described in previous studies (Miao et al., 2018; Miller et al., 2019; Qian et al., 2020; Zeng et al., 2022; Chen et al., 2023; Xu et al., 2023), and the criteria for detection positivity were as follows: 1) at least one species-specific read for *Mycobacterium tuberculosis*, *Nocardia* and *Legionella pneumophila* detection; 2) for other bacteria, fungi, virus, and parasites, at least three unique reads were needed; 3) pathogens were excluded if the ratio of microorganism reads per million of a given sample versus NTC was < 10.

2.6 Statistics analysis

The statistical analysis was carried out using the R software (v4.2.1) (R Core Team, 2021). Alpha diversity was estimated by Shannon index and Simpson index based on the taxonomic profile of each sample. Beta diversity was assessed by Bray-Curtis measure. PERMANOVA was performed using the R package "vegan" to analyze the Bray-Curtis distance in different P and Non-P groups. In all cases, two-tailed analysis was performed and considered. Differences were regarded as significant at $P < 0.05$. Differential relative abundance of taxonomic groups at the genus/species level between groups was tested using the Kruskal-Wallis rank sum test (R package "kruskal.test") (Kruskal and Wallis, 1952). Statistical

TABLE 1 Patient and sample characteristics including biochemical parameters, underlying disease and clinical features.

	Pneumoconiosis (P) (n=25)	Non-Pneumoconiosis (Non-P) (n=19)
Age(years) (mean ± SD)	51.68 ± 11.51	62.2 ± 14.4
Gender		
Male	25	14
Female	0	5
Inflammatory index		
WBC($\times10^9$/L) (mean ± SD)	8.32 ± 2.41	8.85 ± 5.35
PCT(μg/L) (mean ± SD)	0.21 ± 0.09	0.19 ± 0.07
CRP (mg/L) (mean ± SD)	57.73 ± 78.00	71.86 ± 70.46
Neutrophils($\times10^9$/L) (mean ± SD)	6.51 ± 2.49	6.94 ± 5.34
Lymphatic cells($\times10^9$/L) (mean ± SD)	1.05 ± 0.59	1.18 ± 0.44
Working years (years) (mean ± SD)	10.76 ± 9.78	/
Underlying disease		
Tuberculosis/history of tuberculosis (n)	6	1
Hypertension (n)	5	2
Hepatitis B (n)	3	1
chronic cor pulmonale	3	0
type 2 diabetes (n)	2	2
chronic obstructive pulmonary disease (n)	2	1
Cancer (n)	0	2
Clinical characterization		
Fever (n)	6	7
Cough (n)	24	18
Expectoration (n)	23	14
Dyspnea (n)	5	1
Hemoptysis (n)	8	4

SD, standard deviation; Working years, Patient's years of pneumoconiosis-related work; WBC, White Blood Count; PCT, Procalcitonin; CRP, C-reactive protein; Neutrophils, Neutrophil count, Lymphatic cells, Lymphocyte count.

analyses and plots were processed by using SPSS statistical software (IBM SPSS Statistics for Windows, Version 25.0. Armonk, NY, United States) and GraphPad Prism software (GraphPad Prism version 8.0.2 for Windows, GraphPad Software, San Diego, CA, United States).

3 Results

3.1 General information of study participants

120 patients suspected of pulmonary infection and pneumoconiosis were screened, 44 eligible patients were included in the final analysis. Including 25 patients with pneumoconiosis and 19 patients with non-pneumoconiosis, 25 patients with pneumoconiosis and 19 patients with non-pneumoconiosis underwent bronchoscopy to obtain BALF. In terms of patient composition, all participants in the study were male and no female patients were enrolled in pneumoconiosis due to occupational characteristics. The main types of dusts causing pneumoconiosis according to clinical data were production dust (indoor work), mineral dust (coal mine, drilling related work), and the average number of years patients were exposed to such work was 10.76 years.

3.2 Characteristics of the pulmonary microbiome of pneumoconiosis patients

We plotted bar charts based on the frequency of species detection in pneumoconiosis patients, with the top 10 genera and top 20 species detected. In BALF samples, 521 bacterial species, 78 fungi species, and 17 viral species were detected in the

pneumoconiosis patient group. At the genus level, the top three bacteria detected were *Streptococcus* (96%), *Acinetobacter* (80%), and *Prevotella* (80%). *Aspergillus* (76.47%), *Candida* (35.29%), *Pneumocystis* (35.29%) for fungi. At the species level, the top 3 bacterial species detected were *Streptococcus pneumoniae* (72%, relative abundance 0.040%), *Stenotrophomonas maltophilia* (72%, relative abundance 0.036%) and *Rothia mucilaginosa* (60%, relative abundance 0.047%), based on frequency of detection and relative abundance of species detected. In terms of fungal detections, the top 3 were *Aspergillus flavus* (52. 94%), *Pneumocystis jirovecii* (35.29%), and *Schizophyllum commune* (35.29%). In addition, we revealed that herpes viruses were detected more frequently in pneumoconiosis patients, with *Human gamma herpesvirus type 4* detected in 61.54% of all patients, and *Human betaherpesvirus type 7* and *Human beta herpesvirus type 5* detection rates of 53.85% and 46.15%, respectively. Meanwhile, RNA viruses were found in two patients, *Human coronavirus NL63*, *Human respiratory virus 3* and *Rhinovirus A*, respectively. Specific detections can be found in Figure 2. Also, we counted the results of conventional microbiological testing of BALF samples. 22 BALF samples were cultured, G test and GM test simultaneously, and 15 samples were cultured only, however, all of these results were negative based on clinical judgment.

3.3 Microbiota analysis between P and Non-P groups

Analysis of microbiome differences in pneumoconiosis patients and non-pneumoconiosis patients will help understand the relationship between microbes and pneumoconiosis and identify biomarkers relevant to pneumoconiosis diagnosis.

Bar graphs were plotted based on the relative abundance of detected species, as shown in Figure 3, and the species with the highest relative abundance at the genus level in the P and Non-P groups were detected as *Streptococcus*. Among the top 10 genera in terms of relative abundance, the relative abundance of *Streptococcus*, *Prevotella*, *Mycobacterium* and *Rothia* in the P group was higher than that Non-P group, while all other genera had higher relative abundance in the Non-P group, the relative abundance of *Corynebacterium* was essentially equal between the two groups.

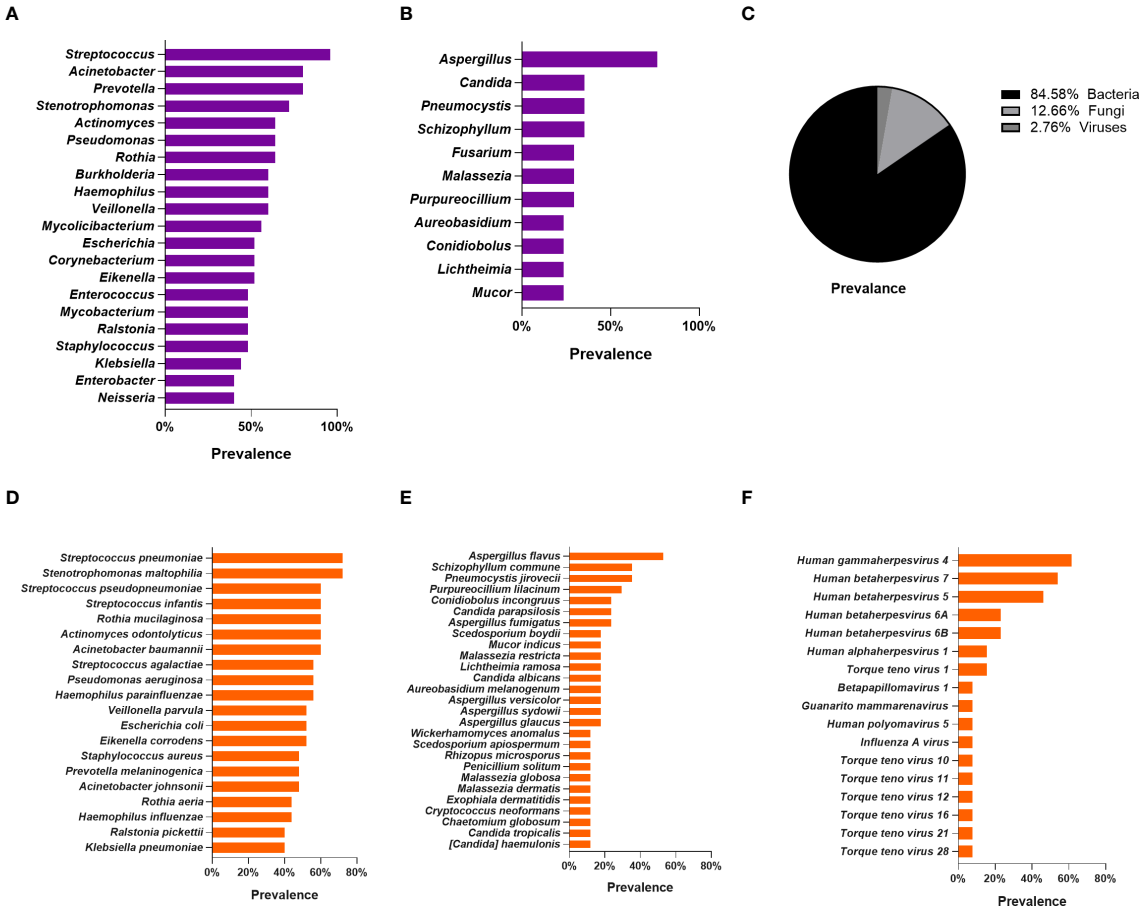

FIGURE 2
Lung microbiome of patients with pneumoconiosis complicated with pulmonary infection (BALF). **(A)** Distribution of bacteria at the genus level. **(B)** Distribution of fungi at the genus level. **(C)** Distribution pie chart of detected bacteria, fungi, and viruses at the species level. **(D)** Distribution of bacteria at the species level. **(E)** Distribution of fungi at the species level. **(F)** Distribution of Viruses at the species level.

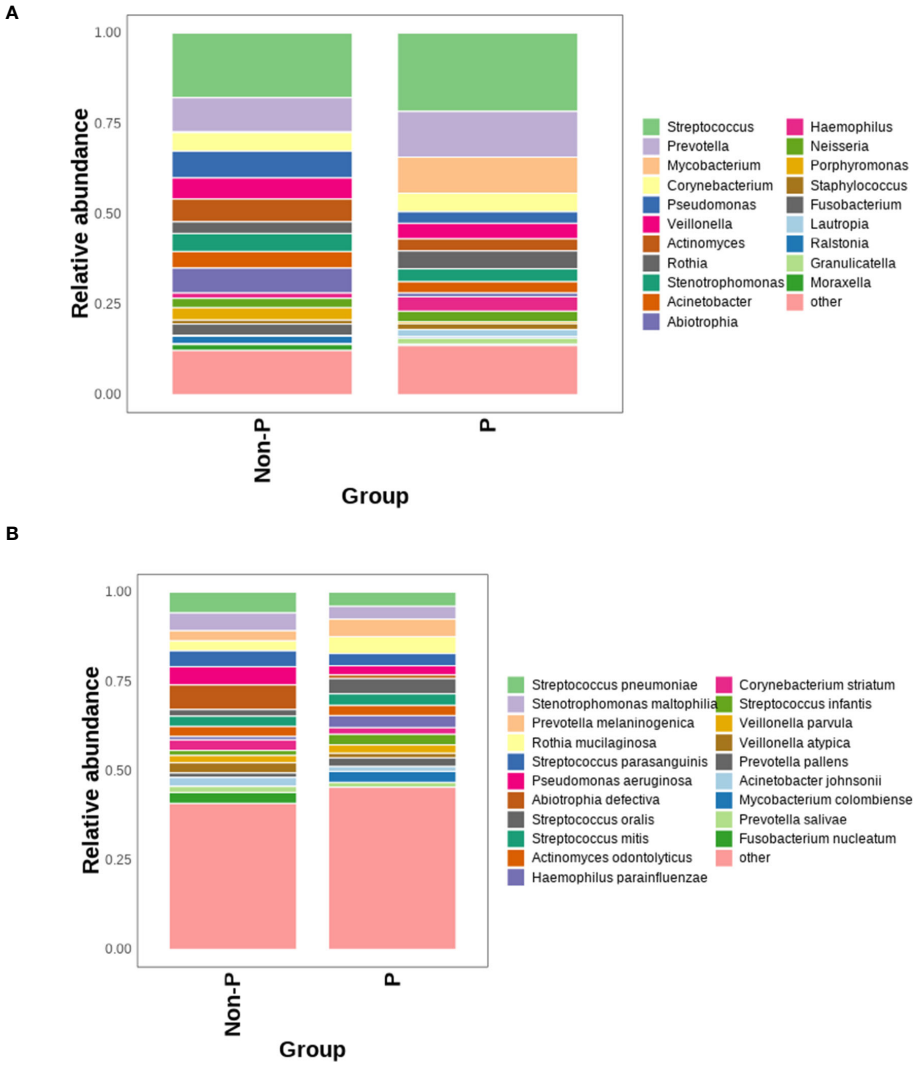

FIGURE 3
Comparison of the relative abundance of microorganisms between P and Non-P groups. **(A)** Distribution of bacteria at the genus level in the P and Non-P groups. **(B)** Distribution of bacteria at the species level in the P and Non-P groups.

At the species level, among the top 10 species by relative abundance, *Prevotella melaninogenica*, *Rothia mucilaginosa*, *Streptococcus oralis*, *Streptococcus mitis* were detected in higher relative abundance in the P group than Non-P group, while the remaining species had higher relative abundance in the Non-P group. Among them, *Pseudomonas aeruginosa* was usually associated with poor patient prognosis (Wang et al., 2019), while *Abiotrophia defectiva* was normal in the oral, genitourinary, and intestinal tracts, may cause sometimes serious infections in humans (Li J et al., 2022).

To analyze the differences in species diversity between the groups, α-diversity and β-diversity were used. The findings proved that there was no significant difference in ACE, Chao1, Shannon or Simpson between the two groups ($P > 0.05$, only the Shannon Diversity Index results were shown), indicating similar species variety. The difference in species between groups was analyzed with β diversity, and $P < 0.01$, suggesting that there was a remarkable difference in species between groups and the grouping was meaningful, as shown in Figure 4.

We tested species differences between P and Non-P groups at phylum, genus and species level. No conspicuous differences were found in the phylum and genus between the groups, However, the distribution of species differed dramatically. *Mycobacterium colombiense* (*M. colombiense*) and *Fusobacterium nucleatum* (*F. nucleatum*) were evidently different in their presence (Figure 5A), with the former being detected mainly in pneumoconiosis patients and the latter mainly in non-pneumoconiosis patients. The study also used LEfSe analysis to explore species that differed strikingly between groups (Figure 5B), with only three species differing between the two groups, including one at the genus level and two at the species level (i.e. the two different species mentioned above), the genus *Capnocytophaga* was enriched in the P group.

Sperman correlation analysis was performed to explore the correlation between clinical parameters such as patient's age, pneumoconiosis years, and inflammatory indicators at admission with significantly different species and the top 18 species in terms of relative abundance (for a total of 20 species, Figure 6). *Prevotella*,

10.3389/fcimb.2023.1200157

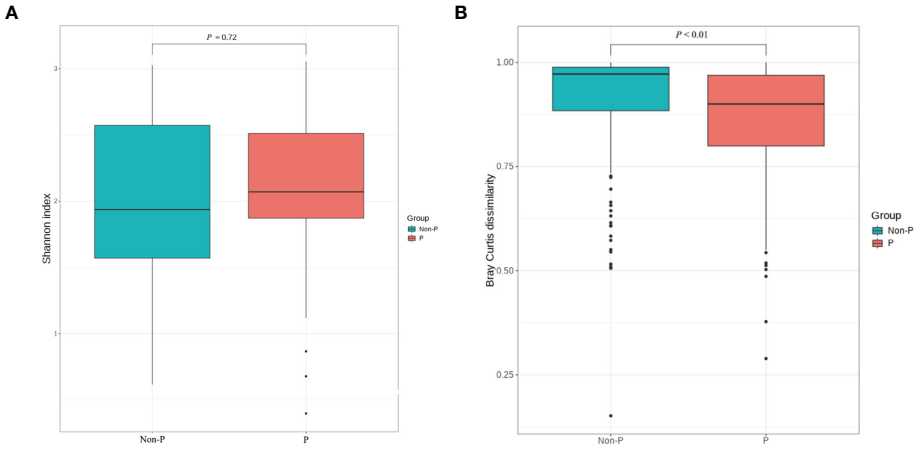

FIGURE 4
α and β diversity analysis between P and Non-P groups. **(A)** Shannon Index analysis. **(B)** Bray Curtis dissimilarity analysis.

Actinomyces and *Rothia* were common colonizing organisms in the mouth, *Prevotella melaninogenica*, *Prevotella pallens*, *Actinomyces odontolyticus*, *Rothia mucilaginosa* and other oral bacteria were distinctly and negatively correlated with patients' age, pneumoconiosis years and lymphocyte count, which may mean that the abundance of these microorganisms decreases as pneumoconiosis progresses. *M. colombiense* was positively correlated with years of work related to pneumoconiosis, suggesting that the likelihood of *M. colombiense* infection increased with the progression of pneumoconiosis, while we observed that the relative abundance of *Pseudomonas aeruginosa* was positively correlated with the length of hospitalization of pneumoconiosis patients, which seemed somewhat unusual and might be related to the small number of patients enrolled.

3.4 Comparison of fungi and virus detection in P and Non-P

The mNGS technology can identify and detect bacteria, fungi and viruses in the same sample, which is more conducive to a fully revealed microbiome signature. The top 20 genera/species were plotted in terms of relative abundance of species detected in the P group, as shown in the Figure 7. At the genus level, the top four genera detected were *Aspergillus*, *Candida*, *Malassezia* and *Pneumocystis*. Among them, more *Malassezia* and *Pneumocystis* were distributed in the P group, while *Aspergillus* and *Candida* were more dominant in the Non-P group. At the species level, among the top five detected species, *Aspergillus sydowii*, *Aspergillus versicolor*, *Candida albicans* were higher in the Non-P group than

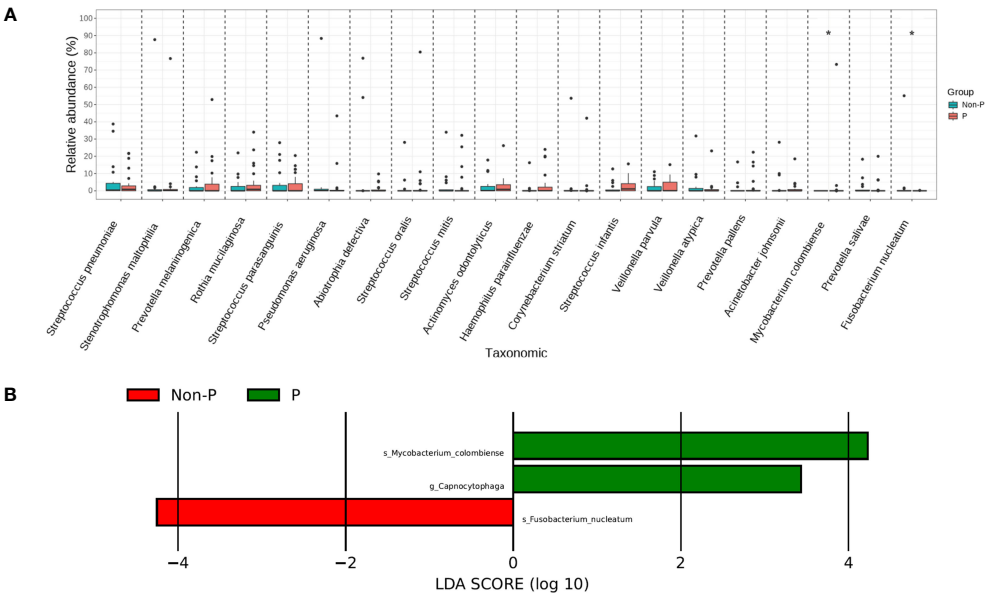

FIGURE 5
Species analysis of differences between P and Non-P groups. **(A)** Analysis of significant differences species. **(B)** LEfSe analysis.

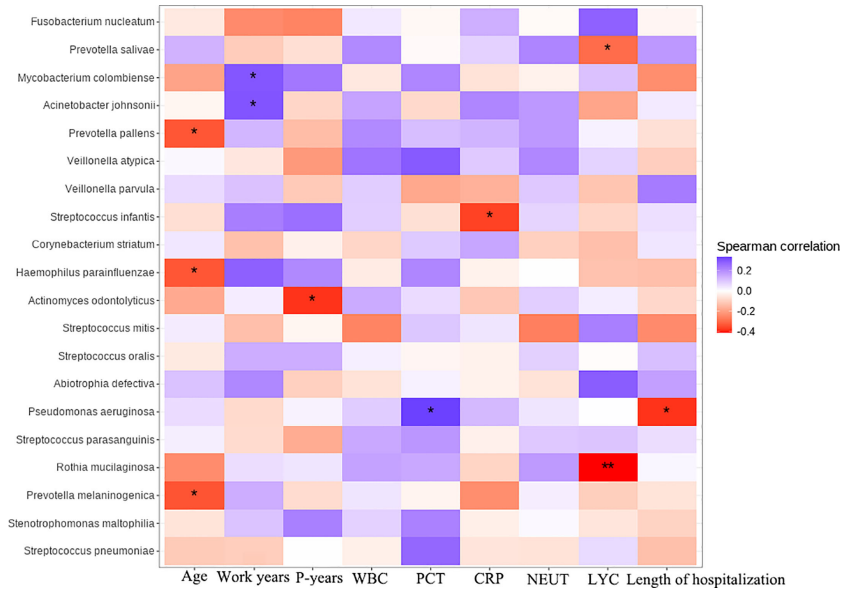

FIGURE 6
Clinical and microbial correlation analysis, Work years, Patient's years of pneumoconiosis-related work; P-years, Pneumoconiosis years; WBC, White Blood Count; PCT, Procalcitonin; CRP, C-reactive protein; NEUT, Neutrophil count; LYC, Lymphocyte count. The symbol * represent significance $p < 0.05$.

in the P group, while *Aureobasidium melanogenum*, *Clavispora lusitaniae* were higher in the P group. The viruses detected were displayed in Figure 7C below, with more viruses detected in the P group, while *Human gammaherpesvirus 4*, *Human betaherpesvirus 5*, *Influenza A virus* were mainly detected in the Non-P group. *Human gammaherpesvirus 4*, *Human betaherpesvirus 5*, *Human betaherpesvirus 7* and *Human betaherpesvirus 6A* were mainly detected in the P group. The *Human gammaherpesvirus* or *Human betaherpesvirus* mentioned above belong to the same family, *Herpesviridae*.

4 Discussion

In this study, mNGS technology was used to comprehensively reveal the pulmonary microbiome of pneumoconiosis patients, including the characteristics of bacteria, fungi and viruses, through BALF samples, and compare the differences in the lung microbiome between the P and Non-P groups so as to compare the microbial differences between the two groups for the exploration of potential biomarkers. To our knowledge, this current study is the first to investigate the lung microbiome of pneumoconiosis patients using a comprehensive and systematic mNGS technique and is also the first study to reveal differences in the lung microbiome of patients with pneumoconiosis versus non-pneumoconiosis.

Due to the chronic progressive disease of pneumoconiosis and the usual damage to the respiratory mucosa in pneumoconiosis patients, pneumoconiosis patients have a high probability of the lower respiratory tract (Xin and Zhang, 2017). Our study is the first to use mNGS to reveal the lung flora of pneumoconiosis complicated with pulmonary infection patients. In a previous study, Druzhinin et al. employed 16S to analyze the microbial composition of sputum samples from coal workers' pneumoconiosis (CWP) and observed a significant increase in the abundance of *Streptococcus* compared to the healthy group (Druzhinin et al., 2022). In addition, Li et al. analyzed the intestinal flora of pneumoconiosis patients and demonstrated a remarkable increase of *Prevotella* abundance in the pneumoconiosis group compared to the control group (Li Y et al., 2022). Similarly, we monitored higher abundance of *Streptococcus* and *Prevotella* in BALF samples from the P group compared to the Non-P group, however, the differences between both groups were non-significant, which we analyzed may be related to differences in sample type, as well as the fact that sputum specimens are susceptible to oral colonization flora compared to BALF samples.

Infections caused by fungi are gradually increasing in the clinic due to the irrational use of antibiotics and the increased use of hormonal drugs. Aspergillus is one of the main pathogens causing invasive fungal diseases, as well as chronic pulmonary aspergillosis, may worsen symptoms in advanced chronic obstructive pulmonary disease (COPD) (Hammond et al., 2020), and is associated with high mortality (Vandewoude et al., 2004). *Aspergillus fumigatus* is the most common agent of invasive aspergillosis and has been widely studied and reviewed (Dewi et al., 2021; Deng et al., 2023). However, *Aspergillus flavus* is the most frequently detected fungi in our studies of the pulmonary microbiome of pneumoconiosis patients, it can produce the most carcinogenic mycotoxin aflatoxins and cause aspergillosis in immune-compromised patients. Meanwhile, *in vivo* experimental studies have shown that the fungi is more toxic than *Aspergillus fumigatus* and other *Aspergillus* species in terms of time to death and initial inoculum in normal and immunocompromised experimental mice

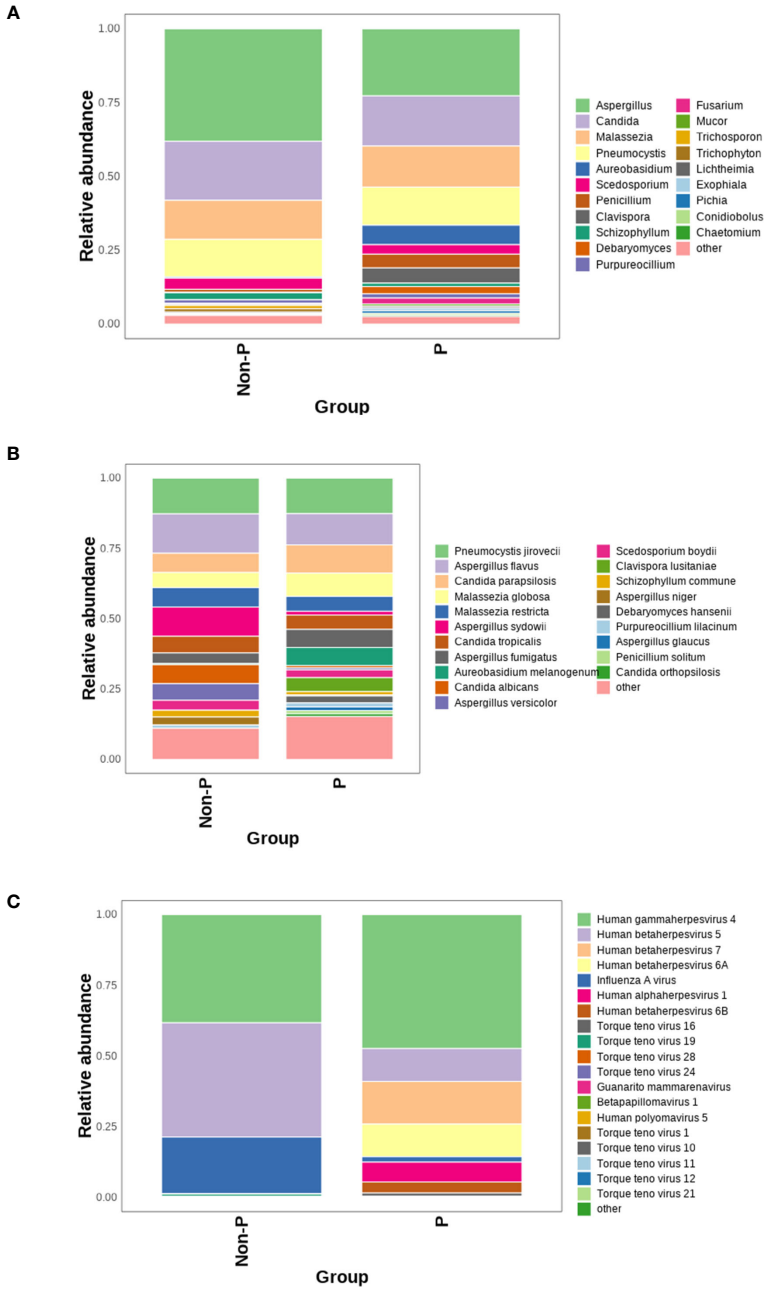

FIGURE 7
Analysis of viruses and fungi in P and Non-P groups. **(A)** Distribution of fungi at the genus level in the P and Non-P groups. **(B)** Distribution of fungi at the species level in the P and Non-P groups. **(C)**. Distribution of viruses at the genus level in the P and Non-P groups.

(Rudramurthy et al., 2019). The G test is widely used for invasive fungal infections (Lu et al., 2011; Li et al., 2015), while the GM test can further identify invasive aspergillosis for early diagnosis (Guo et al., 2010). In our study, some of the BALF samples were subjected to both G test and GM test, however, their negative results indicated the limitations of the traditional testing method to some extent, while the culture of BALF samples seemed to be unsatisfactory. Due to the specificity of the pneumoconiosis patient population, most of the patients have been on long-term antibiotic and antifungal medication prior to the relevant tests, which we speculate may be one of the reasons for the unsatisfactory results of the traditional tests, while some studies have reported that the detection rate of mNGS is relatively less affected by the use of antibiotics compared to the traditional testing modalities (Miao et al., 2018; Diao et al., 2021). Beyond this, a combination of guidelines and consensus, mNGS will be conducted when conventional tests fail to clarify the pathogen, which may be due to the high cost limitations of sequencing (Chinese Thoracic Society, 2023). We expect the reduced cost of mNGS technology in the future to make this tool more accessible, especially for low resource settings where the burden of infectious diseases is high and the availability of many pathogen-specific assays is low (Ramachandran et al., 2022).

The high detection rate of *Mycobacterium* in pneumoconiosis patients has been confirmed in large number of studies, including *Mycobacterium tuberculosis* and *NTM* (Kim et al., 2009). *M. colombiense* is mainly found in patients with pneumoconiosis and is an emerging species in the complex group of *Mycobacterium avium*, characterized by acid resistance, immobility, rod-shaped structure, and slow growth. It was first isolated and described by Murcia in 2006, and can be isolated in blood, sputum, and lymph nodes (Murcia et al., 2006; Tang et al., 2023). The bacterium is prone to cause severe pulmonary infection in immunodeficient or immunosuppressed patient (Yu and Jiang, 2021), disseminated diseases (Pena et al., 2019), ganglionar mycobacteriosis related diseases (Larry et al., 2019), and disseminated diseases associated with immunocompetent patients have also been reported (Esparcia et al., 2008; Tang et al., 2023). Cases of the bacterium have been reported in Europe, America, and Asia (Vuorenmaa et al., 2009; Poulin et al., 2013; Gao et al., 2014). However, there is a lack of attention to this bacterium, and it is often ignored in clinical diagnosis (Van Ingen et al., 2018). Our study identified for the first time that *M. colombiense* was substantially enriched in BALF samples of P group, which may be related to lung damage of these patients. The detection of this bacterium requires special attention as it could be a potential biomarker to distinguish pneumoconiosis from non-pneumoconiosis. However, this result has not been reported in previous studies of flora associated with pneumoconiosis (Druzhinin et al., 2022; Li Y. et al., 2022), which may be due to differences in sample types. Although our study inaugurally evaluates the lung microbiota of pneumoconiosis complicated with pulmonary infection patients and reveals a notable enrichment of *M. colombiense* in the P group, further validation with larger sample sizes still is needed at a later stage to characterize the lung microbiota of pneumoconiosis complicated with pulmonary infection patients.

More and more studies have found the relationship between viruses and human diseases. Viruses may cause serious respiratory diseases, tumors, and neuropsychiatric related diseases in humans (Gaglia and Munger, 2018; Bjornevik et al., 2022; Domingo and Rovira, 2020), where respiratory tract viral infection is one of the most common diseases in the human worldwide (Zhang et al., 2020). We found more virus species in pneumoconiosis patients in this study, suggesting that patients like this may be more susceptible to viral attack, and the viruses detected were mainly *Human gammaherpesvirus 4* and Human gammaherpesvirus-like viruses. Like other herpesviruses, the above viruses are double-stranded linear DNA viruses that exhibit a biphasic lifecycle, which are carried for life after infection, and overproduce when immunity is low or compromised, leading to human infection. Studies have shown that herpesviridae reactivation is associated with worse clinical outcomes, possibly as a direct cause or as a manifestation of the outcome of exacerbation of diseases (Huang and He, 2020). We only detailed the lung viruses in pneumoconiosis patients, and the relationship between viruses and the development, diagnosis and treatment of pneumoconiosis patients remains to be explored in more studies.

Overall, our study analyzed the differences in pulmonary microorganisms between pneumoconiosis with pulmonary infection and non-pneumoconiosis with pulmonary infection patients and screened for differential flora between the two groups, such as *M. colombiense*, *F. nucleatum* and the genus *Capnocytophaga*. These species could be used as potential biomarkers for the diagnosis of patients with pneumoconiosis with pulmonary infection. In addition, *M. colombiense* was also confirmed to be positively correlated with the number of years of work related to pneumoconiosis, tentatively suggesting a correlation between pneumoconiosis and microorganisms. This study contributes to the understanding of the relationship between microorganisms and pneumoconiosis and provides potential biomarkers for the diagnosis of pneumoconiosis with pulmonary infection, as well as basic data for the investigation of the pathogenesis of the disease.

This study still has some shortcomings. First, this is a single-center study and the patients enrolled only represent the lung microbiome of pneumoconiosis patients around that center. In addition, the number of patients in this cross-sectional study is relatively small due to the reduced number of pneumoconiosis patients and the fact that the patients are scattered in different hospitals, so more centers are needed to participate and enroll more patients to study the lung microbiome of pneumoconiosis in depth.

5 Conclusion

In this study, mNGS technology was used to fully expose the microbiome characteristics of the lungs of patients who had pneumoconiosis. Among the bacterial microbiota in the lungs of pneumoconiosis patients, *Streptococcus* were mainly detected, with *Streptococcus pneumoniae* as the main organism. Fungi were mainly detected in *Aspergillus* with *Aspergillus flavus* as the main organism, and the most frequently detected virus was *Human gammaherpesvirus 4*. The P and Non-P groups had different species at the species level, namely *M. colombiense* and *F. nucleatum*, with the former mainly detected in pneumoconiosis patients and the latter mainly in non-pneumoconiosis patients. As a result, we uncovered microbiome characteristics and differences between pneumoconiosis and non-pneumoconiosis with pulmonary infection patients, which provides a good basis for better understanding the relationship between pneumoconiosis and microorganisms, as well as discovering potential biomarkers.

Data availability statement

The data presented in the study are deposited in the SRA (https://www.ncbi.nlm.nih.gov/sra/) repository, accession number PRJNA985087.

Ethics statement

The studies involving human participants were reviewed and approved by Ethics Committee of West China Fourth Hospital

Sichuan University. The patients/participants provided their written informed consent to participate in this study.

Author contributions

MZ and XY designed the study and drafted the manuscript. LX collected the patients' samples and clinical information. ZZS performed the mNGS sequencing and analyzed the data. All the authors read and approved the final manuscript.

Acknowledgments

We sincerely thank Dinfectome Inc., Nanjing, China for providing the help in mNGS sequencing and results interpretation.

Conflict of interest

ZZS was employed by the company Dinfectome Inc.

The remaining authors declare that the research was conducted in the absence of any commercial or financial relationships that could be construed as a potential conflict of interest.

Publisher's note

References

Barnes, H., Goh, N. S. L., Leong, T. L., and Hoy, R. (2019). Silica-associated lung disease: an old-world exposure in modern industries. *Respirology* 24 (12), 1165–1175. doi: 10.1111/resp.13695

Bjornevik, K., Cortese, M., Healy, B. C., Kuhle, J., Mina, M. J., Leng, Y., et al. (2022). Longitudinal analysis reveals high prevalence of Epstein-Barr virus associated with multiple sclerosis. *Science* 375 (6578), 296–301. doi: 10.1126/science.abj8222

Cao, B., Huang, Y., She, D. Y., Cheng, Q. J., Fan, H., Tian, X. L., et al. (2018). Diagnosis and treatment of community-acquired pneumonia in adults: 2016 clinical practice guidelines by the Chinese Thoracic Society, Chinese Medical Association. *Clin. Respir. J.* 12 (4), 1320–1360. doi: 10.1111/crj.12674

Chen, Z., Cheng, H., Cai, Z., Wei, Q., Li, J., Liang, J., et al. (2021). Identification of microbiome etiology associated with drug resistance in pleural empyema. *Front. Cell Infect. Microbiol.* 11. doi: 10.3389/fcimb.2021.637018

Chen, H., Liang, Y., Wang, R., Wu, Y., Zhang, X., Huang, H., et al. (2023). Metagenomic next-generation sequencing for the diagnosis of Pneumocystis jirovecii Pneumonia in critically pediatric patients. *Ann. Clin. Microbiol. Antimicrob.* 22 (1), 6. doi: 10.1186/s12941-023-00555-5

Chinese Thoracic Society (2023). [Consensus of clinical pathways of metagenomic next-generation sequencing test in diagnosis of lower respiratory tract infections in China]. *Zhonghua Jie He He Hu Xi Za Zhi* 46 (4), 322–323. doi: 10.3760/cma.j.cn112147-20220701-00553

Chiu, C. Y., and Miller, S. A. J. N. R. G. (2019). Clinical metagenomics. *Nat. Rev. Genet.* 20 (6), 341–355. doi: 10.1038/s41576-019-0113-7

Dahyot, S., Lemee, L., and Pestel-Caron, M. (2017). Description and role of bacteriological techniques in the management of lung infections. *Rev. Mal Respir.* 34 (10), 1098–1113. doi: 10.1016/j.rmr.2016.07.007

Deng, W., Jiang, Y., Qin, J., Chen, G., Lv, Y., Lei, Y., et al. (2023). Metagenomic next-generation sequencing assists in the diagnosis of mediastinal aspergillus fumigatus abscess in an immunocompetent patient: a case report and literature review. *Infect. Drug Resist.* 16, 1865–1874. doi: 10.2147/IDR.S399484

Dewi, I. M., Janssen, N. A., Rosati, D., Bruno, M., Netea, M. G., Brüggemann, R. J., et al. (2021). Invasive pulmonary aspergillosis associated with viral pneumonitis. *Curr. Opin. Microbiol.* 62, 21–27. doi: 10.1016/j.mib.2021.04.006

D'Humières, C., Salmona, M., Dellière, S., Leo, S., Rodriguez, C., Angebault, C., et al. (2021). The potential role of clinical metagenomics in infectious diseases: therapeutic perspectives. *Drugs* 81 (13), 1453–1466. doi: 10.1007/s40265-021-01572-4

Diao, Z., Han, D., Zhang, R., and Li, J. (2021). Metagenomics next-generation sequencing tests take the stage in the diagnosis of lower respiratory tract infections. *J. Adv. Res.* 38, 201–212. doi: 10.1016/j.jare.2021.09.012

Dickson, R. P., Schultz, M. J., van der Poll, T., Schouten, L. R., Falkowski, N. R., Luth, J. E., et al. (2020). Lung microbiota predict clinical outcomes in critically ill patients. *Am. J. Respir. Crit. Care Med.* 201 (5), 555–563. doi: 10.1164/rccm.201907-1487OC

Domingo, J. L., and Rovira, J. (2020). Effects of air pollutants on the transmission and severity of respiratory viral infections. *Environ. Res.* 187, 109650. doi: 10.1016/j.envres.2020.109650

Druzhinin, V. G., Baranova, E. D., Matskova, L. V., Demenkov, P. S., Volobaev, V. P., Larionov, A. V., et al. (2022). Sputum microbiota in coal workers diagnosed with pneumoconiosis as revealed by 16S rRNA gene sequencing. *Life* 12 (6), 830. doi: 10.3390/life12060830

Esparcia, O., Navarro, F., Quer, M., and Coll, P. (2008). Lymphadenopathy caused by Mycobacterium colombiense. *J. Clin. Microbiol.* 46 (5), 1885–1887. doi: 10.1128/JCM.01441-07

Gaglia, M. M., and Munger, K. (2018). More than just oncogenes: mechanisms of tumorigenesis by human viruses. *Curr. Opin. Virol.* 32, 48–59. doi: 10.1016/j.coviro.2018.09.003

Gao, W., Chen, H., Jiang, H., Wang, Q., Tang, M., and Wang, H. S. (2014). Disseminated cutaneous infection caused by Mycobacterium colombiense. *Acta Derm. Venereol.* 94 (6), 727–728. doi: 10.2340/00015555-1828

GBD 2017 Disease and Injury Incidence and Prevalence Collaborators. (2018). Global, regional, and national incidence, prevalence, and years lived with disability for 354 diseases and injuries for 195 countries and territories, 1990–2017: a systematic analysis for the Global Burden of Disease Study 2017. *Lancet* (London, England), 392 (10159), 1789–1858. doi: 10.1016/S0140-6736(18)32279-7

GBD 2013 Mortality and Causes of Death Collaborators. (2015). Global, regional, and national age-sex specific all-cause and cause-specific mortality for 240 causes of death, 1990–2013: a systematic analysis for the Global Burden of Disease Study 2013. *Lancet* 385 (9963), 117–117. doi: 10.1016/S0140-6736(14)61682-2

GraphPad Software Inc. (2019). *GraphPad prism version 8.0.2 for windows* (San Diego, CA: GraphPad Software Inc).

Guo, Y. L., Chen, Y. Q., Wang, K., Qin, S. M., Wu, C., and Kong, J. L. (2010). Accuracy of BAL galactomannan in diagnosing invasive aspergillosis: a bivariate metaanalysis and systematic review. *Chest* 138 (4), 817–824. doi: 10.1378/chest.10-0488

Hammond, E. E., McDonald, C. S., Vestbo, J., and Denning, D. W. (2020). The global impact of Aspergillus infection on COPD. *BMC Pulm. Med.* 20 (1), 241. doi: 10.1186/s12890-020-01259-8

Honma, K., Abraham, J. L., Chiyotani, K., De Vuyst, P., Dumortier, P., Gibbs, A. R., et al. (2004). Proposed criteria for mixed-dust pneumoconiosis: definition, descriptions, and guidelines for pathologic diagnosis and clinical correlation. *Hum. Pathol.* 35 (12), 1515–1523. doi: 10.1016/j.humpath.2004.09.008

Huang, H., and He, H. (2020). Herpesviridae reactivation for poor outcome in ARDS patients with ECMO: criminal or witness? *Ann. Intensive Care* 10 (1), 10. doi: 10.1186/s13613-020-0626-4

IBM Corp. (2017). *IBM SPSS Statistics for windows, version 25.0* (Armonk, NY: IBM Corp).

Ju, C. R., Lian, Q. Y., Guan, W. J., Chen, A., Zhang, J. H., Xu, X., et al. (2022). Metagenomic next-generation sequencing for diagnosing infections in lung transplant recipients: a retrospective study. *Transpl. Int.* 35. doi: 10.3389/ti.2022.10265

Jun, J. S., Jung, J. I., Kim, H. R., Ahn, M. I., Han, D. H., Ko, J. M., et al. (2013). Complications of pneumoconiosis: radiologic overview. *Eur. J. Radiol.* 82 (10), 1819–1830. doi: 10.1016/j.ejrad.2013.05.026

Kim, Y. M., Kim, M., Kim, S. K., Park, K., Jin, S. H., Lee, U. S., et al. (2009). Mycobacterial infections in coal workers' pneumoconiosis patients in South Korea. *Scand. J. Infect. Dis.* 41 (9), 656–662. doi: 10.1080/00365540903089468

Kruskal, W. H., and Wallis, W. A. (1952). Use of ranks in one-criterion variance analysis. *J. Am. Stat. Assoc.* 47 (260), 583–621. doi: 10.1080/01621459.1952.10483441

Langelier, C., Kalantar, K. L., Moazed, F., Wilson, M. R., Crawford, E. D., Deiss, T., et al. (2018). Integrating host response and unbiased microbe detection for lower

respiratory tract infection diagnosis in critically ill adults. *Proc. Natl. Acad. Sci. USA* 115 (52), E12353–E12362. doi: 10.1073/pnas.1809700115

Langmead, B., and Salzberg, S. L. (2012). Fast gapped-read alignment with Bowtie 2. *Nat. Methods* 9 (4), 357–359. doi: 10.1038/nmeth.1923

Larry, M. R., Daniel, M. R., and Santiago, O. N. (2019). Ganglionar Mycobacteriosis associated to Mycobacterium colombiense in a Seropositive HIV Patient. Case report a literature review. *J. AIDS & Clinical Research*. 10 (4). 1000792.

Levy, L., Juvet, S. C., Boonstra, K., Singer, L. G., Azad, S., Joe, B., et al. (2018). Sequential broncho-alveolar lavages reflect distinct pulmonary compartments: clinical and research implications in lung transplantation. *Respir. Res.* 19 (1), 102. doi: 10.1186/s12931-018-0786-z

Li, W. J., Guo, Y. L., Liu, T. J., Wang, K., and Kong, J. L. (2015). Diagnosis of pneumocystis pneumonia using serum (1-3)-β-D-Glucan: a bivariate meta-analysis and systematic review. *J. Thorac. Dis.* 7 (12), 2214–2225. doi: 10.3978/j.issn.2072-1439.2015.12.27

Li, Y., Xiao, K., Xiao, S., Wang, M., Pei, S., Liu, H., et al. (2022). Difference in intestinal flora and characteristics of plasma metabonomics in pneumoconiosis patients. *Metabolites* 12 (10), 917. doi: 10.3390/metabo12100917

Li, J., Zhou, L., Gong, X., Wang, Y., Yao, D., and Li, H. (2022). Abiotrophia defectiva as a rare cause of mitral valve infective endocarditis with mesenteric arterial branch pseudoaneurysm, splenic infarction, and renal infarction: a case report. *Front. Med. (Lausanne)* 9. doi: 10.3389/fmed.2022.780828

Liu, W., Liang, R., Zhang, R., Wang, B., Cao, S., Wang, X., et al. (2022). Prevalence of coal worker's pneumoconiosis: a systematic review and meta-analysis. *Environ. Sci. pollut. Res. Int.* 29 (59), 88690–88698. doi: 10.1007/s11356-022-21966-5

Lu, Y., Chen, Y. Q., Guo, Y. L., Qin, S. M., Wu, C., and Wang, K. (2011). Diagnosis of invasive fungal disease using serum (1→3)-β-D-glucan: a bivariate meta-analysis. *Intern. Med.* 50 (22), 2783–2791. doi: 10.2169/internalmedicine.50.6175

Mac Aogáin, M., Narayana, J. K., Tiew, P. Y., Ali, N. A. B. M., Yong, V. F. L., Jaggi, T. K., et al. (2021). Integrative microbiomics in bronchiectasis exacerbations. *Nat. Med.* 27 (4), 688–699. doi: 10.1038/s41591-021-01289-7

McGrath, E. E., and Bardsley, P. (2009). An association between Mycobacterium malmoense and coal workers' pneumoconiosis. *Lung* 187 (1), 51–54. doi: 10.1007/s00408-008-9104-8

Miao, Q., Ma, Y., Wang, Q., Pan, J., Zhang, Y., Jin, W., et al. (2018). Microbiological diagnostic performance of metagenomic next-generation sequencing when applied to clinical practice. *Clin. Infect. Dis.* 67 (suppl_2), S231–S240. doi: 10.1093/cid/ciy693

Miller, S., Naccache, S. N., Samayoa, E., Messacar, K., Arevalo, S., Federman, S., et al. (2019). Laboratory validation of a clinical metagenomic sequencing assay for pathogen detection in cerebrospinal fluid. *Genome Res.* 29 (5), 831–842. doi: 10.1101/gr.238170.118

Mingjing Chen, T. L., Li, S., Zuo, H., and Pei, X. (2017). Drug resistance of pathogens and epidemiological analysis on 348 cases of silicosis with pulmonary infections. *Modern Prev. Med.* 44 (13), 5.

Murcia, M. I., Tortoli, E., Menendez, M. C., Palenque, E., and Garcia, M. J. (2006). Mycobacterium colombiense sp. nov., a novel member of the Mycobacterium avium complex and description of MAC-X as a new ITS genetic variant. *Int. J. Syst. Evol. Microbiol.* 56 (Pt 9), 2049–2054. doi: 10.1099/ijs.0.64190-0

Pena, E., Machado, D., Viveiros, M., and Jordão, S. (2019). A case report of disseminated Mycobacterium colombiense infection in an HIV patient. *Int. J. Mycobacteriol.* 8 (3), 295–297. doi: 10.4103/ijmy.ijmy_100_19

Perret, J. L., Plush, B., Lachapelle, P., Hinks, T. S., Walter, C., Clarke, P., et al. (2017). Coal mine dust lung disease in the modern era. *Respirology* (Carlton, Vic.) 22 (4), 662–670. doi: 10.1111/resp.13034

Poulin, S., Corbeil, C., Nguyen, M., St-Denis, A., Côté, L., Le Deist, F., et al. (2013). Fatal Mycobacterium colombiense/cytomegalovirus coinfection associated with acquired immunodeficiency due to autoantibodies against interferon gamma: a case report. *BMC Infect. Dis.* 13, 24. doi: 10.1186/1471-2334-13-24

Qi, X. M., Luo, Y., Song, M. Y., Liu, Y., Shu, T., Liu, Y., et al. (2021). Pneumoconiosis: current status and future prospects. *Chin. Med. J. (Engl.)* 134 (8), 898–907. doi: 10.1097/CM9.0000000000001461

Qian, L., Shi, Y., Li, F., Wang, Y., Ma, M., Zhang, Y., et al. (2020). Metagenomic next-generation sequencing of cerebrospinal fluid for the diagnosis of external ventricular and lumbar drainage-associated ventriculitis and meningitis. *Front. Microbiol.* 11. doi: 10.3389/fmicb.2020.596175

Ramachandran, P. S., Ramesh, A., Creswell, F. V., Wapniarski, A., Narendra, R., Quinn, C. M., et al. (2022). Integrating central nervous system metagenomics and host response for diagnosis of tuberculosis meningitis and its mimics. *Nat. Commun.* 13 (1), 1675. doi: 10.1038/s41467-022-29353-x

R Core Team (2021). *R: a language and environment for statistical computing* (Vienna, Austria: R Foundation for Statistical Computing).

Rudramurthy, S. M., Paul, R. A., Chakrabarti, A., Mouton, J. W., and Meis, J. F. (2019). Invasive aspergillosis by aspergillus flavus: epidemiology, diagnosis, antifungal resistance, and management. *J. Fungi (Basel)* 5 (3), 55. doi: 10.3390/jof5030055

Shi, Y., Huang, Y., Zhang, T. T., Cao, B., Wang, H., Zhuo, C., et al. (2019). Chinese Guidelines for the diagnosis and treatment of hospital-acquired pneumonia and ventilator-associated pneumonia in adults, (2018 Edition). *J. Thorac. Dis.* 11 (6), 2581–2616. doi: 10.21037/jtd.2019.06.09

Shi, P., Xing, X., Xi, S., Jing, H., Yuan, J., Fu, Z., et al. (2020). Trends in global, regional and national incidence of pneumoconiosis caused by different aetiologies: an analysis from the Global Burden of Disease Study 2017. *Occup. Environ. Med.* 77 (6), 407–414. doi: 10.1136/oemed-2019-106321

Tang, M., Zeng, W., Qiu, Y., Fang, G., Pan, M., Li, W., et al. (2023). Clinical features of rare disseminated mycobacterium colombiense infection in nine patients who are HIV-negative in Guangxi, China. *Int. J. Infect. Dis.* 128, 321–324. doi: 10.1016/j.ijid.2023.01.002

Vandewoude, K., Blot, S., Benoit, D., Depuydt, P., Vogelaers, D., and Colardyn, F. (2004). Invasive aspergillosis in critically ill patients: analysis of risk factors for acquisition and mortality. *Acta Clin. Belg.* 59 (5), 251–257. doi: 10.1179/acb.2004.037

Vangara, A., Gudipati, M., Chan, R., Do, T. V., Bawa, O., and Shyam Ganti, S.. (2022). Chronic pulmonary aspergillosis infection in coal workers pneumoconiosis with progressive massive fibrosis. *J. Investig. Med. High Impact Case Rep.* 10, 23247096221127100. doi: 10.1177/23247096221127100

Van Ingen, J., Turenne, C. Y., Tortoli, E., Wallace, R. J.Jr, and Brown-Elliott, B. A. (2018). A definition of the Mycobacterium avium complex for taxonomical and clinical purposes, a review. *Int. J. Syst. Evol. Microbiol.* 68 (11), 3666–3677. doi: 10.1099/ijsem.0.003026

Vuorenmaa, K., Ben Salah, I., Barlogis, V., Chambost, H., and Drancourt, M. (2009). Mycobacterium colombiense and pseudotuberculous lymphadenopathy. *Emerg. Infect. Dis.* 15 (4), 619–620. doi: 10.3201/eid1504.081436

Wang, T., Hou, Y., and Wang, R. (2019). A case report of community-acquired pseudomonas aeruginosa pneumonia complicated with MODS in a previously healthy patient and related literature review. *BMC Infect. Dis.* 19 (1), 1–6. doi: 10.1186/s12879-019-3765-1

Wood, D. E., Lu, J., and Langmead, B. (2019). Improved metagenomic analysis with Kraken 2. *Genome Biol.* 20 (1), 257. doi: 10.1186/s13059-019-1891-0

Wu, L., Zeng, T., Deligios, M., Milanesi, L., Langille, M. G. I., Zinellu, A., et al. (2020). Age-related variation of bacterial and fungal communities in different body habitats across the young, elderly, and centenarians in Sardinia. *Msphere* 5 (1), e00558–19. doi: 10.1128/mSphere.00558-19

Xin, Y., and Zhang, N. (2017). [The analysis of pathogens distribution and drug resistance of bacteria in sputum samples of pneumoconiosis patients combined with lower respiratory tract infection.]. *Zhonghua Lao Dong Wei Sheng Zhi Ye Bing Za Zhi* 35 (1), 58–61. doi: 10.3760/cma.j.issn.1001-9391.2017.01.015

Xu, J., Zhou, P., Liu, J., Zhao, L., Fu, H., Han, Q., et al. (2023). Utilizing metagenomic next-generation sequencing (mNGS) for rapid pathogen identification and to inform clinical decision-making: results from a Large real-world cohort. *Infect. Dis. Ther.* 12 (4), 1175–1187. doi: 10.1007/s40121-023-00790-5

Yu, X., and Jiang, W. (2021). Mycobacterium colombiense and Mycobacterium avium complex causing severe pneumonia in a patient with HIV identified by a novel molecular-based method. *Infect. Drug Resist.* 14, 11–16. doi: 10.2147/IDR.S282190

Zeng, X., Wu, J., Li, X., Xiong, W., Tang, L., Li, X., et al. (2022). Application of metagenomic next-generation sequencing in the etiological diagnosis of infective endocarditis during the perioperative period of cardiac surgery: a prospective cohort study. *Front. Cardiovasc. Med.* 9. doi: 10.3389/fcvm.2022.811492

Zhang, N., Wang, L., Deng, X., Liang, R., Su, M., He, C., et al. (2020). Recent advances in the detection of respiratory virus infection in humans. *J. Med. Virol.* 92 (4), 408–417. doi: 10.1002/jmv.25674

Zhimin Ma, W. B. (2020). Distribution of pathogens and their drug resistance in occupational pneumoconiosis with pulmonary infections. *Med. Diet Health* 18 (7), 2.

frontiers | Frontiers in Cellular and Infection Microbiology

TYPE Original Research
PUBLISHED 08 September 2023
DOI 10.3389/fcimb.2023.1223090

OPEN ACCESS

EDITED BY
Veeranoot Nissapatorn,
Walailak University, Thailand

REVIEWED BY
Igori Balta,
University Of Life Sciences "King Mihai I", Romania
Gisli G. Einarsson,
Queen's University Belfast, United Kingdom

*CORRESPONDENCE
Jiangchao Zhao
jzhao77@uark.edu

RECEIVED 15 May 2023
ACCEPTED 23 August 2023
PUBLISHED 08 September 2023

CITATION
Howe S, Kegley B, Powell J, Chen S and Zhao J (2023) Effect of bovine respiratory disease on the respiratory microbiome: a meta-analysis. *Front. Cell. Infect. Microbiol.* 13:1223090. doi: 10.3389/fcimb.2023.1223090

Effect of bovine respiratory disease on the respiratory microbiome: a meta-analysis

Samantha Howe[1], Beth Kegley[1], Jeremy Powell[1], Shicheng Chen[2] and Jiangchao Zhao[1]*

[1]Department of Animal Science, Division of Agriculture, University of Arkansas, Fayetteville, AR, United States, [2]Medical Laboratory Sciences Program, College of Health and Human Sciences, Northern Illinois University, DeKalb, IL, United States

Background: Bovine respiratory disease (BRD) is the most devastating disease affecting beef and dairy cattle producers in North America. An emerging area of interest is the respiratory microbiome's relationship with BRD. However, results regarding the effect of BRD on respiratory microbiome diversity are conflicting.

Results: To examine the effect of BRD on the alpha diversity of the respiratory microbiome, a meta-analysis analyzing the relationship between the standardized mean difference (SMD) of three alpha diversity metrics (Shannon's Diversity Index (Shannon), Chao1, and Observed features (OTUs, ASVs, species, and reads) and BRD was conducted. Our multi-level model found no difference in Chao1 and Observed features SMDs between calves with BRD and controls. The Shannon SMD was significantly greater in controls compared to that in calves with BRD. Furthermore, we re-analyzed 16S amplicon sequencing data from four previously published datasets to investigate BRD's effect on individual taxa abundances. Additionally, based on Bray Curtis and Jaccard distances, health status, sampling location, and dataset were all significant sources of variation. Using a consensus approach based on RandomForest, DESeq2, and ANCOM-BC2, we identified three differentially abundant amplicon sequence variants (ASVs) within the nasal cavity, ASV5_*Mycoplasma*, ASV19_*Corynebacterium*, and ASV37_*Ruminococcaceae*. However, no ASVs were differentially abundant in the other sampling locations. Moreover, based on SECOM analysis, ASV37_*Ruminococcaceae* had a negative relationship with ASV1_*Mycoplasma_hyorhinis*, ASV5_*Mycoplasma*, and ASV4_*Mannheimia*. ASV19_*Corynebacterium* had negative relationships with ASV1_*Mycoplasma_hyorhinis*, ASV4_*Mannheimia*, ASV54_*Mycoplasma*, ASV7_*Mycoplasma*, and ASV8_*Pasteurella*.

Conclusions: Our results confirm a relationship between bovine respiratory disease and respiratory microbiome diversity and composition, which provide additional insight into microbial community dynamics during BRD development. Furthermore, as sampling location and sample processing (dataset) can also affect results, consideration should be taken when comparing results across studies.

KEYWORDS

meta-analysis, respiratory microbiome, bovine respiratory disease, alpha diversity, differential abundance

1 Introduction

Bovine respiratory disease (BRD), also referred to as bovine bronchopneumonia, is the most devastating disease affecting North American cattle producers (Taylor et al., 2010). BRD is the leading cause of death in pre-weaned dairy calves (Dubrovsky et al., 2020) and is one of the leading causes of disease affecting feedlot cattle, specifically in the first 50 days post feedlot arrival (Timsit et al., 2016). It accounts for 70-80% of total feedlot morbidity and 40-50% of total feedlot mortality (Edwards, 2010). The USDA APHIS Feedlot study estimated that BRD costs, on average, $23.60/case (USDA-APHIS, 2013). The costs associated with BRD can be attributed to the cost of treatment and decreased carcass quality grade. In the early 2000s, BRD was estimated to cost approximately $800-900 million annually (Brooks et al., 2011), and more recently, it has been estimated to be between $1-3 billion annually in the United States (Cozens et al., 2019).

BRD is considered a multifactorial disease complex with multiple causative agents, the most common being a bacterial infection, typically with *Mannheimia haemolytica, Pasteurella multocida, Histophilus somni*, or *Mycoplasma bovis*. However, the commonly isolated bacterial "pathogens" are often found in the upper respiratory tract (URT) of healthy cattle. Nevertheless, historically most research has focused on these opportunistic pathogens. Recently the role of the respiratory microbiome in BRD has become a major research area of interest. Major differences exist in the URT and lower respiratory tract (LRT) microbiomes of beef and dairy cattle with and without BRD (Lima et al., 2016; Gaeta et al., 2017; Johnston et al., 2017; Zeineldin et al., 2017; Timsit et al., 2018; Klima et al., 2019; McMullen et al., 2019; McMullen et al., 2020; Zeineldin et al., 2020; Raabis et al., 2021; Centeno-Martinez et al., 2022). However, results regarding alpha diversity (intra-sample diversity) and differentially abundant taxa are inconclusive.

In human medicine, it is well-accepted that a loss of microbial diversity in the gastrointestinal tract leads to many diseases (Mosca et al., 2016). Additionally, in cystic fibrosis patients, reduced respiratory microbial diversity has been correlated with reduced respiratory function (van der Gast et al., 2011; Fodor et al., 2012; Zhao et al., 2012). Moreover, decreased alpha diversity is linked to COVID-19 infection and severity (Xu et al., 2021). Decreased richness (Holman et al., 2015; Timsit et al., 2018; McMullen et al., 2019) and decreased Shannon Diversity Index (Timsit et al., 2018) have been observed in the URT of calves with BRD compared to healthy calves. However, several studies have found no significant difference or pattern of change in alpha diversity metrics between BRD and healthy calves (Zeineldin et al., 2017; McMullen et al., 2019; McMullen et al., 2020). Furthermore, it has been observed that calves that developed BRD had decreased richness at arrival compared to those that remained healthy (Holman et al., 2015). However, this has also been disputed, as others observed no difference (Zeineldin et al., 2017). Many studies report slightly different results for observed sequence variants, including observed operational taxonomic units (OTUs) (Holman et al., 2015), species (Zeineldin et al., 2017; McMullen et al., 2019), amplicon sequence variants (ASVs), and the number of reads (Lima et al., 2016), which can make comparisons among studies difficult. Furthermore, previous results have varied regarding differentially abundant and significantly enriched bacterial taxa as well (Lima et al., 2016; Zeineldin et al., 2017; McMullen et al., 2020; Zeineldin et al., 2020; Raabis et al., 2021; Centeno-Martinez et al., 2022; Li et al., 2022).

More and more studies show that meta-analysis is a very powerful tool to evaluate a scientific question when current research is heterogenous, if there are conflicting results, or if there is a lack of consensus regarding a certain scientific question (Siddaway et al., 2019; Tawfik et al., 2019). As both culture-dependent and -independent microbiome studies attempt to describe microbial ecology (Gray and Head, 2008), formal meta-analyses can likely be used to examine microbiome-associated metrics and remove the "noise" that may contribute to conflicting results due to hiding the underlying "biological pattern" (Duvallet et al., 2017; Nikolova et al., 2021). For example, Nikolova et al. (2021) performed a meta-analysis to analyze the effect of gut microbiome alpha diversity associated with numerous psychiatric conditions (Nikolova et al., 2021). Moreover, Avalos-Fernandez et al. (2022) conducted a meta-analysis to determine the effect of respiratory microbiome alpha diversity's relationship with chronic lung disease (Avalos-Fernandez et al., 2022). However, analyzing reported metrics for relative abundance presents some issues, such as differences in bioinformatic analyses pipelines, classification databases, and differential abundance method, as all of these can affect taxonomic classification and relative and differential abundance results (Edgar, 2018; López-García et al., 2018; Prodan et al., 2020; Nearing et al., 2022). Therefore, compiling and re-analyzing sequences may be a preferred method to examine individual taxa abundances across studies. As a result, a "formal" meta-analysis was conducted to examine the development of BRD on commonly analyzed alpha diversity metrics, including Shannon Diversity Index, Chao1, and variations of observed sequence variants (OTUs, species, ASVs, reads), hereon referred to as "observed features." Additionally, four datasets [(Nicola et al., 2017) (Nicola), (Johnston et al., 2017) (Johnston), (Centeno-Martinez et al., 2022) (Centeno-Martinez), and PRJNA532923 (PRJNA) (Arkansas, U.o, 2019)] of publicly available sequences were re-analyzed to examine the effect of BRD on individual bacterial abundances.

2 Materials and methods

2.1 Literature search, data extraction, and effect size calculation

A detailed literature search was conducted using Preferred Reporting Items for Systematic Reviews and Meta-analyses (PRISMA) methods on May 5, 2022, and again on November 21, 2022 (Figure 1) (Moher et al., 2009). The search terms "bovine respiratory disease" OR "bovine bronchopneumonia" AND "microbiome OR microbiota" were used to search the following databases: Agricola, NCBI PubMed, Web of Science, and NCBI BioProject. Databases were searched to acquire relevant literature

10.3389/fcimb.2023.1223090

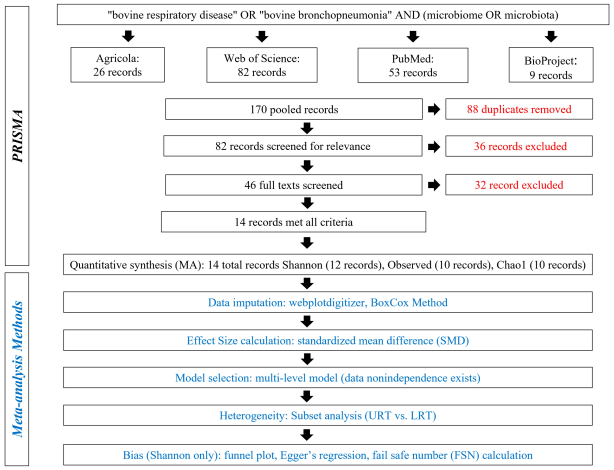

FIGURE 1
Preferred Reporting Items for Systematic Reviews and Meta-Analyses (PRISMA) for alpha diversity analysis.

and deposited but not published sequences. A total of 170 records were pooled, and 88 duplicates were removed. Then, 82 records were screened for relevance, and 36 were excluded for being not of interest (i.e., were review papers, not in cattle, not microbiome, etc.). The remaining 46 records were screened in more detail and were required to meet the following criteria: compare 16S rDNA sequences from healthy and BRD cattle and report one of the three alpha diversity metrics or contain publicly available data. Finally, 32 records were excluded for not meeting the criteria, and 14 were included in the meta-analysis (Figure 1).

Available data]i.e., alpha diversity metrics' (Shannon Index, Chao1, and Observed features) mean, standard deviation, and the number of samples in each group (BRD, control)] was extracted from each study. If the mean and standard deviation values were not readily presented in the paper, Webplotdigitizer was used to extract the data from published figures (Rohatgi, 2021). If the only available figures did not provide the mean and standard deviation (i.e., boxplot), these values were imputed using the following website https://smcgrath.shinyapps.io/estmeansd/ using S2 and the Box-Cox method (McGrath et al., 2020; McGrath et al., 2022) as it does not assume normality as demonstrated previously (Avalos-Fernandez et al., 2022). For graphics with error bars, the average standard error of the mean (SEM) or standard deviation was used, and the SEM was computed to standard deviation by multiplying the SEM by the square root of the sample size. Due to variable alpha diversity metrics reported and lack of available data, all metrics (Shannon, Chao1, and Observed features) could not be extracted from all studies. Therefore, studies without the metric of interest were excluded from the effect size calculation for that metric. Two records had sequencing data but did not report alpha diversity metrics. Therefore, these sequences were analyzed using QIIME2 (as described in section 3.3 below), and the Shannon's Diversity Index, Chao1, and Observed ASVs were calculated.

A database containing relevant metadata and data was constructed (Supplementary Table 1). The SMD of both metrics was calculated for each record using the escalc function, where 1 (n1i (sample size), m1i (mean), sd1i (standard deviation) referred to healthy calves, and 2 (n2i, m2i, and sd2i) referred to BRD calves, in the R package metafor (v3.8-1) in R (v4.2.1) (Viechtbauer, 2010; Team, R.C, 2022).

2.2 Meta-analytical model, subset analysis, and publication bias

A multi-level meta-analytical model was run to determine the overall effect of BRD on Shannon SMD, Observed features SMD, and Chao1 SMD and to account for potential non-independence and heterogeneity introduced by calculating multiple effect sizes for specific records, as some studies reported metrics of interest for differing sample locations (upper vs. lower respiratory tract) or time points (feedlot entry vs. diagnosis, see Supplementary Table 1). This was accomplished using the rma.mv function in the metafor package and by setting "random = ~1|paper_num/count", in which paper_num is the study number and count is the entry number (Supplementary Table 1), and the model was fitted using restricted maximum likelihood (REML).

Subgroup analysis was then conducted to determine if sampling location (URT vs. LRT) was a source of residual heterogeneity. Therefore, the previous multi-level model was altered by setting "mods = ~factor(location)-1". Forest plots of the Shannon, Observed features, and Chao1 SMDs were then created using the forest function in the metafor package (Figures 1–3).

To assess publication bias for the Shannon SMD, a random effects model was run and used to generate a funnel plot, which

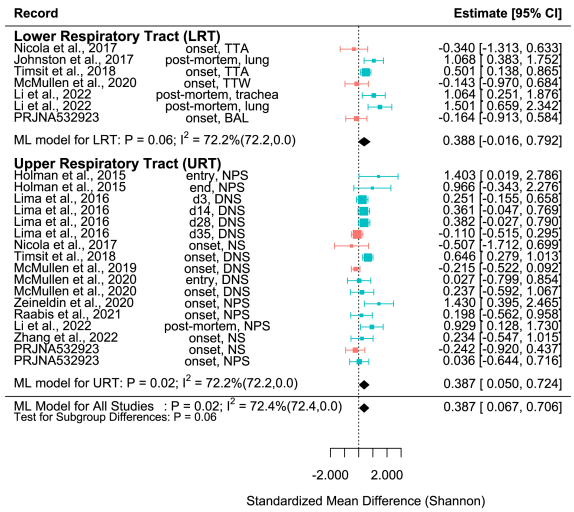

FIGURE 2
SMD of Shannon Diversity Index in Healthy and BRD Calves. Data located right (blue) or left (pink) of the dotted line indicates that healthy or BRD calves have higher SMD, respectively. Datapoint size corresponds to precision. Bars depict 95% confidence interval. I^2 indicates total heterogeneity. Values in parentheses indicate between- and within-group heterogeneity. Middle column indicates sampling collection time and sample type [transtracheal aspiration (TTA), transtracheal wash (TTW), bronchoalveolar lavage (BAL), nasopharyngeal swab (NPS), deep nasal swab (DNS), and nasal swab (NS)].

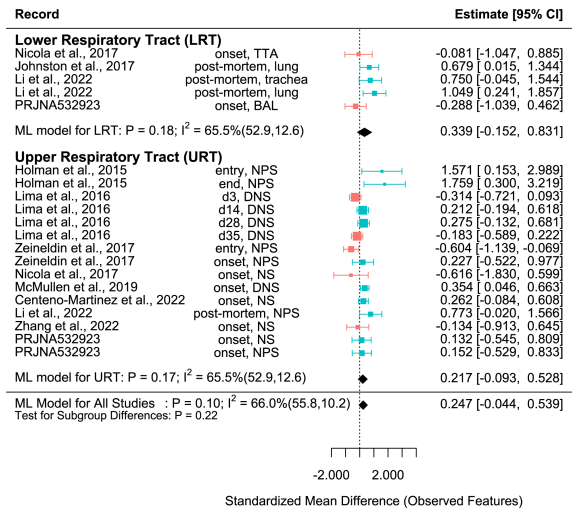

FIGURE 3
SMD of Observed features in Healthy and BRD Calves. Data located right (blue) or left (pink) of the dotted line indicates that healthy or BRD calves have higher SMD, respectively. Datapoint size corresponds to precision. Bars depict 95% confidence interval. I^2 indicates total heterogeneity. Values in parentheses indicate between- and within-group heterogeneity. Middle column indicates sampling collection time and sample type [transtracheal aspiration (TTA), transtracheal wash (TTW), bronchoalveolar lavage (BAL), nasopharyngeal swab (NPS), deep nasal swab (DNS), and nasal swab (NS)].

was created using the funnel function in the metafor package. Additionally, Egger's regression test was performed using the regtest function in the metafor package in R. The failsafe number was calculated using the fsn function in the metafor package in R.

2.3 Sequencing analysis

The search terms "bovine respiratory disease" OR "bovine bronchopneumonia" AND "microbiome OR microbiota" were used to search NCBI BioProject. To be selected, datasets had to be comprised of 16S sequencing data from the bovine respiratory microbiome from BRD calves and controls, have available metadata indicating which samples were BRD and controls, and be at least overlapping the V4 region. Four datasets met these requirements and were downloaded from the SRA database using prefetch and fasterqdump from the SRA toolkit and were analyzed by QIIME2 (version 2022.8) as previously described (Wang et al., 2019; Wang et al., 2021; Wang et al., 2022). Briefly, data from each dataset were individually imported into QIIME2 (Bolyen et al., 2019). Demultiplexed paired-end V3V4 sequences were trimmed to the V4 region using cutadapt (Martin, 2011) with the forward primer (515F: GTGCCAGCMGCCGCGGTAA) and reverse primer (806R: GGACTACHVGGGTWTCTAAT). The forward and reverse adapters used were the reverse complements of the reverse and forward primer, respectively (forward adapter: ATTAGAWACCCBDGTAGTCC; reverse adapter TTACCGCGGCKGCTGGCAC), and untrimmed reads were discarded. Then for each dataset, forward and reverse reads were joined, reads were filtered, and Deblur was used to further trim and denoise sequences (Amir et al., 2017). Identical filtering and Deblur parameters were used for each dataset. The feature table and representative sequences for each dataset were then merged, and data were rarefied to 1108 reads. Shannon diversity index, Chao1, and Observed ASVs were calculated for alpha diversity analysis (see sections 3.1 and 3.2), and Bray-Curtis and Jaccard distances were calculated using QIIME2 and visualized using PCoA plots created with R (v.4.2.1). ASVs were then classified against the Greengenes database (version 13_8_99), and both relative abundance and count ASV tables were created. Then, Bray Curtis and Jaccard distances were calculated using the distance function in the phyloseq R package (v1.40), and sources of variation were assessed using the anosim function from the vegan package (v2.6-4) (McMurdie and Holmes, 2013).

2.4 Differential abundance and taxa interactions

To further investigate the role of BRD on the respiratory microbiome, differential abundance tests were conducted to determine control- and BRD-associated ASVs for each sample type [nasal swabs (NS), nasopharyngeal swabs (NPS), bronchoalveolar lavage (BAL), and trans-tracheal aspiration (TTA)]. Only one of the datasets (Centeno-Martinez) included negative control samples. One ASV (ASV6_*Pseudoalteromonas*) was highly abundant in all negative control samples. This ASV was excluded from NS differential abundance analysis since the Centeno-Martinez dataset was comprised of only NS samples. A consensus approach was used to select differentially abundant taxa for each health status in each sampling location, as recommended by Nearing et al. (2022) (Nearing et al., 2022). To be classified as a control- or BRD- associated taxa, ASVs must have been in the top 25 RandomForest predictors and selected as differentially abundant using both DESeq2 and Analysis of Compositions of Microbiomes with Bias Correction 2 (ANCOM-BC2) for the respective health status. Briefly, RandomForest (v4.7-1.1) was performed on the first 500 ASVs from the rarefied relative abundance table; for each location, a differing number of variables were tried at each branch (mtry) to attempt to optimize results (Breiman, 2001). For DESeq2 and ANCOM-BC2 analysis, the top 1500 ASVs in the rarefied count ASV table were converted into a phyloseq object (McMurdie and Holmes, 2013). For DESeq2 analysis, the phyloseq object was converted to a DESeq2 object, size factors were estimated with the argument type = "poscounts", and taxa with less than 5 reads in 3 samples were filtered out. Then, DESEq2 (v1.36) with the fittype = "local", was used to analyze differentially abundant taxa at the ASV level. ASVs were considered differentially abundant using DESeq2 if Padj < 0.05 (Love et al., 2014). For ANCOM-BC2 (v1.6.4) analysis, ASVs with no variances were removed. The following arguments were set as follows, prv_cut = 0.1, p_adj_method = "hochberg", struc_zero = TRUE, neg_lb = FALSE. ASVs were considered differentially abundant using ANCOM-BC2 if Q < 0.05 (Lin and Peddada, 2020; Lin et al., 2022).

To further examine bacterial relationships at the species level, Sparse Estimation of Correlations among Microbiomes (SECOM) was used to determine both linear and non-linear relationships. The full rarefied count ASV table (excluding the ASV highly abundant in negative controls) was converted into a phyloseq object. Monotonic/linear relationships were quantified using the Spearman correlation coefficient. The secom_linear function in the ANCOMBC package (v2.0.2) was used with the following arguments: pseudo = 0, prv_cut = 0.1, lib_cut = 0, corr_cut = 0.5, wins_quant = c(0.05, 0.95), method = "spearman", soft = FALSE, n_cv = 10, thresh_hard = 0, thresh_len = 100, max_p = 0.05, n_cl = 2. In order to be further analyzed, taxa had to co-occur in at least ten samples and have $P < 0.05$. Non-linear relationships were quantified using the distance correlation coefficient. The secom_dist function in the ANCOMBC package was used with the following arguments: pseudo = 0, prv_cut = 0.1, lib_cut = 0, corr_cut = 0.5, wins_quant = c(0.05, 0.95), R = 100, max_p = 0.05, n_cl = 10, thresh_hard = 0 (Lin et al., 2022).

3 Results

The literature search resulted in 14 records, including published studies and unpublished deposited sequences. The final database consisted of 27 entries. Information for each entry, such as study sample size, calf age, sample date, and individual study effect sizes can be found in Supplementary Table 1. The effect size calculated for both metrics was the standardized mean difference (SMD), also referred to as Hedges g. This method compares the differences between two means, is standardized, and bias-corrected because it takes the sample size into account (Nakagawa et al., 2015). As both metrics were not available for all records, a total of 24, 20, and 18 effect sizes were calculated from 12, 10, and 10 records for Shannon SMD, Observed features SMD, and Chao1 SMD, respectively (Figure 1; Supplementary Table 1).

3.1 Healthy calves have increased Shannon SMD

The SMD varied considerably for each record for all metrics. Among them, many records of Shannon SMD were highly positive, showing that the SMD was greater in healthy calves than in BRD calves. This observation demonstrated that the healthy calves had greater microbial diversity. However, there were still many records with negative SMDs, which signified that the SMD was higher in BRD calves than in healthy calves (Figure 2). The same trends were shown in Observed features SMD and Chao1 SMD (Figures 3, 4).

A meta-analytical model determined BRD's overall effect on the diversity and richness of the respiratory microbiome. Considering the non-independence and heterogeneity introduced by calculating multiple effect sizes from one study, the multi-level meta-analytical model was selected. In this combined analysis, regardless of location, the Shannon SMD was significantly higher in healthy calves than that in calves with BRD (SMD: 0.387, $P < 0.05$, 95% CI: 0.067 – 0.706). Among them, high heterogeneity was observed

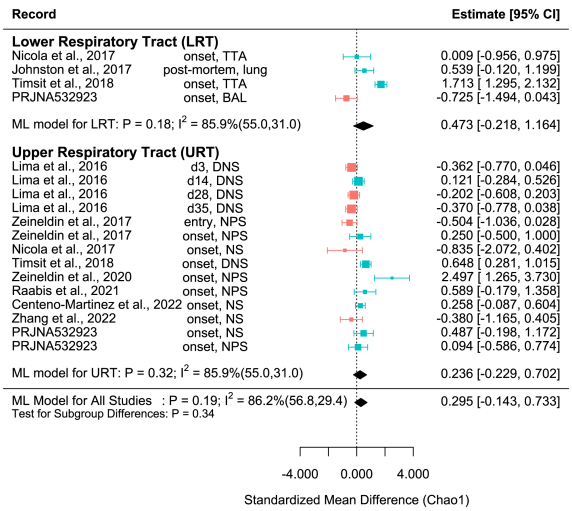

FIGURE 4
SMD of Chao1 in Healthy and BRD Calves. Data located right (blue) or left (pink) of the dotted line indicates that healthy or BRD calves have higher SMD, respectively. Datapoint size corresponds to precision. Bars depict 95% confidence interval. I^2 indicates total heterogeneity. Values in parentheses indicate between- and within-group heterogeneity. Middle column indicates sampling collection time and sample type [transtracheal aspiration (TTA), transtracheal wash (TTW), bronchoalveolar lavage (BAL), nasopharyngeal swab (NPS), deep nasal swab (DNS), and nasal swab (NS)].

(I^2 = 72.4%) (Figure 2). However, there were no significant differences between healthy and BRD calves for Observed features SMD (SMD: 0.247, $P > 0.05$, 95% CI: -0.044 – 0.539) and only moderate heterogeneity was observed (I^2 = 66.0%) (Figure 3). Similar results were observed for Chao1 SMD (SMD: 0.295, $P > 0.10$, 95% CI: -0.143 – 0.733) and high heterogeneity was observed (I^2 = 86.2%) (Figure 4). Shannon SMD was next analyzed for publication bias because it was the only significant metric observed. Our result showed that the funnel plot was not asymmetrical and publication bias did not exist based on Egger's regression test ($P > 0.1$). The fail-safe number (FSN) was also calculated, indicating the number of insignificant studies needed to decrease the observed significance to the target significance. The FSN for the Shannon SMD model was 215, showing that it would take 215 insignificant results to decrease the observed significance ($P < 0.0001$) to the target significance ($P = 0.05$) (Figure 5). Additionally, the FSN value was greater than 5k + 10 (where k is the number of effect sizes calculated) (Robert, 1979). Therefore, it was concluded that the Shannon SMD lacked publication bias.

3.2 Sampling location (URT vs. LRT) could not explain residual heterogeneity

It is well known that the structure and composition of the upper respiratory tract (URT) and lower respiratory tract (LRT) microbiomes differ (Timsit et al., 2018). In this study, subset analysis was conducted to determine if the sampling sites affected the SMD. In the URT, the Shannon SMD was significantly higher in healthy calves than that in BRD calves (SMD: 0.387, $P < 0.05$, 95%

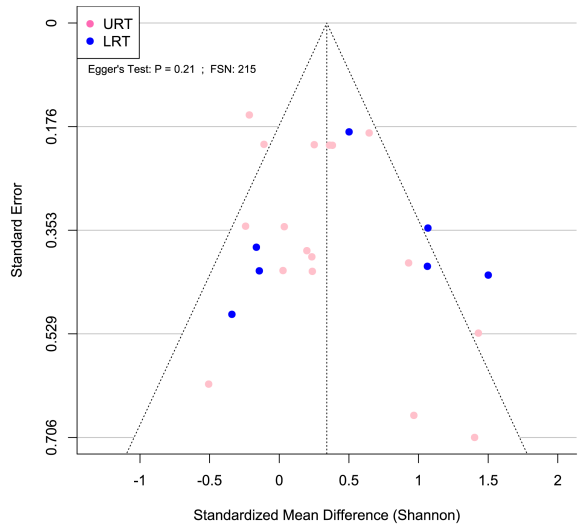

FIGURE 5
Publication bias was not detected for Shannon SMD. Asymmetrical funnel plot indicates lack of publication bias. Blue and pink circles indicate effect sizes from the lower and upper respiratory tract, respectively. Egger's test P > 0.05 and FSN > 130 indicate lack of publication bias.

CI: 0.05 – 0.724). Instead, in the LRT, healthy calves tended to have a higher Shannon SMD compared to BRD calves (SMD: 0.388, P = 0.06, 95% CI: -0.016 – 0.792). Additionally, high heterogeneity still existed after subgroup analysis (I^2 = 72.2%), indicating that the URT vs. LRT did not explain the heterogeneity observed (Figure 2).

For the Observed features SMD, no differences were observed between healthy and BRD calves in the URT (SMD: 0.217, P > 0.1, 95% CI: -0.093 - 0.528) or LRT (SMD: 0.339, P > 0.1, 95% CI: -0.152 – 0.831), and moderate heterogeneity was still observed (I^2 = 65.5%) (Figure 3). Similarly, for the Chao1 SMD, no differences were observed between healthy and BRD calves in the URT (SMD: 0.236, P > 0.1, 95% CI: -0.229 – 0.702) or LRT (SMD: 0.473, P > 0.1, 95% CI: -0.218 – 1.164), and high heterogeneity was still observed (I^2 = 85.9%) (Figure 4).

3.3 Sampling location and dataset are major sources of microbiome variation

Four datasets [(Nicola et al., 2017) (Nicola), (Johnston et al., 2017) (Johnston),(Centeno-Martinez et al., 2022) (Centeno-Martinez), and PRJNA532923 (PRJNA) (Arkansas, U.o, 2019)] were used for this study because they contained V4 or V3-V4 16S rDNA sequencing data from the respiratory tract of cattle with and without BRD and included available metadata to identify controls or calves with BRD. However, due to the lack of available data for all time points and unclear metadata, we only used sequences from samples (BRD vs. control) taken at BRD diagnosis/onset or post-mortem samples. Thus, no feedlot entry samples were included in this study. The datasets contained different read numbers; therefore, all samples were further rarefied to 1,108 reads to better examine results evenly across samples.

Both Bray-Curtis and Jaccard distances were calculated and next visualized using PCoA plots. Furthermore, an Analysis of Similarity (ANOSIM) was performed to assess sources of variation. Based on the Bray-Curtis PCoA plot, clustering did not occur due to different health status (*e.g.*, BRD vs. controls). However, it occurred when the analysis was done on location within the respiratory tract and dataset (Figure 6). This observation was further confirmed by ANOSIM analysis (Table 1). Health status, URT vs. LRT, dataset, and sampling location were sources of variation. However, the sampling location (R: 0.6474, P < 0.001) was the most significant source of variation, followed by dataset (R: 0.6032, P < 0.001). Health status contributed the least to variation (R: 0.0399, P < 0.05). Similar results were observed in the analysis of Jaccard distances. Samples did not cluster based on health status and appeared to cluster based on dataset or sampling location (Figure 7). Additionally, ANOSIM analysis of Jaccard distances showed that all tested variables were significant sources of variation. However, the main sources were dataset (R: 0.7614, P < 0.001), followed by sampling location (R: 0.7486, P < 0.001); the health status was the least important source of variation (R: 0.0475, P < 0.05) (Table 1).

3.4 Control- and BRD- associated ASVs

Our results showed that sampling location was the largest source of variation based on Bray Curtis distances and the second largest source of variation based on Jaccard distances (Table 1); therefore, control- and BRD- associated ASVs were determined based on sampling site, including nasal (NS) (Centeno-Martinez, Nicola, PRJNA), nasopharyngeal (NPS) (PRJNA), lung (Johnston), bronchoalveolar lavage (PRJNA), and trans tracheal aspiration (TTA) (Nicola). ASV6 was removed from NS differential abundance analysis because it was highly abundant in the negative controls of the Centeno-Martinez dataset. A consensus approach was used to determine differentially abundant ASVs, as recommended by Nearing et al. (2022). To be considered differentially abundant, an ASV had to be ranked among the top 25 RandomForest predictors and be selected as differentially abundant using both DESeq2 and ANCOM-BC2. Using these criteria, only one sampling location (NS) contained differentially abundant ASVs. Using DESeq2, 16 ASVs were identified as differentially abundant in the nasal cavity, and 8 of them were RandomForest predictors (Supplementary Figures 1A, B). Using ANCOM-BC2, 3 ASVs were identified as differentially abundant in the nasal cavity, which overlapped with those identified by RandomForest and DESeq2. Therefore, the consensus-based approach allowed us to identify 3 differentially abundant ASVs in the nasal cavity. ASV5_*Mycoplasma* was differentially abundant in BRD calves (*DESeq2:* $\log_2$fold change (lfc): -1.85, $p_{adj} < 0.05$; *ANCOM-BC2:* $W_{control}$: -4.00, Q < 0.05), and ASV19_*Corynebacterium* (*DESeq2:* lfc: 0.97, $p_{adj} < 0.05$; *ANCOM-BC2:* $W_{control}$: 4.02, Q < 0.05) and ASV37_*Ruminococcaceae* (*DESeq2:* lfc: 0.82, $p_{adj} < 0.05$; *ANCOM-BC2:* $W_{control}$: 3.91, Q < 0.05) were differentially abundant in controls (Figure 8). Furthermore, the abundance of the three control- or BRD- associated ASVs were also broken down by dataset to ensure that they were present in more than one dataset (Supplementary Figure 2).

10.3389/fcimb.2023.1223090

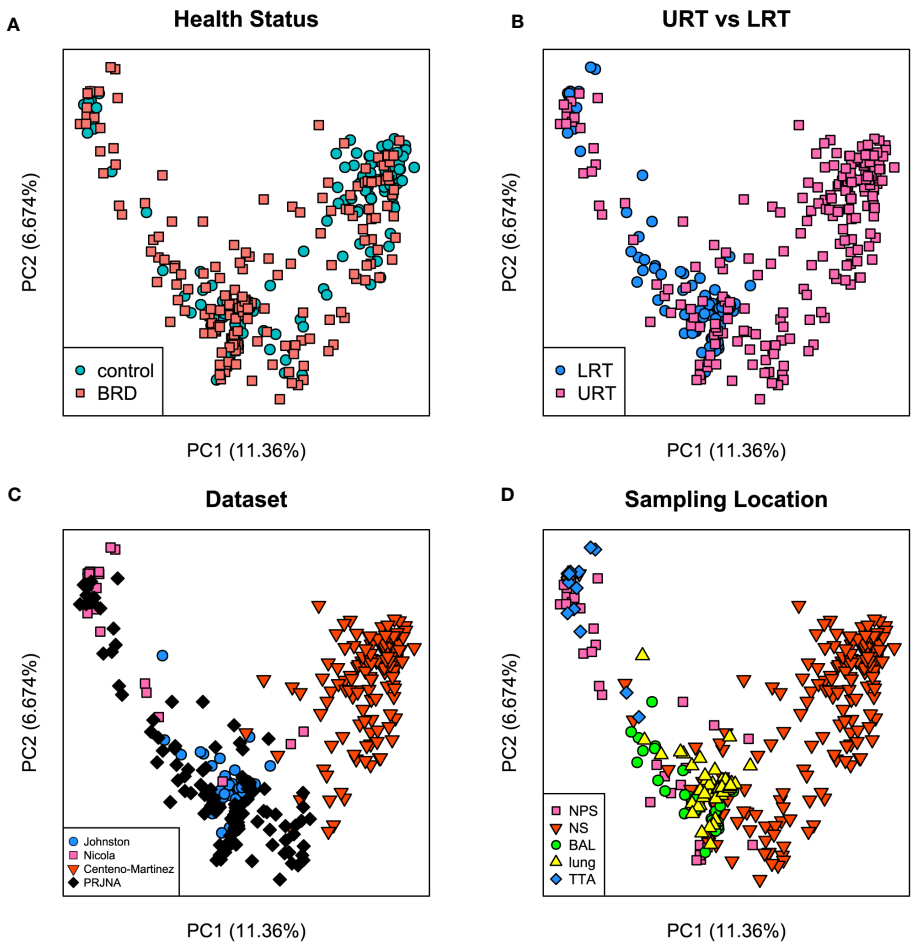

FIGURE 6
Principal coordinate analysis (PCoA) plots based on Bray-Curtis distances. **(A)** illustrates health status [ANOSIM: R: 0.03, P < 0.05 (Table 1)], **(B)** URT vs. LRT [ANOSIM: R: 0.47, P < 0.001 (Table 1)], **(C)** dataset [ANOSIM: R: 0.6, P < 0.001 (Table 1)], and **(D)** sampling location [ANOSIM: R: 0.64, P < 0.001 (Table 1)]. Legends for each plot indicate sample breakdown.

In NPS samples, 4 ASVs were differentially abundant using DESeq2. Furthermore, two ASVs overlapped with RandomForest predictors. However, no ASVs were identified as differentially abundant using ANCOM-BC2 (Supplementary Figures 3A, B). Similar results were observed in the LRT samples. For example, for lung samples, 6 ASVs were differentially abundant when DESeq2 was applied. In this analysis, 1 ASV was found to be differentially abundant using ANCOM-BC2 While no ASVs overlapped with each other. Among TTA samples, only 1 ASV was differentially abundant using DESeq2, while none were differentially abundant using ANCOM-BC2. Moreover, no ASVs were identified as differentially abundant in BAL samples when both DESeq2 and ANCOM-BC2 were used.

TABLE 1 Analysis of Similarities (ANOSIM) of Bray-Curtis and Jaccard Distances.

	Bray-Curtis R	Jaccard R
Health Status	0.0399**	0.04753***
URT vs LRT	0.4711***	0.5403***
Dataset	0.6032***	0.7614***
Sampling Location	0.6474***	0.7486***

**P < 0.01.
***P < 0.001.

3.5 Linear and non-linear interactions exist between bacterial taxa in the nasal cavity

To further investigate the possible role(s) of the control- and BRD-associated ASVs, we used SECOM to analyze both linear and non-linear relationships between different taxa (at the ASV level). The nasal cavity was chosen for SECOM analysis because it was the only location with differentially abundant ASVs and contained multiple datasets for comparison. ASV5_*Mycoplasma*, ASV19_*Corynebaterium*, and ASV37_ *Ruminococcaceae* were of interest at the ASV level (Supplementary Tables 2, 3). It is noted that there can be non-linear relationships between taxa when no linear relationship exists. However, if a linear relationship exists, a non-linear one should also; if one does not, results should be interpreted carefully. Therefore, only linear

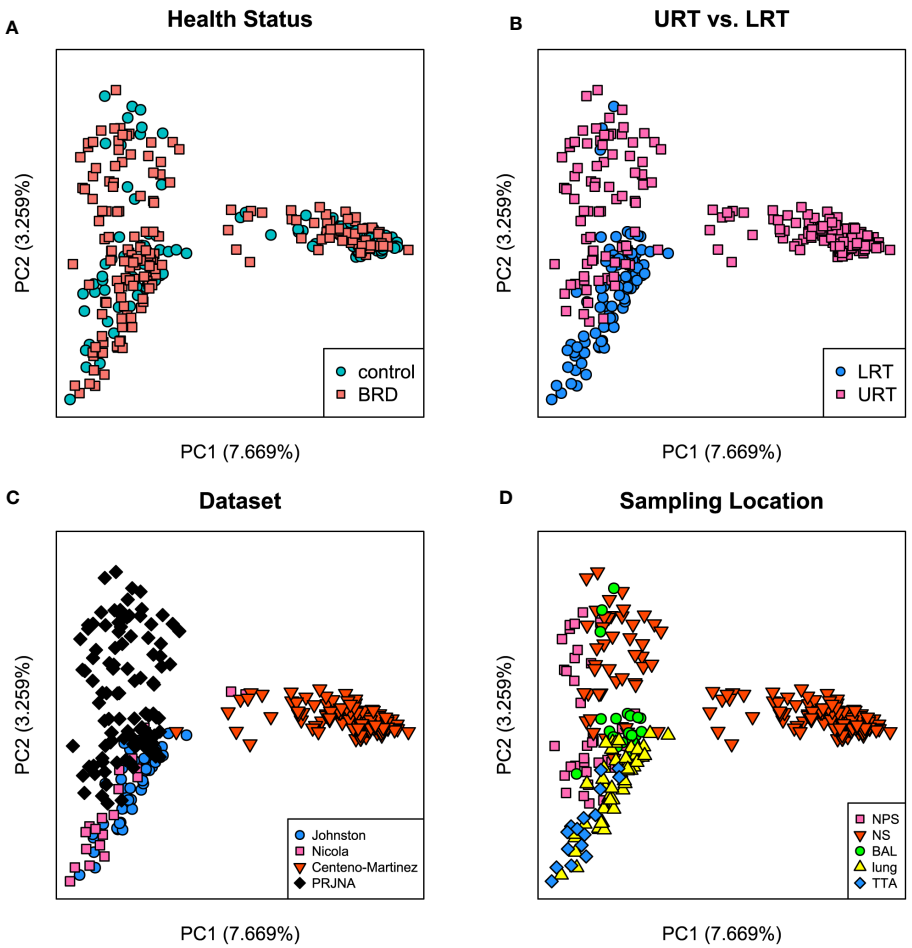

FIGURE 7
Principal coordinate analysis (PCoA) plots based on Jaccard distances. **(A)** Illustrates health status [ANOSIM: R: 0.047, P < 0.05 (Table 1)], **(B)** URT vs. LRT [ANOSIM: R: 0.54, P < 0.001 (Table 1)], **(C)** dataset [ANOSIM: R: 0.76, P < 0.001 (Table 1)], and **(D)** sampling location [ANOSIM: R: 0.74, P < 0.001 (Table 1)]. Legends for each plot indicate sample breakdown.

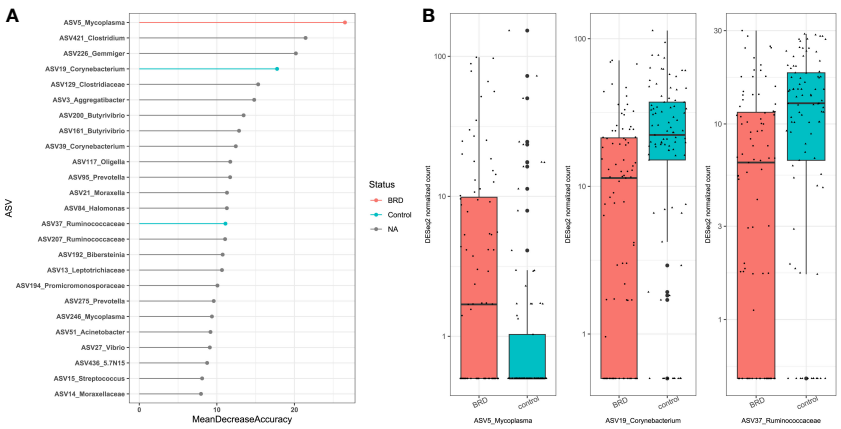

FIGURE 8
Differentially abundant ASVs within the nasal cavity. ASVs were determined differentially abundant if they were selected as a RandomForest predictors (top 25) and were differentially abundant using both DESeq2 (Padj < 0.05), and ANCOM-BC (Q < 0.05). **(A)** Top 25 RandomForest predictors; pink indicates BRD-associated ASV; blue indicates healthy control-associated ASV. **(B)** Boxplot of DESeq2 counts; Pink indicates abundance in BRD samples; blue indicates abundance in control samples.

10.3389/fcimb.2023.1223090

relationships with overlapping non-linear relationships were reported. It should also be noted that the non-linear relationship (distance correlation) was only non-zero and does not have a direction, as it only described a general dependency between taxa (Lin et al., 2022). As this was a meta-analysis and combining datasets could introduce lots of "noise," the primary goal was to identify general dependencies between the selected taxa and any ASVs associated with *Mycoplasma, Mannheimia, Histophilus*, and *Pasteurella*. Therefore, the SECOM distance matrix was primarily used to determine relationships (Table 2; Supplementary Table 2), and SECOM Spearman2 (p-value filtering) was used to determine the direction of the relationship (Table 3; Supplementary Table 3). ASV19_*Corynebacterium* had a negative relationship with ASV1_*Mycoplasma_hyorhinis* (distance: 0.38; ρ: -0.41; $P < 0.05$), ASV4_*Mannheimia* (distance: 0.46; ρ: -0.31; $P < 0.05$), ASV54_*Mycoplasma* (distance: 0.4; ρ: -0.41; $P < 0.05$), ASV7_*Mycoplasma* (distance: 0.31; ρ: -0.28, $P < 0.05$), and ASV8_*Pasteurella* (distance: 0.38; ρ: -0.4; $P < 0.05$) and a positive relationship with ASV376_*Mycoplasma* (distance: 0.64; ρ: 0.67; $P < 0.05$). ASV37_*Ruminococcaceae* had a negative relationship with ASV1_*Mycoplasma_hyorhinis* (distance: 0.31; ρ: -0.29; $P < 0.05$), ASV4_*Mannheimia* (distance: 0.39; ρ: -0.3; $P < 0.05$), and ASV5_*Mycoplasma* (distance: 0.3; ρ: -0.28; $P < 0.05$). ASV5_*Mycoplasma* had a positive relationship with ASV1_*Mycoplasma_hyorhinis* (distance: 0.43; ρ: 0.42; $P < 0.05$), ASV10_*Histophilus_somni* (distance: 0.52; ρ: 0.50; $P < 0.05$), and ASV346_*Mycoplasma* (distance: 0.88; ρ: 0.87; $P < 0.05$) (Tables 2, 3). Finally, ASV37_*Ruminococcaceae* had a relationship with ASV7_*Mycoplasma* (distance: 0.22; $P < 0.05$), but the direction could not be determined (Table 2). Furthermore, ASV19_*Corynebacterium* and ASV37_*Ruminococcaceae* had a positive relationship with each other (distance: 0.63; ρ: 0.56; $P < 0.05$) (Tables 2, 3). These data indicated that, in the nasal cavity, the healthy control-associated ASVs potentially interact with the BRD-associated ASV and other opportunistic pathogens within the nasal cavity and that the BRD opportunistic pathogens were likely interacting with each other.

TABLE 2 Sparse Estimation of Correlations among Microbiomes (SECOM) Distance. Matrix quantifying non-linear relationships between taxa in the bovine nasal cavity.

	ASV1 *Mycoplasma_hyorhinis*	ASV10 *Histophilus_somni*	ASV346 *Mycoplasma*	ASV37 *Ruminococcaceae*	ASV376 *Mycoplasma*	ASV4 *Mannheimia*	ASV5 *Mycoplasma*	ASV54 *Mycoplasma*	ASV7 *Mycoplasma*	ASV8 *Pasteurella*
ASV19 *Corynebacterium*	0.379826	0	0	0.626393	0.642521	0.461004	0	0.399021	0.314158	0.377679
ASV37 *Ruminococcaceae*	0.307754	0	0	1	0	0.395374	0.299882	0	0.222071	0
ASV5 *Mycoplasma*	0.433682	0.52168	0.8803	0.299882	0	0	1	0	0	0

Values are distance correlation coefficients.
Non-zero values indicate general dependency/relationship between taxa ($P < 0.05$).
Zeroes indicate no dependency/relationships exist between taxa.

4 Discussion

Our study provides the first meta-analysis examining BRD's effect on the respiratory microbiome alpha diversity. Overall, healthy calves had a greater Shannon diversity index of 0.39 standard deviations, indicating that the respiratory microbiome of healthy calves had increased microbial diversity compared to calves that developed BRD ($P < 0.05$). These results agreed with the previous observations: healthy calves had increased alpha diversity metrics compared to those with BRD (Holman et al., 2015; Timsit et al., 2018; McMullen et al., 2019). However, no difference was observed for either the Chao1 or Observed features metrics. There could be many reasons for this. First, the Shannon Diversity Index is a measure of evenness and richness, meaning that it considers both bacterial presence/absence and bacterial abundance (Kim et al., 2017). Whereas both Chao1 and Observed features measure bacterial richness, meaning they only take into account bacterial presence/absence (Hughes et al., 2001). Therefore, this might indicate that the abundance of specific bacteria, rather

10.3389/fcimb.2023.1223090

TABLE 3 Sparse Estimation of Correlations among Microbiomes (SECOM) Spearman (P value filtering) Matrix quantifying monotonic/linear relationships between taxa in the bovine nasal cavity.

	ASV1 *Mycoplasma_hyorhinis*	ASV10 *Histophilus_somni*	ASV346 *Mycoplasma*	ASV37 *Ruminococcaceae*	ASV376 *Mycoplasma*	ASV4 *Mannheimia*	ASV5 *Mycoplasma*	ASV54 *Mycoplasma*	ASV7 *Mycoplasma*	ASV8 *Pasteurella*
ASV19 *Corynebacterium*	-0.411968738	0	0	0.558790593	0.666666667	-0.312895125	0	-0.406967023	-0.284981088	-0.39992
ASV37 *Ruminococcaceae*	-0.291410913	0	0	1	0	-0.301406873	-0.284311214	0	0	0
ASV5 *Mycoplasma*	0.417471755	0.505609498	0.866666667	-0.284311214	0	0	1	0	0	0

Non-zero values indicate a monotonic/linear relationship between taxa ($P < 0.05$).
Negative values indicate a negative relationship, and positive values indicate a positive relationship ($P < 0.05$).
Zero values indicate no monotonic/linear relationships between taxa.

than just their presence, accounted for BRD. However, it is also possible that this difference is not related to disease but rather the effect of different data analytical methods. Chiarello et al. (2022) observed that data analysis pipeline significantly influenced presence/absence indices. Furthermore, richness estimates were also influenced using either ASVs or OTUs. They also noted that this affected both the richness metric values and sample ranking (Chiarello et al., 2022). Therefore, it is possible that the data analysis method had a greater effect on the richness alpha diversity metrics (Chao1, Observed features) than on the Shannon Diversity Index. The effect of data analytical pipeline on alpha diversity SMD could be addressed by re-analyzing publicly available sequencing data. However, many of the included studies did not have publicly available sequencing data and metadata. Future studies should make all sequencing data and metadata publicly available to address this question.

Furthermore, the URT of healthy calves had a greater Shannon diversity index of 0.38 standard deviations than BRD calves ($P < 0.05$), and no differences were observed in the LRT between BRD and healthy calves. This could indicate that the URT microbiome's Shannon Diversity Index is more affected by BRD, but it could also be due to the small sample size for the LRT. Although the LRT samples had by far the smallest sample size, the sample size for the entire meta-analysis (total records/effect sizes) is small, indicating a need for additional research into the bovine respiratory microbiome and its role in BRD. In addition, subset analysis based on sampling location did not explain the high heterogeneity observed for Shannon SMD. This indicates that other unexplained factors, such as sampling time, diet, age, and/or management factors, etc., likely also affect the respiratory microbiome, leading to the observed high residual heterogeneity. Future meta-analyses should attempt to explain this heterogeneity if possible. Nevertheless, no publication bias was observed for the Shannon SMD in this study. Therefore, although high residual heterogeneity was observed for Shannon SMD, the lack of publication bias and significant effect size, especially for the URT, clearly demonstrate that the URT microbiome Shannon diversity index is higher in healthy calves than in those with BRD. However, it remains unclear if the decreased diversity in BRD calves is due to disease development or if decreased diversity predisposes the calf to BRD because all sampling time points were analyzed together due to a lack of available data.

To assess the effect of BRD on the respiratory microbiome, publicly available sequences with available metadata were compiled and analyzed as a singular dataset. Previous datasets with available data could not be included due to a lack of available metadata or the use of a non-overlapping 16S hypervariable region. Beta diversity analysis indicated that all tested variables (health status, URT vs. LRT, sampling location, and dataset) were significant sources of variation on both Bray Curtis and Jaccard distances. Interestingly, health status was the smallest source of variation for both beta diversity metrics, whereas either sampling location or dataset were the greatest sources of variation. This indicates that sampling location and other outside influences affect the microbiome more than health status alone. Chai et al. (2022b) performed a meta-

analysis on metagenomic sequencing data from the bovine respiratory microbiome. Their results showed that microbial structure and function were significantly affected by both geographical location and sampling niche. Therefore, this indicates that respiratory tract location and environmental factors, such as diet or climate, likely affect the respiratory microbiome more than health status alone, as these differed for each geographic location included in the study (Chai et al., 2022b).

To address these issues, we split samples into individual sampling locations (NS, NPS, BAL, lung tissue, and TTA) to examine control- and BRD-associated ASVs. ASVs were considered differentially abundant using a consensus approach of RandomForest, DESeq2, and ANCOM-BC2. Nearing et al. (2022) showed that differing differential abundance analysis methods yielded differing results and recommended applying a consensus approach to determine robust biological interpretations (Nearing et al., 2022). In the nasal cavity, ASV19_*Corynebacterium* and ASV37_*Ruminococcaceae* were identified as healthy control-associated ASVs, as they were higher in abundance in controls, and ASV5_*Mycoplasma* was identified as the only BRD-associated ASV. While *Mycoplasma* is present in the microbiome of clinically healthy cattle also (Chai et al., 2022a), it is clear that ASV5_*Mycoplasma* is associated with BRD.

To further evaluate the nasal cavity microbiome, Sparse Estimation of Correlations among Microbiomes (SECOM) was used to examine both linear and non-linear relationships between taxa. Pearson and Spearman correlation coefficients have been deemed inappropriate for use with microbiome data; however, SECOM takes into account the sparsity of microbiome data (Lin et al., 2022). Using SECOM at the ASV-level, both ASV37_*Ruminococcaceae* and ASV19_*Corynebacterium* were positively correlated with each other and were negatively correlated with ASV4_*Mannheimia* and many *Mycoplasma* ASVs. Furthermore, ASV19_*Corynebacterium* was negatively correlated with ASV8_*Pasteurella*, and, interestingly, positively correlated with ASV376_*Mycoplasma*. It should be noted that *Mannheimia, Mycoplasma*, and *Pasteurella* are not opportunistic pathogens themselves and that other species exist within these genera as well (Slack, 2010; Suástegui-Urquijo et al., 2015; Parker et al., 2018). *Ruminococcaceae* is a normal and abundant member of the bovine gastrointestinal tract microbiome (Lopes et al., 2019). It has also been observed in the upper respiratory tract as well, and it is thought that its presence is due to contact with feces, manure, or digesta due to rumination (Amat et al., 2019a; Crosby et al., 2022). Additionally, Crosby et al. (2022) observed that *Ruminococcaceae* abundance was decreased in the upper respiratory tract of cattle with BRD and speculated that this might be due to decreased rumination in sick calves (Crosby et al., 2022). Therefore, our observation of ASV37_ *Ruminococcaceae* as a healthy control-associated ASV within the bovine nasal cavity indicates a need for further research into the role of gastrointestinal tract-associated microbes in respiratory health. Amat et al. (2019b) observed that three *Corynebacterium* isolates from the nasopharyngeal tract of healthy cattle were able to inhibit the growth of *M. haemolytica in vitro* (Amat et al., 2019b). One can assume that *Corynebacterium* may repress the growth of BRD pathogens in the animal hosts. It is well established that *Corynebacterium* is part of normal microbiota in the bovine nasal cavity and nasopharyngeal tract regardless of health status (Gaeta et al., 2017; Holman et al., 2017; Nicola et al., 2017; Zeineldin et al., 2017; McDaneld et al., 2018; Timsit et al., 2018; Amat et al., 2019a; Chai et al., 2022a). However, *Corynebacterium* sp. have often been associated with human respiratory disease (Yang et al., 2018) and cause disease in cattle, albeit not in the respiratory tract (Smith et al., 2020; Lücken et al., 2022). Regardless, our results and Amat et al. (2019b) showed that *Corynebacterium* may be involved in maintaining microbiome stability of the bovine URT and preventing BRD opportunistic pathogen invasion and colonization. However, additional research is needed to evaluate the role of *Corynebacterium* within the bovine respiratory tract and the role of gastrointestinal microbes in the upper respiratory tract.

It should be noted that our study has some limitations. First, all data included in this study was based on 16S sequencing data. Future studies utilizing shotgun metagenomics, metabolomics, or quantifying total bacterial load would provide additional insight into the respiratory microbiome's role in BRD development and progression. Additionally, due to a lack of available data, all time points were analyzed together when analyzing the effect of BRD on different alpha diversity metrics SMD. However, our multi-level model attempted to account for the potential non-independence introduced by calculating multiple effect sizes for some studies. Although, it should be noted that the inclusion criteria for this study were very broad; therefore, only broad conclusions can be drawn. It remains unclear if the decreased Shannon SMD observed in BRD calves is due to disease development or if decreased diversity predisposes the calf to BRD. Future studies should aim to make all data, including sequencing data or calculated alpha diversity metrics (even if the metric is not significant), publicly available to aid in answering this question. Moreover, subset analysis based on sampling location did not explain the high heterogeneity observed for Shannon SMD, indicating that other unexplained factors exist that also affect the respiratory microbiome. Future studies should aim to make all data publicly available and have clear, descriptive metadata, so future meta-analyses can explain the residual heterogeneity observed. Additionally, other factors, such as breed, age, geographical location, climate, and management practices all affect the respiratory microbiome, and we cannot rule out the effects of these factors in our study. Future studies comparing the respiratory microbiome of BRD calves would also need to be standardized in this field, as in the human microbiome project, including sample collection, storage, DNA extraction, the hypervariable region of the bacterial 16S rRNA gene, and analytical pipelines. The definition and diagnosis of BRD, the application of antibiotics, and the sampling time after feedlot arrival should also need to be considered when comparing the bovine respiratory microbiome between studies. Finally, as previously noted, the sample size of our study is small, and many studies could not be included due to either a lack of publicly available data or unclear metadata. Our study would be strengthened by the inclusion of additional data, so future studies

should aim to make all sequencing data and descriptive metadata publicly available.

5 Conclusion

Our study investigated the effect of BRD on the alpha (intra-sample) diversity of the cattle respiratory microbiome, which fills the knowledge gap between respiratory microbiome alpha diversity and BRD. The multi-level model concluded that healthy calves had an increased Shannon Diversity Index, and no difference was observed for richness measures (Observed or Chao1). Overall, these results indicate that Shannon Index in calves with BRD is lower than in healthy calves. Furthermore, publicly available sequences were combined and re-analyzed for four datasets. ANOSIM, based on Bray-Curtis and Jaccard distances, found that, although significant, health status was the smallest source of variation, and sampling location and dataset were the largest sources of variation, respectively. Additionally, in the nasal cavity, ASV19_*Corynebacterium* and ASV37_*Ruminococcaceae* were healthy control-associated ASVs, and ASV5_*Mycoplasma* was the only BRD-associated ASV. Based on SECOM analysis, ASV19_*Corynebacterium* was negatively associated with ASV4_*Mannheimia*, ASV1_*Mycoplasma_hyorhinis*, ASV54_*Mycoplasma*, ASV7_*Mycoplasma*, and ASV8_*Pasteurella*, and positively correlated with ASV376_*Mycoplasma*, and ASV37_*Ruminococcaceae*, the other healthy control-associated ASV. Taken together, these results indicate that additional research is needed into the role of *Corynebacterium* in the bovine respiratory microbiota and that sampling location and other factors significantly affect microbial structure and need to be considered.

Data availability statement

Publicly available datasets were analyzed in this study. This data can be found here: All sequencing data used in this study were obtained and were previously available on NCBI Bioproject under the following accessions: PRJNA532923, PRJNA746809, PRJNA383722, PRJNA335827.

Author contributions

JZ and SH contributed to conception. SH contributed to data collection, analysis, interpretation, and drafted the manuscript. SH, JZ, JP, BK, and SC contributed to critically revised the manuscript. All authors contributed to the article and approved the submitted version.

Funding

This project was supported by Agriculture and Food Research Initiative Competitive Grant no. 20196701629869 from the USDA National Institute of Food and Agriculture.

Acknowledgments

We would like to thank Adam Siepielski, PhD from the University of Arkansas Department of Biology for his assistance with the alpha diversity formal meta-analyses methods.

Conflict of interest

The authors declare that the research was conducted in the absence of any commercial or financial relationships that could be construed as a potential conflict of interest.

Publisher's note

Supplementary material

The Supplementary Material for this article can be found online at: https://www.frontiersin.org/articles/10.3389/fcimb.2023.1223090/full#supplementary-material

SUPPLEMENTARY FIGURE 1
ASVs identified as differentially abundant in nasal cavity using only RandomForest and DESeq2. ASVs were selected if they were selected as a RandomForest predictors (top 25) and were differentially abundant using DESeq2 (Padj < 0.05). **(A)** Top 25 RandomForest predictors; pink indicates BRD-associated ASV; blue indicates healthy control-associated ASV. **(B)** Boxplot of DESeq2 counts; Pink indicates abundance in BRD samples; blue indicates abundance in control samples.

SUPPLEMENTARY FIGURE 2
Differentially abundant ASVs in the nasal cavity broken down by health status and datasets. ASVs were determined differentially abundant if they were selected as a RandomForest predictors (top 25) and were differentially abundant using both DESeq2 (Padj < 0.05), and ANCOM-BC (Q < 0.05). Boxplots formed based on DESeq2 counts. Pink indicates abundance in BRD samples; blue indicates abundance in control samples.

SUPPLEMENTARY FIGURE 3
ASVs identified as differentially abundant in nasopharyngeal cavity using RandomForest and DESeq2. ASVs were selected if they were selected as a RandomForest predictors (top 25) and were differentially abundant using DESeq2 (Padj < 0.05). **(A)** Top 25 RandomForest predictors; pink indicates BRD-associated ASV; blue indicates healthy control-associated ASV. **(B)** Boxplot of DESeq2 counts; Pink indicates abundance in BRD samples; blue indicates abundance in control samples.

References

Amat, S., Holman, D. B., Timsit, E., Schwinghamer, T., and Alexander, T. W. (2019a). Evaluation of the nasopharyngeal microbiota in beef cattle transported to a feedlot, with a focus on lactic acid-producing bacteria. *Front. Microbiol.* 10. doi: 10.3389/fmicb.2019.01988

Amat, S., Timsit, E., Baines, D., Yanke, J., and Alexander, T. W. (2019b). Development of bacterial therapeutics against the bovine respiratory pathogen *Mannheimia haemolytica*. *Appl. Environ. Microbiol.* 85 (21), e01359–01319. doi: 10.1128/aem.01359-19

Amir, A., McDonald, D., Navas-Molina, J. A., Kopylova, E., Morton, J. T., Zech Xu, Z., et al. (2017). Deblur rapidly resolves single-nucleotide community sequence patterns. *mSystems* 2 (2), e00191–00116. doi: 10.1128/mSystems.00191-16

Arkansas, U.o. (2019). *Cattle respiratory metagenome Genome sequencing and assembly* (National Library of Medicine (US): BioProject [Internet]). Available at: http://www.ncbi.nlm.nih.gov/bioproject/PRJNA532923.

Avalos-Fernandez, M., Alin, T., Métayer, C., Thiébaut, R., Enaud, R., and Delhaes, L. (2022). The respiratory microbiota alpha-diversity in chronic lung diseases: first systematic review and meta-analysis. *Respir. Res.* 23 (1), 214. doi: 10.1186/s12931-022-02132-4

Bolyen, E., Rideout, J. R., Dillon, M. R., Bokulich, N. A., Abnet, C. C., Al-Ghalith, G. A., et al. (2019). Reproducible, interactive, scalable and extensible microbiome data science using QIIME 2. *Nat. Biotechnol.* 37 (8), 852–857. doi: 10.1038/s41587-019-0209-9

Breiman, L. (2001). Random forests. *Mach. Learn.* 45 (1), 5–32. doi: 10.1023/A:1010933404324

Brooks, K. R., Raper, K. C., Ward, C. E., Holland, B. P., Krehbiel, C. R., and Step, D. L. (2011). Economic effects of bovine respiratory disease on feedlot cattle during backgrounding and finishing phases. *Prof. Anim. Scientist* 27 (3), 195–203. doi: 10.15232/S1080-7446(15)30474-5

Centeno-Martinez, R. E., Glidden, N., Mohan, S., Davidson, J. L., Fernández-Juricic, E., Boerman, J. P., et al. (2022). Identification of bovine respiratory disease through the nasal microbiome. *Anim. Microbiome* 4 (1), 15. doi: 10.1186/s42523-022-00167-y

Chai, J., Capik, S. F., Kegley, B., Richeson, J. T., Powell, J. G., and Zhao, J. (2022a). Bovine respiratory microbiota of feedlot cattle and its association with disease. *Vet. Res.* 53 (1), 4. doi: 10.1186/s13567-021-01020-x

Chai, J., Liu, X., Usdrowski, H., Deng, F., Li, Y., and Zhao, J. (2022b). Geography, niches, and transportation influence bovine respiratory microbiome and health. *Front. Cell. Infection Microbiol.* 12. doi: 10.3389/fcimb.2022.961644

Chiarello, M., McCauley, M., Villéger, S., and Jackson, C. R. (2022). Ranking the biases: The choice of OTUs vs. ASVs in 16S rRNA amplicon data analysis has stronger effects on diversity measures than rarefaction and OTU identity threshold. *PloS One* 17 (2), e0264443. doi: 10.1371/journal.pone.0264443

Cozens, D., Sutherland, E., Lauder, M., Taylor, G., Berry, C. C., and Davies, R. L. (2019). Pathogenic *Mannheimia haemolytica* invades differentiated bovine airway epithelial cells. *Infect. Immun.* 87 (6), 00078–00019. doi: 10.1128/iai.00078-19

Crosby, W. B., Pinnell, L. J., Richeson, J. T., Wolfe, C., Castle, J., Loy, J. D., et al. (2022). Does swab type matter? Comparing methods for *Mannheimia haemolytica* recovery and upper respiratory microbiome characterization in feedlot cattle. *Anim. Microbiome* 4 (1), 49. doi: 10.1186/s42523-022-00197-6

Dubrovsky, S. A., Van Eenennaam, A. L., Aly, S. S., Karle, B. M., Rossitto, P. V., Overton, M. W., et al. (2020). Preweaning cost of bovine respiratory disease (BRD) and cost-benefit of implementation of preventative measures in calves on California dairies: The BRD 10K study. *J. Dairy Sci.* 103 (2), 1583–1597. doi: 10.3168/jds.2018-15501

Duvallet, C., Gibbons, S. M., Gurry, T., Irizarry, R. A., and Alm, E. J. (2017). Meta-analysis of gut microbiome studies identifies disease-specific and shared responses. *Nat. Commun.* 8 (1), 1784. doi: 10.1038/s41467-017-01973-8

Edgar, R. (2018). Taxonomy annotation and guide tree errors in 16S rRNA databases. *PeerJ* 6, e5030. doi: 10.7717/peerj.5030

Edwards, T. A. (2010). Control methods for bovine respiratory disease for feedlot cattle. *Veterinary Clinics North America: Food Anim. Pract.* 26 (2), 273–284. doi: 10.1016/j.cvfa.2010.03.005

Fodor, A. A., Klem, E. R., Gilpin, D. F., Elborn, J. S., Boucher, R. C., Tunney, M. M., et al. (2012). The adult cystic fibrosis airway microbiota is stable over time and infection type, and highly resilient to antibiotic treatment of exacerbations. *PloS One* 7 (9), e45001. doi: 10.1371/journal.pone.0045001

Gaeta, N. C., Lima, S. F., Teixeira, A. G., Ganda, E. K., Oikonomou, G., Gregory, L., et al. (2017). Deciphering upper respiratory tract microbiota complexity in healthy calves and calves that develop respiratory disease using shotgun metagenomics. *J. Dairy Sci.* 100 (2), 1445–1458. doi: 10.3168/jds.2016-11522

Gray, N. D., and Head, I. M. (2008). "Microbial ecology," in *Encyclopedia of ecology*. eds. S. E. Jørgensen and B. D. Fath (Oxford: Academic Press), 2357–2368.

Holman, D. B., McAllister, T. A., Topp, E., Wright, A. D., and Alexander, T. W. (2015). The nasopharyngeal microbiota of feedlot cattle that develop bovine respiratory disease. *Vet. Microbiol.* 180 (1-2), 90–95. doi: 10.1016/j.vetmic.2015.07.031

Holman, D. B., Timsit, E., Amat, S., Abbott, D. W., Buret, A. G., and Alexander, T. W. (2017). The nasopharyngeal microbiota of beef cattle before and after transport to a feedlot. *BMC Microbiol.* 17 (1), 70. doi: 10.1186/s12866-017-0978-6

Hughes, J. B., Hellmann, J. J., Ricketts, T. H., and Bohannan, B. J. (2001). Counting the uncountable: statistical approaches to estimating microbial diversity. *Appl. Environ. Microbiol.* 67 (10), 4399–4406. doi: 10.1128/aem.67.10.4399-4406.2001

Johnston, D., Earley, B., Cormican, P., Murray, G., Kenny, D. A., Waters, S. M., et al. (2017). Illumina MiSeq 16S amplicon sequence analysis of bovine respiratory disease associated bacteria in lung and mediastinal lymph node tissue. *BMC Vet. Res.* 13 (1), 118. doi: 10.1186/s12917-017-1035-2

Kim, B. R., Shin, J., Guevarra, R., Lee, J. H., Kim, D. W., Seol, K. H., et al. (2017). Deciphering diversity indices for a better understanding of microbial communities. *J. Microbiol. Biotechnol.* 27 (12), 2089–2093. doi: 10.4014/jmb.1709.09027

Klima, C. L., Holman, D. B., Ralston, B. J., Stanford, K., Zaheer, R., Alexander, T. W., et al. (2019). Lower respiratory tract microbiome and resistome of bovine respiratory disease mortalities. *Microb. Ecol.* 78 (2), 446–456. doi: 10.1007/s00248-019-01361-3

Li, C., Zaheer, R., Kinnear, A., Jelinski, M., and McAllister, T. A. (2022). Comparative microbiomes of the respiratory tract and joints of feedlot cattle mortalities. *Microorganisms* 10 (1), 134. doi: 10.3390/microorganisms10010134

Lima, S. F., Teixeira, A. G., Higgins, C. H., Lima, F. S., and Bicalho, R. C. (2016). The upper respiratory tract microbiome and its potential role in bovine respiratory disease and otitis media. *Sci. Rep.* 6, 29050. doi: 10.1038/srep29050

Lin, H., Eggesbø, M., and Peddada, S. D. (2022). Linear and nonlinear correlation estimators unveil undescribed taxa interactions in microbiome data. *Nat. Commun.* 13 (1), 4946. doi: 10.1038/s41467-022-32243-x

Lin, H., and Peddada, S. D. (2020). Analysis of compositions of microbiomes with bias correction. *Nat. Commun.* 11 (1), 3514. doi: 10.1038/s41467-020-17041-7

Lopes, D. R. G., La Reau, A. J., Duarte, M. S., Detmann, E., Bento, C. B. P., Mercadante, M. E. Z., et al. (2019). The bacterial and fungal microbiota of nelore steers is dynamic across the gastrointestinal tract and its fecal-associated microbiota is correlated to feed efficiency. *Front. Microbiol.* 10. doi: 10.3389/fmicb.2019.01263

López-García, A., Pineda-Quiroga, C., Atxaerandio, R., Pérez, A., Hernández, I., García-Rodríguez, A., et al. (2018). Comparison of Mothur and QIIME for the analysis of rumen microbiota composition based on 16S rRNA amplicon sequences. *Front. Microbiol.* 9. doi: 10.3389/fmicb.2018.03010

Love, M. I., Huber, W., and Anders, S. (2014). Moderated estimation of fold change and dispersion for RNA-seq data with DESeq2. *Genome Biol.* 15 (12), 550. doi: 10.1186/s13059-014-0550-8

Lücken, A., Woudstra, S., Wente, N., Zhang, Y., and Krömker, V. (2022). Intramammary infections with *Corynebacterium* spp. in bovine lactating udder quarters. *PloS One* 17 (7), e0270867. doi: 10.1371/journal.pone.0270867

Martin, M. (2011). Cutadapt removes adapter sequences from high-throughput sequencing reads. *EMBnet.journal* 17 (1), 10–12. doi: 10.14806/ej.17.1.200. *Next Generation Sequencing Data Analysis*.

McDaneld, T. G., Kuehn, L. A., and Keele, J. W. (2018). Evaluating the microbiome of two sampling locations in the nasal cavity of cattle with bovine respiratory disease complex (BRDC). *J. Anim. Sci.* 96 (4), 1281–1287. doi: 10.1093/jas/sky032

McGrath, S., Katzenschlager, S., Zimmer, A. J., Seitel, A., Steele, R., and Benedetti, A. (2022). Standard error estimation in meta-analysis of studies reporting medians. *Stat. Methods Med. Res.* 32 (2), 373–388. doi: 10.1177/09622802221139233

McGrath, S., Zhao, X., Steele, R., Thombs, B. D., and Benedetti, A. (2020). Estimating the sample mean and standard deviation from commonly reported quantiles in meta-analysis. *Stat. Methods Med. Res.* 29 (9), 2520–2537. doi: 10.1177/0962280219889080

McMullen, C., Alexander, T. W., Orsel, K., and Timsit, E. (2020). Progression of nasopharyngeal and tracheal bacterial microbiotas of feedlot cattle during development of bovine respiratory disease. *Vet. Microbiol.* 248, 108826. doi: 10.1016/j.vetmic.2020.108826

McMullen, C., Orsel, K., Alexander, T. W., van der Meer, F., Plastow, G., and Timsit, E. (2019). Comparison of the nasopharyngeal bacterial microbiota of beef calves raised without the use of antimicrobials between healthy calves and those diagnosed with bovine respiratory disease. *Vet. Microbiol.* 231, 56–62. doi: 10.1016/j.vetmic.2019.02.030

McMurdie, P. J., and Holmes, S. (2013). phyloseq: an R package for reproducible interactive analysis and graphics of microbiome census data. *PloS One* 8 (4), e61217. doi: 10.1371/journal.pone.0061217

Moher, D., Liberati, A., Tetzlaff, J., and Altman, D. G. (2009). Preferred reporting items for systematic reviews and meta-analyses: the PRISMA statement. *BMJ* 339, b2535. doi: 10.1136/bmj.b2535

Mosca, A., Leclerc, M., and Hugot, J. P. (2016). Gut microbiota diversity and human diseases: should we reintroduce key predators in our ecosystem? *Front. Microbiol.* 7. doi: 10.3389/fmicb.2016.00455

Nakagawa, S., Poulin, R., Mengersen, K., Reinhold, K., Engqvist, L., Lagisz, M., et al. (2015). Meta-analysis of variation: ecological and evolutionary applications and beyond. *Methods Ecol. Evol.* 6 (2), 143–152. doi: 10.1111/2041-210X.12309

Nearing, J. T., Douglas, G. M., Hayes, M. G., MacDonald, J., Desai, D. K., Allward, N., et al. (2022). Microbiome differential abundance methods produce different results across 38 datasets. *Nat. Commun.* 13 (1), 342. doi: 10.1038/s41467-022-28034-z

Nicola, I., Cerutti, F., Grego, E., Bertone, I., Gianella, P., D'Angelo, A., et al. (2017). Characterization of the upper and lower respiratory tract microbiota in Piedmontese calves. *Microbiome* 5 (1), 152. doi: 10.1186/s40168-017-0372-5

Nikolova, V. L., Hall, M. R. B., Hall, L. J., Cleare, A. J., Stone, J. M., and Young, A. H. (2021). Perturbations in gut microbiota composition in psychiatric disorders: a review and meta-analysis. *JAMA Psychiatry* 78 (12), 1343–1354. doi: 10.1001/jamapsychiatry.2021.2573

Parker, A. M., Sheehy, P. A., Hazelton, M. S., Bosward, K. L., and House, J. K. (2018). A review of mycoplasma diagnostics in cattle. *J. Vet. Intern. Med.* 32 (3), 1241–1252. doi: 10.1111/jvim.15135

Prodan, A., Tremaroli, V., Brolin, H., Zwinderman, A. H., Nieuwdorp, M., and Levin, E. (2020). Comparing bioinformatic pipelines for microbial 16S rRNA amplicon sequencing. *PloS One* 15 (1), e0227434. doi: 10.1371/journal.pone.0227434

Raabis, S. M., Quick, A. E., Skarlupka, J. H. T., Suen, G., and Ollivett, T. L. (2021). The nasopharyngeal microbiota of preweaned dairy calves with and without ultrasonographic lung lesions. *J. Dairy Sci.* 104 (3), 3386–3402. doi: 10.3168/jds.2020-19096

Robert, R. (1979). The file drawer problem and tolerance for null results. *Psychol. Bull.* 86, 638–641. doi: 10.1037/0033-2909.86.3.638

Rohatgi, A. (2021). *Webplotdigitizer: version 4.5*.

Siddaway, A. P., Wood, A. M., and Hedges, L. V. (2019). How to do a systematic review: a best practice guide for conducting and reporting narrative reviews, meta-analyses, and meta-syntheses. *Annu. Rev. Psychol.* 70, 747–770. doi: 10.1146/annurev-psych-010418-102803

Slack, M. P. E. (2010). "Chapter 172 - gram-negative coccobacilli," in *Infectious diseases*, *3rd ed.* Eds. J. Cohen, S. M. Opal and W. G. Powderly (London: Mosby), 1738–1756.

Smith, J. S., Krull, A. C., Schleining, J. A., Derscheid, R. J., and Kreuder, A. J. (2020). Clinical presentations and antimicrobial susceptibilities of *Corynebacterium cystitidis* associated with renal disease in four beef cattle. *J. Vet. Intern. Med.* 34 (5), 2169–2174. doi: 10.1111/jvim.15844

Suástegui-Urquijo, Z., Jaramillo-Arango, C. J., Martínez-Hernández, F., Ureta, E., Trigo-Tavera, F., Suárez-Güemes, F., et al. (2015). Identification and phylogenetic relationship of *Mannheimia varigena* using the 16S rRNA subunit and the rpoB gene. *Ann. Microbiol.* 65 (3), 1781–1787. doi: 10.1007/s13213-014-1017-6

Tawfik, G. M., Dila, K. A. S., Mohamed, M. Y. F., Tam, D. N. H., Kien, N. D., Ahmed, A. M., et al. (2019). A step by step guide for conducting a systematic review and meta-analysis with simulation data. *Trop. Med. Health* 47, 46. doi: 10.1186/s41182-019-0165-6

Taylor, J. D., Fulton, R. W., Lehenbauer, T. W., Step, D. L., and Confer, A. W. (2010). The epidemiology of bovine respiratory disease: What is the evidence for predisposing factors? *Can. Veterinary J.* 51 (10), 1095–1102.

Team, R.C (2022). *R: a language and environment for statistical computing* (Vienna, Austria: R Foundation for Statistical Computing). 4.2.1.

Timsit, E., Holman, D., Hallewell, J., and Alexander, T. (2016). The nasopharyngeal microbiota in feedlot cattle and its role in respiratory health. *Anim. Front.* 6 (2), 44–50. doi: 10.2527/af.2016-0022

Timsit, E., Workentine, M., van der Meer, F., and Alexander, T. (2018). Distinct bacterial metacommunities inhabit the upper and lower respiratory tracts of healthy feedlot cattle and those diagnosed with bronchopneumonia. *Vet. Microbiol.* 221, 105–113. doi: 10.1016/j.vetmic.2018.06.007

USDA-APHIS (2013). Types and costs of respiratory disease treatments in U.S. feedlots.

van der Gast, C. J., Walker, A. W., Stressmann, F. A., Rogers, G. B., Scott, P., Daniels, T. W., et al. (2011). Partitioning core and satellite taxa from within cystic fibrosis lung bacterial communities. *Isme J.* 5 (5), 780–791. doi: 10.1038/ismej.2010.175

Viechtbauer, W. (2010). Conducting meta-analyses in R with the metafor package. *J. Stat. Software* 36 (3), 1–48. doi: 10.18637/jss.v036.i03

Wang, X., Howe, S., Wei, X., Deng, F., Tsai, T., Chai, J., et al. (2021). Comprehensive cultivation of the swine gut microbiome reveals high bacterial diversity and guides bacterial isolation in pigs. *mSystems* 34 (5), e0047721. doi: 10.1128/mSystems.00477-21

Wang, X., Tsai, T., Deng, F., Wei, X., Chai, J., Knapp, J., et al. (2019). Longitudinal investigation of the swine gut microbiome from birth to market reveals stage and growth performance associated bacteria. *Microbiome* 7 (1), 109. doi: 10.1186/s40168-019-0721-7

Wang, X., Tsai, T., Zuo, B., Wei, X., Deng, F., Li, Y., et al. (2022). Donor age and body weight determine the effects of fecal microbiota transplantation on growth performance, and fecal microbiota development in recipient pigs. *J. Anim. Sci. Biotechnol.* 13 (1), 49. doi: 10.1186/s40104-022-00696-1

Xu, R., Lu, R., Zhang, T., Wu, Q., Cai, W., Han, X., et al. (2021). Temporal association between human upper respiratory and gut bacterial microbiomes during the course of COVID-19 in adults. *Commun. Biol.* 4 (1), 240. doi: 10.1038/s42003-021-01796-w

Yang, K., Kruse, R. L., Lin, W. V., and Musher, D. M. (2018). *Corynebacteria* as a cause of pulmonary infection: a case series and literature review. *Pneumonia (Nathan)* 10, 10. doi: 10.1186/s41479-018-0054-5

Zeineldin, M., Elolimy, A., and Barakat, R. (2020). Meta-analysis of bovine respiratory microbiota: link between respiratory microbiota and bovine respiratory health. *FEMS Microbiol. Ecol.* 96 (8), fiaa127. doi: 10.1093/femsec/fiaa127

Zeineldin, M., Lowe, J., de Godoy, M., Maradiaga, N., Ramirez, C., Ghanem, M., et al. (2017). Disparity in the nasopharyngeal microbiota between healthy cattle on feed, at entry processing and with respiratory disease. *Vet. Microbiol.* 208, 30–37. doi: 10.1016/j.vetmic.2017.07.006

Zhao, J., Schloss, P. D., Kalikin, L. M., Carmody, L. A., Foster, B. K., Petrosino, J. F., et al. (2012). Decade-long bacterial community dynamics in cystic fibrosis airways. *Proc. Natl. Acad. Sci. U.S.A.* 109 (15), 5809–5814. doi: 10.1073/pnas.1120577109

frontiers | Frontiers in Cellular and Infection Microbiology

TYPE Original Research
PUBLISHED 26 September 2023
DOI 10.3389/fcimb.2023.1220943

OPEN ACCESS

EDITED BY
Jianmin Chai,
Foshan University, China

REVIEWED BY
Haojiang Zuo,
Sichuan University, China
Gangfeng Yan,
Fudan University, China
Kun Qin,
National Institute for Viral Disease Control and Prevention (China CDC), China

*CORRESPONDENCE
Yongping Lin
18928868278@163.com
Wenyan Qin
wenyanqin@capitalbiotech.com

†These authors have contributed equally to this work and share first authorship

RECEIVED 11 May 2023
ACCEPTED 04 September 2023
PUBLISHED 26 September 2023

CITATION
Xu Y, Jiang Y, Wang Y, Meng F, Qin W and Lin Y (2023) Metagenomic next-generation sequencing of bronchoalveolar lavage fluid assists in the diagnosis of pathogens associated with lower respiratory tract infections in children.
Front. Cell. Infect. Microbiol. 13:1220943.
doi: 10.3389/fcimb.2023.1220943

Metagenomic next-generation sequencing of bronchoalveolar lavage fluid assists in the diagnosis of pathogens associated with lower respiratory tract infections in children

Yunjian Xu[1†], Yueting Jiang[1†], Yan Wang[2], Fanlin Meng[2], Wenyan Qin[2*] and Yongping Lin[1,3*]

[1]Department of Clinical Laboratory, The Key Laboratory of Advanced Interdisciplinary Studies Center, The First Affiliated Hospital of Guangzhou Medical University, National Center for Respiratory Medicine, National Clinical Research Center for Respiratory Disease, Guangzhou, China, [2]CapitalBio Technology Inc., Beijing, China, [3]Department of Laboratory Medicine, Cancer Hospital Chinese Academy of Medical Sciences, Shenzhen Center, Shenzhen, China

Worldwide, lower respiratory tract infections (LRTI) are an important cause of hospitalization in children. Due to the relative limitations of traditional pathogen detection methods, new detection methods are needed. The purpose of this study was to evaluate the value of metagenomic next-generation sequencing (mNGS) of bronchoalveolar lavage fluid (BALF) samples for diagnosing children with LRTI based on the interpretation of sequencing results. A total of 211 children with LRTI admitted to the First Affiliated Hospital of Guangzhou Medical University from May 2019 to December 2020 were enrolled. The diagnostic performance of mNGS versus traditional methods for detecting pathogens was compared. The positive rate for the BALF mNGS analysis reached 95.48% (95% confidence interval [CI] 92.39% to 98.57%), which was superior to the culture method (44.07%, 95% CI 36.68% to 51.45%). For the detection of specific pathogens, mNGS showed similar diagnostic performance to PCR and antigen detection, except for *Streptococcus pneumoniae*, for which mNGS performed better than antigen detection. *S. pneumoniae*, cytomegalovirus and *Candida albicans* were the most common bacterial, viral and fungal pathogens. Common infections in children with LRTI were bacterial, viral and mixed bacterial-viral infections. Immunocompromised children with LRTI were highly susceptible to mixed and fungal infections. The initial diagnosis was modified based on mNGS in 29.6% (37/125) of patients. Receiver operating characteristic (ROC) curve analysis was performed to predict the relationship between inflammation indicators and the type of pathogen infection. BALF mNGS improves the sensitivity of pathogen detection and provides guidance in clinical practice for diagnosing LRTI in children.

KEYWORDS

lower respiratory tract infections, pathogen diagnosis, bronchoalveolar lavage fluid, metagenomic next-generation sequencing, traditional methods, medication adjustment, children

1 Introduction

Lower respiratory tract infections (LRTI) are the deadliest infectious diseases worldwide and the fourth leading cause of death (World Health Organization, 2020). Early and accurate identification of the etiology of LRTI is essential for effective pathogen targeted therapy. However, pathogen identification is limited due to the limitations of traditional microbiological detection. Diagnosis is further complicated by noninfectious inflammatory syndromes that mimic LRTI (Langelier et al., 2018a). Currently, traditional detection methods, including microscopy, pathogen culture and isolation, biochemical testing, immunology, and polymerase chain reaction (PCR) testing, are used mainly to identify LRTI pathogens in children. However, these methods have shortcomings in terms of sensitivity, specificity, timeliness, and amount of information obtained (Jain et al., 2015; Zhang et al., 2018; Rajapaksha et al., 2019). Moreover, it is impossible to quickly identify unknown or rare pathogenic microorganisms. In the absence of a clear microbiological diagnosis, clinicians may assume that symptoms are caused by noninfectious inflammation and prescribe empirical corticosteroids, which can exacerbate occult infections (Wilson et al., 2014).

Metagenomic next-generation sequencing (mNGS) is a novel technique for rapid, efficient, and unbiased acquisition of nucleic acid sequence information that can be used to identify pathogens in a given sample. Moreover, the advent of rapid mNGS has extended its applications from laboratory research to clinical diagnostics (Goldberg et al., 2015). mNGS has been used mainly to diagnose emerging pathogens and rare infectious diseases (Yao et al., 2016). For example, in the unusual pneumonia outbreak reported in Wuhan in December 2019, mNGS was performed using RNA extracted from patient bronchoalveolar lavage fluid (BALF), which rapidly identified a novel coronavirus pathogen (SARS-CoV-2) present in high abundance (Chen et al., 2020). Rapid and accurate diagnostic methods for detecting pathogenic microorganisms are extremely crucial for disease control and treatment. mNGS is already being successfully applied for pneumonia, meningitis, liver abscess, endometritis, and endophthalmitis diagnosis using BALF, sputum, cerebrospinal fluid, pleural fluid, and vitreous humor specimens (Ai et al., 2018; Langelier et al., 2018b; Moreno et al., 2018; Miller et al., 2019).

In recent years, the feasibility of mNGS for etiological detection and identification of respiratory tract infections has been demonstrated (Miao et al., 2018; Li et al., 2020). However, numerous challenges remain, including the interpretation of mNGS results, human genome interference and other common issues. In addition, there are few studies on BALF mNGS in a large cohort of children with LRTI, which needs to be addressed. Here, we summarize the mNGS results for 229 BALF samples from 211 children with LRTI and sought to validate the value of mNGS for diagnosing children with LRTI based on the interpretation of sequencing results.

2 Materials and methods

2.1 Patients

This study retrospectively analyzed the medical records of 211 children with LRTI who were admitted to the First Affiliated Hospital of Guangzhou Medical University from May 2019 to December 2020. The study was approved by the institutional ethics committee of the First Affiliated Hospital of Guangzhou Medical University (No. 2021K-40). The medical records contained patient information, clinical diagnosis and symptoms, results of mNGS and traditional microbiological assays, information on relevant clinical laboratory tests and clinical medication information. The inclusion criteria were as follows: 1) chest imaging revealing abnormalities; 2) infection symptoms that did not improve after empirical treatment; patients presenting with persistent expectoration, fever, and shortness of breath, and patients with unsatisfactory clinical outcomes; re-examination of chest imaging showed no improvement, and the etiology needed to be clarified; and 3) for immunocompromised patients complicated with septic shock or multiple organ failure, the attending physician may have advised the use of mNGS. The exclusion criteria were patients unable to fulfill the required medical follow-up. In this study, 229 BALF samples from 211 children with LRTI were assessed using mNGS (DNA and RNA) assays. Resampling for testing occurred in the following circumstances: 1) results were not consistent with diagnosis or treatment; 2) infection improved but was not cured; 3) samples were resampled for mNGS detection in cases with negative mNGS results but clinical manifestations of infection; and 4) repeated infection was observed for a long time.

A total of 39 patients were considered immunocompromised when clinically diagnosed, including 1) patients with blood-related diseases (e.g., aplastic anemia, thalassemia, and congenital neutrophil deficiency) or 2) cancers (e.g., solid malignancy and hematological malignancy), 3) patients who received invasive surgery (e.g., heart surgery and a patient with tumor resection), and 4) patients diagnosed with kidney diseases (e.g., uremia and nephrotic syndrome) or 5) multiple organ failure and other autoimmune deficiencies (Ramírez, 2013; Tecklenborg et al., 2018; Spoor et al., 2019; Zinter et al., 2019; El Hasbani et al., 2022; Xi et al., 2022; Zaimoku et al., 2022).

2.2 Flow of BALF sample collection

BALF specimen collection was performed as previously described with some modifications (Collins et al., 2014; Hogea et al., 2020). 1) Site selection: Lesion segments were selected for patients with limited lesions. For diffuse lesions, the right middle lobe of the lung or the lingual segment of the left upper lobe of the lung was selected. 2) Local anesthesia: 1-2 mL of 2% lidocaine was injected into the biopsy hole of the lavage lung segment to perform local anesthesia; 1-2 mL of 2% lidocaine could also be administered to patients under intravenous combination anesthesia who had

strong airway reactions. 3) Saline injection: After the tip of the bronchoscope was wedged in the opening of the target bronchial segment or inserted subterminal, sterile saline (37°C or room temperature) was rapidly injected through the operating channel in a total volume of 20-30 mL, and multiple injections (3-10 mL each time) were performed. 4) Negative pressure suction: Immediately after the injection of saline, BALF was obtained by suction with an appropriate negative pressure (commonly recommended below 100-200 mm Hg), and the total recovery rate was more than 40%. 5) BALF collection: The recovered fluid contained approximately 10 mL of secretions from bronchial terminals and alveoli. The potentially contaminated portion from the front was discarded, and the remaining portion of at least 3 mL was collected for immediate inspection.

2.3 Traditional methods detection

Simultaneously, sputum, throat swab and blood samples were collected. All the above samples, including BALF samples, were immediately subjected to the following laboratory tests. Culture: Blood agar, Sabouraud dextrose agar, chocolate agar, and MacConkey agar used to manually inoculate and culture pathogens were purchased from Autobio Diagnostics Co., Ltd. (China). Bacteria were cultured at 35°C for 24 to 48 hours, and fungi were cultured for 7 days. The VITEK® 2 system (France) was used for automated bacterial and fungal identification. The sample types included BALF, sputum, blood, pleural effusion, cerebrospinal fluid, urine, or stool samples. Nucleic acid detection: The processes were carried out according to the protocols of commercial kits. In this study, 15 nucleic acid detection kits were used from seven suppliers; the detection kits were for *Mycobacterium tuberculosis* (MTB) and *Chlamydia trachomatis* (Qiagen, Shenzhen, China), cytomegalovirus (CMV), Epstein–Barr virus (EBV), enterovirus, coxsackievirus, human herpes simplex virus 1 (HSV1), and *Mycoplasma pneumoniae* (MP) (Daan Gene, China), adenovirus (HAdV) (Hecin, China), respiratory syncytial virus (RSV) and influenza virus A/B (Huayin, China), HSV2 (Biot Gene, China), hepatitis B virus (Amplly, China), and hepatitis C virus (Sansure, China). The sample types included BALF, sputum, swab, blood, pleural effusion, cerebrospinal fluid, urine, or stool samples. Antibody detection: In this study, the MP antibody detection test kit (passive agglutination method) was purchased from Fujirebio (Japan). This kit only detects MP antibodies (IgM and IgG) and does not directly detect MP. Therefore, a positive result does not confirm MP infection, and comprehensive evaluation of the patient's condition should be made by combining clinical symptoms and test results. The sample type was blood. Antigen detection: The processes were carried out according to the protocols of the commercial kits. In this study, five antigen detection kits were used from four suppliers; the detection kits were for *S. pneumoniae* (colloidal gold method) (Abbott, USA), rotavirus (colloidal gold method) (Wantai, China), *Aspergillus* spp. (ELISA), *Cryptococcus* (ELISA) (Genobio, China), and seven respiratory viruses (namely, influenza A/B virus, human parainfluenza virus 1-3 (HPIV 1-3), RSV, HAdV) (immunofluorescence method) (B&C, China). The sample types for detecting *S. pneumoniae* were cerebrospinal fluid and urine, those for detecting *Aspergillus* spp. or *Cryptococcus* were BALF and blood, those for detecting rotavirus were stool, and those for detecting the seven respiratory viruses were nasal swabs. The commercial kits used in this study were all certified and approved for clinical testing by the China National Medical Products Administration.

Quality control of the manual culture method: The quality control strains were *Pseudomonas aeruginosa* ATCC 27853, *Escherichia coli* ATCC 25922, *Escherichia coli* ATCC 35218, *Staphylococcus aureus* ATCC 25923, and *Staphylococcus aureus* ATCC 29213. Quality control of automated culture and identification: conducted every two weeks. The quality control strains were *Staphylococcus sciuri* ATCC 29061, *Candida albicans* ATCC 14053, *Eikenella corrodens* BAA-1152, *Enterobacter aerogenes* ATCC 13048 and *Enterobacter hormaechei* ATCC 700323. Positive controls for Hepatitis B/C virus nucleic acid testing were obtained from Conchestan (China). Controls are included in the remaining commercial kits used for clinical testing.

2.4 Metagenomic next-generation sequencing using BALF samples

BALF samples were obtained; 3 mL of BALF was placed in a sterile sputum container, stored at 4°C, and sent to CapitalBio (Guangzhou, China) for mNGS detection. DNA from each BALF sample (0.5 mL) was extracted using a QIAamp DNA Microbiome Kit (Cat#51704, QIAGEN, Germany), and RNA was extracted using a QIAamp Viral RNA Mini Kit (Cat#52904, QIAGEN, Germany). The extracted RNA was reverse transcribed using random primers, and cDNA was pooled with DNA from the same sample for sequencing library preparation. The pooled nucleic acid was enzymatically fragmented to a size of 200-300 bp, and sequencing libraries were constructed through end repair, adapter ligation and PCR amplification. Sequencing templates were prepared with OneTouch2 System (Life Technologies, USA), and after quality control, sequencing was performed using a BioelectronSeq 4000 sequencer (CapitalBio, China) based on a semiconductor platform Ion Torrent Proton™ sequencer. A negative control sample consisting of water was used in each run to monitor potential contamination.

The original sequencing data were subjected to quality control, and adapter reads, low quality, reads with N (represents uncertain base information) > 5, reads with lengths less than 50 bp, or low complexity were removed. The remaining high-quality sequencing data were mapped to the human reference genome grch38 for depletion of human host sequences using Bowtie2 software. Subsequently, nonhuman sequences were classified by simultaneous alignment to the genomic sequence databases downloaded from the NCBI and PATRIC, which contain 13,992 bacterial species, 1,659 fungal species, 13,000 viral species and 287 parasitic pathogens. To judge the suspected pathogens in the clinical samples, we reviewed data for different types of samples

from healthy people and calculated relevant reference values, including the hit read number and coverage of all bacteria, fungi, viruses and parasites detected. Moreover, pathogens detected in the negative control sample (water) were removed from the results for the clinical samples. The final pathogen detection results included a list of suspected pathogens, the number of hit reads and genome-level coverage statistics.

Human nucleic acid depletion is one of the challenges of mNGS (Diao et al., 2021). In this study, the following two methods were mainly used to remove human nucleic acids. 1) The processed BALF sample was centrifuged, and pathogens were distributed in the supernatant and precipitate based on their different structures. The precipitate contains the majority of human host cells and pathogens with cellular structures such as bacteria and fungi. Differential lysis was performed based on the different structures of human host cells and pathogen cells, and the nucleic acids released from human host cells were digested using nucleases for the first depletion of host nucleic acids. This process was repeated once. 2) The supernatant containing viral nucleic acids and a small portion of human host cells was subjected to two rounds of centrifugation to remove as many human host cells as possible. Then, the pathogen sequences were enriched. After filtering and deduplication, the average total number of reads was 9,518,921 (320,578-26,524,467). Human reads accounted for an average of 69.96% (6.56%-93.69%); microorganism reads accounted for an average of 6.70% (0.12%-66.81%); and unmapped reads accounted for an average of 23.34% (6.06%-60.30%).

mNGS for each BALF cost approximately $600, and the result could be obtained about 24 hours of the sample's arrival at the testing laboratory.

2.5 Criteria for a positive mNGS result

1) Positive indicators of comprehensive interpretation were as follows: microbial characteristics (cell wall thickness, genome size), number of detected sequences, genome coverage percent and estimated concentration (copies/mL). Above the threshold of the parameter, the organism was judged as a high- or medium-confidence pathogen. 2) Additional positive indicators were as follows: bacteria, fungi, or parasites: cover length > 3000 bp; viruses: cover length > 300 bp. 3) When clinically confirming pathogenic microorganisms, a comprehensive judgment was made based on the pathogen, sample, and clinical characteristics.

2.6 Statistical analysis

The sensitivity (TPR), specificity (TNR), positive predictive value (PPV), and negative predictive value (NPV) were calculated and compared between mNGS and traditional pathogen detection methods. Statistical analyses were performed using SPSS software v.24.0. Pearson's chi-square test or Fisher's exact test was used for discrete variables where appropriate. P values < 0.05 were considered significant, and all tests were two-tailed.

3 Results

3.1 Samples and patient characteristics

A total of 211 children with LRTI were the subjects of this study (Supplementary Table 1). There were 121 males and 90 females. Their average age was 5.00 ± 4.30 years. Among the 211 patients, 172 were non-immunocompromised, and 39 were immunocompromised (Table 1). Among the 39 immunocompromised children with LRTI were diagnosed with nine kinds of diseases, namely, aplastic anemia, thalassemia, congenital neutrophil deficiency, invasive surgery, solid malignancy, kidney disease, multiple organ failure, hematological malignancy, and other autoimmune deficiencies (Table 1; Supplementary Table 1).

3.2 Comparison of diagnostic performances between mNGS and traditional methods in non-immunocompromised children with LRTI

Supplementary Tables 2, 3 list the etiological detection results for 172 enrolled non-immunocompromised children with LRTI, including the results for 186 samples by mNGS, 177 samples by culture, 165 samples by PCR detection, 136 samples by antibody detection (serological assay) for MP, 137 samples by antigen detection for bacteria and fungi, and 154 samples by antigen detection for viruses. The etiological detection results for the non-immunocompromised children with LRTI showed 176

TABLE 1 Characteristics of 211 children with LRTI.

Characteristic	mNGS (n = 211)
Age (years)	5.00 ± 4.30
Sex	
Female, n (%)	90 (42.65%)
Male, n (%)	121 (57.35%)
Non-immunocompromised, n (%)	172 (81.52%)
Immunocompromised, n (%)	39 (18.48%)
Aplastic anemia	2 (5.13%)
Thalassemia	3 (7.69%)
Congenital neutrophil deficiency	1 (2.56%)
Hematological malignancy	19 (48.72%)
After invasive surgery	2 (5.13%)
Solid malignancy	3 (7.69%)
Kidney disease	2 (5.13%)
Multiple organ failure	1 (2.56%)
Other autoimmune deficiency	6 (15.38%)

10.3389/fcimb.2023.1220943

TABLE 2 Diagnostic performance of mNGS compared with traditional methods for non-immunocompromised children with LRTI.

	Pathogen	Sample number	Corresponding mNGS positive	Traditional method positive	Double positive	Concordance rate (%)	P value
PCR	MTB	142	1	2	1	99.30	1
	MP	104	12	19	6	81.73	0.242
	Chlamydia trachomatis	23	1	0	0	95.65	1
	CMV	65	12	16	8	81.54	0.393
	HAdV	79	16	20	12	84.81	0.448
	RSV	8	2	1	1	87.5	1
	Influenza A virus	21	1	2	1	95.24	1
	Influenza B virus	20	0	0	0	100.00	/
	EBV	30	0	4	0	86.67	0.112
	Enterovirus	8	0	0	0	100.00	/
	Coxsackie virus	3	0	0	0	100.00	/
	Hepatitis B virus	1	0	1	0	0.00	1
	Hepatitis C virus	2	0	0	0	100.00	/
	HSV 1	2	0	0	0	100.00	/
	HSV 2	2	0	0	0	100.00	/
Detection of antibody (serological assay)	MP	136	10	78	8	47.06	**< 0.001**
Detection of bacterial and fungal antigens	*S. pneumoniae*	88	36	7	6	64.77	**< 0.001**
	Aspergillus spp.	67	4	0	0	94.03	0.119
	Cryptococcus	68	0	1	0	98.53	0.181
Detection of viral antigens	Influenza A virus	153	2	1	1	99.35	1
	Influenza B virus	153	0	0	0	100.00	/
	HPIV 1	153	2	2	0	97.39	1
	HPIV 2	153	0	0	0	100.00	/
	HPIV 3	153	11	3	3	94.77	0.052
	RSV	153	11	11	8	96.08	1
	HAdV	153	18	8	7	92.16	0.063
	Rotavirus	14	0	0	0	100.00	/

MTB, Mycobacterium tuberculosis; MP, Mycoplasma pneumoniae; CMV, cytomegalovirus; HAdV, adenovirus; EBV, Epstein-Barr virus; RSV, respiratory syncytial virus; RhV, rhinovirus; HPIV, human parainfluenza virus; HSV, herpes simplex virus. "Concordance rate" represents the total of the positive and negative concordance rates.
The bold represent significant differences in data and can be replaced with regular fonts in this table.

cases to be positive when using BALF for mNGS, with a positive rate of 94.62% (176/186, 95% CI 91.35% to 97.90%). Seventy-eight cases were positive based on the culture method, with a positive rate of 44.07% (78/177, 95% CI 36.68% to 51.45%). The culture method is regarded as the gold standard for the clinical diagnosis of bacterial and fungal infections. Comparing the culture method with the corresponding mNGS results, the TPR, TNR, PPV and NPV of mNGS were 98.72%, 7.07%, 45.56% and 87.50%, respectively. A

total of 95.48% (169/177, 95% CI 92.39% to 98.57%) of the BALF mNGS results were positive, which was superior to the culture method (χ^2= 110.92, P <.001) (Supplementary Table 3). Antibody detection (serological assay) is the main method for the clinical diagnosis of MP. The positive rate of the serological assay for MP was 57.35% (78/136, 95% CI 48.93% to 65.77%). The corresponding BALF mNGS positive rate was 7.35% (10/136, 95% CI 2.91% to 11.80%), which was lower than that for serological detection (χ^2= 77.68, P <.001). The concordance rate between mNGS and serological detection for MP was 47.06%, while the concordance rate between mNGS and PCR was 81.73%, indicating that there may be a high false-positive rate for serological detection of MP (Table 2, Supplementary Table 3). PCR and antigen detection were used for clinically suspected specific pathogens. Most of the concordance rates of mNGS and the traditional methods were above 85%. The positive rates of mNGS and traditional methods (PCR, antigen detection for viruses) for specific pathogens differed, but there were no significant differences (Table 2). Antigen detection of *Aspergillus* spp. and *Cryptococcus*, did not differ significantly from mNGS, while for *S. pneumoniae*, the positive rate of BALF mNGS was 40.91% (36/88, 95% CI 30.43% to 51.39%), which was superior to the rate for antigen detection of *S. pneumoniae* (7.95%, 7/88, 95% CI 2.19% to 13.72%) (χ^2= 25.88, P <.001) (Table 2).

The results showed no significant differences in the detection of pathogens between mNGS and PCR or in antigen detection, except for *S. pneumoniae*. In addition, BALF mNGS was superior to the culture method and antigen detection for *S. pneumoniae*, but the positive rate for diagnosing MP was lower than that of the serological assay.

3.3 Comparison of pathogens detected by the culture method and mNGS in non-immunocompromised children with LRTI

The culture method is the primary method used in clinical microbiology laboratories for identifying bacterial and fungal pathogens of LRTI. Comparison of the results for mNGS and culture for the identification of suspected pathogens in all 177 samples is shown in Figure 1. mNGS and culture were both positive for 77 of the 177 samples (43.50%). Seven were both negative (3.95%), 92 samples were positive only by mNGS (51.98%), and only one sample was positive by culture (0.56%). For the 77 double-positive samples, the concordance between mNGS and culture was assessed as match (34, 44.16%), partly match (9, 11.69%), and mismatch (34, 44.16%) (Figure 1D). For culture results, 36 kinds of pathogens were detected, namely, 30 kinds of bacteria and six kinds of fungi (Figures 1A, B). The most frequently detected bacteria were *Pseudomonas aeruginosa* (10/177), *Klebsiella pneumoniae* (10/177) and *Haemophilus influenzae* (10/177), followed by *Staphylococcus aureus* (8/177) (Figure 1A). *Candida albicans* (4/177) was the most frequently detected fungus (Figure 1B). According to mNGS, 90 kinds of microorganisms were determined, namely, 24 kinds of viruses, 53 kinds of bacteria, 10 kinds of fungi, one *Mycoplasma* and two kinds of *Chlamydia* (Figure 1). Among the microbes detected, *S. pneumoniae* (74/177) was the most frequently detected bacterium, followed by *Staphylococcus aureus* (30/177), *Haemophilus influenzae* (25/177), *Staphylococcus epidermidis* (20/177) and *Pseudomonas aeruginosa* (13/177) (Figure 1A). The top six detected viruses were CMV (25/177), rhinovirus subtype A (RhV-A) (20/177), HAdV-B (18/177), RhV-C (12/177), human parainfluenza virus type 3 (HPIV3) and RSV (11/177) (Figure 1C). *Candida albicans* (15/177) was the most frequently detected fungus (Figure 1B). Among all BALF samples, only one case of MTB was detected (Figure 1A). A total of 38 species of bacteria and six species of fungi were detected only by mNGS. Fifteen kinds of bacteria and two kinds of fungi were detected only by culture. mNGS has a broader spectrum for pathogen detection and can detect more definite or probable pathogens than culture.

3.4 Comparison of types of pathogens detected in non-immunocompromised and immunocompromised children with LRTI

According to the mNGS results, the most frequently detected pathogens were bacteria, followed by viruses and fungi (Figures 1A–C, 2A). For the 186 samples from 172 non-immunocompromised children, except for 10 samples for which no pathogens were detected, 44.32% of the infected children were diagnosed with single bacterial, viral, fungal, or *Mycoplasma* infection (30.11%, 53/176; 11.93%, 21/176; 1.14%, 2/176; 1.14%, 2/176). The mixed infections observed were mainly bacterial-viral (34.09%, 60/176) and bacterial-viral-fungal (10.23%, 18/176) (Figures 1, 2B). For the 43 samples from 39 immunocompromised children, except for 4 samples for which no microbes were detected, 41.03% of the children were diagnosed with single bacterial or viral infections (25.64%, 10/39; 15.38%, 6/39). Mixed infections were mainly bacterial-viral (33.33%, 13/39) and bacterial-viral-fungal (17.95%, 7/39) (Figure 2C). Compared with the non-immunocompromised children with LRTI, the immunocompromised children with LRTI were more susceptible to mixed infections (58.97% > 55.68%, P = 0.708) and fungal infections (25.64% > 17.05%, P = 0.212); however, there were no significant differences.

3.5 Medication strategy adjustment according to mNGS detection

Complete information on medication orders was available for 125 of the 211 patients (Supplementary Table 4). Forty-six patients underwent medication adjustments within three days of obtaining the mNGS results. Thirty-two patients had their medication adjusted within 24 hours based on the mNGS results, and in five patients, their medication was adjusted within two days of obtaining the mNGS results. For the 37 patients (29.60%, 37/125) whose medications were adjusted based on the mNGS results within two days, the adjustments were as follows: antibacterial drugs were increased for 13 patients; antibacterial drugs were changed for 10; antifungal drugs were increased for six; antifungal drugs were reduced for two; antiviral drugs were increased for three; the antibacterial drug was replaced and the antifungal drug increased

10.3389/fcimb.2023.1220943

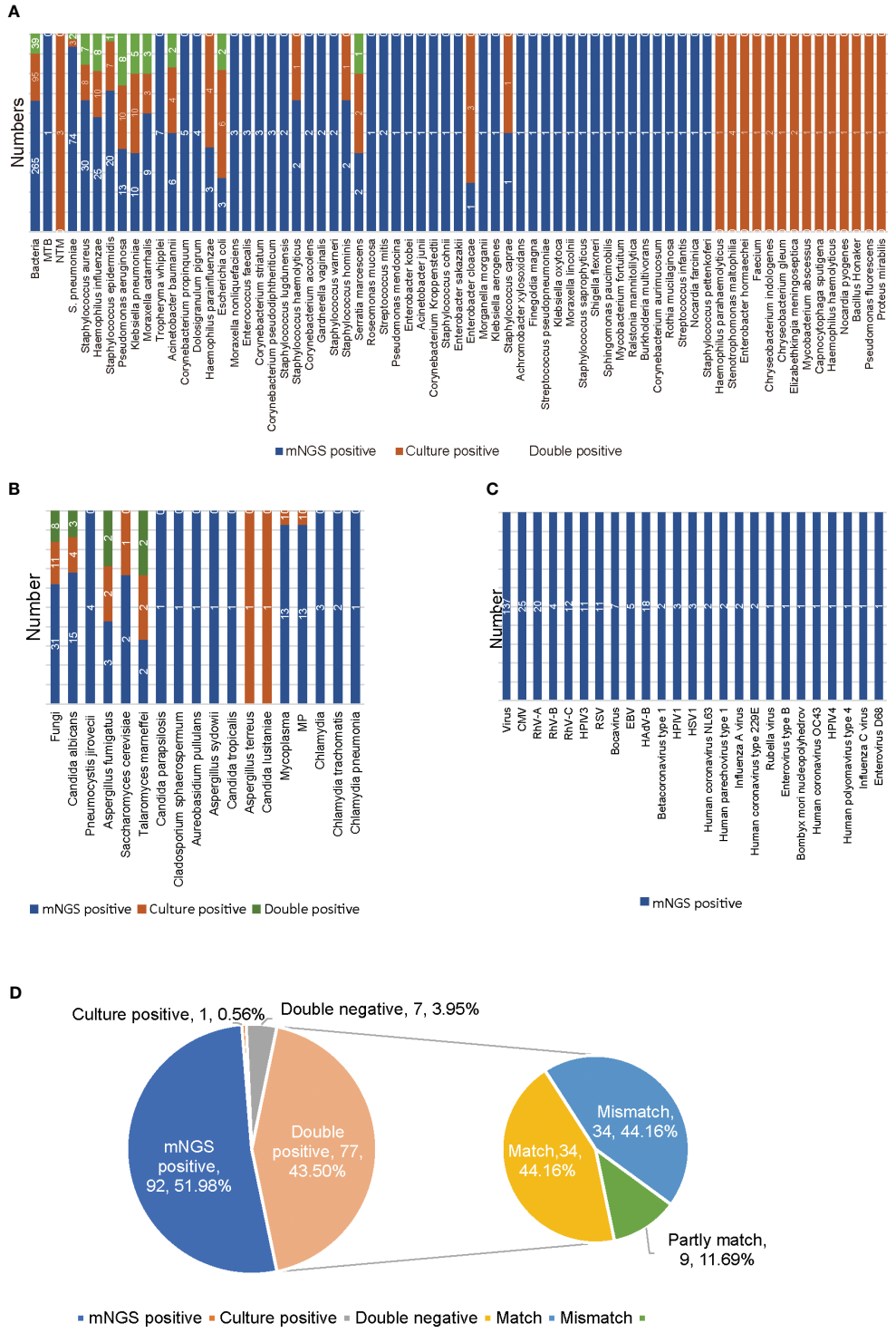

FIGURE 1
Results of mNGS and culture for non-immunocompromised children with LRTI. **(A)** The distribution of bacterial infections in 177 non-immunocompromised LRTI samples detected by mNGS and culture. **(B)** The distribution of fungal, *Mycoplasma* and *Chlamydia* infections in 177 non-immunocompromised LRTI samples detected by mNGS and culture. **(C)** The distribution of viral infections in 177 non-immunocompromised LRTI samples detected by mNGS. **(D)** The concordance between mNGS and culture for 177 non-immunocompromised LRTI samples. Culture results were used as the standard. Match indicates that all the pathogens detected by culture were also found by mNGS. Mismatch indicates that all the microorganisms detected by culture were not found by mNGS. Partly match indicates that some of the pathogens detected by culture were found by mNGS. MTB, *Mycobacterium tuberculosis*; NTM, nontuberculous mycobacteria; MP, *Mycoplasma pneumoniae*; CMV, cytomegalovirus; RhV, rhinovirus; HAdV, adenovirus; EBV, Epstein-Barr virus; RSV, respiratory syncytial virus; HPIV, human parainfluenza virus; HSV, herpes simplex virus.

10.3389/fcimb.2023.1220943

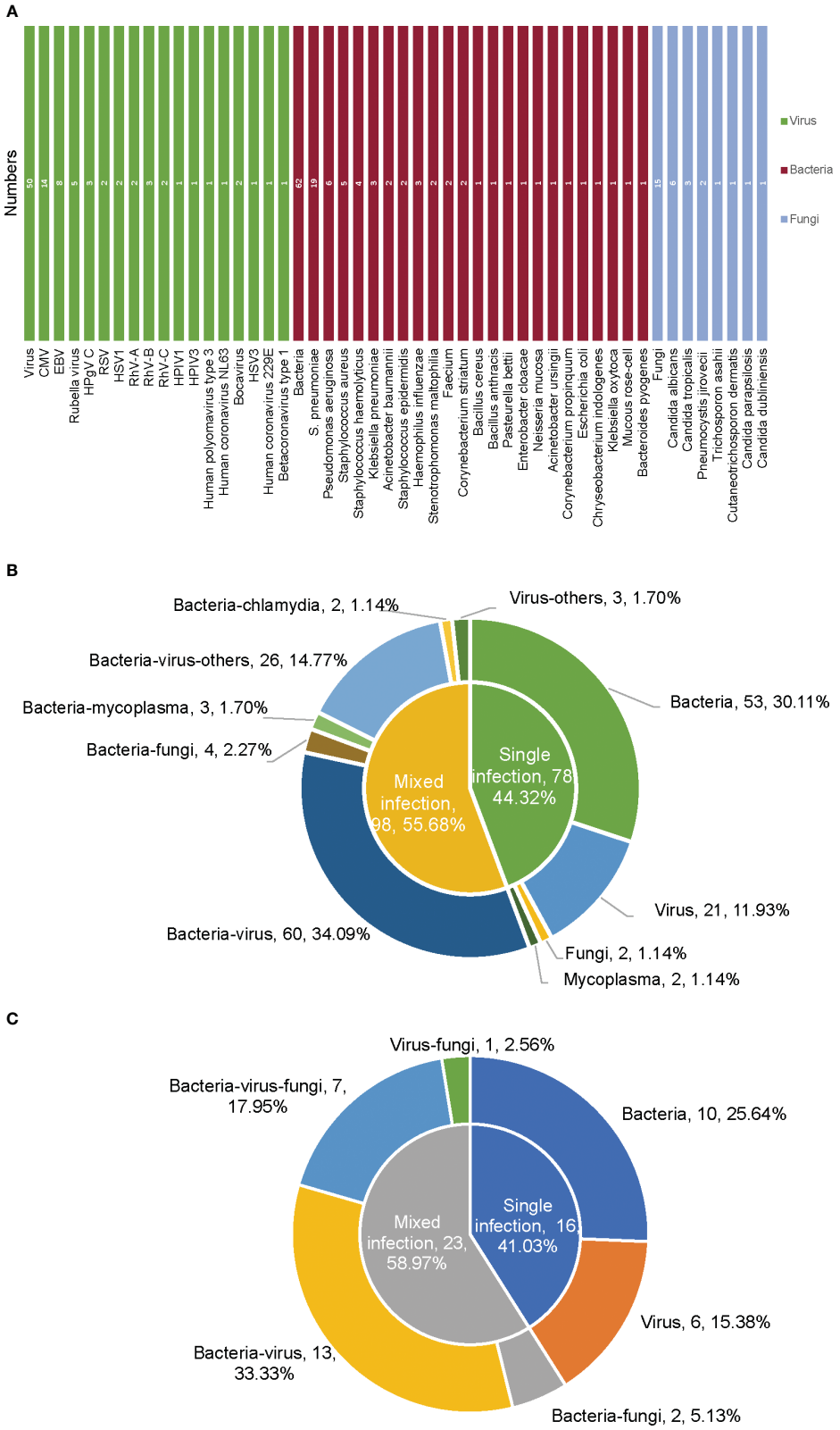

FIGURE 2
Types of pathogens based on mNGS in non-immunocompromised and immunocompromised children with LRTI. **(A)** Pathogen spectrum of infection in 39 immunocompromised children with LRTI detected by mNGS. **(B)** Pathogen types of infection in 172 non-immunocompromised children with LRTI detected by mNGS. **(C)** Pathogen types of infection in 39 immunocompromised children with LRTI detected by mNGS. CMV, cytomegalovirus; EBV, Epstein–Barr virus; RSV, respiratory syncytial virus; RhV, rhinovirus; HPIV, human parainfluenza virus; HSV, herpes simplex virus.

for one, the antiviral drug was reduced and the antibacterial drug replaced for one; and the antibacterial drug was reduced and the antifungal drug increased for one. 63.20% (79/125) of cases were abandoned for adjustment due to consistent results between previous antibiotic usage and mNGS testing. All 125 patients with mNGS test and complete medication information on medication orders were improved and discharged.

3.6 Inflammation indicators predict types of pathogen infection in children with LRTI

Receiver operating characteristic (ROC) curve analysis was performed to assess the predictive performance of inflammation indicators and the type of pathogen infection and to calculate the area under curve (AUC). In this study, 78 samples, namely, 28 bacterial, 12 viral, and 38 bacterial-viral infection samples with complete procalcitonin (PCT), C-reactive protein (CRP) and routine blood data, were used for analysis of inflammation indicators and types of infectious pathogens (Supplementary Table 5). Univariate logistic regression analysis showed that neutrophils (NEUT) were able to distinguish single (bacterial or viral) and mixed (bacterial and viral) infections, and the AUC value was 0.711 (Figure 3A). PCT, CRP and eosinophils (EO) were also able to distinguish bacterial infections from viral infections, with AUC values of 1, 1 and 0.929, respectively (Figures 3B-D). Multivariate logistic regression analysis showed that four indicators, NEUT, lymphocyte (LYMPH), monocyte (MONO) and basophil (BASO), were able to distinguish single infections from mixed infections (Figure 3E), with an AUC value of 0.767. However, there were no significant differences in the logistic regression analysis, and more samples from children with LRTI are needed to further study the relationship between inflammatory indicators and different types of infection.

4 Discussion

For LRTI, early etiological diagnosis is necessary. However, traditional culture methods are time-consuming and have low positive detection rates. mNGS is suitable for detecting pathogens that cannot be identified by other detection technologies and for patients who do not respond to standard antibacterial treatments (Li et al., 2020). For rare and slow-growing pathogenic microorganisms, mNGS has considerable advantages, such as reducing the time required for diagnosis and confirmation of mixed infections, facilitating targeted antibacterial therapy, and improving patient prognosis.

We know that the lung is not sterile and supports the existence of a different microbiota in the upper and lower compartments (Cabrera-Rubio et al., 2012). Given its operability, several noninvasive and invasive procedures have been used to surrogate or proxy lung tissue for sampling of the pulmonary environment (Yi et al., 2022). BALF, a common method for sampling the lung microbiome, is more similar to the lower airway than sputum, and has limited contamination from the upper airway or oral cavity. While other microbial sampling methods include bronchial brushing and tracheal aspirate, the application range is limited (Yi et al., 2022). BALF specimen collection in children should be carried out according to the corresponding standard requirements, but different medical institutions have their own procedures for BAL operations. During the collection of BALF samples, it is not possible to establish a personalized sample collection procedure based on the type of unknown microbe that causes pediatric lung infections. For this study, BALF sample collection was adapted from literature and the Guidelines for Specimen Collection, Transportation and Detection of Microorganisms in Respiratory Infections in Chinese Children and modified according to clinical practice. Approximately 20-30 mL of lavage fluid was used in this study, with a recovery volume of approximately 10 mL.

Among 229 BALF samples from 211 children with LRTI, 215 (93.89%) tested positive by mNGS. Thirteen patients underwent resampling tests. No. 4 underwent five mNGS tests, and No. 100 underwent four mNGS tests. The first four tests of No. 4 detected *S. pneumoniae*, and the last test did not detect it. mNGS testing can also indirectly reflect the treatment effect. No. 100 was an immunocompromised child who tested positive for rubella virus in all four tests, CMV and *S. pneumoniae* in three tests, and *Pseudomonas aeruginosa* in two tests. Although the pathogens were detected, the patient eventually died of X-linked immunodeficiency combined with severe pneumonia. Additionally, 11 patients underwent two mNGS tests. One patient tested negative in the first test but tested positive for *Enterococcus faecalis* and *Staphylococcus epidermidis* in the second test. One patient had completely different pathogen results in the two tests, while the remaining nine patients had partial overlap in the detected pathogens. mNGS resampling could quantitatively reflect the dynamic changes in pathogens and the treatment effect in patients. For 37 of the 125 patients who underwent mNGS, medication adjustments were performed to facilitate the optimization of clinical interventions based on the mNGS results. This suggests that the clinical value of mNGS using BALF in children with LRTI is substantial. Indeed, the mNGS detection method was superior to the culture method and was the same as the PCR identification method (Table 2), proving its effectiveness and accuracy in our research (Miao et al., 2018; Chen et al., 2021). BALF mNGS for MP had a lower positive rate than serological assays. There are three reasons for this result. One reason is that mNGS does not perform as well as serological assays for MP detection. Another reason is that MP might cause infection in other systems of the patient, such as the central nervous system, cardiovascular system, hematopoietic system, kidneys, or gastrointestinal system, and is not present in the LRTI samples (Narita, 2016; Al Busaidi et al., 2017). The third reason is that the high false-positive rate for MP in serological assays may affect the comparison of diagnostic performance between the two methods. The antibodies detected by MP serology in this study were IgM and IgG and could have indicated a past MP infection. On the other hand, for a reliable diagnosis of MP infection, paired sera, that is, acute and convalescent phase sera, are used to demonstrate a 4-fold titer increase or decrease. However, convalescent serum is difficult to obtain from children (Youn et al., 2010). In previous reports, a

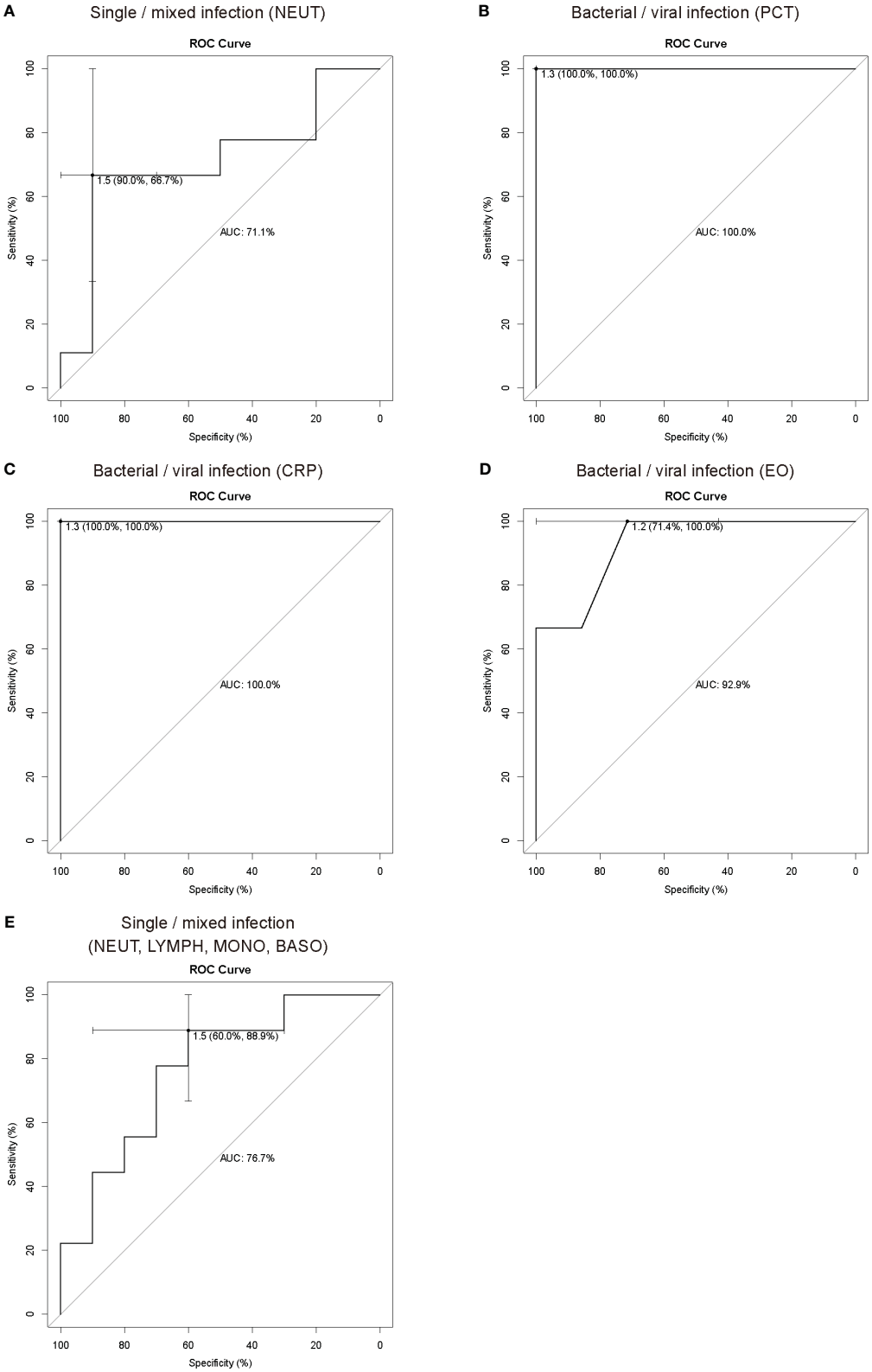

FIGURE 3
ROC curve analysis of inflammation indicators and pathogen types. ROC curve analysis showed that NEUT **(A)** could be used as an indicator to distinguish single infections from mixed infections, and PCT **(B)**, CRP **(C)** and EO **(D)** could be used as indicators to distinguish bacterial infections and viral infections. **(E)** ROC curve analysis showed that NEUT, LYMPH, MONO and BASO could be used in combination with multiple inflammation indicators to distinguish single infections from mixed infections. In ROC analysis, the sample size for the training set was fifty-nine, and the sample size for the test set was nineteen for distinguishing single (bacterial or viral) and mixed (bacterial-viral) infections. The sample size for the training set was thirty, and the sample size for the test set was ten for distinguishing single bacterial and viral infections. PCT, procalcitonin; CRP, C-reactive protein; NEUT, neutrophils; LYMPH, lymphocyte; MONO, monocyte; EO, eosinophils; BASO, basophil.

single titer ≥ 1:160 or 1:640 was considered to indicate acute MP infection (Matas et al., 1998; Kim et al., 2007). In our study, a single titer ≥ 1:40 was considered to indicate MP infection, possibly resulting in a high false-positive rate.

In this study, *S. pneumoniae*, CMV and *Candida albicans* were the most common bacterium, virus and fungus in children with LRTI, as in a previous report (Yang et al., 2022). However, the complete pathogen spectrum in our study differed from the study by Yang et al. Analyze the possible reason, our study utilized mNGS for DNA and RNA codetection, which can better assess the diagnostic value of mNGS in identifying RNA viruses causing LRTI, such as RSV, influenza virus, HPIV, and coronavirus. Compared to previous reports, the pathogen spectrum differs in children and adults or among different severity levels of disease (Huang et al., 2020; Li et al., 2020; Tsitsiklis et al., 2022; Xi et al., 2022). For hospitals with limited testing capabilities, empirical therapy based on local epidemiological characteristics detected by mNGS is recommended.

LRTI encompass a large and heterogeneous group of infections caused by bacteria, viruses, fungi and other etiologies. Inflammation indicators, such as CRP, PCT, and the white blood cell (WBC) count, are quantifiable, commonly available, and reflect underlying biological processes as well as disease severity, and their combination can characterize some specific infections. For example, PCT and CRP have been proven useful for helping to differentiate between pure SARS-CoV-2 or secondary bacterial infection and guiding the use of antibiotic therapy (Pink et al., 2021), and the PCT, CRP and WBC count can be combined as effective indicators for the identification of acute bacterial or nonbacterial infections in children (Li et al., 2021). Thus, the combination of multiple inflammation indicators has crucial clinical value. mNGS is high throughput and unbiased and simultaneously identifies bacterial, fungal, viral, parasitic, atypical and novel pathogens (Gu et al., 2019). In contrast, traditional culture methods can only identify culturable bacteria and fungi. Although PCR and antigen detection are rapid and accurate for pathogen identification, it requires prior knowledge or assumption of the pathogen type, and the detection throughput is relatively limited (Qian et al., 2020; Diao et al., 2021). Therefore, only mNGS can completely distinguish different types of pathogen infections. According to the results of mNGS in this study, the common infections in children with LRTI were bacterial, viral, and mixed bacterial-viral infections. In this study, univariate and multivariate logistic regression were used to assess the relationship between inflammation indicators and the types of infectious pathogens. NEUT were used to distinguish single and mixed infections; PCT, CRP or EO were used to distinguish bacterial and viral infections. Multivariate logistic regression analysis showed that NEUT, LYMPH, MONO and BASO could be used to distinguish single infections from mixed infections. Despite no significant difference, these measures are feasible and have important clinical value. The lack of significance might be due to an insufficient sample size. PCT or CRP has a high AUC value for distinguishing bacterial and viral infections, consistent with previous reports (Simon et al., 2004), but the inadequate sample size contributed to the exceptionally high AUC values. More samples from children with LRTI are needed to further investigate the relationship between inflammatory indicators and different types of infection.

mNGS is changing the way physicians diagnose and treat infectious diseases due to its wide range of applications, including assessing antimicrobial resistance, the microbiome, human host gene expression and oncology (Chiu and Miller, 2019). Empirical use of broad-spectrum antibiotics early in the course of treatment results in false-negatives when using traditional detection methods, although mNGS is less affected by antibiotic use (Miao et al., 2018; Diao et al., 2021). mNGS may reveal a massive amount of clinically irrelevant pathogens in the diagnosis of pulmonary infections, but it may improve the diagnostic yield, which might actually benefit clinical decision-making (Qian et al., 2020). Clinicians should combine traditional tests, clinical manifestations, immune status, underlying diseases and antibiotic use to determine the clinical significance of the microbe. In a subset of patients with underlying diseases or low immunity, colonization may lead to LRTI (Langelier et al., 2018b; Diao et al., 2021). Although mNGS is considered a promising experimental technique, there are several barriers to overcome, such as depletion of human nucleic acids, discrimination between colonization and infection, and high cost, before large scale clinical application (Diao et al., 2021).

This study is not without limitations. The BALF mNGS results were not confirmed by PCR or other traditional methods; thus, the results for microorganisms detected by mNGS should be combined with epidemiological and clinical characteristics before a pathogenic microbe can be identified. In addition, the sample size was insufficient to evaluate the relationship between the combination of inflammation indicators and the types of infectious pathogens based on the results of mNGS. For mNGS, there is no uniform standard for modifying or guiding clinical treatment strategies (Li et al., 2020). Finally, we suggest that mNGS may have high sensitivity for identifying early pathogens for which detection is usually time-consuming. With proper patient selection, sample processing and data interpretation, mNGS is expected to be a promising technique for the diagnosis and tailored treatment of clinical infectious diseases.

In conclusion, mNGS was found to be effective for pathogen diagnosis and informative for medication adjustment in children with LRTI in this retrospective study. Although mNGS has limitations, it has advantages compared with traditional methods. More pathogens can be detected using BALF mNGS, and it is also suitable for use as a supplementary method.

Data availability statement

The data presented in the study are deposited in the FigShare repository, accession number: 10.6084/m9.figshare.24164913.

Ethics statement

The studies involving humans were approved by Medical Ethics Committee of the First Affiliated Hospital of Guangzhou Medical University. The studies were conducted in accordance with the local legislation and institutional requirements. The ethics committee/institutional review board waived the requirement of written informed consent for participation from the participants or the participants' legal guardians/next of kin because this study was an anonymous retrospective analysis, the ethics committee approved the application for waiver of informed consent.

Author contributions

All authors have materially participated in this study and manuscript preparation. YX and YJ carried out all the molecular genetic analyses, participated in the design of the work and wrote the manuscript. YW and FM collected the clinical data, analyzed the data, and participated in conceiving the work. YL and WQ designed the work, drafted, and revised the manuscript. All authors contributed to the article and approved the submitted version.

Funding

This study were funded by the project of Guangdong Dengfeng Hospital specialist team construction (No. 310139). This study was also funded by the Guangzhou Science and Technology Project (No. 2023A03J0363).

Acknowledgments

We thank the clinicians of the First Affiliated Hospital of Guangzhou Medical University for their cooperation and the patients who participated in this study.

Conflict of interest

Authors YW, FM and WQ were employed by CapitalBio Technology Inc.

The remaining authors declare that the research was conducted in the absence of any commercial or financial relationships that could be construed as a potential conflict of interest.

Publisher's note

Supplementary material

The Supplementary Material for this article can be found online at: https://www.frontiersin.org/articles/10.3389/fcimb.2023.1220943/full#supplementary-material

SUPPLEMENTARY TABLE 1
Clinical information for 211 children with LRTI.

SUPPLEMENTARY TABLE 2
The mNGS sequencing data of 229 samples.

SUPPLEMENTARY TABLE 3
Results of pathogenic microorganisms' detection in non-immunocompromised children with LRTI.

SUPPLEMENTARY TABLE 4
Medication information before and after mNGS detection in children with LRTI.

SUPPLEMENTARY TABLE 5
Inflammation indicator data.

References

Ai, J.-W., Weng, S.-S., Cheng, Q., Cui, P., Li, Y.-J., Wu, H.-L., et al. (2018). Human endophthalmitis caused by pseudorabies virus infection, China 2017. *Emerg. Infect. Dis.* 24, 1087–1090. doi: 10.3201/eid2406.171612

Al Busaidi, I., Al-Amin, M., Ibrahim, S., Balkhair, A., and Gaifer, Z. (2017). Multi-system manifestations of Mycoplasma pneumoniae infection in a young patient. *JMM Case Rep.* 4, e005117. doi: 10.1099/jmmcr.0.005117

Cabrera-Rubio, R., Garcia-Núñez, M., Setó, L., Antó, J. M., Moya, A., Monsó, E., et al. (2012). Microbiome diversity in the bronchial tracts of patients with chronic obstructive pulmonary disease. *J. Clin. Microbiol.* 50, 3562–3568. doi: 10.1128/JCM.00767-12

Chen, Y., Feng, W., Ye, K., Guo, L., Xia, H., Guan, Y., et al. (2021). Application of metagenomic next-generation sequencing in the diagnosis of pulmonary infectious pathogens from bronchoalveolar lavage samples. *Front. Cell. Infect. Microbiol.* 11. doi: 10.3389/fcimb.2021.541092

Chen, L., Liu, W., Zhang, Q., Xu, K., Ye, G., Wu, W., et al. (2020). RNA based mNGS approach identifies a novel human coronavirus from two individual pneumonia cases in 2019 Wuhan outbreak. *Emerg. Microbes Infect.* 9, 313–319. doi: 10.1080/22221751.2020.1725399

Chiu, C. Y., and Miller, S. A. (2019). Clinical metagenomics. *Nat. Rev. Genet.* 20, 341–355. doi: 10.1038/s41576-019-0113-7

Collins, A. M., Rylance, J., Wootton, D. G., Wright, A. D., Wright, A. K. A., Fullerton, D. G., et al. (2014). Bronchoalveolar lavage (BAL) for research; obtaining adequate sample yield. *J. Vis. Exp. JoVE* 28, 4345. doi: 10.3791/4345

Diao, Z., Han, D., Zhang, R., and Li, J. (2021). Metagenomics next-generation sequencing tests take the stage in the diagnosis of lower respiratory tract infections. *J. Adv. Res.* 38, 201–212. doi: 10.1016/j.jare.2021.09.012

El Hasbani, G., Musallam, K. M., Uthman, I., Cappellini, M. D., and Taher, A. T. (2022). Thalassemia and autoimmune diseases: absence of evidence or evidence of absence? *Blood Rev.* 52, 100874. doi: 10.1016/j.blre.2021.100874

Goldberg, B., Sichtig, H., Geyer, C., Ledeboer, N., and Weinstock, G. M. (2015). Making the leap from research laboratory to clinic: challenges and opportunities for next-generation sequencing in infectious disease diagnostics. *mBio* 6, e01888–e01815. doi: 10.1128/mBio.01888-15

Gu, W., Miller, S., and Chiu, C. Y. (2019). Clinical metagenomic next-generation sequencing for pathogen detection. *Annu. Rev. Pathol.* 14, 319–338. doi: 10.1146/annurev-pathmechdis-012418-012751

Hogea, S.-P., Tudorache, E., Pescaru, C., Marc, M., and Oancea, C. (2020). Bronchoalveolar lavage: role in the evaluation of pulmonary interstitial disease. *Expert Rev. Respir. Med.* 14, 1117–1130. doi: 10.1080/17476348.2020.1806063

Huang, J., Jiang, E., Yang, D., Wei, J., Zhao, M., Feng, J., et al. (2020). Metagenomic next-generation sequencing versus traditional pathogen detection in the diagnosis of peripheral pulmonary infectious lesions. *Infect. Drug Resist.* 13, 567–576. doi: 10.2147/IDR.S235182

Jain, S., Self, W. H., Wunderink, R. G., Fakhran, S., Balk, R., Bramley, A. M., et al. (2015). Community-acquired pneumonia requiring hospitalization among U.S. Adults. *N. Engl. J. Med.* 373, 415–427. doi: 10.1056/NEJMoa1500245

Kim, N. H., Lee, J. A., Eun, B. W., Shin, S. H., Chung, E. H., Park, K. W., et al. (2007). Comparison of polymerase chain reaction and the indirect particle agglutination antibody test for the diagnosis of Mycoplasma pneumoniae pneumonia in children during two outbreaks. *Pediatr. Infect. Dis. J.* 26, 897–903. doi: 10.1097/INF.0b013e31812e4b81

Langelier, C., Kalantar, K. L., Moazed, F., Wilson, M. R., Crawford, E. D., Deiss, T., et al. (2018a). Integrating host response and unbiased microbe detection for lower respiratory tract infection diagnosis in critically ill adults. *Proc. Natl. Acad. Sci. U. S. A.* 115, E12353–E12362. doi: 10.1073/pnas.1809700115

Langelier, C., Zinter, M. S., Kalantar, K., Yanik, G. A., Christenson, S., O'Donovan, B., et al. (2018b). Metagenomic sequencing detects respiratory pathogens in hematopoietic cellular transplant patients. *Am. J. Respir. Crit. Care Med.* 197, 524–528. doi: 10.1164/rccm.201706-1097LE

Li, Y., Min, L., and Zhang, X. (2021). Usefulness of procalcitonin (PCT), C-reactive protein (CRP), and white blood cell (WBC) levels in the differential diagnosis of acute bacterial, viral, and mycoplasmal respiratory tract infections in children. *BMC Pulm. Med.* 21, 386. doi: 10.1186/s12890-021-01756-4

Li, Y., Sun, B., Tang, X., Liu, Y.-L., He, H.-Y., Li, X.-Y., et al. (2020). Application of metagenomic next-generation sequencing for bronchoalveolar lavage diagnostics in critically ill patients. *Eur. J. Clin. Microbiol. Infect. Dis.* 39, 369–374. doi: 10.1007/s10096-019-03734-5

Matas, L., Dominguez, J., De Ory, F., García, N., Galí, N., Cardona, P. J., et al. (1998). Evaluation of Meridian ImmunoCard Mycoplasma test for the detection of Mycoplasma pneumoniae-specific IgM in paediatric patients. *Scand. J. Infect. Dis.* 30, 289–293. doi: 10.1080/00365549850160954

Miao, Q., Ma, Y., Wang, Q., Pan, J., Zhang, Y., Jin, W., et al. (2018). Microbiological diagnostic performance of metagenomic next-generation sequencing when applied to clinical practice. *Clin. Infect. Dis.* 67, S231–S240. doi: 10.1093/cid/ciy693

Miller, S., Naccache, S. N., Samayoa, E., Messacar, K., Arevalo, S., Federman, S., et al. (2019). Laboratory validation of a clinical metagenomic sequencing assay for pathogen detection in cerebrospinal fluid. *Genome Res.* 29, 831–842. doi: 10.1101/gr.238170.118

Moreno, I., Cicinelli, E., Garcia-Grau, I., Gonzalez-Monfort, M., Bau, D., Vilella, F., et al. (2018). The diagnosis of chronic endometritis in infertile asymptomatic women: a comparative study of histology, microbial cultures, hysteroscopy, and molecular microbiology. *Am. J. Obstet. Gynecol.* 218, 602.e1–602.e16. doi: 10.1016/j.ajog.2018.02.012

Narita, M. (2016). Classification of extrapulmonary manifestations due to mycoplasma pneumoniae infection on the basis of possible pathogenesis. *Front. Microbiol.* 7. doi: 10.3389/fmicb.2016.00023

Pink, I., Raupach, D., Fuge, J., Vonberg, R.-P., Hoeper, M. M., Welte, T., et al. (2021). C-reactive protein and procalcitonin for antimicrobial stewardship in COVID-19. *Infection* 49, 935–943. doi: 10.1007/s15010-021-01615-8

Qian, Y.-Y., Wang, H.-Y., Zhou, Y., Zhang, H.-C., Zhu, Y.-M., Zhou, X., et al. (2020). Improving pulmonary infection diagnosis with metagenomic next generation sequencing. *Front. Cell. Infect. Microbiol.* 10. doi: 10.3389/fcimb.2020.567615

Rajapaksha, P., Elbourne, A., Gangadoo, S., Brown, R., Cozzolino, D., and Chapman, J. (2019). A review of methods for the detection of pathogenic microorganisms. *Analyst* 144, 396–411. doi: 10.1039/c8an01488d

Ramírez, M. (2013). Multiple organ dysfunction syndrome. *Curr. Probl. Pediatr. Adolesc. Health Care* 43, 273–277. doi: 10.1016/j.cppeds.2013.10.003

Simon, L., Gauvin, F., Amre, D. K., Saint-Louis, P., and Lacroix, J. (2004). Serum procalcitonin and C-reactive protein levels as markers of bacterial infection: a systematic review and meta-analysis. *Clin. Infect. Dis.* 39, 206–217. doi: 10.1086/421997

Spoor, J., Farajifard, H., and Rezaei, N. (2019). Congenital neutropenia and primary immunodeficiency diseases. *Crit. Rev. Oncol. Hematol.* 133, 149–162. doi: 10.1016/j.critrevonc.2018.10.003

Tecklenborg, J., Clayton, D., Siebert, S., and Coley, S. M. (2018). The role of the immune system in kidney disease. *Clin. Exp. Immunol.* 192, 142–150. doi: 10.1111/cei.13119

Tsitsiklis, A., Osborne, C. M., Kamm, J., Williamson, K., Kalantar, K., Dudas, G., et al. (2022). Lower respiratory tract infections in children requiring mechanical ventilation: a multicentre prospective surveillance study incorporating airway metagenomics. *Lancet Microbe* 3, e284–e293. doi: 10.1016/S2666-5247(21)00304-9

Wilson, M. R., Naccache, S. N., Samayoa, E., Biagtan, M., Bashir, H., Yu, G., et al. (2014). Actionable diagnosis of neuroleptospirosis by next-generation sequencing. *N. Engl. J. Med.* 370, 2408–2417. doi: 10.1056/NEJMoa1401268

World Health Organization. (2020). *The top 10 causes of death*. Available at: www.who.int/news-room/fact-sheets/detail/the-top-10-causes-of-death (Accessed October 24, 2022).

Xi, Y., Zhou, J., Lin, Z., Liang, W., Yang, C., Liu, D., et al. (2022). Patients with infectious diseases undergoing mechanical ventilation in the intensive care unit have better prognosis after receiving metagenomic next-generation sequencing assay. *Int. J. Infect. Dis.* 122, 959–969. doi: 10.1016/j.ijid.2022.07.062

Yang, A., Chen, C., Hu, Y., Zheng, G., Chen, P., Xie, Z., et al. (2022). Application of metagenomic next-generation sequencing (mNGS) using bronchoalveolar lavage fluid (BALF) in diagnosing pneumonia of children. *Microbiol. Spectr.* 10, e0148822. doi: 10.1128/spectrum.01488-22

Yao, M., Zhou, J., Zhu, Y., Zhang, Y., Lv, X., Sun, R., et al. (2016). Detection of listeria monocytogenes in CSF from three patients with meningoencephalitis by next-generation sequencing. *J. Clin. Neurol. Seoul Korea* 12, 446–451. doi: 10.3988/jcn.2016.12.4.446

Yi, X., Gao, J., and Wang, Z. (2022). The human lung microbiome—A hidden link between microbes and human health and diseases. *iMeta* 1, e33. doi: 10.1002/imt2.33

Youn, Y.-S., Lee, K.-Y., Hwang, J.-Y., Rhim, J.-W., Kang, J.-H., Lee, J.-S., et al. (2010). Difference of clinical features in childhood Mycoplasma pneumoniae pneumonia. *BMC Pediatr.* 10, 48. doi: 10.1186/1471-2431-10-48

Zaimoku, Y., Patel, B. A., Shalhoub, R., Groarke, E. M., Feng, X., Wu, C. O., et al. (2022). Predicting response of severe aplastic anemia to immunosuppression combined with eltrombopag. *Haematologica* 107, 126–133. doi: 10.3324/haematol.2021.278413

Zhang, D., Bi, H., Liu, B., and Qiao, L. (2018). Detection of pathogenic microorganisms by microfluidics based analytical methods. *Anal. Chem.* 90, 5512–5520. doi: 10.1021/acs.analchem.8b00399

Zinter, M. S., Dvorak, C. C., Mayday, M. Y., Iwanaga, K., Ly, N. P., McGarry, M. E., et al. (2019). Pulmonary metagenomic sequencing suggests missed infections in immunocompromised children. *Clin. Infect. Dis.* 68, 1847–1855. doi: 10.1093/cid/ciy802

frontiers | Frontiers in Cellular and Infection Microbiology

TYPE Original Research
PUBLISHED 16 October 2023
DOI 10.3389/fcimb.2023.1261284

OPEN ACCESS

EDITED BY
Jianmin Chai,
Foshan University, China

REVIEWED BY
Valeriy Poroyko,
Laboratory Corporation of America Holdings (LabCorp), United States
Haipeng Sun,
Rutgers, The State University of New Jersey, United States

*CORRESPONDENCE
Ling Li
liling25@fmmu.edu.cn
Ke Wang
wangke@fmmu.edu.cn
Jian Zhang
zjfmmu19700227@163.com

†These authors have contributed equally to this work

RECEIVED 19 July 2023
ACCEPTED 20 September 2023
PUBLISHED 16 October 2023

CITATION
Zhang Y, Chen X, Wang Y, Li L, Ju Q, Zhang Y, Xi H, Wang F, Qiu D, Liu X, Chang N, Zhang W, Zhang C, Wang K, Li L and Zhang J (2023) Alterations of lower respiratory tract microbiome and short-chain fatty acids in different segments in lung cancer: a multiomics analysis. *Front. Cell. Infect. Microbiol.* 13:1261284. doi: 10.3389/fcimb.2023.1261284

Alterations of lower respiratory tract microbiome and short-chain fatty acids in different segments in lung cancer: a multiomics analysis

Yong Zhang[1,2†], Xiangxiang Chen[1†], Yuan Wang[3†], Ling Li[4], Qing Ju[1], Yan Zhang[1], Hangtian Xi[1], Fahan Wang[5], Dan Qiu[1], Xingchen Liu[5], Ning Chang[1], Weiqi Zhang[6], Cong Zhang[7], Ke Wang[2*], Ling Li[2*] and Jian Zhang[1*]

[1]Department of Pulmonary and Critical Care of Medicine, The First Affiliated Hospital of Fourth Military Medical University, Xi'an, China, [2]National Translational Science Center for Molecular Medicine & Department of Cell Biology, Fourth Military Medical University, Xi'an, China, [3]Department of Microbiology, School of Basic Medicine of Fourth Military Medical University, Xi'an, China, [4]Department of Pediatrics, The First Affiliated Hospital of Fourth Military Medical University, Xi'an, China, [5]School of Basic Medicine, Fourth Military Medical University, Xi'an, China, [6]Department of Radiology, The First Affiliated Hospital of Fourth Military Medical University, Xi'an, China, [7]Department of Radiation Oncology, The First Affiliated Hospital of Fourth Military Medical University, Xi'an, China

Introduction: The lower respiratory tract microbiome is widely studied to pinpoint microbial dysbiosis of diversity or abundance that is linked to a number of chronic respiratory illnesses. However, it is vital to clarify how the microbiome, through the release of microbial metabolites, impacts lung health and oncogenesis.

Methods: In order to discover the powerful correlations between microbial metabolites and disease, we collected, under electronic bronchoscopy examinations, samples of paired bronchoalveolar lavage fluids (BALFs) from tumor-burden lung segments and ipsilateral non-tumor sites from 28 lung cancer participants, further performing metagenomic sequencing, short-chain fatty acid (SCFA) metabolomics, and multiomics analysis to uncover the potential correlations of the microbiome and SCFAs in lung cancer.

Results: In comparison to BALFs from normal lung segments of the same participant, those from lung cancer burden lung segments had slightly decreased microbial diversity in the lower respiratory tract. With 18 differentially prevalent microbial species, including the well-known carcinogens *Campylobacter jejuni* and *Nesseria polysaccharea*, the relative species abundance in the lower respiratory tract microbiome did not significantly differ between the two groups. Additionally, a collection of commonly recognized probiotic metabolites called short-chain fatty acids showed little significance in either group independently but revealed a strong predictive value when using an integrated model by machine learning. Multiomics also discovered particular species related to SCFAs, showing a

positive correlation with *Brachyspira hydrosenteriae* and a negative one with *Pseudomonas* at the genus level, despite limited detection in lower airways. Of note, these distinct microbiota and metabolites corresponded with clinical traits that still required confirmation.

Conclusions: Further analysis of metagenome functional capacity revealed that genes encoding environmental information processing and metabolism pathways were enriched in the lower respiratory tract metagenomes of lung cancer patients, further supporting the oncogenesis function of various microbial species by different metabolites. These findings point to a potent relationship between particular components of the integrated microbiota-metabolites network and lung cancer, with implications for screening and diagnosis in clinical settings.

KEYWORDS

lung cancer, lower respiratory tract microbiome, metagenomic sequencing, short chain fatty acids, machine learning

Introduction

A growing body of evidence implies that perturbations of the compositions within the human microbiome exert great influence on a broad array of human diseases, including a set of cancer types (Cullin et al., 2021; Sepich-Poore et al., 2021; Yang et al., 2023). As a widely accepted perspective, gut microbiota, due to vast microbial coverage and quantity within the digestive tract, is confirmed to shed bidirectional light on lung cancer by crosstalk between microbiota and host cells (Liu et al., 2019; Dong et al., 2021; Dohlman et al., 2022). Compared with remote modulation by gut microbiome-released metabolites, microbiota in local pulmonary microecological environments, which were previously considered to be sterile, is gradually receiving widespread attention in oncogenesis, development, and drug resistance of lung cancer (Routy et al., 2018; Tsay et al., 2018; Patnaik et al., 2021; Zitvogel and Kroemer, 2021). Importantly, colonization of microbes in the lungs, especially those in the lower respiratory tract, features much lower bacterial biomass but higher relative diversity, which may be reversed with elevated bioburden and descending bacterial diversity followed by several taxa in a significant proportion in suppurative and infectious diseases (Lanaspa et al., 2017; Man et al., 2017; Singh et al., 2017). However, only limited research focused on the potential role of the lower respiratory tract microbiome in the initiation and development of lung cancer and further studies are still needed for a detailed exploration of this.

Analysis of the lower respiratory tract microbiome is still intractable, partially due to the complexity of sample detection and the low biomass planted in the local respiratory tract, impeding the accuracy and sensitivity of bacterial community processing and sequencing (Drengenes et al., 2019). Different from conventional 16S rRNA gene sequencing, metagenomics seems more effective in eliminating latent hosted and operational contamination, making it an alternative to further uncover the microbial composition of the lower respiratory tract microbiome (Kurian et al., 2020; Fromentin et al., 2021; Lamoureux et al., 2022). Of note, although characterized with significantly lower bacterial communities than those detected by oropharyngeal swabs or washes, sputum samples, and bronchial aspirates from the upper airway, bronchoalveolar lavage fluids (BALFs) are usually given preference to sequence lower respiratory tract microbiome and their metabolites (Glendinning et al., 2017; Tsang et al., 2021).

Short-chain fatty acids (SCFAs), which are chemically composed of a carboxylic acid moiety and a small hydrocarbon chain under six including acetic, propionic, and butyric acids, are a subset of intermediate fatty acid metabolites mainly produced by anaerobic bacteria in the intestinal tract during the fermentation of fibers and dietary carbohydrates. SCFAs perform a beneficial function in the maintenance of health and in guarding against cancers (Sivaprakasam et al., 2016; Mirzaei et al., 2021; Van Der Hee and Wells, 2021). Mechanically, SCFAs are known to modify extensive cellular processes by direct activation of G protein-coupled receptors (GPCRs) (Kim et al., 2013), inhibition of histone deacetylases (HDACs) (Shen et al., 2017), and stabilization of the hypoxia-inducible factor (HIF) signaling pathway (Shen et al., 2017) in a ligand-receptor interaction by regulating epithelial homeostasis and stimulating anti-tumor immune activity (Trompette et al., 2014; Kim et al., 2016; Zou et al., 2018; Matsushita et al., 2021). Intriguingly, with the further exploration of the microbiome in a liquid layer on the surface of the respiratory tract and alveoli, it has been observed that lower respiratory tract-derived SCFAs might also be involved in the

Abbreviations: LC, lung cancer; NSCLC, Non-Small Cell Lung Cancer; BALF, Broncho Alveolar Lavage Fluid; NLS(Normal), Normal lung segment; TBLS (Tumor), Tumor-burden lung segment; SCFAs, Short Chain Fatty Acids; AA, Acetic Acid; PA, Propionic Acid; BA, Butyric Acid; IBA, Isobutyric Acid; VA, Valeric Acid; IVA, Isovaleric Acid; CA, Caproic Acid.

modulation of the host metabolism and immunity homeostasis. The inhibitory function of SCFAs on lung cancer deserves additional attention.

In order to address the correlation of lower respiratory tract microbiome and SCFAs, as well as their potential interaction with lung cancer, we investigated the microbial communities and SCFAs of the lower respiratory tract by metagenomic and targeted metabolome sequencing in BALF from tumor-burden lung segments and ipsilateral non-tumor sites of the same lung cancer patients. Employing an in-depth multiomics combined analysis, we aimed to validate the predictive role of SCFAs and specific microbiota in tumorigenesis and their predictive effects in the diagnosis and prevention of lung cancer in clinical practice.

Materials and methods

Study design and participant recruitment

The study cohort consisted of a subset of hospitalized subjects enrolled in our Clinical Humoral Biological Sample Library. We collected 128 cases that, according to their CT scanning characteristics, were suspected lung cancer (LC) cases, and excluded the inappropriate patients in light of our clinical research design (#2021LC2115). Details of inclusion and exclusion criteria and workflow are displayed in Table 1; Figure S1. A final diagnosis of LC depended on pathological characteristics of tissue samples from electronic bronchoscopy-mediated needle aspiration biopsy after BALF collection. At enrollment, we included patients with lung cancer who had not been treated with pharmacological interventions for the previous 3 months, such as anti-tumor regimes, antibiotics, probiotics intake, and other potential preparations that might affect local and extensive microbial compositions. Exclusion criteria included patients with concomitant infectious or inflammatory respiratory diseases, tumor-associated obstructive pneumonia, and patients using glucocorticoid drugs in the preceding 6 months. All patients fully understood the objectives and were volunteers for potential inspection risks. Each subject signed an informed consent approved by the Ethics Committee of the First Affiliated Hospital of the Air Force Medical University; the Academic Integrity Supervision Committee of Air Force Military Medical University carried out supervision of the whole course within the study.

TABLE 1 Demographic and clinical characteristics of the cohort.

Variable	Number (Mean ± SD or %)
Age (yrs)	63.59 ± 8.95
Sex (male,%)	20 (74.07)
BMI (kg/m^2)	23.12 ± 2.35
Smoking status (Yes,%)	15 (55.56)
Pathological types (%)	
Adenocarcinoma	12 (44.44)
Squamouscarcinoma	9 (33.33)
Small cell lung cancer	5 (18.52)
Others	1 (3.70)
Mutations (%)	
EGFR	7 (25.93)
Others	2 (7.40)
None	18 (66.67)
Clinical stages (%)	
I	0 (0)
II	2 (7.41)
III	2 (7.41)
IV	16 (59.25)
Unknown	7 (25.93)

Sample collection and preservation

Samples processed for microbiota analysis were collected from patients consulting for medical assistance in our center who needed electronic bronchoscopy-mediated needle aspiration biopsy to reach a definite diagnosis. Before that, bronchial and alveolar lavage fluid was obtained from normal lung segment (NLS) and tumor-burden lung segments (TBLS) successively within the same lung lobe. Each lavage was treated with preheated sterile physiological saline for 50-60ml, maintaining a stable recovery rate of >60%. All samples intended for microbial analysis were under centrifugation at 4°C 12000rpm for 40 min. Centrifugal sedimentation and supernatant were segregated and restored at -80°C for microbial and targeted metabolomics analysis concurrently until processing. All processes strictly abided by sterile operating standards.

DNA isolation and shotgun metagenomics sequencing

BALF precipitation samples (1-3mg) were weighed in 2 ml microcentrifuge tubes and placed on ice. Total DNA from the lower respiratory tract microbiotas was extracted using the QIAamp Fast DNA Stool Mini Kit (QIAGEN, Germany) per the manufacturer's instructions (see the QIAamp Fast DNA Stool Mini Kit Handbook, www.qiagen.com/handbooks). The degradation degree and potential contamination of the DNA were analyzed using 1% agarose gels. The DNA purity was determined using the NanoPhotometer® spectrophotometer (IMPLEN, CA, USA). DNA samples were further diluted with sterile water to an OD value between 1.8 and 2.0, measuring with the Qubit® dsDNA Assay Kit in Qubit® 2.0 Fluorometer (Life Technologies, CA, USA). One microgram of qualified DNA was used to construct the library via NEBNext® Ultra DNA Library Prep Kit for Illumina (NEB, USA). DNA samples were fragmented to 350 bp by sonication, and then the DNA fragments were end-polished, A-tailed, and ligated with the full-length adaptor for Illumina sequencing with further PCR amplification. Libraries were analyzed for size distribution

using the Agilent2100 Bioanalyzer (Agilent, USA) and quantified via real-time PCR to keep size distribution of DNA fragments >3nM. The libraries were then sequenced on an Illumina PE150 HiSeq platform.

Preprocessing of sequencing results and metagenomic assembly

Raw data obtained from the Illumina PE150 sequencing platform were preprocessed by Readfq (V8, https://github.com/cjfields/readfq) to obtain clean data for subsequent analysis. The clean data were utilized for assembly analysis with MEGAHIT software (v1.0.4-beta in a –presets meta-large (–end-to-end, –sensitive, -I 200, -X 400) parameter settings, and the Scaftigs were obtained by breaking the resulted scaffolds from the N junction. All the sample details on the quality of their assemblies are present in Table S1.

Gene prediction and abundance analysis

The Scaftigs (≥ 500 bp) were submitted to predict the open reading frame (ORF) using MetaGeneMark (V2.10; http://topaz.gatech.edu/GeneMark/) to filter out the excessive information with a length less than 100nt, and CD-HIT software (V4.5.8; http://www.bioinformatics.org/cd-hit/) to eliminate redundancy. Clean data of each sample was aligned to the initial gene catalog by using Bowtie2 (V2.2.4; https://bowtie-bio.sourceforge.net/bowtie2/) to calculate the number of reads of the genes on each sample alignment, with parameter settings: –end-to-end, –sensitive, -I 200, -x 400. Genes with reads ≤2 in each sample were filtered out to finally determine the gene catalog (Unigenes) for subsequent analysis (Tables S2, S3). Based on the number of reads aligned and the length of the gene, the abundance of each gene in each sample was calculated by the following formula:

$$G_k - \frac{r_k}{L_k} \times \frac{1}{\sum_{i=1}^{n} \frac{r_i}{L_i}}$$

in which r is the number of gene reads on alignment, and L is the length of the gene (Qin et al., 2010). Based on the abundance of each gene in the gene catalog in each sample, basic information statistics, core-pan gene analysis, correlation analysis between samples, and Venn diagram analysis of gene number were performed.

Species annotation

The obtained unigenes were used to blast the sequences for the bacteria, fungi, archaea, and viruses, which were extracted from the NR database (V20180102; https://www.ncbi.nlm.nih.gov/) of NCBI using DIAMOND software (V0.9.9.110; https://github.com/bbuchfink/diamond/). We used the lowest common ancestor (LCA) algorithm to obtain the number of genes and abundance information for each sample in each taxonomic hierarchy (kingdom, phylum, class, order, family, genus, and species). DIAMOND software was also used to blast unigenes to functional databases, including the KEGG (V20180101; http://www.kegg.jp/kegg/) databases, for the blast results, and the best blast hit was used for subsequent analysis.

Advanced analysis of metagenomic data

According to the alignment results, the relative abundance at different functional levels was calculated (the relative abundance at each functional level was equal to the sum of the relative abundance of genes annotated at that functional level). The gene number table of each sample at each taxonomy level was derived from the result of functional annotation and gene abundance table. The number of genes with a certain function in a sample was equal to the number of genes whose abundance was non-zero among the genes annotated with this function. Based on the abundance table at each taxonomy level, annotated genes statistics, relative abundance overview, and abundance clustering heat map were carried out, combined with PCA and NMDS analysis of dimension reduction, ANOSIM analysis of inter-/intra-group differences based on functional abundance, metabolic pathway comparative analysis, as well as Metastat and LEfSe analysis on the inter-group functional difference.

Quantification of BALF metabolites

SCFA contents in BALF supernatant were detected by Metware Biotechnology Co., Ltd. (Wuhan, China) with gas chromatography-tandem mass spectrometry analysis. Briefly, BALF samples were thawed and vortexed for 1 min prior to analysis. A total of 50μL of samples were mixed with 100μL of phosphoric acid (0.5% v/v) solution, vertexing for 3 min and ultrasonicating for 5 min. After that, the mixture was centrifuged at 12000 rpm for 10 min at a temperature of 4°C. The supernatant was collected and used for GC-MS/MS analysis. Agilent 7890B gas chromatograph coupled to a 7000D mass spectrometer with a DB-5MS column (30m length × 0.25mm inner diameter × 0.25μm film thickness; J&W Scientific, Folsom, CA) was used. Helium was used as the carrier gas, at a flow rate of 1.2mL/min. Injections were made in the spitless mode, and the injection volume was 2μL. The oven temperature was held at 90°C for 1 min, raised to 100°C at a rate of 25°C/min, raised to 150°C at a rate of 20°C/min, and held at 150°C for 0.6 min. Then, the temperature was further raised to 200°C at a rate of 25°C/min and held at 200°C for 0.5 min. After running for 3 min, all samples were analyzed in multiple reaction monitoring mode. The temperature of the injector inlet and transfer line were held at 200°C and 230°C, respectively.

Random forest and machine learning prediction models

The random forest algorithm was applied to elucidate the influence of candidates on lung cancer prediction by repeated cross-validation. Further analyses were carried out in R software (v3.5.2). The LASSO logistic regression model was performed to select the most useful prognostic risk factors for SCFA candidates in BALFs collected from lower respiratory tracts. All samples were identified using dummy variables. We used R software version 3.6.1 and the "glmnet" package (R Foundation for Statistical Computing, Vienna, Austria) to perform the LASSO logistic regression analysis.

Statistical analysis

The significance of the differences between groups was analyzed using the Wilcoxon rank-sum test and ANOSIM with P value< 0.05 (5% level of probability) with VEGAN of R package being considered to be significant and denoted as follows: $^{*}P<0.05$, $^{**}P<0.01$, and $^{***}P<0.001$. The statistical significance was adjusted for multiple testing using FDR correction with the cutoff adjusted p-value< 0.05 unless otherwise stated. The receiver operating characteristic curve (ROC) analysis was performed using the R project, and the discriminative power of the predictor was assessed by calculating the area under the receiver operating characteristic curves (AUC). A variable with an AUC above 0.7 was considered useful. Significant differences between corresponding subgroups were determined via an unpaired t-test and a false discovery rate approach using the two-stage linear step-up procedure with a false discovery rate (Q) of 1%. Testing conditions were analyzed individually, without assuming a consistent SD. Statistical analysis was performed with GraphPad Prism (V9.0.0 for Windows; www.graphpad.com).

Results

Study group enrollment and clinical characteristics

From May 2022 to December 2022, we collected 128 patients with highly suspected lung cancer based on computed tomography scanning (CT) with typical malignant imaging features, including solitary or multifocal mass nodular shadow, unsmooth edges with a burr, and microvascular insertion, in light of independent judgment from our Pulmonary Nodule Diagnosis and Treatment Center. Typical CT scanning and corresponding 3D view of the targeted lesion within a representative patient among this cohort was displayed as follows (Figures 1A, B). All subjects were evaluated to undergo lung malignant lesion biopsy after bronchoalveolar lavage in adjacent normal segments of the ipsilateral lobe and tumor-burden lung segment via electronic bronchoscope (Figure 1C). After the exclusion of benign lesions and other interference factors of sample acquisition, only those patients with pathological diagnoses of malignancy were successfully enrolled, with follow-up sequencing and analysis being carried out (Figure 1D). The demographics of the participants are shown in Table 1 and specific inclusion criteria and other exclusion criteria are displayed as a flowchart in Figure S1. Since the samples were also taken as the self-control of the same patient, we did not set up a blank control group in this study.

Lower respiratory tract microbiome diversity decreased in tumor-burden segments

To determine compositional diversity between tumor-burden lung segment (TBLS) and ipsilateral normal lung segment (NLS),

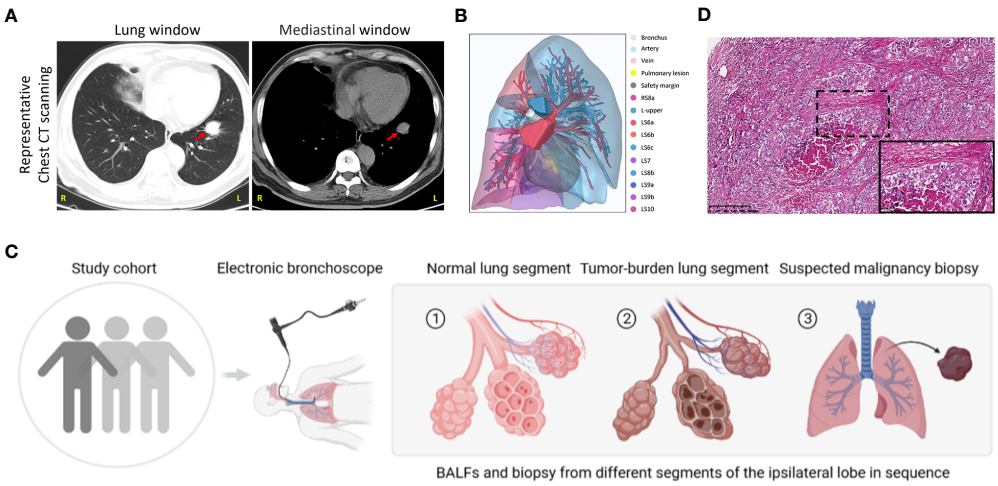

FIGURE 1
Study group enrollment and clinical characteristics. **(A)** Chest CT scan images in lung and mediastinal windows of a representative patient in the same slice. Red arrow, suspected malignant lesion. R, right; L, left. **(B)** 3D reconstruction of lung lesions within the vulnerable segment. Indicated annotations are listed on the right. **(C)** Sample collection scheme and corresponding processes. **(D)** Representative images of HE staining in the patient mentioned above. Scale bar, 200μm (10×) and 50μm (40×, inset).

we drafted those precipitations of BALF samples collected from corresponding pulmonary segments or subsegments profiling with shotgun metagenomics sequencing, generating 1.3Gbp of sequencing data on average, and further analyzed their alpha diversity indices for the subset of final enrolled samples. Consequently, multidimensional scaling (MDS), an ordination plot based on Bray-Curtis dissimilarities, revealed distinct lower respiratory tract microbial compositions among both groups at the species level (Stress=0.1311; ADONIS P^{**}=0.001; ANOSIM P^{**}<0.001), with the majority of TBLS samples overlapping with the NLS subjects (Figure 2A). Additionally, the alpha-diversity comparison of indicated groups also demonstrated low taxonomic abundance in the TBLS-BALF subgroup by Simpson index (**P<0.001, Wilcoxon rank sum test), which had no significance in the Shannon index (Figure 2B). Across the board, however, the lower respiratory tract microbiome at both the phylum and genus levels rarely fluctuated no matter which samples we sequenced (Figures S2A, B, 2E, F). Other beta diversity analyses seemed to reach the same conclusion as mentioned above (Figures S2C, D). These results suggested a perspective that despite restricted loaded biomass, minor alterations in the lower respiratory tract microbiota, especially several key species, facilitated a microbiota prone to oncogenesis and tumor development.

To further explore the differences among species that presented spatially in NLS and TBLS at the time of microscopic examination, we identified 18 differentially abundant microbial species in the comparison between both groups (FDR P<0.05, Wilcoxon rank-sum test) (Figure 2C). Meanwhile, linear discriminant analysis

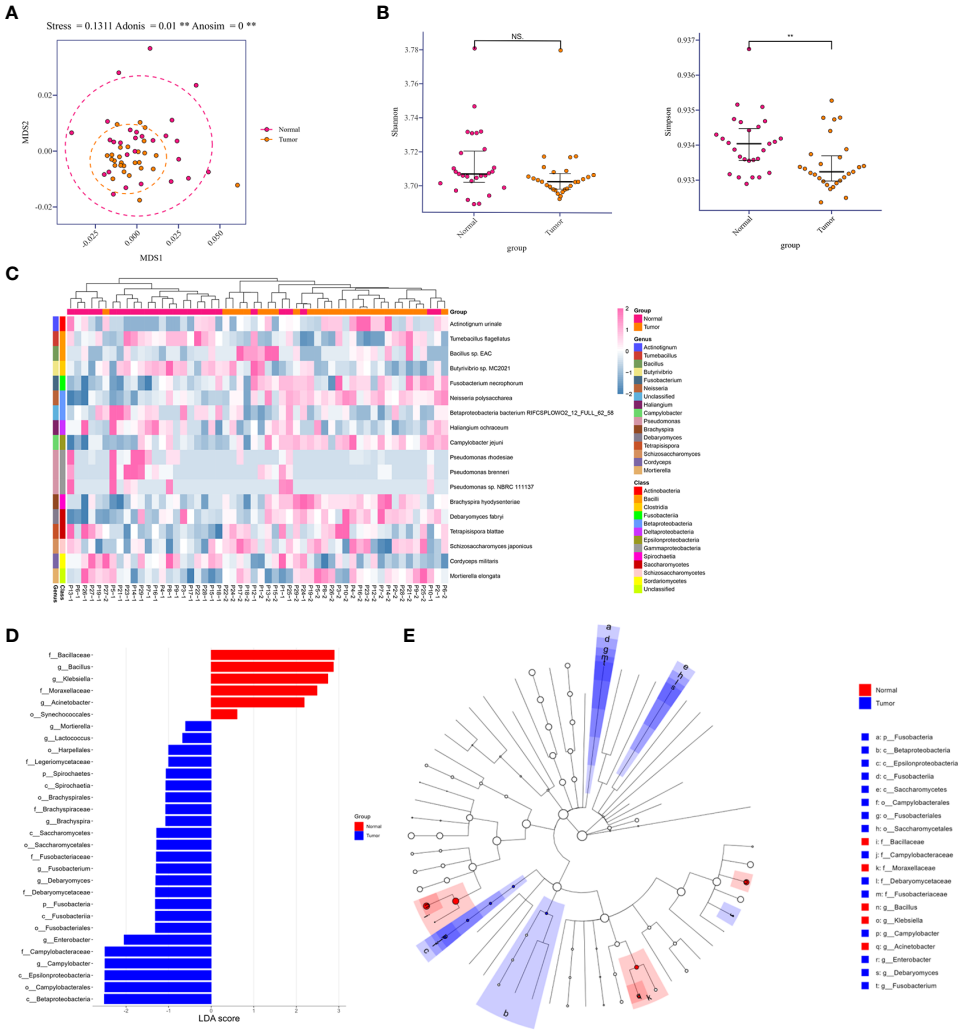

FIGURE 2
Relative abundances in lower respiratory tract microbiome and comparison of diversity analysis. **(A)** MDS plot of normal and tumor-burden lung segments in the same lung cancer patients based on the lower respiratory tract microbial compositions using Bray-Curtis dissimilarities (Stress=0.1311; ADONIS P=0.001; ANOSIM P<0.001). Intra-patient samples are linked to each other. **(B)** Alpha-diversity comparison of indicated groups by the Shannon index (No significance, Wilcoxon rank sum test) and Simpson index (**P<0.001, Wilcoxon rank sum test). **(C)** Heatmap of differentially abundant species detected in the comparison of two groups within each sample. **(D)** Distribution diagram of the LDA score in both groups and results of the LEfSe analysis based on the LDA score to screen the candidate biomarkers. **(E)** Cladogram based on different candidates from **(D)**. The red and blue nodes represent the microorganisms that mattered most in each group. MDS, multidimensional scaling. Normal, normal lung segments; Tumor, tumor-burden lung segments. NS, no significance.

effect size (LefSe) was performed to uncover the potential the tumor-related species biomarkers. We compared the microbiota compositions of the above candidates by the LDA score of the species (log10) to enlighten the distribution diagram of species differences (Figure 2D), finding that the relatively abundant microbial species were differentiated in TBLS and NLS (Figure S3A). CIRCOS plot of taxonomic abundance within each sample also verified the outcomes mentioned above (Figure S2G). A species co-abundance network among this differential genus between both lung segments further suggested that the high abundance of *C. jejuni* in TBLS might promote the dominance of *Firmicutes* and impede *Bacillota* by their intra-phylum positive associations along with the negative associations with *Bacillota* species (Figure S3B). Particularly, a Cladogram based on differential candidates also revealed that specific taxa related to lung cancer differed from those in normal lung segments, characterized by genus enrichment of *Campylobacter*, *Enterobacter*, *Debaryomyces*, and *Fusobacterium* in tumor-burden lung segments, which were replaced by *Bacillus*, *Klebsiella*, and *Acinetobacter* in normal lung segments (Figure 2E and Table S4), indicating the consistency of pathogenic microbial genus from biological evolutional perspectives. Collectively, these results further illustrated that compositional variations existed in cancer-loaded segments, some of which were quite distinct from those in healthy lower respiratory tract. Given the transient and significantly variable nature of normal lung microbiota in a relatively open environment (Dickson et al., 2015), the presence of a specific community could signal an ongoing pathological process providing bacteria with nutrients, a process that also deserves additional attention.

Conjoint predictive value of multicomponent SCFAs in tumoral associations

Except for the direct cytotoxic effects of the majority of viruses and quite limited bacteria species, metabolites accounted for the interaction between microorganisms and hosts (Bhatt et al., 2017; Sepich-Poore et al., 2021). Short-chain fatty acids derived from the intestine are important protective lipid metabolites released by anaerobic or facultative anaerobic microbiomes to regulate distant primary tumors (Kim et al., 2016). Despite the extensive literature on the inhibitory function of gut microbiome-derived SCFAs, several lower respiratory tract microbiota at the distal end of the tumor lesion could utilize SCFAs to regulate the local ecological environment (Jin et al., 2018; Yue et al., 2020). Correspondingly, to examine the dominant SCFAs in lung cancer blockade, except for the influences from the gut microbiome, we further detected SCFAs in BALF samples mentioned above to screen out the predictive components of SCFAs in lung cancer initiation or those associated with clinical diagnosis. To our surprise, SCFAs were generally expressed at a low level in the lower respiratory tract and were slightly increased in the TBLS group but with no significance (Figure 3A). This outcome seemed difficult to confront in light of the probiotic effects of SCFAs in preventing tumor process, and inevitable bias or other unknown correlated noise could have contributed to the outcome. If anything, the release of SCFAs-oriented from the lower respiratory tract within different lung segments of the same lung cancer patient was prone to be identical, regardless of the differentiated microbial composition, which was in line with previous studies.

From a practical perspective, however, exploring the predictive value of a single metabolite under sophisticated circumstances in lower airways seemed unacceptable, due to the potent interactional multiplicities between the microbiome and the host. Thus, we reconstructed a machine learning-based multivariate prediction model to clarify the predictive function of SCFAs. LASSO regression coefficient profiles of the seven SCFA candidates showed that priorities for prediction were given to combined metabolites of three SCFAs, namely, CA, VA, and IBA (Figures 3B, S4A), which was also confirmed by the Random forest prediction model and ROC curve based on repeated cross-validation from SCFA candidates (Figures 3C–E, S4B). Despite restricted accuracy of under 50%, the predictive value of this combined model should be highlighted, probably because it presented a new lung cancer diagnostic approach based on metabolic exhalation detection, deserving further validation in clinical settings.

Metagenomic and targeted metabolomic analysis with clinical characteristics

The production of SCFAs bears a tight correlation with anaerobic or facultative anaerobic microbiome in guts, supported by sufficient findings that the fluctuation of microbial metabolites may be attributed to microbiome compositional diversity (Asnicar et al., 2021). Next, we implemented an integrated analysis of the candidate microbial species and SCFAs, in order to screen out dominant SCFA-associated microbes in tumor-burden lower respiratory tract. As a consequence, CCA profiling showed that the potential correlation between SCFAs and differential microbes mattered in tumor-burden segments with merely low efficiency (Figure 4A), partially due to restricted abundance and sample capacity. Heatmap of microbial species and SCFAs might present explicit correlations of differential microbes and SCFAs (Figure 4B), indicating a positive SCFA correlation with *Brachyspira hydysenteriae* and a negative connection with *Pseudomonas* at the genus level. These results further illustrated that the microbial-metabolic prediction model facilitated cancer screening and diagnosis by bronchoscopy-dependent BALF examination, which still deserves detailed evaluation in a large-scale population. Furthermore, as to significant correlations with clinical characteristics mentioned in other studies (Ubachs et al., 2021), we found that SCFAs and differential microbes were bound up with various clinical factors (Figures 4C, D), including sex, smoking status, TNM stages, and tumor gradings, although these correlations might be triggered indirectly by other unverified factors. Owing to the lack of experimental verifications of indicated candidates correlated with these characteristics,

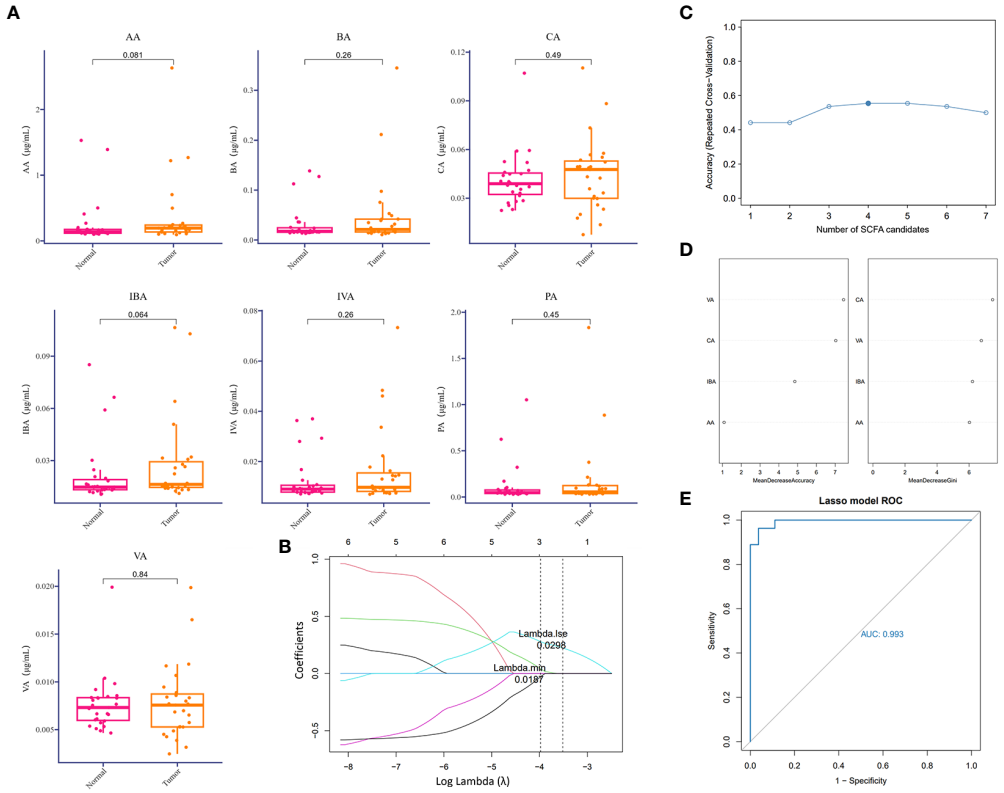

FIGURE 3
Difference analysis of SCFAs in the lower respiratory tract. **(A)** Relative detection (μg/ml) of indicated SCFAs in BALF samples collected from corresponding groups. P values are listed on each histogram. **(B)** LASSO regression coefficient profiles of the seven variables within SCFAs. Each line represents a variable. Lambda.min, the vertical dotted line at 3; Lambda.1se, the vertical dotted line at 2. **(C)** Accuracy of random forest prediction model based on repeated cross-validation from SCFA candidates. **(D)** Variable importance ranking in the effective SCFAs random forest prediction model with Mean Decrease Accuracy and Gini, respectively. LASSO, least absolute shrinkage, and selection operator. **(E)** ROC curve of SCFA-based LASSO predictive model, AUC=0.993.

additional preferences should be given in clinical studies to further demonstrate the underlying role of the lower respiratory tract microbiome.

Microbial metabolite-mediated host cell signaling activated in TBLS

The Bray-Curtis dissimilarities based on KEGG pathway abundances illustrated the marginally separate clusters of NLS and TBLS (ANOSIM, $^{**}P<0.01$) (Figure 5A). The KEGG pathway enrichment analysis of the metagenomic data showed that activated pathways in TBLS overlapped with those in NLS, whereas minor differences were detected only in environmental information processing and metabolism-related cascades, including cellular community-prokaryotes, signaling transduction, membrane transport, metabolism of cofactors and vitamins, and carbohydrate metabolism (Figures 5B, S5A, B). It is reasonable to speculate that microbe-mediated host interactions were achieved by microbial metabolites, which might induce oncogenesis or other tumor processing in a complicated microenvironment in lower respiratory tracts, further validated by a restricted proportion of functional cascades based on the KEGG pathways (Figures 5C, S5C). These results were also in accordance with various previous works that showed that the utilization of complex metabolites to induce local chronic inflammatory stimulation may be one of the dominant factors in microbial-mediated tumor development and progression (Hosseinkhani et al., 2021).

Discussion

In this study, we aimed to address the compositional discrepancy between the microbial components detected in BALF samples obtained from healthy lung segments and tumor-burden lung segments in the same patient by electronic bronchoscopy mediated invasive sampling approach, focusing on adults with untreated lung cancer. Our findings confirmed niche specificity of microbiota in malignant lesions loaded segments and normal bronchial surface but indicated that the architecture of the bacterial communities in two types of different segments slightly differed with quite limited differential bacterial abundance, which might contribute to oncogenesis in a dynamic process. Of the intermediate metabolites of lipid metabolism detection, our observations collectively supported that the specific original microbiota related closely with the production and release of

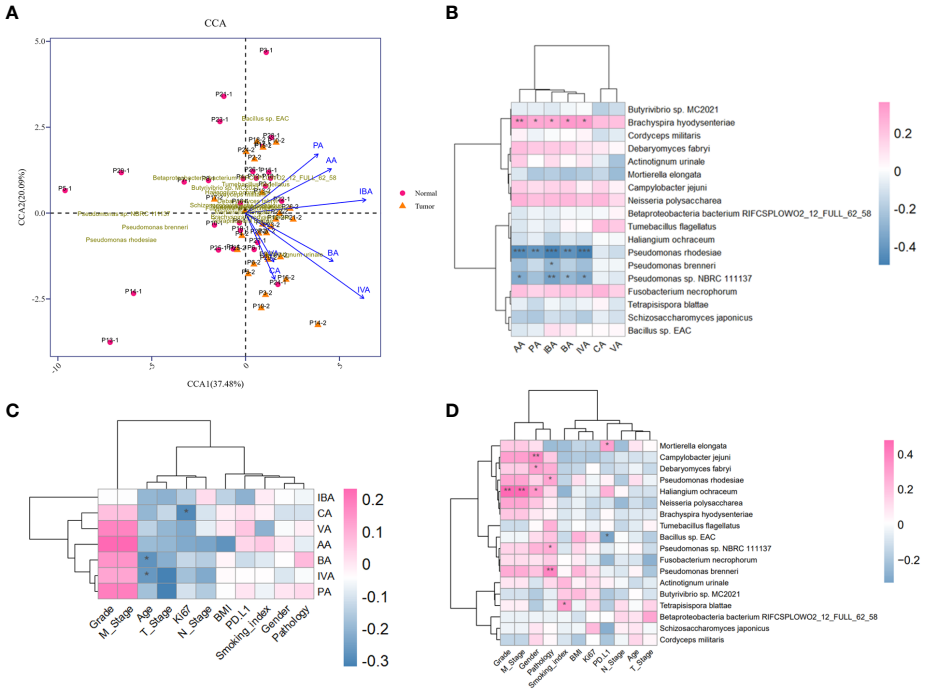

FIGURE 4
Metagenomic and metabolomic combined analysis and indicated correlation with clinical characteristics. **(A)** CCA biplot of the candidate microbial species and SCFAs. Each microbial sample is marked in the plot. **(B)** Heatmap of the correlation between candidate microbial species and SCFAs. **(C, D)** Heatmaps of potent correlation between candidate microbial species, SCFAs, and clinical information of enrolled cohort, respectively. *P<0.05, **P<0.01, and***P<0.001. CCA, Canonical correspondence analysis.

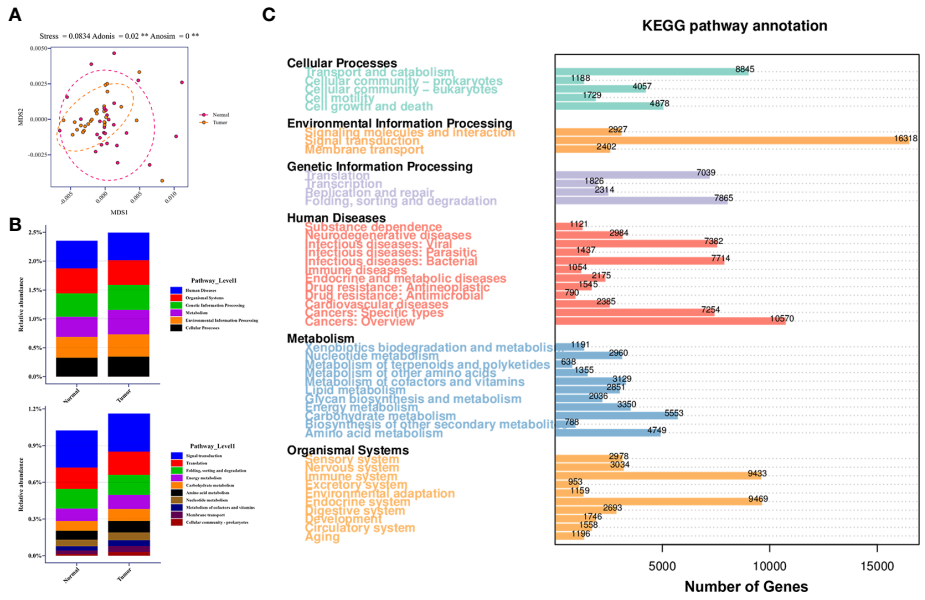

FIGURE 5
Relative abundance of KEGG pathway in lower respiratory tract microbiome. **(A)** MDS plot of samples based on KEGG pathway abundances using Bray-Curtis dissimilarities (Stress=0.0834; ADONIS P=0.02; ANOSIM P<0.001). **(B)** Relative abundance of candidate pathways at Level 1 and Level 2 in healthy and tumor-burden lung segments, respectively. **(C)** Distribution of differentially abundant KEGG pathways (FDR, Wilcoxon rank-sum test) detected in the comparison of corresponding samples. ** means P<0.01.

SCFAs in this cohort, recognizing that the dominance of a set of candidate species in tumor-burden lung segments might be the main genus of bacteria producing SCFAs, supporting that a single metabolite weakened the predictive value and that a combined model would be a priority. Additionally, our analyses by multiple approaches consistently found that microbiota willingly promotes oncogenesis by activating host cell signaling by microbial metabolites, including SCFAs. This finding might be opposite to those of previous studies, suggesting that this deserves experimental verifications and clinical analysis in detail.

Commensal microbial dysbiosis has been regarded as a primary carcinogenic factor to carcinogenesis and progression by bilateral interaction between microbiota and the host, including microbes in tumor-resident intracellular microbiota (Fu et al., 2022), intratumoral extracellular microbiota (Nejman et al., 2020), gut microbiome (Sepich-Poore et al., 2021), and those in localized microenvironment. Technically, the outburst of metagenomic sequencing dispelled the cloud overhead that the lower respiratory tract is sterile (Teague et al., 1981), accelerating the extensive explorations of lower respiratory tract microbiomes in lung carcinogenesis and malignant biological behaviors. Various studies have reported the frequent association of *Streptococcus*, *Staphylococcus*, *Pseudomonas*, and *Veillonella* in lung cancer (Fu et al., 2022), which could be altered dynamically by primary lesion types and progression, metastatic sites formation, and complications accompanied in clinical settings (Garg et al., 2017). In accordance with other microbe-mediated oncogenesis, the lower respiratory tract microbiome is also prone to trigger tumor initiation by inducing DNA damage, activating oncogenic and inflammatory pathways, breaking anti-tumor immunity balance, and most likely, releasing microbe-oriented cytotoxic metabolites (Sepich-Poore et al., 2021). Segal's studies illustrated that the exposure of airway epithelial cells to tumor-associated microbes upregulated ERK and PI3K pathways by lower airway transcriptome in patients with cancer, possibly by activating IL-17 inflammatory phenotype (Tsay et al., 2018). In our study, we found that the abundance of *Campylobacter jejuni*, also detected by other groups (Canning et al., 2013; Zheng et al., 2021), shared a close connection with lung cancer, and several species were also sequenced in normal segments, which perhaps dressed up as probiotics in localized microenvironment. Unfortunately, as the same with other studies, we failed to demonstrate the specific oncogenic or anti-oncogenic roles of these diverse microbiota in lung cancer due to the lack of appropriate models *in vivo* and the complexity of microbial pathogenesis. Given that the majority of studies on lower respiratory tract microbiome concentrated on its potential relevance with lung cancer clinically (Table S5), in-depth studies are still needed to shed light on mechanical insights, owing to microbial compositional diversity and differential pathogenicity of lower respiratory tract microbiome.

SCFAs are mainly generated by non-digestive and fermentable carbohydrates from the gut microbiome, some of which can also be produced by host cells during normal cellular processes, performing as widely recognized protective metabolites in multiple cancer types. With total intestinal concentration exceeding 100mM, SCFAs released by the gut microbiome exert beneficial effects on gastrointestinal cancer and can also mediate tumoral inhibition of distant organs by large amounts of SCFA influx into the bloodstream via several gut axes (Liu et al., 2021). As to lung cancer, the lower respiratory tract microbiome should also be viewed as a vital source of SCFAs besides intestinal tracts, even if with a quite limited concentration, which is in line with the perspective that elevated SCFAs in the cancer group act as a sign of abnormal bacterial growth in the damaged lung (Dickson et al., 2015). Unfortunately, few studies have focused on the determination of respiratory microbiota-derived SCFAs in mediating lung cancer, which limits the understanding of their possible functions in the maintenance of respiratory immunity homeostasis. Based on the above, our study examined the concentration of SCFAs from BALF samples in different lung segments, finding that a slight difference of SCFAs was detected in tumor-burden lung segments compared to healthy segments, which was in agreement with previous findings (Yue et al., 2020). After excluding the detection errors induced by lavage liquids, machine learning profiles supported that the results that integrated prediction models of SCFA candidates, including VA, CA, and IBV, were more important compared to a single agent in lung cancer screening and diagnosis. It is still well-established that the lower respiratory tract microbiota is linked to lung cancer either directly via secreted SCFAs that stop the disease's progression or by producing other substances on host cells that start metabolic reprogramming. However, more research is necessary to fully understand this association's powerful mechanical effects.

As to the crucial prerequisite for revealing the compositional role of the microbiome, accurately measuring the low biomass microbiota in the lower airways is still challenging in the deep sequencing era (Huang and Boushey, 2015). Bacterial DNA density is at least 100 times lower in the lower respiratory tract than in the upper airways, compromising accuracy due to potential sampling and processing contamination (Dickson et al., 2017; Schneeberger et al., 2019). In this study, we standardized protected sampling of the lower respiratory tract to minimize artificial and systematic contamination, including homogeneous samples of ipsilateral lung segments from the same patient to reduce individual differences, strict aseptic technique processes and materials to restrict man-made interferences, and precise sequencing data of metagenomic and metabolic detection to lower confounding bias to a certain extent. Cohorts from the same center additionally ensured a uniform approach for operating processes from healthy segments to tumor-burden ones, as well as for electronic bronchoscope evaluation. Additionally, the simultaneous processing, storage, and testing of the two sets of samples reduced unanticipated growth and metabolic activity. Briefly, except for inevitable noises from collecting sequence, such as bronchoalveolar lavages in tumor-burden segments after those in healthy ones and microbiota compositional diversities in different lung segments in the same patient, the uniformity of sample collection and processing greatly reduces systematic errors and further guarantees the accuracy of a realistic composition of the lower respiratory tract microbiota and corresponding metabolism in lung cancer compared with healthy controls. Even though a degree of cross-contamination was inevitable, the confounding factors have

been minimized in the design and actual implementation of this study.

Another issue that deserves additional attention is the causality between malignant lesion formation and microbial composition alteration in a spatiotemporal dynamic manner. Due to the abnormal outward proliferation that breaks through the basement membrane, the distal end of alien organisms in the airway was prone to be in a relatively hypoxic state (West, 1978), which may facilitate the proliferation of anaerobic bacteria and weaken the aerobic bacterial content accordingly. The dominant presence of specific bacterial genera, especially anaerobic or facultative anaerobic organisms, causes ripples throughout the tumor partly and even entirely via abnormal production of bacterial metabolites. This restrictive interaction makes tumors settle at a certain stage and forms a specific tumor microenvironment, which can be switched by perturbation of microbiota or rapid changes in tumor cell load. On the other hand, unrelenting nutrient transformation within the local microecological environment surrounding tumors inevitably contributes to competition between microorganisms and host cells, leading to dynamic changes in both species and quantity of microbial community. Although tumor cell-mediated nutritional deprivation undermines the energy supply of the microbial community, the slight variations induced by the imbalance of the microbiota in the lower respiratory tract still matter in tumor progression as a non-negligible biological point. According to our study sampling the microbiome and targeted metabolites at a restricted time, dynamic monitoring based on different stages of tumor progression still requires additional attention from large-scale examinations, which should aim to further uncover in detail microbial dysbiosis-mediated oncogenesis or vice versa.

Several limitations may shadow the outcomes of this study. First, restricted participants in a single center probably magnified the selective bias, leading to a distanced state from genuine microbial communities and metabolites in the lower respiratory tract with its densely packed low biomass. Additionally, due to successive sample collection from different lung segments in the same lung cancer patient and lack of negative control from healthy subjects and those with benign respiratory disease, BALFs were prone to be affected by operational sequence, inducing nuances of microbial composition and metabolic content. Furthermore, a complex composition of various microbiota-released metabolites detected from BALF in the lower respiratory tract was not distinguished in this study, which was liable to weaken the protective role of SCFAs. Finally, the dynamic interaction between the host and microbiota via metabolites makes it challenging to determine the actual source of these microbiota-oriented metabolites, leading to confounding bias in our data. *In vitro* experiments detaching from the whole dimmed the holistic influence on lung cancer, inspired by complicated microbial and microbe-host interactions.

Conclusions

In our 28-participant-enrolled cohort, the lower respiratory tract microbiome and relative SCFAs detected in paired bronchoalveolar lavage fluids from normal lung segments and tumor-burden lung segments of the same patient were investigated. We found that different regions of the same patients' lower respiratory tract microbiomes exhibit distinct signals. Furthermore, neither group's SCFAs had any value as a single predictor, but combined analysis may be able to forecast the connection of SCFAs to oncogenesis. Additionally, by the production of specific metabolites, such as SCFAs, some microbial species in lung regions with tumor load were able to influence oncogenesis or serve as a predictor. Therefore, self-control studies of extended samples may be advantageous for future studies intended to clarify the preventative, diagnostic, and therapeutic significance of lower respiratory tract microbiota contributing to tumor blocking.

Data availability statement

All data generated or analyzed in this study were oriented from a standardized clinical process and are included in this published article. Sequence data that support the findings of this study have been deposited in the NCBI Short Read Archive with the primary Bioproject accession code PRJNA991321 on the following link: https://www.ncbi.nlm.nih.gov/sra/PRJNA991321.

Ethics statement

This research presented here has been performed in accordance with the Declaration of Helsinki and was approved by the Ethics Committee of the First Affiliated Hospital of the Air Force Medical University (#XJYY-LL-FJ-002). The patients included in this research have signed informed consent forms based on the voluntary principle before sample collection performance.

Author contributions

YoZ: Data curation, Visualization, Writing – original draft. XC: Data curation, Formal Analysis, Resources, Writing – original draft. YW: Investigation, Methodology, Writing – original draft. LL: Formal Analysis, Project administration, Software, Writing – review & editing. QJ: Investigation, Validation, Writing – review & editing. YaZ: Methodology, Resources, Validation, Writing – review & editing. HX: Methodology, Validation, Writing – review & editing. FW: Methodology, Validation, Writing – review & editing. DQ: Resources, Software, Writing – original draft. XL: Formal Analysis, Visualization, Writing – review & editing. NC: Project administration, Resources, Writing – review & editing. WZ: Project administration, Software, Writing – review & editing. CZ: Formal Analysis, Validation, Writing – review & editing. KW: Funding acquisition, Investigation, Writing – review & editing. LL: Funding acquisition, Supervision, Writing – review & editing. JZ: Conceptualization, Funding acquisition, Supervision, Writing – review & editing.

Funding

The authors declare financial support was received for the research, authorship, and/or publication of this article. This study was funded by grants from the Booster project of the Air Force Military Medical University (#2021LC2115), Science and Technology Project of Shaanxi Province (#2021PT-047), Young Elite Scientist Sponsorship Program by China Association for Science and Technology (#2020QNRC001), National Natural Science Foundation of China (#81872349) and Key Project Program of the State Key Laboratory of Cancer Biology in Fourth Military Medical University (#CBSKL2022ZZ09).

Acknowledgments

We thank the lung cancer patients who participated in this research and all the clinical staff who assisted with the sample collections and preliminary processing. We also would like to thank *Novogene Technology Co., Ltd* and *Metware Technology Co., Ltd* for providing support in the sequencing experiments as well as bioinformatics support for the taxonomic profiling and metabolomics analysis.

Conflict of interest

The authors declare that the research was conducted in the absence of any commercial or financial relationships that could be construed as a potential conflict of interest.

Publisher's note

All claims expressed in this article are solely those of the authors and do not necessarily represent those of their affiliated organizations, or those of the publisher, the editors and the reviewers. Any product that may be evaluated in this article, or claim that may be made by its manufacturer, is not guaranteed or endorsed by the publisher.

Supplementary material

The Supplementary Material for this article can be found online at: https://www.frontiersin.org/articles/10.3389/fcimb.2023.1261284/full#supplementary-material

SUPPLEMENTARY FIGURE 1
Workflow of study cohort enrollment with inclusion and exclusion criteria.

SUPPLEMENTARY FIGURE 2
Microbial composition and diversity comparison within each sample. **(A, B)** Relative abundance of the lower respiratory tract microbiota in the indicated groups at phylum and genus level, respectively. **(C, D)** 3D PCA and PCoA analysis plot of lower respiratory tract microbiome in normal and tumor burden lung segments. PCA, principal component analysis. PCoA, principal coordinates analysis. **(E, F)** Relative abundance of the lower respiratory tract microbiota in each sample at phylum and genus level, respectively. **(G)** CIRCOS plot of taxonomic abundance among each samples.

SUPPLEMENTARY FIGURE 3
Differential microbiota comparison and co-occurrence network. **(A)** Box plots of relative abundance within indicated significant differential microbiota among both groups. **(B)** Microbial co-occurrence network of different candidates from Figure S3A. Each node represents a species and edges correspond to significant species-species associations. The size of each node is proportional to the mean relative abundance at the phylum level. The 95% credible criteria were used to assess significance, and estimated correlations were then filtered with the correlation coefficient≥0.4 in a line thickness-dependent format. Color labels are marked by orange (positive correlation) and blue (negative correlation), respectively.

SUPPLEMENTARY FIGURE 4
Key parameter supplementation of LASSO and Random Forest. **(A)** Profiles of LASSO regression regarding partial likelihood deviance and misclassification error. The lines indicate the 95% confidence interval of the regression, and the dotted line represents the optimal number of variables. **(B)** Representative OOB error estimate based on random forest among indicated groups. OOB, out-of-bag.

SUPPLEMENTARY FIGURE 5
Relative abundance of KEGG pathways in both groups. **(A, B)** Relative abundance of KEGG levels 1 and 2 within both groups. **(C)** Distribution diagram of the KEGG pathways based on LDA score among indicated groups.

References

Asnicar, F., Berry, S. E., Valdes, A. M., Nguyen, L. H., Piccinno, G., Drew, D. A., et al. (2021). Microbiome connections with host metabolism and habitual diet from 1,098 deeply phenotyped individuals. *Nat. Med.* 27, 321–332. doi: 10.1038/s41591-020-01183-8

Bhatt, A. P., Redinbo, M. R., and Bultman, S. J. (2017). The role of the microbiome in cancer development and therapy. *CA Cancer J. Clin.* 67, 326–344. doi: 10.3322/caac.21398

Canning, C., Sun, S., Ji, X., Gupta, S., and Zhou, K. (2013). Antibacterial and cytotoxic activity of isoprenylated coumarin mammea A/AA isolated from Mammea africana. *J. Ethnopharmacol.* 147, 259–262. doi: 10.1016/j.jep.2013.02.026

Cullin, N., Azevedo Antunes, C., Straussman, R., Stein-Thoeringer, C. K., and Elinav, E. (2021). Microbiome and cancer. *Cancer Cell* 39, 1317–1341. doi: 10.1016/j.ccell.2021.08.006

Dickson, R. P., Erb-Downward, J. R., Freeman, C. M., Mccloskey, L., Falkowski, N. R., Huffnagle, G. B., et al. (2017). Bacterial topography of the healthy human lower respiratory tract. *mBio* 8(1), e02287–16. doi: 10.1128/mBio.02287-16

Dickson, R. P., Erb-Downward, J. R., and Huffnagle, G. B. (2015). Homeostasis and its disruption in the lung microbiome. *Am. J. Physiol. Lung Cell Mol. Physiol.* 309, L1047–L1055. doi: 10.1152/ajplung.00279.2015

Dohlman, A. B., Klug, J., Mesko, M., Gao, I. H., Lipkin, S. M., Shen, X., et al. (2022). A pan-cancer mycobiome analysis reveals fungal involvement in gastrointestinal and lung tumors. *Cell* 185, 3807–3822.e3812. doi: 10.1016/j.cell.2022.09.015

Dong, Q., Chen, E. S., Zhao, C., and Jin, C. (2021). Host-microbiome interaction in lung cancer. *Front. Immunol.* 12, 679829. doi: 10.3389/fimmu.2021.679829

Drengenes, C., Wiker, H. G., Kalananthan, T., Nordeide, E., Eagan, T. M. L., and Nielsen, R. (2019). Laboratory contamination in airway microbiome studies. *BMC Microbiol.* 19, 187. doi: 10.1186/s12866-019-1560-1

Fromentin, M., Ricard, J. D., and Roux, D. (2021). Respiratory microbiome in mechanically ventilated patients: a narrative review. *Intensive Care Med.* 47, 292–306. doi: 10.1007/s00134-020-06338-2

Fu, A., Yao, B., Dong, T., Chen, Y., Yao, J., Liu, Y., et al. (2022). Tumor-resident intracellular microbiota promotes metastatic colonization in breast cancer. *Cell* 185, 1356–1372.e1326. doi: 10.1016/j.cell.2022.02.027

Garg, N., Wang, M., Hyde, E., Da Silva, R. R., Melnik, A. V., Protsyuk, I., et al. (2017). Three-dimensional microbiome and metabolome cartography of a diseased human lung. *Cell Host Microbe* 22, 705–716.e704. doi: 10.1016/j.chom.2017.10.001

Glendinning, L., Collie, D., Wright, S., Rutherford, K. M. D., and Mclachlan, G. (2017). Comparing microbiotas in the upper aerodigestive and lower respiratory tracts of lambs. *Microbiome* 5, 145. doi: 10.1186/s40168-017-0364-5

Hosseinkhani, F., Heinken, A., Thiele, I., Lindenburg, P. W., Harms, A. C., and Hankemeier, T. (2021). The contribution of gut bacterial metabolites in the human immune signaling pathway of non-communicable diseases. *Gut Microbes* 13, 1–22. doi: 10.1080/19490976.2021.1882927

Huang, Y. J., and Boushey, H. A. (2015). The sputum microbiome in chronic obstructive pulmonary disease exacerbations. *Ann. Am. Thorac. Soc.* 12 Suppl 2, S176–S180. doi: 10.1513/AnnalsATS.201506-319AW

Jin, Y. Y., Shi, Z. Q., Chang, W. Q., Guo, L. X., Zhou, J. L., Liu, J. Q., et al. (2018). A chemical derivatization based UHPLC-LTQ-Orbitrap mass spectrometry method for accurate quantification of short-chain fatty acids in bronchoalveolar lavage fluid of asthma mice. *J. Pharm. BioMed. Anal.* 161, 336–343. doi: 10.1016/j.jpba.2018.08.057

Kim, M. H., Kang, S. G., Park, J. H., Yanagisawa, M., and Kim, C. H. (2013). Short-chain fatty acids activate GPR41 and GPR43 on intestinal epithelial cells to promote inflammatory responses in mice. *Gastroenterology* 145, 396–406.e391-310. doi: 10.1053/j.gastro.2013.04.056

Kim, M., Qie, Y., Park, J., and Kim, C. H. (2016). Gut microbial metabolites fuel host antibody responses. *Cell Host Microbe* 20, 202–214. doi: 10.1016/j.chom.2016.07.001

Kurian, S. M., Gordon, S., Barrick, B., Dadlani, M. N., Fanelli, B., Cornell, J. B., et al. (2020). Feasibility and comparison study of fecal sample collection methods in healthy volunteers and solid organ transplant recipients using 16S rRNA and metagenomics approaches. *Biopreserv. Biobank* 18, 425–440. doi: 10.1089/bio.2020.0032

Lamoureux, C., Surgers, L., Fihman, V., Gricourt, G., Demontant, V., Trawinski, E., et al. (2022). Prospective comparison between shotgun metagenomics and sanger sequencing of the 16S rRNA gene for the etiological diagnosis of infections. *Front. Microbiol.* 13, 761873. doi: 10.3389/fmicb.2022.761873

Lanaspa, M., Bassat, Q., Medeiros, M. M., and Muñoz-Almagro, C. (2017). Respiratory microbiota and lower respiratory tract disease. *Expert Rev. Anti Infect. Ther.* 15, 703–711. doi: 10.1080/14787210.2017.1349609

Liu, F., Li, J., Guan, Y., Lou, Y., Chen, H., Xu, M., et al. (2019). Dysbiosis of the gut microbiome is associated with tumor biomarkers in lung cancer. *Int. J. Biol. Sci.* 15, 2381–2392. doi: 10.7150/ijbs.35980

Liu, Q., Tian, X., Maruyama, D., Arjomandi, M., and Prakash, A. (2021). Lung immune tone via gut-lung axis: gut-derived LPS and short-chain fatty acids' immunometabolic regulation of lung IL-1β, FFAR2, and FFAR3 expression. *Am. J. Physiol. Lung Cell Mol. Physiol.* 321, L65–l78. doi: 10.1152/ajplung.00421.2020

Man, W. H., De Steenhuijsen Piters, W. A., and Bogaert, D. (2017). The microbiota of the respiratory tract: gatekeeper to respiratory health. *Nat. Rev. Microbiol.* 15, 259–270. doi: 10.1038/nrmicro.2017.14

Matsushita, M., Fujita, K., Hayashi, T., Kayama, H., Motooka, D., Hase, H., et al. (2021). Gut microbiota-derived short-chain fatty acids promote prostate cancer growth via IGF1 signaling. *Cancer Res.* 81, 4014–4026. doi: 10.1158/0008-5472.CAN-20-4090

Mirzaei, R., Afaghi, A., Babakhani, S., Sohrabi, M. R., Hosseini-Fard, S. R., Babolhavaeji, K., et al. (2021). Role of microbiota-derived short-chain fatty acids in cancer development and prevention. *BioMed. Pharmacother.* 139, 111619. doi: 10.1016/j.biopha.2021.111619

Nejman, D., Livyatan, I., Fuks, G., Gavert, N., Zwang, Y., Geller, L. T., et al. (2020). The human tumor microbiome is composed of tumor type-specific intracellular bacteria. *Science* 368, 973–980. doi: 10.1126/science.aay9189

Patnaik, S. K., Cortes, E. G., Kannisto, E. D., Punnanitinont, A., Dhillon, S. S., Liu, S., et al. (2021). Lower airway bacterial microbiome may influence recurrence after resection of early-stage non-small cell lung cancer. *J. Thorac. Cardiovasc. Surg.* 161, 419–429.e416. doi: 10.1016/j.jtcvs.2020.01.104

Qin, J., Li, R., Raes, J., Arumugam, M., Burgdorf, K. S., Manichanh, C., et al. (2010). A human gut microbial gene catalogue established by metagenomic sequencing. *Nature* 464, 59–65. doi: 10.1038/nature08821

Routy, B., Le Chatelier, E., Derosa, L., Duong, C. P. M., Alou, M. T., Daillère, R., et al. (2018). Gut microbiome influences efficacy of PD-1-based immunotherapy against epithelial tumors. *Science* 359, 91–97. doi: 10.1126/science.aan3706

Schneeberger, P. H. H., Prescod, J., Levy, L., Hwang, D., Martinu, T., and Coburn, B. (2019). Microbiota analysis optimization for human bronchoalveolar lavage fluid. *Microbiome* 7, 141. doi: 10.1186/s40168-019-0755-x

Sepich-Poore, G. D., Zitvogel, L., Straussman, R., Hasty, J., Wargo, J. A., and Knight, R. (2021). The microbiome and human cancer. *Science* 371(6536), eabc4552. doi: 10.1126/science.abc4552

Shen, H., Lu, Z., Xu, Z., Chen, Z., and Shen, Z. (2017). Associations among dietary non-fiber carbohydrate, ruminal microbiota and epithelium G-protein-coupled receptor, and histone deacetylase regulations in goats. *Microbiome* 5, 123. doi: 10.1186/s40168-017-0341-z

Singh, N., Vats, A., Sharma, A., Arora, A., and Kumar, A. (2017). The development of lower respiratory tract microbiome in mice. *Microbiome* 5, 61. doi: 10.1186/s40168-017-0277-3

Sivaprakasam, S., Prasad, P. D., and Singh, N. (2016). Benefits of short-chain fatty acids and their receptors in inflammation and carcinogenesis. *Pharmacol. Ther.* 164, 144–151. doi: 10.1016/j.pharmthera.2016.04.007

Teague, R. B., Wallace, R. J. Jr., and Awe, R. J. (1981). The use of quantitative sterile brush culture and gram stain analysis in the diagnosis of lower respiratory tract infection. *Chest* 79, 157–161. doi: 10.1378/chest.79.2.157

Trompette, A., Gollwitzer, E. S., Yadava, K., Sichelstiel, A. K., Sprenger, N., Ngom-Bru, C., et al. (2014). Gut microbiota metabolism of dietary fiber influences allergic airway disease and hematopoiesis. *Nat. Med.* 20, 159–166. doi: 10.1038/nm.3444

Tsang, N. N. Y., So, H. C., Ng, K. Y., Cowling, B. J., Leung, G. M., and Ip, D. K. M. (2021). Diagnostic performance of different sampling approaches for SARS-CoV-2 RT-PCR testing: a systematic review and meta-analysis. *Lancet Infect. Dis.* 21, 1233–1245. doi: 10.1016/S1473-3099(21)00146-8

Tsay, J. J., Wu, B. G., Badri, M. H., Clemente, J. C., Shen, N., Meyn, P., et al. (2018). Airway microbiota is associated with upregulation of the PI3K pathway in lung cancer. *Am. J. Respir. Crit. Care Med.* 198, 1188–1198. doi: 10.1164/rccm.201710-2118OC

Ubachs, J., Ziemons, J., Soons, Z., Aarnoutse, R., Van Dijk, D. P. J., Penders, J., et al. (2021). Gut microbiota and short-chain fatty acid alterations in cachectic cancer patients. *J. Cachexia Sarcopenia Muscle* 12, 2007–2021. doi: 10.1002/jcsm.12804

Van Der Hee, B., and Wells, J. M. (2021). Microbial regulation of host physiology by short-chain fatty acids. *Trends Microbiol.* 29, 700–712. doi: 10.1016/j.tim.2021.02.001

West, J. B. (1978). Regional differences in the lung. *Chest* 74, 426–437. doi: 10.1378/chest.74.4.426

Yang, L., Li, A., Wang, Y., and Zhang, Y. (2023). Intratumoral microbiota: roles in cancer initiation, development and therapeutic efficacy. *Signal Transduct. Target Ther.* 8, 35. doi: 10.1038/s41392-022-01304-4

Yue, M., Kim, J. H., Evans, C. R., Kachman, M., Erb-Downward, J. R., D'souza, J., et al. (2020). Measurement of short-chain fatty acids in respiratory samples: keep your assay above the water line. *Am. J. Respir. Crit. Care Med.* 202, 610–612. doi: 10.1164/rccm.201909-1840LE

Zheng, L., Sun, R., Zhu, Y., Li, Z., She, X., Jian, X., et al. (2021). Lung microbiome alterations in NSCLC patients. *Sci. Rep.* 11, 11736. doi: 10.1038/s41598-021-91195-2

Zitvogel, L., and Kroemer, G. (2021). Lower airway dysbiosis exacerbates lung cancer. *Cancer Discov* 11, 224–226. doi: 10.1158/2159-8290.CD-20-1641

Zou, J., Chassaing, B., Singh, V., Pellizzon, M., Ricci, M., Fythe, M. D., et al. (2018). Fiber-mediated nourishment of gut microbiota protects against diet-induced obesity by restoring IL-22-mediated colonic health. *Cell Host Microbe* 23, 41–53.e44. doi: 10.1016/j.chom.2017.11.003

frontiers | Frontiers in Cellular and Infection Microbiology

TYPE Original Research
PUBLISHED 06 November 2023
DOI 10.3389/fcimb.2023.1269726

OPEN ACCESS

EDITED BY
Li Min,
Guangdong Academy of Agricultural Sciences (GDAAS), China

REVIEWED BY
Wang Tianwei,
Chinese Academy of Sciences (CAS), China
Chun Chang,
Peking University Third Hospital, China

*CORRESPONDENCE
Jianmin Chai
jchai@uark.edu
Ying Li
yingli@fosu.edu.cn

†These authors share first authorship

RECEIVED 30 July 2023
ACCEPTED 06 October 2023
PUBLISHED 06 November 2023

CITATION
Zhang Z, Zhang C, Zhong Y, Yang S, Deng F, Li Y and Chai J (2023) The spatial dissimilarities and connections of the microbiota in the upper and lower respiratory tract of beef cattle. *Front. Cell. Infect. Microbiol.* 13:1269726. doi: 10.3389/fcimb.2023.1269726

The spatial dissimilarities and connections of the microbiota in the upper and lower respiratory tract of beef cattle

Zhihao Zhang[1†], Chengqian Zhang[1†], Yikai Zhong[1†], Shuli Yang[1], Feilong Deng[1,2], Ying Li[1*] and Jianmin Chai[1,2*]

[1]Guangdong Provincial Key Laboratory of Animal Molecular Design and Precise Breeding, College of Life Science and Engineering, Foshan University, Foshan, China, [2]Division of Agriculture, Department of Animal Science, University of Arkansas, Fayetteville, AR, United States

Bovine respiratory disease (BRD) causes morbidity and mortality in cattle. The critical roles of the respiratory microbiota in BRD have been widely studied. The nasopharynx was the most popular sampling niche for BRD pathogen studies. The oral cavity and other niches within the respiratory tract, such as nostrils and lung, are less assessed. In this study, oropharyngeal swabs (OS), nasal swabs (NS), nasopharyngeal swabs (NP), and bronchoalveolar lavage (BAL) were collected from calves located in four countries and analyzed for investigation of the dissimilarities and connections of the respiratory microbiota. The results showed that the microbial diversity, structure, and composition in the upper and lower respiratory tract in beef cattle from China, the USA, Canada, and Italy were significantly different. The microbial taxa for each sampling niche were specific and associated with their local physiology and geography. The signature microbiota for OS, NS, NP, and BAL were identified using the LEfSe algorithm. Although the spatial dissimilarities among the respiratory niches existed, the microbial connections were observed in beef cattle regardless of geography. Notably, the nostril and nasopharynx had more similar microbiomes compared to lung communities. The major bacterial immigration patterns in the bovine respiratory tract were estimated and some of them were associated with geography. In addition, the contribution of oral microbiota to the nasal and lung ecosystems was confirmed. Lastly, microbial interactions were characterized to reveal the correlation between the commercial microbiota and BRD-associated pathogens. In conclusion, shared airway microbiota among niches and geography provides the possibility to investigate the common knowledge for bovine respiratory health and diseases. In spite of the dissimilarities of the respiratory microbiota in cattle, the spatial connections among these sampling niches not only allow us to deeply understand the airway ecosystem but also benefit the research and development of probiotics for BRD.

KEYWORDS

respiratory microbiota, bovine respiratory disease, geography, oral cavity, nostrils, nasopharynx, lung

Introduction

Bovine respiratory disease (BRD), causing huge economic costs worldwide, is one of the most common diseases in beef cattle (Chai et al., 2022a). The respiratory microbiota in cattle associated with disease has been confirmed, and several bacterial pathogens in BRD have been identified, such as *Mycoplasma bovis*, *Mannheimia haemolytica*, *Histophilus somni*, and *Pasteurella multocida* (Nicola et al., 2017; McMullen et al., 2020b). However, since the physiological and biochemical environments of different niches along the bovine respiratory tract result in the dissimilarities of microbial compositions, these opportunistic pathogens do not have great agreement with BRD onset (Dickson et al., 2016; Cirone et al., 2019). Moreover, the variation of geographic climate causes changes in the respiratory microbiota even in healthy cattle (Chai et al., 2022b), resulting in challenges to understanding the microbial ecology, and identifying pathogens and probiotics. Therefore, a deep investigation into the spatial dissimilarity and connection of the respiratory microbiota in healthy cattle is necessary and provides insights into bovine respiratory disease.

Nasopharynx is the most frequent sampling niche used to investigate bovine respiratory microbiota (Holman et al., 2015; Amat et al., 2019; Holman et al., 2019; McMullen et al., 2020a; Zeineldin et al., 2020). Notably, the upper airway microbiota associated with respiratory diseases has also been widely investigated in humans (Wang et al., 2020; Losol et al., 2021; Wang et al., 2022). Microbiota colonizing in other niches, such as nostrils and lungs, are less studied but also important as the physiological environment of the whole respiratory tract is changed in BRD cattle (Man et al., 2017; Fahkrajang et al., 2021). A study found different microbial structures and dominant bacteria between the upper and lower respiratory tract in Piedmontese calves (Nicola et al., 2017), indicating that niche physiology influences the microbial community. Thus, investigation of nasal and lung microbiota in healthy or BRD calves is also necessary to elucidate respiratory homeostasis or dysbiosis. It was previously suggested that bovine nasal bacterial communities provide a potential pen-side diagnostic testing for BRD (Centeno-Martinez et al., 2022). In the meantime, the dispersal of the microbiota within the respiratory system exists as shared bacterial taxon among different niches of the bovine respiratory tract was observed (McMullen et al., 2020a), and oral microbiota being one of the main sources of lung community was reported in humans (Venkataraman et al., 2015) and determines two microbiota pneumo-types associated with health status (Zhang et al., 2022). In cattle, the pathogens in the lungs could be from the nostrils or mouth based on the theory that "disease enters by the mouth". Similarly, the genera associated with common BRD pathogens such as *Mycoplasma*, *Mannheimia*, and *Pasteurella* are observed in the nostrils and oral cavity in healthy and BRD cattle (Nicola et al., 2017; McMullen et al., 2020a). All these imply that the microbial composition of the nostril and mouth is critical to the lung microbiome community in cattle. However, to our knowledge, there are fewer studies to specifically investigate spatial dissimilarity and connection of the bovine respiratory microbiota.

In this study, bovine respiratory samples from China, the United States, Canada, and Italy were collected to estimate the geographic effects, and the dissimilarities among niches, including oropharynx, nostrils, nasopharynx, and lungs were determined. Notably, the microbial connection or migration from the upper airway or mouth to the lungs in bovines were first confirmed and characterized, which provides the fundamental knowledge for understanding the bovine respiratory system.

Materials and methods

The experiment protocol was approved by the Animal Ethics and Humane Animal Care of the Foshan University.

Sample collection

A total of thirteen steers, twelve to eighteen months old, of two breeds (Gayal (Bos gaurus frontalis): n=5 and Zebu (Bos taurus indicus): n=8) from Yunnan province, China were selected in October 2022 (Supplementary Table S1). All steers were clinically healthy and did not receive any recorded therapeutic or prophylactic antibiotic treatments. In this study, all calves were sampled using oropharyngeal swabs (OS), nasal swabs (NS), nasopharyngeal swabs (NP), and bronchoalveolar lavage (BAL). OS was collected by swirling two Puritan Opti-Swabs (Puritan Medical Products Co. LLC, Guilford, Maine) in the end and over the tongue until saturation. NS were collected by swirling swabs in the right nostril until saturation. NP was collected by inserting a double guarded culture swab (Jorgensen Labs, Loveland, Colorado) up the nares until reaching the nasopharynx where the swab was advanced through the guard, rotated against the nasopharyngeal mucosa, then retracted back into the guard and removed from the nares. For a BAL sample, a tube (MILA International, Florence, KY) was passed through the nares, guided through the larynx into the trachea, and advanced until resistance was met. Sterile 0.9% saline was administered in aliquots of 60 ml (up to 240 ml) and aspirated. All samples were transported on dry ice to the laboratory, and stored at −80°C pending further processing.

Simultaneously, our study collected public datasets published by Nicola et al. (Nicola et al., 2017), Holman et al. (Holman et al., 2017; Holman et al., 2018; Holman et al., 2019), McMullen et al. (McMullen et al., 2020a), Zeineldin et al. (Zeineldin et al., 2017b) and Centeno −Martinez et al. (Centeno-Martinez et al., 2022) (Supplementary Table S2). These datasets contained 400 respiratory tract samples from healthy calves, which contained 18 OS samples, 160 NS samples, 87 NP samples, and 135 BAL samples, collected in different countries. In the meantime, these calves were from different elevations which was described in Supplementary Table S1. All sequences were downloaded from the NCBI SRA database.

DNA extraction and next-generation sequencing

All samples were thawed on ice and DNA was extracted using a commercial DNA Kit (Omega Bio-tek, Norcross, GA, U.S.) according to the manufacturer's instructions. Sterile Opti-Swab Amies buffer was taken through the extraction process representing a negative control. Total DNA quality was analyzed using a NanoDrop 2000 UV spectrophotometer (ThermoFisher, Waltham, MA, USA) and 1% agarose gel electrophoresis. The V3 - V4 region of the bacterial 16S ribosomal RNA genes were amplified by PCR (95°C for 3 min, followed by 30 cycles at 98°C for 20 s, 58°C for 15 s, and 72°C for 20 s and a final extension at 72°C for 5 min) using indexes and adaptor-linked universal primers (338F: ACTCCTACGGGAGGCAGCA; 806R: GGACTACHVGGGTWTCTAAT). PCR reactions were performed in 30 μL mixtures containing 15 μL of 2 × KAPA Library Amplification Ready Mix, 1 μL of each primer (10 μM), and 50 ng of template DNA and ddH2O. All PCR products were normalized and quantified by a Qubit 2.0 Fluorometer (Thermo Fisher Scientific, Waltham, MA, USA). Amplicon libraries were mixed using all qualified products and sequenced with an Illumina HiSeq platform at Biomarker Technologies Corporation (Beijing, China).

Sequence processing

The software package QIIME2 (version 2020.6) (Bolyen et al., 2019) was applied to analyze the next-generation sequencing data from the Illumina MiSeq platform. After fastq files were imported together into QIIME2, the Deblur program was used to process the raw reads. Deblur, a novel sub-operational-taxonomic-unit approach, uses error profiles to obtain putative error-free sequences, resulting in high-quality amplicon sequence variants (ASVs) (Amir et al., 2017). After the quality filtering step was completed, high-quality reads were normalized to minimize the effects of sequencing depth on alpha and beta diversity measures. The Bray-Curtis and Jaccard distance metrics were calculated to investigate the dissimilarities in community structure. The ANalysis Of SIMilarity was employed to compare the significance of beta diversity. Then, clean reads were classified using the Greengenes reference database (13-8 version) (DeSantis et al., 2006) which classifies 99% similarity. A bacterial ASVs table was generated using the QIIME2 command.

Statistical analyses

Determination of alpha and beta diversity was performed in the QIIME2 platform. Alpha diversity (Shannon index) was calculated using the Kruskal-Wallis test to explore the difference between different groups. Beta diversity was evaluated using Bray-Curtis (Bray and Curtis, 1957) and Jaccard (Chao et al., 2005) distances. The analysis of similarities (ANOSIM) was performed to calculate the P value and correlation coefficient (R-value), and explored similarity and dissimilarity between members of different groups. For all analyses, statistical significance was determined at $p < 0.05$. The algorithm of linear discriminant analysis (LDA) effect size (LEfSe) was performed using the non-parametric Kruskal–Wallis and pair Wilcoxon rank sum tests to determine the features with significantly different abundances between groups. The LEfSe's threshold on the logarithmic score of LDA was set to 4.0, the remaining settings were default parameters. All figures were generated with the ggplot2 and pheatmap packages in R (Wickham, 2011).

To analyze the microbial associations among niches (oropharynx, nostrils, nasopharynx, and lung), we first detected the shared bacterial taxa among them. Then, using Pearson correlation between niches, the microbial community similarity was calculated by accounting for both the rank order of ASVs and the magnitude of relative abundances. Subsequently, the important taxa were deeply analyzed to reveal micro aspiration.

Results

Sample characteristics and sequencing analysis

A total of 441 samples from our lab and publicly available datasets were included in this study. The characteristics of the samples are summarized in Table S2. The beef cattle were from four geographic locations, including China, the USA, Canada, and Italy. The respiratory microbial samples were collected from oropharynx, nostrils, nasopharynx, and lung using oral swabs (OS), nasal swabs (NS), nasopharyngeal swabs (NPS), and bronchoalveolar lavage (BAL). A total of 25,991,588 high-quality reads were generated with an average of 58,937 reads per sample. After rarefaction of sample reads to 2000, a total of 19,295 ASVs from 428 samples were included for downstream analysis, which identified 644 genera. The other thirteen samples with sequence read numbers below 2000 were excluded from further analysis.

The respiratory microbiota in beef cattle is affected by geographic locations and sampling niches

The microbiota from the upper (U) and lower (L) respiratory tract in the beef cattle associated with geography was found. The beef calves from China, the USA, Canada, and Italy showed significant differences in the U and L microbial diversity (Figure 1A). The U airway microbiota diversity from Canada was significantly lower than that from China and the USA. The L microbial diversity in cattle from China was the greatest followed by the USA, Canada, and Italy had the least. In the meantime, except in China, the U alpha diversity was significantly higher ($p < 0.05$) compared to the L in the calves from the same country.

Regarding the beta diversity based on Bray-Curtis distance, the geography affecting the microbial structure in the U and L was also observed (Figure 1B). The U airway microbiota in cattle from the USA showed a distinct cluster compared to other countries

10.3389/fcimb.2023.1269726

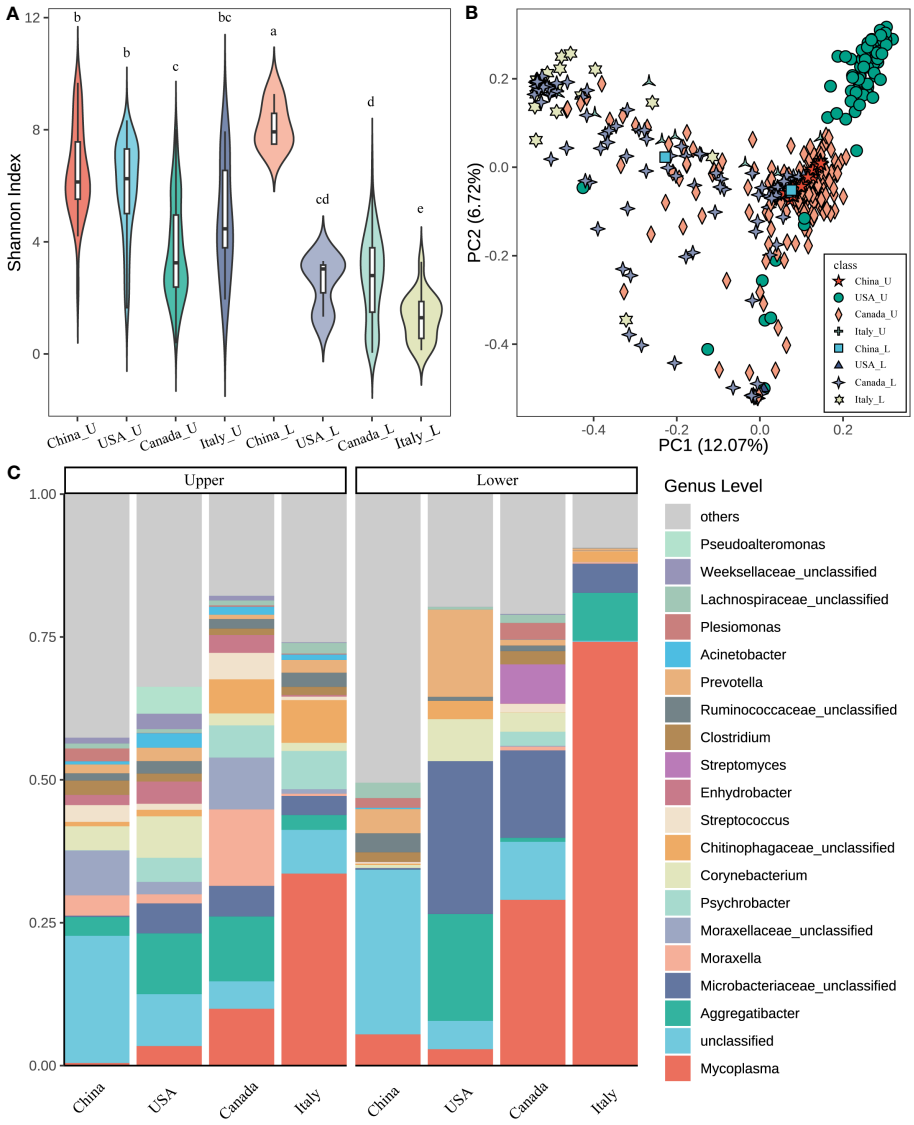

FIGURE 1
Microbial diversity and structure of the respiratory tract in different countries. **(A)** Alpha diversity (Shannon index) of the upper and lower respiratory tract in different countries. The letters on the box, which was the same between different groups mean that the difference is not significant ($p > 0.05$). On the contrary, the difference is significant ($p < 0.05$). **(B)** The principal coordinate analysis (PCoA) is based on the beta diversity (Bray–Curtis) of microbes in each sample (a point represents a sample) of different countries. **(C)** The composition of the top 20 microbes of the genus level in the average relative abundance of the respiratory tract in different countries. ***_U means the upper respiratory tract microbes of *** cattle; ***_L means the lower respiratory tract microbes of *** cattle (*** indicates any one of China, USA, Canada, and Italy).

(ANOSIM, USA vs China: R = 0.767; USA vs Italy: R = 0.625, P = 0.001 for both). Similarly, the L airway microbial structure was also influenced by geographic locations. Moreover, the differences between the U and L airway microbiota in the same country were also observed (Supplementary Table S3).

Next, the microbial composition in the U and L respiratory tracts of cattle from different countries was estimated. At the phylum level, the dominant bacteria were Proteobacteria (33.99%), Firmicutes (18.90%), Tenericutes (16.07%), Actinobacteria (15.90%), and Bacteroidetes (10.84%) across all samples. Notably, in the U airway, Proteobacteria was greater in China, the USA, and Canada compared to Italy, while Tenericutes was higher in Italy (Figure S1). For the L respiratory tract, Tenericutes was higher in Italy followed by Canada, China, and the USA. Higher Actinobacteria were observed in the USA and Canada. In addition, across the four countries, the L airway had lower abundances of Proteobacteria but higher abundances of Tenericutes compared to the U airway.

At the genus level, the five most predominant genera were *Mycoplasma* (19.87%), *Microbacteriaceae unclassified* (7.71%), *Aggregatibacter* (6.95%), *Moraxellaceae unclassified* (2.50%), and *Moraxella* (2.48%) across all samples (Figure 1C). The relative abundances of top taxa among the four countries were significantly different. For example, *Mycoplasma* had the highest abundance in the U and L airways of cattle from Italy followed by Canada, the USA, and China. *Aggregatibacter* had high abundance

in the U airway of cattle from the USA and Canada, but abundant in the L airway of cattle from the USA and Italy. *Microbaceriaceae unclassified* were greater in both the U and L airways of cattle from the USA, Canada, and Italy. *Moraxella* was enriched in the U airway of cattle from Canada but lower in other niches of cattle from other countries. Moreover, the different microbial compositions between the U and L airways were also observed. For instance, *Mycoplasma* was higher in the L airway of cattle from all four countries, *Microbaceriaceae unclassified* had a similar pattern especially in cattle from the USA and Canada.

The bovine airway bacterial features influenced by geography were identified by using LEfSe (Figure 2). *Porphyromonadaceae unclassified*, *Porphyromonas*, *Plesiomonas*, *Helcococcus*, and *Clostridium* were abundant in the U airway of cattle from China (Figure 2A). The U airway of USA cattle had a high abundance of *Corynebacterium*, *Microbacteriaceae unclassified*, *Pseudoalteromonas*,

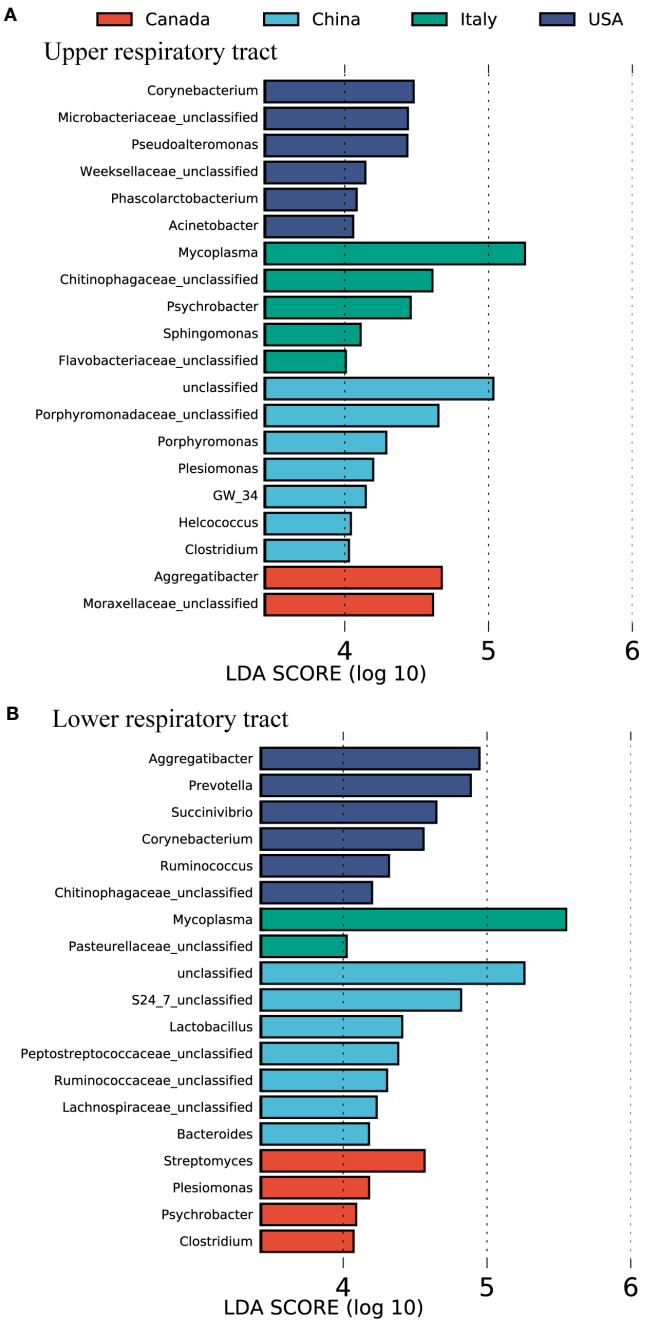

FIGURE 2
The featured microbes of the calve respiratory tract in different countries identified by LEfSe analysis. **(A)** The featured microbes of the upper respiratory tract identified. **(B)** The featured microbes of the lower respiratory tract identified. Samples were collected from four countries. The general accounting for > 0.1% of the average relative abundance of each genus were selected for LEfSe analysis. Genera in this figure were significant ($p < 0.05$), had an LDA Score > 4, and set the less strict multi-class analysis, which was considered a significant effect size.

and *Acinetobacter*. The bacteria, including *Aggregatibacter* and *Moraxellaceae unclassified*, were enriched in the U airway of Canadian cattle. *Mycoplasma*, *Chitinophagaceae unclassified*, *Psychrobacter*, and *Sphingomonas* were over-represented in the U airway of cattle from Italy. The same analysis for the L airway microbiota among four countries was also performed (Figure 2B). Some gut microbiotas, including *S24_7 unclassified*, *Lactobacillus*, *Peptostreptococcaceae unclassified*, *Ruminococcaceae unclassified*, *Lachnospiraceae unclassified*, and *Bacteroides*, were enriched in the L airway of cattle from China. *Mycoplasma* was over-represented in the lungs of cattle from Italy, and *Aggregatibacter*, *Prevotella*, and *Corynebacterium* were abundant in USA cattle.

Distribution of the main microbes in different niches

As the physiology of different respiratory niches influences the microbial composition, LEfSe analysis and correlation analysis were performed to screen out the signature microbes for the major niches (OS, NS, NP, and BAL) along the bovine respiratory tract (Figures 3, S2). In Chinese cattle, *Aggregatibacter*, *Moraxella*, *Streptococcus*, *Weeksellaceae unclassified*, *Haemophilus*, *Flavobacteriaceae unclassified*, and *Pasteurellaceae unclassified* had higher abundances in the OS (Figure 3). In the NS, only the *Enhydrobacter* genus was more abundant. In the NP, the abundance of *Corynebacterium*, *Microbacteriaceae unclassified*, *Janibacter*, and *Kineosporiaceae unclassified* was greater. In BAL, bacterial genera, including *Mycoplasma*, *Prevotella*, *Lactobacillus*, *Akkermansia*, *Ruminococcaceae unclassified*, *Lachnospiraceae unclassified*, *Ruminococcus*, *Oscillospira*, *Pseudomonadaceae unclassified*, *Parabacteroides*, and *Faecalibacterium*, were more abundant. In Canadian cattle, *Aggregatibacter*, *Streptococcus*, *Fusobacterium*, *Pasteurellaceae unclassified*, and *Weekselllaceae unclassified* had higher abundance in the OS. In the NS, *Moraxella*, *Moraxellaceae unclassified*, *Chitinophagaceae unclassified*, *Ruminococcaceae unclassified*, *Macrococcus*, *Planococcaceae unclassified*, *Demequina*, *Lactobacillus*, and *Solibacillus* were more abundant. In the NP, the abundance of *Psychrobacter*, *Acinetobacter*, and *Pseudomonadaceae unclassified* was higher. In the BAL, the abundances of *Mycoplasma*, *Microbacteriaceae unclassified*, *Streptomyces*, *Corynebacterium*, *Plesiomonas*, *Aerococcus*, and *Micrococcus* were high.

Moreover, some signature bacteria for one niche were found across countries. For example, *Aggregatibacter* and *Streptococcus* were abundant in the OS of both Chinese and Canadian cattle (Figure 3), and they were also identified as OS signatures in the LEfSe outputs using all samples from four countries (Figure S2). *Mycoplasma* abundant in the BAL had a similar pattern. Overall, although the niche-specific microbiota was associated with geography, shared microbiotas were found and detected in all four niches.

The spatial dissimilarities and connections of the microbiota in the respiratory tract of beef cattle

After the different microbial compositions in the niches along the bovine respiratory tract were characterized, the spatial dynamics of the bovine respiratory microbiota from the same cattle were estimated. When excluding the geographic effects, distinct microbial structures between the oral cavity, upper, and lung were also observed, which had a similar pattern in samples of different countries (Figures 4A–C). For example, regarding the beta diversity based on Bray-Curtis distance, in the different geographies, microbiota in different niches showed distinct clusters (Figures 4A–C) (ANOSIM, in Canada, NS vs BAL: R = 0.365; in

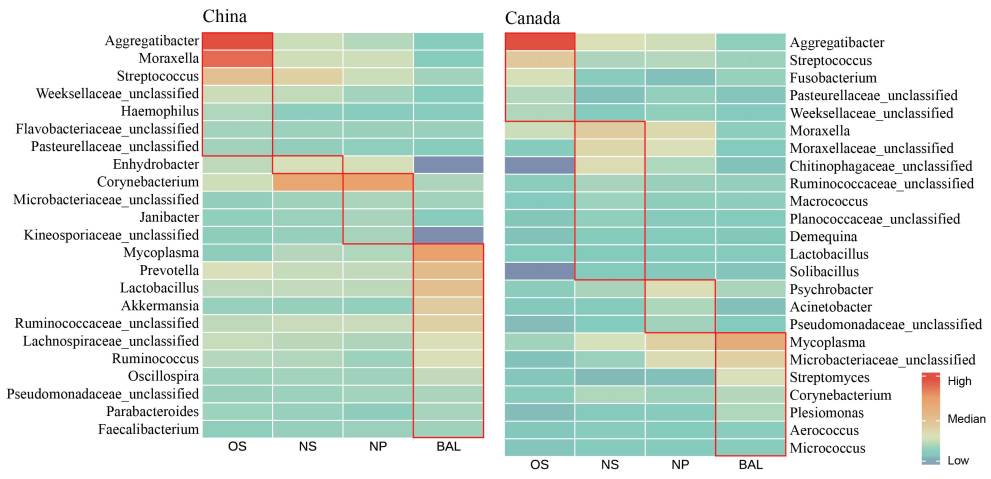

FIGURE 3
Abundance profile of featured microbes in different ecological niches in the respiratory tract of cattle in China and Canada. The average value of the relative abundance of the single bacteria was compared after making the logarithm in different niches. The red box represents featured microbes that have the highest relative abundance in this niche. The featured microbes were selected based on the results of LEfSe analysis (LDA > 2) across various niches and the significant co-efficient relationship (Pearson rank correlation coefficient > 0.4 or < -0.4) with specific bacteria. OS (Oropharynx); NS (Nasal); NP (Nasopharyngeal); BAL (Bronchoalveolar lavage).

China, NS vs BAL: R = 0.285; in Italy, NS vs BAL: R = 0.529, $P < 0.05$, Supplementary Table S4). However, regardless of the countries, bigger differences between NP and BAL were observed compared to NS and BAL (Supplementary Table S5). Moreover, oropharyngeal microbiota seemed to be independent of the respiratory microbiota in beef cattle as it showed a large distance from NS, NP, and BAL.

Next, we sought to analyze the microbial associations among niches (oropharynx, nostrils, nasopharynx, and lung) as shared bacteria taxa existed and the anatomical connections may lead to microbial migration within the respiratory systems. We assessed the similarities between niches by measuring the Pearson correlation between sampling niches, thus accounting for both the rank order of ASVs and the magnitude of relative abundances between sampling sites being compared. In the Canadian beef cattle, the correlation between OS vs NS was higher than OS vs NP and OS vs BAL (Pearson, OS vs NS: R = 0.41; OS vs NP: R = 0.36; OS vs BAL: R = 0.37) (Figures 4D–F). The NS microbiota was highly correlated with that of the NPS (r=0.68, p<0.001) (Figure 4G). The correlation between NPS and BAL microbiota (r=0.50, p<0.001) was greater

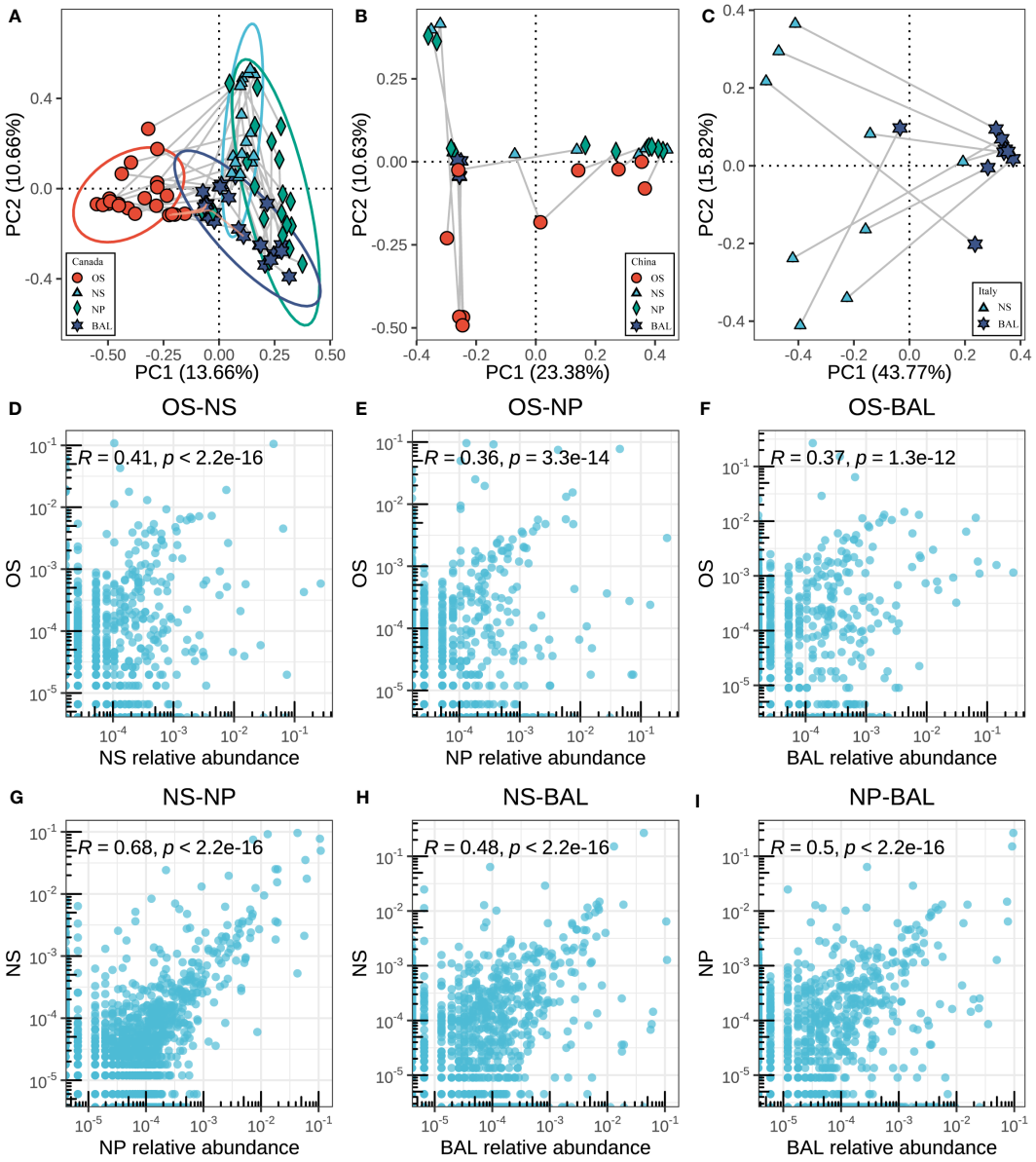

FIGURE 4
Associations between microbes in different niches of the respiratory tract. **(A–C)** The principal coordinate analysis (PCoA) is based on the beta diversity (Bray–Curtis) of microbes in each sample between different niches in different countries. The Connected points represent samples from the same animal. The length of the line reflects the similarity between samples, and the longer lines represent the lower similarity. **(D–I)** The correlation of the respiratory tract microbes in different niches in Canadian samples. Each point corresponds to the average relative abundance of a feature across all animals for each of the respiratory tract sampling niches. To measure correlation, Pearson's r was calculated based on the features abundance of two niches.

than that between NS and BAL microbiota than that of BAL (r=0.48, p<0.001) (Figures 4H, I), which is consistent with the ANOSIM data based on microbial structure. In the other countries, the microbial similarities between niches had a similar pattern (Figure S3). Overall, the microbial connection within the respiratory tract of beef cattle existed although we observed the microbial dissimilarities among niches.

The microaspiration in the respiratory tract of beef cattle

To deeply understand the microbial connection within the respiratory tract of beef cattle, the microaspiration of the major taxa were assessed. As we observed, *Mycoplasma* associated with bovine respiratory disease existed in four sampling niches of the Canadian beef cattle and increased from the oropharynx and upper to the lung although its abundances were different (Figure 5). A similar pattern was also observed in the cattle from China and Italy (Figure S4A). In the meantime, *Streptococcus* migration among niches was the same among countries with high abundance in OS followed by NS, BAL, and NPS (Figures 5D, E, S4B). In contrast, the microaspiration of other major respiratory microbiota among countries were different. In Chinese beef cattle, *Moraxella* was higher in the oral cavity followed by NS, NPS, and lung (Figure 5B). However, in Canada, it was higher in NS and NPS followed by oral and lung (Figures 5C, S4B). Other important respiratory microbiota, such as *Pasteurellaceae unclassified*, *Moraxellaceae unclassified*, *Microbacteriaceae unclassified*, *Mogibacteriaceae unclassified*, *Corynebacterium*, *Pseudomonadaceae unclassified*, and *Roseburia* were abundant in the upper airway or oropharynx, but their abundance in lung varied among countries (Figures S5, S6). The microbiota commonly found in the gut showed higher abundances in NS and NPS followed by OS and BAL, such as *Ruminococcaceae unclassified* and *Turicibacter* (Figures 5F, G, S4B, C). Other gut microbiotas, including *Prevotellaceae unclassified*, *Clostridium*, *Lactobacillus*, *Lachnospiraceae unclassified*, and *Bifidobacterium*, were more enriched in the oral cavity or the upper respiratory tracts regardless of country (Figure S7).

Network analysis to reveal the microbial interactions among respiratory niches

The microbial interactions were determined using network analysis (Figures 6, S8). When using Chinese and Canadian bovine airway microbial samples, four and seven modules were observed respectively. In the meantime, more edges and nodes were found in airway samples of Chinese cattle compared to that of Canadian bovines. Interestingly, in both countries, the featured microbes within the same niche exhibited a stronger correlation in the same module. For example, in China cattle, genera for BAL identified by LEfSe that correlated with other commensal microbiotas formed a module, including *Mycoplasma*, *Lactobacillus*, *Akkermansia*, *Ruminococcaceae unclassified*, *Lachnospiraceae unclassified*, *Ruminococcus*, *Oscillospira*, and *Pseudomonadaceae unclassified* (Figure 6). In addition, these signature microbiotas were identified as the bridge nodes to connect different modules. The BAL signature microbiotas for the bovines from Canada, including *Corynebacterium, Aerococcus*, *Micrococcus*, were the key nodes to bright two modules. Additionally, network analysis using all four countries' samples showed that the niches' effects on the bacterial interaction were slight (Figure S8). All these results indicated that geographic effects on the bovine respiratory microbiome system were greater than niche effects, and the signature microbiota affected the microbial interactions.

Discussion

Investigation of the respiratory microbiota in healthy bovines aid in understanding the critical roles of the microbiota in health and provide microbial insights for prevention and diagnosis of BRD. Until now, the nasopharynx has been the most popular sampling site to investigate bovine respiratory microbiota (McMullen et al., 2020a), but microbiota colonization in the nostrils and lungs is less studied and important. In this study, we found that significant differences in the respiratory microbial composition and structure of the bovine were associated with geography and sampling niches. Despite the greater variations of the upper and lower airway microbiota being observed, geographic effects on both were also identified. It is confirmed that geography influenced the physiological and biochemical environments of the bovine respiratory tract; however local physiology of niches also shaped its microbial community. The abundant bacteria for each respiratory niche were identified, and they were associated with geography. In the meantime, shared taxa among these sampling niches were found, indicating that microaspiration might exist in the bovine airway. However, the spatial connection of the bovine airway microbiota is still less studied. This study determined the spatial dynamics of the respiratory microbiota from the nostrils to the nasopharynx to the lung and found that NS and NPS microbiota were more similar compared to the lung community. The oral microbiota also showed similarities to the respiratory microbiota. In addition, the spatial connection of the bovine respiratory microbiota from worldwide geographic locations was also characterized, which allows us to understand the microaspiration of the microbiota deeply. This study elucidated the fundamental knowledge of the bovine respiratory microbiota.

Geography serving an important role in affecting the bovine respiratory microbiota has been confirmed in our previous study (Chai et al., 2022b). In this study, we also found that either the upper or lower airway microbiota in the beef cattle from China (Asia), Canada and the United States (North America), and Italy (Europe) had different diversities and composition. Calves living in worldwide geographic locations experienced environmental variations, including feed strategy, diet, altitude, temperature, etc. In this study, the dominant bacteria varied across the four countries. For instance, *Mycoplasma* was abundant in the upper and lower airway of Italy cattle but lower in other countries, and *Moraxella* was enriched in the upper airway of cattle from Canada but lower in

other niches of cattle from other countries. Previously, a study found that, in Canada, the most prominently identified bacteria in the bovine nasopharynx were *Mycoplasma*, *Lactococcus*, *Moraxella*, *Histophilus*, and *Pasteurella*, while *Mannheimia*, *Mycoplasma*, *Moraxella*, *Psychrobacter*, and *Pseudomonas* were the top five genera in the nasopharynx of calves from the United States (Lima et al., 2016; McMullen et al., 2018). Thus, it's not surprising that bovine airway microbiota from three continents showed differences.

In addition, the current study first characterized the altitude effects on the bovine airway microbiota. We found that more significant differences in airway microbiota among cattle from 200 m, 500 m, 1000 m, and 1500 m masl were observed although breed and diet effects may exist. Thus, geography or external environment may have a greater influence on the bovine airway microbiota. Further studies need to deepen the environmental effects, which might benefit the probiotics production from high-altitude cattle.

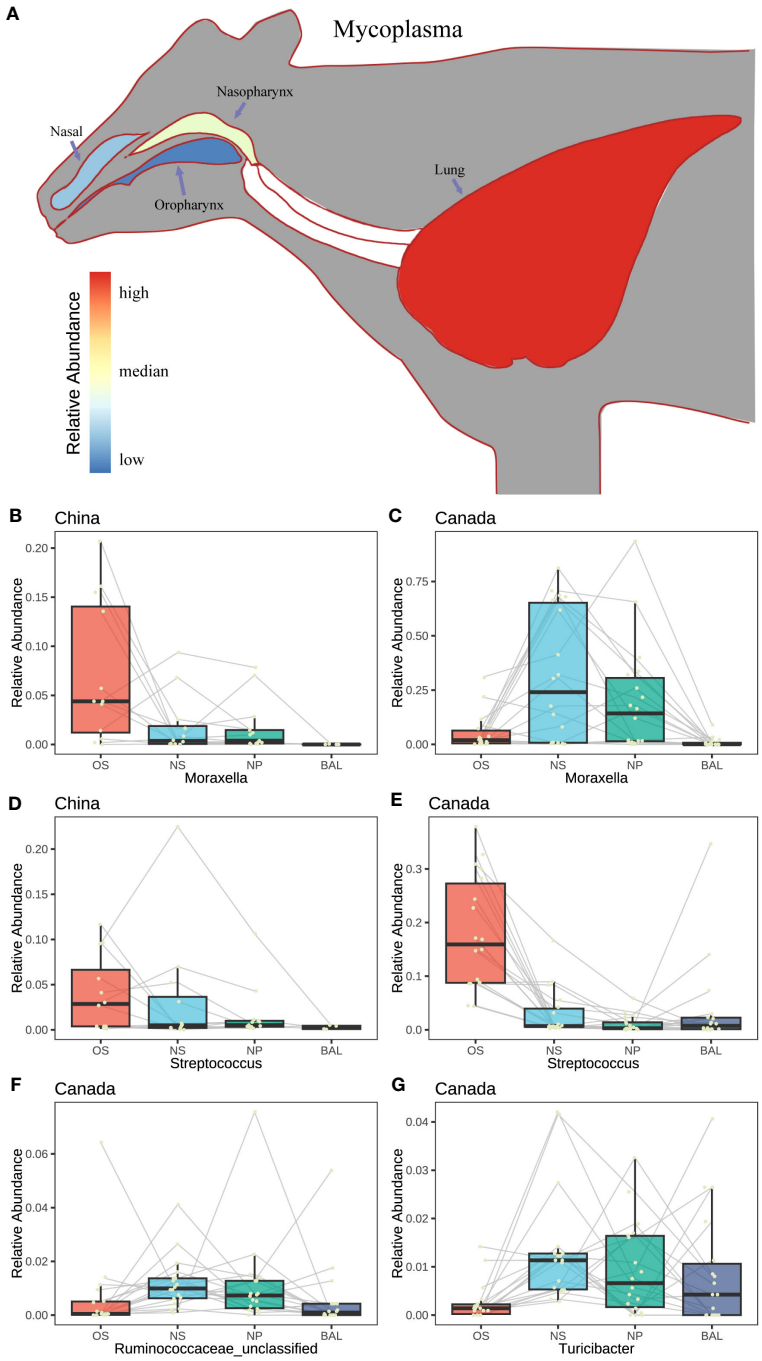

FIGURE 5
The characteristics in abundance change of the featured microbes. **(A)** Model diagram of the relative abundance change of a single bacterium (*Mycoplasma*) at different niches in the respiratory tract of animals. **(B–G)** The change of the relative abundance of the featured microbes with different niches in different countries. A yellow point represents a sample. The Connected points represent samples from the same animal.

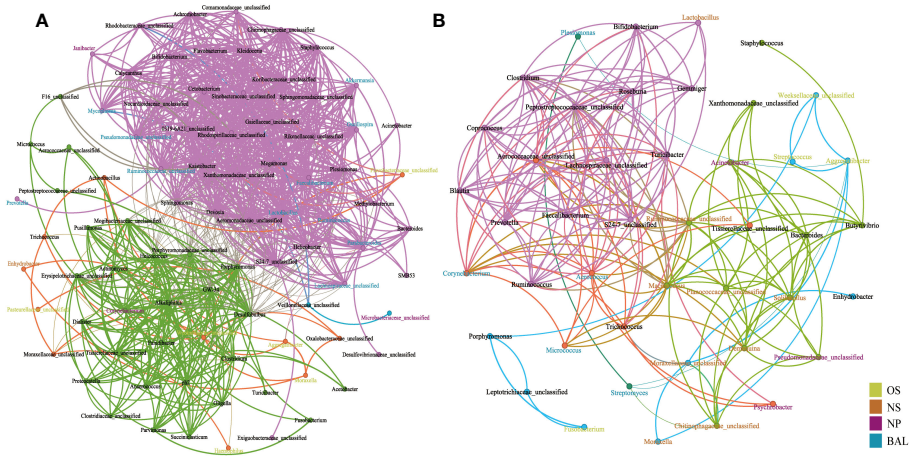

FIGURE 6
Network analysis of interactions between genus level interactions in the respiratory tract of cattle in **(A)** China and **(B)** Canada. Each node denotes a particular genus within the network and the different colors denote the featured bacteria in different niches. Each line (edge) represents a significant co-efficiency relationship (Pearson rank correlation coefficient in China > 0.5 or < −0.5 and in Canada > 0.4 or < −0.4). The network has divided all bacteria into communities of different colors through modularization. OS (Oropharynx); NS (Nasal); NP (Nasopharyngeal); BAL (Bronchoalveolar lavage).

Anatomical niches within the respiratory tract have different local environments (Chai et al., 2022a). Differences in microbial composition and structure in the upper and lower respiratory tract of bovine were found in the current study. The bovine nostrils had higher abundances of *Enhydrobacter, Corynebacterium, Pseudoalteromonas*, and *Phascolarctobacterium*, while the dominant genera in the nasopharynx were *Psychrobacter, Moraxella, Pseudomonadaceae unclassified, Ruminococcaceae unclassified, Roseburia, Moraxellaceae unclassified*, and *Acinetobacter*. In the lungs, we classified *Streptomyces, Plesiomonas, Turicibacter, Microbacteriaceae unclassified*, and *Mycoplasma*. Previous studies reported dominant genera in the bovine nasal cavity, such as *Psychrobacter*, *Aggregatibacter*, *Sphingomonas*, *Corynebacterium*, and *Coprococcus* (Nicola et al., 2017; McDaneld et al., 2018). The nasopharynx (the region near the caudal aspect of the nose) colonized with *Pseudomonas*, *Psychrobacter*, *Actinobacillus*, *Clostridium*, *Acinetobacter*, *Bacillus*, *Proteus*, *Bifidobacterium*, *Rathayibacter*, *Cellulomonadaceae*, *Corynebacterium*, *Jeotgalicoccus*, and *Planomicrobium* (Gaeta et al., 2017; Holman et al., 2017; Zeineldin et al., 2017a; Timsit et al., 2018; Amat et al., 2019). In the clinically healthy bovine lungs, previous studies found the genera *Mycoplasma*, *Moraxella*, *Pasteurella*, *Mannheimia*, *Bacteroides*, *Clostridium*, *Bibersteinia*, and *Prevotella* (Nicola et al., 2017; Zeineldin et al., 2017b; Klima et al., 2019). Overall, except for the variations among cattle or studies, the bacterial composition and abundances among the three popular sampling niches (nostrils, nasopharynx, and lungs) in the bovine are different but shared taxon could be observed. Investigation of the global microbial ecosystem in calves allows us to identify BRD pathogens well.

Microbial movement or dispersion within the respiratory tract is new and essential research direction as it could potentially explain the contribution of the upper airway microbiota to the lung microbiota and the respiratory health to disease (Zeineldin et al., 2019; Chai et al., 2022a). This study found that microbial communities in the nostrils and nasopharynx were correlated with those in the lungs regardless of geographic effects. One recent study concluded that nasopharyngeal microbiota may serve as the primary source for the lung microbiota in healthy calves since the nasopharyngeal region shared a similar bacterial composition with the lungs compared to other sampling niches (McMullen et al., 2020a). Similarly, bacterial overlaps between the upper and lower tracts in cattle have also been reported (Nicola et al., 2017; Zeineldin et al., 2017b; Timsit et al., 2018), indicating microbial aspiratory within the bovine respiratory tract. In healthy subjects, microbiota from the upper airway could enter the lungs via an active and continuous process in several ways, such as inhalation of air, direct mucosal dispersal, and microaspiration (Dickson et al., 2014). Furthermore, an adapted island model was applied in healthy humans, and the hypothesis is that the lung microbiome and its growth rate are more affected by microbial entry and removal processes than by the effects of the local growth environments. However, for ruminants, there is no specific statistical model to investigate the respiratory microbial movement. Thus, the current study mapped the relative abundance of the major microbiota along the bovine airway. We found that immigration of some microbiotas was similar in different countries, such as *Mycoplasma* and *Moraxella* abundant in the upper airway rather than the lungs. However, geography affecting the microaspiration of a specific bacterium was also observed. For example, the abundances of *Pasteurellaceae* and *Microbacteriaceae* were high in the upper air way but varied among countries in lung communities. Overall, the microaspiration of the bovine respiratory microbiota existed and some bacteria showed same immigration pattern no matter whatever geographies, which may help us explain the common pattern of respiratory microbiome in the world.

Oral microbiome in cattle is starting to be studied as its importance in humans has been confirmed (Dickson and Huffnagle, 2015; Dickson et al., 2016). The specific ruminating activity in cattle may cause more oral microbiota to enter into the lungs (Glendinning et al., 2017). Moreover, social grooming may cause oral bacteria to

migrate into the upper airway. All these movements of microbiota are relevant to our understanding of pathogenesis in bovine health and disease (Segal and Blaser, 2014). In this study, the major bacterial signatures, including *Aggregatibacter, Streptococcus, Pasteurellaceae unclassified, Clostridium, Ruminococcus, Lactobacillus, Prevotellaceae unclassified*, and *Bifidobacterium*, were identified for the bovine oral cavity. A previous study found that *Pasteurellaceae*, *Moraxellaceae*, and *Neisseriaceae* associated with the BRD pathogens were detected in the oral cavity of calves (Barden et al., 2020). Another study found that *Pseudomonas*, *Burkholderia*, and *Actinobacteria* were the most prevalent bacteria in the mouth of healthy cattle, but *Prevotella*, *Fusobacterium*, and *Porphyromonas* were significantly increased in cattle with periodontitis (Borsanelli et al., 2018). Although the dominant species may be different, shared taxa were observed compared to these studies. Our results also found that some oral bacteria were associated with the upper and lower airway microbiota in cattle, which showed a similar pattern to a previous study (McMullen et al., 2020a). For example, *Moraxella* and *Mogibacteriaceae unclassified* were higher in both the oral cavity and nostrils. Considering cattle often lick their noses and can actually reach farther into their nostrils than other species, this is not surprising. However, the composition of the oral microbiome and its association with the bovine respiratory microbial communities is still largely unknown. The oral and oropharyngeal microbiome for health and BRD calves should be further investigated.

Conclusions

Bacterial 16S rRNA gene sequencing demonstrated that geography affected both the upper and lower respiratory microbiota in bovine. The factors related to geography, including altitude and temperature, may contribute to microbial changes. Although the dominant genera among countries were different, shared taxa were observed, indicating that the similarities in research on bovine respiratory microbiota may elucidate the microbial roles in health and disease. Beyond the most popular sampling niche (nasopharynx) in the current studies, the microbiome in nostrils and lungs showed their specifications, which should be further investigated for better understanding of bovine respiratory disease. In addition to the effects of geography and niche on the bovine airway ecosystem, the common taxa and their immigration pattern were characterized in this study, providing some insights into bovine respiratory microbiome and health. Moreover, oral microbiota with its specific composition compared to the respiratory microbiome was associated with the nostril and lung microbial community in cattle. Therefore, all the results in this study support the notion that bacterial isolations or probiotics could be administrated into the bovine mouth or nostrils to improve lung community.

Data availability statement

Sequences were deposited in the NCBI sequence read archive (SRA) database under Bioproject PRJNA952496, BioSamples SAMN34074578-SAMN34074618.

Ethics statement

The animal studies were approved by Animal Ethics and Humane Animal Care of the Foshan University. The studies were conducted in accordance with the local legislation and institutional requirements. Written informed consent was obtained from the owners for the participation of their animals in this study.

Author contributions

ZZ: Data curation, Formal Analysis, Investigation, Writing – original draft. CZ: Data curation, Investigation, Writing – original draft. YZ: Data curation, Investigation, Writing – original draft. SY: Data curation, Methodology, Resources, Writing – review & editing. FD: Data curation, Investigation, Writing – original draft. YL: Funding acquisition, Project administration, Writing – review & editing. JC: Project administration, Writing – review & editing, Conceptualization, Data curation, Formal Analysis, Investigation, Methodology, Resources, Software, Supervision, Writing – original draft.

Funding

This project was supported by Agriculture and Food Research Initiative Competitive Grant No. 20196701629869 from the USDA National Institute of Food and Agriculture, National Natural Science Foundation of China (No. 32170430), Guangdong Provincial Key Laboratory of Animal Molecular Design and Precise Breeding (2019B030301010), and Key Laboratory of Animal Molecular Design and Precise Breeding of Guangdong Higher Education Institutes (2019KSYS011).

Conflict of interest

The authors declare that the research was conducted in the absence of any commercial or financial relationships that could be construed as a potential conflict of interest.

Publisher's note

Supplementary material

The Supplementary Material for this article can be found online at: https://www.frontiersin.org/articles/10.3389/fcimb.2023.1269726/full#supplementary-material

References

Amat, S., Holman, D. B., Timsit, E., Schwinghamer, T., and Alexander, T. W. (2019). Evaluation of the nasopharyngeal microbiota in beef cattle transported to a feedlot, with a focus on lactic acid-producing bacteria. *Front. Microbiol.* 10, 1988. doi: 10.3389/fmicb.2019.01988

Amir, A., Mcdonald, D., Navas-Molina, J. A., Kopylova, E., Morton, J. T., Zech Xu, Z., et al. (2017). Deblur rapidly resolves single-nucleotide community sequence patterns. *mSystems* 2, 10–1128. doi: 10.1128/mSystems.00191-16

Barden, M., Richards-Rios, P., Ganda, E., Lenzi, L., Eccles, R., Neary, J., et al. (2020). Maternal influences on oral and faecal microbiota maturation in neonatal calves in beef and dairy production systems. *Anim. Microbiome* 2, 31. doi: 10.1186/s42523-020-00049-1

Bolyen, E., Rideout, J. R., Dillon, M. R., Bokulich, N. A., Abnet, C. C., Al-Ghalith, G. A., et al. (2019). Reproducible, interactive, scalable and extensible microbiome data science using QIIME 2. *Nat. Biotechnol.* 37, 1091–1091. doi: 10.1038/s41587-019-0252-6

Borsanelli, A. C., Lappin, D. F., Viora, L., Bennett, D., Dutra, I. S., Brandt, B. W., et al. (2018). Microbiomes associated with bovine periodontitis and oral health. *Vet. Microbiol.* 218, 1–6. doi: 10.1016/j.vetmic.2018.03.016

Bray, J. R., and Curtis, J. T. (1957). An ordination of the upland forest communities of southern Wisconsin. *Ecol. Monogr.* 27, 326–349. doi: 10.2307/1942268

Centeno-Martinez, R. E., Glidden, N., Mohan, S., Davidson, J. L., Fernández-Juricic, E., Boerman, J. P., et al. (2022). Identification of bovine respiratory disease through the nasal microbiome. *Anim. Microbiome* 4, 15. doi: 10.1186/s42523-022-00167-y

Chai, J., Capik, S. F., Kegley, B., Richeson, J. T., Powell, J. G., and Zhao, J. (2022a). Bovine respiratory microbiota of feedlot cattle and its association with disease. *Vet. Res.* 53, 4. doi: 10.1186/s13567-021-01020-x

Chai, J., Liu, X., Usdrowski, H., Deng, F., Li, Y., and Zhao, J. (2022b). Geography, niches, and transportation influence bovine respiratory microbiome and health. *Front. Cell Infect. Microbiol.* 12, 961644. doi: 10.3389/fcimb.2022.961644

Chao, A., Chazdon, R. L., Colwell, R. K., and Shen, T. J. (2005). A new statistical approach for assessing similarity of species composition with incidence and abundance data. *Ecol. Lett.* 8, 148–159. doi: 10.1111/j.1461-0248.2004.00707.x

Cirone, F., Padalino, B., Tullio, D., Capozza, P., Losurdo, M., Lanave, G., et al. (2019). Prevalence of pathogens related to bovine respiratory disease before and after transportation in beef steers: preliminary results. *Animals* 9, 1093. doi: 10.3390/ani9121093

DeSantis, T. Z., Hugenholtz, P., Larsen, N., Rojas, M., Brodie, E. L., Keller, K., et al. (2006). Greengenes, a chimera-checked 16S rRNA gene database and workbench compatible with ARB. *AEM* 72, 5069–5072. doi: 10.1128/AEM.03006-05

Dickson, R. P., Erb-Downward, J. R., Martinez, F. J., and Huffnagle, G. B. (2016). The microbiome and the respiratory tract. *Annu. Rev. Physiol.* 78, 481–504. doi: 10.1146/annurev-physiol-021115-105238

Dickson, R. P., and Huffnagle, G. B. (2015). The lung microbiome: new principles for respiratory bacteriology in health and disease. *PLoS Pathog.* 11, e1004923. doi: 10.1371/journal.ppat.1004923

Dickson, R. P., Martinez, F. J., and Huffnagle, G. B. (2014). The role of the microbiome in exacerbations of chronic lung diseases. *Lancet* 384, 691–702. doi: 10.1016/S0140-6736(14)61136-3

Fahkrajang, W., Sudaryatma, P. E., Mekata, H., Hamabe, S., Saito, A., and Okabayashi, T. (2021). Bovine respiratory coronavirus enhances bacterial adherence by upregulating expression of cellular receptors on bovine respiratory epithelial cells. *Vet. Microbiol.* 255, 109017. doi: 10.1016/j.vetmic.2021.109017

Gaeta, N. C., Lima, S. F., Teixeira, A. G., Ganda, E. K., Oikonomou, G., Gregory, L., et al. (2017). Deciphering upper respiratory tract microbiota complexity in healthy calves and calves that develop respiratory disease using shotgun metagenomics. *J. Dairy Sci.* 100, 1445–1458. doi: 10.3168/jds.2016-11522

Glendinning, L., Collie, D., Wright, S., Rutherford, K. M. D., and Mclachlan, G. (2017). Comparing microbiotas in the upper aerodigestive and lower respiratory tracts of lambs. *Microbiome* 5, 145. doi: 10.1186/s40168-017-0364-5

Holman, D. B., Mcallister, T. A., Topp, E., Wright, A.-D. G., and Alexander, T.W.J.V.M. (2015). The nasopharyngeal microbiota of feedlot cattle that develop bovine respiratory disease. *Vet. Microbiol.* 180, 90–95. doi: 10.1016/j.vetmic.2015.07.031

Holman, D. B., Timsit, E., Amat, S., Abbott, W., Buret, A. G., and Alexander, T. W. (2017). The nasopharyngeal microbiota of beef cattle before and after transport to a feedlot. *BMC Microbiol.* 17, 1–12. doi: 10.1186/s12866-017-0978-6

Holman, D. B., Timsit, E., Booker, C. W., and Alexander, T.W.J.V.M. (2018). Injectable antimicrobials in commercial feedlot cattle and their effect on the nasopharyngeal microbiota and antimicrobial resistance. *Vet. Microbiol.* 214, 140–147. doi: 10.1016/j.vetmic.2017.12.015

Holman, D. B., Yang, W., and Alexander, T. W. (2019). Antibiotic treatment in feedlot cattle: a longitudinal study of the effect of oxytetracycline and tulathromycin on the fecal and nasopharyngeal microbiota. *Microbiome* 7, 7–86. doi: 10.1186/s40168-019-0696-4

Klima, C. L., Holman, D. B., Ralston, B. J., Stanford, K., Zaheer, R., Alexander, T. W., et al. (2019). Lower respiratory tract microbiome and resistome of bovine respiratory disease mortalities. *Microb. Ecol.* 78, 446–456. doi: 10.1007/s00248-019-01361-3

Lima, S. F., Teixeira, A. G., Higgins, C. H., Lima, F. S., and Bicalho, R. C. (2016). The upper respiratory tract microbiome and its potential role in bovine respiratory disease and otitis media. *Sci. Rep.* 6, 1–12. doi: 10.1038/srep29050

Losol, P., Choi, J.-P., Kim, S.-H., and Chang, Y.-S. (2021). The role of upper airway microbiome in the development of adult asthma. *Immune Netw.* 21 (3), e19. doi: 10.4110/in.2021.21.e19

Man, W. H., De Steenhuijsen Piters, W. A., and Bogaert, D. (2017). The microbiota of the respiratory tract: gatekeeper to respiratory health. *Nat. Rev. Microbiol.* 15, 259–270. doi: 10.1038/nrmicro.2017.14

McDaneld, T. G., Kuehn, L. A., and Keele, J. W. (2018). Evaluating the microbiome of two sampling locations in the nasal cavity of cattle with bovine respiratory disease complex (BRDC). *J. Anim. Sci.* 96, 1281–1287. doi: 10.1093/jas/sky032

McMullen, C., Alexander, T. W., Leguillette, R., Workentine, M., and Timsit, E. (2020a). Topography of the respiratory tract bacterial microbiota in cattle. *Microbiome* 8, 91. doi: 10.1186/s40168-020-00869-y

McMullen, C., Alexander, T. W., Orsel, K., and Timsit, E. (2020b). Progression of nasopharyngeal and tracheal bacterial microbiotas of feedlot cattle during development of bovine respiratory disease. *Vet. Microbiol.* 248, 108826. doi: 10.1016/j.vetmic.2020.108826

McMullen, C., Orsel, K., Alexander, T. W., van der Meer, F., Plastow, G., and Timsit, E. (2018). Evolution of the nasopharyngeal bacterial microbiota of beef calves from spring processing to 40 days after feedlot arrival. *Vet. Microbiol.* 225, 139–148. doi: 10.1016/j.vetmic.2018.09.019

Nicola, I., Cerutti, F., Grego, E., Bertone, I., Gianella, P., D'angelo, A., et al. (2017). Characterization of the upper and lower respiratory tract microbiota in Piedmontese calves. *Microbiome* 5, 152. doi: 10.1186/s40168-017-0372-5

Segal, L. N., and Blaser, M. J. (2014). A brave new world: the lung microbiota in an era of change. *Ann. Am. Thorac. Soc.* 11 Suppl 1, S21–S27. doi: 10.1513/AnnalsATS.201306-189MG

Timsit, E., Workentine, M., van der Meer, F., and Alexander, T. (2018). Distinct bacterial metacommunities inhabit the upper and lower respiratory tracts of healthy feedlot cattle and those diagnosed with bronchopneumonia. *Vet. Microbiol.* 221, 105–113. doi: 10.1016/j.vetmic.2018.06.007

Venkataraman, A., Bassis, C. M., Beck, J. M., Young, V. B., Curtis, J. L., Huffnagle, G. B., et al. (2015). Application of a neutral community model to assess structuring of the human lung microbiome. *MBio* 6, e02284–e02214. doi: 10.1128/mBio.02284-14

Wang, J., Chai, J., Sun, L., Zhao, J., and Chang, C. (2020). The sputum microbiome associated with different sub-types of AECOPD in a Chinese cohort. *BMC Infect. Dis.* 20, 1–12. doi: 10.1186/s12879-020-05313-y

Wang, J., Chai, J., Zhang, L., Zhang, L., Yan, W., Sun, L., et al. (2022). Microbiota associations with inflammatory pathways in asthma. *Clin. Exp. Allergy* 52, 697–705. doi: 10.1111/cea.14089

Wickham, H. (2011). ggplot2. *Computational Statistics* 3, 180–185. doi: 10.1002/wics.147

Zeineldin, M., Lowe, J., and Aldridge, B. (2019). Contribution of the mucosal microbiota to bovine respiratory health. *Trends Microbiol.* 27, 753–770. doi: 10.1016/j.tim.2019.04.005

Zeineldin, M., Lowe, J., and Aldridge, B. (2020). Effects of tilmicosin treatment on the nasopharyngeal microbiota of feedlot cattle with respiratory disease during the first week of clinical recovery. *Front. Vet. Sci.* 7, 115. doi: 10.3389/fvets.2020.00115

Zeineldin, M., Lowe, J., De Godoy, M., Maradiaga, N., Ramirez, C., Ghanem, M., et al. (2017a). Disparity in the nasopharyngeal microbiota between healthy cattle on feed, at entry processing and with respiratory disease. *Vet. Microbiol.* 208, 30–37. doi: 10.1016/j.vetmic.2017.07.006

Zeineldin, M. M., Lowe, J. F., Grimmer, E. D., De Godoy, M. R. C., Ghanem, M. M., Abd El-Raof, Y. M., et al. (2017b). Relationship between nasopharyngeal and bronchoalveolar microbial communities in clinically healthy feedlot cattle. *BMC Microbiol.* 17, 1–11. doi: 10.1186/s12866-017-1042-2

Zhang, J., Wu, Y., Liu, J., Yang, Y., Li, H., Wu, X., et al. (2022). Differential oral microbial input determines two microbiota pneumo-types associated with health status. *Adv. Sci.* 9, 2203115. doi: 10.1002/advs.202203115

Frontiers in
Cellular and Infection Microbiology

Investigates how microorganisms interact with their hosts

Explores bacteria, fungi, parasites, viruses, endosymbionts, prions and all microbial pathogens as well as the microbiota and its effect on health and disease in various hosts.

Discover the latest Research Topics

See more →

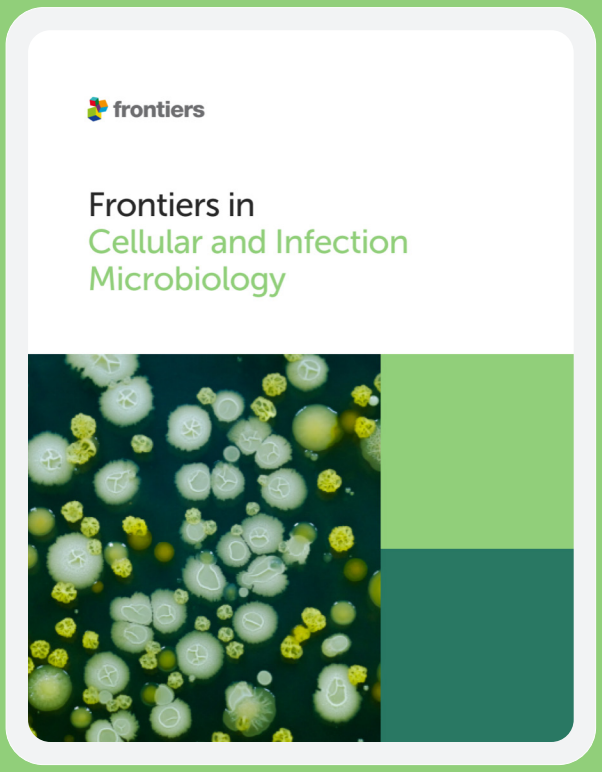

Frontiers

Avenue du Tribunal-Fédéral 34
1005 Lausanne, Switzerland
frontiersin.org

Contact us

+41 (0)21 510 17 00
frontiersin.org/about/contact